GEOLOGICAL SURVEY RESEARCH 1968

Chapter B

GEOLOGICAL SURVEY PROFESSIONAL PAPER 600–B

Scientific notes and summaries of investigations in geology, hydrology, and related fields

UNITED STATES GOVERNMENT PRINTING OFFICE, WASHINGTON: 1968

UNITED STATES DEPARTMENT OF THE INTERIOR

STEWART L. UDALL, Secretary

GEOLOGICAL SURVEY

William T. Pecora, Director

For sale by the Superintendent of Documents, U.S. Government Printing Office
Washington, D.C. 20402 - Price $2

CONTENTS

GEOLOGIC STUDIES

GEOLOGICAL SURVEY RESEARCH 1968

This collection of 44 short papers is the first published chapter of "Geological Survey Research 1968." The papers report on scientific and economic results of current work by members of the Geologic, Topographic, and Water Resources Divisions of the U.S. Geological Survey.

Chapter A, to be published later in the year, will present a summary of significant results of work done during fiscal year 1968, together with lists of investigations in progress, reports published, cooperating agencies, and Geological Survey offices.

"Geological Survey Research 1968" is the ninth volume of the annual series Geological Survey Research. The eight volumes already published are listed below, with their series designations.

Geological Survey Research 1960—Prof. Paper 400
Geological Survey Research 1961—Prof. Paper 424
Geological Survey Research 1962—Prof. Paper 450
Geological Survey Research 1963—Prof. Paper 475
Geological Survey Research 1964—Prof. Paper 501
Geological Survey Research 1965—Prof. Paper 525
Geological Survey Research 1966—Prof. Paper 550
Geological Survey Research 1967—Prof. Paper 575

X-RAY AND CHEMICAL ANALYSIS OF ORTHOPYROXENES FROM THE LOWER PART OF THE BUSHVELD COMPLEX, SOUTH AFRICA[1]

By GEORGE A. DESBOROUGH and HARRY J. ROSE, JR.,
Denver, Colo., Washington, D.C.

Abstract.—Seven orthopyroxene concentrates from rocks of the lower part of the eastern Bushveld Complex were analyzed by X-ray fluorescence and rapid rock analysis methods. The composition of the orthopyroxenes is correlated with the (060) X-ray reflection. Measurement of this X-ray reflection for "Bushveld-type" orthopyroxenes provides a method of determining the En content with a standard error of about ±1.0 mol percent for the composition range En_{86} to En_{76}.

An effort to establish a rapid and precise method for the determination of the average composition of bulk concentrates of orthopyroxenes from the Bushveld Complex, South Africa, has provided an X-ray determination curve with a standard error of about ±1.0 mol percent En for "Bushveld-type" orthopyroxenes. The position of the (060) spacing is measured for seven high-purity orthopyroxene concentrates separated from 6 pyroxenites and 1 norite from a 9,000-foot-thick stratigraphic interval of the eastern Bushveld Complex (Cameron, 1963, fig. 4). Because of the small range in composition of these orthopyroxenes, between about En_{86} and En_{76}, a precise method for determination of composition is required in order to demonstrate fractionation trends in this part of the Bushveld Complex.

Himmelberg and Jackson (1967) prepared an X-ray determinative curve for some orthopyroxenes of composition En_{48-85} from the Stillwater Complex (Precambrian, Montana) using the (131) spacing of orthopyroxene. The method of Himmelberg and Jackson (1967) should be compared with the method described here to ascertain if both methods are applicable to the Bushveld Complex and to the Stillwater Complex.

The orthopyroxene of the interval studied is "Bushveld type" as described by Hess (1952). It is characterized by fine exsolution lamellae composed of Ca-rich clinopyroxene oriented parallel to the (100) face of orthopyroxene as discussed by Poldervaart and Hess (1951), Hess (1952), Bown and Gay (1951), and Hess (1960). Hess (1960, p. 34) reported between 3.1 and 5.6 percent (by volume) of diopside lamellae in an orthopyroxene ($En_{85.6}$) from the Bushveld Complex, Transvaal; these lamellae range in thickness from 0.0001 to 0.0008 millimeter. Thus, two phases are present in virtually all grains of the mineral referred to as orthopyroxene. Although the clinopyroxene content of the orthopyroxene is small, the lack of good data regarding the quantities present in the orthopyroxene precludes the use of chemical data alone for the determination of the composition of the orthopyroxene phase.

X-ray powder techniques seemed most suitable for the determination of the composition of the orthopyroxene, inasmuch as the cell parameters appear to have for the most part a linear variation with composition (Hess, 1952). Also, X-ray diffraction techniques permit use of concentrates which are not of very high purity, in contrast to those required for wet chemical techniques or X-ray fluorescence. By using the diffractometer, a high degree of precision is obtainable, and also bulk samples of powder can be used to obtain an average composition for orthopyroxene in each rock specimen.

The $d(060)$ reflection was selected because it is the most intense (0k0) reflection, it is at a suitable 2θ value for precise measurement, and it has been demonstrated by Hess (1952) that the b-cell dimension varies considerably with composition. Ni-filtered Cu$K\alpha_1$ radiation was used in the present study and was chosen only because of availability. Standard aluminum holders were back-packed manually under high pressure against a polished stainless steel plate. Settings were: 35 kilovolt and 18 milliampere, 1° Soller and divergence slits. The (060)$K\alpha_1$ peak was traversed in 0.01° 2θ increments and graphed, using a fixed count and variable

[1] Work done in cooperation with Prof. E. N. Cameron, University of Wisconsin, under National Science Foundation Grant GP2901.

time. By so doing the center of the peak could be established; generally, 3 to 5 separate mounts were prepared, and run, and the average value was used. An internal standard was not used for the routine analysis of orthopyroxene concentrates from about 280 Bushveld specimens. Instead, an empirical determinative curve was prepared using orthopyroxenes analyzed by rapid rock analysis and X-ray fluorescence methods (table 1). X-ray data for these specimens are given in table 2. In figure 1 the determinative curve, based on results of rapid rock analyses, is mol percent En=°2θ (060) −61.322/0.02071. In figure 2 the determinative curve, based on X-ray fluorescence analyses, is mol percent En=°2θ (060) −61.428/0.01968.

TABLE 1.—*Analysis of seven orthopyroxenes from the eastern Bushveld Complex, South Africa*

Lab. No. / *Field No.*	*W-166979* *J-8*	*W-166980* *J-1*	*W-166981* *61-46-251*	*W-166982* *16-276½A*	*W-166983* *15-2117*	*W-166984* *15-1248-4*	*W-166985* *US-9-1190-5-A*
Rapid rock analysis [1]							
SiO_2	56.2	56.1	56.0	56.4	55.8	55.3	54.6
Al_2O_3	1.8	1.6	2.0	1.6	1.7	1.6	1.6
Fe_2O_3	.45	.27	.30	.30	.22	.00	.16
FeO	8.5	8.3	9.0	9.0	10.8	12.9	14.4
MgO	31.3	31.2	31.3	31.4	29.7	28.5	27.4
CaO	1.1	1.6	1.0	.90	.95	.85	.87
Na_2O	.00	.20	.00	.00	.00	.00	.00
K_2O	.04	.11	.00	.00	.04	.00	.00
H_2O-	.16	.12	.00	.08	.08	.04	.12
H_2O+	.00	.00	.00	.12	.12	.20	.08
TiO_2	.09	.11	.14	.11	.18	.16	.24
P_2O_5	.00	.00	.00	.00	.00	.00	.00
MnO	.23	.22	.16	.00	.22	.22	.41
Sum	100	100	100	100	100	100	100
$En=\frac{100Mg^{+2}}{Mg^{+2}+Fe^{+2}+Fe^{+3}}$	86.51	86.85	85.92	85.96	82.92	79.75	77.14
X-ray fluorescence [2]							
Total iron as FeO	9.1	9.0	9.5	9.9	11.2	13.1	15.0
Calculated En	85.8	85.9	85.1	84.4	82.2	79.0	75.5

[1] Analysis by method described by Shapiro and Brannock (1962) supplemented by atomic-absorption techniques. Analyst: Paul Elmore.
[2] Analyst: H. J. Rose, Jr.

TABLE 2.—*X-ray data for seven orthopyroxenes from the eastern Bushveld*
[Cu$K\alpha_1$ radiation]

Field No.	°2θ(060) (*no internal standard*)	°2θ(LiF)$_{220}$ −°2θ(*ortho-pyroxene*)$_{060}$	°2θ(060) (LiF *internal standard*)
J-8	63.107	2.440	63.060
J-1	63.098	2.436	63.064
61-46-251	63.120	2.460	63.040
16-276½A	63.112	2.460	63.040
15-2117	63.050	2.515	62.985
15-1248-4	62.969	2.583	62.917
US-9-1190-5-A	62.918	2.633	62.867

In order to make an internally consistent means of referring to mol percent enstatite in orthopyroxene, that is, a curve for conversion of the chemically determined iron oxide components to mol percent En, some of the chemical analyses of Hess (1952, 1960) were used (mol percent En=100 $Mg^{+2}/Mg^{+2}+Fe^{+2}$) as some of the analyses here are for total Fe calculated as FeO. The formula, mol percent En=100 $Mg^{+2}/Mg^{+2}+Fe^{+2}+Fe^{+3}$, was used for the rapid rock analysis data. The conversion curve was constructed so that the uncertainty between calculation of mol percent En by both the formulas above could be evaluated. The uncertainty involved is as great as 0.3 mol percent En. Orthopyroxenes from the western Bushveld Complex have been chemically analyzed for total Fe calculated as FeO by McDonald (1964), and concentrates of seven of McDonald's specimens were examined by X-ray diffractometer determination of the (060) reflection as described above (table 3). Results of these determinations are illustrated in figure 3. The slope of the line (mol percent En=°2Θ(060)−61.382/0.02021) differs

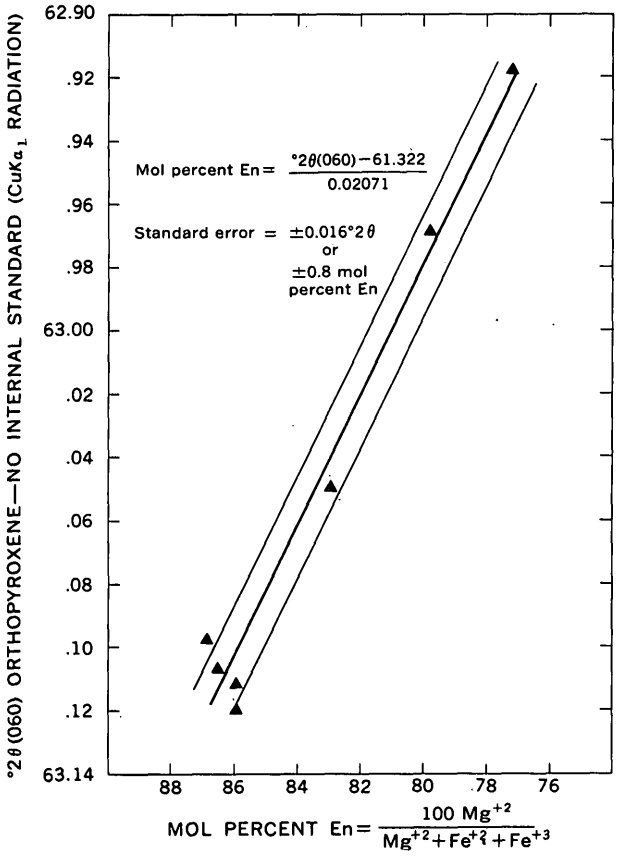

FIGURE 1.—X-ray diffraction determinative curve for seven eastern Bushveld orthopyroxenes based on rapid rock analyses. No internal X-ray diffraction standard.

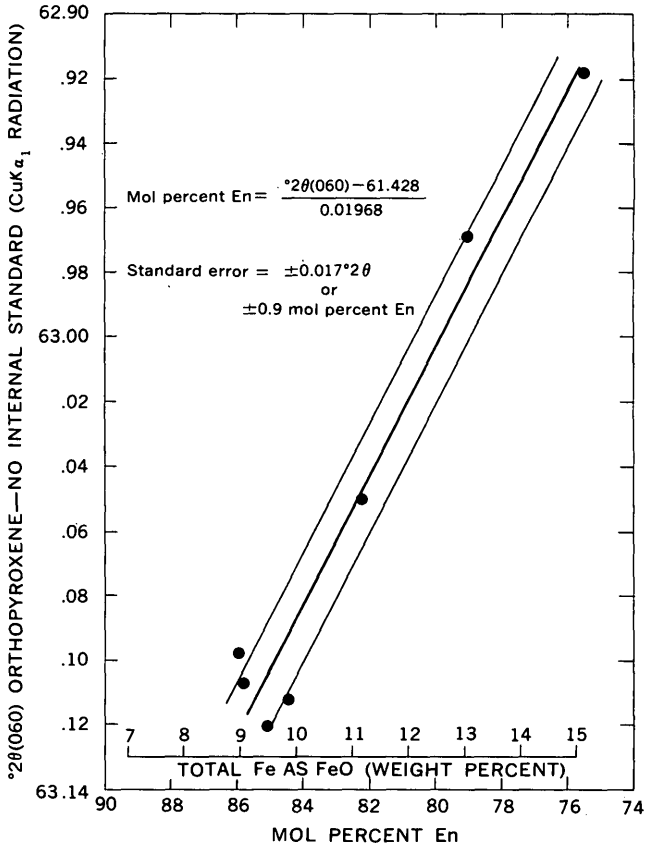

FIGURE 2.—X-ray diffraction determinative curve for seven eastern Bushveld orthopyroxenes based on X-ray fluorescence analyses. No internal X-ray diffraction standard.

very slightly from that of the eastern Bushveld orthopyroxenes analyzed for total Fe as FeO by the U.S. Geological Survey, but the correlation of $°2\Theta(060)_{CuK\alpha_1}$ with composition is much better and shows that the precision of McDonald's analysis is very high and that the precision of measurement of the (060) reflection is also very high.

TABLE 3.—*X-ray and chemical data for seven orthopyroxenes from the western Bushveld*

°2Θ(060) [1] (no internal standard)	FeO [2] (weight percent)
63.140	8.15
63.152	8.30
63.098	9.65
63.068	10.60
63.024	11.81
63.014	12.17
63.008	12.50

[1] $CuK\alpha_1$ radiation.
[2] Analyses from McDonald (1964).

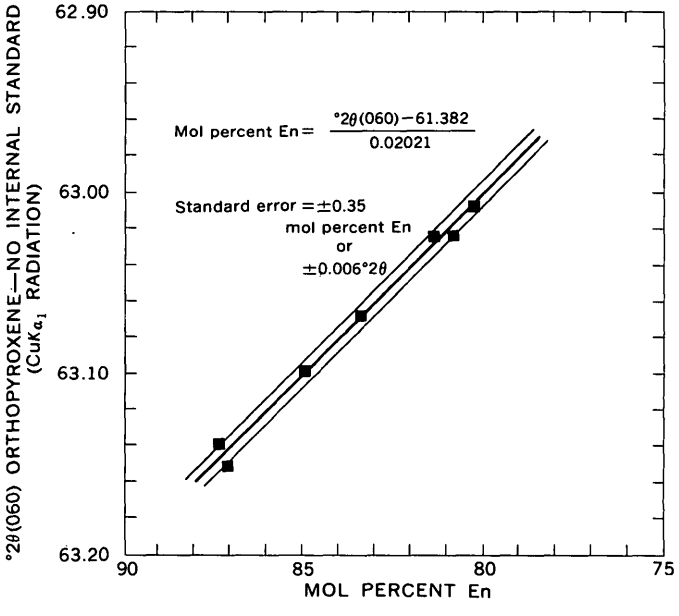

FIGURE 3.—X-ray diffraction determinative curve for seven western Bushveld orthopyroxenes based on chemical analyses of FeO by McDonald (1964). No internal X-ray diffraction standard.

LINEARITY OF $(060)_{CuK\alpha 1}$ VERSUS COMPOSITION FOR En_{86} TO En_{76}

In order to evaluate the linear relationship between composition and the $d(060)$ of the orthopyroxenes, the 7 orthopyroxene concentrates from the eastern Bushveld Complex were mixed with reagent grade LiF to provide an internal standard for determination of the actual value of $d(060)$ (figs. 4 and 5). The LiF $(220)^{CuK\alpha_1}$ reflection is less than 3.0° 2Θ from the orthopyroxene $(060)^{CuK\alpha_1}$ reflection. The separation of these 2 peaks was measured for 5 to 7 separate powder mounts for each of the 7 analyzed specimens, and the value of the $d(060)^{CuK\alpha_1}$ was thus obtained (table 2). The standard deviation of each set of observations did not exceed 0.01° 2Θ. Settings used were the same as for the method previously described except that the peaks were recorded on chart paper at a speed of 1/4° 2Θ per minute and 2 inches equals 1° 2Θ.

The regression equations for figure 4 and figure 5, respectively, are mol percent En=° 2Θ(060)−61.396/0.01936 and mol percent En=° 2Θ (060)−61.31/0.02015.

PRECISION AND ACCURACY OF THE METHODS

Collective assessment of the determinative curves indicates that for the eastern Bushveld specimens studied, the standard error of estimate of composition by measuring $d(060)^{CuK\alpha_1}$ is between about ±0.8 and ±1.0 mol percent En, when no internal standard is used, and ±0.3 to ±0.6 when an internal standard is used. McDonald's western Bushveld analyses show a standard error of ±0.35 mol percent En without an internal standard, so that if five analyses and an internal standard could be used, it seems that the precision is potentially very high. However, because there is an intergrown clinopyroxene phase in all the orthopyroxene concentrates, it is not possible to determine the accuracy of the X-ray method discussed here because chemical analysis of the concentrates included the finely intergrown clinopyroxene phase. This problem is discussed by Howie and Smith (1966, p. 447) in regard to correlation of electron microprobe data and gravimetric analyses of orthopyroxenes. For the present work, however, it was desirable to obtain a high precision at the expense of accuracy in order to evaluate fractionation trends in the lower 11,000 feet of the eastern Bushveld Complex.

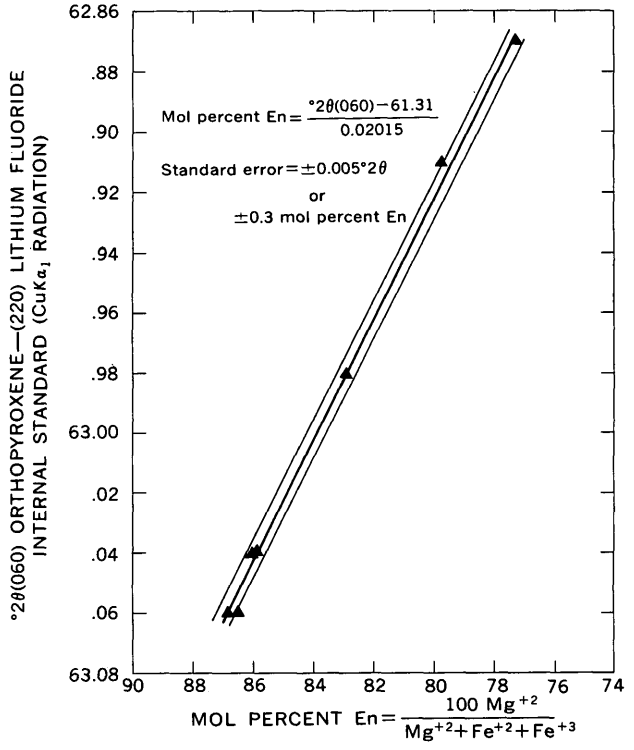

FIGURE 5.—X-ray diffraction determinative curve for seven eastern Bushveld orthopyroxenes based on rapid rock analyses. Internal X-ray diffraction standard used.

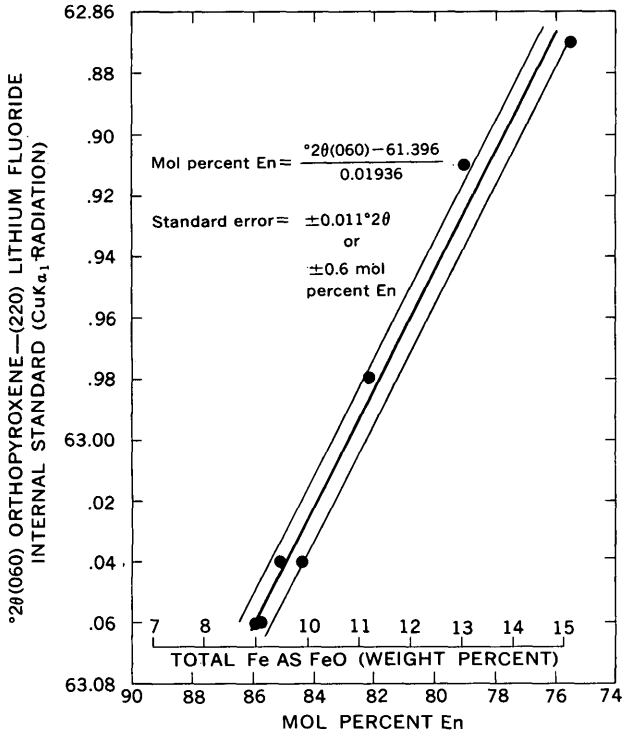

FIGURE 4.—X-ray diffraction determinative curve for seven eastern Bushveld orthopyroxenes based on X-ray fluorescence analyses. Internal X-ray diffraction standard used.

REFERENCES

Bown, M. G., and Gay, Peter, 1959, The identification of oriented inclusions in pyroxene crystals: Am. Mineralogist, v. 44, nos. 5–6, p. 592–602.

Cameron, E. N., 1963, Structure and rock sequences of the critical zone of the Eastern Bushveld Complex: Mineralog. Soc. America Spec. Paper 1, p. 93–107.

Hess, H. H., 1952, Orthopyroxenes of the Bushveld type, ion substitutions and changes in unit cell dimensions: Am. Jour. Sci., Bowen volume, pt. 1, p. 173–187.

——— 1960, Stillwater igneous complex, Montana: Geol. Soc. America Mem. 80, 230 p.

Himmelberg, G. R., and Jackson, E. D., 1967, X-ray determinative curve for some orthopyroxenes of composition Mg_{46-85} from the Stillwater Complex, Montana, *in* Geological Survey research 1967: U.S. Geol. Survey Prof. Paper 575–B, p. B101–B102.

Howie, R. A., and Smith, J. V., 1966, X-ray emission microanalysis of rock-forming minerals—[pt.] 5, Orthopyroxenes: Jour. Geology, v. 74, no. 4, p. 443–462.

McDonald, J. A., 1964, Evolution of part of the critical zone, Farm Ruighoek, Western Bushveld: Univ. Wisconsin, Ph. D. thesis, 132 p.

Poldervaart, Arie, and Hess, H. H., 1951, Pyroxene in the crystallization of basaltic magma: Jour. Geology, v. 59, no. 5, p. 472–489.

Shapiro, Leonard, and Brannock, W. W., 1962, Rapid analysis of silicate, carbonate, and phosphate rocks: U.S. Geol. Survey Bull. 1144–A, 56 p.

OCCURRENCE AND COMPOSITION OF BIOTITES FROM THE CARTRIDGE PASS PLUTON OF THE SIERRA NEVADA BATHOLITH, CALIFORNIA

By F. C. W. DODGE and JAMES G. MOORE, Menlo Park, Calif.

Abstract.—Composition of analyzed biotites from the Cartridge Pass pluton, a zoned granitic intrusion of the Sierra Nevada batholith, shows little correlation with bulk rock composition. Systematic variations of minor elements suggest that the micas originally crystallized over a range of temperatures, but constant major-element composition suggests that all the biotites were equilibrated with respect to the same oxygen partial pressure. Buildup of fluid pressure late in the crystallization history of the pluton, and permeation of the entire pluton by a late H_2O-rich fluid of a specific oxygen partial pressure may be responsible for the homogeneity of major-element composition.

Many individual plutonic bodies of the Sierra Nevada batholith are compositionally zoned. One of the best examples of a concentrically zoned body is provided by the granodiorite of Cartridge Pass—a small pluton that crops out over an area of about 20 square miles near the crest of the Sierra Nevada (fig. 1). This paper relates the occurrence and composition of biotites from different parts of this pluton to general features of the zoning.

GENERAL FEATURES OF THE CARTRIDGE PASS PLUTON

The regional geologic setting of the area of the Sierra Nevada in which the Cartridge Pass pluton is exposed has recently been summarized by Bateman and Wahrhaftig (1966). Field relations and general petrographic features of the pluton have been described by Moore (1963) and are briefly restated and, in part, elaborated upon here.

Systematic compositional variations from the core to the margin of the Cartridge Pass pluton are shown by chemical and modal analyses (table 1) and plots of modes (fig. 2) and norms (fig. 3). The trend of norms of rocks from the pluton follows closely the trend of norms of granitic rocks from several plutons of the

TABLE 1.—*Composition of granitic rocks of the Cartridge Pass pluton*

Number / *Field No.*	*1* *M-127*	*2* *M-131*	*3* *M-139*	*4* *M-135*	*5* *M-133*
Chemical analyses [1]					
SiO_2	59. 14	65. 95	68. 12	69. 09	68. 43
Al_2O_3	18. 23	16. 49	15. 77	15. 57	15. 99
Fe_2O_3	2. 32	1. 80	1. 47	1. 25	1. 44
FeO	3. 62	1. 91	1. 53	1. 44	1. 37
MgO	2. 50	1. 37	1. 01	. 84	. 77
CaO	5. 92	3. 99	3. 36	2. 94	3. 25
Na_2O	3. 81	3. 68	3. 80	3. 87	4. 03
K_2O	2. 19	3. 34	3. 53	3. 72	3. 50
H_2O+	. 82	. 57	. 43	. 46	. 40
H_2O-	. 04	. 03	. 05	. 05	. 02
TiO_2	. 79	. 54	. 47	. 41	. 42
P_2O_5	. 30	. 19	. 17	. 14	. 16
MnO	. 11	. 07	. 06	. 06	. 06
CO_2	. 01	. 01	. 03	. 01	. 01
Total	99. 80	99. 94	99. 80	99. 85	99. 85
CIPW norms					
Q	11. 69	21. 18	24. 00	24. 79	23. 66
C	0	. 05	. 07	. 19	. 07
or	12. 97	19. 76	20. 91	22. 03	20. 72
ab	32. 32	31. 17	32. 24	32. 81	34. 16
an	26. 24	18. 51	15. 41	13. 64	15. 04
mt	3. 37	2. 61	2. 14	1. 82	2. 09
il	1. 50	1. 03	. 90	. 78	. 80
ap	. 71	. 45	. 40	. 33	. 38
di	. 96	0	0	0	0
hy	9. 42	4. 68	3. 46	3. 14	2. 67
cc	. 02	. 02	. 07	. 02	. 02
Total	99. 20	99. 46	99. 60	99. 55	99. 61
Modal analyses					
Quartz	13. 4	20. 9	22. 1	24. 7	21. 9
K-feldspar	4. 5	17. 3	20. 0	21. 4	19. 8
Plagioclase	60. 1	49. 1	46. 3	44. 7	50. 6
Biotite	12. 8	7. 2	6. 2	4. 8	4. 8
Chlorite	1. 4	. 9	. 4	1. 2	. 6
Hornblende	5. 1	2. 4	2. 8	. 5	. 2
Magnetite	. 6	1. 1	1. 1	1. 1	1. 0
Nonopaque accessories	2. 2	1. 1	1. 1	1. 6	1. 1
Total	100. 0	100. 0	100. 0	100. 0	100. 0

[1] By E. L. Munson.

U.S. GEOL. SURVEY PROF. PAPER 600-B, PAGES B6-B10

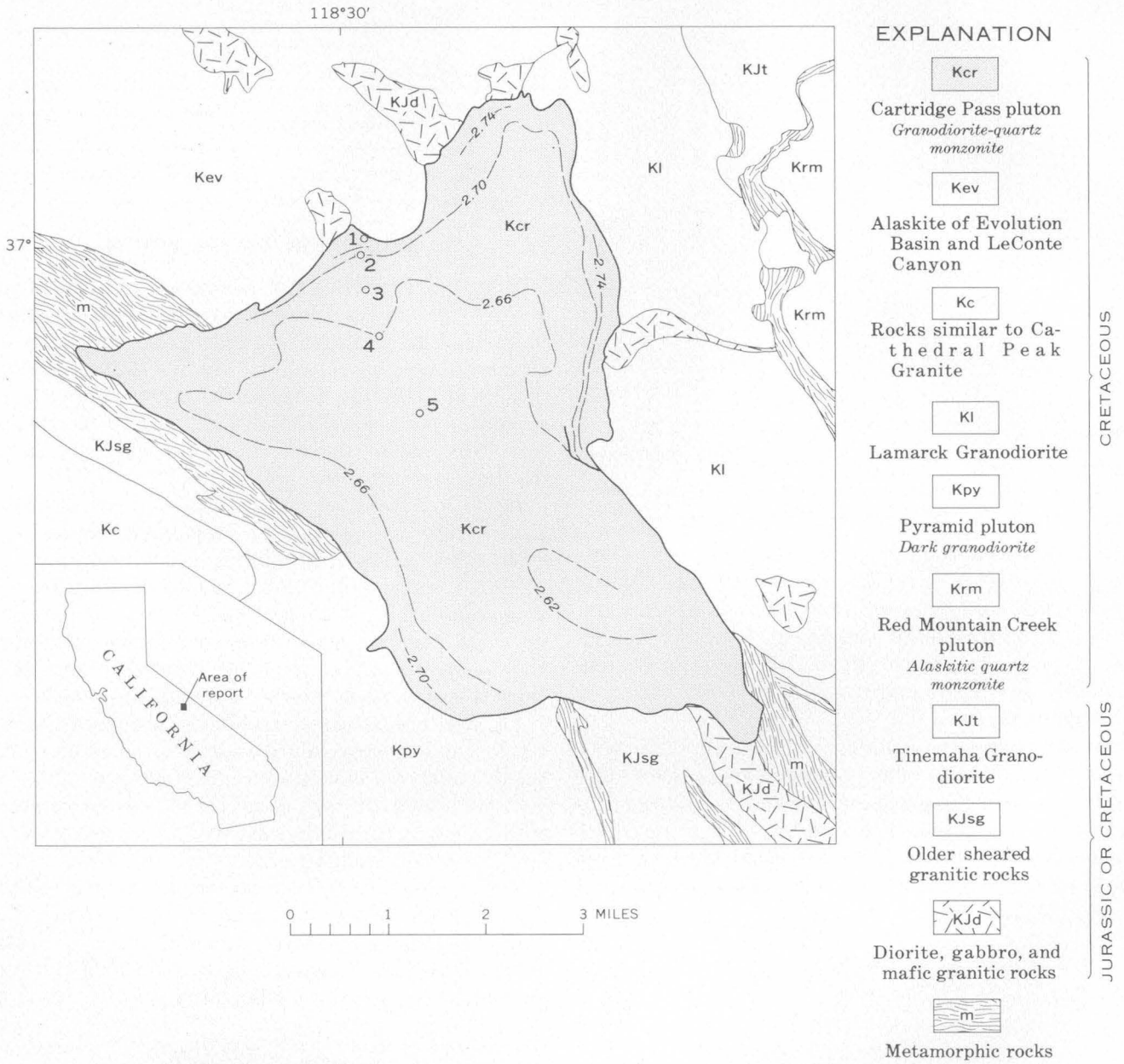

FIGURE 1.—Map showing the Cartridge Pass pluton and surrounding region. Small numbered circles indicate location of samples listed in tables 1–4. Dashed lines are contours of equal specific gravity of hand specimens. Modified from Bateman (1965), Bateman and Moore (1965), and Moore (1963).

east-central Sierra Nevada. In addition to the 5 analyzed samples, approximately 130 other samples have been collected and examined in less detail.

The pluton grades from a porphyritic quartz monzonite in its core to equigranular quartz diorite some places along its margins. Quartz and potassium feldspar are increasingly more abundant toward the center of the pluton, and crystals of the feldspar increase in size as the center is approached. Plagioclase decreases in amount and changes in average composition from andesine to oligoclase from the margin to the core of the pluton. Hornblende and biotite—the predominant mafic minerals—also decrease in amount in the center of the pluton. Hornblende is absent in some of the lightest colored rocks, but biotite and magnetite are ubiquitous. Nonopaque accessories, including sphene, allanite, epidote, zircon, and apatite are also present in all rocks of the pluton, but in such small amounts that variations in abundance are not readily apparent. Specific gravities of whole-rock samples range systematically from 2.61 in the center to more than 2.74 at the edge of the body. Mafic inclusions, common in many Sierra Nevada granitic rocks, are smaller and less abundant in the core than in the margins. Changes in

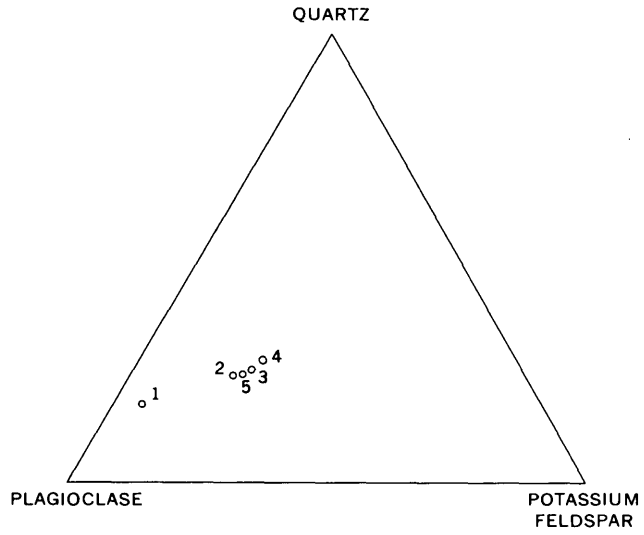

FIGURE 2.—Modal analyses of granitic rocks of the Cartridge Pass pluton.

composition and texture are gradational everywhere except in one area on the east side of the pluton where light-colored core rock is intrusive into darker marginal rock. The intrapluton contact can be traced for less than a mile—to the north it becomes diffuse and gradually disappears and to the south it terminates at the edge of the body.

The Cartridge Pass pluton intrudes all rocks with which it is in contact. The potassium-argon age of biotite from one of the granodiorite samples (table 2) indicates that the pluton is a member of a group of intrusions of the Sierra Nevada batholith which were emplaced during Late Cretaceous time (Kistler and others, 1965).

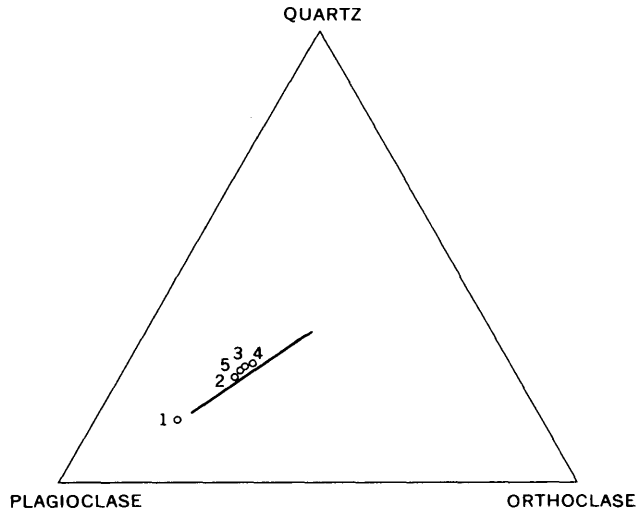

FIGURE 3.—Plot of norms of granitic rocks of the Cartridge Pass pluton. Line represents the median line of norms of 27 granitic rocks from various plutonic bodies of the east-central Sierra Nevada (from Bateman and others, 1963).

TABLE 2.—*K-Ar age determination on biotite from the granodiorite of Cartridge Pass*

[Analysts: Potassium, H. C. Whitehead; argon, J. D. Obradovich]

Sample No.	K_2O *(weight percent)*	rAr^{40}/K^{40}	*Age (m.y.)*	*rAr (percent)*
5 (field No. M–133)	7. 34	4.82×10^{-3}	81 ± 3	92

DESCRIPTION OF THE BIOTITE

Biotite fractions were recovered by centrifuging washed, disaggregated rock powders in bromoform–methylene iodide mixtures, and by concentration in a Frantz isodynamic separator. Minus-140-mesh material estimated to contain less than 0.3 percent impurity was submitted for chemical analysis; a second biotite fraction, between 40 and 80 mesh, was used for the age determination given in table 2.

Rock of the pluton contains about 2 to 13 percent biotite. The mica occurs in irregularly shaped plates with an average size of 1 millimeter. In the darker rocks there is a tendency for biotite to fill interstices between plagioclase grains. Euhedral apatite crystals and small numbers of zircon, plagioclase, epidote, sphene, quartz, and magnetite grains have been noted as inclusions; chlorite is sometimes interlayered with the mica.

Physical properties of the biotites are markedly constant. The following values were determined on each of the five analyzed biotites: specific gravity = $3.05\pm.03$; $\gamma=1.609\pm.003$; $2V=0°$, or nearly 0°; dispersion strong with $r<v$; pleochroism strong with X=pale straw yellow, Y=Z=dark olive green.

The invariability of the major elements in biotites from rock representing all zones of the Cartridge Pass pluton is illustrated by the chemical analyses of table 3. The "average" formula based on 24(O, OH, F) for biotites from rocks of the pluton is

$$(K_{1.71}Na_{0.03}Ca_{0.05})(Fe^{+2}{}_{1.78}Mn_{0.08}Mg_{2.71}Fe^{+3}{}_{0.42}Ti_{0.28}Al_{0.39})(Al_{2.39}Si_{5.61})\ O_{20.15}(OH,\ F)_{3.85}.$$

Individual biotites differ only slightly from this composition (table 4). Variations in hydroxyl may be due to determinative errors in H_2O+. Relative differences in amounts of most of the minor elements (table 3) are much greater than those of major elements.

RELATION BETWEEN BIOTITE COMPOSITION AND CONDITIONS OF FORMATION

Systematic variation in content of minor elements in the analyzed micas suggests that biotites may have crystallized in the Cartridge Pass pluton over a range of temperatures. Cr, Ni, and V tend to be present in greatest amounts in biotites from the relatively mafic rock near the margin of the pluton, whereas the same

TABLE 3.—*Composition of biotites from rocks of the Cartridge Pass pluton*

Number / *Field No.*	*1* / *M-127*	*2* / *M-131*	*3* / *M-139*	*4* / *M-135*	*5* / *M-133*
Major elements as oxides (weight percent)					
SiO_2	37.4	37.0	37.1	37.5	37.3
Al_2O_3	16.1	15.7	15.5	15.8	15.6
Fe_2O_3	3.3	4.4	3.8	3.3	3.7
FeO	15.1	13.4	13.7	14.7	14.0
MgO	11.6	12.1	12.5	12.1	12.2
CaO	.29	.28	.52	.23	.24
Na_2O	.15	.11	.11	.11	.15
K_2O	9.0	8.8	9.0	8.8	8.9
H_2O+	3.3	3.9	3.4	3.7	4.3
H_2O-	.20	.35	.32	.22	.30
TiO_2	2.7	2.5	2.6	2.2	2.2
MnO	.41	.61	.62	.69	.76
F	.12	.30	.23	.32	.33
O≡F	.05	.13	.10	.14	.14
Total	99.6	99.3	99.3	99.5	99.8
Minor elements (weight percent)					
Ba	0.22	0.30	0.30	0.22	0.30
Co	.0060	.0065	.0050	.0065	.0055
Cr	.0014	.0014	.0012	.0008	.0004
Cu	.011	.013	.013	.0085	.016
Ga	.0034	.0046	.0044	.0055	.0055
Ni	.0030	.0024	.0020	.0018	.0015
Sc	.0012	.0036	.0024	.0038	.0032
Sr	<.0002	.0012	.0008	.0008	.0010
V	.033	.027	.025	.025	.023
Zn	.060	.080	.10	.10	.10
Zr	<.002	<.002	.004	.006	.005

Looked for but not found: Ag, As, Au, B, Be, Bi, Cd, Ce, Eu, Ge, Hf, Hg, In, La, Mo, P, Pb, Pd, Pt, Re, Sb, Sn, Ta, Te, Th, Tl, U, W, Y, Yb.

Major elements determined by methods described by Shapiro and Brannock (1962) supplemented by atomic absorption. Analyzed by U.S. Geol. Survey, Washington, D.C. analytical laboratories under the direction of Leonard Shapiro, except F in all samples determined by J. J. Warr, Jr., and H_2O+ in M-127 by W. W. Brannock.

Minor elements determined by quantitative spectrographic analysis using methods described by and detectibilities given by Bastron and others (1960). R. E. Mays, analyst.

TABLE 4.—*Number of ions in analyzed biotites on the basis of 24*(O, OH, F) *per formula unit*

Number / *Field No.*	*1* / *M-127*		*2* / *M-131*		*3* / *M-139*		*4* / *M-135*		*5* / *M-133*	
Si	5.66	8.00	5.56	8.00	5.62	8.00	5.64	8.00	5.56	8.00
Al^{IV}	2.34		2.44		2.38		2.36		2.44	
Al^{VI}	.53		.34		.38		.43		.29	
Ti	.31		.28		.30		.25		.25	
Fe^{+3}	.38	5.79	.50	5.59	.43	5.74	.37	5.70	.41	5.50
Fe^{+2}	1.91		1.68		1.73		1.85		1.74	
Mn	.05		.08		.08		.09		.10	
Mg	2.61		2.71		2.82		2.71		2.71	
Ca	.05		.05		.08		.04		.04	
Na	.04	1.83	.03	1.77	.03	1.85	.03	1.76	.04	1.77
K	1.74		1.69		1.74		1.69		1.69	
F	.06	3.39	.14	4.05	.11	3.54	.15	3.86	.16	4.43
OH	3.33		3.91		3.43		3.71		4.27	
100(Fe/Fe+Mg)	46.7		44.6		43.4		45.0		44.2	

biotites are depleted in Sc, Sr, and Zn compared to those from the core. The Co content is fairly uniform, and the Cu and Ba content appears to be erratic. A relation between Sc content of biotite and temperature of formation has been noted by previous workers (Oftedal, 1944; Ingerson, 1955; Herz and Dutra, 1964), and, at least in a relative sense, their observations seem valid. Absolute values probably cannot be placed on temperatures of formation solely on the basis of the trace-element content of a single mineral, but the Sc content suggests that biotite in rock at the margin formed at higher temperatures than biotite in rock of the core. Herz and Dutra (1964) have noted that Co, Ni, and Cr also indicate temperature—all tend to be less abundant or absent in biotites formed at lower temperatures. Nockolds and Mitchell (1948) have shown that in biotites of Caledonian plutonic rocks Cr, V, Cu, Ni, Co, and Sr decrease, and Ga increases, as the biotites range from early to late. These observations support the interpretation that trace-element variation may be the result of temperature variation and generally suggest that biotite in the margin of the pluton crystallized at higher temperatures than biotite in the core.

Uniformity of major-element composition of the biotites is particularly striking in view of the systematic variation of host-rock composition. Atomic ratios of 100 Fe/(Fe+Mg) of analyzed biotites are constantly 45, the maximum deviation from this value being less than 2 (table 4). Recent experimental work by Wones and Eugster (1965) relates this ratio to the fugacity of oxygen and the temperature at which biotite is stable. Biotites with a ratio of 45, coexisting with potassium feldspar and magnetite, define an oxygen fugacity of approximately 10^{-13} bars (fig. 4). This biotite composition defines an oxygen fugacity that will remain almost constant regardless of temperature changes. Wones and Eugster (1965) have stressed that different total pressures will have little effect on the spatial relations of equilibrium shown in figure 4; increased pressure will merely shift the biotite isopleths to higher temperatures. Thus the biotites in rocks of the Cartridge Pass pluton all appear to have been in equilibrium with the constant oxygen fugacity of 10^{-13} bars regardless of temperature and total pressure.

The biotite of the Cartridge Pass pluton probably acquired its present uniform composition late in its crystallization history. Field evidence indicates that the marginal rocks crystallized before those in the core, and presumably the volatile content of the residual melt in the core increased during solidification. Hence the porphyritic interior of the pluton might have been subjected to higher volatile pressures during the crystallization of its biotite than was the fine-grained mafic margin.

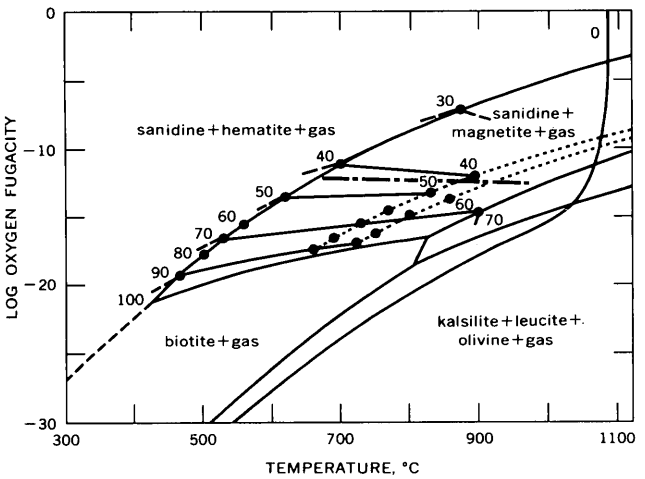

FIGURE 4.—Stability of biotites of specific Fe/(Fe+Mg) values as a function of oxygen fugacity and temperature at 2,070 bars total pressure. Heavy lines represent contours of constant 100 Fe/(Fe+Mg) values. Dash-dot line represents compositions of biotites from the Cartridge Pass pluton. Diagram from Wones and Eugster (1965, fig. 4).

The biotite from all zones is probably homogeneous because late water-rich fluids permeated the entire pluton and perhaps even its walls. Existing biotite recrystallized in equilibrium with this late fluid, resulting in homogeneous biotite compositions throughout the cooling body.

The Rocky Hill stock, a zoned pluton in the Sierra Nevada foothills described by Putnam and Alfors (1965), offers an interesting comparison with the Cartridge Pass pluton. In the Rocky Hill stock, when vapor pressure of the core magma exceeded load pressure, more rigid portions of the stock ruptured and loss of water pressure was rapid. Probably because of its greater depth, as well as the higher temperature of its walls, rupture did not occur in the Cartridge Pass body and loss of water pressure was slow. A striking contrast is shown by the textures of the core rocks. Contacts between core and marginal rocks are generally gradational in both bodies. In the Rocky Hill stock, rise of the solidus temperature was caused by the rapid isothermal loss of water pressure from the residual core fluid; consequently nucleation and crystallization were rapid. Core rocks have a fine-grained matrix of quartz, albite, and K-feldspar. In the Cartridge Pass pluton, the solidus temperature was depressed by the gradual buildup of water pressure during final stages of crystallization. Nucleation rates under these conditions may have been gradually retarded. Core rocks contain K-feldspar phenocrysts. Hence in a pluton like the Rocky Hill stock one would expect contrasting composition of biotites from rim to core as the entire cooling unit was never subjected to late uniform fluids, as may have been the case in the Cartridge Pass pluton.

REFERENCES

Bastron, Harry, Barnett, P. R., and Murata, K. J., 1960, Method for the quantitative spectrochemical analysis of rocks, minerals, ores, and other materials by a powder d-c arc technique: U.S. Geol. Survey Bull. 1084–G, p. 165–182.

Bateman, P. C., 1965, Geology and tungsten mineralization of the Bishop district, California: U.S. Geol. Survey Prof. Paper 470, 208 p.

Bateman, P. C., Clark, L. D., Huber, N. K., Moore, J. G., and Rinehart, C. D., 1963, The Sierra Nevada batholith—a synthesis of recent work across the central part: U.S. Geol. Survey Prof. Paper 414–D, p. D1–D46.

Bateman, P. C., and Moore, J. G., 1965, Geologic map of the Mount Goddard quadrangle, Fresno and Inyo Counties, California: U.S. Geol. Survey Geol. Quad. Map GQ–429, scale 1: 62,500.

Bateman, P. C., and Wahrhaftig, Clyde, 1966, Geology of the Sierra Nevada, *in* Bailey, E. H., ed., Geology of northern California: California Div. Mines and Geology Bull. 190, p. 107–172.

Herz, Norman, and Dutra, C. V., 1964, Cobalt, nickel, chromium, scandium and niobium in biotite and the scandium geological thermometer: Soc. Brasileira Geol. Bol. 13, no. 1/2, p. 23–42.

Ingerson, Earl, 1955, Methods and problems of geologic thermometry: Econ. Geology, 50th Anniversary Volume, pt. 1, p. 341–410.

Kistler, R. W., Bateman, P. C., and Brannock, W. W., 1965, Isotopic ages of minerals from granitic rocks of the central Sierra Nevada and Inyo Mountains, California: Geol. Soc. America Bull., v. 76, no. 2, p. 155–164.

Moore, J. G., 1963, Geology of the Mount Pinchot quadrangle, southern Sierra Nevada, California: U.S. Geol. Survey Bull. 1130, 152 p.

Nockolds, S. R., and Mitchell, R. L., 1948, The geochemistry of some Caledonian plutonic rocks; a study in the relationship between the major and trace elements of igneous rocks and their minerals: Royal Soc. Edinburgh Trans., v. 61, 2, p. 533–575.

Oftedal, Ivar, 1944, Scandium in biotite as a geologic thermometer: Norsk. Geol. Tiddsk., v. 23, no. 4, p. 202–213.

Putnam, G. W., and Alfors, J. T., 1965, Depth of intrusion and age of the Rocky Hill stock, Tulare County, California: Geol. Soc. America Bull., v. 76, no. 3, p. 357–364.

Shapiro, Leonard, and Brannock, W. W., 1962, Rapid analysis of silicate, carbonate, and phosphate rocks: U.S. Geol. Survey Bull. 1144–A, p. A1–A56.

Wones, D. R., and Eugster, H. P., 1965, Stability of biotite—experiment, theory, and application: Am. Mineralogist, v. 50, no. 9, p. 1228–1272.

PHOSPHATE NODULES FROM THE WILLS POINT FORMATION, HOPKINS COUNTY, TEXAS

By CHARLES MILTON [1] and ALLAN P. BENNISON [2], Washington, D.C., Tulsa, Okla.

Abstract.—Phosphate nodules, several centimeters in size, generally rounded, consisting principally of carbonate-fluorapatite with calcite (mostly foraminiferal tests) and glauconite and very minor quartz, occur in glauconitic clay in the basal part of the Wills Point Formation (upper part of Midway Group) of Paleocene age in Hopkins County, Tex. The nodules are a stratigraphic marker of an angular unconformity, and occur along the Mexia-Talco fault zone from Limestone County to Hopkins County in northeast Texas, a distance of about 100 miles. A chemical analysis of the nodules and an X-ray powder pattern are given, and the petrography of the nodules is described and illustrated.

Phosphatic nodules are of rapidly developing interest to stratigraphers and marine geologists. As early as 1922 it was recognized that nodular phosphate associated with glauconite indicated a break in stratigraphic succession (Goldman, 1922), these minerals being accumulated on the floor of an advancing sea, over eroded strata, and thus marking the base of a new stratigraphic series. An equally significant relationship, of phosphate nodules and manganese oxide deposition, has been described by Pratt and McFarlin (1966): the continental shelf off the Georgia coast is floored by hundreds of square miles with manganese oxide in continuous sheets several inches thick, with the bottom usually phosphatic; the sheets grade into areas of nodular deposition of both manganese oxide and phosphate. Pecora and others (1962) have described a notable occurrence of Cretaceous phosphate-nodule deposition in Montana, at the base of the marine Colorado Shale. This present note describes Paleocene glauconite-bearing phosphate nodules from the basal Wills Point Formation in Texas.

Acknowledgments.—We are indebted to Z. S. Altschuler, Harry A. Tourtelot, and Carter B. Hearn, Jr., of the U.S. Geological Survey, for critical reading of this report and for helpful discussions.

LOCATION AND STRATIGRAPHY OF PHOSPHATE NODULES

The Wills Point Formation (upper part of Midway Group) of Paleocene age, along its outcrop belt from Kaufman County northward to Hopkins County in northeast Texas, truncates and oversteps progressively older members of the Tehuacana and Pisgah Members of the Kincaid Formation (lower part of Midway Group) at a rate of about 2 feet per mile.

The blanketing 400–500-foot-thick Wills Point Formation is composed mainly of dark clays, which are silty near the top of the formation. A basal conglomeratic zone 1 to 5 feet thick contains pebbles, which are mainly black phosphatic nodules in a green amorphous glauconite-rich clay. Nodules diminish in abundance upward through the basal 1 to 5 feet, and are sparse in the overlying 5–8-foot shaly zone. This shale contains abundant planktonic Foraminifera indicative of an outer-shelf or basinal environment. The pebbles are viewed as a lag concentrate evolved by subaqueous erosion and winnowing of the underlying Kincaid Formation, which had been deposited in a shallow environment, and of the basal part of the Wills Point sediments in a reducing outer-shelf environment. Although the clay matrix is usually decomposed by profound weathering, the nodules locally weather out in such great profusion that the basal Wills Point contact can be readily traced through low hilly regions of sparse outcrops. One of the more accessible localities for collecting abundant Wills Point phosphate nodules is along and just west of the road 2 miles north of Ridgeway, Hopkins County (fig. 1). Other localities occur in a discontinuous band about a hundred miles in length along the Mexia fault zone from Groesbeck in Lime-

[1] The George Washington University and U.S. Geological Survey.
[2] Sinclair Oil and Gas Co.

285-544 O—68——2

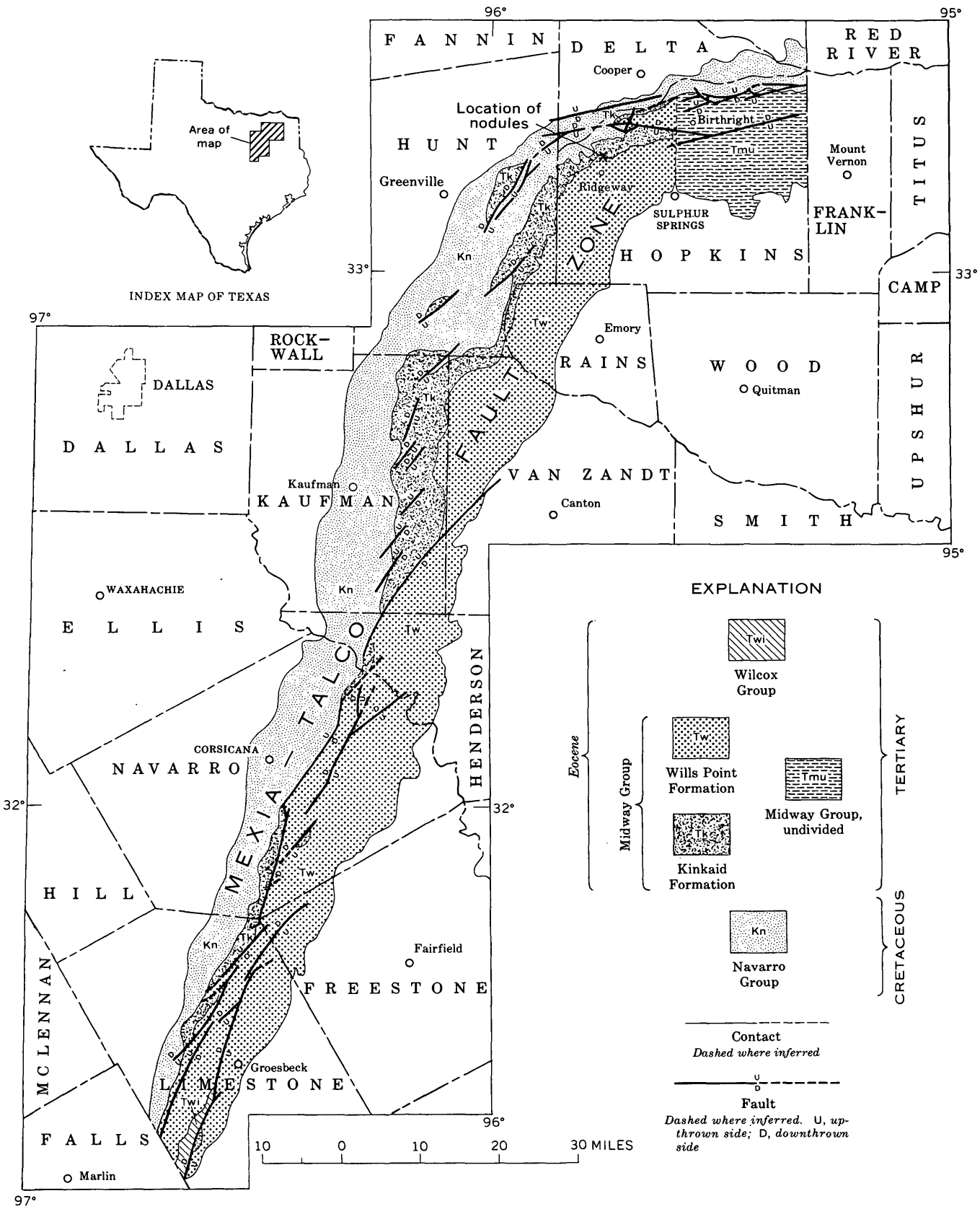

FIGURE 1.—Map of part of northeast Texas, showing generalized geology along the outcrop belt of phosphate nodules in the Wills Point Formation. Modified from Texas University, Bureau of Economic Geology (1966) and Darton and others (1937).

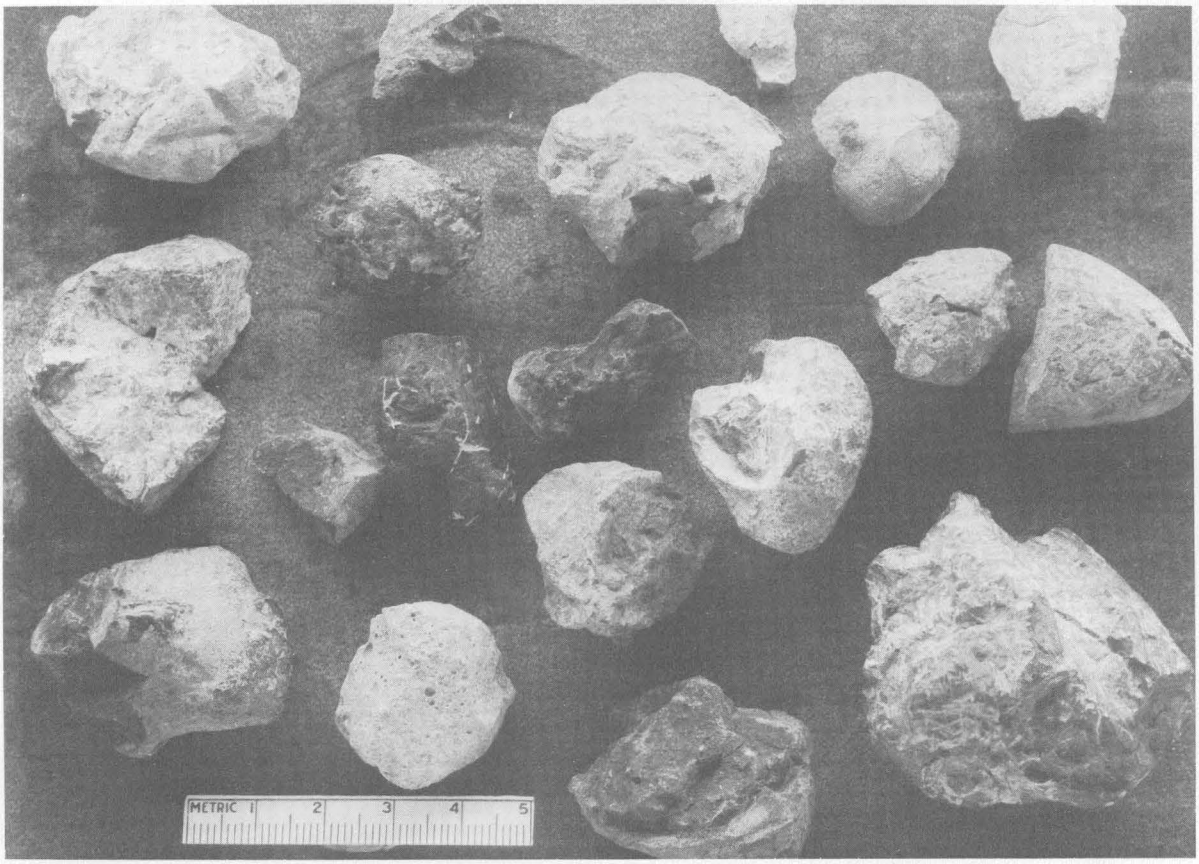

FIGURE 2.—Typical, moderately rounded phosphate nodules from Wills Point Formation, Texas. White streaks on nodule at left center are calcite. Scale in centimeters.

stone County northward to Birthright in Hopkins County.

Typical nodules are shown in figure 2. Most are rounded to subrounded to botryoidal; some are obviously internal molds of mollusks. Median diameter ranges from 2 to 10 centimeters. The rounded dark-gray surfaces are streaked and mottled with whitish calcite, which is the only conspicuous accessory mineral in these nodules other than glauconite. Some of the nodules internally show slightly contrasting areas because of minor variation in tint and perhaps grain size (fig. 3), but no compositional difference has been detected.

Under the microscope, calcite occurs in irregular patches and as the principal constituent of the many Foraminifera tests. Scattered grains of glauconite are usually green, but some are yellow brown. Glauconite and areas of crystalline calcite and calcite foraminiferal tests are shown in figure 4. Diagenetic features such as described by Pecora and others (1962) and, in particular, spherulitic structure, were not seen in any of the specimens examined. Detrital minerals are inconspicuous; only silt-size particles of quartz and mica were observed.

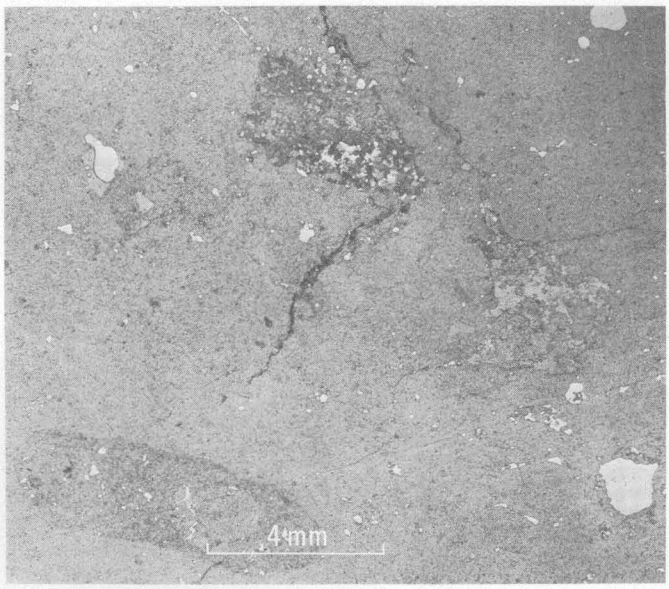

FIGURE 3.—Photomicrograph of thin section showing composite character of phosphate nodule. In lower left, the elliptical area and the lighter colored area enclosed within it are phosphate, similar in composition and texture to the surrounding phosphate, differing only slightly in color. Two large irregular calcite patches are shown in upper center and center right. The thin dark band in center is limonitic calcite. Ordinary light.

CHEMICAL COMPOSITION AND X-RAY POWDER DATA

A chemical analysis of a representative specimen of the Hopkins County, Tex., nodules is given in table 1, and X-ray powder data in table 2.

It is not possible to compute a formula for the apatite mineral in these nodules, because of uncertainty as to what part of the 5.2-percent CO_2 is in calcite and what part is in the apatite mineral and because of uncertainty as to how much of the 3.2-percent H_2O+ represents (OH) in the apatite. Because neither optical nor X-ray examination indicates any fluorite to be present in these nodules, the 3.8-percent F of the analysis may be allocated entirely to the apatite. In theoretical fluorapatite, $Ca_{10}(PO_4)_6F_2$, the fluorine percentage is 3.8, the same as that of the nodules. However, the nodules contain substantial amounts of calcite, glauconite, quartz, and other minerals in addition to apatite; the latter actually has more fluorine than the 3.8 percent found in the analysis, and, again, more than the 3.8 percent required by the stoichiometric fluorapatite $Ca_{10}(PO_4)_6F_2$. Altschuler and others (1958) have shown that sedimentary carbonate-fluorapatites normally contain more than 3.8-percent F; the substitution of CO_3^{-2} for PO_4^{-3} causes a charge imbalance which is compensated by F^{-1} or $(OH)^{-1}$. In other words, besides the 3.8-percent F represented by the F_2 of the stoichiometric formula of fluorapatite, carbonate-fluorapatite requires more fluorine to balance the charge.

TABLE 1.—*Analysis of phosphate nodules from the Wills Point Formation, Hopkins County, Tex.*

[X-ray fluorescence analysis supplemented by methods described by Shapiro and Brannock (1962). Analysts: Paul Elmore, S. D. Botts, Gillison Chloe, Lowell Artis, Joe Budinsky, and H. Smith]

Constituent	*Amount (weight percent)*
SiO_2	5.7
Al_2O_3	1.9
Fe_2O_3	1.1
FeO	.28
MgO	1.3
CaO	45.0
Na_2O	1.0
K_2O	.77
H_2O-	.87
H_2O+	3.2
TiO_2	.02
P_2O_5	28.4
F	3.8
S	1.6
CO_2	5.2
MnO	.08
	100.2
Less 0 for F	1.6
	98.6

TABLE 2.—*X-ray powder data for carbonate-fluorapatite, Hopkins County, Tex.*

I	d (*A*) *observed*	d (*A*)*calculated*	hkl
14	8.08	8.081	100
9	5.25	5.249	101
		4.666	110
11	4.042	4.041	200
11	3.867	3.865	111
		3.487	201
43	3.451	3.451	002
21	3.174	3.174	102
22	3.061	3.054	210
100	2.792	2.793	211
55	2.775	2.775	112
57	2.694	2.694	300
21	2.625	2.624	202
10	2.508	2.509	301
		2.333	220
44	2.287	2.287	212
		2.241	310
		2.213	103
		2.210	221
		2.132	311
		2.123	302
11	2.064	2.064	113
		2.020	400
		1.939	401
29	1.932	1.933	222
16	1.880	1.880	312
		1.854	320
32	1.837	1.838	213
18	1.791	1.790	321
18	1.764	1.763	410
		1.750	303
17	1.744	1.744	402
18	1.726	1.726	004
		1.709	411
		1.688	104
		1.638	223
		1.633	322
		1.618	114
		1.616	500
		1.605	313
		1.587	204
		1.574	501
		1.570	412

$c=0.6902$, $a=0.9331$, $c/a=0.7397$, $\lambda=1.5405$(Cu/Ni).

Thus the chemical data indicate a carbonate-fluorapatite in these nodules. This is confirmed by X-ray data: the c/a ratio computed from d-spacings of the X-ray powder is 0.7397. This may be compared with ratios listed by Deer and others (1962, p. 324):

Fluorapatite	0.735
Chlorapatite	.704
Hydroxyapatite	.731
Carbonate-apatite	.736

Evidently the ratio in question approximates that of either fluorapatite or carbonate-fluorapatite. Five carbonate-apatite analyses listed by Deer and others (1962, p. 328) have a fluorine content ranging from 2.80 to 5.60 percent as compared with 3.8 percent in the Texas nodules (but more in the apatite, as discussed

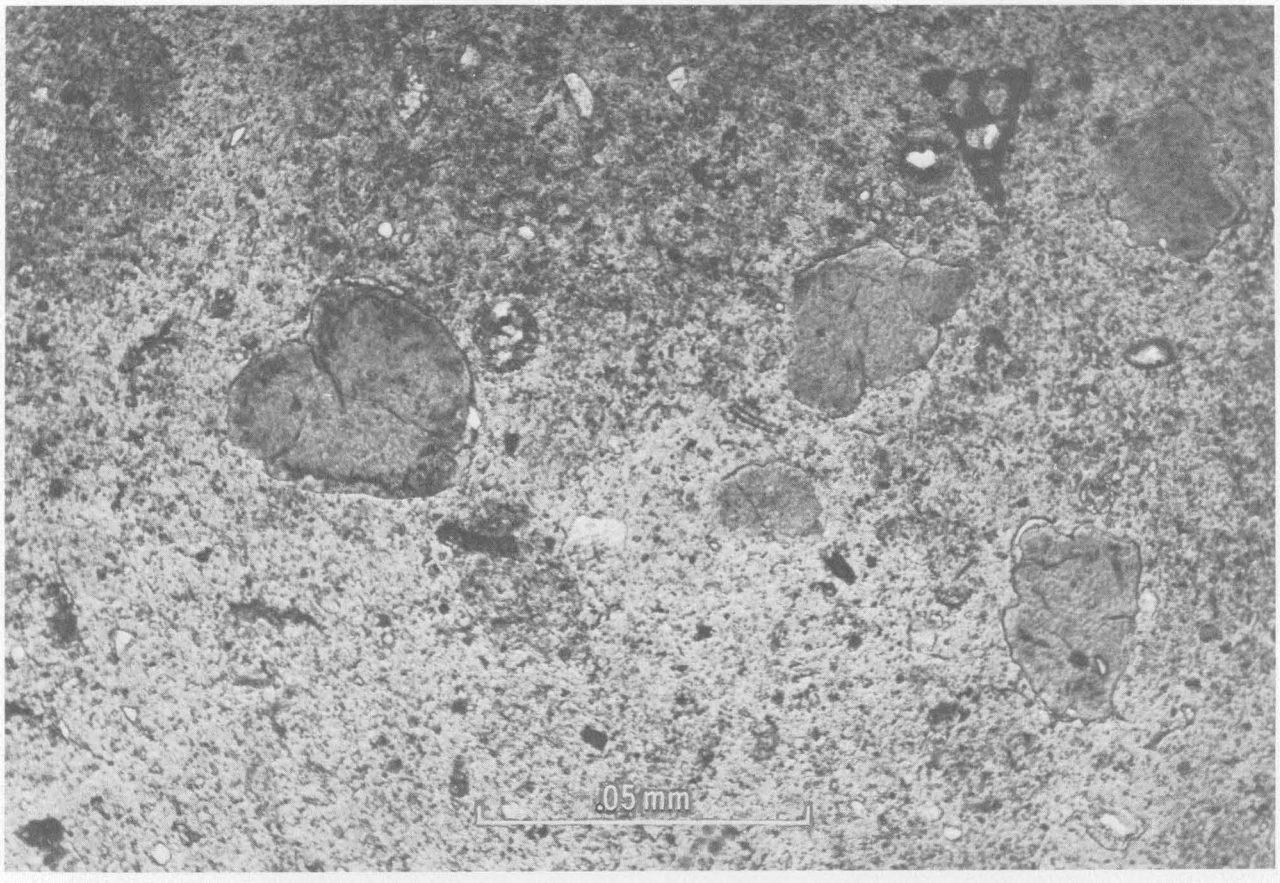

FIGURE 4.—Photomicrograph of thin section showing interior of nodule. The darker outlined areas are glauconite. Foraminifera are fairly abundant; one is seen in upper right. Ordinary light.

above), with corresponding carbon dioxide ranging from 0.36 to 4.43 percent as compared with 5.2 percent in the Texas nodules (with some obviously present in calcite). In summary, both chemical and X-ray data indicate that the phosphate contains fluorine and carbonate, and therefore is a carbonate-fluoroapatite as are most if not all marine apatites.

REFERENCES

Altschuler, Z. S., Clarke, R. S., Jr., and Young, E. J., 1958, Geochemistry of uranium in apatite and phosphorite: U.S. Geol. Survey Prof. Paper 314–D, p. 45–90.

Darton, N. H., Stephenson, L. W., and Gardner, J. A., 1937, Geologic map of Texas: U.S. Geol. Survey, 4 sheets, scale 1:500,000.

Deer, W. A., Howie, R. A., and Zussman, J., 1962, Rock-forming minerals, v. 5. Non-silicates: New York, John Wiley and Sons, 371 p.

Goldman, Marcus, 1922, Basal glauconite and phosphate beds: Science, v. 56, p. 171–173.

Pecora, W. T., Hearn, B. C., Jr., and Milton, Charles, 1962, Origin of spherulitic phosphate nodules in basal Colorado Shale, Bearpaw Mountains, Montana: Art 12 *in* U.S. Geol. Survey Prof. Paper 450–B, p. B30–B35.

Pratt, R. M., and McFarlin, P. F., 1966, Manganese pavements on the Blake Plateau: Science, v. 151, p. 1080–1082.

Shapiro, Leonard, and Brannock, W. W., 1962, Rapid analysis of silicate, carbonate, and phosphate rocks: U.S. Geol. Survey Bull. 1144–A, 56 p.

Texas University, Bureau of Economic Geology, 1966, Geologic atlas of Texas, Texarkana sheet: Austin, Tex., Univ. Texas Bur. Econ. Geology, scale 1:250,000.

INTRUSIVE ROCKS OF NORTH-CENTRAL PUERTO RICO

By ARTHUR E. NELSON, Beltsville, Md.

Work done in cooperation with the Economic Development Administration of Puerto Rico

Abstract.—In north-central Puerto Rico, Late Cretaceous to early Tertiary intrusive rocks, which range from gabbro to granodiorite, cut chemically similar Albian to Maestrichtian volcanic rocks. The chemical affinities between the two kinds of igneous rocks present suggest that this area is part of a calc-alkalic igneous terrane.

This report presents new mineralogic and chemical data on intrusive rocks ranging from gabbro to granodiorite that occur in north-central Puerto Rico (fig. 1). The data suggest that most of these intrusive rocks form a chemically related rock series which is chemically similar to a distinctive suite of older volcanogenic rocks also present in the area (Nelson, 1966).

North-central Puerto Rico, centered 30 miles west-southwest of San Juan, is underlain by a variety of volcanic rocks ranging in age from Early Cretaceous (Albian) to early Tertiary. These rocks are unconformably overlain to the north by middle Tertiary marine calcareous and minor epiclastic deposits (Berryhill, 1965; Nelson, 1967a, 1967b; Nelson and Monroe, 1966). Most of the Cretaceous rock units have been intruded by gabbroic and dioritic rocks. The volcanic rock units have complex intertonguing relations and are folded and complexly faulted; the middle Tertiary deposits are for the most part undeformed, having been only gently warped. Evidence of pervasive deformation in the intrusive rocks is lacking.

Flat-stage methods were used to determine the anorthite content of the plagioclase, and the Rosiwal method was used to determine the modes.

DISTRIBUTION AND AGE OF THE INTRUSIVE ROCKS

Figure 1 shows the general distribution of the intrusive rocks in the report area. Most of these rocks occur as irregularly-shaped masses of various sizes; numerous small dikes and, in places, some sills also are present. Granodiorite and quartz diorite form the bulk of the plutonic rocks; more mafic types are limited in occurrence. Many of the intrusive bodies, especially the dikes and small stocks, seem to have been emplaced along faults or fault intersections. Small areas of gabbro and diorite occur locally along the margins of large quartz diorite-granodiorite masses. The large area of intrusive rock in the western part of the map area is quartz diorite and granodiorite and forms part of the Utuado pluton (Weaver, 1958; Nelson, 1967b).

Small discontinuous tabular dikes of both aplite and andesite occur throughout the area and most commonly are found in large bodies of granodiorite and quartz diorite. They are too small to be shown on the map, ranging from less than 15 centimeters to 16 meters in width. Generally the aplite dikes are smaller but more plentiful than the andesite dikes.

Geologic evidence indicates that most of the intrusive rocks were emplaced in the Late Cretaceous (late Maestrichtian) to middle Paleocene-Eocene interval (Tertiary). However, some small dioritic stocks and an andesite sill cut rocks of Paleocene-Eocene age.

Two lead-alpha age determinations on zircon collected from two samples of quartz diorite in the eastern part of north-central Puerto Rico yielded an age of 60 ± 10 million years. The lead content was determined by Harold Westley and Charles Annel, U.S. Geological Survey; sample 616 contained 4.4 parts per million and sample 620 contained 2.5 ppm. The alpha activity, which was determined by T. W. Stern, was $170a$ and $97a$ per milligram-hour, respectively. The age was calculated using the formula given by Gottfried and others (1959, p. 19), and a value of 2,485 was determined for the factor c. A lead-alpha age of 70 ± 20 million years has been reported for zircon from granodiorite (Berryhill, 1965, p. 68), and a 60 ± 10 m.y. age has been calculated for granodiorite and quartz diorite collected south of the report area (T. W. Stern, written commun., March 1962.)

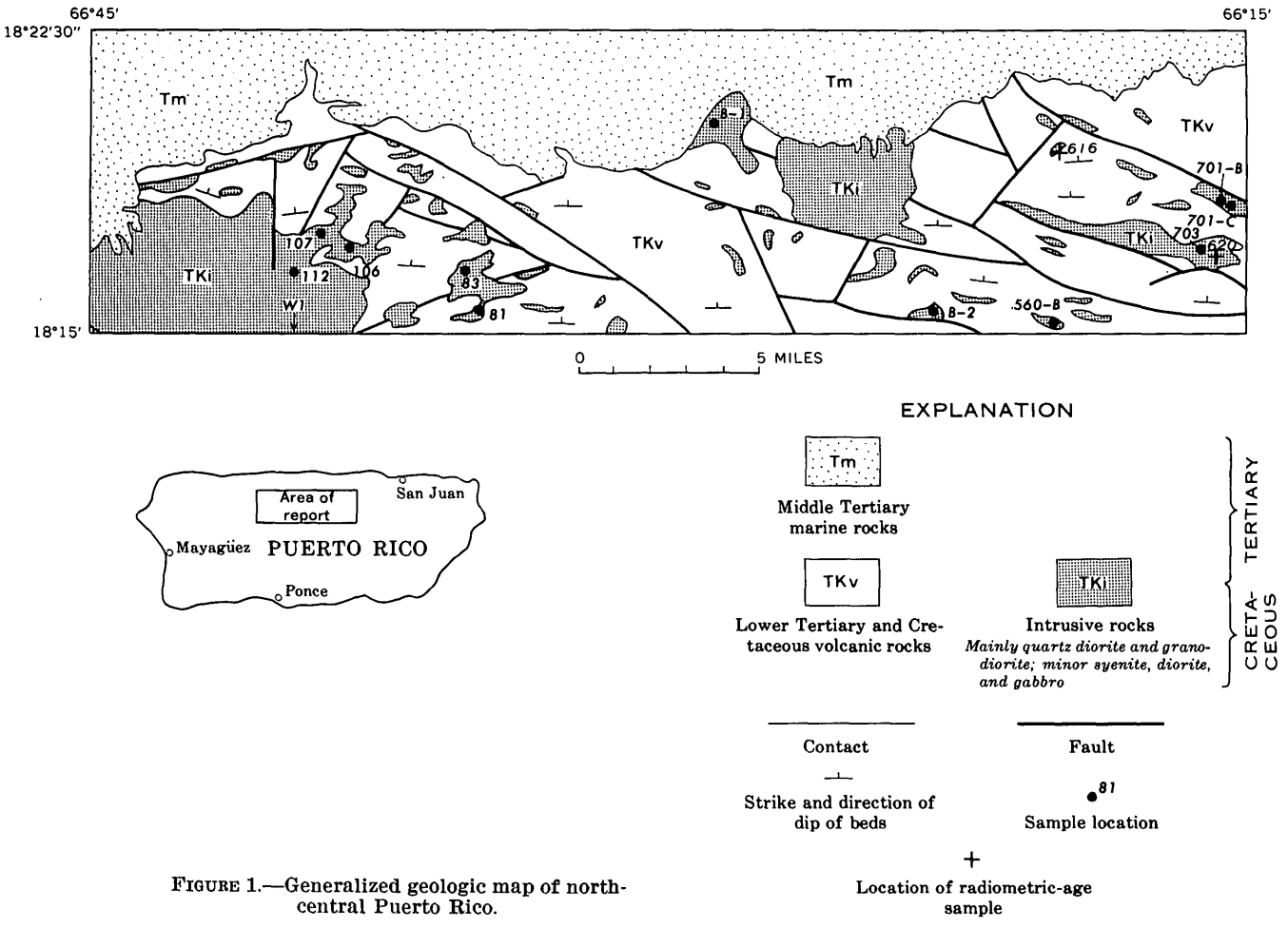

FIGURE 1.—Generalized geologic map of north-central Puerto Rico.

MEGASCOPIC AND MICROSCOPIC DESCRIPTION

Contacts between the intrusive and country rocks are sharp; the volcanic rocks generally dip steeply away from the intrusive rocks. Contact metamorphic effects on the volcanic rocks are slight; hornfelsic textures are developed locally.

The plutonic rocks are commonly massive and without apparent planar structure, but in places a faint randomly oriented foliation is present. Jointing is well developed, but faulting within the bodies is not common. Texture of the intrusive rocks ranges from granitic to xenomorphic, and grain size ranges from fine to medium and rarely to coarse. Locally, the rocks are porphyritic. Hornblende, plagioclase, potassium feldspar, and quartz are the principal minerals, and magnetite, biotite, pyroxene, and olivine are present in lesser abundance. Accessory minerals include apatite, sphene, and zircon, and secondary minerals include albite(?), sericite, biotite, chlorite, and calcite. Table 1 present modes for some of the intrusive rock types.

The more silicic rocks—quartz diorite and granodiorite—have a uniform appearance throughout north-central Puerto Rico; they range from pinkish gray to light gray to gray. Locally, they are spotted by small clusters of mafic minerals. In these rocks, plagioclase ranges from An_{22} to An_{40} and occurs in the groundmass and as phenocrysts; it locally is complexly twinned and normally zoned. Quartz is anhedral, and its percentage in the rock varies videly. Potassium feldspar is mostly orthoclase(?), but it includes some microcline. Potassium feldspar, which is usually cloudy and partly altered, occurs principally between larger minerals in the groundmass and only locally embays plagioclase; in places, potassium feldspar is graphically intergrown with quartz. Hornblende usually occurs as needlelike forms, but in places it also occurs as stubby crystals 4 to 6 millimeters long; it rarely exceeds 2 cm in length. Hornblende seems to alter to biotite and magnetite; chlorite also replaces hornblende and biotite. Tiny grains of pyroxene occur locally in the groundmass.

TABLE 1.—*Modes, in volume percent, of some intrusive rocks occurring in north-central Puerto Rico*

Sample No.	*560–B*	*81*	*83*	*703*	*701–C*	*112*	*701–B*	*106*	*107*
Rock type	*Gabbro*	*Gabbro*	*Diorite*	*Granodiorite*	*Granodiorite*	*Granodiorite*	*Granodiorite*	*Granodiorite*	*Granodiorite*
Type of plagioclase	*(An_{53})*	*(An_{64})*	*(An_{40})*	*(An_{37})*	*(An_{35})*	*(An_{32})*	*(An_{33})*	*(An_{40})*	*(An_{38})*
Plagioclase	20	[1] 46	[1] 67	55	45	[1] 49	55	[1] 56	[1] 51
Sericite	19	------	------	6	7	--------	3	--------	---------
K-Feldspar	------	------	------	17	21	16	15	13	19
Quartz	------	------	------	9	17	21	15	18	21
Hornblende	------	10	[2] 8	10	8	11	10	10	8
Biotite	4	5	------	1	--------	--------	--------	--------	---------
Chlorite	3	------	------	--------	--------	--------	--------	--------	---------
Pyroxene	25	34	[2] 20	--------	--------	--------	--------	--------	---------
Olivine	25	------	------	--------	--------	--------	--------	--------	---------
Magnetite	4	5	5	1	1	2	1	2	<1
Calcite	------	------	------	Tr.	--------	--------	--------	--------	---------
Accessory minerals: sphene, apatite, zircon.	Tr.	Tr.	------	<1	1	<1	<1	<1	<1
Total	100	100	100	99+	100	99+	99+	99+	99+

[1] Includes some sericite.
[2] Includes some chlorite.

TABLE 2.—*Chemical compositions for some intrusive rocks occurring in or near north-central Puerto Rico*

Sample No.	*560–B* [1]	*W–1*	*81* [1]	*83* [1]	*B–2*	*703* [1]	*B–1*	*701–C* [1]	*112* [2]	*701–B* [1]	*106* [2]	*107* [2]	*Alkali gabbro*	*Hornblende granodiorite*
Rock type	*Gabbro*	*Gabbro*	*Gabbro*	*Diorite*	*Alkali syenite*	*Granodiorite*	*Granodiorite*	*Granodiorite*	*Granodiorite*	*Granodiorite*	*Granodiorite*	*Granodiorite*	*(Nockolds, 1954, p. 1020)*	*(Nockolds, 1954, p. 1014)*
SiO_2	45	46. 21	47. 2	50. 2	57. 3	59	61. 3	63	63. 7	64	64. 2	67. 2	43. 94	65. 50
Al_2O_3	15	18. 92	15. 6	17. 3	16. 9	21	16. 4	19	15. 6	18	15. 7	15. 7	14. 87	15. 65
Fe_2O_3	6	4. 97	6. 0	4. 6	2. 9	3	3. 0	3	2. 7	3	2. 6	2. 3	4. 35	1. 63
FeO	10	7. 19	6. 4	5. 8	3. 2	3	2. 7	3	2. 6	3	2. 2	1. 8	7. 80	2. 79
MgO	15	6. 45	7. 9	5. 1	2. 2	1	2. 1	<1	2. 3	1	2. 2	1. 6	9. 31	1. 86
CaO	6	12. 49	11. 8	9. 3	2. 6	5	5. 1	4	5. 2	3	4. 6	4. 1	12. 37	4. 10
Na_2O	2	1. 86	2. 2	3. 0	4. 1	4	3. 4	3	3. 6	5	4. 4	4. 0	2. 32	3. 84
K_2O	<1	. 33	. 78	. 96	6. 8	3	3. 4	4	2. 6	3	2. 0	2. 1	. 92	3. 01
H_2O-	-----	. 50	. 10	. 10	1. 9	-----	1. 1	-----	. 04	-----	. 18	. 06	-----	------
H_2O+	<1	. 10	. 38	1. 6	------	<1	------	<1	. 45	<1	. 62	. 63	. 66	. 69
TiO_2	-----	1. 07	1. 2	. 91	. 91	-----	. 56	-----	. 48	-----	. 44	. 36	2. 86	. 61
P_2O_5	-----	. 15	. 2	. 26	. 63	-----	. 40	-----	. 21	-----	. 21	. 18	. 44	. 23
MnO	-----	. 20	. 2	. 20	------	-----	. 18	-----	. 10	-----	. 14	. 07	. 10	. 09
CO_2	-----	. 00	. 05	. 89	<. 05	<1	. 07	-----	. 05	-----	. 05	. 05	-----	------
Total	99+	100. 44	100	100	100	99+	100	99+	100	100+	99	100	99. 94	100

[1] Chemical composition only approximate, based on calculation of modes.
[2] Samples analyzed by methods described by Shapiro and Brannock (1962). Analysts: Paul Elmore, Samuel Botts, Gillison Chloe, Lowell Artis, and H. Smith.

560–B Gabbro. Dark-gray olivine pyroxene gabbro with medium-grained granitic texture. Plagioclase is highly sericitized. Olivine and clinopyroxene (augite?) are the principal mafic minerals. Magnetite is widely dispersed in rock. Alteration minerals are biotite and chlorite.

W–1 Gabbro. Collected by J. D. Weaver (1958, p. 1133).

81 Gabbro. Dark-gray medium-grained clinopyroxene-hornblende gabbro, with granitic texture. Plagioclase (An_{64}), pyroxene, and hornblende are chief minerals with lesser amounts of biotite, chlorite, and magnetite.

83 Diorite. Medium-gray to dark-gray diorite with phenocrysts of plagioclase and hornblende in very fine textured groundmass. Principal minerals are partly sericitized plagioclase, and hornblende, pyroxene, some magnetite, chlorite, and a trace of calcite.

B–2 Alkali syenite. Collected by H. L. Berryhill (1965, p. 67).

703 Granodiorite. Light- to medium-gray hornblende quartz diorite with granitic texture. Highly sericitized plagioclase, cloudy K-feldspar, quartz, and hornblende are the principal minerals. Biotite is sparse, and small grains of magnetite are uniformly distributed in rock.

B–1 Granodiorite. Collected by H. L. Berryhill (1965, p. 67).

701–C Granodiorite. Light-gray fine- to medium-grained granodiorite with granitic texture. Partly sericitized plagioclase, altered K-feldspar, and quartz are the principal minerals. Hornblende is not widely distributed, and magnetite is sparse.

112 Granodiorite. Gray medium-grained hornblende granodiorite, with automorphic-granular texture. Contains partly sericitized plagioclase, quartz, cloudy K-feldspar, hornblende, and magnetite.

701–B Granodiorite. Light-gray fine- to medium-grained hornblende granodiorite, with granitic texture. Highly sericitized plagioclase, altered K-feldspar, and quartz are principal minerals; hornblende occurs as slender needlelike laths and is uniformly distributed in rock.

106 Granodiorite. Gray to light-gray mostly fine grained hornblende granodiorite, with porphyritic texture. Contains zoned, partly sericitized plagioclase (andesine) phenocrysts, quartz, K-feldspar, and partly chloritized laths of hornblende.

107 Granodiorite. Medium-gray to light-gray hornblende granodiorite with phenocrysts of plagioclase and some hornblende in a fine-grained groundmass with xenomorphic granular texture. Plagioclase (An_{38}) is complexly twinned and partly sericitized; hornblende occurs as needlelike laths. K-feldspar, pyroxene, and magnetite occur as tiny grains between larger minerals.

The mafic rocks are massive and range from dark gray to black or dusky blue. In these rocks, the plagioclase commonly ranges from calcic oligoclase to andesine, but one sample does contain labradorite. Hornblende, clinopyroxene, and, locally, olivine are the principal mafic minerals. Biotite is locally present, but never in large amounts. Quartz and potassium feldspar occur in small quantities in the diorite, but they have not been observed in the gabbros. Hornblende, some of which contains ragged relict cores of augite, occurs as slightly biotized and (or) chloritized subhedral prisms; in places, kelyphitic rims of magnetite and hornblende envelop clinopyroxene. Subhedral biotite flakes, pleochroic from pale yellow to dark brown or greenish brown, generally are associated with magnetite and probably are alteration products of hornblende.

CHEMICAL RELATIONS OF THE INTRUSIVE ROCKS

Table 2 presents chemical data of the intrusive rocks sampled. Five new chemical analyses, four rock compositions calculated from modes, and three previously published chemical analyses are shown (Weaver, 1958, p. 1133; Berryhill, 1965, p. 67). As indicated, these analyses cover a compositional range from gabbro to granodiorite. All the analyzed samples were collected within the report area except for one sample (W–1) of gabbro (Weaver, 1958, p. 1133), which was collected from the southern part of the Utuado pluton just south of the report area.

Chemical analyses of the intrusive rocks sampled are close to the average compositions given by Nockolds (1954) for corresponding rock types. Some of the calculated compositions, which are based on Rosiwal modes, are higher in total iron than similar rocks for which chemical analyses are available. Generally, however, most of the differences in oxide percentage are not great, and the computed compositions for the given rock types are reasonable. The alkali-lime index for the intrusive rocks, excluding the alkali syenite, is 58 to 59 percent SiO_2; this suggests that as a whole these rocks should be classed as calc-alkalic.

Figure 2 shows the position plots for the analyses given in table 2. Superposed is a curved line representing the trend of fractional crystallization of calc-alkali rocks (Hess, 1960, pl. 11). Plots for the volcanic rocks (Nelson, 1966) are also shown. As indicated, the points for the intrusive rocks are clustered around the crystallization curve and fall within the field of similar plots for the volcanic rocks that range from basalt to rhyolite (Nelson, 1966).

The intrusive rocks, in general, correspond in chemical composition to the volcanic rocks in the report area

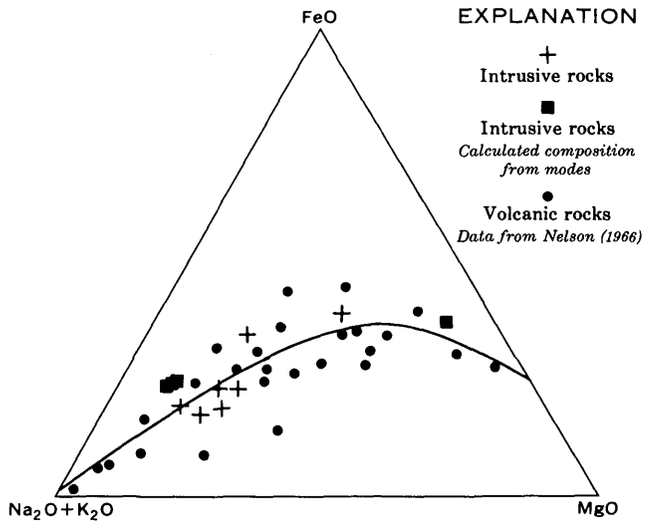

FIGURE 2.—Iron-magnesium-alkalies (FMA) diagram for igneous rocks in north-central Puerto Rico. Curve is trend of fractional crystallization of calc-alkalic rocks from Hess (1960, pl. 11).

(Nelson, 1966) as follows: gabbros correspond to basalts and andesitic basalts, diorite to andesite lava, and granodiorite and syenite to the more acidic andesites and dacitic volcanic rocks.

SUMMARY

Areal and chemical relationships between most of the intrusive rock bodies show that these bodies were derived from magma that gave rise to chemically related intrusive rocks throughout the report area, and that these rocks form part of a calc-alkalic suite. The close chemical affinity between the intrusive and volcanic rock suites suggests that north-central Puerto Rico is part of a calc-alkalic petrographic terrane. The source magmas for the intrusive and volcanic rocks must have been somewhat similar in bulk chemical composition; this suggests that a genetic relationship might have existed between the respective source magmas.

The origin of the intrusive rock magma is at present unknown. Possibly the magma was generated by fusion of older but chemically similar volcanic rocks or, alternatively, the magma might have been a derivative of the magma type that gave rise to the earlier volcanic rocks, thus suggesting that the intrusive rocks represent a later phase of a long igneous episode.

REFERENCES

Berryhill, H. L., 1965, Geology of the Ciales quadrangle, Puerto Rico: U.S. Geol. Survey Bull. 1184, 116 p.

Gottfried, David, Jaffe, H. W., and Senftle, F. E., 1959, Evaluation of the lead-alpha (Larsen) method for determining ages of igneous rocks: U.S. Geol. Survey Bull. 1097–A, 63 p.

Hess, H. H., 1960, Stillwater igneous complex, Montana: Geol. Soc. America Mem. 80, 230 p.

Nelson, A. E., 1966, Significant changes in volcanism during the Cretaceous in north-central Puerto Rico, *in* Geological Survey Research 1966: U.S. Geol. Survey Prof. Paper 550–D, p. D172–D177.

———1967a, Geologic map of the Corozal quadrangle, Puerto Rico: U.S. Geol. Survey Misc. Geol. Inv. Map I–473.

———1967b, Geologic map of the Utuado quadrangle, Puerto Rico: U.S. Geol. Survey Misc. Geol. Inv. Map I–480.

Nelson, A. E., and Monroe, W. H., 1966, Geology of the Florida quadrangle, Puerto Rico: U.S. Geol. Survey Bull. 1221–C, 22 p.

Nockolds, S. R., 1954, Average chemical compositions of some igneous rocks: Geol. Soc. America Bull., v. 65, no. 10, p. 1007–1032.

Shapiro, Leonard, and Brannock, W. W., 1962, Rapid analysis of silicate, carbonate, and phosphate rocks: U.S. Geol. Survey Bull. 1144–A, p. A1–A56.

Weaver, J. D., 1958, Utuado pluton, Puerto Rico: Geol. Soc. America Bull., v. 69, p. 1125–1142.

SERPENTINIZATION IN A SHEARED SERPENTINITE LENS, TIBURON PENINSULA, CALIFORNIA

By NORMAN J PAGE, Menlo Park, Calif.

Abstract.—A well-exposed sheared serpentinite lens occurring on the Tiburon Peninsula, Marin County, Calif., in rocks of the Franciscan Formation was mapped and sampled in detail. Remnant olivine (Fo_{90}) and enstatite (En_{85-90}) indicate that the parent material was a peridotite which is now 95 to 100 percent serpentine with local magnetite and carbonate minerals. The composition of mesh texture (chrysotile + lizardite), vein (chrysotile), and bastite (lizardite) serpentines increases in FeO content during serpentinization as shown by combined electron microprobe, X-ray, and textural studies. Brucite was not identified, although it has been reported in other California Coast Range ultramafic bodies. Its absence may be caused by reaction with SiO_2 carried by large volumes of water through the sheared serpentinite to form the abundant late chrysotile veins that crosscut all other structural and mineralogical features in the lens.

Sheared serpentinites are so abundant in the Coast Ranges of California and elsewhere that it is worthwhile studying an isolated and well-exposed sheared serpentinite lens. The lens selected for mapping and sampling is within an area 340 feet by 170 feet on the Tiburon Peninsula in southeastern Marin County, Calif., (fig. 1) on the corner of Endeavor Cove Road and Endeavor Drive in the township of Corte Madera. The whole outcrop is included in a steep roadcut that exposed unweathered rocks at the time of mapping.

The detailed map (fig. 2) of the sheared serpentinite lens and surrounding country rocks was prepared with an alidade and planetable. The contour lines indicate the height of the outcrop relative to an arbitrary zero contour.

Earlier investigators of the region include Lawson (1914), who mapped the Tiburon Peninsula and surrounding region at a scale of 1:62,500, and Taliaferro (1943). Lawson's map more accurately portrays the actual distribution of rock types around and within the serpentinite.

The present study on the serpentinite lens of the Tiburon Peninsula represents results of research that was done concurrently at the University of California and by the U.S. Geological Survey. The geologic map was prepared jointly with Priscilla Dudley, University of California. All sample numbers are those of specimens in the collections of the University of California (Berkeley), Department of Geology and Geophysics.

Acknowledgments.—In addition to Priscilla Dudley, whose help in preparing the geologic map is warmly acknowledged, special thanks are due Professors W. S. Fyfe, A. Pabst, and H. E. Hawkes, of the University of California, who acted as advisors in work on the serpentine group, and B. W. Evans, University of California, who gave invaluable assistance in the microprobe work. The University also provided part of the financial support. The suggestions of R. A. Loney and G. R. Himmelberg, U.S. Geological Survey, in preparation of the paper were very helpful.

GENERAL GEOLOGY

The rock units differentiated in the field and mapped are massive graywacke interbedded with shale and siltstone layers, highly fractured and sheared graywacke and shale, chert, conglomerate, glaucophane-bearing schist, serpentinite undivided, blocky serpentinite, sheared serpentinite, and outcrop cover caused by sliding and slumping (fig. 2). These form part of the sequence of rocks that compose the Franciscan Formation of Jurassic and Cretaceous age on the Tiburon Peninsula. Traceable filled shear zones, minor faults, folds, and bedding attitudes have also been mapped.

Lithology

Massive graywacke with interbedded shale.—The most abundant rock type, which makes up most of the country rock of the serpentinite, is massive graywacke with interbedded shale. The bedding strikes generally

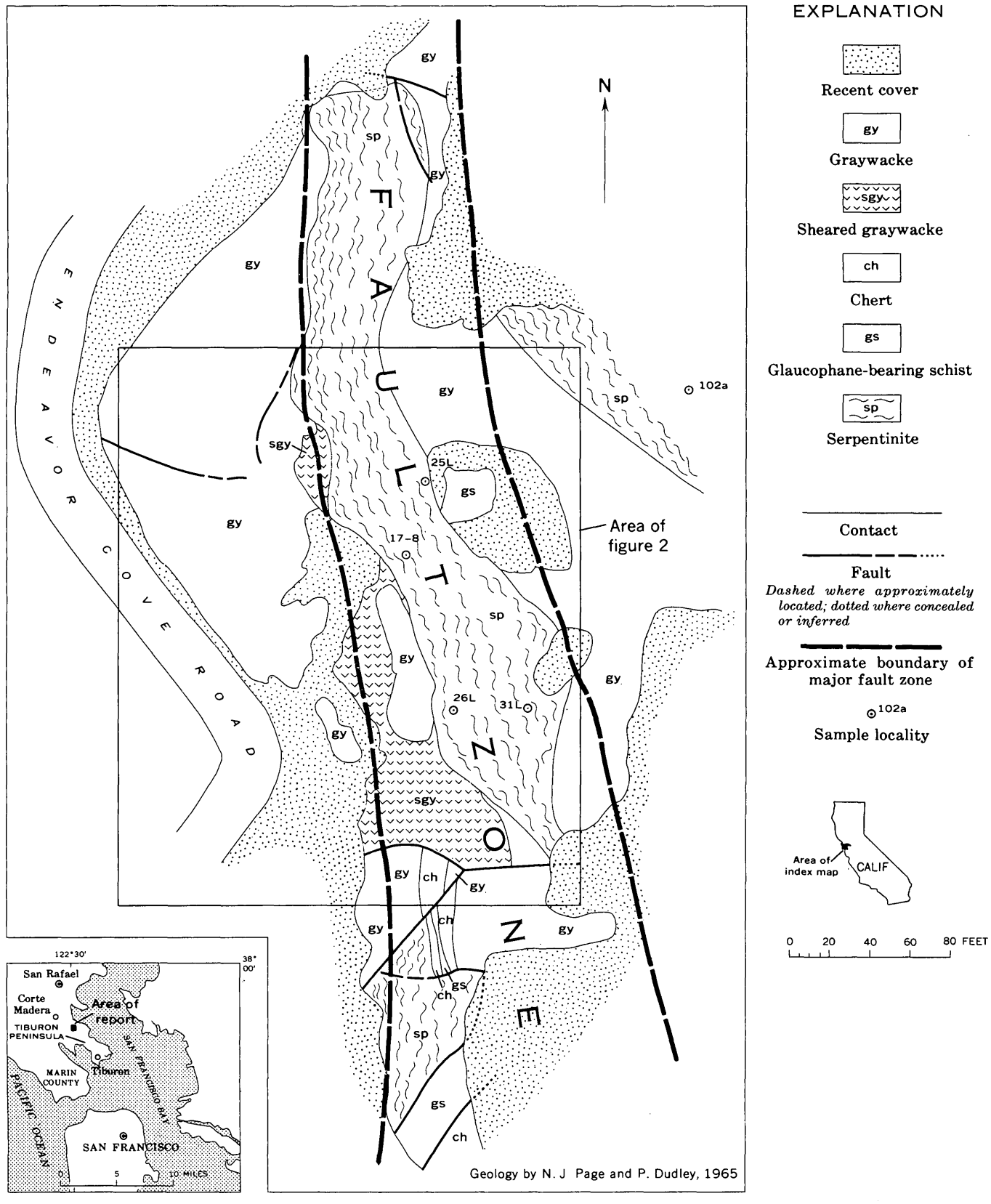

FIGURE 1.—Geologic sketch map of serpentinite lens, Tiburon Peninsula, Calif.

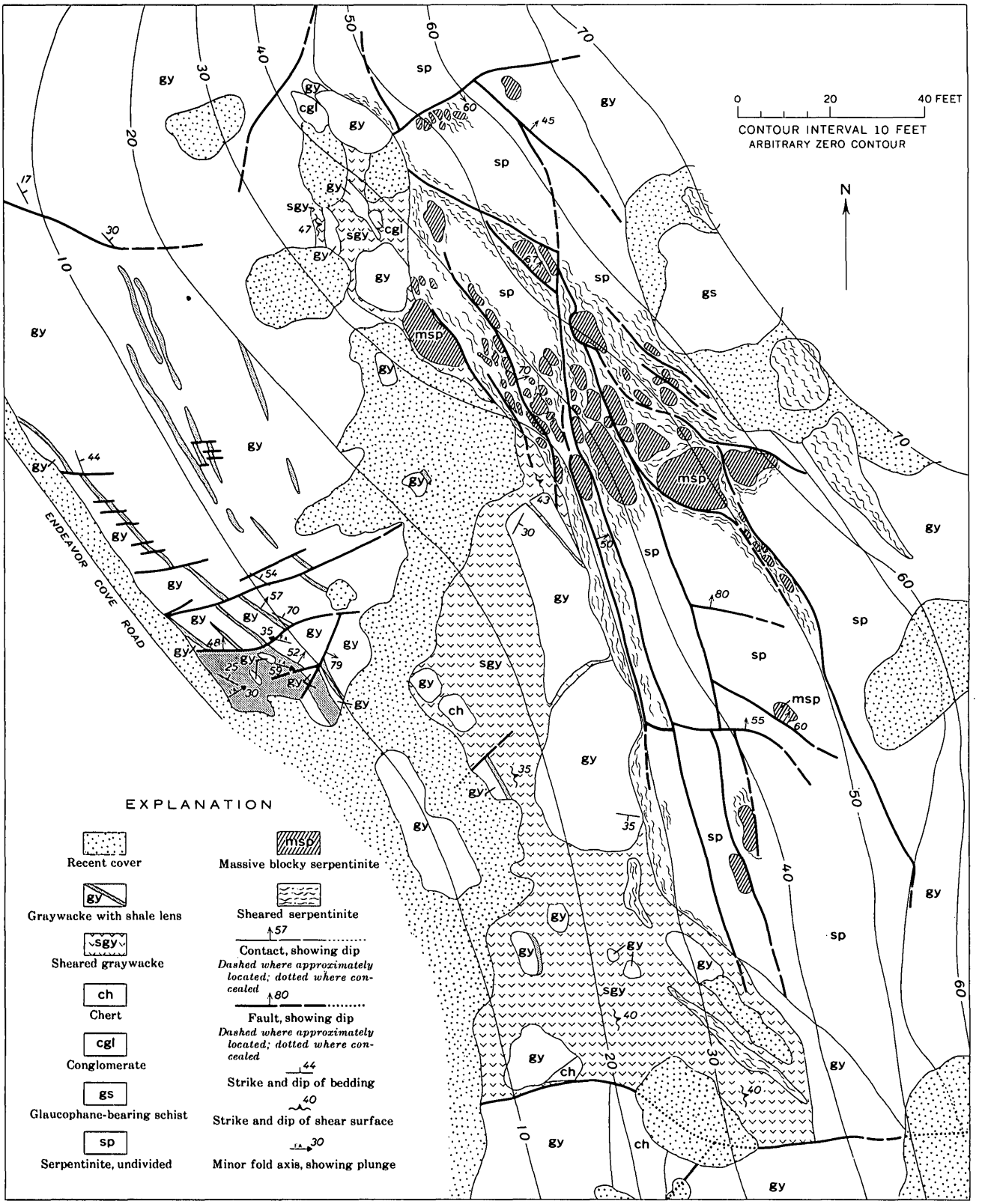

FIGURE 2.—Detailed geologic map of area outlined in figure 1.

north-south and dips eastward at moderate angles. The beds of graywacke range in thickness from 0.5 inch to tens of feet and are separated by thin 0.5- to 6-inch shaly layers. The shale beds serve as distinct markers that make it possible to map the small faults and folds (fig. 2).

The graywacke is composed of quartz, albite, carbonate, hydrogrossularite, epidote, chlorite, and opaque minerals; the shale, predominantly of quartz and chlorite. The texture is that of a typical clastic rock with much of the matrix material altered to chlorite.

Fractured and sheared graywacke.—Sheared graywacke that contains blocks of massive graywacke occupies the area below the serpentinite lens (fig. 2). Some of these blocks appear to be rotated, as is indicated by bedding planes within them. Chert and conglomerate blocks are also enclosed in the sheared graywacke, and highly sheared serpentinite lenses are found locally within the sheared graywacke. In general, the shear planes in sheared graywacke strike north-south and dip eastward at moderate angles, very similar to strike and dip of the shales interbedded with massive graywacke. Contacts of this unit with other rocks appear to be faults.

Sheared graywacke contains the same minerals as massive graywacke, but it has a greater abundance of chlorite.

Chert.—Chert occurs only in the southern part of the mapped area (fig. 2) and is mostly interbedded with massive graywacke; a few minor chert blocks are found in the sheared graywacke. The chert is predominantly green with an occasional shaly parting in one fault block; in another, it is red with shaly partings.

Conglomerate.—Conglomerate only occurs as blocks in the sheared graywacke.

Glaucophane-bearing schist.—Glaucophane-bearing schist occurs only in the southern part of the area mapped (fig. 1) and is separated from all other types of rocks, except red chert, by faults. The contact between the one serpentine lens and the glaucophane schist is probably a shear surface. These rocks have a moderate foliation which appears to be almost perpendicular to the contact of chert and schist.

The minerals present in the schist are a glaucophane-like amphibole, quartz, vermiculite, stilpnomelane, lawsonite, albite, and aragonite(?) or calcite.

A pumpellyite-green soda pyroxene-glaucophane-lawsonite-sphene block occurs only as a boulder or "knocker" about 15 feet in diameter above the main serpentine lens (fig. 2). The contacts are covered.

Ultramafic rocks.—All ultramafic rocks within the area studied are now either blocky or sheared serpentinite. The blocky type is found on the top of the hill outside the fault zone (northeastern map area, fig. 1). It also comprises all of the massive serpentinite blocks within the mapped sheared serpentinite lens. The serpentinite body located on the top of the hill contains relict olivine and pyroxene, as do the blocks in the sheared lens, indicating that the parent rock type of both serpentinites probably was a peridotite. The sheared serpentinite was developed by tectonic processes from the blocky massive serpentinite. The contact of the sheared serpentinite lens with the country rocks is generally sharp and is composed of numerous slickensided surfaces within both the ultramafic and country rocks. Locally, late feathery carbonates (aragonite and hydromagnesite) formed in the contact zone.

Structure

Most of the mapped area (fig. 2) represents a major fault zone. Priscilla Dudley (oral commun., 1966) believes that the fault extends northward across the mapped area, intersecting the serpentinite lens in the region of intense shearing and faulting (fig. 1). All the structures present—folds, faults, rotated blocks, and shear zones—are probably directly related to this major fault.

Folds.—Three minor folds were observed and the orientation of their axial planes and axes measured. They show no recognizable preferred orientation nor do they appear to be penetrative structures. All of them occur in highly crumpled and fractured shale and appear to be the result of the intense shearing caused by faulting.

Faults and shear fractures.—Shear zones within the country rocks are true faults, and some amount of displacement can be demonstrated. Those occurring within the serpentinite lens are more aptly termed shear zones in which there may or may not be demonstrable displacement, but such structures are continuous and mappable. At least two sets of faults occur, a northeast-trending set and a northwest-trending set. The jumbling and rotation of fault blocks makes a very complex picture, probably owing to movement within the major fault zone that was responsible for emplacing the serpentinite lens in its present position in the crust. The lens probably represents a part of a larger ultramafic body from which it was separated by faults on the Tiburon Peninsula.

PETROLOGY, MINERALOGY, AND TEXTURE OF THE ULTRAMAFIC ROCK

Parent material of the serpentinite

Only a few minute remnants of olivine, orthopyroxene, clinopyroxene, and chromite are within the lens.

Estimates of the percentages of olivine and pyroxene in the original rock, based on the ratio of bastite to mesh-structure serpentine, range from 10 to 20 volume percent pyroxene and 90 to 80 volume percent olivine.

Figure 3*A* presents partial microprobe analyses[1] for MgO, FeO,and SiO_2 of olivine and enstatite from the upper serpentinite. The compositions are very similar to those of minerals of Burro Mountain (Page, 1967) and other "alpine" ultramafic bodies. Olivine and enstatite occur as remnants in the mesh (olivine) and bastite (enstatite) structure. Small grains of diopside are present as individuals and as lamellae in enstatite. Reddish-brown spinel is rimmed and veined by magnetite. Serpentine minerals compose about 95 percent or more by volume of the rock.

Serpentinite

There are two structural types of serpentinite within the lens: blocky massive, and sheared serpentinite. Blocky serpentinites consist of lizardite, chrysotile, magnetite, remnant clinopyroxene lamellae, remnant enstatite, remnant olivine, carbonate minerals, and vermiculite. All the minerals have been identified by either X-ray diffraction or by microscopic examination in thin section, or by both methods. Relative abundances of lizardite and chrysotile determined by X-ray analysis vary, but lizardite appears to be the more abundant. Lizardite comprises the bastites and is combined with chrysotile in the meshes. Brucite was not observed in any specimen. Most of the carbonate is argonite or hydromagnesite. Vermiculite is found only in weathered rocks. Magnetite appears to be most abundant in the later veins. No antigorite was identified, but it has been found in stream boulders at other localities on the peninsula (E. J. Essene, oral commun., 1966). Serpentine minerals in the blocky massive type form the "classical" mesh texture after olivine and bastite texture after pyroxene. The last serpentine mineral to form in the mesh texture is nearest the center of the structure, or nearest the remnant olivine grain.

Each block of massive serpentinite is veined by cross-fiber chrysotile veins. In most examples, these veins extend from the margin of the block inward, some even as far as the center; many generations of crosscutting veins are present. Also, gashlike cross-fiber veins develop within the blocks. Sparse lizardite veins are observed to follow patterns similar to the cross-fiber veins. All vein types contain abundant magnetite, mostly euhedral but locally as fine filigrees and clots.

[1] The microprobe techniques used for these analyses are discussed by Page (1966).

Some specimens have large plates of lizardite developing possibly from the mesh structure. In other samples, wormy textures of small crystals develop at the edges of meshes. These textures suggest a later period of recrystallization of serpentine. Locally, ribbon-structured serpentinite blocks develop and indicate that some of the individual blocks have been affected by tectonic processes. The development of the ribbon-structured serpentine has been detailed by Francis (1955).

All the blocks of massive serpentinite enclosed in sheared serpentinite have slickensided and polished serpentine on each face. The sheared serpentinite shows a variety of textures. Sheared serpentinites are composed of chrysotile, lizardite, magnetite, and carbonates. Chrysotile is the dominant serpentine mineral. The dominant texture is represented by well-foliated, finely ground and shredded, platy serpentine and fibrous serpentine. The magnetite included in the sheared serpentinite is fractured. Fibrous chrysotile vein fragments often show kinked structures. Other textures are apparently randomly oriented pieces of serpentine cut by fine, irregular fractures and very small sheared lenses of massive ribbon-textured serpentinite. Sheared serpentinites are also veined by late chrysotile and lizardite, both parallel and crosscutting the foliations.

Serpentine composition

Numerous electron microprobe analyses of serpentine minerals from six specimens (fig. 3*B–G*) show (1) the variation in the total iron content of the various serpentine minerals, (2) the diversity of serpentine composition among different serpentine grains in a thin section and between samples, and (3) information concerning the "polymorphic" relation of chrysotile and lizardite. The following textural varieties of serpentine were analyzed for Fe, Si, and Mg: bastite texture (lizardite), mesh-texture serpentine (lizardite + chrysotile), mesh-texture centers (lizardite + chrysotile), mesh-texture margins (lizardite + chrysotile), chrysotile veins, lizardite veins, platelets (lizardite), and ribbon-structured serpentine (chrysotile + lizardite). Many spots were analyzed and fall within the outlined areas in the diagrams where average compositions are plotted (fig. 3*B*, *D*, *E*), except for mesh-textured serpentine, lizardite platelets, and ribbon-structure serpentine (fig. 3*C*, *F*. *G*), where individual spots are plotted.

Textural relations indicate that bastite and mesh-texture serpentine have formed simultaneously and in stages. Imprinted upon these two types of serpentine are chrysotile veins which were formed at many later

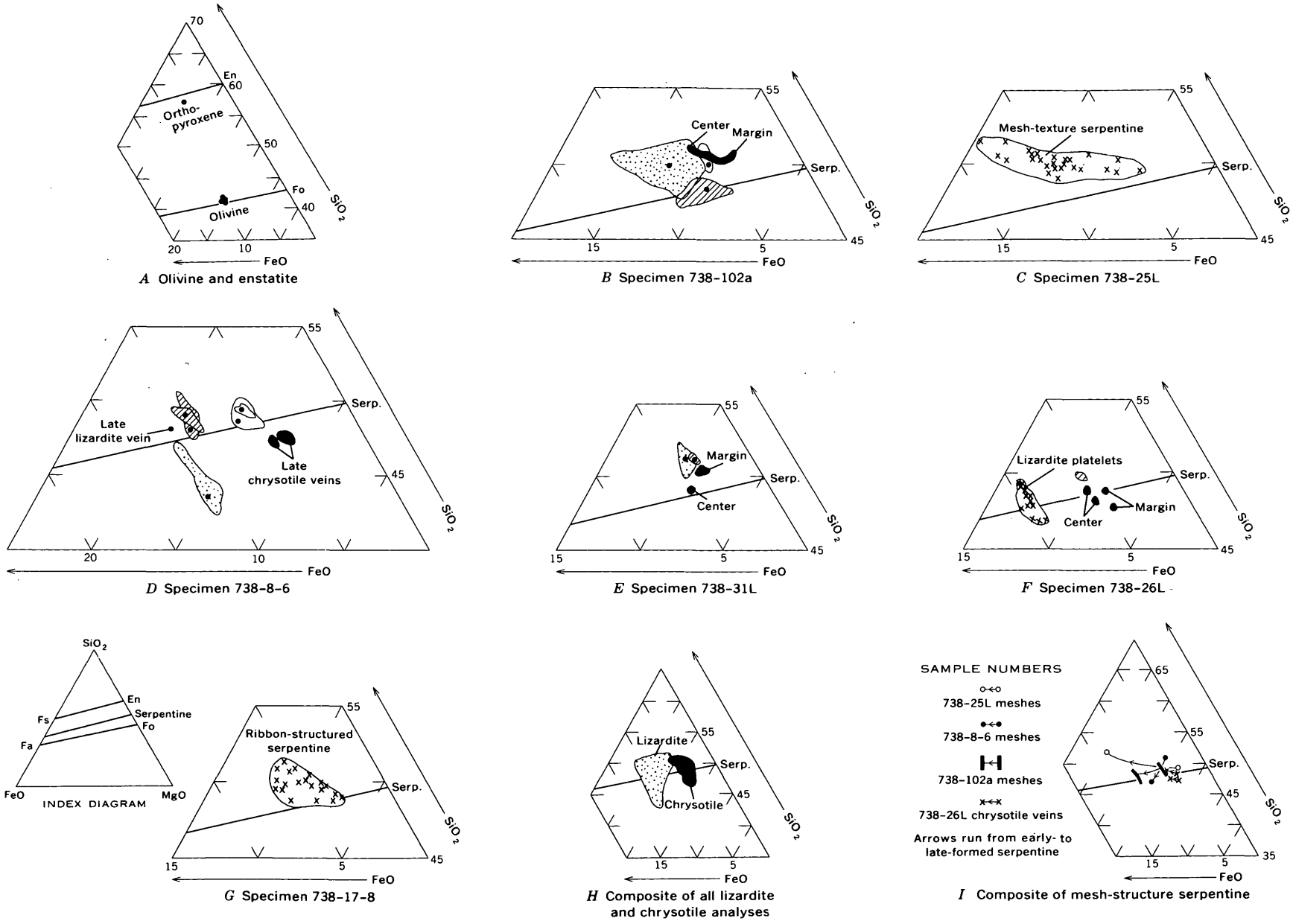

FIGURE 3.—Electron microprobe analyses of olivine, enstatite, and serpentine plotted on portions of the triangular diagram MgO–FeO–SiO_2 in weight percent. Sample locations given in figure 1. Stippled pattern, bastites; crossruled, mesh centers; plain, mesh margins; black, chrysotile veins; dots, average analyses; ex, spot analyses.

stages after the initial stages of formation of the bastites and mesh textures. At a stage later than the majority of the chrysotile veins, platelets of lizardite replaced the mesh-texture serpentine, and ribbon-structured serpentine was formed. Chrysotile and lizardite veins continued to form. All the varieties of serpentine minerals are enriched in total iron (calculated as FeO) as a function of time, as demonstrated by the analyses.

The analyses also show that there is a larger variation in total iron content of serpentine from different samples than there is within an individual sample; that is, each sample appears unrelated to any other sample. This means that one rock will not be representative of a small serpentine body, nor is it possible to unravel the process of serpentinization without a very detailed study. In the following discussion of composition, the serpentines will be described in order of their apparent paragenetic sequence.

Figure 3*H* shows composites of all analyses made on bastite (lizardite) and vein chrysotile. The bastite is iron rich, similar to bastite from Burro Mountain (Page 1967). This diagram indicates that lizardite and chrysotile have distinct chemical compositions and could not be considered polymorphs. In the Tiburon serpentine lens, vein chrysotile and bastite lizardite have a restricted range of total iron content, as is shown in figure 3*H*. Bastite and chrysotile vary in composition by about 5 weight percent FeO. Mesh-texture serpentine (fig. 3*B*, *C*, *D*) shows a trend of iron enrichment from earliest serpentine to latest serpentine.

Wherever crosscutting chrysotile veins were observed and analyzed, the younger veins were found to be richer in iron than the older veins. In general, for an individual chrysotile vein (fig. 3*B*, *E*, *F*), the center of the vein is more iron enriched than the margin. Late lizardite veins also occur, and the analysis of one of them is plotted in figure 3*D*. Figure 3*I* summarizes the data that indicate iron enrichment of younger serpentines.

Two other types of serpentine have formed later than the mesh textures, bastite, and some of the chrysotile veins. These are ribbon-structured serpentine (fig. 3*G*) and lizardite platelets. Platelets of lizardite, apparently forming from mesh-structure serpentine, were analyzed (fig. 3*F*); such formation represents an enrichment of total iron in the lizardite.

For all types of serpentine studied, the general trend is one of progressively greater iron enrichment in younger serpentines. All the interrelationships between various types of serpentine are unclear except that lizardite is always richer in iron than the associated chrysotile.

285-544 O—68——3

PETROGENESIS OF THE SERPENTINITE LENS

Only if and after the peridotite was emplaced in the crust at an appropriate temperature for serpentinization, and the system was open to water, could various reactions proceed to cause alteration. Using an equilibrium model, some features of serpentinization can be related to temperature by textural studies, assuming that the body cooled during serpentinization. One of these features is the increase in iron content of the serpentine phases with decrease in temperature. Another is the abundance of magnetite at late stages or low temperatures in the alteration process. Other features of importance are the absence of brucite in the altered rock, as compared with Burro Mountain (Page, 1967) and other described bodies containing occurrences of brucite (Hostetler and others, 1966), and the absence of large amounts of magnesite which might have developed by a reaction of CO_2 with brucite or Mg^{+2} ions in the altering solutions. The postulated events and the evidence for them are:

Olivine (Fo_{90}) + enstatite (Fo_{10}) + H_2O + O_2 = Fe^{+2}, Mg-chrysotile + Fe^{+2}, Fe^{+3}, Mg-lizardite + magnetite, and (1)

Olivine (Fo_{90}) + enstatite (Fo_{10}) + H_2O + O_2 = Fe^{+2}, Mg-chrysotile + Fe^{+2},Fe^{+3}, Mg-lizardite. (2)

Most early serpentinization takes place by reaction 2, as is suggested by the absence of magnetite associated with early serpentine. As temperature falls, both the lizardite and chrysotile become richer in iron. These reactions are suggested by the compositions of mesh and bastite structures in partially serpentinized rocks. Since brucite is not present in these rocks, there is no evidence to suggest that the following reactions ever took place. Bowen and Tuttle's investigation (1949) of the forsterite-serpentine-brucite reaction suggests that these reactions occur at lower temperatures than reactions 1 and 2:

Olivine (Fo_{90}) + H_2O + O_2 = Mg, Fe^{+2}-brucite + Fe^{+2}, Mg-chrysotile + Fe^{+3}, Fe^{+2}, Mg-lizardite + magnetite (3)

Olivine (Fo_{90}) + H_2O + O_2 = Mg, Fe-brucite + Fe^{+2}, Mg-chrysotile + Fe^{+3}, Fe^{+2}, Mg-lizardite. (4)

As is well known, use of reactions 1 to 4 implies a volume change, and any other type of reaction involves the transport by solution of large amounts of MgO, SiO_2, or both. Perhaps, before appropriate tempera-

tures for these reactions were reached, the development of sheared serpentinite from blocky serpentite took place, making a very open system in which the documented partial recrystallization took place. In this way, large volumes of water could be flushed through the lens to remove MgO and add SiO_2. Or more likely, the shearing took place after reactions 3 and 4 were completed and the system was opened to such an extent that enough SiO_2 could readily be brought into the system in enormous volumes of water, the recrystallized platelets and late chrysotile veins being the result of the reaction

$$\text{Mg, Fe}^{+2}\text{-brucite} + SiO_2\ (\text{in solution}) \rightarrow \text{iron-bearing chrysotile and lizardite.} \quad (5)$$

Whichever mechanism is accepted to explain the absence of brucite, the one given here or that discussed by Thayer (1966), serpentinization or the development of serpentine continued after the formation of the sheared serpentinite, as evidenced by the crosscutting nature of the very late chrysotile and lizardite veins.

A factor disregarded so far in the discussion is the partial pressure of oxygen (Page, 1967). Throughout reactions 1 through 4, as temperature decreases, the partial pressure of oxygen also decreases; but at lower temperatures, the partial pressure decreases at a slower rate than does the temperature. Evidence for this is the abundance of magnetite in late stages, which requires a relatively higher P_{O_2}.

REFERENCES

Bowen, N. L., and Tuttle, O. F. ,1949, The system MgO–SiO_2–H_2O: Geol. Soc. America Bull., v. 60, no. 3, p. 439–460.

Francis, G. H., 1955, Zoned hydrothermal bodies in the serpentine mass of Glen Urquhart (Inverness-shire) : Geol. Mag., v. 92, no. 6, p. 433–447.

Hostetler, P. B., Coleman, R. G., Mumpton, F. A., and Evans, B. W., 1966, Brucite in Alpine serpentinites: Am. Mineralogist, v. 51, nos. 1–2, p. 75–98.

Lawson, A. C., 1914, Description of the San Francisco, district; Tamalpais, San Francisco, San Mateo, and Hayward quadrangles: U.S. Geol. Survey Geol. Atlas, Folio 193, 24 p.

Page, N. J, 1966, Mineralogy and chemistry of the serpentine group minerals and the serpentinization process: California Univ., Berkeley, Ph.D. thesis, 390 p.

———1967, Serpentinization at Burro Mountain, California: Contr. Mineralogy and Petrology, v. 14, p. 321–342.

Taliaferro, N. L., 1943, The Franciscan-Knoxville problem: Am. Assoc. Petroleum Geologists Bull., v. 27, no. 2, p. 109–219.

Thayer, T. P., 1966, Serpentinization considered as a constant-volume metasomatic process: Am. Mineralogist, v. 51, p. 685–710.

THE SOURCE OF TRAVERTINE IN THE CREEDE FORMATION, SAN JUAN MOUNTAINS, COLORADO

By T. A. STEVEN and IRVING FRIEDMAN, Denver, Colo.

Work done in cooperation with the Colorado State Mining Industrial Development Board

Abstract.—The Creede Formation and its included travertine were deposited in a closed basin around the periphery of the Creede caldera shortly after final subsidence and resurgent doming of the caldera core. Geologic and isotopic evidence favors derivation of the carbonate in the travertine by upwelling resurgent magma intruding or approaching a sedimentary carbonate unit, and remobilizing the calcium carbonate by some process related to contact metamorphism or solution and replacement.

Travertine and related calcareous deposits are widespread in the Creede Formation, a sedimentary formation localized around the periphery of the Creede caldera near the center of the San Juan volcanic field in southwestern Colorado (fig. 1). Only negligible quantities of carbonate minerals are associated with either earlier or later rocks in this part of the volcanic field; why, then, during a given brief interval of time in a long sequence of related geologic events, was such a large quantity of calcium carbonate deposited in such a local area? The time and place of deposition of the Creede Formation in the sequence of volcanic eruptions, cauldron subsidence, and resurgence suggest that the carbonate in the travertine may have been derived by a magma body approaching or intruding limestone at depth beneath and adjacent to the Creede caldera and remobilizing the calcium carbonate. The only sedimentary carbonate units that can be projected beneath this area are the Pony Express Limestone Member and the marl member of the Wanakah Formation, limy beds in the Morrison Formation, and equivalents of the Niobrara Formation and Greenhorn Limestone in the lower part of the Mancos Shale. Independent evidence favoring an origin from these units is given by carbon- and oxygen-isotope data.

In the discussion that follows, the geologic evidence is based on fieldwork by T. A. Steven and J. C. Ratté, and the isotopic data on analyses by Irving Friedman. Geologic work is continuing in the central San Juan area, and this report presents in preliminary form the conclusions on a limited part of the more comprehensive investigation. Other preliminary results bearing on different aspects of the geology have been given by Steven and Ratté, (1960, 1963, 1964), Steven (1964),

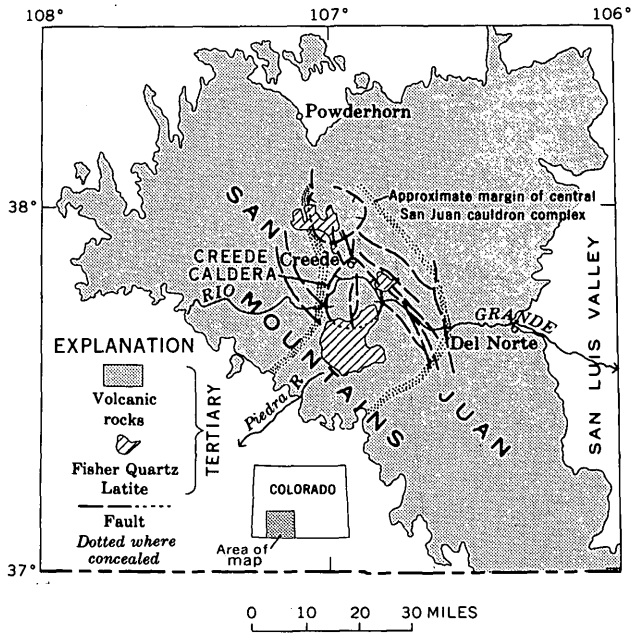

FIGURE 1.—Map of San Juan volcanic field, southwestern Colorado.

U.S. GEOL. SURVEY PROF. PAPER 600-B, PAGES B29-B36

and Ratté and Steven (1964, 1967). A detailed study of the Creede mining district, which includes much of the area underlain by the Creede Formation and contained travertine, has been published (Steven and Ratté, 1965).

Many of the geologic ideas expressed herein had their origin during the investigation of the Creede mining district by Steven and Ratté (1965). J. C. Ratté not only contributed toward the background geologic data upon which this report is based, but also participated in developing the concept of a shallow batholithic body beneath the Creede caldera; his contributions are gratefully acknowledged. W. J. Hail, Jr., provided samples of three sedimentary carbonate units in the San Juan Basin south of the volcanic field, and advised us about their areal extent and geologic relations. H. A. Tourtelot made petrographic and X-ray studies of our samples to determine their suitability for isotopic analysis.

GEOLOGIC SETTING

The central San Juan Mountains, including the Creede caldera area, are underlain largely by ash flows and lava flows making up one of the youngest major assemblages of units in the Tertiary San Juan volcanic field (Steven and Ratté, 1960, 1964, 1965). These rocks were erupted from a source area now marked by a cauldron complex at least 50 miles long and as much as 25 miles wide extending southward through the Creede caldera (fig. 1). The eruptions from this source area were preceded in the eastern San Juan Mountains by accumulation of a great mass of andesitic to rhyodacitic flows and breccias of the Conejos Formation (Larsen and Cross, 1956, pl. 1), and in the western San Juan Mountains by the San Juan Formation and the Silverton Volcanic Group (Luedke and Burbank, 1963). Units in the Potosi Volcanic Group as used by Luedke and Burbank (1963) in the western San Juan Mountains accumulated in part concurrently with units from the central San Juan source area, but are older than the Creede Formation and associated units of particular interest here. Late basaltic lava flows of the Hinsdale Formation are widespread in the central and eastern San Juan Mountains, but are apparently unrelated in time or genesis with any of the events leading to deposition of the Creede Formation (Steven and others, 1967).

The Creede Formation, and its contained travertine, is among the youngest units in the central San Juan Mountains (Steven and Ratté, 1964), where it was deposited around the margin of the Creede caldera, the youngest and most conspicuous of the cauldron subsidence structures in this source area (fig. 2). Incomplete evidence indicates that the Creede caldera area subsided time and again in response to voluminous ash-flow eruptions, but only the last main subsidence can be documented in detail. This last period of subsidence accompanied eruption of the Snowshoe Mountain Quartz Latite, a crystal-rich ash-flow tuff that accumulated within the core of the caldera concurrent with subsidence (Steven and Ratté, 1964, p. D61; 1965, p. 39). After collapse, the caldera appears to have been a flat-floored basin whose bottom was below the present altitude of 8,000 feet. The core of the caldera was then resurgently domed, presumably by magmatic pressure, until parts near the center stood more than 4,000 feet above a topographic moat left all around the margin. Tangential grabens extending northwestward and southeastward out from the caldera developed concurrent with either final subsidence or resurgence, or both.

After doming, volcanic eruptions along the broken caldera margin extruded viscous quartz latitic lavas to form thick local flows and domes of Fisher Quartz Latite, particularly along the eastern and southern margins of the Creede caldera. Elsewhere, the closed basin marking the structural and topographic moat around the caldera margin was the site of deposition of volcanic ash, stream and lake deposits, and travertine from mineral springs, which together constitute the Creede Formation. These largely sedimentary deposits accumulated to a depth of at least 2,000 feet until the low point of the rim was reached along the southeastward-extending tangential graben, and external drainage was established eastward toward the San Luis Valley. The subsequent history has been largely one of erosion; the Rio Grande has cut a deep narrow gorge east of the Creede caldera and has excavated most of the soft Creede Formation around the margin of the caldera and reexposed the domed core.

The Creede Formation (fig. 2) consists of several facies, whose distribution depends on local conditions of deposition and on proximity to sources of the different constituent materials. Primary igneous materials, largely ash, are abundant along the eastern margin of the caldera and increase southward toward their probable source in the Fisher Quartz Latite vent areas south of the caldera. Nonwelded ash-flow deposits form the largest bulk of this primary igneous material, although airfall ash is widespread and a few thin layers of welded tuff are present locally. Lava flows of Fisher Quartz Latite intertongue with the ashy deposits of the Creede Formation and indicate that the Creede and the Fisher accumulated concurrently. Most of the Creede

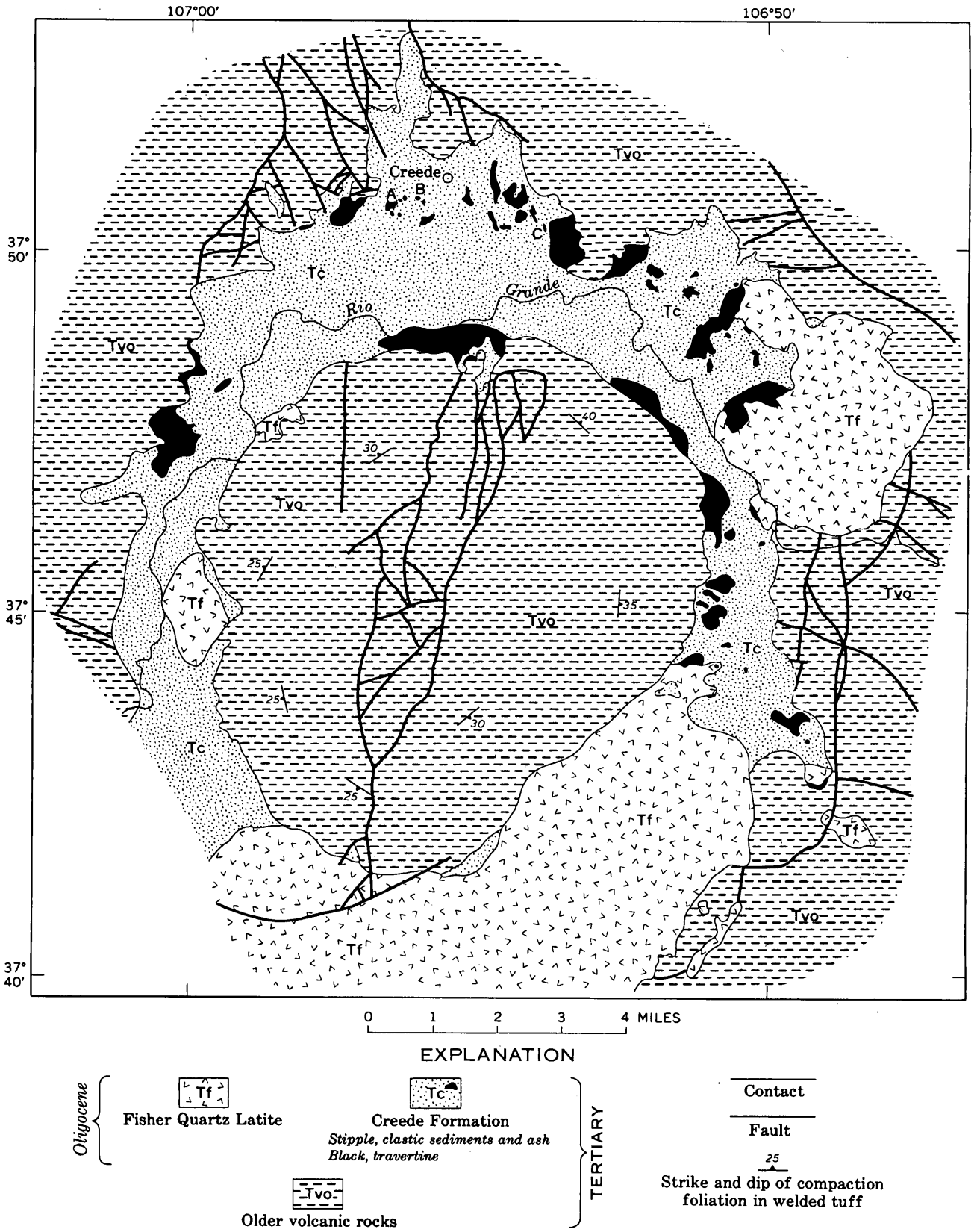

FIGURE 2.—Geologic map of the Creede caldera. Letters (*A*, *B*, *C*) show locality of samples collected for isotope analysis.

Formation along the northern and western margins of the caldera consists of reworked ashy sediments or of volcanic sands and gravels, and ranges from thin-bedded shallow-lake deposits to conglomeratic stream deposits. Most commonly the stream deposits are in tributary valleys in the outer wall of the caldera or they are interbedded with the lake-deposit facies opposite the mouths of such tributary valleys. Some layers of nearly pure bentonite representing ashfall deposits are interlayered with the reworked sedimentary deposits. The steep outer walls of the caldera commonly are mantled with a layer of talus-regolith which grades outward or intertongues laterally with stream or lake deposits toward the middle of the moatlike basin.

The travertine in the Creede Formation (fig. 2) occurs in a wide variety of local deposits. Some was deposited by mineral springs that issued well above the level of concurrent sedimentation, and forms inclined sheetlike masses cementing talus or regolith deposits along the steep outer walls of the caldera. In places the lower ends of these tabular marginal masses split into a series of tongues that are interlayered with the clastic sedimentary beds and wedge out toward the center of the basin. In other places, masses of the travertine are completely surrounded by sedimentary rocks and commonly grade from a central mass of travertine, through a marginal zone of intertongued wedges of travertine and sedimentary beds, into normal stream or lake deposits with little or no travertine. Some of these masses show structures suggesting original travertine terrace form, but more commonly this is not apparent in present exposures. Some masses show local tubular openings that probably represent original spring orifices. Hard beds, ranging from sedimentary strata highly cemented with calcite to nearly pure limestone, occur in the Creede Formation in the vicinity of some of the irregular travertine masses, and probably resulted from carbonate deposition in shallow ponds fed by the mineral springs.

Although the travertine constitutes only a small percentage of the total volume of the Creede Formation, it is widely distributed, and many bodies measuring several thousand feet across and of unknown thickness have been mapped (fig. 2). Some individual masses clearly contain many millions of tons of calcium carbonate. The relatively large quantity of calcium carbonate deposited during the brief period encompassed by deposition of the Creede Formation stands in marked contrast with the nearly complete absence of carbonate minerals in older or younger rocks in the volcanic field. Clearly some unique circumstances, or combination of circumstances, obtained during this interval to account for this anomalous constituent in the otherwise predominantly volcanic assemblage of rocks.

POSSIBLE SOURCE OF THE CARBONATE

Possibly the most significant factors bearing on the origin of the travertine are its geographic restriction to the periphery of the Creede caldera and its place in the local sequence of geologic events immediately following the strong resurgent doming (Smith and Bailey, 1962) of the caldera core. This doming is postulated (Steven and Ratté, 1960, p. B14; 1965, p. 63) to have resulted from magmatic pressure in much the manner illustrated by Smith and others (1961, p. D148) for the Valles caldera, New Mexico. In the Creede caldera, no lavas breached the core itself, but doming was followed shortly by extrusion of viscous lava at many places around the broken margin. The domed core of the Creede caldera is believed to mark the roof of a major cupola on a batholithic magma chamber that once must have underlain the whole irregularly collapsed caldera complex in the central San Juan Mountains (Steven and Ratté, 1963).

The close association in time and space of travertine deposition with the postulated upward movement of magma into shallow depths beneath the Creede caldera area suggests that the magma body may have intruded or approached near a limestone unit beneath the volcanic edifice and have released the primary constituents for the travertine by some process related to contact metamorphism or solution and replacement. This hypothesis is difficult to test by direct evidence, as none of the units underlying the valcanic rocks are exposed in the central San Juan Mountains. A review of the sedimentary rocks exposed in adjacent areas indicates that the volcanic rocks of the San Juan Mountains were deposited in large part on an old positive area, the Uncompahgre–San Luis highland, that stood high and was subjected to erosion in late Paleozoic and early Mesozoic time. The Entrada Sandstone of Jurassic age overlaps the beveled edges of Paleozoic sedimentary units northward onto Precambrian crystalline rocks in the canyon of the Piedra River south of the central San Juan Mountains area (Read and others, 1949), and the Morrison Formation of Jurassic age rests on the Precambrian rocks in the Powderhorn area north of the central San Juan Mountains (Larsen and Cross, 1956, pl. 1). No evidence is known that would indicate any sedimentary rocks older than Jurassic under the volcanic rocks between these areas.

The Jurassic and younger sedimentary units underlying the volcanic rocks of the central San Juan Mountains include the Entrada Sandstone, Wanakah Formation, Morrison Formation, Dakota Sandstone, Man-

cos Shale, and Blanco Basin Formation. The only sedimentary carbonate units present in this section are the Pony Express Limestone Member of the Wanakah Formation, limy siltstone forming the marl member of the Wanakah Formation (Bush and others, 1959, p. 327-328), minor local limestone lenses in the Morrison Formation, and equivalents of the Niobrara Formation and Greenhorn Limestone in the lower part of the Mancos Shale. Most of these units are thin, and only the limy shale in the Niobrara equivalent exceeds a few tens of feet in maximum thickness; it seems probable that some combination of units is necessary to provide an adequate source for the remobilized carbonate. All the limy units extend under the volcanic cover along the southern margin of the volcanic pile, but only the Morrison Formation emerges from beneath that cover along the northern margin; the Pony Express apparently laps out against the underlying Precambrian rocks, and the Cretaceous units have been beveled by prevolcanic erosion. Present exposures do not permit establishing the position of the wedging edges of any of the sedimentary carbonate units beneath the volcanic rocks, but it is permissive that any or all of them be present beneath the Creede caldera area.

ISOTOPIC ANALYSIS

To test the hypothesis that the calcium carbonate in the Creede Formation travertine might have been derived from underlying sedimentary carbonate units, seven representative samples were analyzed for their carbon and oxygen isotopes. Two samples were of typical Pony Express Member, one each of the Niobrara and Greenhorn equivalents in the Mancos Shale, and three samples of Creede travertine. Of the travertine samples, C 1022 (locality *A*, fig. 2; lab. No. 3202–31) was collected adjacent to a cylindrical hole in a small travertine mass, and is believed to represent deposition adjacent to a former spring orifice; sample C 1008 (locality *B*; lab. No. 3202–33) is from a nearby bulbous mass of travertine completely surrounded by lake-facies sedimentary rocks; and sample C 910 (locality *C*; lab. No. 3203–32) is from a sheetlike mass extending basinward into lake facies sedimentary rocks from the lower part of an inclined mass of travertine cementing talus.

The calcium carbonate samples were reacted with 100-percent phosphoric acid. The CO_2 formed was analyzed on a mass spectrometer by the methods described by McCrea (1950), and the raw data were corrected for mass spectrometric errors according to the method described by Craig (1957). The C^{13} and O^{18} values are correct to $\pm 0.1‰$ (per mil). The C^{13} results are given relative to the PDB standard,[1] and the O^{18} relative to SMOW[2] as well as PDB. The results of the analyses are given in table 1.

DISCUSSION

Several methods of remobilizing the sedimentary carbonate under the influence of a nearby intrusive mass can be envisaged. During the thermal decomposition ($Ca(Mg)\ CO_3 \rightarrow Ca(Mg)O + CO_2$) or silication ($Ca(Mg)CO_3 + SiO_2 \rightarrow Ca(Mg)SiO_3 + CO_2$) of limestone or dolomite in response to contact metamorphism all the carbon is released as CO_2, and the isotopic composition (C^{13}/C^{12} ratio) of the evolved CO_2 is the same as that in the original limestone. In a natural environment, the CO_2 so evolved moves upward toward the surface either as a gas to issue as a CO_2 fumerole, or in solution to mix with ground water and perhaps issue from a hot or cold spring. If all the evolved CO_2 dissolves in water, the resulting carbon isotopic composition of the solution will again be equal to that in the original limetone. A major difficulty in this mechanism is that an outside source of calcium is required if travertine is to be deposited at the surface.

Total or partial replacement of a sedimentary carbonate bed by silica, sulfides, or some combination of these and similar materials is common near many intrusive igneous contacts, and is a mechanism that could provide both the calcium and the CO_2 required for the travertine. The limestone might be dissolved and replaced by meteoric water alone or mixed in part with volcanic water not closely connected with magmatic intrusion, but the close association in time and space of travertine deposition in the Creede Formation with resurgent doming of the Creede caldera suggests that the process was in some way tied closely with intrusive activity. Either an influx of magmatic water from an intrusion or an increase in chemical activity of meteoric water with added magmatic constituents in a zone near an intrusive could account for the time-space relationship.

Whether derived by contact metamorphism, by solution and replacement, or by some combination, where dissolved CO_2 is in equilibrium with the bicarbonate ion, HCO_3^{-1}, the bicarbonate ion will tend to be enriched in C^{13}. This enrichment is a function of temperature and will tend to decrease with increasing temperature. At 22°C, approximating average surface temperatures, the bicarbonate ion will be enriched by about 8‰ relative to the CO_2. As the temperatures at which CO_2 will

[1] The PDB standard is CO_2 prepared from a Cretaceous belemnite (*Belemnitella americana*) collected from the Peedee Formation in South Carolina.

[2] SMOW refers to standard mean ocean water as defined by Craig (1961).

TABLE 1.—*Relative* C^{13} *and* O^{18} *content of samples*

Lab. No. and (field No.)	*Locality*	*Description*	C^{13} *PBD* (‰)	O^{18} *PDB* (‰)	O^{18} *SMOW* (‰)
3202–30 (Ds 30).	Leopard Creek, San Miguel County, Colo.	Pony Express Limestone Member	+0.3	−8.7	+26.5
3257–9 (H 59).[1]	Chimney Rock, Archuleta County, Colo.	----do----	+.1	--------	+19.5
3257–10 (H 60).[1]	Oneal Park, Archuleta County, Colo.	Greenhorn Limestone equivalent in the Mancos Shale.	.0	--------	+21.0
3257–11 (H 61).[1]	----do----	Niobrara Formation equivalent in the Mancos Shale.	+.6	--------	+22.9
3202–31 (C 1022).	*A*, fig. 2.	Travertine, Creede Formation, near original spring orifice.	+.4	−4.2	+25.2
3202–33 (C 1008).	*B*, fig. 2.	Travertine, Creede Formation, from bulbous mass.	+2.0	−9.3	+22.9
3202–32 (C 910).	*C*, fig. 2.	Travertine, Creede Formation, from sheet-like mass.	−.7	−8.2	+21.1

[1] Collected by W. J. Hail, Jr., U.S. Geological Survey.

equilibrate with the bicarbonate ion in the circulating hot water at depth will be above 22°C, we can predict that the carbon in solution will be no more than 8‰ heavier in C^{13} than the original limestone, and probably will not deviate significantly in isotopic composition from the decomposing limestone. In the steady-state situation outlined above, where all the CO_2 dissolves in the water without fractionation, the precipitation of carbonate minerals (travertine) by reaction of bicarbonate ion with calcium ion should also take place with little fractionation. Vogel (1960) found that at 22°C the precipitated limestone will in turn be enriched in C^{13} over the bicarbonate ion by about 1‰. Therefore we can expect that the travertine formed from CO_2 liberated by dissolving or thermally decomposing a limestone should have a C^{13} content within a few per mil of that in the original limestone, as suggested by Vogel (1960).

The isotopic compositions (C^{13}/C^{12} ratios) obtained from the samples of limestone from the Pony Express, Niobrara equivalent, and Greenhorn equivalent as well as of the Creede travertine all are near the middle of the range found by Craig (1953, fig. 3) to be typical of sedimentary carbonate rocks. Equally important, all other sources of carbon tested by Craig, including atmospheric CO_2, had significantly lower C^{13}/C^{12} ratios. Unfortunately, however, Craig did not test CO_2 from volcanic gasses and no comparison could be made with one of the more important possible sources of CO_2 for the Creede travertine. Although volcanic CO_2 should have been available in comparable quantities throughout the period of volcanic activity in the vicinity of the Creede caldera, calcium carbonate deposition was almost completely restricted to the period during which the Creede Formation accumulated. This seems to require a unique combination of circumstances provided for by remobilizing sedimentary carbonate but not by a process involving volcanic CO_2. The source of the abundant calcium would be a major problem were the CO_2 of volcanic derivation, whereas it can readily be derived from a sedimentary carbonate by several mechanisms. Thus the relatively high C^{13} content of the travertine indicates that the CO_2 could most readily have been derived by thermal decomposition, silication, or solution and replacement of a sedimentary limestone, and more specifically of a limestone having a C^{13}/C^{12} ratio close to that in the travertine.

The oxygen isotopic composition of the travertine reflects the isotopic composition of the water from which it was precipitated, as well as the temperature of precipitation. From the data of Epstein and others (1953) and Clayton (1959) on oxygen isotopic fractionation in the system calcium carbonate–water, we can calculate the isotopic composition of the water from which the travertine precipitated, assuming that the temperature of precipitation was between 10° and 90°C. Table 2 compares the per mil difference in O^{18} relative to SMOW for different temperatures of deposition for one of the Creede Formation travertine samples.

TABLE 2.—*Comparison of oxygen isotopic composition with possible temperatures of deposition*

Sample	*Measured* O^{18} *SMOW* (‰)	*Possible temperatures of deposition* (° C)	O^{18}, *SMOW of water* (‰)
3202–31, travertine near spring orifice.	+25.2	10	−9
		20	−7
		30	−5
		40	−3
		90	+3

The isotopic composition of present-day ground water in a similar volcanic and climatic environment and elevation in the Jemez Mountains of New Mexico, about 125 miles to the south, was measured by Friedman

and Smith (1958). Assuming a similar deuterium content of ground water in the Creede area at the time the travertine was deposited, and applying the relation between deuterium and O^{18} given by Friedman (1953), we get a value of −7‰ SMOW for O^{18} in the Creede region, in good agreement with the values given in table 2 for 20°C.

The assumption that the isotopic composition of modern ground waters in the Jemez Mountains is similar to that of the ground waters around the Creede caldera during the period the travertine was deposited is based on two factors:

1. Hot-spring waters in such volcanic and thermal regions as Italy, Yellowstone Park (Craig and others, 1956), and Iceland (Friedman and others, 1963, 1964) have the same isotopic compositions as the meteoric waters in the same regions.

2. The isotopic composition of metoric water in any area depends on broad regional factors such as distance from oceanic sources for the water, and general orographic conditions between the oceanic sources and the given locality (Friedman and others, 1964).

The distance between the San Juan–Jemez Mountains area and either the Pacific Ocean or the Gulf of Mexico has not changed significantly since the Creede Formation was deposited in late Oligocene time (Steven and others, 1967), but the differences in orographic conditions, particularly as they may have affected atmospheric circulation, cannot be adequately assessed. However, even near seacoasts, rainwater gives values of −2 to −3‰ SMOW, which for the measured per mil deviation in O^{18} from SMOW of sample 3202–31 of Creede travertine would give an estimated temperature of deposition of only about 40°C. It seems probable therefore that the mineral springs from which the Creede Formation travertine was deposited were relatively cool (Craig, 1953).

SUMMARY

Geologic and isotopic evidence suggests that the carbonate in travertine in the Creede Formation was derived from a sedimentary carbonate unit, and that remobilization probably resulted from resurgent igneous intrusion beneath the Creede caldera. The Creede Formation travertine thus may represent, in fossil form, the surface conditions above a shallow zone of contact metamorphism or solution and replacement of limestone beds around an intrusive that rose high enough to approach or cut the thin wedge of sedimentary rocks underlying the volcanic rocks of the central San Juan Mountains.

The limited data available will not support further speculation concerning details of remobilization, transport, or deposition of the carbonate in the travertine, although these problems probably would benefit from additional intensive study. In addition to scientific data and interpretations that might derive from such an investigation, perhaps tentative conclusions might be reached on a question of definite economic significance: was the limestone unit simply thermally decomposed or silicated by the intruding magma, or did metasomatic replacement involving deposition of metallic sulfides contribute to the remobilized carbonate? Elsewhere, the Pony Express Limestone Member is a host for replacement ore in the Uncompahgre district near Ouray, Colo., where mineralized rock occurs in a halo around an intrusive center of Late Cretaceous or early Tertiary age (Burbank, 1930; 1940).

REFERENCES

Burbank, W. S., 1930, Revision of geologic structure and stratigraphy in the Ouray district of Colorado, and its bearing on ore deposition: Colorado Sci. Soc. Proc., v. 12, no. 6, p. 151–232.

———1940, Structural control of ore deposition in the Uncompahgre district, Ouray County, Colorado; U.S. Geol. Survey Bull, 906–E, p. 189–265.

Bush, A. L., Bromfield, C. S., and Pierson, C. T., 1959, Areal geology of the Placerville quadrangle, San Miguel County, Colorado: U.S. Geol. Survey Bull. 1072–E, p. 299–384.

Clayton, R. N., 1959, Oxygen isotope fractionation in the system calcium carbonate-water: Jour. Chem. Physics, v. 30, p. 1246–1250.

Craig, Harmon, 1953, The geochemistry of the stable carbon isotopes: Geochim. et Cosmochim. Acta, v. 3, p. 53–92.

———1957, Isotopic standards for carbon and oxygen and correction factors for mass-spectrometric analysis of carbon dioxide: Geochim. et Cosmochim. Acta, v. 12, p. 133–149.

———1961, Standard for reporting concentrations of deuterium and oxygen-18 in natural waters: Science, v. 133, p. 1833–1834.

Craig, Harmon, Boato, Giovanni, and White, D. E., 1956, Isotopic geochemistry of thermal waters, [chap.] 5 *of* Nuclear processes in geologic settings: Natl. Research Council, Comm. Nuclear Sci., Nuclear Sci. Ser. Rept. 19, p. 29–38.

Epstein, S., Buchsbaum, R., Lowenstam, H. A., and Urey, H. C., 1953, Revised carbonate-water isotopic temperature scale: Geol. Soc. America Bull., v. 64, no. 11, p. 1315–1325.

Friedman, Irving, 1953, Deuterium content of natural waters and other substances: Geochim. et Cosmochim. Acta, v. 4, p. 89–103.

Friedman, Irving, Redfield, A., Schoen, B., and Harris, J., 1964, The variation of the deuterium content of natural waters in the hydrologic cycle: Rev. Geophysics, v. 2, p. 177–224.

Friedman, Irving, Sigurgeirsson, Thorbjörn, and Gardarsson, Örar, 1963, Deuterium in Iceland waters: Geochim. et Cosmochim. Acta, v. 27, p. 553–561.

Friedman, Irving, and Smith, R. L., 1958, The deuterium content of water in some volcanic glass: Geochim. et Cosmochim. Acta, v. 15, p. 218–228.

Larsen, E. S., Jr., and Cross, Whitman, 1956, Geology and petrology of the San Juan region, southwestern Colorado: U.S. Geol. Survey Prof. Paper 258, 303 p.

Luedke, R. G., and Burbank, W. S., 1963, Tertiary volcanic stratigraphy in the western San Juan Mountains, Colorado: Art. 70 *in* U.S. Geol. Survey Prof. Paper 475–C, p. C39–C44.

McCrea, J. M., 1950, On the isotopic chemistry of carbonates and a paleotemperature scale: Jour. Chem. Physics, v. 18, p. 849–857.

Ratté, J. C., and Steven, T. A., 1964, Magmatic differentiation in a volcanic sequence related to the Creede caldera, Colorado: Art. 131 *in* U.S. Geol. Survey Prof. Paper 475–D, p. D49–D53.

———1967, Ash flows and related volcanic rocks associated with the Creede caldera, San Juan Mountains, Colorado: U.S. Geol. Survey Prof. Paper 524–H, 58 p.

Read, C. B., Wood, G. H., Wanek, A. A. ,and Mackee, P. V., 1949, Stratigraphy and structure in the Piedra River Canyon, Archuleta County, Colorado: U.S. Geol. Survey Oil and Gas Inv. Prelim. Map 96, scale 1:48,000.

Smith, R. L., and Bailey, R. A., 1962, Resurgent cauldrons—their relation to granitic ring complexes and large volume rhyolitic ash-flow fields [abs.]: Internat. Assoc. Volcanology, Symposium, Japan, 1962, p. 67–68.

Smith, R. L., Bailey, R. A., and Ross, C. S., 1961, Structural evolution of the Valles caldera, New Mexico, and its bearing on the emplacement of ring dikes: Art. 340 *in* U.S. Geol. Survey Prof. Paper 424–D, p. D145–D149.

Steven, T. A., 1964, Geologic setting of the Spar City district, San Juan Mountains, Colorado: Art. 146 *in* U.S. Geol. Survey Prof. Paper 475–D, p. D123–D127.

Steven, T. A., and Ratté, J. C., 1960, Relation of mineralization to caldera subsidence in the Creede district, San Juan Mountains, Colorado: Art. 8 *in* U.S. Geol. Survey Prof. Paper 400–B, p. B14–B17.

——— 1963, Resurgent cauldrons in the Creede area, San Juan Mountains, Colorado [abs.]: Am. Geophys. Union 44th Ann. Mtg., 1963, Program, p. 112–113.

——— 1964, Revised Tertiary volcanic sequence in the central San Juan Mountains, Colorado: Art. 132 *in* U.S. Geol. Survey Prof. Paper 475–D, p. D54–D63.

——— 1965, Geology and structural control of ore deposition in the Creede district, San Juan Mountains, Colorado: U.S. Geol. Survey Prof. Paper 487, 90 p.

Steven T. A., Mehnert, H. H., and Obradovich, J. D., 1967, Age of volcanic activity in the San Juan Mountains, Colorado, *in* Geological Survey Research 1967: U.S. Geol. Survey Prof. Paper 575–D, p. D47–D55.

Vogel, J. C., 1960, Isotopic separation factors in the equilibrium system CO_2–HCO_3^{-1}–CO_3^{-2}: Laboratorio di Geologia Nucleare, Pisa, Summer course in nuclear geology, Varenna, Italy, 1960, p. 216–221.

LAMINAR FLOWAGE IN A PLIOCENE SODA RHYOLITE ASH-FLOW TUFF, LAKE AND HARNEY COUNTIES, OREGON

By GEORGE W. WALKER and DONALD A. SWANSON, Menlo Park, Calif.

Abstract.—A simple cooling unit of texturally zoned soda rhyolitic ash-flow tuff has laminar flowage structures that formed during the end phase of movement after partial welding. The structures, consisting of a lineation of stretched pumice fragments in the plane of foliation and an asymmetric ramp, show that movement was southward from two vents at opposite ends of the Wagontire Mountain domal uplift. The ash-flow tuff, exposed over many tens of square kilometers on the south slope of Wagontire Mountain, is 2 to more than 40 meters thick and has a total volume of less than 1 cu km. Several Pliocene ash-flow tuffs of comparable or vastly greater volume, but with compositions near calc-alkaline rhyolite and with less evidence of laminar flowage, occur in the same region. Eruption at a near-liquidus temperature onto depositional slopes steep enough to create unstable load conditions may have caused laminar flowage. Comparisons with other ash-flow tuffs showing laminar flowage suggest, however, that high sodium-potassium ratios and above-average total iron also are important in reducing glass viscosity sufficiently to permit mass laminar flowage.

Recent investigations by Hoover (1964) and Schmincke and Swanson (1966, 1967) suggest that structures indicative of viscous laminar flowage, such as lineations, crenulations and folds, tension fractures, imbricated disks of collapsed pumice, and ramp structures may be common and widespread in parts of some ash-flow tuffs. Some of these flowage structures have been recognized at several places in southeast Oregon, and are particularly well displayed by a low-alumina soda rhyolite ash-flow tuff of small extent on the south and southwest flanks of Wagontire Mountain (fig. 1). This paper describes the ash-flow tuff of Wagontire Mountain and discusses factors that could have promoted its laminar flowage.

We are grateful to D. L. Hoover, U.S. Geological Survey, for permission to use the unpublished chemical analyses of an ash-flow tuff from Nye County, Nev.

GEOLOGIC SETTING

Wagontire Mountain, a complexly faulted exogenous dome of platy, flow-banded and jointed rhyolite or rhyodacite, lies near the western margin of a large structural basin filled with widespread Pliocene ash-flow tuffs, local interlayers of diktytaxitic olivine basalt, and extensive lenses of continental tuffaceous sedimentary rocks. West of Wagontire Mountain, the sequence of Pliocene rocks thins and is covered by younger Pliocene and Pleistocene basalt flows. Several exogenous domes of silicic rocks similar to Wagontire Mountain occur in nearby parts of the region, including Little Juniper Mountain and Horsehead Mountain, about 23 kilometers to the south and southeast of Wagontire Mountain; Sheep Mountain, about 9 km to the north; and Egli Ridge, 10 km to the east. Numerous basaltic cinder cones—the vents for some of the flows—are present within 30 km of Wagontire Mountain. Pleistocene and Recent surficial deposits thinly cover most of the downfaulted basins and stream valleys.

All the Tertiary rocks of the region have been broken and displaced by normal faults that belong either to a northwest-trending set or to a less conspicuous northeast-trending set. The amount of displacement is commonly less than a few tens of meters in the Pliocene rocks. Some of the faults extend with decreasing displacement into late Pliocene and Pleistocene rocks, and some extend into Miocene rocks of adjoining regions where displacements of a kilometer have been measured. Much of the faulting and tilting of fault blocks was concurrent with volcanism, and some rocks were deformed by intrusion of silicic domes.

Most of the Pliocene ash-flow cooling units are several meters to more than a hundred meters thick and

U.S. GEOL. SURVEY PROF. PAPER 600-B, PAGES B37-B47

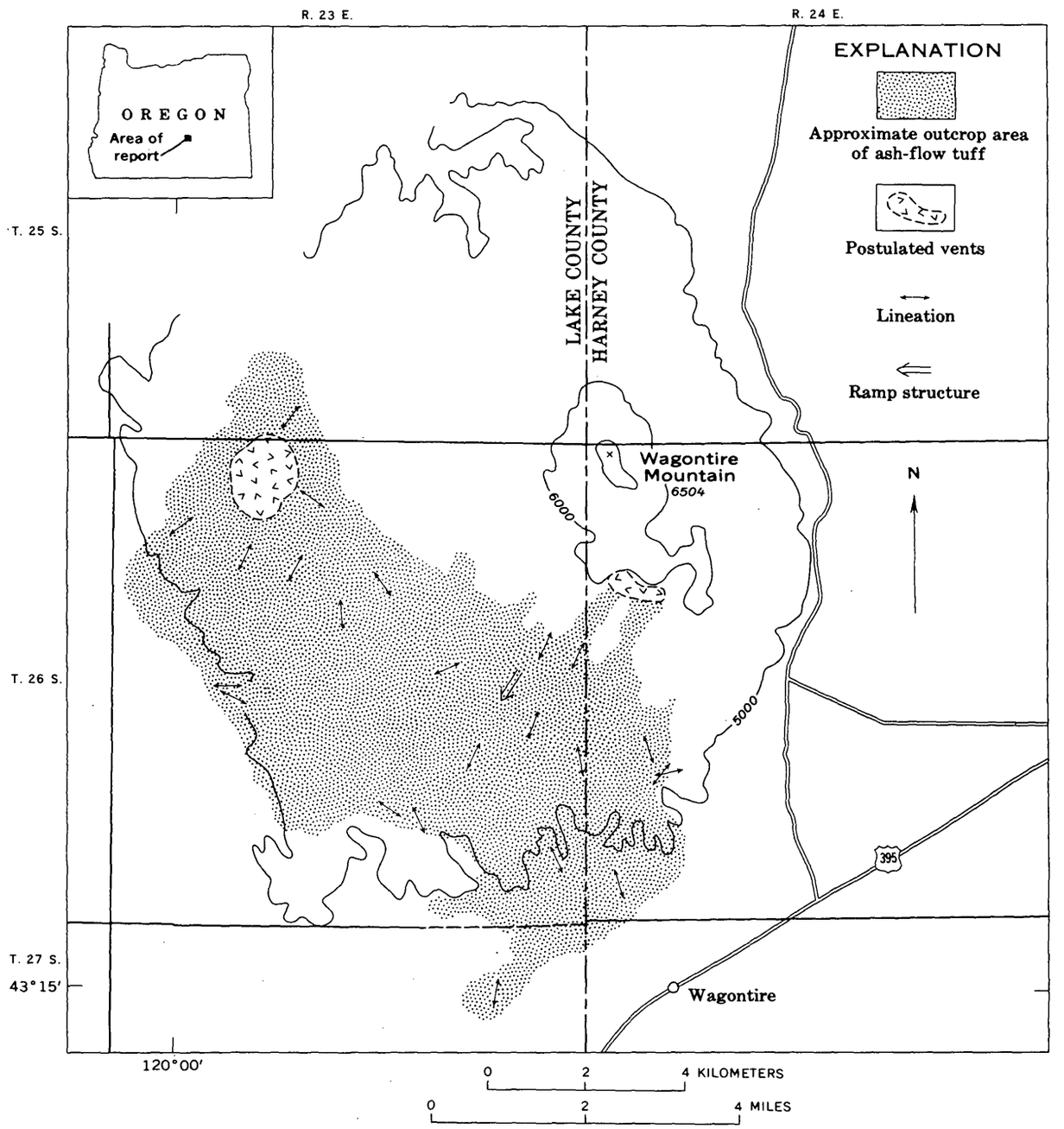

FIGURE 1.—Sketch map showing approximate outcrop area of ash-flow tuff of Wagontire Mountain, Oreg., and orientation of lineations and ramp structure.

cover hundreds or thousands of square kilometers. Petrographic examination and a few chemical analyses indicate they are chiefly of calc-alkaline to alkali rhyolite composition. Some of the tuffs are crystal rich, but most are composed almost entirely of glass shards and pumice lapilli. The products of vapor-phase crystallization are conspicuous in many of the cooling units. Laminar flowage structures are rare or lacking in these widespread ash-flow tuffs.

ASH-FLOW TUFF OF WAGONTIRE MOUNTAIN

The ash-flow tuff of Wagontire Mountain is presumed to be of Pliocene age, but it differs from other nearby Pliocene ash-flow sheets in its small areal extent, its probable local source atop Wagontire Mountain, and its soda-rich chemical composition. The ash-flow tuff overlies steeply flow-banded and jointed rhyolite or rhyodacite of the Wagontire Mountain dome and, locally, basalt flows of probable late Miocene to

early Pliocene age. From field relations it seems to be part of the Wagontire Formation of Smith (1926, p 207–214), which was considered by him to be of Eocene(?) age.

The ash-flow tuff presently covers about 85 sq km (fig. 1). Owing to the irregular topography of the surface it buries, the thickness of the tuff is highly varied, ranging from about 40 m, 6 km south-southwest of the top of Wagontire Mountain, to about 2 m near eroded ends of the ash flow; the average thickness is probably about 8 m. These figures indicate that the present volume of the ash-flow tuff is probably less than 1 cu km, and that its original volume before erosion was not much greater. In contrast, some of the widespread Pliocene ash-flow sheets of the region contain many tens or hundreds of cubic kilometers of pyroclastic material.

LITHOLOGIC ZONES

The tuff of Wagontire Mountain is a simple cooling unit composed predominantly of crystallized vitroclastic debris, minor amounts of crystals and crystal fragments, and rare rock fragments. Five lithologic zones (fig. 2) have been recognized, although all five zones have nowhere been found in a single continuous sequence.

The zonation results from different degrees of compaction and resultant welding of the shards and pumice lapilli and from primary and vapor-phase crystallization of internal parts of the ash flow. The zones are easily distinguishable by their textural characteristics and by their coloration. They display different shades of gray green, brown, and red corresponding to increasing degree of oxidation of iron-bearing minerals; the oxidation is especially pronounced in upper zones of the cooling unit. The individual zones are comparable to those described by Smith (1960a, p. 145–159; 1960b, p. 830–831) and Ross and Smith (1961, p. 20–22) and do not represent different flow units. They are described from bottom to top in the following discussion.

Zone 1

A dense, slightly foliated vitrophyre makes up the lowest zone in the ash-flow tuff; no nonwelded ash was recognized below the vitrophyre, but exposures are poor. The vitrophyre is a black to dark-gray obsidianlike glass that has a bright vitreous luster and conchoidal fracture. Several pieces of the vitrophyre from different localities have specific gravities near 2.365, which is near the maximum of published specific-gravity data for rhyolitic ash-flow tuffs (Smith, 1960b, fig. 5). In most places, the vitrophyre is poorly exposed and, where present, is only a meter or two thick.

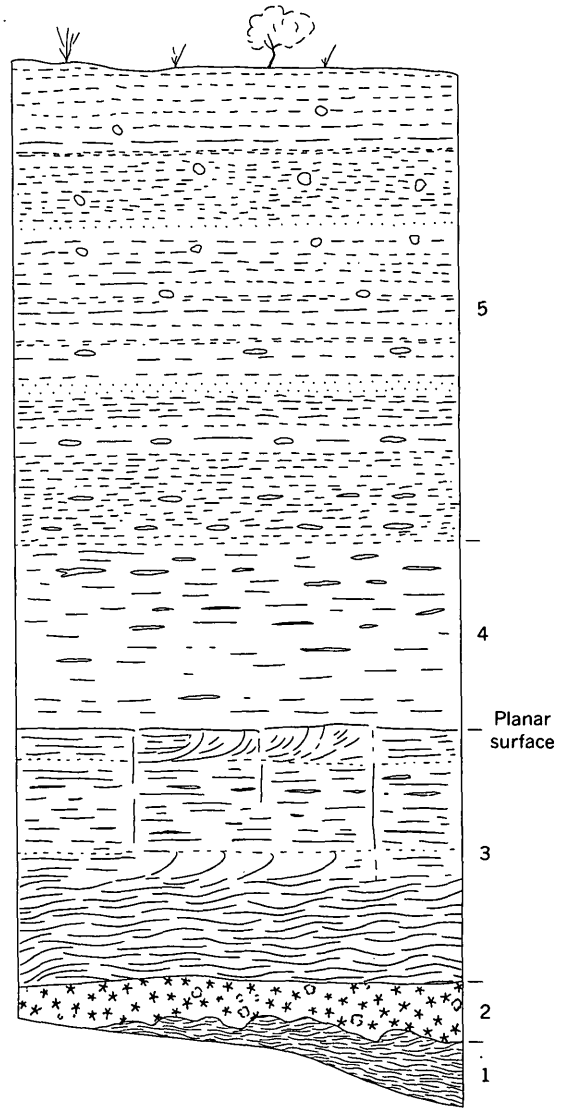

FIGURE 2.—Diagrammatic sketch section showing zones in ash-flow tuff. Base (zone 1) is composed of dense, black to gray-black vitrophyre with eutaxitic texture that grades into zone 2, characterized by abundant lithophysae. Completely crystallized light-olive-gray to yellowish-gray tuff in zone 3 exhibits widespread foliation, common lineation, and rare ramp structures. Zone 4 contains partly flattened pumice fragments forming vague foliation in moderately dense, light-olive-gray tuff; no lineations or ramps are present. Pumice fragments decrease in abundance upward and, in zone 5, show less flattening. Lower part of zone 5 is moderately dense, brownish-gray tuff, and upper part is slightly welded grayish-red tuff.

About 99 percent of the basal zone is composed of flattened glass shards that have been compacted and welded to form a striking eutaxitic texture (fig. 3). The shards, less than 1 millimeter in length, are colorless clear glass (index of refraction of about 1.495 ± 0.005), but their borders and the surrounding fine ash are

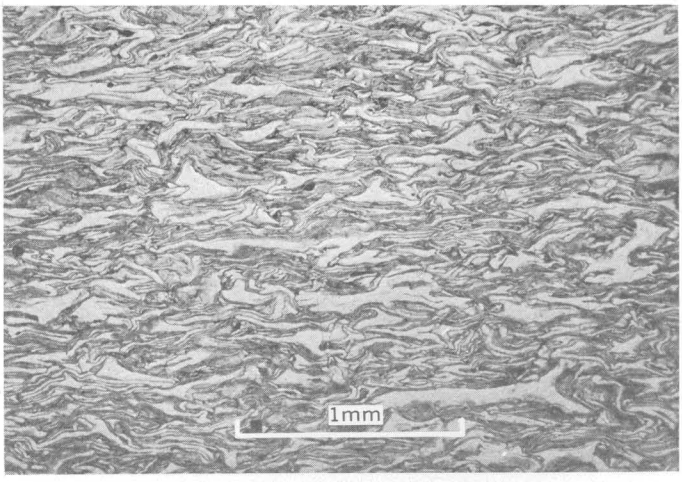

FIGURE 3.—Photomicrograph of dense vitrophyre (GWW–82–66), showing eutaxitic texture in zone 1 of ash-flow tuff.

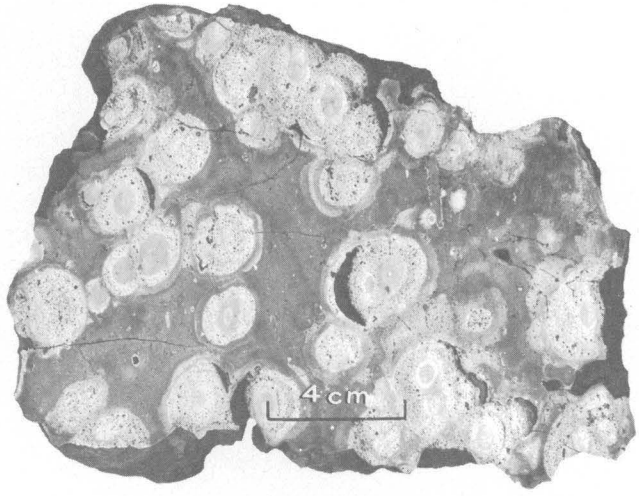

FIGURE 4.—Lithophysae in crystallized ash-flow tuff from zone 2.

slightly reddish, probably owing to oxidation. Pumice fragments are highly flattened—the largest in thin section is 10 mm long and only 0.3 mm thick—into dense glass, but they are not elongate in the plane of foliation.

Phenocrysts total less than 1 percent of the vitrophyre; they are predominantly alkali feldspar, quartz, and pleochroic green and yellow-green aegirine-augite ($2V(-) \approx 65°–70°$). Small microphenocrysts of magnetite are also present. Small inclusions of tuff and other volcanic rocks are uncommon.

A chemical analysis of one sample (GWW–82–66) (table 1, column 2) of the vitrophyre shows that the rock is a soda rhyolite which is richer in Na_2O and total iron and poorer in Al_2O_3, K_2O, MgO, CaO, and TiO_2 than Nockolds' (1954) average calc-alkaline rhyolite. Its normative composition (table 1) is principally alkali feldspar, quartz, and magnetite.

Zone 2

This zone is characterized by abundant concentrically banded lithophysae (fig. 4)—most about 2 centimeters in diameter but some as large as 5 cm—that impart a mottled appearance to hand specimens and outcrops. The lithophysal zone is gradational over several centimeters into the underlying vitrophyre of zone 1 and across several tens of centimeters into the overlying zone 3. It is generally less than 2 m thick, and in places is much thinner or absent. It thickens with the cooling unit and reaches a maximum of about 10 m where the cooling unit is nearly 40 m thick.

Matrix ash between lithophysae is comparatively dense, finely crystalline, and is mostly light olive gray. The lithophysae are finely crystalline and contain abundant vesicles less than 0.5 mm in diameter, many of which are crescent shaped. Most of the lithophysae are concentrically color banded in shades of yellowish gray, pale grayish orange, and, rarely, light olive gray. Intermediate zones in the lithophysae contain numerous ragged vesicles, whereas outer zones are nonvesicular. The lithophysae are spherical to only slightly ellipsoidal, indicating that they formed after most of the compaction and laminar flowage of the ash flow. Abundant gas pockets impart a rough pock-marked surface to outcrops of the zone (fig. 5).

FIGURE 5.—Lithophysal zone (zone 2) in ash-flow tuff that locally shows slight laminar flowage and abundant gas pockets.

The lithophysae are composed of alkali-feldspar fibers which radiate from local spherulites and from the center of each lithophysa. Cristobalite coats many of the vesicle walls in the intermediate concentric layers and may also occur in the cores of lithophysae. The grain size of the vesicular layer is smaller than that of the other layers, possibly because the volatiles exsolved into bubbles and thus could not promote coarse crystallization of the glass. The matrix between lithophysae is crystallized to alkali feldspar and quartz of finer grain size than any concentric layer except the vesicular layer. A relict eutaxitic texture is visible in both the matrix and the lithophysae.

Zone 3

The most continuous and widespread of all the zones consists of well-indurated, thoroughly crystallized, strongly foliated ash-flow tuff that in many places contains laminar flowage structures. The zone is normally 4–5 m thick, but thins toward distal ends of the ash-flow tuff and thickens to about 30 m where the ash flow locally filled low areas. A gradation across several tens of centimeters—locally a meter or two—into the underlying lithophysal zone is characteristic, whereas the top of the zone is a widespread, relatively sharp, nearly planar surface. Sheet jointing and columnar jointing are prevalent (fig. 6).

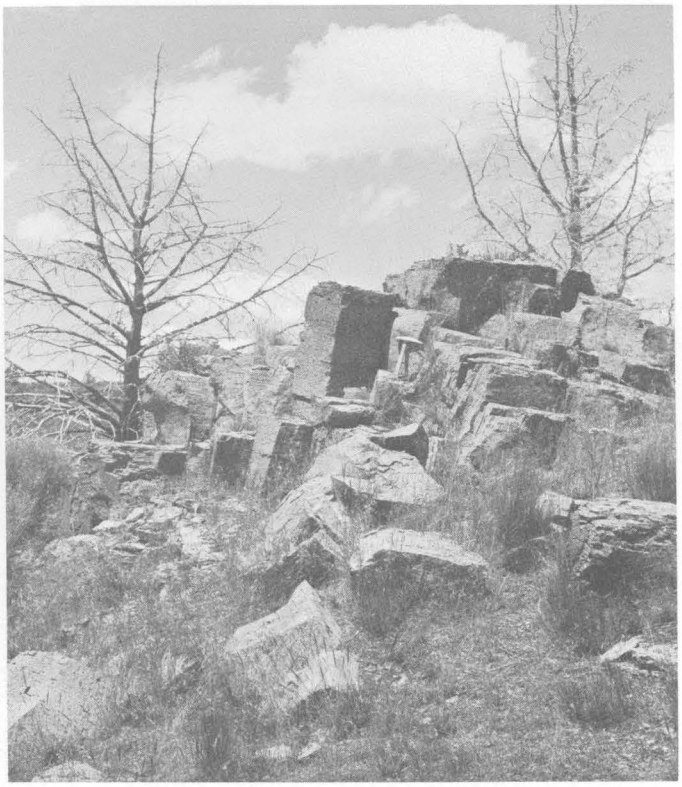

FIGURE 6.—Well-developed columnar jointing in zone 3 of ash-flow tuff, which shows strong foliation and sheet jointing at 90° to columns. Lineation in plane of foliation is not visible, but is shown on figure 9*B*.

Before crystallization the zone was composed of glass shards, pumice fragments of various sizes, and less than 1 percent mineral and rock fragments. The rocks are now holocrystalline, but the eutaxitic texture of the groundmass is still recognizable, owing to contrasting grain sizes of the crystallization products of the flattened shards (fig. 7). Many lensoid cavities that represent highly flattened pumice fragments impart a pronounced foliation to rocks of this zone. The cavities apparently result partly from exsolution of the volatiles within pumice fragments to form bubbles and partly from volume reduction through crystallization of the pumice.

The pumice fragments and cavities average about 8–10 mm in length, but range from 2 mm to several tens of centimeters. They are flattened to produce a pronounced foliation, which in places simulates fine, discontinuous flow banding.

Pumice fragments are also greatly stretched and elongate parallel to one another in the plane of foliation. Measurements of the degree of elongation in a typical specimen give length-width ratios of from 1:4 to 1:12. Such lineation clearly indicates that the pumice fragments were stretched principally in one direction, presenting good evidence that the ash flow moved with laminar flowage after the pumice fragments had collapsed and had become welded together into a coherent mass.

One ramp structure (fig. 8) was found during rapid reconnaissance of the area. It probably formed by suc-

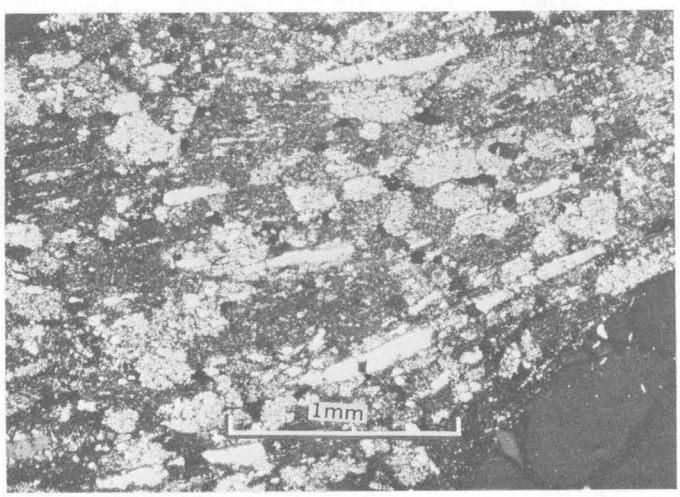

FIGURE 7.—Specimen (GWW–84–66) from zone 3 of ash-flow tuff that shows pronounced laminar flowage. Phenocryst (dark area) is fractured and partly rounded quartz in a crystallized groundmass composed of alkali feldspar and quartz. Lensoid texture of groundmass reflects the original eutaxitic texture. Partly crossed nicols.

FIGURE 8.—Ramp structure in zone 3 of ash-flow tuff. Lineation—not visible on photograph—is principally parallel to scarp and perpendicular to strike of ramp. Asymmetry shows sense of movement (from right to left.)

cessive imbricate thrusts of the already welded, viscous, fluidlike ash flow, much as ramping occurs in viscous lava flows and in some other ash-flow tuffs which have undergone laminar flowage (Schmincke and Swanson, 1967).

The cavities, once pumice fragments, are now partly filled with alkali feldspar and quartz, and the matrix shards and ash are crystallized chiefly to these minerals. The alkali feldspar and quartz are coarser grained and more nearly euhedral in the cavities than in the matrix. In addition, alkali amphiboles of three different kinds occur sparsely among the primary crystallization and vapor-phase minerals. One amphibole is pleochroic in shades of blue and blue green; another is less strongly pleochroic in shades of green and yellow green; and a third is highly pleochroic in shades of murky red brown. All are of such fine grain size that further identification was not attempted, but they are similar to the riebeckite, aenigmatite-rhönite, and green hornblende of Walker (1961), which also occur in soda rhyolite flows and domes in southeast Oregon.

The composition of the alkali feldspar in the crystallized pumice fragments is Or_{10-15}, based on X-ray determination of d spacings of $(\bar{2}01)$ (Bowen and Tuttle, 1950). Groundmass alkali feldspar is so poorly crystalline that X-ray determination of its composition is unsatisfactory, though suggestive of Or_{90}. Normative alkali feldspar of the whole rock is about Or_{40}. The alkali feldspars in the crystalline pumice fragments are slightly zoned and may be cryptoperthitic, though the $(\bar{2}01)$ peak is not an obvious doublet.

Phenocrysts, which total less than 1 percent of the zone, are alkali feldspar, quartz, aegirine-augite, and a blue amphibole (probably riebeckite). Some of the aegirine-augite phenocrysts are surrounded by opaque blackish, presumably oxidized margins, which in turn are mantled by the blue amphibole.

A holocrystalline sample of zone 3 showing the effects of intense vapor-phase crystallization, a high degree of compaction, and evidence of laminar flowage is of soda rhyolitic composition (table 1, column 1), like the vitrophyre. In fact, the two chemical analyses

(table 1, columns 1 and 2) are surprisingly similar, despite the glassiness of one rock and the completely crystalline nature of the other.

Zone 4

Many lithologic features that characterize zone 3 are present in zone 4, but foliation is not as pronounced and laminar flowage structures were not found. In most places, zone 4 is a few meters thick and consists of well-indurated, mottled, light-olive-gray tuff with very pale pinkish-gray oxidized patches. Joints are common, both parallel and at random angles to cooling surfaces, but no columnar joints were recognized. The rock is holocrystalline, and shard structure has been almost completely destroyed by primary crystallization to quartz and alkali feldspar; sodic amphiboles are much less abundant than in zone 3. The pumice fragments are not collapsed as completely as in zone 3, and they have been converted by vapor-phase crystallization to a porous aggregate of relatively coarse grained (several tenths of a millimeter) alkali feldspar and quartz. In addition, coarse single crystals of quartz and alkali feldspar are sprinkled throughout the finely crystalline groundmass; they may also be vapor-phase products. Numerous small vesicles, a few tenths of a millimeter in diameter, occur in the groundmass and are lined by thin rims of alkali feldspar and cristobalite.

Zone 5

Within zone 5, a moderately well indurated, pinkish to brownish-gray ash-flow tuff, similar in lithology to parts of zone 4, grades upward into a soft, slightly welded, grayish-red tuff containing partly collapsed to largely unflattened pumice fragments. Rocks of zone 5 are not present on the high parts of Wagontire Mountain, owing to nondeposition or to erosional stripping, but they are exposed near the distal ends of the cooling unit, where the zone attains a maximum thickness of several meters. Most of the shards have been crystallized to alkali feldspar, quartz, and minor cristobalite, but many of their outlines are still visible in thin section, largely because of a coating of reddish iron oxide around each crystallized shard. The iron oxide probably formed by oxidation of matrix ash and is concentrated near the top of the cooling unit. All the pumice fragments are holocrystalline, but the grain size of the minerals varies significantly from fragment to fragment, perhaps reflecting different amounts of gases held in each pumice fragment. Cristobalite lines small vesicles, but quartz is dominant in the groundmass and in the centers of crystallized pumice fragments. The phenocrysts are similar to those of the other zones.

285-544 O—68——4

LAMINAR FLOWAGE

Laminar flowage structures in zone 3 of the ash-flow tuff of Wagontire Mountain consist of (1) pumice lapilli which are stretched parallel to one another and form a lineation in the plane of foliation (fig. 9) and (2) a ramp structure. Only one ramp structure was found during the incomplete reconnaissance of the area, but more are likely to be present. The lineations radiate from two areas at opposite ends of Wagontire Mountain (fig. 1) which were suspected of being vent areas even before the lineations had been mapped. Most of the lineations trend southward, and the asymmetry

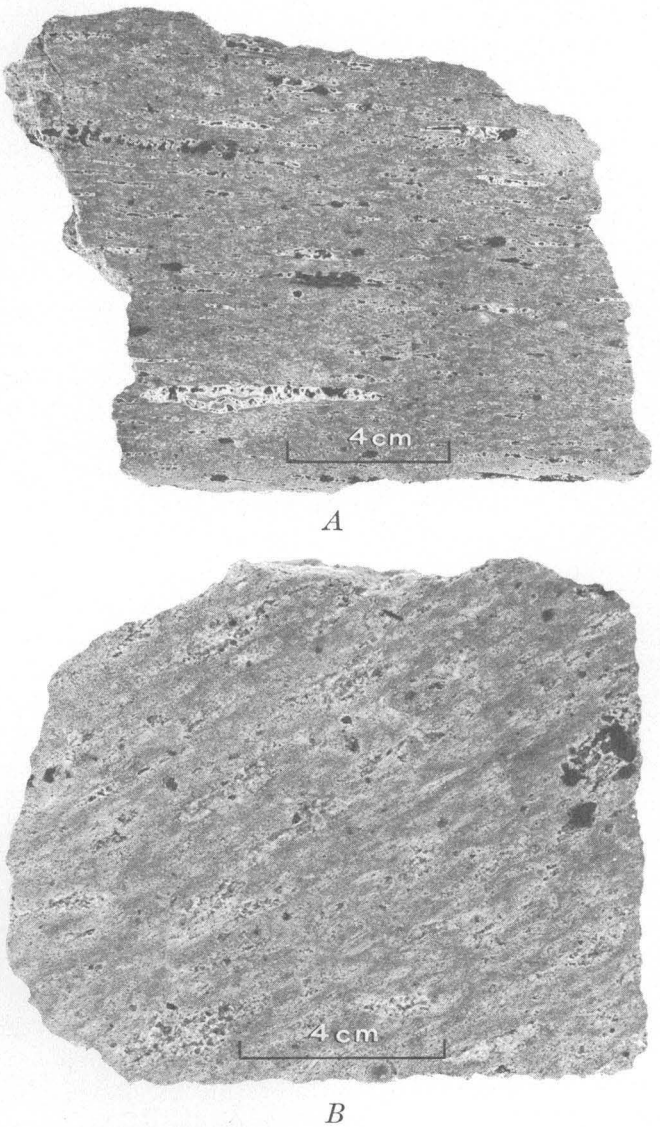

FIGURE 9.—Foliation and lineation in specimen of ash-flow tuff showing laminar flowage (zone 3). Specimen (GWW–84–66) obtained from outcrop shown on figure 6. *A*, Foliation defined principally by flattened pumice lapilli—commonly represented by lensoid miarolitic cavities. *B*, Sawed surface in plane of foliation normal to surface shown in *A*. The lineation results from stretched and elongated pumice fragments and possibly glass shards.

of the ramp structure indicates that flowage was to the south, away from the two postulated vent areas. Several measurements of the lineation near distal ends, however, show random orientations that probably result from flowage down local cross slopes of the now-buried pre-flow surface. The ash flow apparently moved down the southern slopes of Wagontire Mountain in two or more lobes which eventually merged to form a nearly continuous sheet. The distribution and zonal features of the ash-flow tuff indicate that it cooled as a single unit; eruptions from the two vents must therefore have been practically synchronous.

The uniformity of most flowage directions suggests that the laminar flowage occurred during spreading of the flow from the vents, not during remobilization of the tuff after initial cessation of movement. Remobilization would probably have taken place locally and at different times throughout the tuff, so that the tuff would have flowed into local surface lows and acquired widely divergent orientations of lineation, as did the tuff that Hoover (1964) described. A similar conclusion, based on more extensive and conclusive evidence, that laminar flowage can occur without remobilization was reached by Schmincke and Swanson (1967) for ash-flow tuffs in the Canary Islands.

The sequence of events leading to compaction, laminar flowage, and vapor-phase crystallization probably was as follows: The ash flow was erupted onto a somewhat irregular surface which probably sloped gently southward. It advanced turbulently to almost its final position. Turbulence subsided, however, as the supply of upward-escaping gases was depleted, and eventually the mass became so deflated that shards and pumice fragments came into contact with each other and welded into a coherent viscous fluid (glass). Flowage continued owing to momentum, but the movement was laminar, not turbulent. The pumice fragments and shards were further flattened and stretched in the direction of movement during the laminar flowage. Finally, internal friction overcame momentum, and the flow stopped. Most of the vapor-phase crystallization began after flowage ceased because the vapor-phase minerals are unfractured and in only a few places do they show a preferred orientation parallel to the stretched pumice lapilli. Also, most of the lithophysae are spherical, or nearly so, indicating formation after most of the compaction and flowage had ceased, probably during vapor-phase crystallization.

Estimates of the distance of laminar flowage in zone 3 are approximate at best. Measurements of the stretched pumice fragments indicate that elongation in the plane of foliation is between 4 and 12 times. This cannot be extrapolated directly into precise flowage distances, but it is commensurate with laminar flowage of a few centimeters at most places. In the ramp structure the distance of laminar flowage was much greater, probably totaling several meters. The distance advanced by laminar flowage of the distal parts of the ash flow, as suggested by the cumulative stretching of myriad pumice fragments, was possibly as much as a few tens or hundreds of meters.

CAUSE OF FLOWAGE

The high degree of compaction and the development of laminar flowage structures suggest either lower than normal glass viscosity, greater than normal load pressures, deposition and compaction on steep slopes, or possibly a combination of these factors.

Field relations do not support high static load conditions. Thick nonwelded tuff does not occur above zone 5 anywhere in the outcrop area, and welding and compaction in the upper part of zone 5 are slight or absent. Also, the degree of oxidation of iron-bearing minerals increases upward through zone 5, and near its top most minerals are thoroughly oxidized; this suggests that the top of the zone was near the top of the entire cooling unit. Compaction and flowage, therefore, took place despite the apparent lack of a significant overlying static load.

Eruption of ash flows onto steep slopes would also affect load conditions and promote tangential or shearing stresses that could lead to laminar flowage, either before or after initial cessation of movement. The present southerly dips of the ash-flow tuff of Wagontire Mountain are mostly about 5°–8°, and there is no evidence to indicate steeper inclinations during emplacement. Inasmuch as the direction of slope coincides with the direction in which the ash flow moved, the slope might have been a factor in the development of laminar flowage. Schmincke and Swanson (1967), however, describe laminar flowage structures in ash-flow tuffs, some of which flowed and compacted on nearly horizontal surfaces. These tuffs and the tuff of Wagontire Mountain have chemical similarities that suggest to us that the viscosity, determined to some degree by chemical composition, may have been important in promoting laminar flowage.

The viscosity of the glass shards and pumice fragments of the ash flow resulted from a combination of factors that include temperature during and after eruption and the chemical composition—including volatile content—of the magma.

A high eruptive temperature, probably only slightly below the liquidus, is suggested by the paucity of phenocrysts in the ash-flow tuff of Wagontire Moun-

tain. The magma was not superheated, however, because the phenocrysts are not resorbed. This high temperature, by itself, does not appear to be the only reason for lower than normal viscosity, however, because many of the other Pliocene ash-flow tuffs of southeast Oregon also contain very small amounts of crystals yet show little or no evidence of lower than normal viscosities or laminar flowage.

The intense vapor-phase crystallization of several zones in the ash-flow tuff of Wagontire Mountain may indicate high amounts of volatiles in the magma, which would tend to decrease glass viscosity. The degree and type of vapor-phase crystallization are comparable to that in other Pliocene ash-flow tuffs of the region, however, so that the differences in viscosity probably cannot be accounted for solely by volatile contents.

The anhydrous chemical composition of the magma probably controlled, to an important degree, the viscosity of the glass in the ash flow, and thus its susceptibility to laminar flowage. Rapid rock analyses of the vitrophyre of zone 1 (table 1, column 2) and of a holo-

TABLE 1.—*Chemical analyses and CIPW norms of ash-flow tuffs from Wagontire Mountain, Oreg., Grand Canary (Canary Islands), and south-central Nye County, Nev., that show laminar flowage structures*

[Abbreviation: nd, not determined]

	1	2	3	4	5	6	7	8	9	10	11	12	13
Chemical analysis													
SiO_2	75.6	75.9	67.1	68.5	68.2	68.4	65.86	70.54	66.28	66.08	71.03	74.4	75.0
Al_2O_3	12.1	12.1	12.0	9.6	14.0	14.0	10.35	11.30	13.27	14.78	12.95	11.3	11.2
Fe_2O_3	1.8	1.4	5.6	7.5	3.6	3.3	6.89	5.09	5.60	1.58	3.98	3.1	3.2
FeO	.80	.96	.8	.1	.1	.3	.62	1.20	.88	1.84	.23	.61	.55
MgO	.00	.02	.7	.1	.2	.2	2.06	.11	.04	.54	.37	.07	.05
CaO	.33	.26	.5	.5	.6	.6	.78	.86	.70	1.52	.27	.10	.16
Na_2O	4.2	4.4	7.0	5.2	6.4	6.4	4.53	5.04	5.61	5.09	5.72	4.7	4.2
K_2O	4.2	4.2	3.8	4.5	4.9	4.8	4.70	3.62	4.23	3.92	4.38	4.4	4.4
H_2O^-	.21	.09	.5	1.7	.5	.6	1.75	.21	.32	.24	.17	.14	.11
H_2O^+	.51	.37					1.50	.89	1.56	3.12	.16	.28	.65
TiO_2	.08	.04	1.1	1.0	.55	.6	1.00	1.00	1.27	1.04	.62	.22	.24
P_2O_5	.03	.00	.17	.10	.07	.08	.08	nd	.13	.07	.05	.06	.05
MnO	.00	.00	.28	.45	.24	.24	.25	.16	.13	.13	.24	.14	.14
CO_2	<.05	<.05	nd	nd	nd	nd	nd	nd	nd	nd	nd	.05	.05
Sum	100.00	100.00	99.6	99.3	99.4	99.5	100.37	100.02	100.02	[1]100.20	[2]100.25	99.57	100.00
CIPW norms													
Q	34.77	33.74	14.94	25.63	13.70	14.16	20.91	27.66	17.80	18.04	21.93	31.66	34.13
C	.12	------	-----	-----	-----	-----	------	------	------	-------	-------	-----	-------
Z	------	------	-----	-----	-----	-----	------	------	------	.38	-------	-----	-------
or	25.03	25.00	22.67	27.26	29.29	28.67	28.60	21.63	25.47	23.92	25.90	26.13	26.01
ab	35.85	37.50	40.96	24.94	45.25	45.78	27.87	38.38	45.55	44.48	42.26	33.79	33.13
an	1.45	.87	-----	-----	-----	-----	------	------	------	6.10	-------	-----	-------
ac	------	------	16.36	17.77	8.40	7.90	10.22	4.17	2.48	-------	-------	5.44	2.14
hl	------	------	-----	-----	-----	-----	------	------	------	-------	.13	-----	-------
ns	------	------	.06	-----	-----	-----	------	------	------	-------	-------	-----	-------
Di wo	------	.18	-----	.21	.58	.58	1.40	.32	.12	.51	.29	.04	.195
Di en	------	.02	.46	.18	.50	.50	1.21	.28	.10	.33	.25	.18	.125
Di fs	------	.18	.05	-----	-----	-----	------	------	------	.15	-------	.01	-------
Hy en	------	.03	1.30	.07	-----	-----	4.08	------	------	1.06	.68	-----	-------
Hy fs	------	.36	.13	-----	-----	-----	------	------	------	.47	-------	-----	-------
mt	2.37	2.05	-----	-----	-----	.01	------	1.51	------	2.37	-------	1.79	1.54
hm	.18	------	-----	1.55	.74	.60	3.56	2.67	4.85	-------	2.28	-----	1.40
il	.15	.08	2.11	1.20	.73	1.15	1.90	1.92	2.18	2.04	1.00	.42	.46
ap	.07	------	.41	.24	.17	.19	.20	------	.31	.17	.12	.14	.12
tn	------	------	-----	.96	.42	-----	.07	------	.36	-------	.23	-----	-------

1. Crystallized ash-flow tuff of Wagontire Mountain from zone showing laminar flowage structures (Sample GWW–84–66). Analysis: P. L. D. Elmore, Lowell Artis, H. Smith, S. D. Botts, G. W. Chloe, and John L. Glenn.
2. Dense glassy base of ash-flow tuff of Wagontire Mountain (Sample GWW–82–66). Analysis: P. L. D. Elmore, Lowell Artis, H. Smith, S. D. Botts, Gillison Chloe, and John L. Glenn.
3–6. Ash-flow tuffs, Grand Canary. Data from Schmincke and Swanson (1967).
7. Ash-flow tuff, Grand Canary. Data from Jérémine (1933).
8–10. Ash-flow tuffs, Grand Canary. Data from Bourcart and Jérémine (1937).
11. Ash-flow tuff, Grand Canary. Data from Hausen (1962, p. 199).
12. Flow-banded ash-flow tuff, south-central Nye County, Nev. Sample (DLH–62–20) collected by D. L. Hoover. Analysis: P. L. D. Elmore, S. D. Botts, G. W. Chloe, Lowell Artis, and H. Smith.
13. Flow-banded ash-flow tuff, south-central Nye County, Nev. Sample (DLH–62–16) collected by D. L. Hoover. Analysis: P. L. D. Elmore, S. D. Botts, G. W. Chloe, Lowell Artis, and H. Smith.

[1] ZrO_2=0.25.
[2] Cl_2=0.08.

crystalline sample from zone 3 that shows well-developed laminar flowage structures (table 1, column 1) denote a low-alumina soda rhyolitic composition in which alkalies total about 8.5 percent and the ratio of Na_2O to K_2O is near unity (Na/K atomic ratio of about 1.51). These analyses are compared with Nockolds' (1954) average calc-alkali rhyolite (fig. 10) and with several analyses of other ash-flow tuffs that show laminar flowage structures (table 1, columns 3–13; fig. 10), from Grand Canary (Schmincke and Swanson, 1967) and from south-central Nevada (D. L. Hoover, 1964; written commun., 1967).

Chemically, the ash-flow tuff of Wagontire Mountain is similar to Nockolds' (1954) average alkali rhyolite and differs mainly in its slightly lower Al_2O_3 and slightly higher SiO_2 and Na_2O contents; the content of $FeO+Fe_2O_3$ is about the same or only slightly greater than that in alkali rhyolite. The other ash-flow tuffs plotted in figure 10 that show laminar flowage structures all diverge from average calc-alkaline rhyolite and

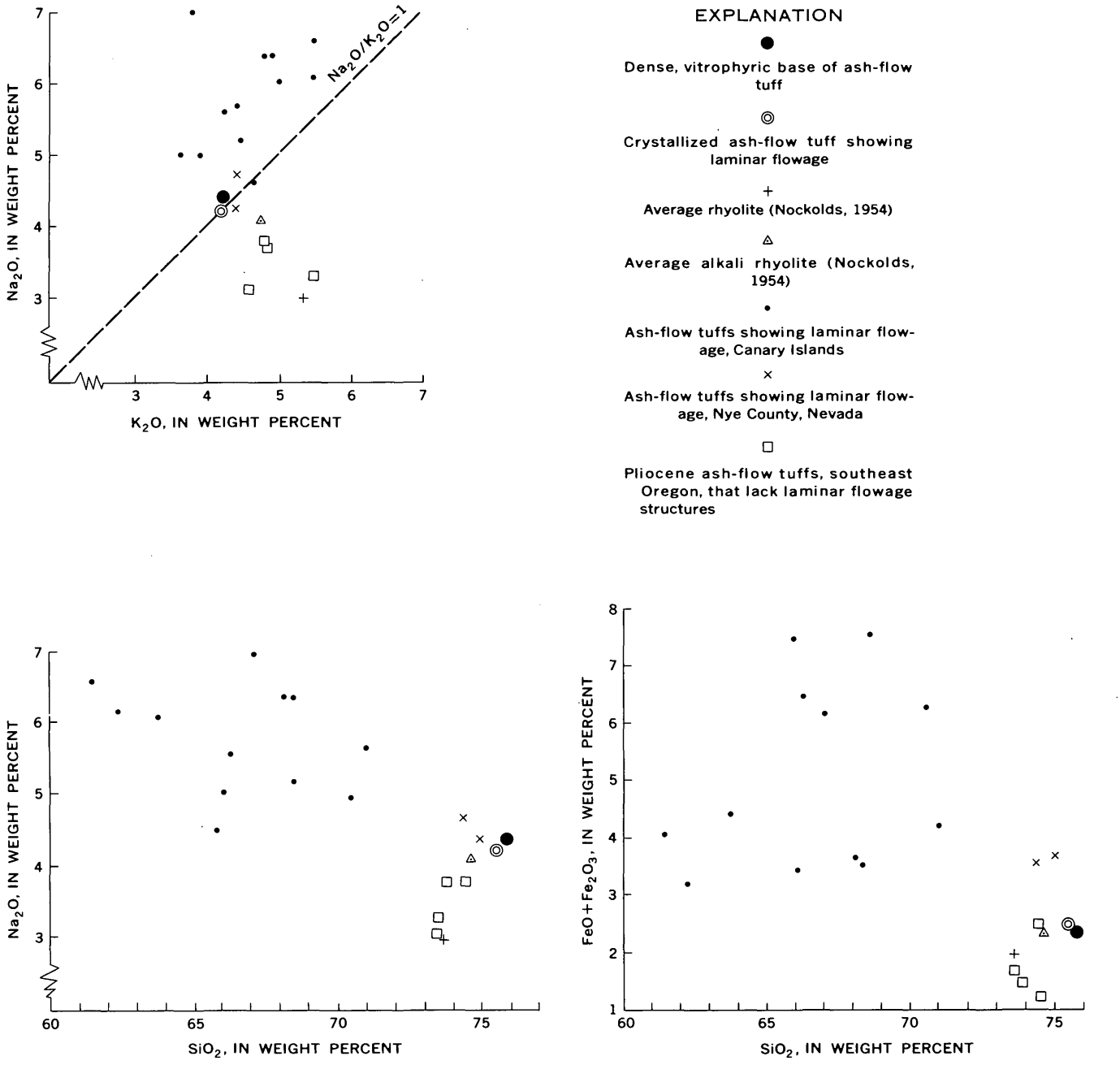

FIGURE 10.—Variation diagrams comparing chemical composition of ash-flow tuff of Wagontire Mountain with several other ash-flow tuffs and with average calc-alkaline rhyolite and alkali rhyolite.

alkali rhyolite by having higher Na_2O/K_2O ratios and higher total alkalis, higher Na_2O, and higher $FeO+Fe_2O_3$ contents; most also contain less Al_2O_3. In contrast, the Pliocene ash-flow tuffs of southeast Oregon that show little or no laminar flowage structures tend toward average calc-alkaline rhyolite and are characterized by appreciably less Na_2O and lower total Fe contents.

A substantial decrease in glass viscosity has been related to a high Fe/Si+Al ratio (Barth, 1962, p. 142), and the ash-flow tuffs listed in table 1 have higher ratios than does Nockolds' average calc-alkali rhyolite. For example, the analysis in column 2 of table 1 has an Fe/Si+Al ratio of 0.023 and all other analyses in table 1 have comparable or higher ratios, whereas Nockolds' average calc-alkali rhyolite has a ratio of only 0.018. Moreover, comparison of alkali ratios in ash-flow tuffs, both with and without laminar flowage structures, suggests that high Na_2O/K_2O ratios also may lower viscosity, as they do in alkali feldspar melts and glasses (Clark, 1966). Thus, those ash-flow tuffs high in both $FeO+Fe_2O_3$ and Na_2O may be particularly susceptible to laminar flowage (Schmincke and Swanson, 1967). Such a composition may largely explain why the Wagontire Mountain ash flow ended its movement by laminar flowage.

The process of deflation, pumice collapse, and welding during movement should promote laminar flowage in some calc-alkaline ash flows. Flowage structures have, in fact, been recognized in ash-flow tuffs of calc-alkaline rhyolite to rhyodacite composition from south-central Nevada (D. L. Hoover, written commun., 1967) and from southwest Montana (H. J. Prostka, written commun., 1967). Nevertheless, most of the ash-flow tuffs known to us that exhibit laminar flowage structures are characterized by low Al_2O_3 and high soda and total iron contents, which suggests that they play a significant role in reducing glass viscosity to the point of allowing plastic creep.

REFERENCES

Barth, T. F. W., 1962, Theoretical petrology, 2d ed.: New York, John Wiley and Sons, 416 p.

Bourcart, Jacques, and Jérémine, E., 1937, La Grande Canarie; étude géologique et lithologique: Bull. Volcanol., ser. 2, v. 2, p. 3–77.

Bowen, N. L., and Tuttle, O. F., 1950, The system $NaAlSi_3O_8$–$KAlSi_3O_8$–H_2O: Jour. Geology, v. 58, no. 5, p. 489–511.

Clark, S. P., Jr., 1966, Viscosity, *in* Clark, S. P., Jr., ed., Handbook of physical constants: Geol. Soc. America Mem. 97, p. 291–300.

Hausen, H. M., 1962, New contributions to the geology of Grand Canary: Societas Scientarium Fennica, Commentationes Physico-mathematicae [Finland] 27, 418 p.

Hoover, D. L., 1964, Flow structures in a welded tuff, Nye County, Nevada [abs.]: Geol. Soc. America Spec. Paper 76, p. 83.

Jérémine, Elisabeth, 1933, Contribution à l'étude petrographique des trois îles de l'archipel Cararien—Tenérife, La Palma, Gran Canaria: Soc. Française Minéralogie Bull., v. 56, no. 4–5, p. 189–261.

Nockolds, S. R., 1954, Average chemical composition of some igneous rocks: Geol. Soc. America Bull., v. 65, no. 10, p. 1007–1032.

Ross, C. S., and Smith, R. L., 1961, Ash-flow tuffs—their origin, geologic relations, and identification: U.S. Geol. Survey Prof. Paper 366, 81 p.

Schmincke, Hans-Ulrich, and Swanson, D. A., 1966, Secondary flowage features in welded pyroclastic flows, Grand Canary, Canary Islands [abs.]: Geol. Soc. America Spec. Paper 87, p. 149.

———1967, Laminar viscous flowage structures in ash-flow tuffs from Gran Canaria, Canary Islands: Jour. Geology, v. 75, p. 641–664.

Smith, R. L., 1960a, Zones and zonal variations in welded ash flows: U.S. Geol. Survey Prof. Paper 354–F, p. 149–159.

———1960b., Ash flows: Geol. Soc. America Bull., v. 71, p. 796–842.

Smith, W. D., 1926, Physical and economic geology of Oregon; the southeastern lake province: Oregon Univ. Commonwealth Rev., v. 8, nos. 2–3, p. 199–253.

Walker, G. W., 1961, Soda rhyolite (pantellerite?) from Lake County, Oregon: Art. 200 *in* U.S. Geol. Survey Prof. Paper 424–C, p. C142–145.

RHABDOPHANE FROM A RARE-EARTH OCCURRENCE, VALLEY COUNTY, IDAHO

By JOHN W. ADAMS, Denver, Colo.

Abstract.—Rhabdophane, a hydrated phosphate of the cerium-group rare-earth elements, occurs in a highly oxidized fault or shear zone near Monumental Summit in Valley County, Idaho. The rhabdophane, which is associated chiefly with hydrated iron oxides, clays, and quartz fragments, is probably of supergene origin. Preliminary analysis shows it to be deficient in cerium like the rhabdophane from Salisbury, Conn. Optical data, X-ray data, and analyses of 10 samples from the rare-earth-bearing zone are given.

Rhabdophane, a hydrated phosphate of the cerium-group elements was found in samples containing high concentrations of rare earths collected in 1966 by geologists of the U.S. Geological Survey during mineral assessment of the Idaho primitive area. The samples were collected from highly altered rock exposed in a roadcut 700 feet east of Monumental Summit, the divide between Roosevelt Lake and Stibnite, in the Yellow Pine 15-minute quadrangle, Valley County, Idaho (fig. 1).

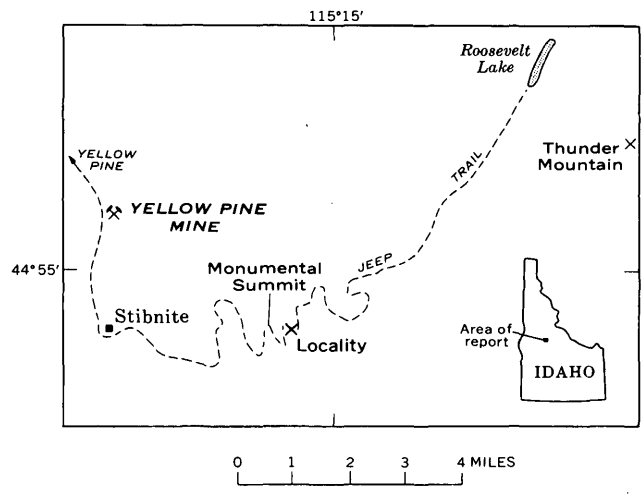

FIGURE 1.—Map showing location of area sampled in Valley County, Idaho.

Because of the occurrence of this rare mineral, and the possible economic significance of the deposit, the locality was visited by the writer, R. L. Parker, and B. F. Leonard in July 1967, and additional samples were collected for analytical and mineralogical work.

The writer acknowledges the assistance of B. F. Leonard, particularly in the description of the regional geology and geologic environment of the rhabdophane deposit.

OCCURRENCE

The rhabdophane occurs in a rare-earth bearing zone in a block-faulted terrane on the west rim of a caldera centered about 8 miles to the northeast of Thunder Mountain. West of Monumental Summit the bedrock consists of granodiorite of the Idaho batholith and northwest-trending complexly folded belts of generally high rank metamorphic rocks of the Hoodoo Quartzite and Yellowjacket Formation of Precambrian age. East of Monumental Summit the bedrock is mainly the Challis Volcanics of Eocene(?) to Miocene(?) age. At Monumental Summit, the Challis has been downdropped, relative to the granitic and metamorphic terrane, along nearly vertical faults. Small blocks of silicified marble of the Yellowjacket Formation have also been downdropped in these faults, and a small patch of this rock is exposed about 50 feet east of the rare-earth-bearing zone.

The relation of the rare-earth-bearing zone to the complex regional structure is not yet known, although faint planar structures preserved within the zone suggest that the zone lies in a north-striking fault. Many faults and shear zones in the region, regardless of their orientation or bedrock association, contain argillic alteration products locally accompanied by quartz, chalcedony, and pyrite or its alteration products, and less commonly by calcite, rutile, and other minerals. Some of the altered zones are barren, but others con-

tain minable quantities of gold, silver, tungsten, antimony, and mercury. Anomalous quantities of the rare earths are not known to occur in any of the altered zones except the rhabdophane-bearing zone east of Monumental Summit.

The outcrop in which the rhabdophane occurs forms the west bank of a roadcut about 120 feet long, 6 feet high, and 5 feet wide through a timbered area at an elevation of 8,300 feet. Except for the artificial exposure of the roadcut, rocks in the immediate vicinity are soil covered. The altered material of the outcrop is an earthy, brown to yellow-brown assemblage consisting largely of hydrated iron oxides, manganese oxides, clays, and fragments of microcrystalline and coarse euhedral quartz. Goethite pseudomorphs of minute pyrite crystals, showing chiefly modified pyritohedral forms, are common. Other minerals noted include pyrite and very sparse rutile, zircon, monazite, and cinnabar.

RHABDOPHANE

Rhabdophane is not readily recognizable in the host material, and as it does not contain appreciable thorium there is no anomalous radioactivity. The mineral is most abundant in a sample (JA–67–26) taken from near the south end of the outcrop. The material used for mineralogical and analytical work was obtained from a 40–80 mesh split of this sample by a combination of heavy-liquid separation, magnetic separation, and hand picking under a binocular microscope.

The rhabdophane occurs as yellowish-brown to white aggregates of intergrown spheroidal forms less than 20 microns in diameter. Under the petrographic microscope individual spheroids show a radial crystalline structure with fibers which are optically length slow. Refractive-index determinations were made by measuring the index of the edge of the spheroids in extinction positions in plane polarized light; indices thus determined are $n_O=1.675$, $n_E=1.705$, $n_E-n_O=0.03$. Whether these indices are the true indices of the mineral is questionable in view of the apparent lack of agreement between optical data obtained from spheroidal and nonspheroidal forms of crystalline materials (Morse and Donnay, 1936). The rhabdophane aggregates, when examined with a microspectroscope, are characterized by strong neodymium-praseodymium absorption bands.

X-ray powder data for the rhabdophane from Idaho and for that from Salisbury, Conn. (Muto and others, 1959), are given in table 1. A weak and broad line at d(A) 4.15 was attributed to goethite. An X-ray diffractometer trace of the sample used for the spectrographic analysis showed that both goethite and kaolinite are present as contaminants.

TABLE 1.—*X-ray diffraction powder data for rhabdophane from Valley County, Idaho, and from Salisbury, Conn.*

[Abbreviations: b, broad; m, moderate; ms, moderately strong; s, strong; vs, very strong; vw, very weak; and w, weak]

Valley County, Idaho [1]		*Salisbury, Conn. (Muto and others, 1959)*	
d(A)	I	d(A)	I
6. 03	m	6. 07	m
4. 39	ms	4. 40	s
3. 49	m	3. 49	m
3. 03	s	3. 02	vsb
2. 83	vs	2. 83	s
2. 36	w	2. 36	w
2. 14	m	2. 15	s
1. 933	vw	1. 920	w
1. 863	m	1. 859	m

[1] Equipment used: Debye-Scherrer camera of 114.59-mm diameter, Cu K_α radiation, Ni filter; not corrected for film shrinkage.

A preliminary spectrographic analysis (table 2) shows that the Idaho rhabdophane, much like the rhabdophane from Salisbury, Conn. (Hildebrand and others, 1957), is deficient in cerium in relation to the other lanthanides. The low cerium content can be attributed to a partial fractionation of the lanthanides through oxidation of Ce^{+3} to Ce^{+4} at some time prior to the formation of the rhabdophane.

GEOCHEMISTRY

Nine samples (JA–67–20 through JA–67–28) of the altered rock were taken at intervals of approximately

TABLE 2.—*Semiquantitative spectrographic analysis, in percent, of rhabdophane from Valley County, Idaho* [1]

[Analysts, H. W. Worthing and J. L. Harris. M, major constituent, greater than 10 percent]

	Sample JA–67–26 [2]		
Si	2. 0	La	M
Al	1. 0	Ce	1. 5
Fe	2. 0	Pr	7
Mg	. 02	Nd	M
Ca	1. 0	Sm	1. 5
Ti	. 07	Eu	. 5
P	M	Gd	5
Mn	. 03	Tb	. 3
As [3]	. 8	Dy	. 3
Ag	. 0005	Ho	. 07
Ba	. 01	Er	. 15
Be	. 007	Tm	. 007
Co	. 005	Yb	. 05
Cr	. 02	Lu	. 05
Cu	. 002	Y	2
Ga	. 001		
Nb	. 007		
Sc	. 015		
Sr	. 01		
Zr	. 0003		

[1] Generally reported to nearest number in the series 1, 0.7, 0.5, 0.3, 0.2, 0.15, and 0.1, and so forth. Looked for but not found: Na, Au, Cd, Ge, Hf, Hg, In, Mo, Ni, Pb, Pd, Pt, Re, Sb, Sn, Ta, Te, Th, Tl, U, V, W, and Zn.

[2] Split II.

[3] Determined on another sample by X-ray fluorescence by J. R. Lindsay.

10 feet along the roadcut exposure, beginning at the north end. An additional sample (JA–67–29) was taken from another roadcut exposure of altered rock about 100 feet to the south. Spectrographic analyses of these samples, together with analyses for mercury and P_2O_5, are given in table 3.

It is apparent from the analytical data that the rare-earth concentration is very high in some samples and is above normal in all. The content of several other metals, such as arsenic, manganese, mercury, and zinc, is also anomalously high in almost all samples.

The distribution of the three major lanthanides and mercury is shown graphically in figure 2. The curves connecting the first nine samples were not extended to include sample JA–67–29 because of the disproportionate sample interval. The changing relationships between the cerium, lanthanum, and neodymium content of the samples suggest that the rare earths are present in more than one phase. Except for a few grains of monazite, only rhabdophane has been recognized. The great excess of cerium over lanthanum and neodymium in sample JA–67–28 might reasonably

TABLE 3.—*Analyses of samples from Monumental Summit area, Valley County, Idaho*

[Semiquantitative spectrographic analyses by N. M. Conklin, P_2O_5 determined by G. D. Shipley, mercury determined by W. W. Janes. Abbreviations and symbols: M, major constituent, greater than 10 percent; A, looked for but not detected, or below limit of detection shown; p, present, but below limit of determination. Si, Al, Fe, Mg, Ca, Na, K, Ti, and P_2O_5 are reported in percent, all other elements in parts per million]

	Sample JA-67-									
	20	21	22	23	24	25	26	27	28	29
Si	M	M	M	M	M	M	M	M	M	M
Al	3	3	2	5	3	7	7	7	5	7
Fe	M	M	M	M	M	M	M	M	M	7
Mg	0.15	0.05	0.05	3	2	0.5	0.3	0.3	0.15	1.5
Ca	.07	.07	.07	0.3	0.3	.15	.15	.15	.07	0.2
Na	.15	A	A	.07	.05	A	.07	A	A	.05
K	A	A	A	A	A	A	A	A	1	A
Ti	.1	.07	.07	.1	.1	.2	.2	.2	.1	.1
P_2O_5	.45	.18	.37	.17	.38	.54	1.42	.63	.26	.48
Mn	15,000	7,000	5,000	70,000	70,000	70,000	15,000	20,000	15,000	200
As	10,000	7,000	10,000	2,000	1,500	5,000	7,000	7,000	1,500	A
B	A	A	A	p	A	p	p	A	A	A
Ba	500	300	150	1,500	700	700	300	200	200	150
Be	7	10	15	15	50	70	30	30	15	3
Ce	1,500	1,500	1,000	1,500	1,000	700	A	1,000	3,000	3,000
Co	30	15	15	70	15	50	30	50	30	7
Cr	15	10	10	30	30	30	50	50	15	30
Cu	70	20	15	70	7	100	150	150	10	70
Ga	10	7	15	20	15	15	30	20	15	10
Hg	1.8	1.9	1.6	3.0	4.0	4.6	7.5	6.5	6.5	1.4
In	A50	A50	A50	A50	A50	A50	A50	A50	A50	A50
La	700	1,500	700	1,500	5,000	1,500	20,000	15,000	300	1,500
Nb	p	p	p	p	p	p	p	10	p	p
Ni	30	30	50	70	70	100	50	100	30	30
Pb	p	p	p	p	p	p	p	10	p	p
Sc	A	A	A	A10	A10	15	15	15	A10	A10
Sr	15	10	10	70	30	30	30	15	10	30
V	10	A	A	20	15	20	20	30	10	10
W	A	p	p	p	p	p	p	p	p	p
Y	150	150	150	200	700	1,500	1,000	700	150	150
Yb	15	15	15	15	20	30	70	50	15	7
Zn	5,000	5,000	7,000	5,000	7,000	10,000	10,000	7,000	7,000	1,000
Zr	200	300	100	150	150	150	200	300	100	150
Pr	A	300	A	300	700	300	3,000	1,500	A	500
Nd	300	700	300	1,500	2,000	1,500	15,000	7,000	300	1,000
Sm	A	A	A	200	300	200	1,500	1,000	A	300
Eu	A	A	A	A	A	A	150	150	A	A
Gd	A	70	A	100	300	150	1,500	700	A	70
Dy	A200	A200	A200	A200	200	200	700	300	A200	A200
Ho	A	A	A	A	30	30	70	50	A	A
Er	A100	A100	A100	A100	A100	A100	A100	A100	A100	A
Tm	A50	A50	A50	A50	A50	A50	A50	A50	A50	A50
Lu	A100	A100	A100	A100	A100	A100	A100	A100	A100	A100

Notes: Elements not detected in any sample; Ag, Au, Bi, Cd, Ge, Hf, Li, Mo, Pd, Pt, Re, Sb, Ta, Tb, Te, Th, Tl, and U. Spectrographic analyses are reported to the nearest number in the series; 1, 0.7, 0.5, 0.3, 0.2, 0.15, 0.1, and so forth.

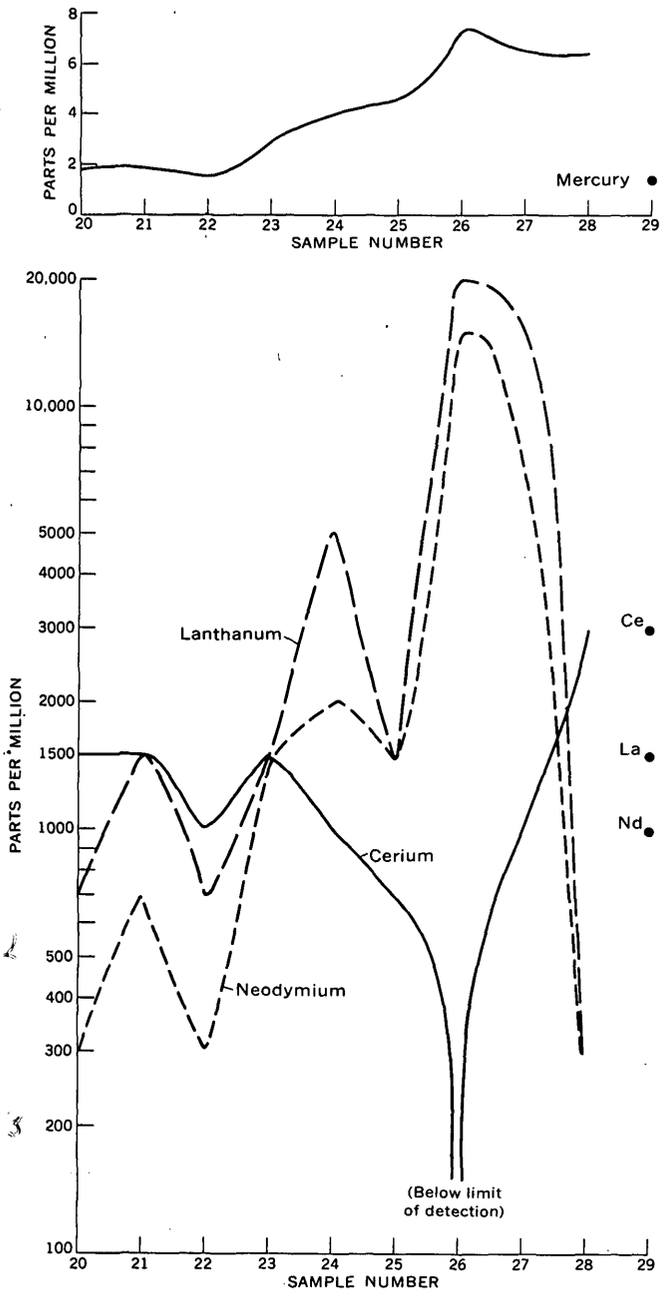

FIGURE 2. Distribution of mercury and rare-earth elements in samples JA–67–20 through JA–67–29.

cause one to expect the presence of cerianite (CeO_2), although this mineral has not yet been found in the iron oxide-rich heavy fraction of the sample. It is also possible that not all the rhabdophane in the deposit is identical in chemical composition to the analyzed sample.

ORIGIN

The origin of the rare-earth concentration is highly speculative. The site of deposition is apparently a mineralized fault or shear zone that has been highly altered by supergene processes. Rhabdophane is commonly a supergene mineral, and a low cerium variety would certainly point to a strongly oxidizing environment. We can assume that the rhabdophane is the alteration product of some preexisting rare-earth mineral. Whether this mineral was in the shear zone prior to the hydrothermal stage that introduced the other ore metals, or whether it formed at the same time is not obvious. The relatively high rare-earth content of sample JA–67–29, in which zinc and mercury are at their lowest values, might suggest that the rare-earth and ore-metal mineralization was not simultaneous. This possibility appears to be refuted, however, by the close correlation of mercury with rare earths in other samples, notably JA–67–26, where the highest mercury content is coincident with the highest concentration of rare earths. It seems probable that the rare earths were introduced at the same time as the other metals, and that their present distribution characteristics are largely the result of supergene alteration.

REFERENCES

Hildebrand, F. A., Carron, M. K., and Rose, H. J., Jr., 1957, Re-examination of rhabdophane (scovillite) from Salisbury, Connecticut [abs.]: Geol. Soc. America Bull., v. 68, no. 12 ,pt. 2, p. 1744–1745.

Morse, H. W., and Donnay, J. D. H., 1936, Optics and structure of three-dimensional spherulites: Am. Mineralogist, v. 21, p. 391–426.

Muto, Tadashi, Meyrowitz, Robert, Pommer, A. M., and Murano, Toru, 1959, Ningyoite, a new uranous phosphate mineral from Japan: Am. Mineralogist, v. 44, p. 633–650.

PRECAMBRIAN ROCKS PENETRATED BY THE DEEP DISPOSAL WELL AT THE ROCKY MOUNTAIN ARSENAL, ADAMS COUNTY, COLORADO

By CHESTER T. WRUCKE and DOUGLAS M. SHERIDAN, Denver, Colo.

Abstract.—The disposal well at the Rocky Mountain Arsenal, Adams County, Colo., about 10 miles northeast of downtown Denver, penetrates Precambrian rocks between a depth of 11,935 feet and the bottom of the hole at 12,045 feet. Migmatitic hornblendic biotite-quartz-feldspar gneiss forms the lower 75 feet of this section. This gneiss is similar in composition and fabric to metasedimentary gneisses found in high-grade metamorphic terrane of the nearby east-central Front Range. A weathered zone of illitic altered gneiss occurs in the upper 35 feet of the Precambrian section and is overlain by the Fountain Formation of Pennsylvanian and Permian age. Fractures, thin veins, and zones of microbreccia that cut the Precambrian gneiss cored in the well resemble structures found along breccia reefs exposed in the mountains west of Denver. This similarity suggests that a fault or fracture zone may occur in the general vicinity of the arsenal well.

The 12,045-foot disposal well at the Rocky Mountain Arsenal, about 10 miles northeast of downtown Denver (fig. 1), is one of the few boreholes that penetrate Precambrian rocks in central Colorado east of the Front Range. The lowermost 110 feet of the well penetrates weathered and relatively unweathered but fractured migmatitic gneiss. Overlying the Precambrian basement is a thick sedimentary section of Paleozoic and younger rocks. A study of the Precambrian rocks from the well was undertaken as one of several investigations by the U.S. Geological Survey in cooperation with the Colorado School of Mines, Regis College, and the University of Colorado to determine the relation of earthquakes in the Denver area to the local and regional geology. The Precambrian rocks at the well have been of interest in these investigations because Evans (1966a, b) suggested that waste fluids injected into them have triggered numerous earthquakes in the surrounding area.

Previous petrographic studies of Precambrian rock from the arsenal well were made by R. B. Taylor (unpub. data, 1961 and 1963), Edwards (1966, p. 26, 28, 199–200), and Sheridan and others (1966). Other studies of the Precambrian rock in the core include age determinations by Hedge (1967), who reported the age to be about 1.75 billion years by Rb–Sr methods.

Material available for this investigation included core of part of the Precambrian rock and samples of drill cuttings from the Precambrian interval not cored (fig. 2), and core and cuttings from the lower part of the overlying sedimentary section. Four thin sections were used by R. B. Taylor in his study, and six more sections were cut from the Precambrian core for the present investigation.

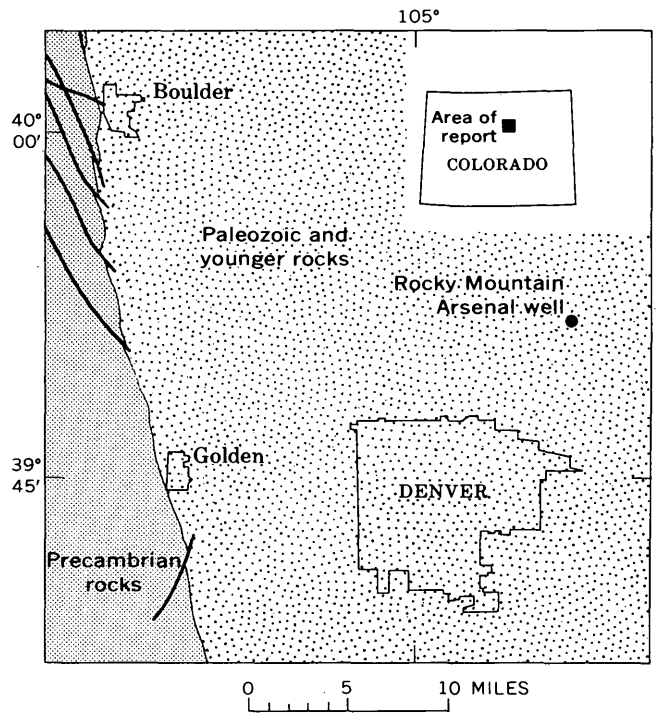

FIGURE 1.—Geologic sketch map of part of north-central Colorado, showing location of the Rocky Mountain Arsenal well. Heavy lines are faults.

U.S. GEOL. SURVEY PROF. PAPER 600-B, PAGES B52-B59

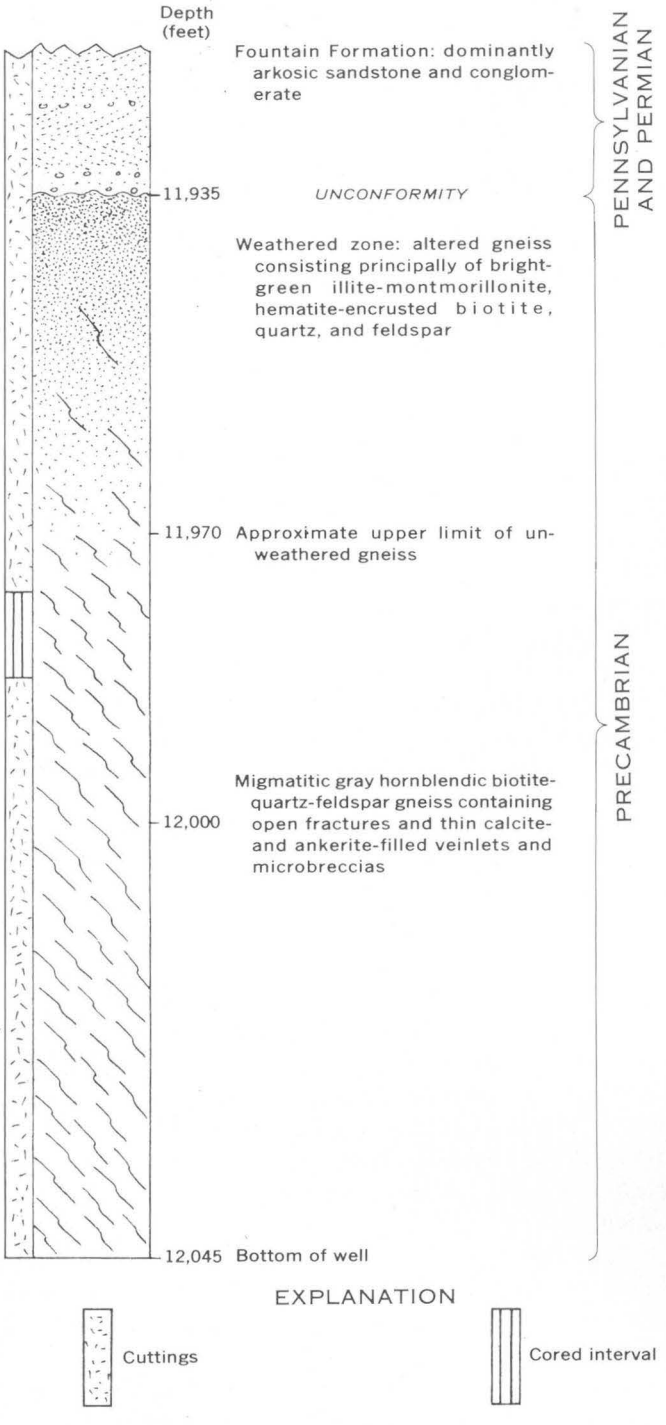

FIGURE 2.—Stratigraphic column of rocks in the lower part of the Rocky Mountain Arsenal well as represented by core and cuttings. Of the cored interval, 6.7 feet was recovered and 2.5 feet was available for this study.

R. E. Wilcox studied several minerals by immersion techniques and contributed interpretations based on the mineralogy. A. J. Gude 3d made X-ray diffractometer patterns of several specimens, L. G. Schultz made X-ray analyses of mixed-layer illite-montmorillonite, F. A. Hildebrand identified anhydrite from X-ray data, and O. B. Raup contributed helpful advice concerning the identification and interpretation of clay minerals in the well cuttings.

MIGMATITIC GNEISS

Drill core

Migmatitic gneiss, as shown in the drill core (fig. 3), has the layered appearance typical of many migmatitic metamorphic rocks in the Front Range. It consists of hornblendic biotite-quartz-feldspar gneiss intercalated with light-colored, reddish-stained pegmatite. Layering, 2 millimeters to 10 centimeters thick, in the gneiss is expressed by differing proportions of dark and light minerals. Layers and irregular lenses of pegmatite commonly parallel the gneissic layers and are less than 2 cm thick, but a mass about 12 cm thick occurs in one piece of core. The gneissic layers are oriented at angles of 60°–70° to the core axis, which suggests a dip of 20°–30°.

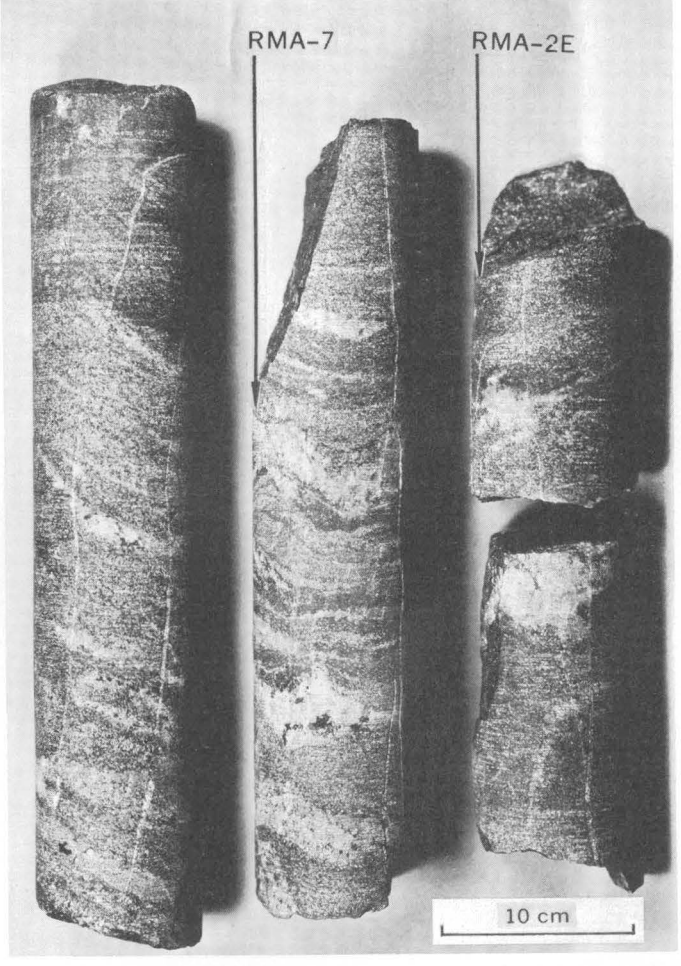

FIGURE 3.—Core of migmatitic gneiss showing location of two of the samples (RMA–7 and RMA–2E) that were studied petrographically. Note fractures parallel to core axis. Photograph by R. B. Taylor.

The gneiss is fine to medium grained and is composed predominantly of plagioclase, quartz, biotite, and hornblende, with lesser amounts of microcline. The major minerals are dominantly 0.3–1 mm across, but range from less than 0.02 mm to as much as 3.5 mm in size. Composition data are summarized in table 1.

TABLE 1.—*Modes (volume percent) of hornblendic biotite-quartz-feldspar gneiss from the Rocky Mountain Arsenal disposal well*

[Modes determined by point-count method; 1,000–1,320 points counted for each mode. Tr., trace]

Mineral	Mode [1]							
	1	2	3	4	5	6	7	8
Plagioclase	42	38	40	42	51	50	52	48
Quartz	31	26	40	33	30	25	29	23
Biotite	8	9	11	15	14	20	8	15
Hornblende	10	16	1.0	2.3	1.3	.8	(2)	(2)
Microcline	7	7	5	4	.5	Tr.	Tr.	1.3
Magnetite-ilmenite	Tr.	1.1	Tr.	.5	Tr.	.5	.5	Tr.
Apatite	Tr.	.6	Tr.	.6	Tr.	Tr.	Tr.	Tr.
Sphene	.9	.8	.6	.4	.7	.9	Tr.	Tr.
Calcite	Tr.	----	.7	1.2	1.1	1.8	Tr.	.5
Zircon	----	Tr.	Tr.	----	----	----	Tr.	Tr.
Hematite	Tr.	Tr.	Tr.	Tr.	.5	Tr.	Tr.	Tr.
Leucoxene	Tr.	Tr.	Tr.	.5	.5	Tr.	Tr.	.5
Sericite	Tr.	Tr.	Tr.	Tr.	Tr.	Tr.	Tr.	Tr.
Alteration products of hornblende:								
Illitic clay	Tr.	Tr.	Tr.	Tr.	Tr.	Tr.	4	2.1
Carbonate minerals	Tr.	Tr.	Tr.	Tr.	Tr.	Tr.	2.9	5
Chlorite	Tr.	----	Tr.	Tr.	Tr.	Tr.	Tr.	1.7
Hematite and magnetite(?)	Tr.	Tr.	----	Tr.	----	----	2.8	1.3

Mode 1. Sample No. 11,988–95B, hornblendic biotite-quartz-feldspar geniss.
2. No. RMA–1F, same as 1.
3. No. 11,988–95A, slightly migmatitic layered hornblendic biotite-quartz-feldspar gneiss.
4. No. RMA–2E, migmatitic hornblendic biotite-quartz-feldspar gneiss.
5. No. RMA–4, slightly migmatitic hornblendic biotite-quartz-feldspar gneiss.
6. No. RMA–3A, same as 5.
7. No. RMA–5, migmatitic hornblendic biotite-quartz-feldspar gneiss in which the hornblende is completely altered.
8. No. 11,988–95D, same as 7.

[1] Modes 3 to 8 are from thin sections of migmatitic gneiss in which the areas of pegmatitic material could not conveniently be separated in making the point counts.
[2] Hornblende altered completely. See description of mode 7 above.

Plagioclase (about An_{25}) is the most abundant mineral in the gneiss and forms the largest grains, which are irregular to somewhat blocky and as much as 3.5 mm across. Albite twinning, distinct in some grains, is weak or absent in others; some twin lamellae are slightly bent. Many of the plagioclase grains contain conspicuous blocky to rounded patches of microcline, forming antiperthite. Most plagioclase shows only weak sericitic alteration, commonly arranged in discontinuous bands parallel to twin lamellae. Quartz occurs as isolated anhedral grains, generally somewhat smaller than plagioclase, and as elongate aggregates. Locally quartz forms myrmekitic intergrowths with plagioclase adjacent to microcline. Biotite sheaves are dark olive brown or brownish green in the direction of maximum absorption. Optical data determined on several grains—$n_x = 1.596–1.598$; birefringence, 0.058; $2V_x < 5°$—indicate high iron content. The hornblende occurs as somewhat ragged to blocky grains that have Z=deep green or slightly bluish green. Other optical data determined for several grains—$n_x = 1.687–1.690$; $2V_x$ about 25° or less; strong dispersion—suggests a hornblende rich in ferrous iron.

Microcline, which forms as much as 7 percent of the gneiss (table 1), occurs as antiperthitic intergrowths in plagioclase and as small grains interspersed among the more abundant minerals of the rock. The microcline is unaltered and generally well twinned. Sphene, apatite, and magnetite-ilmenite are common accessory minerals; zircon is sparse. Irregular grains of calcite form an integral part of the granoblastic fabric in several thin sections and are assumed to be part of the metamorphic mineral suite of the rock, as distinct from the carbonate minerals in veins.

Some thin sections show hornblende altered partly or completely to a complex intergrowth of micaceous material and fine-grained carbonate minerals together with less abundant pale-green chlorite and hematite (fig. 4*A*). The micaceous material is illitic clay, determined by X-ray diffraction patterns. It occurs as very fine grained aggregates of colorless to pale-brown grains that locally are sufficiently integrated optically to indicate that they are biaxial negative with low $2V$ and have a birefringence of about 0.03. Hematite in the altered hornblende occurs approximately along former cleavage traces. Biotite is fresh even where hornblende is completely altered. Thin platelets of hematite are common and chlorite is rare along the cleavage traces of the biotite. Leucoxene forms partial to complete pseudomorphs after sphene, and, together with hematite, coats grains of magnetite-ilmenite.

The gneiss is characterized by a predominately granoblastic texture and a metamorphic foliation expressed by a weakly to moderately well developed preferred planar orientation of biotite and hornblende. As shown in figure 4*B*, the granoblastic fabric has been modified by cataclastic granulation that produced mortar trains of fine-grained minerals. The complexly interlocking borders between quartz and feldspar grains in these mortar trains suggest that recrystallization occurred during cataclasis.

Pegmatite forms about 10 percent of the drill core. The average grain size is about 1.5 mm, but plagioclase grains are as much as 7 mm across. Large grains of albite and oligoclase and somewhat smaller grains of quartz are the principal constituents. Minor minerals are microcline (most commonly as antiperthitic intergrowths in plagioclase), biotite, hornblende, apatite, and zircon. The pegmatite owes its pale-reddish color to finely crystalline hematite that occurs along minute fractures and as disseminated "dust." Mortar trains generally do not occur in the pegmatite.

Well cuttings

Cuttings from the Precambrian section above and below the cored interval (fig. 2) consist of angular

fragments, generally 0.5 to 5 mm across, of Precambrian rocks and younger strata, particularly the Fountain Formation. Material from Precambrian rocks in the interval 11,935–11,976 feet makes up 30–50 percent of the cuttings, whereas in the interval 11,985–12,045 feet it increases in abundance to as much as 70 percent.

The Precambrian constituents in the cuttings include many biotite-bearing quartzofeldspathic grains that probably are fragments of gneiss similar to that of the core. Also present are abundant grains—probably from the gneiss—of quartz, feldspar, and biotite. Much of the feldspar is reddish, but some grains from the lowest 5-foot interval drilled are transparent. A few muscovite books 3 mm across and feldspar fragments 8 mm across suggest a pegmatite source.

Comparison with gneisses in the Front Range

The migmatitic hornblendic biotite-quartz-feldspar gneiss seems to be a variety gradational in composition between microcline gneiss and hornblende gneiss, two metasedimentary rocks that are common in the high-grade metamorphic terrane of the east-central Front Range west of Denver. Although similar in general composition to microcline gneiss, the gneiss of the drill core is somewhat more mafic and contains more hornblende and less microcline than most of the specimens of microcline gneiss described by Sims and Gable (1964, p C11) and Moench (1964, p. A22–A23). The presence of noteworthy amounts of hornblende, sphene, apatite, and metamorphic calcite suggests a gradation in composition toward that of hornblende gneiss in which minerals are more typical.

The granoblastic texture and the foliation by planar orientation of biotite and hornblende in the cored rock are identical with textural features of metasedimentary gneisses in the east-central Front Range. In that area this fabric is interpreted to be the result of relatively early Precambrian plastic deformation accompanied by metamorphism to a grade generally equivalent to the sillimanite zone of regional metamorphism. The superimposed mortar trains in the gneiss of the drill core produce a fabric found in the Front Range (Wells and others, 1964, p. O15–O16) in rocks cataclastically sheared during a Precambrian deformation probably considerably younger than the events that developed the granoblastic texture.

WEATHERED ZONE ON THE PRECAMBRIAN GNEISS

We believe that a weathered zone formed on the Precambrian gneiss prior to deposition of the overlying Paleozoic sedimentary rocks. This zone probably extends from the top of the Precambrian interval at 11,935 feet down to about 11,970 feet, below which the gneiss is relatively fresh. Our conclusion that the top of the weathered zone occurs at 11,935 feet differs from the 11,950-foot position reported by Scopel (1964, p. 40) for the unconformity on the top of the Precambrian section.

Evidence for the weathered zone is based in part on the presence of abundant soft green micaceous material of waxy appearance in the cuttings from the upper part of the Precambrian interval. This material is absent above the Precambrian section but makes up perhaps 50 percent of the Precambrian fragments in the interval 11,935–11,970 feet, and it decreases in abundance markedly below a depth of 11,970 feet. Additional evidence for weathering of the gneiss is provided by some of the feldspar grains, which are altered to light-colored material in the uppermost part of the Precambrian section. With increasing depth, the amount of the altered feldspar decreases.

The greenish material was determined from X-ray analyses (made before and after treatment with ethylene glycol) to consist of 10–20 percent illite and 80–90 percent mixed-layer illite-montmorillionite. For simplicity this material is referred to here as illite-montmorillonite. Some of the illite-montmorillonite occurs in fragments of gneiss and has irregular and indistinct boundaries with the quartzofeldspathic minerals. These relations suggest an origin from alteration. Much of the illite-montmorillonite occurs in nearly pure masses that contain small amounts of biotite, commonly reddish brown or copper colored from hematite. This hematite probably formed from weathering of the biotite. Some of the biotite is fresh, as would be expected in rocks weathered incompletely. The possibility that the illite-montmorillonite might be glauconite was checked carefully by comparison with numerous samples of glauconite-bearing rock from Cambrian and Ordovician strata in Colorado. The habit and color of the illite-montmorillonite from the well is unlike that of glauconite in the younger strata.

We conclude that the illite-montmorillonite, altered feldspar, and hematitic biotite resulted from weathering of the Precambrian gneiss. Outcrops of weathered Precambrian rocks below the Fountain Formation in the Front Range are also reported to contain illite and mixed-layer illite-montmorillonite (Raup, 1966, p. 261).

OVERLYING PALEOZOIC SEDIMENTARY ROCKS

We believe that strata of the Fountain Formation of Pennsylvanian and Permian age directly overlie the unconformity at 11,935 feet at the top of the weathered zone of altered Precambrian gneiss. In an earlier

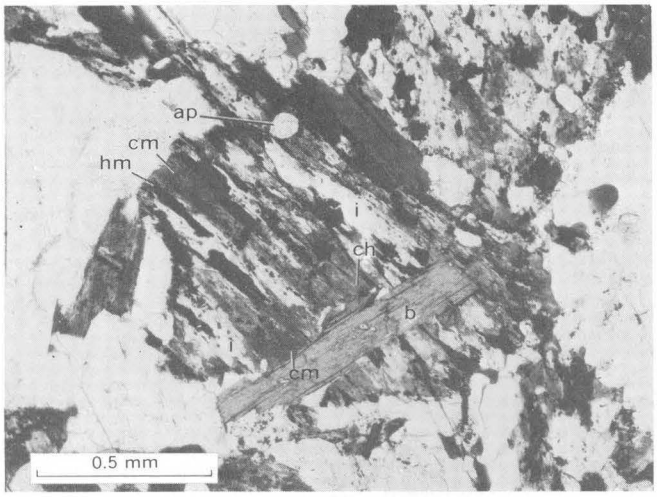

A

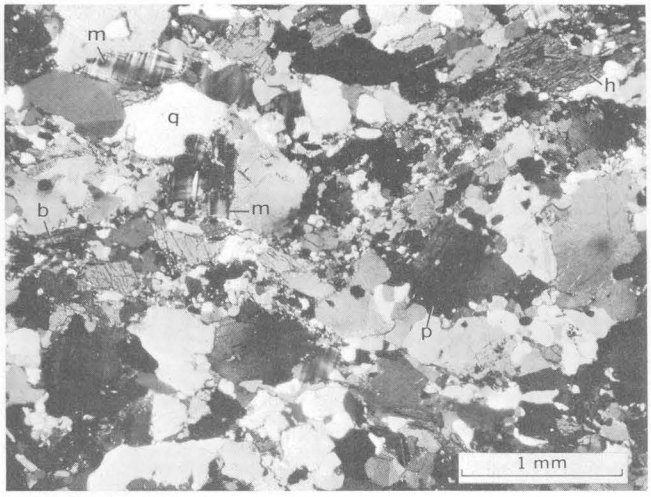

B

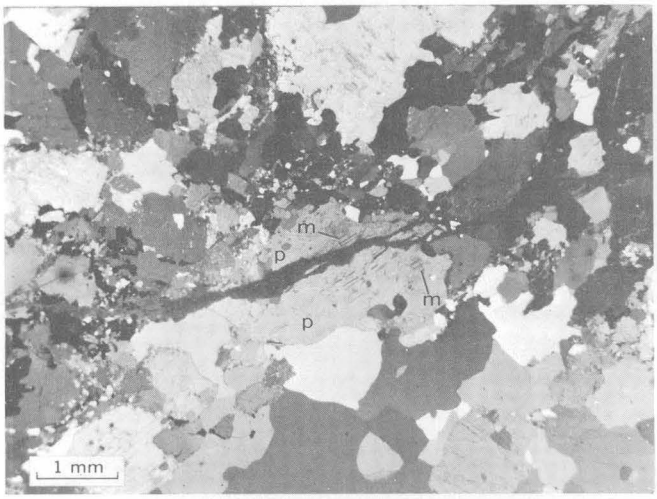

C

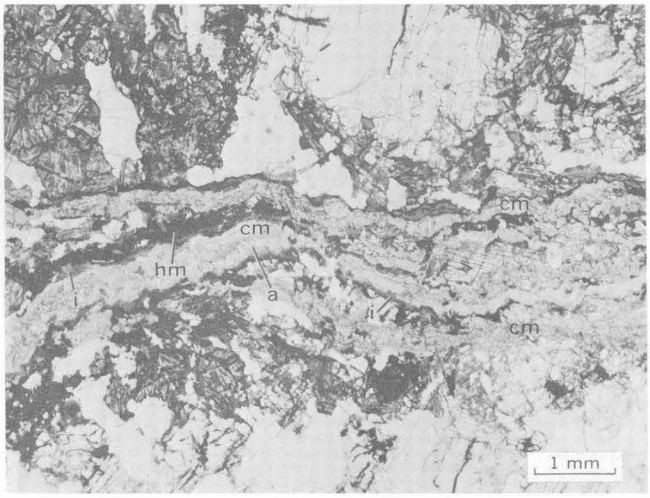

D

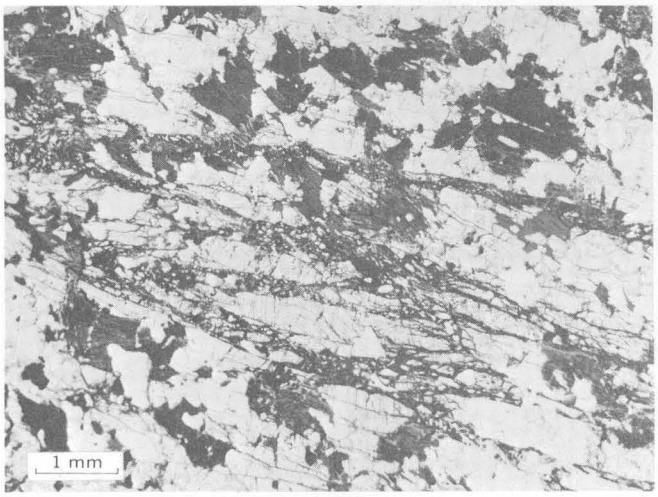

E

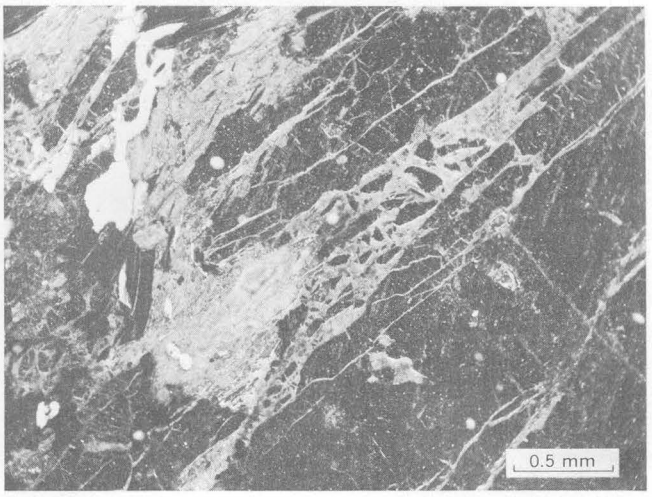

F

FIGURE 4.

study, Scopel (1964, p. 40–41) noted the presence of shale, dolomite, and conglomerate fragments in cuttings from the interval directly above the Precambrian rocks and concluded that these represent about 55 feet of strata of Cambrian(?) or Ordovician(?) age. However, we found dolomite fragments in every sample of cuttings from immediately above the Precambrian rocks to the stratigraphic horizons well within the Fountain Formation. Ellis (1966) described limestone and dolomite that occur in the usually arkosic lower part of the Fountain Formation about 35 miles south of Denver. Furthermore, Taylor (1958, fig. 4) reported that dolomite beds occur in the Fountain Formation in the northern Denver basin; he also noted (1958 p. 64) that the continental facies characteristic of mountain-front outcrops of the Fountain grades eastward over very short distances in the subsurface to marine facies. We believe that the dolomite fragments were derived from the marine facies of the Fountain rather than from Cambrian and Ordovician strata. Furthermore, the shale and conglomerate fragments that occur with the dolomite grains represent lithologies typical of the continental beds in the Fountain Formation.

Although Scopel (1964, p. 40) reported about 15 feet of regolith between his Cambrian and Ordovician section and the Fountain Formation, our study indicates that this interval (11,880–11,895 feet) is more probably a normal sequence of shaly mudstones from within the Fountain. We conclude that the only weathered zone is the one we have described as lying beneath the unconformity at the top of the Precambrian gneiss.

FIGURE 4.—Photomicrographs of gneiss from the Rocky Mountain Arsenal well (*A–E*, by W. N. Sharp; *F*, by R. B. Taylor).

A, Gneiss showing large blocky grain of hornblende completely altered to a complex intergrowth of illitic clay (i), fine-grained carbonate minerals (cm), and less abundant chlorite (ch) and hematite (hm), arranged approximately along former cleavage traces. Biotite (b) and apatite (ap) are fresh. Plane polarized light. Sample RMA–5.

B, Gneiss showing granoblastic fabric modified by cataclastic granulation that produced mortar trains of finely granulated minerals. Principal minerals are plagioclase (p), quartz (q), biotite (b), hornblende (h), and microcline (m). Crossed nicols. Sample RMA–1F.

C, Gneiss showing open fracture extending from left to right (thin section cut from specimen showing megascopic open fractures). Rounded to blocky patches of microcline (m) occur in large grains of plagioclase (p), forming antiperthite. Nicols partly crossed. Sample RMA–4.

D, Thin sinuous vein cutting gneiss. Bands of carbonate minerals (cm), illitic clay (i), hematite (hm), and anhydrite (a) are parallel to vein walls. Plane polarized light. Sample RMA–7.

E, Gneiss cut by branching and intersecting subparallel zones of microbreccia. Angular wallrock fragments making up the microbreccia are cemented by carbonate minerals, illitic clay, and hematite. Plane polarized light. Sample RMA–5.

F, Microbreccia in fractures cutting gneiss. Angular wallrock fragments making up the microbreccia are cemented by carbonate minerals, illitic clay, and hematite. Reflected light. Sample 11,988–95D.

FRACTURES, VEINS, AND MICROBRECCIA IN THE GNEISS

The gneiss in the drill core is cut by open fractures and by thin veins and zones of microbreccia. The open fractures have fairly smooth walls and show little or no displacement (fig. 4*C*). Commonly they parallel the core axis, indicating a vertical or nearly vertical attitude, but one dips as low as 20°. Some of the veins also cut the gneissic layering at large angles; other veins and the zones of microbreccia are subparallel to the layering. Individual veins are less than 3 mm thick. Some of them formed along simple fractures, whereas others were deposited along sinuous fractures that contained a few angular fragments of the host rock (fig. 4*D*). The microbreccia also occurs in single fractures, but more commonly it forms zones of branching and intersecting subparallel fractures (figs. 4*E*, 4*F*), each choked with abundant angular angular wallrock fragments cemented by vein minerals. The distribution of fractures, veins, and microbreccias in the core is not uniform: some thin sections contain many of these features and others none.

The principal vein minerals are calcite and ankerite, both identified from X-ray diffractometer patterns. Other vein minerals are illitic clay, anhydrite, and hematite. Although the X-ray analysis showed that ankerite and calcite occur in approximately equal amounts, the distinction between the two is difficult to make in thin section. The calcite probably forms relatively coarse grains that contain less hematite than the ankerite. Illitic clay forms an aggregate of very fine micaceous grains, colorless to pale brown in thin section, that are biaxial (—) and have a low $2V$ and a birefringence judged to be about 0.030–0.035. This material is thus optically similar to the conspicuous alteration product of hornblende in the gneiss. The anhydrite seems to be the latest of the vein minerals. One vein contains all these minerals arranged in bands parallel to the vein walls: bands of carbonate minerals alternate with discontinuous zones of illitic clay and hematite; the central zone contains anhydrite (fig. 4*D*). Variable amounts of hematite occur in the vein minerals and as coatings on the angular fragments of wallrock in the microbreccias.

The hornblende of the host gneiss is partly to completely altered (fig. 4*A*) in most thin sections that contain abundant microbreccia or thin veins. This alteration may have occurred during weathering of the Precambrian rocks or it may be hydrothermal in origin and possibly much younger than the weathered zone.

The microbreccias, veins, and fractures that cut the gneiss of the drill core are strikingly similar to structures found along and near the breccia-reef faults and fracture zones in the Precambrian of the Front Range

(Adams and Stugard, 1956, p. 194, 199). Along the eastern margin of the Front Range the Fountain Formation and the Permian Lyons Sandstone also are intensely fractured in the vicinity of southeastward continuations of breccia-reef faults and along related faults. Scopel (1964, p. 39–40) described the abundant fractures in the Lyons Sandstone and fractures in the upper third of the Fountain Formation, as cored in the well, and he noted that circulation was lost during drilling of these formations. It is also worth noting that an analysis of water obtained from the Precambrian rocks of the well before injection of wastes showed a high concentration of radium (U.S. Geological Survey, Water Resources Division, open-file analysis, laboratory No. 4668, Denver, Colo.). This abnormal amount of radium suggests a possible derivation from pitchblende, which is common in vein deposits associated with breccia-reef faults in the east-central part of the Front Range (Sims and Sheridan, 1964, p. 85).

Breccia-reef faults and fracture zones in the Front Range (fig. 1) commonly trend about N. 30° W. and dip steeply, generally to the northeast, but branching faults of other trends and variable dip are common in complexly faulted areas (Lovering and Goddard, 1950, pls. 1 and 2; Wells, 1963). Tweto and Sims (1963, p. 1001) noted that the breccia-reef faults range from single fractures through complex fault zones to broad granulated zones; they also give evidence indicating that these faults were first active in Precambrian time but that complex movements occurred along them again during the Laramide orogeny. Open spaces are today abundant in veins that occur along breccia-reef faults (Sims and Sheridan, 1964, p. 24). Apparent vertical or horizontal displacements along the faults are as much as hundreds of feet, but in many areas no offset is evident.

Although none of the Precambrian core available for this study is megascopically as strongly brecciated as the material found within Front Range fault zones, the similarity between many features of the microbreccias in the gneiss at the Rocky Mountain Arsenal well and the breccia reefs seems clear. However, a seismic-reflection study reported by Healy and Hoover (1967) provided ". . . no indication of any faulting very near the well." In our opinion, though, the seismic method would not readily detect the presence of a steep fault if the vertical offset were small or if the offset were dominantly strike-slip. Moreover, we believe that the petrographic indications of fracturing cannot be ignored. The microbreccias in the Precambrian rocks and the fractures in the Lyons Sandstone and the upper third of the Fountain Formation do exist, and they suggest that a fault or fracture zone may occur in the general vicinity of the well at the Rocky Mountain Arsenal.

REFERENCES

Adams, J. W., and Stugard, Frederick, Jr., 1956, Wall-rock control of certain pitchblende deposits in Golden Gate Canyon, Jefferson County, Colorado: U.S. Geol. Survey Bull. 1030–G, p. 187–209.

Edwards, Jonathan, Jr., 1966, The petrology and structure of the buried Precambrian basement of Colorado: Colorado School Mines Quart., v. 61, no. 4, 436 p.

Ellis, C. H., 1966, Paleontologic age of the Fountain Formation south of Denver, Colorado: The Mountain Geologist, v. 3, no. 4, p. 155–160.

Evans, D. M., 1966a, The Denver area earthquakes and the Rocky Mountain arsenal disposal well: The Mountain Geologist, v. 3, no. 1, p. 23–36.

———1966b, Man-made earthquakes in Denver: Geotimes, v. 10, no. 9, p. 11–18.

Healy, J. H., and Hoover, D. B., 1967, Microearthquakes near the Rocky Mountain Arsenal well, Denver, Colorado [abs.]: Geol. Soc. America Rocky Mtn. Sec. Mtg. 1967, Golden, Colo., Program p. 38.

Hedge, C. E., 1967, The age of the gneiss at the bottom of the Rocky Mountain Arsenal well: The Mountain Geologist, v. 4, no. 3, p. 115–117.

Lovering, T. S., and Goddard, E. N., 1950, Geology and ore deposits of the Front Range, Colorado: U.S. Geol. Survey Prof. Paper 223, 319 p.

Moench, R. H., 1964, Geology of Precambrian rocks, Idaho Springs district, Colorado: U.S. Geol. Survey Bull. 1182–A., p. A1–A70,

Raup, O. B., 1966, Clay mineralogy of Pennsylvanian redbeds and associated rocks flanking ancestral Front Range of central Colorado: Am. Assoc. Petroleum Geologists Bull., v. 50, no. 2, p. 251–268.

Scopel, L. J., 1964, Pressure injection disposal well, Rocky Mountain Arsenal, Denver, Colorado: The Mountain Geologist, v. 1, no. 1, p. 35–42.

Sheridan, D. M., Wrucke, C. T., and Wilcox, R. E., 1966, Petrography of the Precambrian rocks from the deep disposal well, Rocky Mountain Arsenal, Adams County, Colorado, *in* Healy, J. H., and others, Geophysical and geological investigations relating to earthquakes in the Denver area, Colorado: U.S. Geo. Survey open-file report, pt. 4, 17 p.

Sims, P. K., and Gable, D. J., 1964, Geology of Precambrian rocks, Central City district, Colorado: U.S. Geol. Survey Prof. Paper 474–C, p. C1–C52.

Sims, P. K., and Sheridan, D. M., 1964, Geology of uranium deposits in the Front Range, Colorado, *with sections by* R. U. King, F. B. Moore, D. H. Richter, and J. D. Schlottmann: U.S. Geol. Survey Bull. 1159, 116 p.

Taylor, J. R., 1958, Pennsylvanian stratigraphy and history of northern Denver basin, *in* Rocky Mtn. Assoc. Geologists, Symposium on Pennsylvanian rocks of Colorado and adjacent areas, 1958: p. 64–68.

Tweto, Ogden, and Sims, P. K., 1963, Precambrian ancestry of the Colorado Mineral Belt: Geol. Soc. America Bull., v. 74, no. 8, p. 991–1014.

Wells, J. D., 1963, Preliminary geologic map of the Eldorado Springs quadrangle, Boulder and Jefferson Counties, Colorado: U.S. Geol. Survey Misc. Geol. Inv. Map I–383.

Wells, J. D., Sheridan, D. M., and Albee, A. L., 1964, Relationship of Precambrian quartzite-schist sequence along Coal Creek to Idaho Springs Formation, Front Range, Colorado: U.S. Geol. Survey Prof. Paper 454–O, p. O1–O25.

285–544 O—68——5

LOCALIZATION AND CONTROL OF URANIUM DEPOSITS IN THE SOUTHERN SAN JUAN BASIN MINERAL BELT, NEW MEXICO—AN HYPOTHESIS

By HARRY C. GRANGER, Denver, Colo.

Abstract.—The Morrison Formation of Late Jurassic age contains primary uranium deposits along the southern margin of the San Juan basin in a belt at least 80 miles long and generally less than 10 miles wide. All known deposits seem to be directly beneath or closely downdip from areas where the structurally uptilted edges of the Morrison sandstones were exposed at the paleosurface by Early Cretaceous erosion. The primary deposits are coextensive with a carbonaceous residue that was presumably derived by solution from decaying vegetal matter, much of which was later incorporated into the Dakota Sandstone of Early(?) and Late Cretaceous age. It is speculated that soluble carbonaceous material was carried downward into the exposed Morrison sandstones by meteoric water and precipitated at the water table. The mineral belt is therefore defined by the intersection of the paleo-ground-water table, which was periodically fluctuating, and the uptilted Morrison aquifers. Because of the probability that the carbonaceous material was not coprecipitated with the uranium but later accumulated uranium from ore-bearing solutions which permeated the rocks, the position of the carbonaceous residue constitutes a primary control of ore.

The southern San Juan basin mineral belt, also known as the Grants mineral belt (Kelley, 1963), contains the greatest concentration of uranium ore known in the United States. Four mining districts—Laguna, Ambrosia Lake, Smith Lake, and Churchrock—lie within a curvilinear belt (fig. 1) known to be about 80 miles long and generally less than 10 miles wide; continuity of the belt is shown by sporadic subeconomic deposits in the intervals between mining areas. Most of the ore in this belt is in sandstones of the Morrison Formation of Jurassic age.

Why does ore occur in this apparently well-defined belt? What is unique about the areal geology that resulted in such unique deposits? Can another geologically similar mineral belt be found that will rival the Southern San Juan belt? This paper is intended to present at least partial answers to these questions and to offer guidelines for further speculation.

Only the uranium deposits in the Morrison Formation are considered in this hypothesis. The many smaller deposits in the underlying Todilto Limestone of Jurassic age (McLaughlin, 1963; Gabelman, 1956) and the few deposits in the overlying Dakota Sandstone of Cretaceous age (Gabelman, 1956) are regarded as genetically distinct, in mineralogy, local ore controls, and lead-uranium ratios (Granger, 1963; Miller and Kulp, 1963; L. S. Hilpert, written commun., 1966). The possibility that Morrison ores are directly related to ores in other rocks is tentatively dismissed.

Geologic studies by Rapaport and others (1952), Craig and others (1955), and Moench and Schlee (1967) contributed much of the fundamental information on which this hypothesis is based. The hypothesis is an outgrowth of studies of the uranium deposits in the Ambrosia Lake district, during which time I was assisted by E. S. Santos.

STRATIGRAPHY

Morrison Formation

The Morrison Formation in New Mexico is a continental fluvial sequence that is part of an assemblage of Jurassic sedimentary rocks ranging from limestones and evaporites to sandstones and mudstones. The salient features—particularly those that may apply to ore deposition—are summarized below from studies by Rapaport and others (1952), Craig and others (1955), Freeman and Hilpert (1956), Granger and others (1961), Santos (1963), Hilpert (1963), and Moench and Schlee (1967).

In the mineral belt, the Morrison Formation (figs. 1, 2) comprises three principal members in ascending

U.S. GEOL. SURVEY PROF. PAPER 600-B, PAGES B60-B70

order the Recapture Shale, Westwater Canyon Sandstone, and Brushy Basin Shale Members. Except for a few small subeconomic deposits, all the known uranium deposits in the Morrison within the belt are in the Westwater Canyon or in an extensive channel sandstone—the Jackpile sandstone of economic usage—in the upper part of the Brushy Basin.

Recapture Shale Member

The Recapture Shale Member seems to have been deposited as a broad alluvial fan (fig. 3) by generally northward-flowing streams from a source area south of Gallup, N. Mex. North and east of Gallup is a lobate area occupied by the conglomeratic sandstone facies. The abundance of pebbles diminishes radially from the conglomeratic sandstone facies leaving a zone characterized largely by sandstones. The sandstone facies, in turn, grades northward and eastward into a broad arcuate zone of finer grained detritus that Craig and others (1955) called the claystone and sandstone facies.

The thickest sections of Recapture—as much as 680 feet—are in northeastern Arizona. In New Mexico some of the thickest sections are in the conglomeratic sandstone facies north of Gallup, and generally the member thins eastward as well as northward toward the toe of the fan and southward toward the source area. Thicknesses are 300–400 feet north of Gallup, 137–232 feet in the Ambrosia Lake area, and less than 50 feet in the Laguna area.

Westwater Canyon Sandstone Member

The Westwater Canyon Sandstone Member is for the most part conformable with the underlying Recapture. The contact is typically sharp and planar although locally either intertonguing or scour-and-fill relations can be seen. Craig and others (1955, p. 156, 157) stated that "facies distribution of the Westwater Canyon member indicates a major source south of Gallup, probably in west-central New Mexico [and] * * * that it formed as a broad fan-shaped alluvial plain or 'fan' * * * It was formed by an alluviating distributary system of braided channels and represents essentially a continuation of Recapture deposition." Craig and others defined a large lobate area of conglomeratic sandstone facies, surrounding Gallup (fig. 4), in which there is a central area characterized by sparse pebbles up to 4 inches across and a peripheral area with scattered pebbles up to 1 inch across. A sandstone facies occupies a broad arcuate zone which borders the conglomeratic sandstone facies on all sides but the south; this facies has fewer pebbles but more interbedded mudstone and mudstone conglomerate units than the conglomeratic sandstone facies.

Craig and others (1955) reported a maximum of 330 feet of Westwater Canyon about 30 miles north of Gallup. From this area the Westwater Canyon seems generally to thin in all directions. In the Ambrosia Lake area as much as 270 feet has been recorded, although this thickness probably includes beds equivalent to the Poison Canyon sandstone of economic usage, a local tongue of sandstone extending from the upper part of the Westwater Canyon into the lower part of the Brushy Basin (fig. 2, section *B–B′*). As little as 18 feet of Westwater Canyon has been measured a few miles east of Grants, and about 8 miles southeast of Grants the Westwater Canyon and underlying Recapture both wedge out depositionally.

In the Laguna district the Westwater Canyon Member is typically lenticular and locally missing. It is ordinarily less than 50 feet thick, although more than 100 feet is present on the northeast side of the district (Moench and Schlee, 1967). The member is probably continuous along the north side, but becomes thin and discontinuous to the south and southwest.

Depositional trends reflected by such features as crossbedding, current lineations, and orientation of fossil logs suggest streams flowing northeastward in the Gallup area in Westwater Canyon time. Filling and choking of these channels probably caused braided, perhaps ephemeral distributaries to spill laterally off the flanks of the fan and resulted in southeasterly and easterly depositional trends in the Ambrosia Lake and Laguna areas. By late Westwater Canyon time the distributary fan had broadened so that many of the depositional trends measured in the upper part of the Westwater Canyon in the Ambrosia Lake area are northeasterly. Individual paleochannels lack continuity because of extensive cut-and-fill processes at the time of sedimentation, but the gross transmissivity of the member probably is greatest in the directions of the depositional trends.

At the outcrop most sandstones of the Westwater Canyon are stained various shades of orange, red, and yellow by iron oxides. The primary ore deposits, however, are surrounded by pyritic light-gray to nearly white sandstones which typically weather at the surface to pale shades of orange and yellow. Opinions regarding the original or early postdepositional color of the sandstones are controversial. It is my belief that most sandstones of the Westwater Canyon in the area under discussion were diagenetically bleached from original drab colors to light gray as the available iron was reduced to sulfide minerals by the activity of sulfate-reducing bacteria shortly after deposition. Within

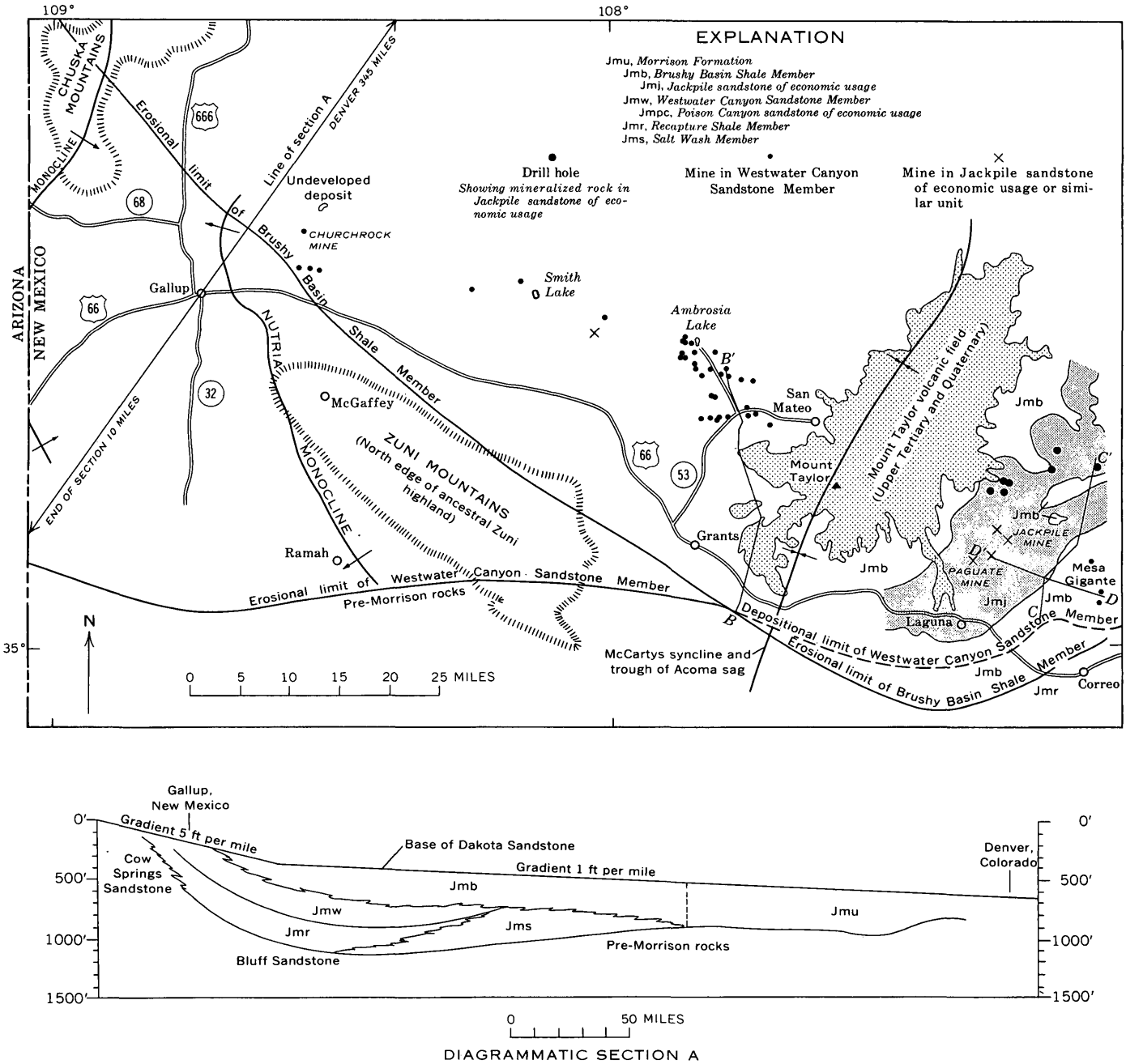

DIAGRAMMATIC SECTION A

FIGURE 1.—Area of southern San Juan basin mineral belt, showing southern limits of the Brushy Basin Shale and Westwater Canyon Sandstone Members of the Morrison Formation in pre-Dakota time, and some later geologic features. The limit of the Westwater Canyon Member in the region south of Gallup is adapted from Craig and others (1955), although Rapaport and others (1952) show the Morrison Formation to be missing 5 miles west of McGaffey and 4½ miles northeast of Ramah. Diagrammatic section A is based on data from Craig and others (1955) and Craig (oral commun., 1967); gradient of the base of the Dakota Sandstone is arbitrarily assumed.

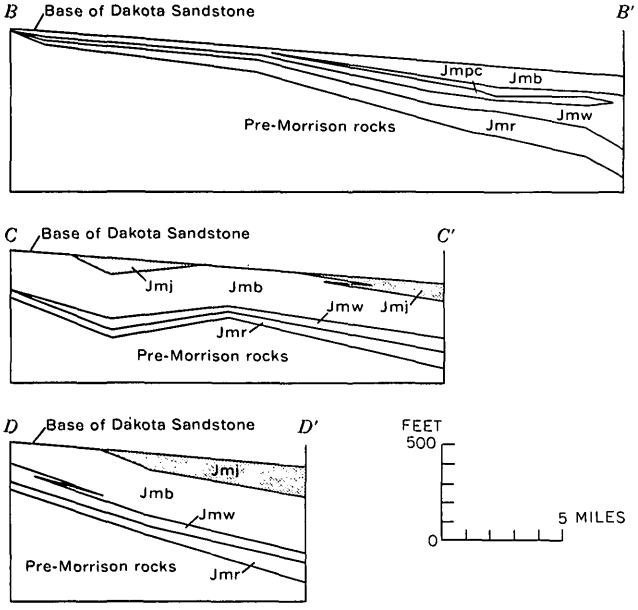

FIGURE 2.—Sections of the Morrison Formation, showing thinning toward the southern edge of San Juan basin. Gradient of the base of the Dakota Sandstone is assumed for diagrammatic purposes to be 10 feet per mile. Section *B–B'* based on private company drilling data and sections measured for this report. Sections *C–C'* and *D–D'* adapted from Moench and Schlee (1967). Line of sections shown on figure 1.

these bleached, reduced rocks the primary ore deposits were formed. The colors of the oxidized rocks (Granger and others, 1961) are largely more recent phenomena related both to surficial weathering and to deep oxidation, which caused partial removal of many of the primary uranium deposits.

Brushy Basin Shale Member

The Brushy Basin Shale Member, a sheet of irregular thickness, overlies the Westwater Canyon throughout its area of deposition except near the apex of the Westwater Canyon fan and sporadically to the southeast along the margin of the Westwater Canyon deposition (figs. 4, 5). The Brushy Basin intertongues so extensively with the top of the Westwater Canyon that the contact must be drawn arbitrarily in many places. Whereas the Westwater Canyon is predominantly sandstone with many thin discontinuous montmorillonitic mudstone and mudstone conglomerate units, the Brushy Basin is predominantly a montmorillonitic mudstone with scattered discontinuous lenticular channel sandstones.

Along the southern edge of outcrops in the San Juan basin the Brushy Basin is typically somewhat less than 100 feet thick, but in the Laguna area it is as much as 370 feet thick. Evidently a northerly trending synclinal warp was forming in this area during Brushy Basin deposition (Moench and Schlee, 1967), so that either a greater thickness of Brushy Basin was deposited or it was preserved from the widespread pre-Dakota erosion.

A channel sand known as the Jackpile sandstone (fig. 1) was deposited in this downwarped zone in the upper part of the Brushy Basin. The unit is as much as 13 miles wide, 200 feet thick, and more than 33 miles long, and is directly overlain by the Dakota. The upper part of the sandstone is white and kaolinite-rich and the lower part is yellowish gray to very pale orange. Contemporaneity between deposition of the Jackpile sandstone and the Brushy Basin mudstones is indicated by interfingering relations.

The Jackpile sandstone contains extensive primary uranium ore bodies similar to those in the Westwater Canyon Member. A few small isolated uranium ore

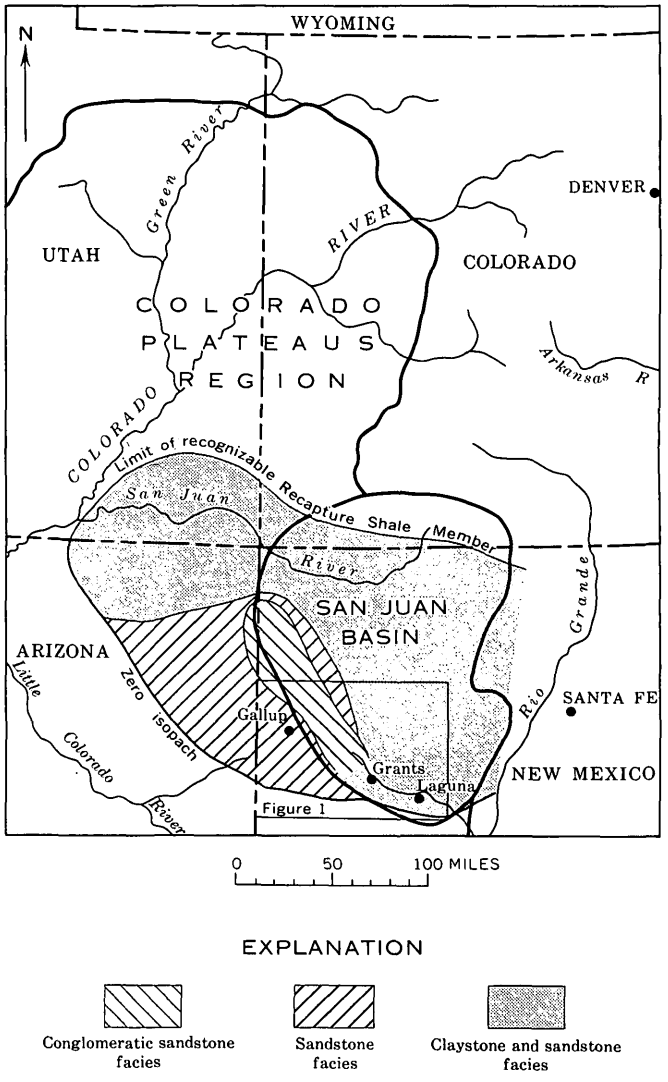

FIGURE 3.—Area of deposition of the Recapture Shale Member of the Morrison Formation, showing facies relations. Adapted from Craig and others (1955).

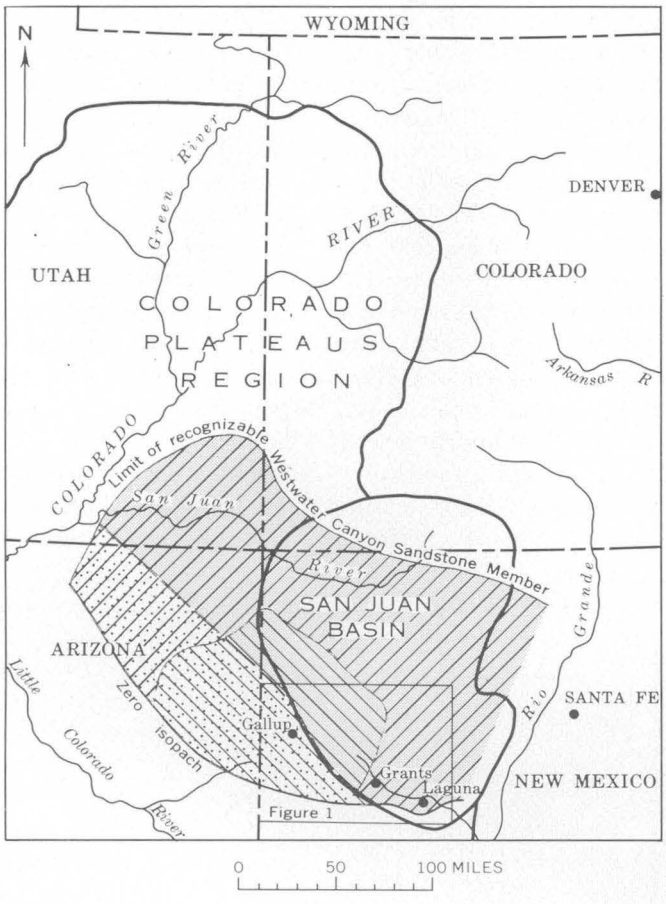

FIGURE 4.—Area of deposition of the Westwater Canyon Sandstone Member of the Morrison Formation, showing facies relations and area of exposure in pre-Dakota time. Adapted from Craig and others (1955).

bodies are also known in other smaller sandstone units in the Brushy Basin between Ambrosia Lake and Gallup; most are in lenses whose upper parts were truncated by pre-Dakota erosion.

Dakota Sandstone

The Dakota Sandstone, of Early(?) and Late Cretaceous age, disconformably overlies the Morrison Formation in the vicinity of the mineral belt and older rocks farther to the south. It is largely a series of massive sandstone units but typically contains carbonaceous shales and silty sandstones as well as thin coaly seams near the base. In the Gallup area Dane and Bachman (1957) described it as a transgressive assemblage of fluvial, lagoonal, and offshore marine deposits. Hilpert (1963) summarized the Dakota as "an accumulation of near-shore continental deposits that were laid down by streams and in swamps during and following a long period of erosion and weathering which must have lasted * * * throughout most of Early Cretaceous time."

Rocks just beneath the Dakota are typically kaolinized (Leopold, 1943; Granger, 1962; Moench and Schlee, 1967) in a layer a few inches to at least 100 feet thick. Permeable feldspathic sandstones such as the Westwater Canyon and Jackpile are most altered, whereas impermeable mudstones such as the Brushy Basin are commonly little affected. Since this kaolinized layer occurs beneath the Dakota regardless of the rock on which it rests, the kaolinization presumably was related to a soil zone (Leopold, 1943) or to humic acids generated under swampy conditions (Young, 1957; Granger, 1962) at the eroded pre-Dakota surface.

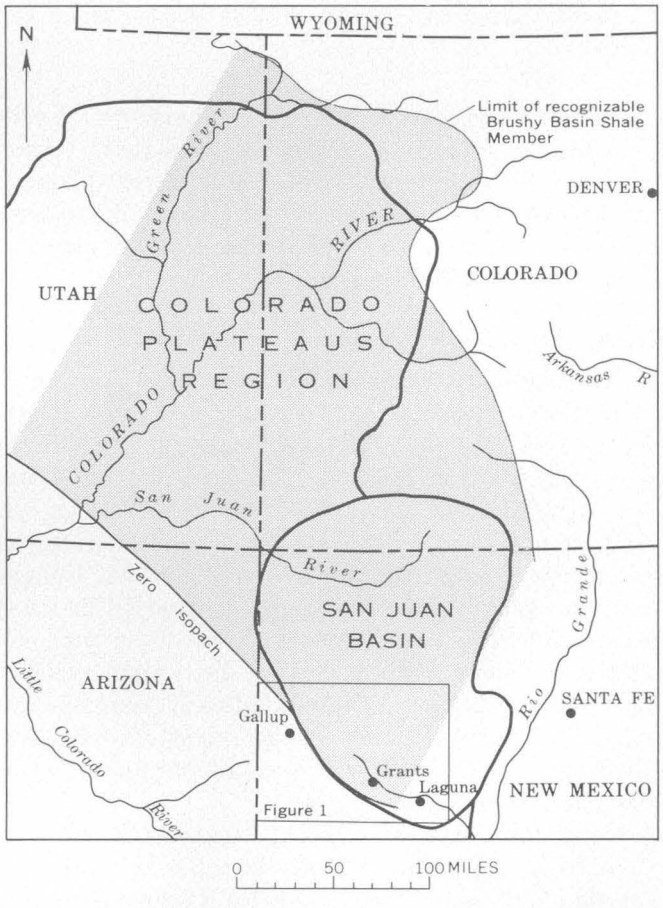

FIGURE 5.—Area (stippled) of deposition of the Brushy Basin Shale Member of the Morrison Formation. Adapted from Craig and others (1955).

Southern margin of the Morrison Formation

All members of the Morrison thin and terminate to the south (fig. 1) along the northern margin of the ancestral Zuni highland (Rapaport and others, 1952). This resulted from three different mechanisms in various places: (1) Depositional thinning and lapping onto the highland, (2) interfingering with windblown and other fluvial units, and (3) truncation at the pre-Dakota erosion surface.

The Recapture Member both thins depositionally and intertongues with the underlying eolian Cow Springs Sandstone south and west of Gallup (Craig and others, 1955). Southeast of Grants it wedges out mainly by depositional thinning. In the Laguna district (Moench and Schlee, 1967) it intertongues with the Bluff Sandstone and thins depositionally, but its complete removal to the south was largely by pre-Dakota erosion.

The Westwater Canyon Member is reported (Craig and others, 1955) to intertongue with the Cow Springs Sandstone south and west of Gallup but all along its southern margin it thins, principally by depositional lapping or by erosion. From some point south or southwest of Grants through the Gallup area and northwestward into Arizona the Westwater Canyon was truncated by pre-Dakota erosion and the Dakota was deposited directly on this extensively exposed surface (figs. 1, 4). From the Grants area southeastward, however, the Westwater Canyon becomes thinner and more discontinuous depositionally and wedges out between the Recapture and Brushy Basin Members. If exposed to pre-Dakota erosion there, it was exposed only locally. East of the downwarp in which Jackpile sandstone was deposited, the Westwater Canyon may have been exposed prior to Dakota deposition. Fifteen miles east of Laguna, at point D on section D–D′ (fig. 2), the Westwater Canyon is about 90 feet thick. Unless it thinned abruptly to the east and southeast, the Westwater Canyon may have been exposed at the pre-Dakota surface in this area.

The thickness of the Brushy Basin Member was everywhere moderated by pre-Dakota erosion. The thickest sections in the southern San Juan basin region may have been protected in downwarps of Early Cretaceous age and, therefore, are probably related more to preservation in these structures than to differences in original deposition. Nevertheless, because the underlying members lapped onto the ancestral Zuni highland the Brushy Basin probably also lapped and thinned to the south. Subsequent pre-Dakota erosion further thinned the Brushy Basin and completely stripped it from the Westwater Canyon Member in a widespread area extending from near Grants northwestward through the Gallup area and into northeast Arizona.

All these relations indicate uplift and erosional planation along the southern edge of the ancestral San Juan basin between the end of Morrison deposition and the start of Dakota deposition. Much but not all of this erosion probably was done by northeasterly flowing streams before the incursion of Cretaceous seas—a continuation of the Jurassic drainage pattern intensified by uplift to the south. A picture emerges, therefore, of layered Jurassic rocks with a northerly regional dip somewhat steeper than the gradients of degrading streams. The steepest dips must have been near and immediately south of the mineral belt where the Dakota overlies successively older beds. To the north of the mineral belt the angular discordance between the pre-Dakota erosion surface and Morrison strata is extremely small.

ORE DEPOSITS

Nearly all investigators of the uranium ore in the mineral belt (Hilpert and Moench, 1960; Granger and others, 1961; Kelley, 1963; Moench and Schlee, 1967) emphasize that individual ore bodies are blanketlike and elongate parallel to the sedimentary trends of the enclosing units. Further, all the primary ore is coextensive with a carbonaceous residue that impregnates the sandstones.

All of this carbonaceous material has been mineralized to some extent with uranium and, conversely, no uranium of undisputably primary origin has been found away from carbonaceous material.

The carbonaceous residue coats sand grains, fills interstices, and locally fills openings in or replaces highly altered detrital grains. Chemical and infrared analyses (Granger and others, 1961; Moench and Schlee, 1967) indicate its similarity to coals and humic acids, prompting the conclusion that it is a residue from a water-soluble humate derived from decaying plant material. There is no convincing evidence that it is a petroleum residue or that it is closely related to hydrocarbons.

Extensive studies of naturally occurring humates have shown that their solubility is strongly dependent on pH and, in some instances, on metal cations in solution (for example, Swanson and Palacas, 1965). Humic acids, abundant naturally occurring varieties of the general family of humates, are readily dissolved or peptized in basic solutions and precipitated in acid solutions. The precipitate, upon drying, forms an amorphous dark-brown to black vitreous material very similar chemically, structurally, and in appearance to

the carbonaceous residue coextensive with ore in the mineral belt.

The carbonaceous residue with ore is not soluble in common acids, bases, or organic solvents and can be likened to coal which went through a gelatinous peat stage but has since solidified to a relatively insoluble mass largely through a process of aging. For the carbonaceous residue, radiation from disintegrating uranium and its daughter products may have produced alterations such as dehydrogenation which would further reduce its solubility.

Whether uranium was deposited concurrently with the carbonaceous material, or later, is unknown. Coalified limbs and trunks of fossil trees within the ore bodies are commonly richly uraniferous. The uranium is not necessarily uniformly distributed in this coaly material, but is localized either in fusain or vitrain zones or along microfractures. The original plant material could not have been highly uraniferous and the uranium presumably was introduced after coalification. Carbonaceous materials tend to create a reducing environment conducive to uranium precipitation, as well as being good adsorbents and partly capable of combining as urano-organic compounds and ligands. If the carbonaceous material accumulated first and was subsequently mineralized by uraniferous solutions—and probably even if uranium and carbonaceous material were deposited simultaneously—ore deposition was controlled largely by the presence of the carbonaceous material. The problem of localization of this material must be solved to determine the extent of the mineral belt and the possibility of similar deposits elsewhere.

Several investigators (Cronk, 1963; Squyres, 1963; Harmon and Taylor, 1963; Moench and Schlee, 1967) have noted the tendency for ore layers to rise stratigraphically to the north or northeast in a direction transverse to the trend of the mineral belt. Where the elongation of the ore bodies is subparallel to the trend of the mineral belt, the ore typically forms irregular monoclinal undulations or rolls, like a flattened "s", that cross the stratification. Although monoclinal rolls with the stratigraphically higher limb on the south side have been observed, there seem to be a greater number that rise to the north. Where the elongation of the ore bodies is transverse to the mineral belt, the ore tends to rise stratigraphically to the northeast in a more regular fashion without such prominent undulations.

This shifting of stratigraphic position suggests that the ore formed horizontal blankets irrespective of the local dip of the beds. For example, in the Laguna district the Jackpile and Paguate ore bodies are almost entirely within 200 feet below the base of the Dakota and seem to rise generally to the northeast until they touch or nearly touch the Dakota (Moench and Schlee, 1967). The only known ore in the Westwater Canyon Member in this district is along the east side of Mesa Gigante about 11 miles southeastward from the Paguate deposit and it is also within 200 feet of the base of the Dakota.

Along the south margin of the main band of deposits in the Ambrosia Lake district the entire Westwater Canyon Member is mineralized (Santos, 1963), although the thicker and richer deposits are in the upper half of the member. Along the north edge of this band almost all the ore is in the upper third of the Westwater Canyon. The band of deposits in the Poison Canyon sandstone along the south edge, however, is stratigraphically high—higher than much of the ore farther north—and contrasts with this general tendency of ore to rise stratigraphically to the north. This will be discussed later.

All evidence concerning the age of the uranium places primary ore deposition at an early stage in the history of the host rocks. All known faults, with the exception of ring faults around circular collapse structures (Granger and Santos, 1963; Moench and Schlee, 1967), displace the carbonaceous layers and therefore postdate them. Folds of pre-Dakota age appear locally to have controlled individual carbonaceous bodies, particularly in the Laguna district (Moench and Schlee, 1967), but folds which affect the Dakota and overlying formations show no such control. Evidence presented by Moench (1963) and Moench and Schlee (1967) indicates that carbonaceous material was deposited in the Jackpile sandstone prior to minor tilting of the rocks in Late Cretaceous or early Tertiary time, but after pre-Dakota folding of low amplitude and after certain pipelike collapse features had formed in the semiindurated rocks. Nash and Kerr (1966) have described a lens of high-grade carbonaceous ore in the Jackpile sandstone that was truncated by erosion at the base of a reworked unit immediately below the Dakota Sandstone. The probability that the carbonaceous material was uranium bearing prior to erosion is established by a private communication from W. Bergloff (Columbia University) to Nash and Kerr citing lead and uranium isotope data which suggest that the age of a coffinite sample from the Jackpile mine is 94 million years or older. Total lead-uranium ratios averaged from several integrated suites of ore samples in the Ambrosia Lake district indicate that the uranium there was deposited at least 100 million years ago (Granger, 1963).

The structural and stratigraphic relations can fix a probable range in age of deposition for the carbonaceous material, but not for the uranium, which could have been introduced later. The ages implied by the isotope and total lead-uranium ratios, however, suggest a minimum age for the carbonaceous material as well as fixing an approximate age for uranium mineralization. Several lines of evidence, therefore, suggest that both the carbonaceous material and uranium were deposited early in the history of the host rock, and there is little or no evidence to the contrary.

SOURCE OF THE CARBONACEOUS MATERIAL

Three sources for the carbonaceous material have been proposed (Granger and others, 1961):

(1) The "Dakota source hypothesis"—an extrinsic epigenetic source from decaying vegetation that contributed to the carbonaceous beds in the lower parts of the Dakota Sandstone. The Morrison Formation was directly overlain by a boggy, vegetated terrain prior to final reworking and Dakota deposition, and humic derivatives from the decaying vegetation were carried downward and laterally into sandstones of the Westwater Canyon and transported to regions where they were precipitated.

(2) The "syngenetic source hypothesis"—an extrinsic penecontemporaneous source from decaying vegetation along the streams that deposited the Westwater Canyon sediments. Humic materials derived from decaying vegetation along the stream courses were dissolved in the stream waters and underflow waters but were precipitated along an interface between underflow and more stagnant ground waters.

(3) The "internal source hypothesis"—an intrinsic diagenetic source from decaying vegetation that was deposited syngenetically with the Westwater Canyon Member. The carbonaceous material was derived from either decaying or petrifying plant materials that were deposited syngenetically with the host rocks. The dissolved humic materials then precipitated wherever they came in contact with precipitating agents.

It was further proposed in each hypothesis that freshly precipitated humic materials would be preserved in areas where they were encroached upon by the waters in which they were insoluble. If they were subsequently enveloped by waters in which they were soluble, on the other hand, they would be redissolved and transported to some other area where they might contact a precipitating environment.

The "Dakota source hypothesis" was considered to be the most probable (Granger and others, 1961) because of the abundant source materials for the soluble humic derivatives and because of the structural relations which would permit the solutions to flow downdip from the source to the vicinity of the deposits. Subsequent investigations of the ore deposits and regional geology have reinforced this conclusion.

SUMMARY AND CONCLUSIONS

The following significant points should be considered in hypothesizing an origin and controls of the ore deposits and in speculating on extensions of the mineral belt.

1. The mineral belt forms a curvilinear trend generally parallel to the southern edge of the ancestral San Juan basin.
2. The mineral belt is seemingly continuous where sandstones of the Morrison Formation are near enough to the surface to have been thoroughly explored.
3. Similar ore is localized both in the Westwater Canyon Member and in the Jackpile sandstone.
4. All ore is beneath or closely downdip from areas where the Dakota Sandstone was deposited directly on the host sandstones.
5. The ore was deposited early in the history of the host rock but after some induration and minor folding.
6. No recognizable structures such as folds or faults are continuous throughout the length of the mineral belt. Uplift at the southern margin of the San Juan basin, however, tended to parallel the mineral belt.
7. Although ore deposits tend to be elongate subparallel to sedimentary trends, they do not seem to extend beyond a relatively narrow elongate mineral belt, regardless of the local direction of the sedimentary trends.
8. Ore is in layers coextensive with an organic residue that was probably originally a water-soluble humate whose solubility was sensitive to changes in pH and concentration of certain metal cations.
9. The carbonaceous residue probably predated and controlled the localization of ore.
10. The ore has a marked tendency to rise stratigraphically in a basinward direction across the trend of the mineral belt.

Visualize now the southern margin of the San Juan basin prior to Dakota deposition. Abundant organic material in the lower part of the Dakota is evidence of boggy, swampy terrain. According to Maxey and Hackett (1963), this type of terrain exists where the underlying rocks are saturated; the swamp waters generally are fed, in part, from ground-water sources rather than contributing to them. The extensive kaolinization in arkosic sandstones immediately beneath

the Dakota, however, strongly suggests that solutions rich in organic acids *did* flow into the underlying rocks from these swampy regions, when the ground-water table was lowered enough to allow drainage from the swamps into the underlying rocks, perhaps during successive minor uplifts along the margin of the basin, or during interpluvial periods.

It is possible that these organically charged surface waters, percolating downdip, encountered conditions where the humates were precipitated. This might take place at the ground-water table or at a horizon where the pH or composition of the ground water changed from that of a humate solvent to a precipitant. In either circumstance this horizon or zone must have been gravity controlled, because the ore layers tend to rise stratigraphically northward but were probably roughly horizontal at the time of deposition. That is, toward the basin the horizons or zone at which the carbonaceous material was precipitated gradually passed upward across the bedding of the northward-dipping beds, as though maintaining a horizontal orientation. Although any one layer of carbonaceous material would rise irregularly to the north, other layers might form at other elevations at other times because of successive uplifts or climatic conditions that would affect the water table or horizon of precipitation. This could explain the stratigraphically high position of the deposits in the Poison Canyon sandstone along the southern margin of the mineral belt in the Ambrosia Lake area.

I prefer the hypothesis that the humate was precipitated at the water table because the humate was soluble in meteoric or vadose pore waters but not in the phreatic ground waters. The flow of vadose water generally could not have been directly downward through the many mudstone and other relatively impermeable layers but was largely lateral along perched water tables and primarily in the directions of the original distributary system. Humate originating in the area of Gallup might well have been transported through the distributary channel system as far east as the Ambrosia Lake area. Successive stages of precipitation and remobilization might have occurred along the way because of a fluctuating water table and interrupted periods of recharge of the vadose water. The Ambrosia Lake area could then have been the ultimate extent of this periodic migration—the sump at the end of the plumbing system. The humate in the Westwater Canyon in the Laguna area was probably more locally derived where the thin and lenticular Westwater Canyon was sparingly exposed at the pre-Dakota surface. Humate in the Jackpile sandstone could have been transported directly downward to the water table by percolating meteoric waters.

The margins formed by the intersection of a horizontal plane or relatively thin zone with the upper and lower surfaces of the Westwater Canyon prior to Dakota deposition would form the lateral limits of a belt subparallel to the margin of the basin. The width of the belt would depend on the thickness of the Westwater Canyon and the local dip of the strata; the position would depend upon the elevation of the plane. One such belt would almost certainly be approximately coincident with the presently known mineral belt. At Laguna, where the dip of strata along the margin of the basin steepened and the Westwater Canyon thinned, the belt of carbonaceous deposits in the Westwater Canyon Member narrowed; but here conditions in the Jackpile sandstone were similarly favorable for precipitation of the organic material Although the belt of deposits in the Westwater Canyon does not seem to widen in the Laguna area, the total belt is wider because of the deposits in the Jackpile sandstone. The Jackpile deposits might be viewed as another mineral belt, in a higher stratigraphic unit, farther north. The mineral belt may not faithfully parallel the zero isopach of the Brushy Basin Member, either because of the lateral changes of dip or because of pre-Dakota erosion subsequent to deposition of the carbonaceous material as reported by Nash and Kerr (1966).

The apparent lack of ore deposits in such permeable rocks as the Bluff Sandstone, which underlies the Morrison Formation, probably indicates (1) that conditions were not conducive for precipitation of carbonaceous material; or (2) that as yet undiscovered carbonaceous material was precipitated, but not mineralized with uranium; or (3) that deposits were formed south of the presently known mineral belt and have since been removed by erosion or have not yet been found.

There is no known reason why the mineral belt should not extend to the northwest in the Westwater Canyon Member across the Nutria monocline or north of the traceable limit of the monocline, but the favorable rocks are deeply buried and have not been thoroughly explored. The Westwater Canyon thins between the Ambrosia Lake area and the southern part of the Laguna area. Through much of this interval the rocks are involved in the Acoma sag, and the Westwater Canyon Member within the trend of the mineral belt is covered to great depth by both sedimentary and volcanic rocks. East of the Laguna district the Morrison Formation is downfaulted into the Rio Grande trough and covered by later rocks. Presumably, the

capacity of the Westwater Canyon to contain ore deposits is diminished to the southeast of the Laguna area but should not be completely ruled out.

This general hypothesis for emplacement of the carbonaceous residue and the width and continuity of the southern San Juan basin mineral belt seems to fit most of the known observations. The further question concerning the source of uranium is not within the scope of this paper. Nevertheless, worldwide occurrence of uranium deposits localized by a variety of local controls in continental fluvial sandstones suggests that uranium-bearing solutions were commonplace in those rocks at some period in their history. Determining the controlling features in such rocks may, therefore, be deemed much more important economically than knowing the source.

If the foregoing hypothesis is correct, the existence of a similar mineral belt basinward is improbable, because the humic material would not be likely to migrate downdip much beyond the water table or zone of precipitation. This would not eliminate the possibility of smaller deposits primarily localized around accumulations of detrital organic trash such as are common in the Uravan mineral belt and other areas farther north on the Colorado Plateau. Neither would it eliminate the possibility, indeed probability, of redistributed deposits formed from oxidative destruction of the primary deposits. From Ambrosia Lake westward a large proportion of the Westwater Canyon within the breadth of the mineral belt is strongly oxidized and, presumably, numerous primary ore deposits have been oxidized and removed. Secondary deposits, therefore, might occur downdip from the mineral belt at the distal ends of oxidized zones in much the same way that roll-type deposits occur in some of the Tertiary basins of Wyoming (Shawe and Granger, 1965). Such deposits are common in the Ambrosia Lake district, but all the presently known redistributed ore bodies are closely associated with their primary progenitors.

The geologic circumstances leading to formation of the deposits in the southern San Juan basin mineral belt are certainly not common, and exploration of the extensions of the presently known mineral belt may prove to be more successful than searching for a similar one.

Along the eastern margin of the San Juan basin, defined by the west edge of the Sierra Nacimiento, the Dakota Sandstone directly overlies a sandstone in the upper part of the Brushy Basin Member that is strikingly similar to the Jackpile sandstone. Much of this sandstone has the bleached appearance that is generally considered to be favorable for the occurrence of primary uranium deposits (D. G. Wyant, oral commun., 1967) and the overlying Dakota Sandstone contains beds rich in organic material. Small uranium deposits—perhaps secondary—in peaty beds in the Dakota have been briefly described by Gabelman (1956). Deduction of the hydrologic and structural relations prior to Dakota time would aid considerably in planning an efficient exploration program in this area.

The Salt Wash Member of the Morrison, which is not present in the area of the mineral belt, is lithologically and depositionally similar to the Westwater Canyon where it occurs farther to the north and northwest on the Colorado Plateau. Southwest of the Escalante River in Utah the Dakota Sandstone rests directly on the Salt Wash, and the general geologic relations show some similarity to those near the mineral belt, with the Salt Wash occupying the position of the Westwater Canyon Member. Results of prospecting the Salt Wash in this region during the late 1940's and 1950's were not encouraging but, perhaps, further efforts should be made.

REFERENCES

Craig, L. C., and others, 1955, Stratigraphy of the Morrison and related formations, Colorado Plateau region—a preliminary report: U.S. Geol. Survey Bull. 1009–E, p. 125–167.

Cronk, R. J., 1963, Geology of the Dysart No. 1 mine, Ambrosia Lake area, *in* Kelley, V. C., Ed., Geology and technology of the Grants uranium region: Soc. Econ. Geologists Mem. 15, New Mexico Bur. Mines and Mineral Resources, p. 60–65.

Dane, C. H., and Bachman, G. O., 1957, The Dakota Sandstone and Mancos Shale in the Gallup area [N. Mex.], in Four Corners Geol. Soc. Guidebook 2d Field Conf., Geology of Southwestern San Juan Basin: p. 95–98.

Freeman, V. L., and Hilpert, L. S., 1956, Stratigraphy of the Morrison formation in part of northwestern New Mexico: U.S. Geol. Survey Bull. 1030–J, p. 309–334.

Gabelman, J. W., 1956, Uranium deposits in paludal black shales of the Dakota Formation, San Juan Basin, New Mexico, *in* Page, L. R., Stocking, H. E., and Smith, H. B., compilers, Contributions to the geology of uranium and thorium by the United States Geological Survey and Atomic Energy Commission for the United Nations International Conference on Peaceful Uses of Atomic Energy, Geneva, Switzerland, 1955: U.S. Geol. Survey Prof. Paper 300, p. 303–319.

Granger, H. C., 1962, Clays in the Morrison Formation and their spatial relation to the uranium deposits at Ambrosia Lake, New Mexico: Art. 124 *in* U.S. Geol. Survey Prof. Paper 450–D, p. D15–D20.

———1963, Radium migration and its effect on the apparent age of uranium deposits at Ambrosia Lake, New Mexico: Art. 17 *in* U.S. Geol. Survey Prof. Paper 475–B, p. B60–B63.

Granger, H. C., Santos, E. S., Deane, B. G., and Moore, F. B., 1961, Sandstone-type uranium deposits at Ambrosia Lake, New Mexico—An interim report: Econ. Geology, v. 56, no. 7, p. 1179–1210.

Granger, H. C., and Santos, E. S., 1963, An ore-bearing cylindrical collapse structure in the Ambrosia Lake uranium district, New Mexico: Art. 100 *in* U.S. Geol. Survey Prof. Paper 475–C, p. C156–C161.

Harmon, G. F., and Taylor, P. S., 1963, Geology and ore deposits of the Cliffside mine, Ambrosia Lake area: *in* Kelly, V. C., ed., Geology and technology of the Grants uranium region: Soc. Econ. Geologists Mem. 15, New Mexico Bur. Mines and Mineral Resources, p. 108–116.

Hilpert, L. S., 1963, Regional and local stratigraphy of uranium-bearing rocks: *in* Kelley, V. C., ed., Geology and technology of the Grants uranium region: Soc. Econ. Geologists Mem. 15, New Mexico Bur. Mines and Mineral Resources, p. 6–18.

Hilpert, L. S., and Moench, R. H., 1960, Uranium deposits of the southern part of the San Juan Basin, New Mexico: Econ. Geology, v. 55, no. 3, p. 429–464.

Kelley, V. C., ed., 1963, Geology and technology of the Grants uranium region: Soc. Econ. Geologists Mem. 15, New Mexico Bur. Mines and Mineral Resources, 277 p.

Leopold, L. B., 1943, Climatic character of the interval between the Jurassic and Cretaceous in New Mexico and Arizona: Jour. Geology, v. 51, no. 1, p. 195–201.

Maxey, G. B., and Hackett, J. E., 1963, Applications of geohydrologic concepts in geology: Jour. Hydrology, v. 1, no. 1, p. 35–45.

McLaughlin, E. D., Jr., 1963, Uranium deposits in the Todilto Limestone of the Grants district, *in* Kelley, V. C., ed., Geology and technology of the Grants uranium region: Soc. Econ. Geologists Mem. 15, New Mexico Bur. Mines and Mineral Resources, p. 136–149.

Miller, D. S., and Kulp, J. L., 1963, Isotopic evidence on the origin of the Colorado Plateau uranium ores: Geol. Soc. America Bull., v. 74, p. 609–630.

Moench, R. H., 1963, Geologic limitations on the age of uranium deposits in the Laguna district, *in* Kelley, V. C., ed., Geology and technology of the Grants uranium region: Soc. Econ. Geologists Mem. 15, New Mexico Bur. Mines and Mineral Resources, p. 157–166.

Moench, R. H., and Schlee, J. S., 1967, Geology and uranium deposits of the Laguna district, New Mexico: U.S. Geol. Survey Prof. Paper 519, 117 p.

Nash, J. T., and Kerr, P. F., 1966, Geologic limitations on the age of uranium deposits in the Jackpile sandstone, New Mexico: Econ. Geology, v. 61, no. 7, p. 1283–1287.

Rapaport, Irving, and others, 1952, Jurassic rocks of the Zuni uplift, New Mexico: U.S. Atomic Energy Comm. RMO–642, issued by the U.S. Atomic Energy Comm. Office of Tech. Inf. Extension, Oak Ridge, Tenn.

Santos, E. S., 1963, Relation of ore deposits to the stratigraphy of the Ambrosia Lake area, *in* Kelley, V. C., ed., Geology and technology of the Grants uranium region: Soc. Econ. Geologists Mem. 15, New Mexico Bur. Mines and Mineral Resources, p. 53–59.

Shawe, D. R., and Granger, H. C., 1964, Uranium ore rolls—An analysis: Econ. Geology, v. 60, no. 2, p. 240–250.

Squyres, J. B., 1963, Geology and ore deposits of the Ann Lee mine, Ambrosia Lake area, *in* Kelley, V. C., ed., Geology and technology of the Grants uranium region: Soc. Econ. Geologists Mem. 15, New Mexico Bur. Mines and Mineral Resources, p. 90–101.

Swanson, V. E., and Palacas, J. G., 1965, Humate in coastal sands of northwest Florida: U.S. Geol. Survey Bull. 1214–B, p. B1–B29.

Young, R. G., 1957, Late Cretaceous cyclic deposits, Book Cliffs, eastern Utah: Am. Assoc. Petroleum Geologists Bull., v. 41, no. 8, p. 1760–1774.

RADIOELEMENT COMPOSITION OF SURFACE SOIL IN ADAMS COUNTY, COLORADO

By CARL M. BUNKER and CHARLES A. BUSH,
Denver, Colo.

Abstract.—Eighty-three samples collected from the Bennett, Manila, Horse Creek, and Sunnydale 7½-minute quadrangle areas near Denver, Colo., were analyzed to determine the radioelement content and distribution. The radioelement concentrations are: 7.7 to 19.0 ppm thorium, 0.7 to 3.3 ppm radium-equivalent uranium, and 2.07 to 3.75 percent potassium. These data provide ground control for a proposed calibration of the U.S. Geological Survey's airborne gamma-radiation detection systems.

Four adjacent 7½-minute quadrangle areas (Bennett, Manila, Horse Creek, and Sunnydale) in Adams County about 30 miles east of Denver, Colo. (fig. 1), are being used to test and evaluate instrumentation systems and data-acquisition techniques of the U.S. Geological Survey's airborne geophysical laboratory. The airborne instruments include a gamma-ray detection system for obtaining measurements of total-gamma radiation and gamma-ray spectra from which individual radioisotopes can be identified. Semiquantitative isotopic data can be obtained with the airborne system if the intensities of the spectral lines can be related to quantities of radioisotopes in the surface soil. The natural radioisotopes measurable with the airborne system include Bi^{214} in the uranium series, Tl^{208} in the thorium series, and K^{40}. The work described here provides the analytical data from the land surface required for calibrating the airborne system when the aeroradioactivity data are acquired. Contours of the analytical results show the distribution of the radioelements and of the total gamma radiation determined from surface soil samples.

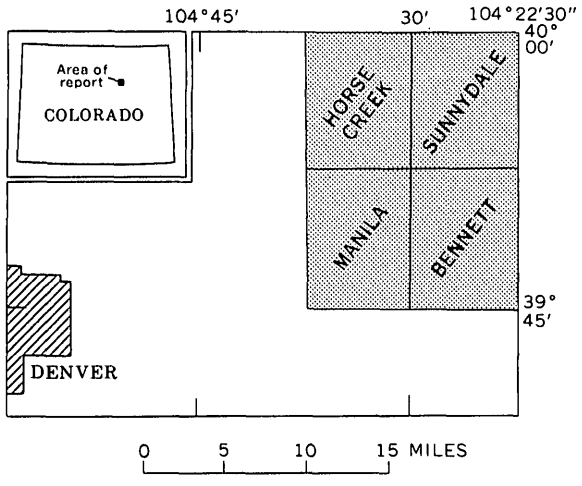

FIGURE 1.—Index map showing area of this report (stippled).

GEOLOGY

Most of the area is covered by eolian sand, alluvium, and loess; exposures of bedrock are scarce. The cover is underlain by lithified sedimentary rocks of the Cretaceous Laramie and Arapahoe Formations and the Cretaceous and Tertiary Denver and Dawson Formations (fig. 2) (Popenoe, 1965). The Laramie Formation, exposed in a narrow band along a stream bottom near the eastern boundary of the area, consists of lagoonal shale, sandstone, and coal. The Arapahoe, Denver, and Dawson (lower part) constitute a transitional zone between the Laramie Formation and the continental clastics of the upper part of the Dawson Formation. This transitional zone is composed of sandstone and conglomerate (Arapahoe Formation); andesitic conglomerate, sandstone, and claystone (Denver Formation); and claystone and siltstone with some pebble conglomerate and arkosic sandstone (Dawson Formation, lower part) (Dane and Pierce, 1936). The upper part of the Dawson Formation consists of a rhyolitic welded tuff and coarse clastic rock derived from the Pikes Peak Granite and associated crystalline rocks of the Front Range (Popenoe, 1965); this geologic unit underlies a small section in the southwestern corner of the report area.

U.S. GEOL. SURVEY PROF. PAPER 600-B, PAGES B71-B75

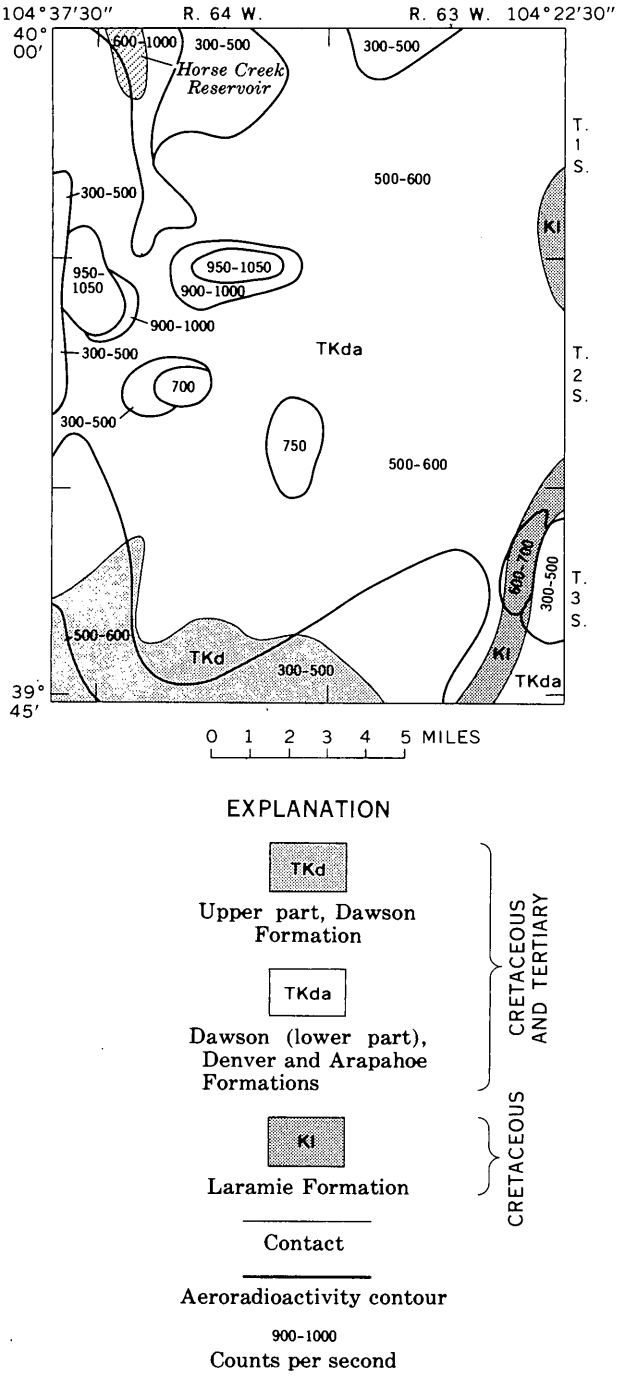

FIGURE 2.—General geologic and aeroradioactivity contour map (from Popenoe, 1965).

INSTRUMENTATION AND OPERATIONAL PROCEDURES

The gamma-ray spectrometer system used for both the laboratory and the field measurements consists of a 400-channel pulse-height analyzer, a high-voltage power supply, two 11½-inch-diameter by 4-inch-thick sodium iodide crystal detectors, a paper tape punch and reader, and an X-Y recorder. During the laboratory measurements the signal output from each detector was routed to separate halves (200 channels) of the analyzer to permit simultaneous analyses of two samples. The field data were obtained by summing the signals from the two crystals to obtain a maximum counting rate.

Most of the soil samples were collected along section lines which are expected to be used as guidelines for the aircraft's flight path (figs. 3, 4). Specific locations were determined from a geologic and aeroradioactivity (fig. 2) map (Popenoe, 1965) to obtain representative samples of the soil overlying the mapped formations and concentrations of samples in areas where significant changes in aeroradioactivity were indicated. The aeroradioactivity data shown in figure 2 were acquired in 1965 with instruments different than those of the airborne spectrometer system which will be calibrated using the results of the present study.

The soil samples were weighed in 600-gram units, enclosed in thin-walled plastic containers 6 inches in diameter by about 1½ inches deep, and sealed with tape to prevent radon or thoron loss. The samples were not analyzed for 2 weeks after being sealed, to permit short-lived radiogenic daughters to approach radioactive equilibrium. The transient equilibrium state thus obtained permits an indirect analysis of long-lived parent radioelements.

While a spectrum is being accumulated, the sample is placed on the top flat surface of the detector which is centered in a 4-inch-thick lead box to minimize external background radiation. Data-accumulation times differ for each sample depending on the radiation intensity. Preset times are in steps of 100, 400, and 1,000 minutes. Samples are analyzed twice at energy ranges of 0 to 0.5 and 0 to 2 Mev (million electron volts), respectively, to measure different isotopes and to obtain verifying energy lines. The spectra are plotted on an X-Y record from which the interpretations are made. The spectrometer system is calibrated empirically with rock samples containing known quantities of natural radioisotopes, and the sample data are compared with the spectra from these samples. Interpretation techniques are virtually the same as those described by Bunker and Bush (1966, 1967). The relative intensity of the total gamma radiation in the samples was determined by summing the counts in the 200-channel groups; a 200-channel group corresponds to an energy range of 0 to 2 Mev.

Gamma-ray spectra were collected in the field along section lines, with the spectrometer system mounted in a vehicle. Each spectrum was accumulated in a 4-minute interval, the time the vehicle took to traverse 1 mile. The spectra were stored on punch tape for sub-

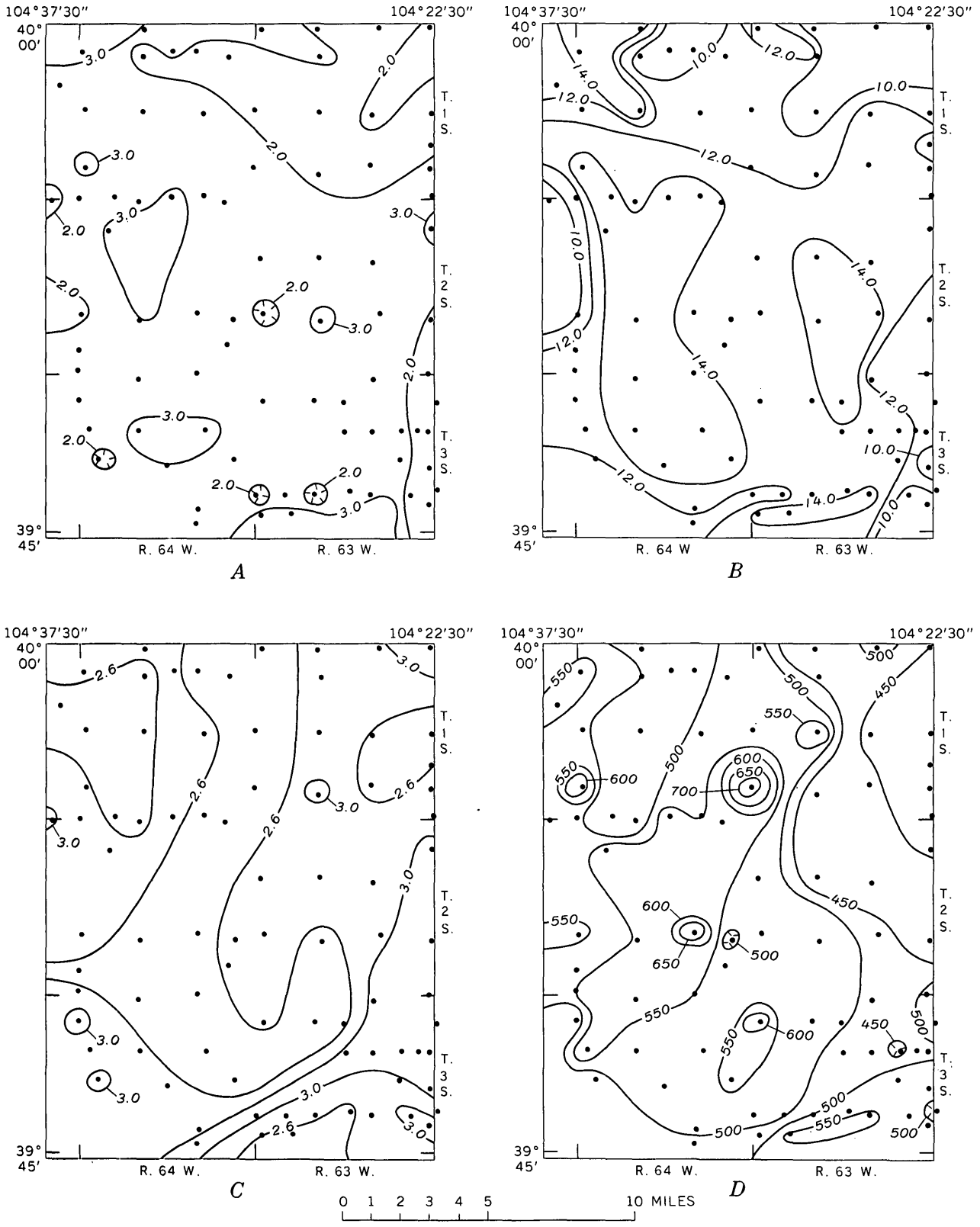

FIGURE 3.—Distribution of radioelement concentration and radiation intensity determined from sample analyses. Black dots are sample localities. *A*, radium-equivalent uranium, in parts per million; *B*, thorium, in parts per million; *C*, potassium, in percent; *D*, total gamma radiation intensity from 0 to 2 Mev, in counts per minute.

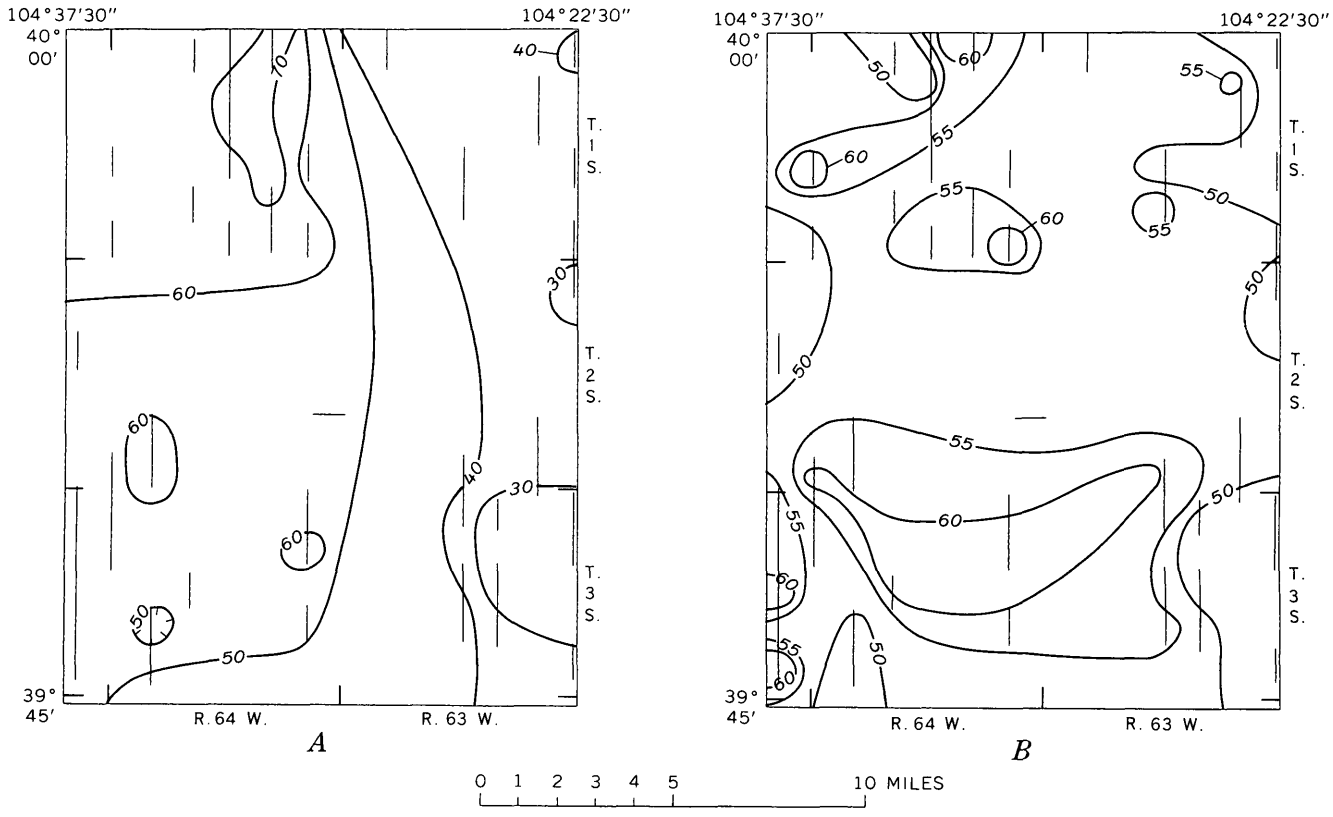

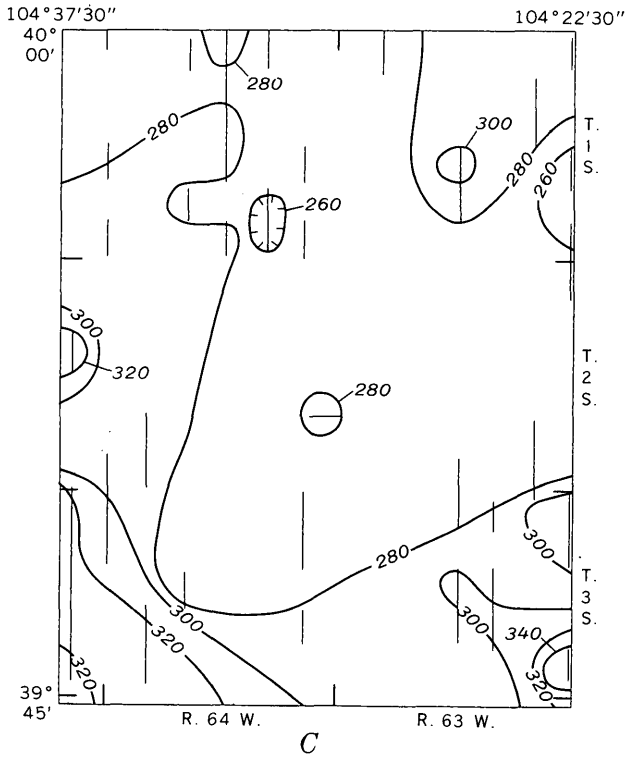

FIGURE 4.—Relative distribution of radioelement concentration determined by mobile traverses (straight lines). *A* radium-equivalent uranium, in counts per minute; *B*, thorium, in counts per minute; *C*, potassium, in counts per minute.

sequent plotting and interpretation. The system was adjusted to accept gamma-ray energies ranging up to 3.0 Mev which includes some different energies than are used for laboratory measurements.

RESULTS

The ranges of the natural radioelement content of the soils are 2.07 to 3.75 percent potassium, 7.7 to 19.0 ppm thorium, and 0.7 to 3.3 ppm radium-equivalent uranium. The possible error in the analytical values are 5 percent for potassium and 10 percent for thorium and radium-equivalent uranium. The analyses of the samples are shown as contours of individual radioelements and of total gamma-radiation intensity within a constant energy range in each spectrum (fig. 3). Parts of the area are slightly contaminated with Cs^{137} from fallout, but the concentration is too low to affect aeroradioactivity measurements or to interfere with natural radioelement analyses.

Contours of radiation intensities of gamma-ray energies related to the radioelements are shown in figure 4; these data were obtained with the mobile spectrometer system. The contours determined from the potassium and thorium gamma-ray energies generally reflect the concentrations of those radioelements determined from sample analyses, but the correlation is insuffici-

ently specific to relate quantitatively the two types of data. The lack of correlation of the radium-equivalent uranium data is probably caused by insufficient sensitivity to the diagnostic energies with the mobile system.

Differences in radioisotopic composition and changes in the aeroradioactivity data of total gamma radiation measured in 1965 are seldom related in this area to geologic contacts indicated by the generalized geologic map (in Popenoe, 1965). Differences in radioisotopic composition and radiation intensity vary more widely within a geologic unit than the differences between units at contacts. The lack of correlation between the radioactivity and the geologic data may be attributable to several factors. The geologic units are composites of several rock types and are not significantly different. Potassium has probably been added in most areas during agricultural fertilization. The mobile traverse data are undoubtedly affected by foreign gravel and paving material on the roads.

The aeroradioactivity detection system used in 1965 to collect the data reported by Popenoe, and used in the above comparative results, has been replaced by more sophisticated equipment. The new instrumentation will undoubtedly provide data which will improve the correlation with radioisotope concentrations.

REFERENCES

Bunker, C. M., and Bush, C. A., 1966, Uranium, thorium, and radium analyses by gamma-ray spectrometry (0.184–0.352 million electron volts), *in* Geological Survey Research 1966: U.S. Geol. Survey Prof. Paper 550–B, p. B176–B181.

———1967, A comparison of potassium analyses by gamma-ray spectrometry and other techniques, *in* Geological Survey Research 1967: U.S. Geol. Survey Prof. Paper 575–B, p. B164–B169.

Dane, C. H., and Pierce, W. G., 1936, Dawson and Laramie Formations in the southeastern part of the Denver basin, Colorado: Am. Assoc. Petroleum Geologists Bull., v. 20, no. 10, p. 1308–1328.

Popenoe, Peter, 1965, Natural gamma aeroradioactivity map of the Denver area, Colorado: U.S. Survey Geophys. Inv. Map GP–505.

285–544 O—68——6

APPLICATION OF COINCIDENCE COUNTING TO NEUTRON ACTIVATION ANALYSIS

By L. PAUL GREENLAND, Washington, D.C.

Abstract.—A fast coincidence-counting technique has been used to simplify the determination of cobalt and cesium in silicate rocks. After neutron irradiation, Co^{60} activity is counted directly in the sample with no chemical separations. Cs^{131} activity is counted after a rapid chemical separation from scandium. Analyses of eight U.S. Geological Survey standard rock reference samples by this technique are presented.

Neutron activation of silicate rocks produces a vast number of radionuclides decaying by gamma-ray emission. Previous attempts at instrumental analysis of silicates have relied on energy discrimination to identify a particular nuclide (Brunfelt and Steinnes, 1966; Stueber and Goles, 1967). For nuclides emitting two or more gamma rays in cascade, greater selectivity may be obtained by adding a time requirement to the energy discrimination.

The technique of fast-coincidence counting enables one to count only those decay events producing two simultaneous gamma rays of specific energies. Unfortunately, the gain in selectivity thus obtained involves a concomitant loss of sensitivity for a given counting time since two gamma rays must be detected simultaneously. However, the signal-to-background ratio is generally improved by coincidence counting, and thus the loss of sensitivity may be recovered if a longer counting time can be tolerated. Because radiochemical separations may be simplified or avoided, the actual man-hours involved may be decreased in spite of longer counting times.

Wing and Wahlgren (1965) have recently calculated γ-γ sensitivities for all the chemical elements. This compilation suggests the possibility of determining many elements in silicate rocks without the need for extensive radiochemical separations. However, application of coincidence counting to neutron activation analyses has been rare and generally restricted to specialized materials, for example, copper in bismuth (Kim and others, 1965), and chlorine in terphenyls (Bramlitt, 1966). The only application of this technique to silicates appears to be the determination of copper in stony meteorites (Schmitt and Smith, 1965; Greenland and Goles, 1966).

Cobalt has been determined previously in silicate rocks by instrumental neutron activation analysis (Brunfelt and Steinnes, 1966; Stueber and Goles, 1967), but the determination of cesium has required extensive radiochemical purifications (Cabell and Smales, 1957; Butler and Thompson, 1962). The present report describes the application of coincidence counting to simplify the determination of cesium and to increase the reliability of cobalt determinations by neutron activation analysis.

REAGENTS AND APPARATUS

Flux monitors

Specpure Cs_2CO_3 and Co_2O_3 were dried at 120°C. Weighed quantities were dissolved in HNO_3 and diluted to volume to give concentrations of 1000 parts per million. A drop ($\approx$0.05 milliliter) of these solutions was weighed onto sufficient Specpure SiO_2 to approximate sample volumes in a polyethylene irradiation vial and evaporated to dryness. The residues were then treated exactly the same as the samples.

Apparatus

The coincidence-counting apparatus is shown in block diagram in figure 1. The sample was centered between two 2- by 2-inch NaI (Tl) detectors. Each detector was connected through a preamplifier and double-delay line amplifier to a jitter-free single-channel pulse-height analyzer. The output from each of the analyzers was put into fast coincidence and the number of coincidence events recorded by a scaler.

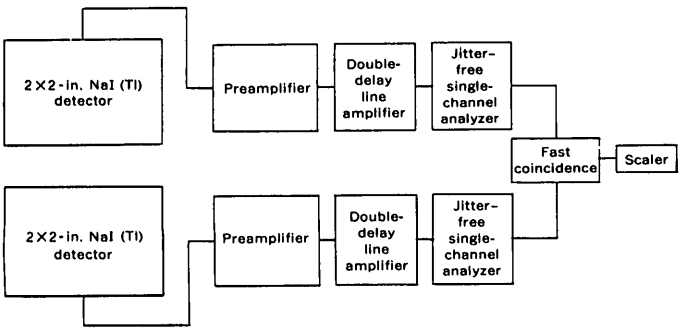

FIGURE 1.—Block diagram of instrument arrangement used for coincidence counting in this investigation.

ANALYTICAL METHODS

Irradiation

Samples of approximately 100 mg were weighed into polyethylene irradiation vials which were then heat sealed. The vials were irridiated for about 15 hours in a thermal neutron flux of 7×10^{12} neutrons per square centimeter per second in the reactor at the Naval Research Laboratory. Short-lived radioactive species were permitted to decay for 2–3 weeks before further work.

Cobalt determination

After cooling, the samples were counted with the experimental arrangement shown in figure 1. The window of each pulse-height analyzer was set to encompass both the 1.17 and 1.33 Mev gamma-ray energies of Co^{60}, and the coincidence resolving time was adjusted to 50 nanoseconds.

In preliminary experiments in which the coincidence output was used to gate a multichannel analyzer, no gamma peaks other than those due to Co^{60} were observed in the spectrum. This demonstrates the high selectivity gained by imposing the coincidence requirement. Since only Co^{60} activity was present in the coincidence spectrum, the arrangement shown in figure 1 was used in subsequent work.

Cesium determination

Attempts to determine cesium directly in the sample, from the coincident gamma peaks at 0.60 and 0.80 Mev of Cs^{134}, were unsuccessful owing to a high coincidence background produced by Compton events from the 0.89 and 1.12 Mev coincident gamma rays of Sc^{46}. This background was removed by a simple chemical separation of cesium from scandium.

After the cobalt was counted, the samples were fused with 1 gram of Na_2O_2 in iron crucibles. The fusion cake was quenched and then decomposed with 30ml of H_2O containing a few milligrams of Cs_2CO_3 carrier for the Cs^{134} activity. The mixture was heated to obtain complete leaching of cesium from the hydroxide precipitate. The precipitate was removed by filtration and the filtrate made to a definite (arbitrary) volume in a polyethylene counting vial. This solution was then counted with the window of each pulse-height analyzer set to encompass both peaks of Cs^{134}. Tracer experiments showed that Cs^{134} appeared quantitatively in the filtrate, thus no correction for chemical yield was required.

Examination of the gamma spectra of the solutions with a multichannel analyzer showed peaks (in Mev) corresponding to 28-day Cr^{51} (0.32), 314-day Mn^{54} (0.84), 84-day Sc^{46} (0.89, 1.12), and 45-day Fe^{59} (1.10, 1.29) as well as 2.1-year Cs^{134}. Although Sc^{46} was not quantitatively separated, it was decreased to such a low level that it no longer interfered with the cesium determination. The efficacy of this separation was demonstrated by attempting to determine cesium in a few achondrite meteorites. These meteorites are known to contain $\approx$ 40 ppm of Sc and $\approx$ 0.01 of Cs (Mason, 1962). All analyses by the present method gave <0.05 ppm of Cs, thus demonstrating that the combination of a simple chemical separation with the coincidence-counting technique removed all interference from the cesium determination.

Analytical sensitivity and precision

With the experimental conditions described here, 0.05 ppm of Cs and 0.02 ppm of Co can be detected at a 2-sigma limit for counting statistics. Analytical precision is affected by neutron flux variation across the irradiation container and by counting statistics. The maximum flux variation has been measured in independent experiments as ±3 percent. At concentrations of 0.1 ppm, these combined errors can be maintained at ±10 percent for both elements employing counting times of less than 1 day. Analyses of several samples in duplicate have confirmed this result. These limits could be easily lowered by shielding the detectors to lower the background and by increasing the sample weight, irradiation time, and counting time.

RESULTS

This method has been applied to the determination of cobalt and cesium in eight U.S. Geological Survey standard rock reference samples. In table 1 these cobalt values are compared with previous emission spectrograph and neutron activation determinations of cobalt. The agreement of the various methods appears to be satisfactory, except for the peridotite and dunite samples where the spectrographic results are considerably lower than the neutron activation figures.

An obvious source of high results from the neutron activation procedure is the production of Co^{60} by

TABLE 1.—*Comparison of cobalt content (in ppm) in eight USGS standard rock reference samples as determined by different analytical methods*

USGS standard rock reference samples	Neutron activation		
	Present report	Brunfelt and Steinnes (1966)	Emission spectrograph [1]
Granite, G–1	2. 1	2. 2	2. 2
Diabase, W–1	48	42	50
Granite, G–2	5. 0	4. 3	6
Granodiorite, GSP–1	8. 5		7
Andesite, AGV–1	17	13	13
Peridotite, PCC–1	140	114	90
Dunite, DTS–1	150	140	115
Basalt, BCR–1	36	36	30

[1] Values for samples G–1 and W–1 are recommended values of Fleischer (1965); other values are averages cited by Flanagan (1967).

reactions other than the $Co^{59}(n,\gamma)Co^{60}$ reaction. Of the various possibilities, the most productive reaction is $Ni^{60}(n,p)Co^{60}$. The extent of this interference has been checked by irradiating and counting Specpure NiO and Co_2O_3 under exactly the same conditions as used for the samples. On an equal weight basis, Co^{60} activity produced from nickel was 1000 times less than that produced from cobalt; since the Ni/Co weight ratio in the peridotite and dunite is only ≈ 20 (Flanagan, 1967), no interference with the neutron activation determination of cobalt is likely. Errors due to isotopes other than Co^{60} should be considered. The compilation of Wing and Wahlgren (1965) shows no other long-lived isotopes with coincident gamma rays of the appropriate energies. Examination of the coincident spectrum with a multichannel analyzer showed no spurious peaks and no Compton scattering from higher energy peaks. High counting rate of a noncoincident gamma ray could produce accidental coincidence counts. Introduction of a delay circuit in one of the single channel analyzers prevents counting of true coincidence events but does not affect the counting rate of accidental coincidences; this test demonstrated that no accidental coincidence events were being mistaken for Co^{60}.

The values of cesium for the eight USGS standard rock reference samples are shown in table 2. The accuracy of neutron activation is confirmed by the reasonable agreement of values of cesium in samples G–1 and W–1 with the recommended values of the same samples.

This work has indicated that the coincidence-counting technique offers considerable advantages in obviating or, at least, simplifying the radiochemical separations usually required by neutron activation analysis. Although this technique is generally applicable to the types of rock studied here, analysis of other materials would require further consideration of possible matrix effects. Work is currently in progress to extend this technique to other elements.

TABLE 2.—*Values of cesium content in eight USGS standard rock reference samples, determined by neutron activation, compared with recommended values*

USGS standard rock reference samples	Cesium values (in ppm)	
	This report	Recommended (Fleischer, 1965)
Granite, G–1	1. 3	1. 5
Diabase, W–1	. 90	1. 1
Granite, G–2	1. 1	
Granodiorite, GSP–1	1. 2	
Andesite, AGV–1	1. 2	
Peridotite, PCC–1	. 08	
Dunite, DTS–1	. 05	
Basalt, BCR–1	. 91	

REFERENCES

Bramlitt, E. T., 1966, Gamma-gamma coincidence counting applied to chlorine analysis by neutron activation: Anal. Chemistry, v. 38, p. 1669–1674.

Brunfelt, A. O., and Steinnes, Eiliv, 1966, Instrumental neutron-activation analysis of "standard rocks": Geochim. et Cosmochim. Acta, v. 30, p. 921–928.

Butler, J. R. and Thompson, A. J., 1962, Different values for caesium in G–1: Geochim. et Cosmochim. Acta, v. 26, p. 1349–1350.

Cabell, M. J., and Smales, A. A., 1957, The determination of rubidium and caesium in rocks, minerals, and meteorites by neutron-activation analysis: Analyst, v. 82, p. 390–406.

Flanagan, F. J., 1967, U.S. Geological Survey silicate rock standards: Geochim. et Cosmochim. Acta, v. 31, p. 289–308.

Fleischer, Michael, 1965, Summary of new data on rock samples G–1 and W–1, 1962–1965: Geochim. et Cosmochim. Acta, v. 29, p. 1263–1283.

Greenland, L. P., and Goles, G. G., 1966, Copper and zinc abundances in chondritic meteorites: Geochim. et Cosmochim. Acta, v. 29, p. 1285–1292.

Kim, J. I., Speecke, A. N., and Hoste, J. R., 1965, Neutron activation analysis of copper in bismuth by γ, γ-coincidence measurement: Anal. Chim. Acta, v. 33, p. 123–130.

Mason, Brian, 1962, Meteorites: New York, John Wiley and Sons, 274 p.

Schmitt, R. A., and Smith, R. H., 1965, Research on elemental abundances in meteoritic and terrestrial matter: General Atomic Div. of General Dynamics rept. GA 6642 to U.S. Natl. Aeronautics and Space Adm., 31 p.

Stueber, A. M., and Goles, G. G., 1967, Abundances of Na, Mn, Sc, Cr, and Co in ultramafic rocks: Geochim. et Cosmochim. Acta, v. 31, p. 75–93.

Wing, James and Wahlgren, M. A., 1965, Detection sensitivities in thermal-neutron activation: Argonne Natl. Lab. Rept. no. 6953, 107 p.

THICKNESS OF VALLEY FILL IN THE JORDAN VALLEY EAST OF THE GREAT SALT LAKE, UTAH

By TED ARNOW and R. E. MATTICK, Salt Lake City, Utah; Denver, Colo

Work done in cooperation with the Utah State Engineer

Abstract.—A seismic-refraction profile in the Jordan Valley, east of the Great Salt Lake, Utah, showed three velocity layers. The upper two are correlated with valley fill of Quaternary and Tertiary age, whereas the lowest is correlated with consolidated rock. The computed thickness of the fill along the seismic profile ranges from about 600 to 4,800 feet.

As part of an investigation of the water resources of Salt Lake County, Utah, the U.S. Geological Survey must determine the amount of ground water that is discharged toward Great Salt Lake through valley fill in the north end of the Jordan Valley. In order to help calculate the thickness of the fill, a refraction seismic study was made across the valley during 1965. On the basis of the seismic work and interpretation of the logs of several nearby wells, the valley fill has been divided into units of Quaternary and Tertiary age and the thickness of each unit calculated.

SEISMIC SURVEY

The refraction survey was based on 10 shotpoints spread over a total length of about 15 miles (fig. 1). Depths to the first refracting horizon were computed by the method of Hawkins (1961), and depths to the deeper refractors were computed using the graphical method of Slotnick (1950). Three major velocity layers were found (fig. 2). The seismic velocity in the near-surface layer ranges from about 5,700 to about 5,900 feet per second, in the second layer it ranges from about 8,700 to about 12,500 fps, and in the third layer it ranges from 15,000 to 15,800 fps. The three layers are interpreted in descending order as Quaternary deposits, Tertiary deposits, and consolidated rocks of several ages.

Quaternary deposits

The uppermost layer is believed to be of Quaternary age. It can be traced continuously along the seismic profile, and the velocity in this layer is characteristic of an unconsolidated water-saturated material. Logs of wells drilled near the profile indicate that this material is predominantly interbedded clay, silt, fine sand, and medium sand. Thin beds of tuff were described by Eardley and Gvosdetsky (1960, pl. 1) and by Berry and Crawford (1932, p. 54) in wells 2 and 4, respectively, at the western and eastern parts of the profile.

The computed thickness of the Quaternary deposits ranges from about 600 to 2,500 feet. The minimum thickness is near the west end of the profile, and the layer thickens to about 1,500 feet at shotpoint 4. It thins east of shotpoint 4, reaching a thickness of about 760 feet between shotpoints 5 and 6, and thickens again toward the east to a calculated thickness of 2,480 feet at shotpoint 9. East and southeast of shotpoint 9, where seismic data are unavailable, the gravity map suggests that the uppermost layer continues to thicken.

The description of well 2 by Eardley and Gvosdetsky (1960) states that the well, which was cored to a total depth of 650 feet, bottomed in sediments of Aftonian age of the Pleistocene. Berry and Crawford (1932, p. 54) report mollusca of Pleistocene age to a depth of 884 feet in well 4. The electrical log for well 3 (fig. 3) does not indicate any change in formation between 512 feet (the top of the log) and a depth of about 970 feet where the marked change in spontaneous potential and gradual change in resistivity indicates a change in the physical characteristics of the sediments. Although neither electrical nor seismic information is

U.S. GEOL. SURVEY PROF. PAPER 600-B, PAGES B79–B82

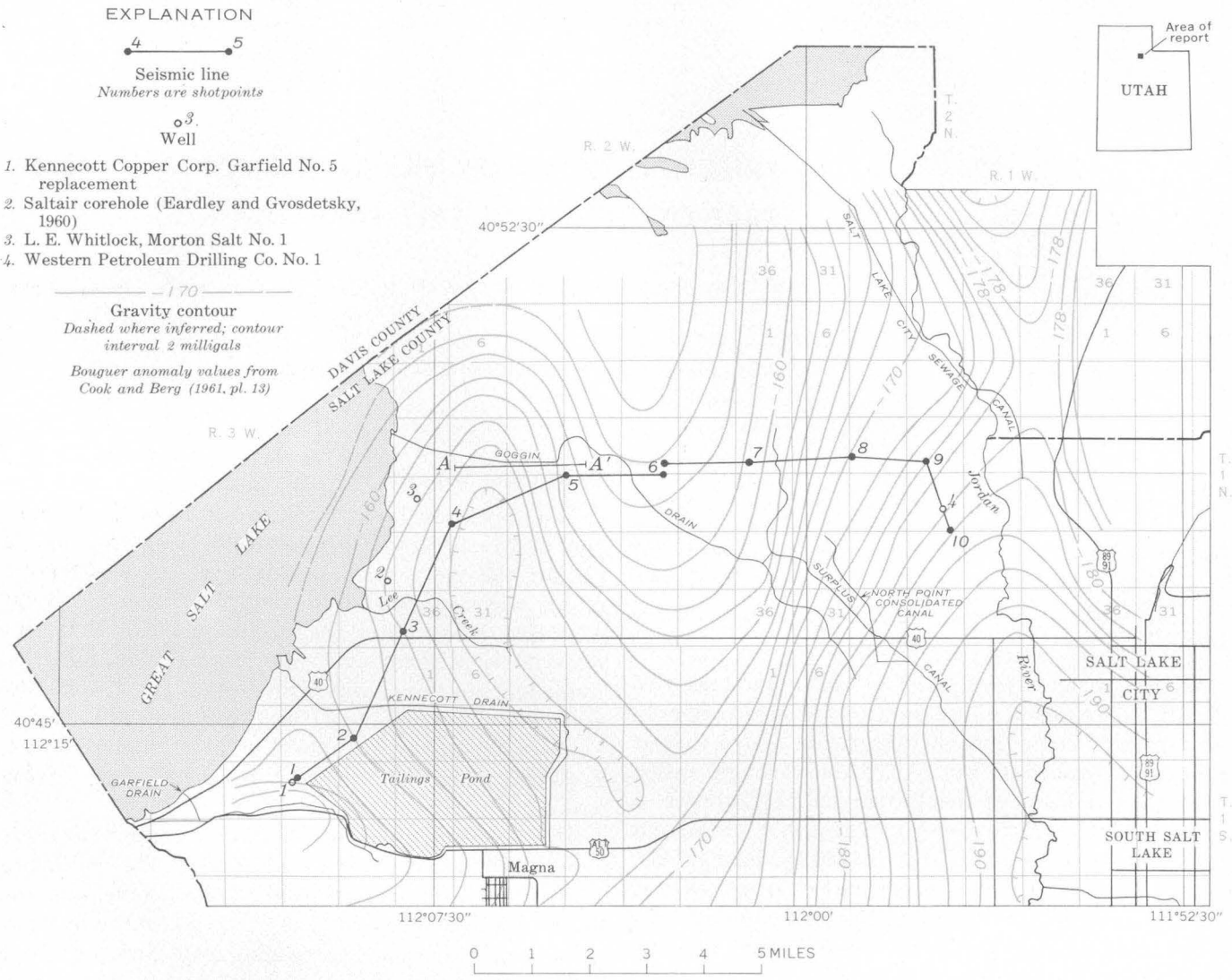

FIGURE 1.—Map of the northern part of the Jordan Valley, Utah, showing line of seismic profile, well locations, and Bouguer gravity anomalies.

diagnostic of age, the decrease of resistivity at about 970 feet in well 3 and the increase of velocity from 5,700 to about 9,000 fps between the upper and middle layers is here correlated with the base of the Quaternary deposits.

Tertiary deposits

The intermediate velocity layer is believed to be of Tertiary age. It appears only in the central and west-central part of the seismic profile, and the velocities in this layer are characteristic of semiconsolidated sediments. Only well 3 near the profile is known to have penetrated this layer. The log of well 3 indicates that the layer primarily contains unconsolidated sediments, but a total of about 300 feet of volcanic rock, possibly andesite, was penetrated between depths of 2,300 and 2,800 feet. Part or all of the second layer may be in the Salt Lake Formation, but without diagnostic fossils or an age determination, a definite identification cannot be made.

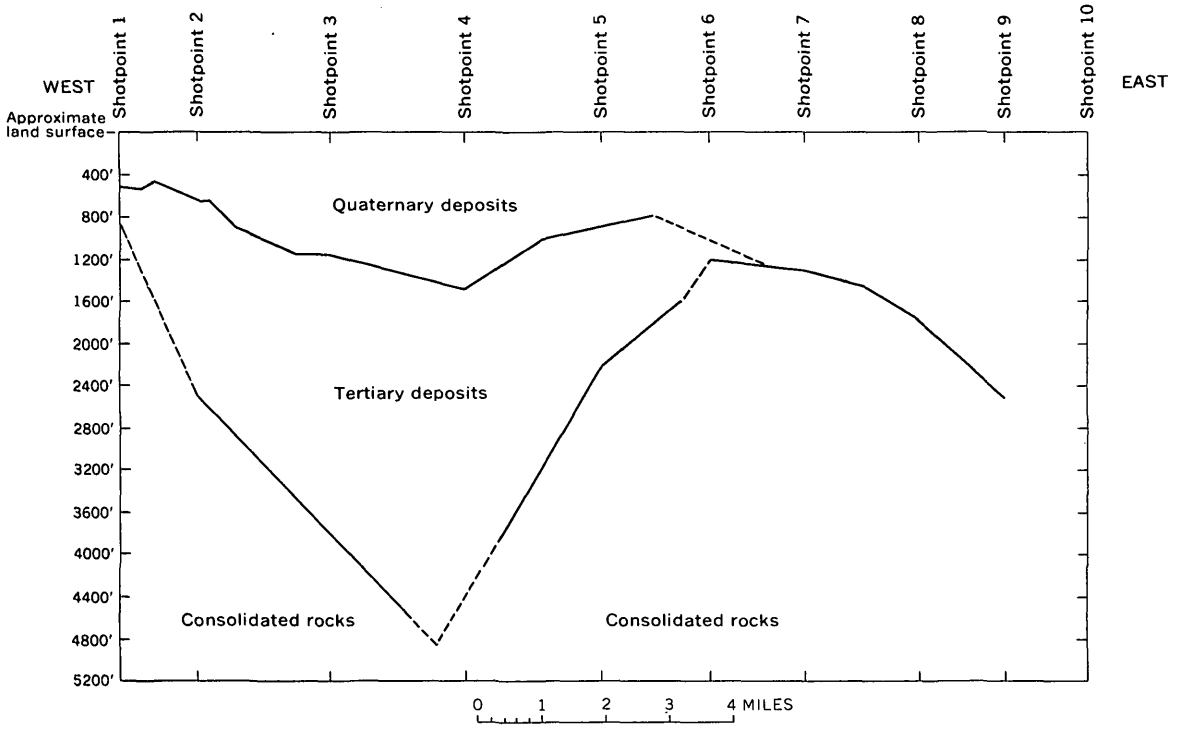

FIGURE 2.—Computed depth of three velocity layers along seismic profile in the Jordan Valley, Utah. Boundaries are dashed where inferred.

The computed thickness of the second layer ranges from 0 to about 3,400 feet. It was traced continuously on the seismic profile between shotpoints 2 and 6, but it did not appear at shotpoint 1 or east of shotpoint 6. It reaches a maximum thickness of about 3,400 feet near shotpoint 4, where the profile crosses a gravity low.

Consolidated rocks

The lowest layer can be traced across almost the entire profile, and the velocities in this layer are characteristic of consolidated rocks. The driller's log for well 1 states that the well penetrated black limestone at a depth of 882 feet (Iorns and others, 1966, p. 88). An increase of resistivity on the electrical log of well 3 at a depth of about 3,650 feet indicates that the well penetrated consolidated rock at about that depth, and a core taken at 4,126 feet suggests that the rock is a conglomerate. Well 3 was correlated with shotpoint 3 because both are located on the —164 milligal gravity contour (fig. 1). The depth to consolidated rock of

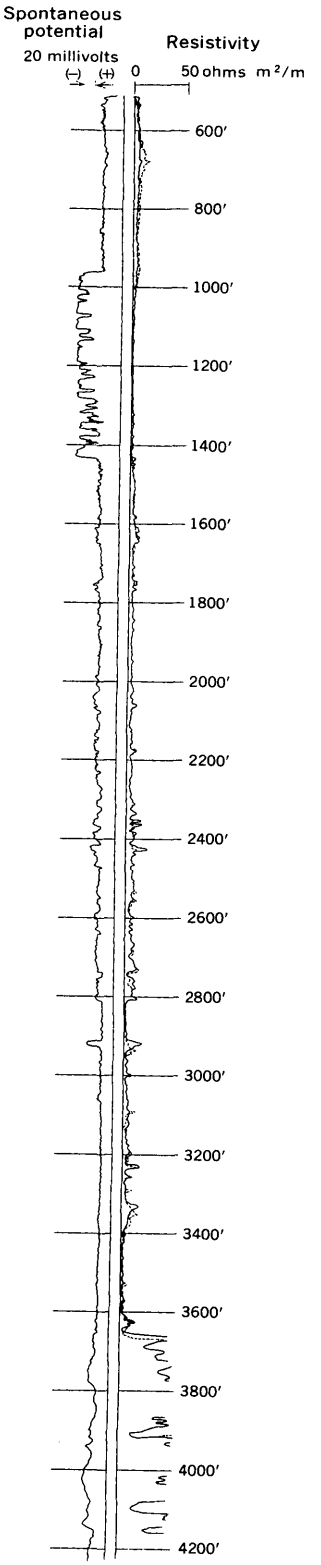

FIGURE 3.—Electrical log of the L. E. Whitlock, Morton Salt No. 1 well, Salt Lake County, Utah.

3,650 feet correlates reasonably well with the calculated depth of about 3,800 feet that was determined at shotpoint 3 to be the depth to the lowest refracting layer.

The depth to consolidated rock between shotpoints 4 and 5 was computed along profile *A–A′* and projected to the line of the profile in figure 2. Because of the projection, the low point on the profile appears to be between shotpoints 3 and 4, rather than being between shotpoints 4 and 5 as indicated by the gravity map.

GRAVITY MAP

A Bouguer gravity map of the area east of the Great Salt Lake (after Cook and Berg, 1961, pl. 13) is shown overlain on figure 1. The results of the gravity interpretation are in reasonable agreement with the computed total thickness of unconsolidated Quaternary and Tertiary sediments, which ranges from about 600 to 4,800 feet along the seismic profile. As density is closely related to velocity, the high velocity contrast between the consolidated rocks (15,000–15,800 fps) and the overlying unconsolidated material (5,700 and about 9,000 fps) suggests that the major part of the gravity anomalies arises from variations in thickness of the unconsolidated sediments. An average density contrast of about 0.3 gram per cubic centimeter between these sediments and the underlying consolidated rocks can account for the change in thickness from 800 to 4,800 feet as computed at shotpoints 1 and 4.

REFERENCES

Berry, E. G., and Crawford, A. L., 1932, Preliminary notes on the mollusca of Lake Bonneville: Utah Acad. Sci., Arts, and Letters Proc., v. 9, p. 53–54.

Cook, K. L., and Berg, J. W., Jr., 1961, Regional gravity survey along the central and southern Wasatch front, Utah: U.S. Geol. Survey Prof. Paper 316–E, p. 75–89.

Eardley, A. J., and Gvosdetsky, Vasyl, 1960, Analysis of Pleistocene core from Great Salt Lake, Utah: Geol. Soc. America Bull., v. 71, p. 1323–1344.

Hawkins, L. V., 1961, The reciprocal method of routine shallow seismic refraction investigations: Geophysics, v. 26, no. 6, p. 806–819.

Iorns, W. V., Mower, R. W., and Horr, C. A., 1966, Hydrologic and climatologic data collected through 1964, Salt Lake County, Utah: U.S. Geol. Survey open-file rept. [Also duplicated as Utah Basic-Data Release No. 11.]

Slotnick, M. M., 1950, A graphical method for the interpretation of refraction profile data: Geophysics, v. 15, no. 2, p. 163–180.

SEISMIC-REFRACTION STUDIES OF THE LOVELAND BASIN LANDSLIDE, COLORADO

By RODERICK D. CARROLL, FITZHUGH T. LEE, JAMES H. SCOTT[1], and CHARLES S. ROBINSON[2], Denver, Colo.

Abstract.—A landslide which developed as a consequence of undercutting along Interstate Route 70 in Colorado was investigated using seismic-refraction methods. The thickness of a low-seismic-velocity layer (1,000 to 2,700 ft/sec), attributed to material involved in movement, was delineated. Bedrock material exhibited seismic velocities ranging from 3,000 to 6,500 ft/sec. Interpretation of the results obtained along a number of lines was difficult, owing to severe energy attenuation and complex arrivals. Consequently the determination of the depth to the slide surface, based solely on seismic-refraction results, was uncertain. However, by combining the seismic results with results of other methods the degree of confidence in the final slide geometry that was derived was greatly increased.

The Loveland Basin landslide (figs. 1 and 2), Clear Creek County, Colo., developed in 1963 as a consequence of undercutting arising from excavation of the plaza area for the eastern approach route of the Straight Creek tunnel. The Straight Creek tunnel is to be a vehicular tunnel which will pass beneath the Continental Divide as part of Interstate Route 70 in Colorado. As evidence was accumulated indicating the nature and extent of the landslide, the need for remedial engineering measures was indicated. Successful planning and application of these measures by the U.S. Bureau of Public Roads and the Colorado Department of Highways required a knowledge of the mass of material involved in the slide and consequently the geometry of the slide. Because of the destruction potential, it was important that the amount of material involved be determined as rapidly as possible. To more confidently define the geometry of the sliding mass three independent methods of investigation were utilized. Surface geologic mapping and seismic-refraction measurements made by the U.S. Geological Survey were combined with the results of electrical-resistivity soundings performed by the U.S. Bureau of Public Roads and the Colorado Department of Highways to provide the necessary data (Robinson and others, 1963). This paper concerns the results of the seismic-refraction surveys performed on the slide.

Published data on the delineation of landslides by seismic methods are meager. Trantina (1963) reported on two landslides in California with depths to the slip plane of approximately 12 and 23 feet which were successfully delineated using a sledge-hammer energy source and seismic-refraction techniques. For these reported cases the slip-plane surface apparently was relatively smooth and the material above the slip plane was relatively uniform so that excellent resolution was obtained. However, favorable seismic conditions such as these do not exist uniformly throughout the Loveland Basin landslide.

GEOLOGY

Bedrock in the landslide area consists primarily of Silver Plume Granite of Precambrian age that contains inclusions of older Precambrian metamorphic rocks belonging to the Idaho Springs Formation. The metamorphic rocks are primarily fine-grained gneiss, schist, and migmatite. In most places the bedrock is overlain by unconsolidated material, 0.5–25 feet thick, consisting of morainal material and colluvial deposits of soil and talus. The area is within the Loveland Pass fault zone, a northeast-trending feature which is about 2 miles wide and consists of numerous faults and shear zones separated by relatively unsheared rock. Individual faults or shear zones range in width from less than a foot to 1,000 feet. Previous work (Robinson and Lee, 1962) determined that the average distance between

[1] U.S. Bureau of Mines.
[2] Consulting geologist; formerly of the U.S. Geological Survey.

U.S. GEOL. SURVEY PROF. PAPER 600-B, PAGES B83–B87

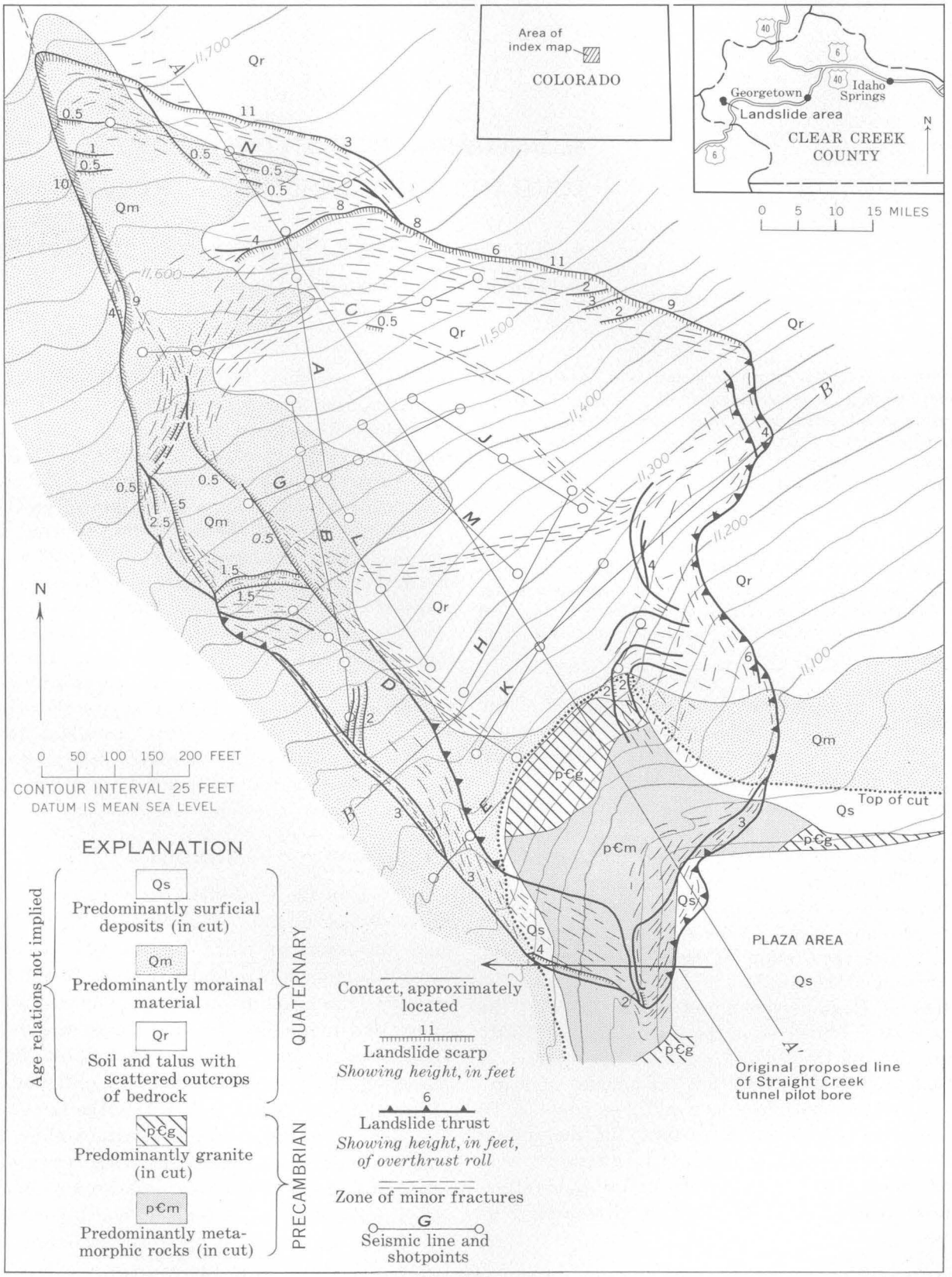

FIGURE 1.—Map of Loveland Basin landslide, Clear Creek County, Colo., showing location of seismic lines. Topographic base modified from base by Continental Engineers, Inc., Denver, Colo.

FIGURE 2.—Loveland Basin landslide, view northward.

fractures in this area ranged from less than 0.1 to 0.5 foot. Bedrock in the landslide area consists of about 75 percent granite and about 25 percent metamorphic rocks. Both rock types are intensely sheared and broken. Few exposures of bedrock existed in the immediate area of the landslide prior to the excavation of the plaza area. During the construction of the portal cut, granite was exposed in the upper part of the cut face and east and south of the cut (fig. 1). The center of the cut exposed altered metamorphic rock.

SLIDE MORPHOLOGY

The landslide is outlined by scarps and thrusts, the scarps occurring where there has been a downward displacement of the landslide mass (fig. 1). The thrusts occur where the landslide mass has moved up and over the preexisting land surface. The scarps are on the western and northeastern sides of the landslide; the southern and southeastern sides are defined by thrusts. The scarp on the western edge of the slide follows an old glacial stream. Zones of minor surface fractures occur over the entire slide area. Near the margins of the slide these fractures are generally parallel to the scarps and thrusts (fig. 1). The scarps, thrusts, and fractures indicate that the landslide did not move as a single homogeneous mass, but rather as several units each somewhat dependent upon the other. Therefore, a slip zone, rather than a single slip plane, probably best represents this landslide. The principal movement was parallel to the long axis of the landslide, but the southwest side exhibits greater movement than the east side. The material involved in movement consists of both morainal and colluvial material as well as intensely sheared and altered bedrock.

EQUIPMENT AND PROCEDURE

Because of the high altitude, steep slopes, and inaccessibility to motor transport, portability was a major consideration in the selection of seismic equipment. Consequently a portable seismic instrument was used. Polaroid film was the recording medium. The entire recording apparatus was contained within a 24-pound package. Standard seismic cables and detectors were used with 12 geophones spaced at 25-foot intervals. Measurements were made along a total of 12 seismic lines in the landslide area (fig. 1). Shotpoints were located at offsets of 25 and 50 or 100 feet on each end of the lines. On a number of the lines a shotpoint was located at the midpoint of the line to obtain more information on variations in the velocity of the near-surface material.

Holes for the emplacement of the seismic charges were driven with a punch bar, and charges averaging five sticks of dynamite (40 percent) per hole were placed at depths of 2 to 4 feet. Energy input to the ground ranged from good to poor, depending on the nature of the near-surface material. The aerated and porous condition of the material above the slip zone was the apparent cause of the poor first arrivals on many lines. Several lines crossed fracture zones visibly open at the surface to depths of a few inches to several feet.

RESULTS

The results of the seismic-refraction survey indicate that two velocity layers in general exist beneath the surface of the landslide—an upper layer in which the velocity ranges from 1,000 to 2,700 ft/sec, overlying a 3,000- to 6,500-ft/sec velocity layer. Differences in velocity are attributed to the relative amounts of dis-

turbed ground present in the two layers. The low-velocity layer contains the scarps, minor fractures, and overthrust rolls which have caused relatively large movement of material. Many of these features are in bedrock. The higher velocity layer probably represents the less disturbed bedrock and morainal and colluvial material. Thickness of the upper layer ranges from 8 to 66 feet. The low-velocity layer is thinner toward the east and south relative to the west and north. Interpretation of the seismic data on the western margin of the slide was hampered by velocity variations in the subsurface. However, the data suggest that the low-velocity layer attains its maximum thickness in this area. Longitudinal and transverse sections through the center of the slide showing the interpreted thickness of the low-velocity layer are shown on figure 3.

Interpretation of the results obtained on a number of lines was hampered by severe attenuation of high-frequency energy and weak arrivals of the first energy. This was further complicated by the occasional presence of an irregular refracting surface as well as some abrupt velocity variations within the near-surface layer. These two features were often inseparable and caused considerable scatter of points on several traveltime plots. Traveltime plots of this nature were generally restricted to seismic lines parallel to the long axis of the landslide. One possible explanation for these features is the presence of relatively competent high-velocity zones within the low-velocity layer. To what extent these zones may act as isolated buttresses within the sliding mass is speculative.

The depths of the low-velocity layer shown in figure 3 are considered representative of the probable minimum amount of material which would be involved in any failure. Resistivity and geologic data indicate the possibility of a deeper slip zone at some locations.

The final calculated mass involved in movement was based upon a conservative estimate of the data from the three disciplines (geologic mapping, and seismic-refraction and electrical-resistivity studies). These procedures resulted in a calculated minimum volume of about 500,000 cubic yards of material weighing about a million tons. Calculations made by R. A. Bohman, of the Bureau of Public Roads, on the basis of these data resulted in placing a buttress load of about 62,000 cubic yards at the toe of the slide. This load was emplaced during September and October 1963. Since this time the slide has stabilized, with only minor additional surficial fracturing. Confirmation of the exact depths involved for the sliding mass is unavailable because of the absence of any definitive drill-hole data. However, it is believed that the seismic and electrical-resistivity interpretations complemented each other sufficiently well to enable a reliable estimate consistent with geologic evidence to be made of the geometry of the sliding mass.

The results of this investigation indicate that the seismic-refraction method is of great utility in delineating the geometry of landslides of a nature similar

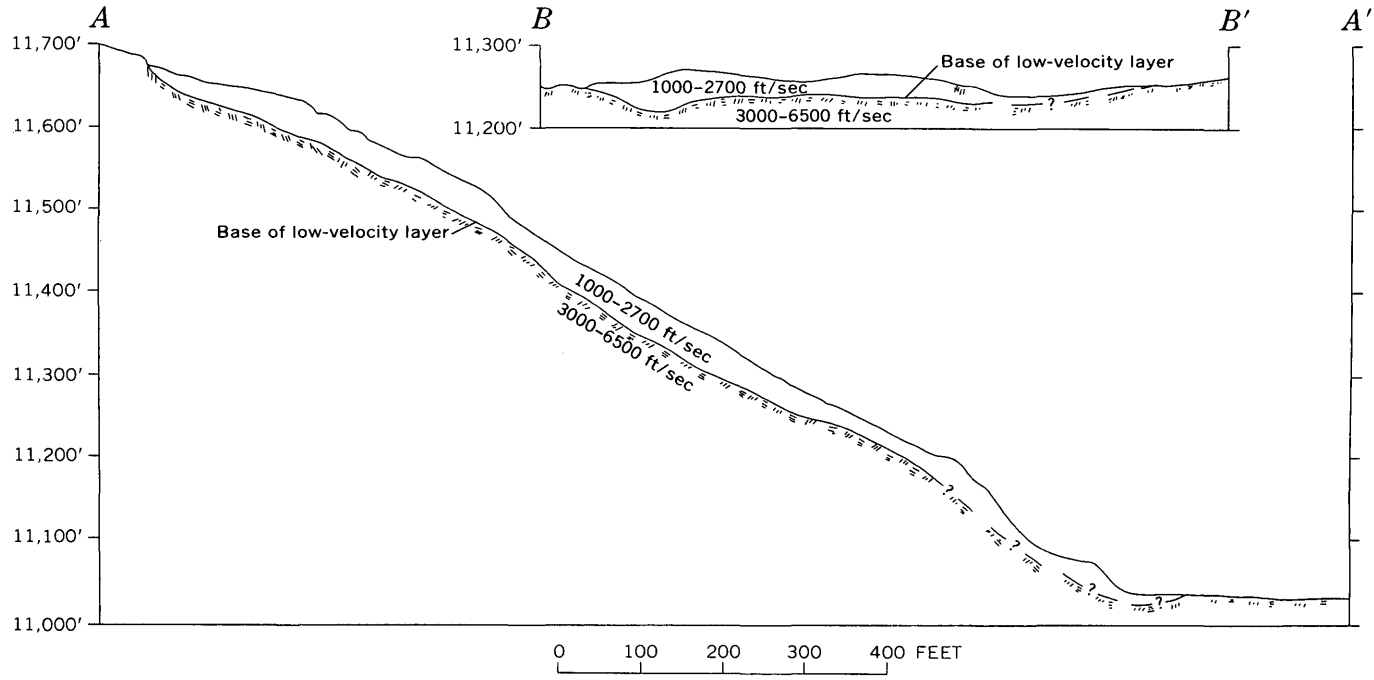

FIGURE 3.—Longitudinal (*A–A'*) and transverse (*B–B'*) sections of the Loveland Basin landslide, showing thickness of low-velocity layer. (See fig. 1 for location.)

to that discussed in this report. Sufficient areas appear to exist within the slide, however, which render the reliability of the interpretation of seismic data uncertain when the seismic method is used without independent criteria for inferring the thickness of the sliding mass. With the availability of several independent criteria for estimating the geometry of the sliding mass—in this case seismic and electrical soundings coupled wth detailed geologic mapping—a large measure of confidence can be obtained in the accuracy of the calculated geometry.

REFERENCES

Robinson, C. S., Carroll, R. D., and Lee, F. T., 1963, Preliminary report of the geologic and geophysical investigations of the Loveland Basin landslide, Clear Creek County, Colorado: U.S. Geol. Survey open-file rept., 5 p.

Robinson, C. S., and Lee, F. T., 1962, Geology of the Straight Creek Tunnel site, Clear Creek and Summit Counties, Colorado, and its predicted effect on tunnel construction: U.S. Geol. Survey open-file rept., 32 p.

Trantina, J. A., 1963, Investigation of landslides by seismic and electrical resistivity methods: Am. Soc. Testing and Materials Spec. Tech. Pub. 322, p. 120–134.

GRAVITY ANOMALIES IN THE RUBY MOUNTAINS, NORTHEASTERN NEVADA

By J. F. GIBBS [1], RONALD WILLDEN [2], and J. E. CARLSON [1],
[1] Menlo Park, Calif., [2] Denver, Colo.

Abstract.—A Bouguer anomaly map of the Ruby Mountains shows steep gradients, interpreted as indicating faults, along most of the east side of the range and at the north and south ends on the west side. The thickness of low-density fill in the south end of Ruby Valley is about 5,500 feet and in the central part is about 4,600 feet. The fill in Huntington Valley is about 5,700 feet thick. Anomaly values over the range are lower than those over topographically lower bedrock areas to the east and west. It is believed that at least some of the low anomaly values are due to a granitic batholith underlying the range.

A gravity survey of the Ruby Mountains and of Ruby Valley to the east was made to determine the external structure of the range and the depth of fill in the valley, and to test the suggestion of Mabey (1964) that the Ruby Mountains may be locally compensated, in contrast to much of the Basin and Range province where isostatic compensation is on a regional scale (Mabey, 1960; Kane and Carlson, 1961). An eastern boundary fault is suggested by the asymmetry of the range, by local scarps, and by the abundant springs near the range front, but evidence for western boundary faults is confined to a scarp in moraines at the mouths of some of the canyons south and southwest of Lamoille. Sharp (1939, pl. 1; 1942, pl. 1) had shown the entire range to be bounded by faults, but Mabey's (1964) gravity work in Huntington Valley to the west indicated no large-displacement boundary fault near Harrison Pass.

The Ruby Mountains are one of the most prominent ranges in northeastern Nevada. North of the low divide of Harrison Pass several peaks are more than 11,000 feet in elevation, and to the south several are more than 10,000 feet. Relief of 4,000–5,000 feet in a horizontal distance of 3–4 miles is common along the east side of the range, where much of Ruby Valley is 5,940–6,000 feet in elevation. The relief is even greater on the west side of the range, where Huntington Valley and Lamoille Valley lie at elevations of 5,400–5,700 feet, but the horizontal distances over which the relief is measured are considerably larger on the west.

GEOLOGY

General description

The northern and southern Ruby Mountains (fig. 1), separated by the broad topographic low at Harrison Pass, are quite dissimilar in the type of rock that is exposed. The northern part is underlain by metamorphosed sedimentary and igneous rocks. The southern part is made up dominantly of sedimentary rocks of Paleozoic age that are cut and locally metamorphosed by a large Tertiary granodiorite pluton. Relatively easy erosion of the granodiorite has resulted in the topographic low of Harrison Pass.

The geology of part of the northern division of the range has been studied in detail by Howard (1966), who recognized seven metamorphosed sedimentary rock formations and tentatively correlated them with Cambrian through Devonian units recognized in other areas. The following description given by Howard (1966, p. 44) is generally appropriate for all of the range lying north of the Tertiary pluton in Harrison Pass:

> The area is a migmatite terrane, with approximately half the total volume of bedrock consisting of granitic rocks. Emplacement was mostly synkinematic and spanned the period of penetrative deformation. The granitic rocks occur in sills, dikes, phacoliths, and irregular bodies intimately injecting the metasedimentary rocks, yet intrusion did not disrupt the structure of the metasedimentary rocks. With rare exception, remnants of metasedimentary rock surrounded by granitic rock are structurally oriented concordantly with foliation in the granitic rock and with the large- and small-scale structural pattern; the remnants outline relic stratigraphy and structure even in areas where granitic rocks greatly predominate.

U.S. GEOL. SURVEY PROF. PAPER 600-B, PAGES B88-B94

The southern division of the range is an area of remarkable contrasts in structural complexity between lower Paleozoic rocks and middle and upper Paleozoic rocks (Willden and Kistler, 1967; Kistler and Willden, 1967). The Cambrian and Lower Ordovician rocks have undergone multiple deformation that resulted in diversely orientated folds, pronounced local tectonic thinning of units, and low-grade metamorphism. The Lone Mountain Dolomite of Silurian and Devonian age and younger units have a simple homoclinal structure that is disrupted by high-angle faults at the south end of the range. A thrust fault of Oligocene or younger age has emplaced Devonian and Mississippian rocks on the deformed lower Paleozoic rocks and on the Harrison Pass pluton along the west side of the range.

The external structure of the northern part of the range was considered by Sharp (1939, p. 898–901) to be a westward-tilted horst with boundary faults dipping 60°–70° basinward. This structure, with gradually decreasing displacement on the western fault, has been postulated to extend as far south as Sherman Creek, beyond which the range probably becomes a simple westward-tilted fault block (Sharp, 1942, p. 683).

Map units

The rock assignments shown on the geologic map (fig. 1) are composites generalized from several larger scale maps. The necessary generalization may have resulted in combining units that would dismay the original workers, but we believe the units described below are significant in terms of density differences between rock types, which might conceivably be related to features of the gravity map.

Gneissic granite is a unit composed of generally coarse grained strongly foliated muscovite granite with locally abundant marble and calc-silicate rock inclusions or roof pendants and minor schist and quartzite inclusions. The gneissic granite is commonly cut by nonfoliated or weakly foliated dikes and sills of granite and pegmatite. Howard (1966, pl. 1) said this unit was of probable Cambrian and Ordovician age and described it as consisting of impure calcite marble, calc-silicate rock, and minor schist and gneiss, although in figure 10 of his text he showed the formation to consist of 40–100 percent pegmatitic granite. The average near-surface density of these rocks, based on specific gravity determinations of 17 samples and an estimated ratio of 70 percent granite to 30 percent metasedimentary rocks, is 2.65 grams per cubic centimeter. If the amount of granite increases downward, as seems likely, the density may fall as low as 2.60 g per cm^3.

The quartzite, marble, and schist map unit includes two thick quartzites and an intervening marble formation tentatively assigned a Cambrian age by Howard (1966, p. 12). Abundant biotite-quartz schist occurs in the southern part of the unit's exposure. In the north part of the Ruby Mountains this unit includes abundant concordant and crosscutting gneissic granite and foliated biotite granodiorite and quartz monzonite intrusive rocks thought by Howard (1966, p. 138, 139) to be of Mesozoic age. One sill-like body, now called a quartz monzonite gneiss (Howard, 1966, p. 45–48) persistently occurs within the marble and has metamorphosed much of it to calc-silicate rock. The near-surface density of these rocks (based on 15 samples) is 2.69 g per cm^3. Calc-silicate rocks near intrusive bodies have densities ranging from 2.83 to 3.15 g per cm^3, and it is quite possible that large masses of high-density rock are present in the northwest part of the range where the gneiss intrudes the marble.

The metacarbonate rocks unit includes all the metamorphic rocks stratigraphically above the quartzite on the upright limb of Howard's (1966, pl. 2) Lamoille Canyon nappe. It consists mainly of calcite marble but includes some dolomite marble and some quartzite. Howard (1966, fig. 3) assigned these rocks a Cambrian through Devonian age. No samples are available for specific-gravity measurements, but the average density may be near the average of 2.66 g per cm^3 for Cambrian and Ordovician rocks in the south part of the range.

The Ordovician and Cambrian rocks unit consists of a thick quartzite formation (Lower Cambrian Prospect Mountain Quartzite) overlain by several thousand feet of interbedded limestone, shale, and shaly limestone which, except for the Lower and Middle Ordovician Pogonip Group at the top of the unit, have not been assigned formational names. The average near-surface density of this unit, based on 14 samples, is 2.66 g per cm^3.

The Devonian and Silurian rocks unit, which is at least 5,000 feet thick, is mostly dolomite with some limestone at the top. It includes the Lone Mountain Dolomite of Silurian and Devonian age, the Nevada Formation and the Devils Gate Limestone of Devonian age, and the Pilot Shale of Devonian and Mississippian age. The Mississippian Joana Limestone is exposed at a few places on the east side of the southern part of the Ruby Mountains, and because it is only about 300 feet thick it has also been included in this map unit. The average near-surface density of these rocks, based on 5 samples, is 2.79 g per cm^3.

The Permian to Mississippian rocks unit in the southern Ruby Mountains is mostly the conglomerate

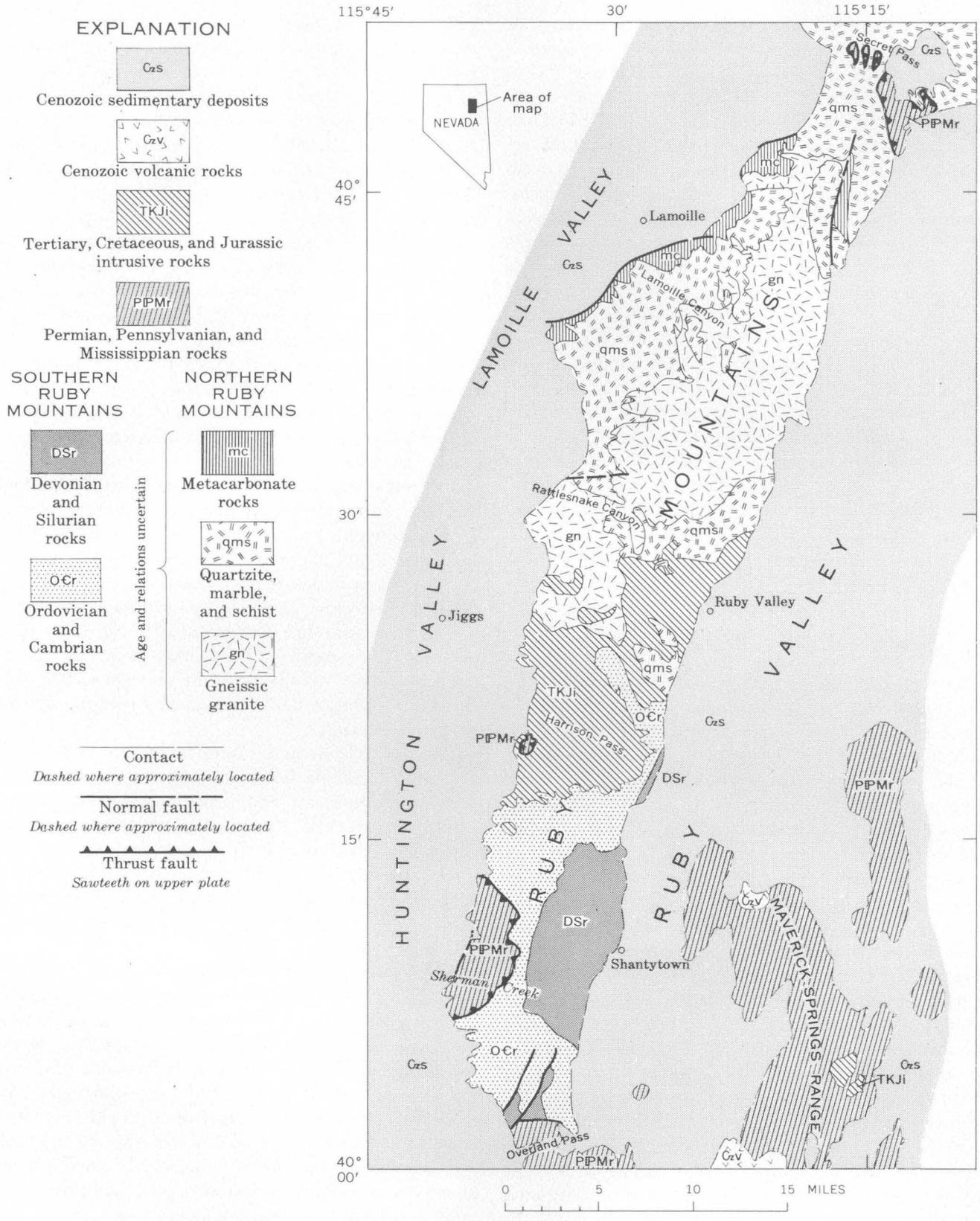

FIGURE 1.—Generalized geologic map of the Ruby Mountains and adjacent areas, Nevada.

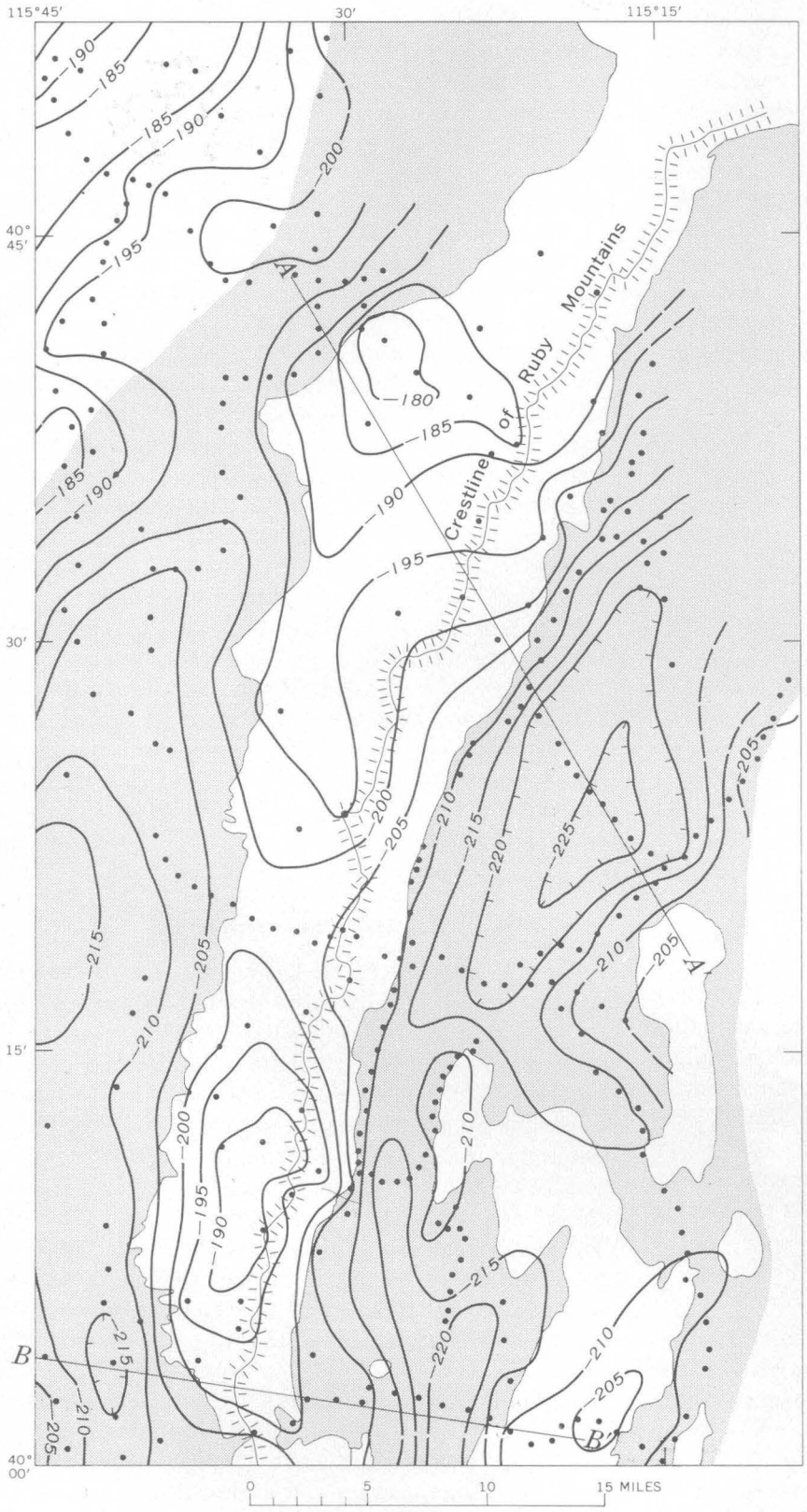

EXPLANATION

—220—

Gravity contour

Dashed where approximately located; hachures indicate closed gravity lows. Contour interval 5 milligals

Gravity station

B——B'

Line of gravity and topographic profile

Mountainous or bedrock area

Valley area

SOURCE OF DATA FOR GEOLOGIC MAP

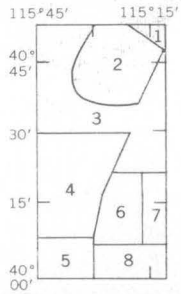

1. Snelson (1957)
2. Howard (1966, pl. 1, fig. 10)
3. Photointerpretation, this report
4. Ronald Willden and R. W. Kistler, this report
5. Sharp (1942, pl. 1)
6. R. A. Hope (written commun., 1967)
7. Collinson (1966)
8. R. K. Hose and M. C. Blake (written commun., 1967)

FIGURE 2.—Bouguer anomaly map of Ruby Mountains and adjacent areas, Nevada.

of the Diamond Peak Formation of Mississippian age. The unit also includes in this area some limestone of possible Pennsylvanian age and some limestone of Devonian age on klippen of a Tertiary thrust sheet. The Diamond Peak is about 3,000 feet thick on the west side of the range. This map unit at the north end of the range consists of limestone in relatively thin thrust plates. In the southeast part of the map area (fig. 1)the unit consists of mostly Permian limestone formations but also includes some Triassic rocks. An average density for these rocks is probably not significant owing to the many rock types included. The average density of the Diamond Peak conglomerate (based on only three samples) is 2.58 g per cm^3. The average density of the limestone included in the map unit is probably nearer 2.70 g per cm^3.

The Tertiary, Cretaceous, and Jurassic intrusive rocks are principally granodiorite to quartz monzonite. One body on the east side of the Ruby Mountains is a weakly foliated muscovite-biotite granite. These rocks are cut by conspicuous joints, are generally coarse grained, and are deeply weathered, which probably accounts for their low average near-surface density of 2.60 g per cm^3 (based on nine samples).

Cenozoic volcanic rocks in the general area include tuffs, flows, and minor intrusive units of rhyolitic to basaltic composition, and some intercalated sedimentary rocks of volcanic origin. The only such rocks identified within the Ruby Mountains are some thin basalt dikes.

Cenozoic sedimentary deposits are generally loosely consolidated or unconsolidated fine- to coarse-grained clastic rocks that are generally locally derived. No deposits older than Quaternary are exposed in Ruby Valley, but Tertiary beds probably underlie the valley just as they do in Huntington and Lamoille Valleys where the Humboldt River tributaries have incised the Quaternary deposits and exposed older material. Specific gravities have not been determined on these deposits, but a density contrast of 0.45 g per cm^3 between them and older rocks has been assumed in calculating the depth of fill in the valleys.

GRAVITY DATA

During this survey in 1964–66, 369 gravity stations were established, of which 295 are in the area of the gravity map (fig. 2). Those outside the area were useful in computing the regional gradient and in tying this survey to a survey to the west by Mabey (1964). A Worden gravity meter with a scale constant of 0.4836 milligals per scale division was used. The observed gravity values are accurate to $\pm$0.25 mgal. The survey is tied to a base station at the Elko airport, established by D. R. Mabey, which is in turn tied to a network that includes stations established by Woollard (1958) at the Las Vegas, Reno, Ely, and Tonopah airports. In the present survey, 3 subbases were established, each by averaging at least 8 separate ties.

Bouguer anomalies were computed from the observations using an elevation correction of 0.06 mgal per ft, which assumes a density of 2.67 g per cm^3 for the rocks above sea level. Terrain corrections were applied using charts through zone L of Hammer (1939) and, for stations at high elevations in the range, modified Hayford-Bowie charts through zone O (Swick, 1942, p. 68). Data presented by Sandberg (1959, p. 326) were used to convert from one chart to the other. Terrain corrections were made on all stations in the range and for part of those at the range front. Corrections were estimated for the remaining range-front stations from nearby stations on which computed corrections had been made. Terrain corrections on stations within the valleys, which were not made, might be as large as 1 mgal.

Bench marks, spot elevations, and vertical-angle bench marks established by the U.S. Coast and Geodetic Survey, U.S. Geological Survey, and the Nevada State Highway Department were used for vertical control. In addition, as part of the gravity survey, one 10-mile line was surveyed across Ruby Valley using planetable methods. For most of the gravity stations the possible error in elevation would not exceed $\pm$5 feet. This corresponds to a gravity error of 0.3 mgal.

INTERPRETATION

The gravity map (fig. 2) has in general borne out the expectation that gravity values would be relatively high in the range and low in the valleys, and that steep gradients would occur over boundary faults. The gravity high over the range, displaced westward from the crestline of the range, is a double feature with a closed high centered near the northwest front of the range. The low area between the two highs is underlain by the Harrison Pass pluton which has an average near-surface density of 2.60 g per cm^3 and a density contrast with rocks to the north and south of 0.05 g per cm^3 and 0.06 g per cm^3, respectively. Gradients are steep along most of the east side of the range, along the west side of the range south of the Harrison Pass pluton, and in the area south of Lamoille, but the gradients are gentle along much of the west side of the range. The steep gradients indicate steep contacts—probably faults—between high density rocks in the range and the less-dense Quaternary and Tertiary deposits in the valleys.

The gravity lows over the valleys are due primarily to an accumulation of low-density fill in the valleys. No wells have been drilled through this material within

the area of the gravity survey (fig. 2), but a well near the confluence of Lamoille Creek and the Humboldt River (14 miles northwest of Lamoille) penetrated 3,150 feet of presumably Cenozoic deposits before going into Paleozoic rocks (Lintz, 1957, p. 39–40). This well is several miles north of the gravity low near Lamoille, and it probably does not represent the total section of the Cenozoic deposits in the central part of the basin. The gravity profiles of figure 3 were used to estimate the thickness of fill in the valleys, assuming a density contrast of 0.45 g per cm^3 between the valley-fill material and the enclosing rocks in the mountains. Steep gradients on the profiles on both sides of the range are interpreted to mark the location of boundary faults. The fill is about 4,600 feet thick (section *A–A′*, fig. 3) in the part of Ruby Valley that underlies the closed gravity low (fig. 2), about 5,500 feet thick in the south end of Ruby Valley (section *B–B′*, fig. 3), and about 5,700 feet thick in the south part of Huntington Valley (section *B–B′*, fig. 3).

Displacement of the gravity highs westward from the crest line of the range cannot be explained by the distribution of dense rock in the range. Density contrasts between various rock units modify the gravity contours (for example the gravity low over the low-density Harrison Pass pluton), but, with the exception of the northwestward elongate −180 mgal high in the northwest part of the range, there is little relationship between the distribution of dense rock and the gross features of the gravity high over the range. The Lamoille Canyon high is centered over an area where calc-silicate rocks of the Cambrian(?) marble of Howard (1966, p. 19–23) are thick. These rocks have densities in excess of 2.80 g per cm^3 and conceivably could be responsible for the gravity high. The only other mass of rock with a density appreciably greater than that assumed in making the corrections is the Devonian and Silurian rocks unit in the southeast part of the range. These rocks, which are thickest on the east side of the range, have an average near-surface density of 2.79 g per cm^3—considerably higher than adjacent rocks—but the gravity high is located over the west side of the range. The eastward bulge in the −190- and −195-mgal contours is over the thickest part of the Devonian and Silurian unit and is the only feature of the southern gravity high that seems clearly related to these dense rocks.

The gravity values over the Ruby Mountains are considerably lower than values over topographically lower bedrock areas to the east and west (fig. 4). Recognition of this feature by Mabey (1964) led him to suggest that the Ruby Mountains might be in partial local isostatic equilibrium. The gravity data (figs. 2 and 3) show, however, that anamolies over the range are too small by an order of magnitude for complete local isostatic compensation. At least part of the low gravity values over the Ruby Mountains, compared to those of adjacent areas, is probably due to an underlying batholith composed of granitic rock much like that in the gneissic granite unit (fig. 1). The average density of the foliated muscovite granite that makes up the bulk of this unit is 2.60 g per cm^3. If the amount of this material increases and the included metasedimentary rocks decrease downward, as

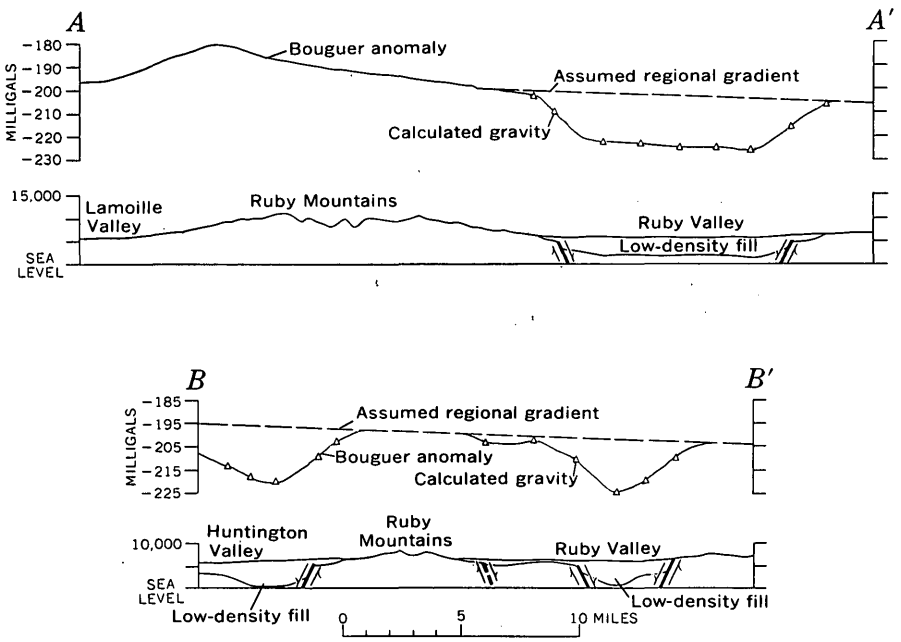

FIGURE 3.—Gravity and topographic profiles across Ruby Mountains and Ruby Valley. Lines of sections shown on figure 2.

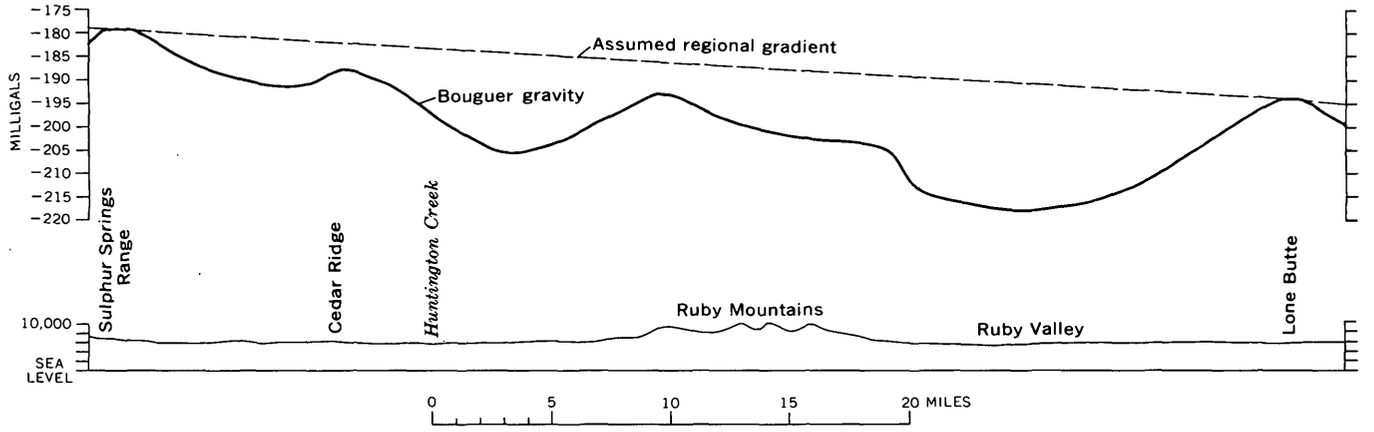

FIGURE 4.—Gravity and topographic profiles from the Sulphur Springs Range across the Ruby Mountains to east of south end of Lone Butte, at approximately lat 40°30′ N.

seems quite likely, a large mass of lower than average density rock may be present beneath the Ruby Mountains. Evidence that the amount of granite in the gneissic granite unit does increase downward can be seen in Lamoille Canyon and one of its principal tributaries, Thomas Canyon, where granite is by far the predominant rock exposed in the canyon bottoms and becomes progressively less abundant upward in the canyon walls (Howard, 1966, fig. 10). The importance of isostatic adjustment of mass anomalies in controlling the position of the Ruby Mountains cannot be evaluated at the present time.

REFERENCES

Collinson, J. W., 1966, Permian and Triassic biostratigraphy of the Medicine Range, Elko County, Nevada: Stanford Univ. unpub. Ph. D. thesis, 130 p.

Hammer, Sigmund, 1939, Terrain corrections for gravimeter stations: Geophysics, v. 4, no. 3, p. 184–194.

Howard, K. A., 1966, Structure of the metamorphic rocks of the northern Ruby Mountains, Nevada: Yale Univ. unpub. Ph. D. thesis, 170 p.

Kane, M. F., and Carlson, J. E., 1961, Gravity anomalies, isostasy, and geologic structure in Clark County, Nevada; Art. 390 *in* U.S. Geol. Survey Prof. Paper 424–D, p. D274–D277.

Kistler, R. W., and Willden, Ronald, 1967, Tectonic and igneous chronology of the southern Ruby Mountains, Nevada: Geol. Soc. America 63d Ann. Mtg., Cordilleran Section, Program, p. 46.

Lintz, Joseph, Jr., 1957, Nevada oil and gas drilling data, 1906–1953: Nevada Bur. Mines Bull. 52, 80 p.

Mabey, D. R., 1960, Regional gravity survey of part of the Basin and Range province; Art 130 *in* U.S. Geol. Survey Prof. Paper 400–B, p. B283–B285.

———1964, Gravity map of Eureka County and adjoining areas, Nevada: U.S. Geol. Survey Geophys. Inv. Map GP–415.

Sandberg, C. H., 1959, Terrain correction charts for transition from Hammer charts to Hayford-Bowie charts: Geophysics, v. 24, p. 323–329.

Sharp, R. P., 1939, Basin-range structure of the Ruby-East Humboldt Range, northeastern Nevada: Geol. Soc. America Bull., v. 50, no. 6, p. 881–920.

———1942, Stratigraphy and structure of the southern Ruby Mountains, Nevada: Geol. Soc. America Bull., v. 53, p. 647–690.

Snelson, Sigmund, 1957, The geology of the northern Ruby Mountains and the Eastern Humboldt Range, Elko County, Nevada: Univ. Washington unpub. Ph. D. thesis, 224 p.

Swick, C. H., 1942, Pendulum gravity measurements and isostatic reductions: U.S. Coast and Geod. Survey Spec. Pub. 232, 82 p.

Willden, Ronald, and Kistler, R. W., 1967, Ordovician tectonism in the Ruby Mountains, Elko County, Nevada, *in* Geological Survey research 1967: U.S. Geol. Survey Prof. Paper 575–D, p. D64–D75.

Wollard, G. P., 1958, Results of a gravity control network at airports in the United States: Geophysics, v. 23, no. 3, p. 520–535.

HAWAIIAN SEISMIC EVENTS DURING 1965

By ROBERT Y. KOYANAGI, Hawaiian Volcano Observatory

Abstract.—During 1965, 565 earthquakes having magnitudes of 2.0 to 4.6, were located in the Hawaiian Islands. These are exclusive of some 300 associated with the December 24–25 eruption of Kilauea Volcano. In all, nearly 30,000 earthquakes were recorded during 1965. The active volcanoes Mauna Loa and Kilauea on the island of Hawaii were zones of highest seismic concentration. In addition to 69 shocks reported as felt by local residents during 1965, many more were felt during the December swarm but were not properly documented.

The following report is a graphical presentation of earthquake locations compiled in the 1965 U.S. Geological Survey Hawaiian Volcano Observatory Summaries 37, 38, 39, and 40 (Okamura and others, 1966; Powers and others, 1966; Koyanagi and others, 1966; Koyanagi and others, in press). It is the fourth of a series of reports (Koyanagi, 1964; Koyanagi and Endo, 1965; Koyanagi and Okamura, 1966) showing locations of Hawaiian earthquakes for specific periods.

Earthquakes of magnitude 2.0 or greater occurring beneath the five volcanoes of the island of Hawaii (fig. 1) and offshore along the Hawaiian Ridge from lat 18° to 23° N. and long 154° to 161° W. are located in figures 2 and 3. The quakes plotted are divided into three depth groups (< 10, 10–20, and 20–60 km) (fig. 4) and two magnitude groups (2.0–3.5, and > 3.5).

Methods and limitations of earthquake determination remain similar to the previous reports. Hawaiian seismic-wave traveltime curves are applied to P-wave arrivals and to S–P values read with 1/10-second accuracy. Earthquakes of magnitude 2.5 or greater beneath the island of Hawaii are generally located within a 5-km sphere of error, although errors as great as 10-km may be expected from earthquakes located offshore or on land at some distance from stations.

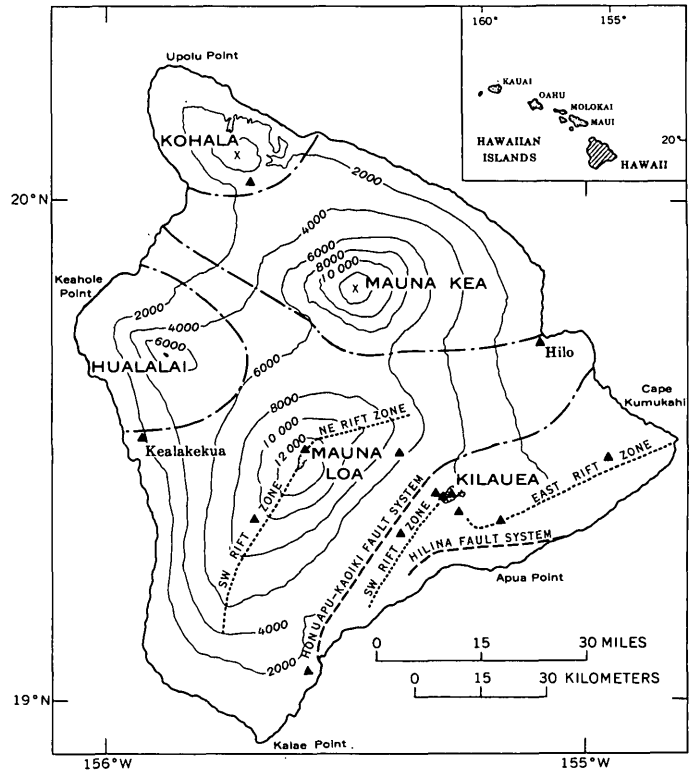

FIGURE 1.—Map of the island of Hawaii, showing the five volcanoes and their principal structural features. Dot-and-dash lines are boundaries of volcanic systems. Locations of seismograph stations are indicated by closed triangles. Contour interval is 2,000 feet, and datum is mean sea level.

1965 CHRONOLOGY OF SEISMIC EVENTS

Of significance during the first quarter of 1965 was the seismic activity that accompanied the March 5–15 flank eruption of Kilauea Volcano. Harmonic tremor and many hundreds of earthquakes occurred during the eruptive period. Except for a few shocks, however, most earthquakes were too small to be located in the usual manner. On March 22 at 09^h33^m,[1] a 4.6-magnitude earthquake was recorded and located about 30 km beneath Mauna Loa's southeast flank. This proved to be the largest event of the year.

[1] All times given are in hours and minutes, Hawaiian standard time.

U.S. GEOL. SURVEY PROF. PAPER 600-B, PAGES B95–B98

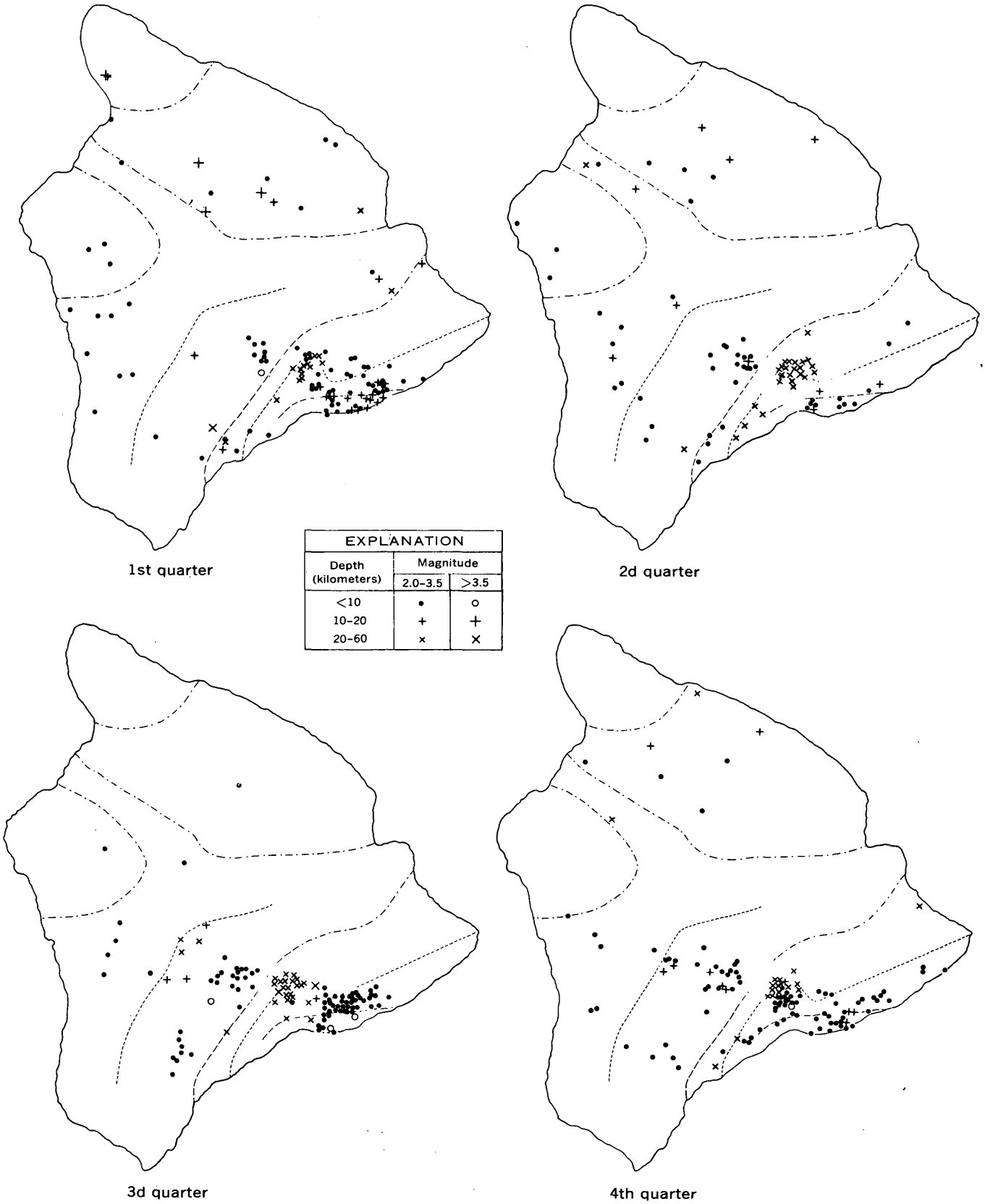

FIGURE 2.—Quarterly plot of epicenters of earthquakes of magnitude 2.0 or greater beneath the island of Hawaii during 1965. Dot-and-dash lines are boundaries of volcanic systems, long-dashed lines are fault systems, and short-dashed lines are rift zones. Geographic names are shown in figure 1.

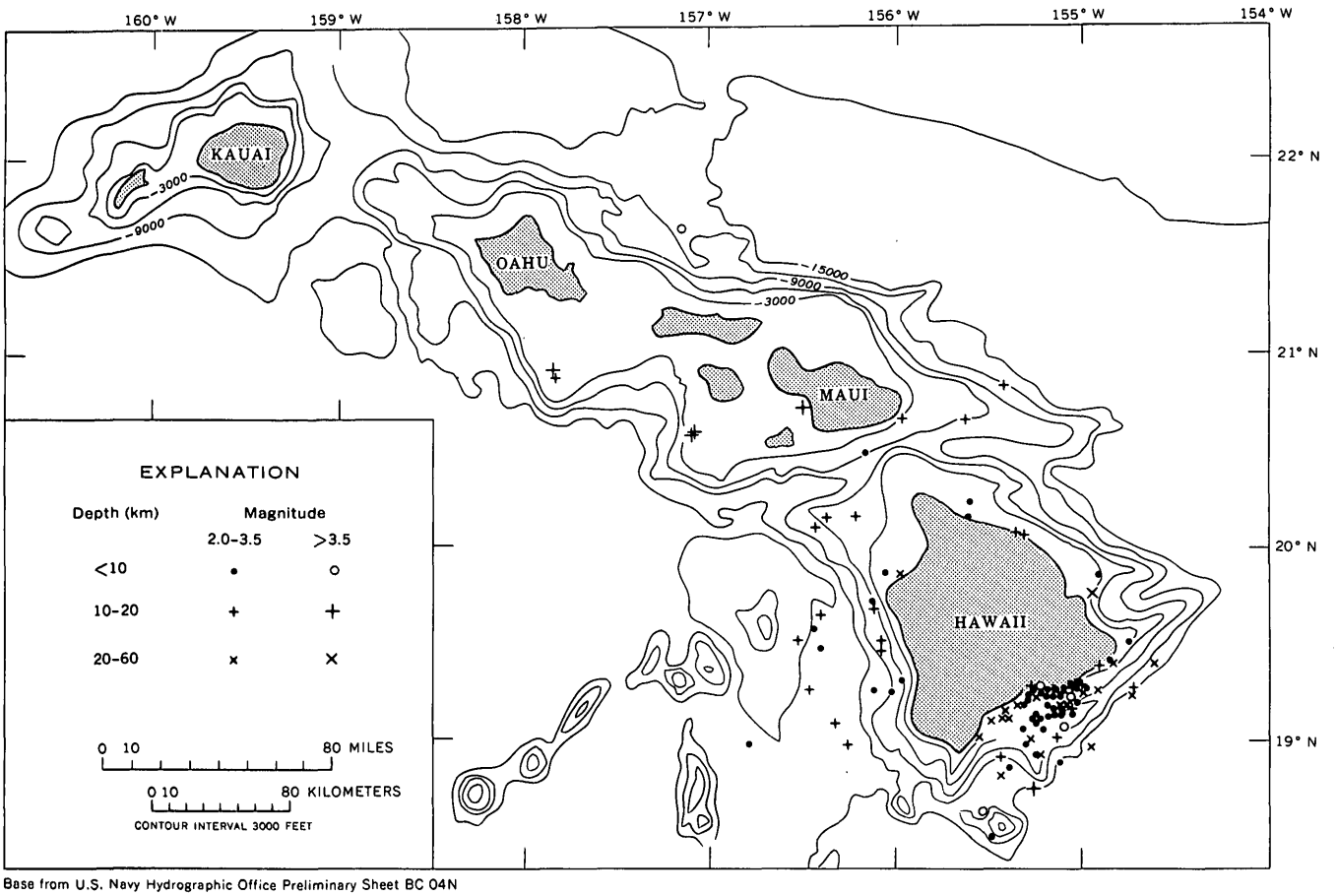

FIGURE 3.—Map of the Hawaiian Islands, showing epicenters of earthquakes having magnitudes of 2.0 or greater that occurred off the island of Hawaii during 1965.

Relative quiescence prevailed throughout the second quarter and early third quarter of 1965. During August 24–26, however, a swarm of more than 500 small earthquakes occurred beneath Kilauea's upper east rift area. Seven of these earthquakes with moderate intensities were reported felt by local residents.

The largest seismic concentration of the year showed at the end of the fourth quarter, during and after a 6-hour flank eruption of Kilauea. Shallow earthquakes, ranging in magnitude from nearly 0 to 4½, numbered many thousands. Most of these quakes were along fault systems curving parallel to the south coastline of Kilauea, south of the summit caldera. Roughly 300 were of magnitude 2 or greater. A special study of this swarm of earthquakes is in preparation, and the details are not presented in this report.

SUMMARY

Nearly 30,000 earthquakes were recorded in Hawaii during 1965; of these, 565 having magnitudes of 2 or greater were located and plotted. As in 1962, 1963, and 1964, the major concentration of earthquakes was near the southeastern part of the Hawaiian Ridge. The

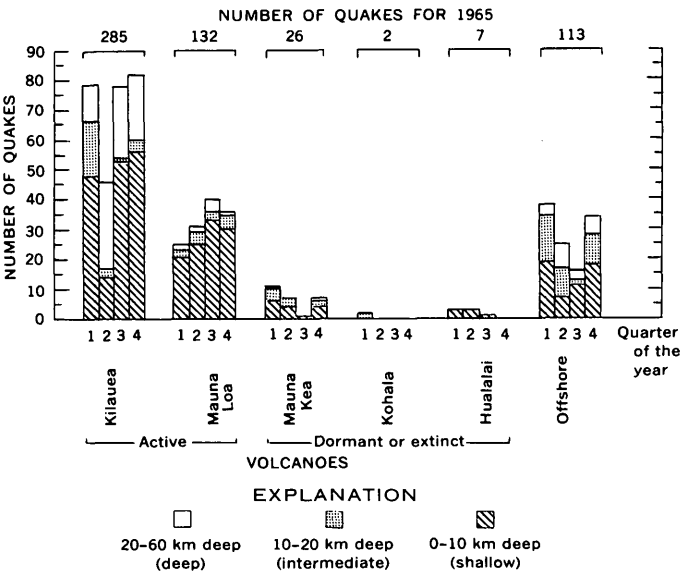

FIGURE 4.—Bar graph showing the geographic location and the distribution, with depth, of earthquakes of magnitude 2.0 and greater which occurred in the Hawaiian Islands during 1965. The graph does not include about 300 Kilauea quakes of shallow origin associated with the December eruption.

epicenters outline active volcanic regions beneath Kilauea and Mauna Loa. Most of the shallow earthquakes occurred beneath Kilauea's caldera region and in areas of recent volcanic eruptions along Kilauea's east rift zone. Many of these small caldera events originate from extremely shallow sources, at depths of 1 km or even less. About 75 percent of the deep earthquakes were concentrated beneath (or several kilometers south of) the Kilauea summit region. These originated from a zone 30 km deep.

In addition to 69 shocks recorded as felt by residents, many dozens felt during the December swarm were not properly reported or documented. Felt earthquakes ranged in magnitude from 2 to 4½. Three of these between 4 and 4½ magnitude were sensed over the entire island.

REFERENCES

Koyanagi, R. Y., 1964, Hawaiian seismic events during 1962: Art. 144 *in* U.S. Geol. Survey Prof. Paper 475–D, p. D112–D117.

Koyanagi, R. Y., and Endo, E. T., 1965, Hawaiian seismic events during 1963, *in* Geological Survey Research 1965: U.S. Geol. Survey Prof. Paper 525–B, p. B13–B16.

Koyanagi, R. Y., and Okamura, A. T., 1966, Hawaiian seismic events during 1964, *in* Geological Survey Research 1966: U.S. Geol. Survey Prof. Paper 550–C, p. C129–C132.

Koyanagi, R. Y., Okamura, A. T., and Kinoshita, W. T., 1966, Hawaiian Volcano Observatory summary: U.S. Geol. Survey Hawaiian Volcano Observatory Summ. 39 (July, Aug., and Sept. 1965).

Koyanagi, R. Y., Okamura, A. T., and Powers, H. A., in press, Hawaiian Volcano Observatory summary: U.S. Geol. Survey Hawaiian Volcano Observatory Summ. 40 (Oct., Nov., and Dec. 1965).

Okamura, A. T., Koyanagi, R. Y., and Powers, H. A., 1966, Hawaiian Volcano Observatory summary: U.S. Geol. Survey Hawaiian Volcano Observatory Summ. 37 (Jan., Feb., and Mar. 1965).

Powers, H. A., Okamura, A. T., and Koyanagi, R. Y., 1966, Hawaiian Volcano Observatory summary: U.S. Geol. Survey Hawaiian Volcano Observatory Summ. 38 (Apr., May, and June 1965).

DETERMINATION OF PALLADIUM AND PLATINUM IN ROCKS

By F. S. GRIMALDI and MARIAN M. SCHNEPFE, Washington, D.C.

Abstract.—Acid-soluble palladium and platinum in rocks are determined spectrophotometrically with α-furildioxime and stannous chloride, respectively. Prior concentration and isolation involve coprecipitation with tellurium and extractions with methyl isobutyl ketone, diethyldithiocarbamate, and α-furildioxime. Approximately 0.01 ppm each of Pd and Pt can be determined as a lower limit on a 10-g sample. The procedure provides for separating up to 50 μg of each element from a total of approximately 50 μg of other platinum metals. The separation and determination processes are examined in detail from the standpoint of both interferences and the measurement of small amounts of palladium and platinum.

This paper presents a sequential procedure for the isolation and spectrophotometric determination of aqua-regia soluble palladium and platinum in rocks. Approximately 0.01 parts per million of Pd and of Pt can be determined as a lower limit on a 10-gram sample. The procedure provides for the separation of up to 50 micrograms of each element from a total of approximately 50 μg of other platinum metals present individually or in mixtures.

The procedure involves preparing the solution, concentrating the noble metals by coprecipitating with tellurium formed by reducing tellurite with stannous chloride, separating tellurium and gold from the platinum metals by extracting into methyl isobutyl ketone (MIBK) from a 4.8*N* HCl solution, separating palladium and platinum from other platinum metals by extracting palladium and platinum diethyldithiocarbamates from a 4*N* HCl solution into chloroform, separating palladium by extracting its α-furildioxime complex from a 1.2*N* HCl solution into chloroform and determining it in this phase, and finally determining platinum in the aqueous phase with stannous chloride.

This procedure integrates known procedures (Ayres and Meyer, 1951; Goto and others, 1958; Grimaldi and Schnepfe, 1967; Ito and others, 1963; Menis and Rains, 1955; Milner and Shipman, 1955; Sandell, 1959, p. 719; Uzumasa and others, 1963; and Yoe and Kirkland, 1954), but a number of modifications were made to improve the results and extend the range to the determination of smaller amounts of palladium and platinum than hitherto attempted. Additional data are given on the individual separation and determination processes to fill some gaps in published information.

EXPERIMENTAL METHOD

Reagents and apparatus

Standard solutions of platinum metals: Prepare from metals or the ammonium chlorosalts stock solutions containing 100μg of metal per milliliter in 2 percent v/v HCl. Prepare other solutions by diluting stock solutions by factors of ten with 2 percent v/v HCl.

Tellurium solution: Prepare a solution containing 1 milligram of Te per milliliter in 10 percent v/v HCl.

Stannous chloride solution A, for the precipitation of tellurium: Dissolve 20 g of $SnCl_2 \cdot 2H_2O$ in 17 ml of HCl. Dilute to 100 ml with water, and filter if necessary. Prepare fresh solutions weekly.

Stannous chloride solution B, for the platinum determination: Dissolve 11.3 g of $SnCl_2 \cdot 2H_2O$ in 17.5 ml of HCl. Dilute to 50 ml with water, and filter if necessary. Prepare fresh solutions weekly.

Sodium chloride solution: 5 mg of NaCl per milliliter.

α-Furildioxime solution: Dissolve 0.500 g of α-furildioxime in 15 ml of absolute alcohol. Dilute to 50 ml with water and filter. Use only a freshly prepared solution. The α-furildioxime shelf reagent should be almost white and yield a low blank. The reagent can be purified by mixing its solution with decolorizing carbon just before filtration, the amount added being determined by the quality of the α-furildioxime. For example, for an old lot of α-furildioxime, a weight ratio of 5 parts Norit to 1 of α-furildioxime was required to reduce the absorbance of the blank from 0.3 to 0.007.

Sodium diethyldithiocarbamate solution, 4 percent w/v aqueous solution: Prepare fresh as needed, and filter if necessary.

Potassium iodide solution, 15 percent w/v aqueous solution: Prepare fresh.

Analyzed reagent grade chloroform and methyl isobutyl ketone.

Beckman model DU spectrophotometer for light-absorption measurements. All cells were made of fused quartz. The "micro" 5-centimeter cells have a volume of approximately 2.5 ml.

U.S. GEOL. SURVEY PROF. PAPER 600-B, PAGES B99-B103

Procedure

1. The sample is decomposed and the tellurium precipitation is made according to the method described by Grimaldi and Schnepfe (1967), except that platinum is not added as a carrier inasmuch as this element is to be determined. Note that nitrates or other oxidants must be thoroughly removed before the tellurium precipitation. A procedural blank should be carried along with the samples.
2. Filter the tellurium precipitate on a Fisher filtrator through a medium-porosity fritted-glass Buchner-type filter funnel having a volume of approximately 20 ml. Wash the tellurium precipitate thoroughly with hot 8-percent-by-volume HCl. Discard the filtrate and the washings.
3. Dissolve the precipitate with several 10-ml portions of hot aqua regia (8 volumes of HCl to 2 of HNO_3 and 5 of H_2O), and collect the filtrate in a 100-ml beaker. With each addition of aqua regia, the vacuum should be turned off for several minutes to permit dissolution of the precipitate. Wash finally with hot 8-percent-by-volume HCl.
4. Evaporate the filtrate and washings to dryness. Remove nitrate by several evaporations to dryness with 3-ml portions of HCl.
5. Add 10-ml of 4.8*N* HCl, warm the mixture briefly on the steam bath to dissolve the salts, and then transfer the solution to a 60-ml separatory funnel; do not wash the beaker.
6. Extract 3 times with 5-ml portions of methyl isobutyl ketone; shake for 1 minute each time. Discard the upper organic layer.
7. Transfer the aqueous phase into a 30-ml beaker. Add 1 ml of the NaCl solution, and evaporate the solution to dryness on the steam bath.
8. Destroy organic matter by treating the residue 2 times with 1 ml of fuming HNO_3, each time digesting the solution for several minutes before evaporating to dryness on the steam bath.
9. Treat the residue with 20 drops of (1+1) HNO_3 and 3 ml of HCl. Evaporate to dryness.
10. Treat the residue 3 times with 1-ml portions of HCl. Evaporate to dryness each time to remove the nitrate.
11. Add 3.33 ml of HCl and 2.67 ml of water. Warm the mixture briefly on the steam bath to dissolve salts, and transfer to a 60-ml separatory funnel. Use two 1-ml portions of water to assist in the transfer.
12. After mixing, add 1 ml of the KI solution. Allow 5 minutes to elapse, while shaking the solution at intervals.
13. Add 1 ml of the sodium diethyldithiocarbamate solution; mix the solution vigorously as the reagent is added. Allow 5 minutes to elapse, again shaking the solution at intervals.
14. Add 5 ml of chloroform and shake for 1 minute. Drain the chloroform extract into a 30-ml beaker.
15. Repeat step 14, and collect the chloroform extract in the same beaker. Reject the aqueous phase.
16. Add 1 ml of the NaCl solution to the combined chloroform extracts, and cautiously evaporate the mixture to dryness.
17. Repeat steps 8, 9, and 10. The residue should be colorless.
18. Add 2 ml of (1+1) HCl and 3 ml of H_2O. After warming the mixture on the steam bath, transfer to a dry 60-ml separatory funnel. Wash the beaker 3 times with 1-ml portions of water. The volume should be 8 ml at this point.
19. In separatory funnels prepare a blank and several palladium standards, each with the same volume and acidity as the samples.
20. Add 2 ml of α-furildioxime solution, and mix.
21. Add 5 ml of chloroform, shake for 1 minute, and drain the chloroform extract into a small beaker. Cover the beaker between extractions to minimize evaporation.
22. Repeat step 21, and combine the chloroform extracts.
23. Mix the combined chloroform extracts thoroughly, and filter through a dry medium-fast 5.5-cm paper on a dry funnel. This procedure quickly removes traces of moisture. Keep the chloroform solutions covered with watch glasses until the absorbances are determined.
24. Determine the absorbance in a 2-cm cell at 380 millimicrons against chloroform. To eliminate differences in cells, the same cell should be used for standards and samples. Correct absorbances of samples for the procedural blank.
25. Drain the aqueous layer in the separatory funnel into a 30-ml beaker. Wash the separatory funnel with small quantities of water, and add the washings to the beaker. Evaporate the solution to dryness.
26. Add 1 ml of fuming HNO_3, digest the solution on the steam bath several minutes, and then evaporate to dryness.
27. Add 1 ml of fuming HNO_3 and 1 ml of $HClO_4$. Evaporate the HNO_3, and bring to fumes of $HClO_4$. Cover the beaker with a watch glass, and reflux on a hotplate until the solution is colorless. Fume off the $HClO_4$ with gentle heat on a hotplate.
28. Add another 1 ml of $HClO_4$, and again gently fume to dryness. There may remain a negligible amount of $HClO_4$ condensate on the upper walls of the beaker.
29. Treat the residue with aqua regia and hydrochloric acid as provided in steps 9 and 10.
30. Add 1 ml of (1+1) HCl, and mix.
31. Add 3 ml of water, then cover and heat briefly on the steam bath to dissolve salts. Cool.
32. Prepare blank and standard solutions of platinum having the same volume and acidity.
33. Add 1 ml of the stannous chloride solution B.
34. Determine the absorbance in a 5-cm cell at 405 mμ against the blank as reference solution. To eliminate differences in cells, the same cell should be used for standards and samples. Correct absorbances of samples for the procedural blank.

RESULTS

Coprecipitation of palladium and platinum with tellurium

Palladium and platinum as well as gold, mercury, and silver are coprecipitated quantitatively with tellurium, and practically all the rhodium and some of the iridium are also coprecipitated (Sandell, 1959, p. 621, 711). Our data confirm that coprecipitation of palladium and platinum is quantitative. Low palladium and platinum recoveries were noted, especially when rhodium and iridium were present, if the tellurium precipitates were ignited and then treated with aqua regia. This may be due to the formation of alloys or metals which are somewhat resistant to the action of aqua regia. For this reason the tellurium precipitates were dissolved without prior ignition.

Methyl isobutyl ketone (MIBK) extraction of tellurium and gold

The percentages of Te(IV), Au(III), Pd(II), and Pt(IV) extracted individually by an equal volume of

MIBK were found to be 98.6, >99, <0.1, and <1, respectively, when 500 μg of each element was taken; the results being independent of the acidity in the range of 4*N* to 6*N* HCl.

Diethyldithiocarbamic acid (DTC) extraction of palladium and platinum

Effect of acidity.—Palladium and platinum are extracted quantitatively as complex diethyldithiocarbamates from solutions ranging in HCl concentration from 1*N* to 9*N*. Rhodium is not extracted in measurable amounts under the same conditions. Tests were made on 10 μg of Pd, 50 μg of Pt, and 50 μg of Rh separately, while the KI and the DTC concentrations were kept fixed at levels recommended in the procedure. Iridium was not tested at this time because it does not represent a serious interference in the determination of either palladium or platinum.

Effect of the potassium iodide concentration.—Palladium and platinum are extracted quantitatively when the KI concentration is varied from 0.05 to 0.25 g per 10 ml and other conditions are kept constant. Rhodium is not extracted in measurable amounts. Tests were made on 3 separate solutions containing 20 μg of Pd, 50 μg of Pt, and 50 μg of Rh, respectively, as well as on 4 mixtures containing 2 μg of Pt and 50 μg of Os, 2 μg of Pt and 50 μg of Rh, 50 μg of Pt and 2 μg of Os, and 50 μg of Pt and 2 μg of Rh.

Effect of DTC concentration.—Recovery of palladium and platinum is quantitative and independent of DTC concentration when this concentration is varied from one half to twice the recommended amount (0.02 to 0.08 g per 10 ml), provided the other conditions are kept constant as prescribed in the procedure. Rhodium and iridium are not extracted in measurable amounts. Tests were made on 4 separate solutions containing 20 μg of Pd, 20 μg of Pt, 50 μg of Rh, and 50 μg of Ir, respectively.

Effect of time.—A slight tendency for rhodium to extract was noted when the reaction time of the potassium iodide was unduly prolonged. With a 20-minute reaction time after the addition of potassium iodide, no rhodium was extracted with a test on 50 μg of Rh. When an hour was allowed to elapse after the potassium iodide addition and before the addition of DTC, approximately 0.8 μg of Rh was extracted; and with a 2-hour wait between additions, approximately 1.4 μg of Rh was extracted.

α-Furildioxime separation and determination of palladium

Reagent concentrations.—Menis and Rains (1955) noted that the palladium—α-furildioxime complex is quantitatively extracted into chloroform independent of the acidity of the aqueous phase in the range of 0.1*N* to 1.4*N* HCl. We adopted a 1.2*N* HCl concentration.

A minimum of 0.3 ml of the 1-percent-weight-per-volume α-furildioxime solution was required to give full color development with 50 μg of Pd. The color intensity for 50 μg of Pd was constant when the volume of α-furildioxime was varied up to 3 ml, the maximum volume of the reagent tested. A volume of 2.0 ml was chosen. That this quantity of α-furildioxime is suitable for small amounts of palladium was shown by a linear working curve of net absorbance versus palladium solution concentration in the 0- to 5-ppm range. The sensitivity by Sandell's definition is 0.0045 μg/cm² at 380 mμ.

Reproductibility of absorbances of blanks and palladium solutions.—The reproducibility of the absorbance of blanks and of palladium solutions sets the minimum amount of palladium that can be determined. Accordingly, the absorbances of 15 blanks, 6 solutions containing 0.05 ppm of Pd, and another 6 containing 1 ppm of Pd, all in chloroform extracts, were determined at 380 mμ when a 2-cm light path was used. The following results were obtained: the maximum difference in the blanks and in the 0.05 ppm of Pd solutions was 0.002, the average difference from the mean being 0.0008 in both series of determinations. The maximum difference in the 1 ppm of Pd solutions was 0.007, the average difference from the mean being 0.0035.

These results indicate that 0.1 μg of Pd in a 10-ml volume yielding a net absorbance of 0.005 is determinable as a lower limit. Thus on a 10-g sample of rock the minimum palladium concentration determinable is approximately 0.01 ppm.

Destruction of organic matter

After each extraction, organic matter needs to be destroyed. Fuming HNO_3 is effective for the destruction of organic matter remaining from the methyl isobutyl ketone and diethyldithiocarbamic acid extractions. The fuming HNO_3 is easily evaporated on the steam bath without subjecting the palladium to elevated temperatures which tend to make palladium difficultly soluble or unreactive. After the palladium is removed, the α-furildioxime remaining in the aqueous phase must be destroyed and requires a more vigorous oxidant than fuming HNO_3. Fortunately, platinum is less sensitive to heating conditions than the palladium. The α-furildioxime is effectively destroyed by a combination of fuming HNO_3 and $HClO_4$. Because of the possibility of reducing the elements to the metallic state during the destruction of organic matter, the residues are treated with aqua regia followed by hydrochloric acid. A small

quantity of sodium chloride is carried along to minimize plating of the metals on glassware.

Test of the DTC and α-furildioxime extractions

The effectiveness of the DTC and the combined DTC–α-furildioxime extractions were tested on synthetic solutions containing various mixtures of platinum metals. In those tests where palladium was absent it was possible to check the DTC extraction directly by evaporating the DTC organic extract to dryness, destroying the organic matter, and applying the stannous chloride method for platinum. A duplicate set of such test solutions was also carried through the combined DTC and α-furildioxime extractions. Where palladium was present an α-furildioxime extraction was made, after the DTC extraction, to separate and determine palladium. The stannous chloride method was applied on all test solutions, even in the absence of platinum, to verify that platinum would not be reported when it is absent. Quantitative results for palladium and platinum without disturbances from other elements, obtained for all the test solutions described below, indicate that palladium and platinum are effectively isolated by a combination of DTC and α-furildioxime extractions. The sets of test solutions are made up as follows: Six 2-μg solutions of Pt, each containing 50 μg of one of the elements Pd (II), Rh(III), Rh(IV), Ir(IV), Os(IV), and Ru(IV); six 50-μg solutions of Pt, each containing 2 μg of one of the forementioned elements; one 2 μg solution and one 50-μg solution of platinum each containing a mixture of 10 μg each of Pd(II), Rh(IV), Ir(IV), Os(IV), and Ru(IV); one 10-μg solution of Pd, one 2-μg solution of Pt, and one 10μg solution of Pt each containing a mixture of 10 μg each of Rh(IV) and Ir(IV); and one solution containing a mixture of 10 μg of Pd and 10 μg of Pt.

Stannous chloride procedure for the determination of platinum

Prior to selecting a stannous chloride procedure for determining platinum, comparative studies were made of the p-nitrosodimethylaniline method of Yoe and Kirkland (1954) and the stannous chloride procedure of Ayres and Meyer (1951). The p-nitrosodimethylaniline method, although more sensitive than the stannous chloride procedure by almost a factor of ten, has more serious interference from platinum metals and iron. But we abandoned it primarily because of poor precision; the absorbances of blank and platinum solutions were critically dependent on the heating technique. The stannous chloride method was adopted because of its exceptionally high precision.

Reagent concentrations.—The color reaction is independent of HCl concentration in the range from 0.7*N* to 6*N*, and independent of $SnCl_2$ concentration in the range from 0.2 to 2 times the recommended amount. However, interference from palladium and rhodium increases with decreasing stannous chloride concentration.

Reproducibility of absorbances of blanks and platinum solutions.—The maximum difference in the absorbances (5-cm light path) of six blanks was found to be 0.001, the average difference from the mean being 0.0003. Similarly, the maximum difference among six 0.04-ppm platinum standards was also 0.001, the average difference being 0.0002. The reproducibilities enable the determination of 0.1 μg of Pt in the prescribed 5-ml volume (net absorbance of 0.0042), corresponding to approximately 0.01 ppm of Pt in a 10-g sample.

The standard curve relating absorbance to concentration of platinum at 405 mμ is linear up to a concentration of 40 ppm of Pt, the maximum amount tested. The concentration range from 0 to 5 ppm was examined in detail for deviation from a straight line; none was found. The sensitivity according to Sandell's definition corresponds to 0.024 μg/cm². No change in the absorbances was observed after 3 hours.

Effect of other elements.—Tolerances for various elements expressed as micrograms of element giving a net absorbance equivalent to 1 μg of Pt are given in table 1. Except for tellurium, absorbances of mixtures are additive. With tellurium there is an interplay of two effects: (1) increase in absorbance due to the formation of a tellurium sol, and (2) decrease in absorbance due to the coprecipitation of platinum. The net effect varies, depending on both the tellurium and platinum concentrations. Interference of palladium is seen to be dependent on the palladium concentration. Palladium, rhodium, and gold form unstable solutions, the extent of interference of each being time dependent.

TABLE 1.—*Tolerances for various elements and certain radicals, and the effect of time, in the stannous chloride procedure for the determination of platinum*

Element or radical	Concentration (ppm)	Micrograms of element equivalent to 1 μg of Pt	
		In zero time	In 30 minutes
Te	2	0.8	0.8
	2+0.4 ppm of Pt	1.1	1.1
	2+2 ppm of Pt	1.3	1.3
	0.6	.9	.9
	0.6+0.4 ppm of Pt	.8	.8
	0.6+2 ppm of Pt	2	2
Pd	1	7	7
	2	7	4.7
	3	5	2.5
	5	5	1.7
	10	2	1.2
	5+5 ppm of Pt	5	1.7
	10+10 ppm of Pt	2	1.2
Rh(III) or (IV)	1	.5	3.2
	2	.5	3.1
	3	.6	3.1
	10	.7	3.1
	10+10 ppm of Pt	.7	3.2
Ru(IV)	2	7	8
	10	4.7	5.3
	10+10 ppm of Pt	4.7	5.3
Os(IV)	2	10	11
	10	8	10
	10+10 ppm of Pt	8	10
Au(III)	2	100	30
	2+2 ppm of Pt	100	30
	10	20	12
	10+2 ppm of Pt	20	12
Ir(IV)	10	100	100
	10+10 ppm of Pt	100	100
	50	100	100
	50+50 ppm of Pt	100	100
Ni	1,000	500	500
	1,000+2 ppm of Pt	500	500
Co	2,000	7,000	7,000
	2,000+2 ppm of Pt	7,000	7,000
Fe(III)	10,000	35,000	35,000
	10,000+2 ppm of Pt	35,000	35,000
Cu	4,000	40,000	40,000
	4,000+2 ppm of Pt	40,000	40,000
Pb	1,000	No interference	No interference.
	1,000+2 ppm of Pt	--do--	Do.
	2,000	$PbCl_2$ precipitates	$PbCl_2$ precipitates.
NO_3	20,000	No interference	No interference.
	20,000+2 ppm of Pt	--do--	Do.
SO_4	4,000	--do--	Do.
	4,000+2 ppm of Pt	--do--	Do.
Ag	40	--do--	Do.
	40+2 ppm of Pt	--do--	Do.
	50	AgCl precipitates	AgCl precipitates

Test of the total procedure

Synthetic solutions containing one of each of the following combinations of elements, 50 μg of Pd and 2 μg of Pt, 10μg of Pd and 10 μg of Pt, 2 μg of Pd and 50 μg of Pt, and 10 μg of Pd in a mixture also containing 10 μg each of Pt, Rh, and Ir, were carried through the entire procedure, starting with the tellurium precipitation. Recoveries of palladium and platinum were better than 94 percent in each experiment. The procedure was also tested on a basalt spiked with identical mixtures of elements. Again, quantitative recoveries of added palladium and platinum were obtained.

REFERENCES

Ayres, G. H., and Meyer, A. S., Jr., 1951, Spectrophotometric study of the platinum(IV)–tin(II) chloride system: Anal. Chemistry, v. 23, no. 2, p. 299–304.

Goto, Hidehiro, Kakita, Yachiyo, and Furukawa, Takeshi., 1958, Methyl isobutyl ketone extraction and determination of metallic salts; I–Extraction of iron, antimony, tin, arsenic, selenium, tellurium, and germanium from solutions containing hydrochloric acid and (or) other acids: Nippon Kagaku Zasshi, v. 79, p. 1513–1520.

Grimaldi, F. S., and Schnepfe, M. M., 1967, Determination of palladium in the parts-per-billion range in rocks, *in* Geological Survey Research 1967: U.S. Geol. Survey Prof. Paper 575–C, p. C141–C144.

Ito, Saburo, Hayashi, Kenjiro, and Uzumasa, Yasumitsu, 1963, Separation of trace amounts of Te from Al, Bi, Cr, Co, Cu, Ni, and Se: Bunsei Kagaku, v. 12, p. 257–261.

Menis, Oscar, and Rains, T. C., 1955, Colorimetric determination of palladium with alpha-furildioxime: Anal. Chemistry, v. 27, no. 12, p. 1932–1934.

Milner, O. I., and Shipman, G. F., 1955, Colorimetric determination of platinum with stannous chloride: Anal. Chemistry, v. 27, no. 9, p. 1476–1478.

Sandell, E. B., 1959, Colorimetric determination of traces of metals, 3d ed.: New York-London, Interscience, 1032 p.

Uzumasa, Yasumitsu, Hayashi, Kenjiro, and Ito, Saburo, 1963, The separation of trace amounts of tellurium from iron by solvent extraction: Chem. Soc. of Japan Bull., v. 36, p. 301–306.

Yoe, J. H., and Kirkland, J. J., 1954, Separation of platinum and palladium and their subsequent colorimetric determination with p-nitrosodimethylaniline: Anal. Chemistry, v. 26, no. 8, p. 1335–1339.

ORIGIN OF THE SODIUM SULFATE DEPOSITS OF THE NORTHERN GREAT PLAINS OF CANADA AND THE UNITED STATES

By I. G. GROSSMAN, Hartford, Conn.

Abstract.—Widespread surficial deposits of sodium sulfate in the northern Great Plains may have been derived from deeply buried evaporites of the Prairie Formation of Devonian age. Ground water from the Rocky Mountain area presumably circulated eastward into the large structural basin underlying the Great Plains in Canada and northern United States, dissolving the evaporites at great depth from late Devonian time onward. In late Pleistocene time, ascending mineralized ground water discharged into melt-water channels in stratified drift overlying buried bedrock valleys. Freezing segregated pure crystals of sodium sulfate which accumulated in meromictic lakes. The residual brines discharged into streams draining southward into the Missouri River system. Rising temperatures and increasing aridity gradually disintegrated the drainage pattern in an area where the deposits are preserved beneath extinct or shrunken lakes.

The northern Great Plains of Canada and the United States are occupied by thousands of shallow lakes and extinct lake basins. Valuable deposits of sodium sulfate underlie many of these basins in a broad area about 100 to 300 miles wide, extending 400 miles from Alberta and Saskatchewan, Canada, southeastward to northwestern North Dakota and northeastern Montana (fig. 1). All the deposits are lacustrine and lie within areas covered by Pleistocene drift; their common stratigraphy and mutual proximity suggest a common origin.

The present paper is a reevaluation of an earlier, limited study of the sodium sulfate deposits in North Dakota by the author (Grossman, 1949a, 1949b), supplemented by a study of the literature on the Canadian deposits.

Acknowledgments.—The fieldwork on the deposits in North Dakota was sponsored by the North Dakota Geological Survey, Dr. Wilson M. Laird, State Geologist. The present paper was critically reviewed and improved by William Back, B. F. Jones, and Q. F. Paulson, but responsibility for the principal conclusions remains my own. I am indebted to Eric Engebrecht for able field assistance, and to Frank Boucher, Dorothy LaBella, and Ann Grossman for able assistance in the physical preparation of the report.

EARLIER THEORIES

The origin of the sodium sulfate deposits has puzzled investigators for at least a half century. Grabau (1920, p. 222) surmised that Chaplin Lake in southern Saskatchewan owed its saline constituents principally to decomposed igneous rocks and perhaps partly to connate salts and older salt beds. Cole (1926, p. 78) suggested that the Canadian deposits originated by base exchange between gypsum and alkali silicates of the bentonite in the glacial drift. Sahinen (1956, p. 4) indicated that such a process could explain the deposits in northeastern Montana but that these also could have been derived by solution from the Fort Union Formation, which directly underlies the drift here. An analysis of the sandy shales in that formation near Plentywood, in extreme northeastern Montana, showed more than 1 percent sodium sulfate. However, glacial drift covers vast areas in Canada and the northern United States that lack sodium sulfate deposits; and the Fort Union Formation also is far more widespread than the area occupied by the deposits.

DEEPLY BURIED EVAPORITES

Intensive drilling resulting from major oil and gas discoveries in the 1950's disclosed the widespread occurrence of thick beds of halite, anhydrite, and potassium salts at great depths throughout the area. The evaporites are buried under a cover of younger rock 1,000 feet thick in Manitoba, about 5,000 feet thick at Regina, Saskatchewan, and about 8,000 feet thick in North Dakota (DeMille and others, 1964, p. 310). The deepest evaporites are Devonian. The principal deposits, in the Prairie Formation, are more than 800

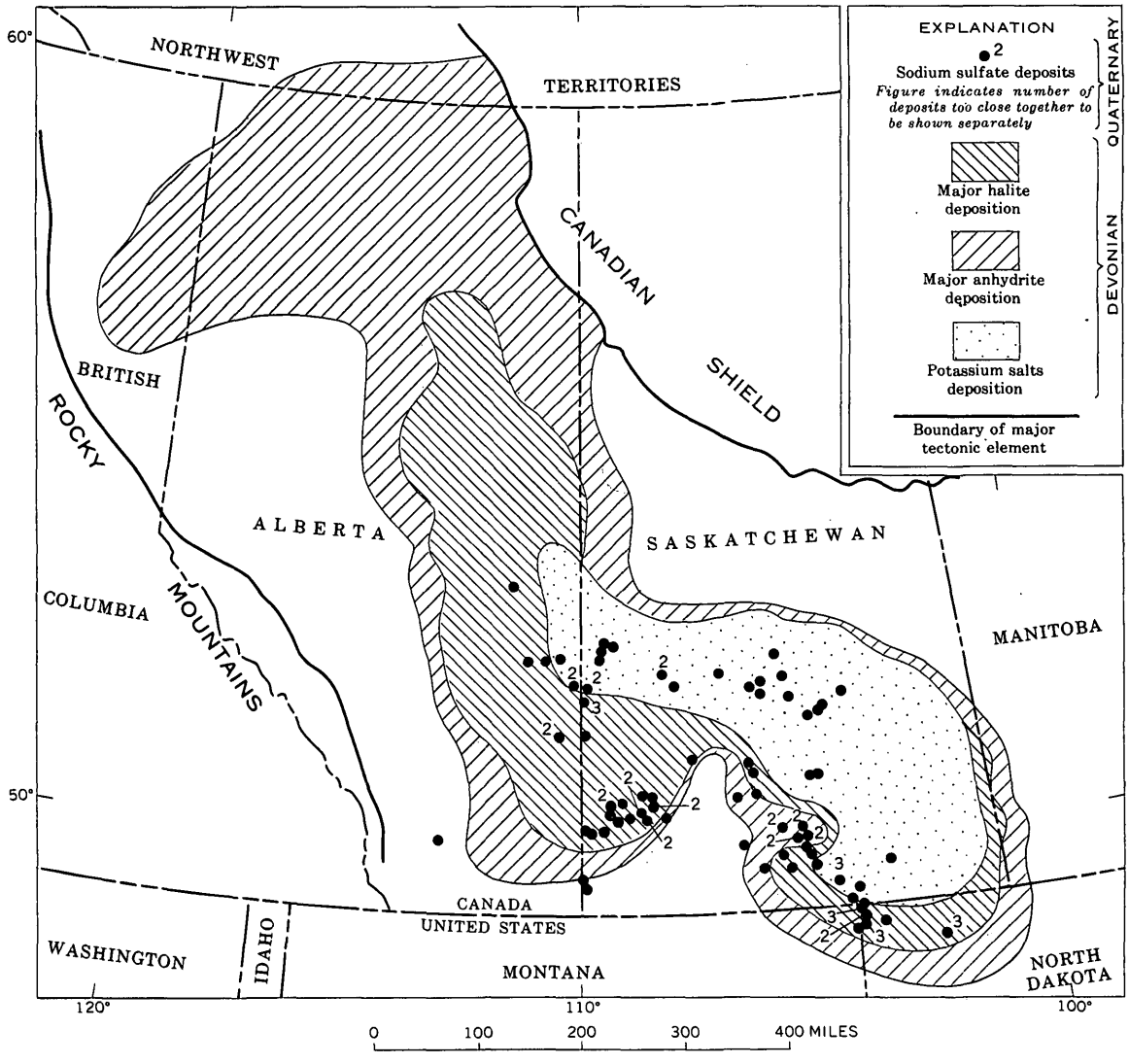

FIGURE 1.—Distribution of surficial sodium sulfate deposits and extent of deeply buried bedrock evaporites in the northern Great Plains of Canada and the United States. Sodium sulfate deposits in Canada from Cole (1926, map 647); in the United States from Binyon (1952, fig. 1); buried evaporites from DeMille and others (1964, fig. 3).

feet thick in Alberta and 670 feet thick in Saskatchewan. The extent of the major types of salt deposits in the Prairie Formation and equivalents as delineated by De Mille and others (1964, fig. 3) is shown in figure 1. It is evident that the surficial sodium sulfate deposits lie almost entirely within the area underlain by the deeply buried evaporites in the Prairie Formation.

Moreover, the surficial deposits occur in three belts whose relation to the deep-lying evaporites is suggestive. The largest and northernmost belt, containing at least 30 surficial deposits, trends approximately east-west with a slightly arcuate southeasterly component. Despite considerable scatter, it is crudely parallel to the main trend of the deeply buried evaporites in the south. The southeastern belt, which contains at least 38 surficial deposits, trends southeastward in a roughly arcuate belt approximately parallel to the southwest margin of the deeply buried beds and parallel to the east side of a pronounced reentrant. The smallest belt, which includes at least 20 surficial deposits, trends southwestward, nearly parallel to the west side of the same reentrant. The reentrant approximately coincides with an area mapped by Bishop (1954, fig. 1) as one in which salt had originally been present but had been removed by solution. It is possible that some new sodium sulfate deposits have recently been discovered, but the distribution of the known deposits and their alinement suggest that they may have been derived from the deeply buried evaporites of the Prairie Formation.

Evidence that the Prairie evaporites have been severely affected by underground solution and that the leaching took place while they were buried under thousands of feet of sediments has been convincingly presented by Bishop (1954, p. 485) and DeMille and others (1964, p. 314). Some of the best evidence consists of depressions in the regional structure. Within these depressions, salt beds present elsewhere are missing and the amount of depression in the overlying beds is nearly equal to the amount of missing salt. The depressions also contain solution or collapse breccias that are restricted to the beds younger than the salt. Significantly, these breccias have not been observed where the salt is still present. The evidence indicates that solution occurred at different geologic ages from Late Devonian to the present. The solution-and-removal theory has been widely accepted, although Klingspor (1966, p. 206) has raised objections.

PALEOHYDROLOGIC CYCLE

Where did the missing salts go? DeMille assumed that ground water moved *downward* in the area before reaching and dissolving the deeply buried evaporites. However, the absence of a local topographically high recharge area to furnish the necessary head for removal of deep salt-laden water to some lower distant area of discharge is a weak link in this otherwise well-documented chain of evidence. The stratigraphy of southern Saskatchewan (DeMille and others, 1964, fig. 2) shows that the area remained a topographic and structural low throughout most of post-Devonian time, receiving vast quantities of clastic and nonclastic sediments. Bishop (1954, p. 480) suggested that in one case perhaps solutions moved *upward* from one "* * * salt" and were redeposited to form stratigraphically higher "* * * salts." However, neither he nor DeMille attempted to trace the circulation of ground water during solution and removal of the Prairie salts.

A credible reconstruction of the hydrologic cycle is deducible from the regional geology and structure. A large structural basin extends from British Columbia and Northwest Territories southeastward into northwestern North Dakota. This major structural low coincides in a general way with the occurrence of the deeply buried evaporates (fig. 1). It is flanked on the west by the Rocky Mountains, a topographic high which was tectonically active from Devonian times onward; on the east, the basin or structural low is flanked by the stable Canadian Shield, worn down to a moderate lowland by repeated erosion. Water entering the upturned flanks of permeable beds interlayered with impermeable beds in high-level recharge areas in the Rocky Mountains moves downdip and eastward into the major structural basin. It continues eastward following the permeable beds updip in the direction of decreasing artesian head to discharge points in areas flanking the Canadian Shield. Some of this eastward-moving water might leak vertically upward through semileaky confining beds. The likelihood and amount of such upward leakage would increase after collapse of overlying beds.

The existence of a regional artesian system with eastward movement, though at a shallower depth, was demonstrated by Darton (1909) in South Dakota. His field studies of deep wells and artesian pressures showed that water entered the upturned flanks of the Dakota Sandstone, the principal bedrock aquifer, in the Black Hills and moved eastward hundreds of miles where it was found in wells at depths of as much as 2,000 feet. Darton also traced the origin of highly mineralized water from deep wells drilled in North Dakota to water that had entered the Dakota Sandstone on the upturned flanks of the Rocky Mountains and had traveled eastward beneath confining beds toward discharge areas in the east. Simpson (1929) showed that the artesian conditions in the Dakota Sandstone extended at least as far north as the Canadian border. In view of the depth and the persistence of the major tectonic basin between the Rocky Mountains and the Canadian Shield, it is likely that ground water at greater depths has generally circulated in an eastward or northeastward direction. A similar conclusion was reached by Milner (1956, p. 111), who stated "The solution of the salt is attributed to movement of subsurface waters across the Province. Studies of the salinity and formation pressures indicate that this movement is in a general northeast direction and is still taking place today. The Prairie evaporites are being dissolved at the present time and local earth movements have been recorded in recent times." Accordingly it is hypothesized that the water which dissolved the huge volumes of salt at various periods from Devonian to Recent moved eastward from areas of higher to lower head. Much of its dissolved load ultimately was discharged at the surface into streams that eventually reached the sea.

INTERIOR DRAINAGE AND EVAPORATION

The pattern and direction of the preglacial surface drainage have been summarized by Lemke and others (1965, fig. 1). In preglacial times the streams of North Dakota drained northward to Hudson Bay. Postglacial streams in all but the north-central and eastern part of the State now flow southward into the Mississippi River and the Gulf of Mexico by way of the Missouri River and its tributaries. However, between

the south-draining area and the area that continues to drain northward lies an intermediate area of essentially interior drainage. This area, which roughly coincides with a belt of glacial moraines (fig. 2), is marked by irregular topography and many small lakes and undrained depressions. Moraines extend northwestward from North Dakota and northeastern Montana into Canada where their extent is not shown. The anions and cations formerly carried to the sea accumulated in closed depressions within this postglacial area of interior drainage.

The map (fig. 2) shows that the sodium sulfate deposits of North Dakota and northeastern Montana lie entirely within the area of interior drainage and also are restricted to the driest part of this belt, west of the approximate 15-inch line of annual average precipitation. Evaporation of water and concentration of dissolved salts in closed basins are favored by a dry climate; hence, evaporation of salt-laden artesian water derived from springs has been used to explain the origin of the sodium sulfate deposits in this area (Witkind 1952, p. 667). However, the relative purity of the deposits is such that they cannot have been derived by total evaporation of ground water discharged into closed lakes. Analyses of water from springs and from wells in glacial drift or bedrock indicate that ground water throughout the area contains substantial amounts of ions other than Na^{+2} and So_4^{-2}. Evaporation of this water would precipitate several salts, the order of deposition being from least soluble (for example, calcium carbonate) to most soluble, with sodium sulfate as as intermediate product.

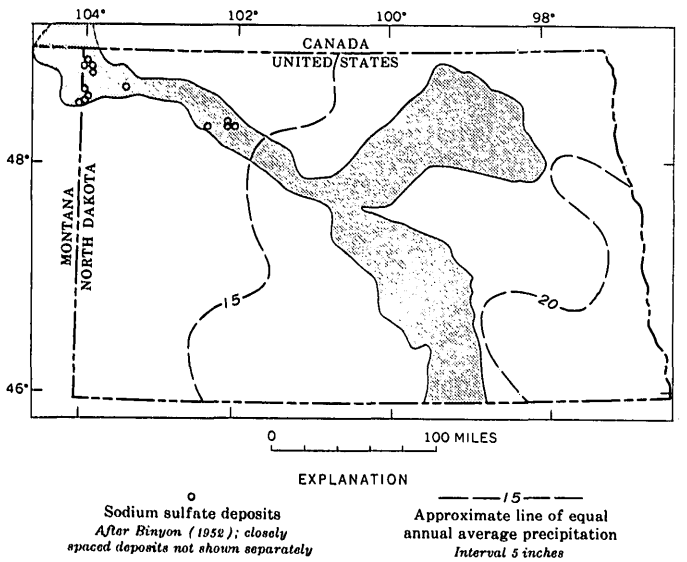

FIGURE 2.—Relation of sodium sulfate deposits of North Dakota and northeastern Montana to arid part of area of interior drainage. Area of interior drainage after Grossman (1949b); small areas in east not shown. Shaded area indicates area of interior drainage.

285-544 O—68——8

BEDROCK VALLEYS AND ICE MARGINAL CHANNELS

The specific location of any group of sodium sulfate deposits within the dry area of interior drainage seems to be controlled by channels in the underlying bedrock. These bedrock channels, some of which are preglacial, recently have been discussed by Howard (1960). Alpha (undated [1937?], p. 7) recognized that the earlier known deposits in North Dakota might be alined along the preglacial course of the Missouri and Yellowstone Rivers. Later discoveries in northwestern North Dakota and Montana suggest that *all* the deposits here overlie these or other buried bedrock valleys. Most of the deposits in North Dakota overlie the preglacial channel of the Missouri River. One deposit overlies the channel of the preglacial Yellowstone River. A group of four other deposits may overlie a buried valley related to the preglacial Little Missouri River. This valley has not been traced as far north as the others, but at least one of the four deposits, White Lake, lies in a bedrock channel thought to be of preglacial origin (Paulson, 1954, p. 1). The coincidence of bedrock valleys and overlying deposits of sodium sulfate is too widespread and consistent to be fortuitous, at least in North Dakota and Montana.

In contrast to control by buried bedrock valleys, Witkind (1952, p. 675; 1959, p. 73) emphasized the role of surficial ice-marginal channels in localizing the deposits. In his view, the sodium sulfate deposits and associated alkali lakes formed only where a "floor" of till prevented subsurface escape of the water carrying dissolved salts. Lakes floored with permeable stratified drift lost their dissolved salts by subsurface flushing. As previously mentioned, an objection to this theory is that complete evaporation in lakes lined with impermeable material would concentrate *all* the salts; hence, the relatively high purity of the deposits is left unexplained. The purity is such that Rawson and Moore (1944, p. 147) noted that only 1 out of 70 deposits in southern Saskatchewan has any important amount of chloride. Moreover, an area in southern Saskatchewan hitherto believed to illustrate control by glacial channels alone is shown on recent maps (Flint, 1957, fig. 10–2) to be underlain, at least in part, by preglacial valleys. It appears that somehow *both* the overlying melt-water channels of glacial origin and the underlying bedrock valleys of largely preglacial origin control the distribution of the deposits.

Stochastic explanations for this dual control can proceed from established hydrologic principles (fig. 3). Water in a regional artesian system ascends along

nearly vertical paths with flow lines converging toward topographic valleys (Toth, 1963, fig. 3). At the interface between bedrock and stratified drift, flow lines are refracted toward the vertical. Water moving farther upward into melt-water channels moves along flow lines bent toward lakes within these channels which act as sinks. The channels were more effective sinks at the end of the Pleistocene when the lakes within them were larger and received and evaporated much more water than they do today.

MEROMICTIC LAKES AND FREEZE SEPARATION OF CRYSTALS

At the end of the Pleistocene, downwasting and retreat of the glaciers exposed a vast drift-covered plain dotted by thousands of lakes of all sizes. Meromictic conditions (thermal or chemical stratification) developed in deep lakes where circulation was poor (fig. 3). Hutchinson (1957, p. 488) has pointed out that in the temperate zones, biogenic meromixis is favored by a markedly continental-type climate and by deep lakes occurring in valleys offering protection from the mixing action of the wind. The persistence of a deep stagnant layer of lake water, the hypolimnion, permitted accumulation of crystallized salts. Here, mirabilite ($Na_2SO_4 10H_2O$) settling to the bottom built up the so-called permanent layers of sodium sulfate. Some of the supernatant water in the epilimnia continued to be flushed from the area, chiefly through temporary drainageways to the south, as long as a plentiful supply of melt water or a pluvial climate prevailed. With the gradual onset of a semi-arid climate, the drainage network gradually disintegrated. When wet cycles or spring freshets temporarily reestablished the broken links in the southward-flowing drainage system, supernatant water was again flushed out of the lakes. Floods or spring freshets also laid down the layers of interbedded mud that protected the "permanent" beds from solution during the next inundation. Swales and shallow channels, now largely dry, indicate the watercourses where lakes formerly overflowed and received overflow in the area of interior drainage.

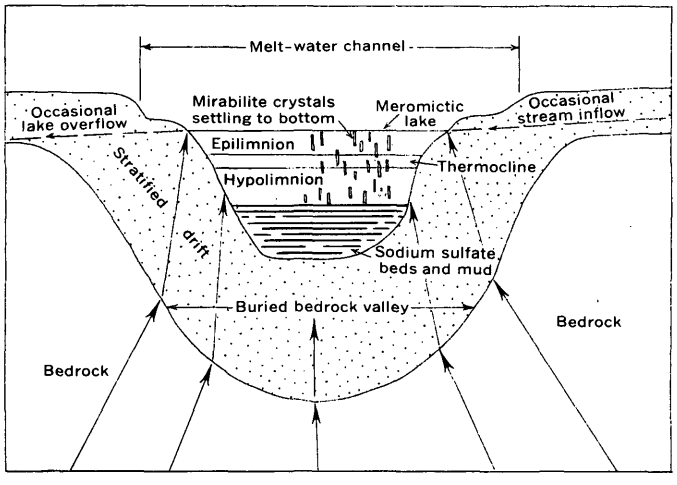

FIGURE 3.—Hypothetical cross section (not to scale) showing deposition of sodium sulfate crystals in a meromictic lake. Lake lies within a melt-water channel that overlies a buried bedrock valley. Large arrows show generalized direction of flow of ground water.

An explanation for the selective concentration of sodium sulfate in lakes subject to periodic overflow is provided by experiments on sea water by Thompson and Nelson (1956, p. 237). They showed that sulfate lakes can form from sea water by freezing followed by removal of the residual brines. They also suggested elsewhere (*in* Hutchinson, 1957, p. 570) that some sulfate deposits have been formed by freezing. Rawson and Moore (1944, p. 148) noted that in Little Manitou Lake in Saskatchewan, "* * * crystals of sodium sulfate (Glauber salt) * * * are frozen out during the winter period and * * * dissolve slowly during the summer." Freezing conditions prevail throughout the area in the winter months and undoubtedly were more prevalent during the waning of the Pleistocene glaciers. It seems clear that the sodium sulfate deposits of the northern Great Plains formed from crystallized mirabilite concentrated in lake bottoms by the sinking of freeze-separated crystals.

REMAINING PROBLEMS

The first hypothesis, that deep salt-laden water has leaked vertically upward to the surface in the northern Great Plains, faces a formidable obstacle—the several thousand feet of largely argillaceous and seemingly impermeable sedimentary rocks above the evaporites of the Prairie Formation. However, Parker (1967, p. 1929) has recently postulated "* * * that salt removal was accomplished by the formation of local and regional fracture systems which allowed ascending water to escape from regional aquifers below the salt beds * * *". He reiterates that solution of Prairie salt and subsequent collapse extended to Recent time in Canada but only to Jurassic time in the United States part of the Williston basin. Thus, a discrepancy in age for the Late Pleistocene to early Recent surficial deposits in the United States remains to be resolved. Perhaps loading by the Pleistocene ice sheet(s) reopened old fractures and stimulated artesian circulation by compression of deep elastic aquifers. Another question is the possible role of shallower but smaller bedrock salt deposits in the area. Some answers may be forthcoming when the results of work now in progress in Canada become available. In the meantime, the foregoing hy-

pothesis are believed to be the most credible ones on the origin of the enigmatic sodium sulfate deposits of the northern Great Plains.

REFERENCES

Alpha, A. G., undated [1937?], General geology of the sodium sulphate district near Grenora, North Dakota: Federal Emergency Relief Administration Project for North Dakota, Project No. S–F2–47.

Binyon, E. O., 1952, North Dakota sodium sulfate deposits: U.S. Bur. Mines Rept. Inv. 4880, 41 p.

Bishop, R. A., 1954, Saskatchewan exploratory progress and problems, *in* Clark, L. M., ed., Western Canada sedimentary basin: American Assoc. Petroleum Geologists, p. 474–485.

Cole, L. H., 1926, Sodium sulphate of western Canada; occurrence, uses and technology: Canada Dept. Mines, Mines Branch, Rept. 646, 160 p.

Darton, N. H., 1909, Geology and underground waters of South Dakota: U.S. Geol. Survey Water-Supply Paper 227, 156 p.

DeMille, G., Shouldice, J. R., and Nelson, H. W., 1964, Collapse structures related to evaporites of the Prairie Formation, Saskatchewan: Geol. Soc. America Bull., v. 75, no. 4, p. 307–316.

Flint, R. F., 1957, Glacial and Pleistocene geology: New York, John Wiley, 553 p.

Grabau, A. W., 1920, Principles of salt deposition: New York, McGraw-Hill, 403 p.

Grossman, I. G., 1949a, Geology of the sodium sulphate deposits of North Dakota [abs.]: North Dakota Acad. Sci. Ann. Proc. v. 2, p. 22.

———1949b, The sodium sulphate deposits of western North Dakota, a progress report: North Dakota Geol. Survey Rept. Inv. 1, 66 p.

Howard, A. D., 1960, Cenozoic history of northeastern Montana and northwestern North Dakota with emphasis on the Pleistocene: U.S. Geol. Survey Prof. Paper 326, 107 p.

Hutchinson, G. E., 1957, A treatise on limnology, v. 1: New York, John Wiley, 1,015 p.

Klingspor, A. M., 1966, Cyclic deposits of potash in Saskatchewan: Bull. Canadian Petroleum Geology, v. 14, no. 2, p. 193–207.

Lemke, R. W., Laird, W. M., Tipton, M. J., and Lindvall, R. M., 1965, Quaternary geology of Northern Great Plains, *in* Wright, H. E., Jr., and Frey, D. G., The Quaternary of the United States: Princeton, N. J., Princeton University Press, p. 15–27.

Milner, R. L., 1956, Effects of salt solution in Saskatchewan [abs.]: North Dakota and Saskatchewan Geol. Societies, Williston Basin Symposium, p. 111.

Parker, J. M., 1967, Salt solution and subsidence structures, Wyoming, North Dakota, and Montana: Am. Assoc. Petroleum Geologists Bull. v. 51 no. 10, p. 1929–1947.

Paulson, Q. F., 1954, Geology and occurrence of ground water in the Stanley area, Mountrail County, North Dakota: North Dakota Ground-Water Studies No. 23.

Rawson, D. S., and Moore, J. E., 1944, The saline lakes of Saskatchewan: Canadian Jour. Research, sec. D, v. 22, no. 6, p. 141–201.

Sahinen, U. M., 1956, Preliminary report on sodium sulphate in Montana: Montana Bur. Mines and Geology Inv. Circ. 11, 9 p. [Reprint]

Simpson, H. E., 1929, Geology and ground-water resources of North Dakota: U.S. Geol. Survey Water-Supply Paper 598, 312 p.

Thompson, T. G., and Nelson K. H., 1956, Concentration of brines and deposition of salts from sea water under frigid conditions: Amer. Jour. Sci., v. 254, no. 4, p. 227–238.

Tóth, J., 1963, A theoretical analysis of ground-water flow in small drainage basins: Jour. Geophys. Research. v. 68, no. 16, p. 4795–4812.

Witkind, I. J., 1952, The localization of sodium sulfate deposits in northeastern Montana and northwestern North Dakota: Amer. Jour. Sci., v. 250, p. 667–676.

———1959, Quaternary geology of the Smoke Creek-Medicine Lake-Grenora area Montana and North Dakota: U.S. Geol. Survey Bull. 1073, 80 p.

COPPER, STRONTIUM, AND ZINC CONTENT OF U.S. GEOLOGICAL SURVEY SILICATE ROCK STANDARDS

By CLAUDE HUFFMAN, JR., Denver, Colo.

Abstract.—Copper, strontium, and zinc values determined by an atomic absorption spectrophotometric method are presented for six U.S. Geological Survey rock standards: granite (G–2), granodiorite (GSP–1), andesite (AGV–1), peridotite (PCC–1), dunite (DTS–1), and basalt (BCR–1).

The U.S. Geological Survey has a series of new reference samples for six silicate rocks to supplement the older reference samples G–1 and W–1. Flanagan (1967) has published complete conventional, rapid rock, and spectrochemical analyses obtained by U.S. Geological Survey analysts for the six samples: granite (G–2), granodiorite (GSP–1), andesite (AGV–1), peridotite (PCC–1), dunite (DTS–1), and basalt (BCR–1). However, in his paper no spectrochemical data are given for zinc, and the data for copper and strontium show a wide range of values for each sample (table 1, this paper). Doe and others (1967) and Peterman and others (1967) reported strontium values for G–2 and GSP–1 based on an isotope-dilution method.

This paper presents copper, strontium, and zinc values determined by atomic absorption spectrophotometry on the six new reference samples and on the well-known samples G–1 and W–1. Duplicate determinations obtained and their means are given in table 2. These duplicates were obtained on independent 1-gram portions of each sample. Previously published data on these samples are given in table 1 for comparison. The atomic absorption values are in reasonable agreement with the mean spectrographic values.

Table 3 shows a comparison of strontium values obtained by atomic absorption, isotope-dilution, and spectrographic methods for reference samples G–2 and GSP–1. All three methods are in good agreement for the strontium content of G–2 (481–490 ppm). Atomic absorption results for GSP–1 (235–250 ppm) are in excellent agreement with those reported by the isotope-dilution method (239–241 ppm), but the average of the spectrographic data for GSP–1 seems high (277 ppm).

TABLE 1.—*Emission spectrochemical determination of copper and strontium in U.S. Geological Survey silicate rock standards*

[Data summarized from Flanagan (1967); values in parts per million]

Sample	Copper		Strontium	
	Range	Mean	Range	Mean
G–2	9–13	10.9	340–760	484
GSP–1	34–60	44.5	200–430	277
AGV–1	55–100	69.1	610–1,000	741
BCR–1	19–35	26.6	300–500	362
PCC–1	5–16	9.9	<2–<10	<4
DTS–1	3–9	6.4	<2–<10	<4

TABLE 2.—*Atomic absorption spectrophotometric determination of copper, strontium, and zinc in U.S. Geological Survey silicate rock standards*

[Analyst: Claude Huffman, Jr.; values in parts per million]

Sample	Slit/position	Copper			Strontium			Zinc		
		HNO_3 solution	HCl solution	Average	Run 1	Run 2	Average	Run 1	Run 2	Average
G–1	.....	17	18	17.5	260	270	265	45	42	43.5
W–1	.....	112	.....	112	190	200	195	78	82	80.0
G–2	19/1	13	14	13.5	480	500	490	84	81	82.5
GSP–1	1/9	38	38	38.0	235	250	243	100	101	100.5
AGV–1	26/25	62	64	63.0	680	700	690	88	83	85.5
BCR–1	64/20	20	19	19.5	345	350	347	125	122	123.5
PCC–1	43/11	10	13	11.5	<10	<10	<10	30	28	29.0
DTS–1	16/20	8	9	8.5	<10	<10	<10	35	32	33.5

TABLE 3.—*Strontium content of standard samples determined by atomic absorption and other methods*

[Values in parts per million]

Sample	Atomic absorption [1]		Isotope dilution [2]		Emission spectrographic [3]	
	Range	Mean	Range	Mean	Range	Mean
G–2	480–500	490	478–486	481	340–760	484
GSP–1	235–250	243	239–241	240	200–430	277

[1] This paper.
[2] Doe and others (1967), Peterman and others (1967).
[3] Flanagan (1967).

PROCEDURE FOR ATOMIC ABSORPTION DETERMINATIONS OF COPPER, STRONTIUM, AND ZINC

Transfer 1.0 g of the rock powder to a platinum dish. Add 10 milliliters demineralized water, 10 ml HNO_3 10 ml HF; cover, and let stand overnight. Add 7 ml $HClO_4$ to the dish. Place dish on a steam bath and evaporate for about 1 hour, then place dish on a hotplate and fume off the acids to near dryness. Wash down the sides of the dish with water, add 5 ml $HClO_4$, and repeat fuming until all acid is evaporated. Cool. Add 25 ml water and 5 ml HCl to the dish, cover and digest on the steam bath for 30 minutes. Transfer the solution to a 100-ml volumetric flash and dilute to volume with water. Atomize a portion of this solution into the flame of the atomic absorption spectrophotometer for copper and zinc determinations. Strontium is also determined on a portion of this solution using the method of Huffman and Mensik (1967). Process a reagent blank with each set of samples.

The copper values shown in table 2 were determined on two sets of sample solutions; one contained 5 percent v/v HCl, and the other 5 percent v/v HNO_3. Dissolution procedure for both acid mediums is that described above. The data indicate that solution in either acid is suitable for determining copper.

The copper, strontium, and zinc values reported by the author were obtained with a Perkin-Elmer model-303 atomic absorption spectrophotometer using an air-acetylene flame and the following instrument parameters recommended by the manufacturer:

	Copper	*Strontium*	*Zinc*
Wavelength--angstroms--	3247	4607	2138
Slit----------	4	4	4
Source current------ma--	15	10	15
Acetylene flow [1]---------	8.5	9.5	8.5
Air flow [1]----------	8.5	8.5	8.5
Flame----------	Oxidizing	Reducing	Oxidizing
Acetylene pressure--psi--	9	9	9
Air pressure--------psi--	30	30	30
Scale----------	×10	×5	×1 and ×5

[1] Arbitrary units.

REFERENCES

Doe, B. R., Tatsumoto, Mitsunobu, Delevaux, M. H., and Peterman, Z. E., 1967, Isotope-dilution determination of five elements in G–2 (granite) with a discussion of the analysis of lead *in* Geological Survey Research 1967: U.S. Geol. Survey Prof. Paper 575–B, p. B170–B177.

Flanagan, F. J., 1967, U.S. Geological Survey silicate rock standards : Geochim. et Cosmochim. Acta, v. 31, p. 289–308.

Huffman, Claude, Jr., and Mensik, J. D., 1967, Strontium content of some standard rocks: Applied Spectroscopy, v. 21, no. 2, p. 125–126.

Peterman, Z. E., Doe, B. R., and Bartel, Ardith, 1967, Data on the rock GSP–1 (granodiorite) and isotope-dilution method of analysis for Rb and Sr *in* Geological Survey Research 1967: U.S. Geol. Survey Prof. Paper 575–B, p. B181–B185.

CONCENTRATION AND MINOR ELEMENT ASSOCIATION OF GOLD IN ORE-RELATED JASPEROID SAMPLES

By T. G. LOVERING, H. W. LAKIN, and A. E. HUBERT,
Denver, Colo.

Abstract.—Sixty-eight samples of jasperoid associated with base- and precious-metal ore deposits in 25 western mining districts were analyzed for gold by a method capable of detecting concentrations as low as 0.04 ppm. All these samples had been analyzed spectrographically for minor elements, and many of them had been analyzed chemically for tellurium and mercury. The gold content of these samples ranged from <0.04 to 32 ppm, with a median content of 0.2 ppm. A statistical comparison of the gold concentrations in these samples with the corresponding concentrations of 16 minor elements indicates that gold is significantly associated with tellurium, mercury, tin, arsenic, and silver.

Sixty-eight samples of jasperoid associated with base- and precious-metal ore deposits in 25 western mining districts of the United States were analyzed for gold (table 1) to determine the distribution of gold and its minor-element association in these jasperoids. Most of the samples included in this study were part of the suite used to establish criteria for the recognition of jasperoid associated with sulfide ore (Lovering and Hamilton, 1962), and many of them were included in a suite analyzed for tellurium and mercury (Lovering and others, 1966). Only those samples containing unusually high concentrations of Ag, Cu, Hg, Pb, Te, or Zn were analyzed for gold. Hence, the data in this paper pertain only to jasperoid samples that are classified as "productive" or "favorable" in the references cited above.

The method used for determining gold in these jasperoids is described by Thompson and others (1968) (p. B130–B132, this chapter). The method involves agitation of the pulverized sample with a hydrobromic acid-bromine solution and the formation of gold bromide; the gold bromide is extracted into methyl isobutyl ketone, and the ketone is washed with 0.1*N* hydrobromic acid. The amount of gold present in the

TABLE 1.—*Gold content of 68 ore-related jasperoid samples*

Sample No.	*Mining district*	*Au content (ppm)*
	Arizona	
32–2	Banner	0.2
29–2	Bisbee	.04
31–1	Courtland-Gleason	.3
30–1	Morenci	.06
30–3	----do	2.6
33–1	San Xavier	.14
33–2	----do	.1
	Colorado	
III–3	Kokomo	0.1
V–1	Leadville	.1
V–2	----do	.2
V–4	----do	.1
I–23	Sacramento	<.04
X–1A	Uncompahgre	.2
	Nevada	
55–3	Antelope	0.16
23–2	Dolly Varden	<.04
23–3	----do	<.04
XIII–9	Ely	.45
XIII–14	----do	.25
XIII–16	----do	2.10
XIII–19	----do	4.25
XIII–20	----do	11.25
XIX–3	Eureka	.35
54–2	Garden Valley	.04
XVIII–4	Hamilton	.35
21–4	Taylor	.2
21–7	----do	.2
34–3	Ward	.2
34–4C	----do	<.04
	New Mexico	
Y–48–62	Lake Valley	0.3
XIV–4	Santa Rita	.1
45–2	Victorio	.08

U.S. GEOL. SURVEY PROF. PAPER 600-B, PAGES B112-B114

TABLE 1.—*Gold content of 68 ore-related jasperoid samples*—Cont.

Sample No.	Mining district	Au content (ppm)
	South Dakota	
35-1B	Lead [1]	<0.04
35-1C	----do	.1
35-1D	----do	<.04
35-1E	----do	3.5
35-2A	----do	2
35-2D	----do	<.04
35-2E	----do	32
35-2F	----do	.2
35-3A	----do	.2
35-3B	----do	.8
35-3C	----do	.1
35-3D	----do	16
35-3E	----do	1
	Utah	
XII-5	Bingham	0.35
XII-6	----do	<.1
36-1	Drum Mountains	<.04
36-3	----do	1.7
36-4	----do	.3
36-5	----do	7.3
36-7	----do	2.9
IX-1C	Mercur	.1
IX-5	----do	1.5
IX-6	----do	.3
IX-10	----do	.1
IX-14	----do	.08
IX-15	----do	.12
VII-6A	Tintic	4.2
VII-7	----do	.7
VII-8	----do	.8
VII-9	----do	1
VII-11A	----do	.1
VII-11B	----do	4.2
VII-12	----do	.75
VII-12B	----do	7
VII-13	----do	.4
VII-14	----do	.2
VII-14A	----do	.15

[1] J. B. McHugh, analyst.

ketone is estimated by atomic absorption. Any gold that is completely enclosed by silica will not be determined by this procedure. However, with samples ground to pass a 100-mesh sieve, but held on a 150-mesh sieve, the method has given good agreement with fire-assay determinations.

Gold concentrations in these samples ranged from < 0.04 to 32 parts per million, with a median of 0.2 ppm; only eight samples assayed less than 0.05 ppm (fig. 1).

In the 68 samples of jasperoid analyzed, the reported concentration of gold was compared statistically with the concentrations of Ag, As, Ba, Be, Bi, Cu, Hg, Mo, Ni, Pb, Sb, Sn, Sr, Te, Zn, and Zr. The concentrations of gold and many of the other minor elements exhibit nonnormal distributions in this suite of samples, and concentrations of some of these elements were below the limit of detection in many samples, resulting in

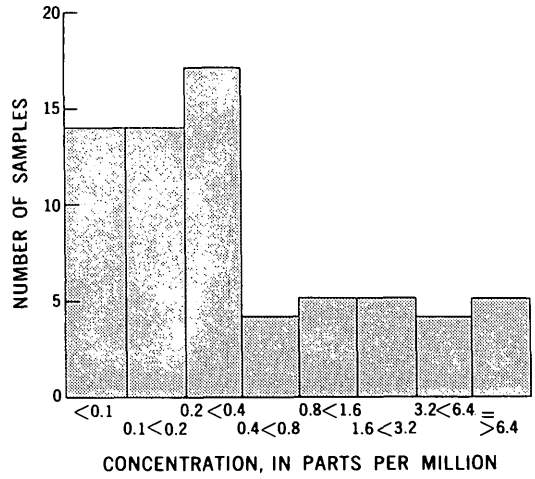

FIGURE 1.—Frequency distribution of gold in jasperoid samples.

censored frequency distributions. The tabulated significance levels for values of the standard product-moment correlation coefficient are predicated on the assumption of a bivariate normal distribution (Dixon and Massey, 1951, p. 162–164). Since our data do not satisfy this assumption, the strength of association between gold and the other minor elements in the ore-related jasperoid samples has been tested by Spearman's nonparametric rank correlation coefficient corrected for tied ranks in the grouped data (Siegel, 1956, p. 202–213).

Rank correlation coefficients between gold and associated minor elements, together with their significance levels calculated from Student's t distribution (Siegel, 1956, p. 212), are tabulated, as follows, in order of decreasing correlation:

Significance level	Gold versus minor element—	Correlation coefficients
Significant at 0.001	Te	+0.49
	Hg	+.42
	Sn	+.39
	As	+.37
Significant at 0.01	Ag	+0.33
Significant at 0.1	Sb	+0.21
	Pb	+.20
Not significant at 0.1	Ba	+0.17
	Bi	+.15
	Cu	+.14
	Be	+.05
	Zr	+.02
	Mo	+.003
	Sr	−0.10
	Zn	−.11
Significant at 0.1	Ni	−0.26

The significance level indicates the likelihood of an observed correlation coefficient occurring by chance alone. Where the significance level is low, the correlation may be ascribed, with high confidence, to geo-

chemical factors. For example, the statement that the correlation of +0.49 between gold and tellurium is significant at the 0.001 level means that a correlation as high as +0.49 between these elements in the group of jasperoid samples could occur by chance less than once in a thousand times. This does not mean that all samples with high tellurium content are rich in gold, or that low concentrations of tellurium preclude relatively high gold content, but it does mean that samples with abundant tellurium are more likely to show high gold values than samples that are low in tellurium. Because all the elements studied are present in low concentrations, it is unlikely that correlations among them result from closed array effects as discussed by Chayes (1960).

The only elements tested that show strong associations with gold in this group of jasperoid samples are tellurium, mercury, tin, arsenic, and possibly silver. Only the last three of these are apt to be present in mineralized samples in sufficient concentrations to be detected by the routine spectrographic analytical methods now in use (Myers and others, 1960).

The six jasperoid samples whose spectrographic analysis showed detectable tin plus detectable arsenic plus >0.005 percent silver all assayed >0.3 ppm in gold. The detection of these three elements in jasperoid samples, by routine spectrographic analysis, might therefore indicate a strong possibility that such samples also contain appreciable concentrations of gold.

REFERENCES

Chayes, Felix, 1960, On correlation between variables of constant sum: Jour. Geophys. Research, v. 65, no. 12, p. 4185–4193.

Dixon, W. J., and Massey, F. J., Jr., 1951, Introduction to statistical analysis: New York, McGraw-Hill Book Co., 370 p.

Lovering, T. G., and Hamilton, J. C., 1962, Criteria for the recognition of jasperoid associated with sulfide ore: Art 63 *in* U.S. Geol. Survey Prof. Paper 450–C, p. C9–C11.

Lovering, T. G., Lakin, H. W., and McCarthy, J. H., 1966, Tellurium and mercury in jasperoid samples, *in* Geological Survey Research 1966: U.S. Geol. Survey Prof. Paper 550–B, p. B138–B141.

Myers, A. T. Havens, R. G., and Dunton, P. J., 1960, A spectrochemical method for the semiquantitative analysis of rocks, minerals, and ores: U.S. Geol. Survey Bull. 1084–I, p. 207–229.

Siegel, Sidney, 1956, Nonparametric statistics for the behavioral sciences: New York, McGraw-Hill Book Co., 312 p.

Thompson, C. E., Nakagawa, H. M., and VanSickle, G. H., 1968, Rapid analysis for gold in geologic materials, *in* Geological Survey Research 1968: U.S. Geol. Survey Prof. Paper 600–B, p. B130–B132.

SPECTROCHEMICAL ANALYSIS OF STREAM WATERS IN GEOCHEMICAL PROSPECTING, NORTH-CENTRAL COLORADO

By EDWARD C. MALLORY, JR., Denver, Colo.

Abstract.—A combined chemical concentration-spectrographic analysis method was used to determine variations in the molybdenum, lead, and zinc concentrations in Clear Creek and its tributaries, which drain known mineralized areas. The variations in concentration correlated closely with the location of the mineralized areas, and the data indicate that this method can be used for rapidly scanning large areas for the presence of mineral concentrations.

Chemical analysis of spring and stream waters has been used for a number of years as a geochemical prospecting technique for minor elements, and considerable progress has been made in recent years in the development of even more sensitive methods for determining minor and trace elements in natural waters.

One of the most sensitive methods combines chemical concentration and spectrographic analysis, and has been described in detail by Silvey and Brennan (1962). Briefly, the minor elements are precipitated at a controlled pH with 8-quinolinol, tannic acid, and thionalide. Indium is added to each sample as a carrier and spectrographic buffer, and palladium is added as an internal standard. The filtered precipitate is ashed and analyzed spectrographically. Thus, major elements that might interfere during spectrographic analysis are removed during chemical concentration, and the waters can be spectrographically analyzed for many elements simultaneously. Silvey and Brennan used this method to quantitatively determine aluminum, cobalt, chromium, copper, iron, gallium, germanium, manganese, nickel, titanium, vanadium, bismuth, lead, molybdenum, cadmium, zinc, and beryllium.

In order to test the effectiveness of the combined chemical concentration-spectrographic method as a means of rapidly scanning a large area for the presence of mineralized areas, a number of water samples from Clear Creek and some of its tributaries were analyzed for molybdenum, lead, and zinc by this method. All samples were filtered through a 0.45-micron average pore diameter membrane filter to remove suspended sediment so that the metal concentrations determined represented only the metals in solution.

Analyses of the first samples collected for determination of the molybdenum content showed that Clear Creek contained more molybdenum than its tributary North Clear Creek, so additional samples were collected farther upstream along Clear Creek and other of its tributaries in an attempt to locate the source of the molybdenum. The molybdenum concentration continued to increase upstream in Clear Creek, West Clear Creek, and Woods Creek, but decreased above the confluence of Woods Creek and West Clear Creek (fig. 1). The concentration in Woods Creek, which flows along the southeast base of Red Mountain and past a molybdenum mine, was more than twice that in Clear Creek and West Clear Creek. However, the highest molybdenum concentration was found in

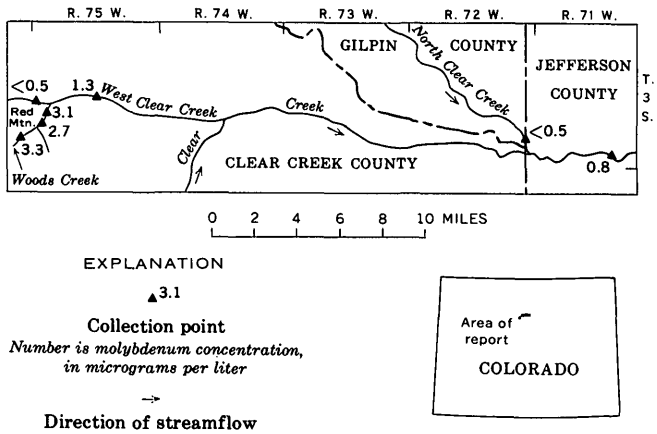

FIGURE 1.—Location of Clear Creek, Colo., and molybdenum concentrations in the waters of the creek and some of its tributaries.

U.S. GEOL. SURVEY PROF. PAPER 600-B, PAGES B115-B116

a sample collected upstream from the mine and the tailings pond, which would indicate at least one additional source of the molybdenum.

A significant variation in concentrations of lead and zinc was found in water samples collected along Clear Creek, Quayle Creek, Grizzly Gulch, and Stevens Gulch (fig. 2). Increasingly higher concentrations were found in an upstream direction, approaching an area where lead and zinc deposits are known to exist (Lovering and Goddard, 1950, p. 137–138, 166).

The zinc concentrations in water samples from Stevens Gulch were considerably higher than in those from Grizzly Gulch. Mining operations were in progress in Stevens Gulch, but no active operations were in evidence for several miles up Grizzly Gulch, which might explain the difference in concentrations.

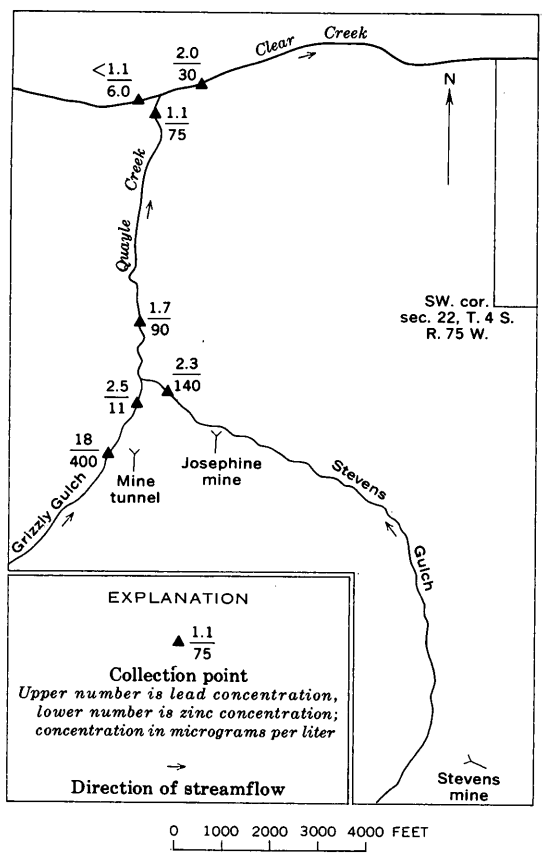

FIGURE 2.—Lead and zinc concentrations in the waters of Clear Creek, Colo., and some of its tributaries.

A sample of drainage from a mine tunnel in Grizzly Gulch contained 18 and 400 micrograms of lead and zinc per liter, respectively. A short distance downstream only 2.5 μg of lead and 11 μg of zince were detected. The marked downstream decrease in lead and zinc concentrations is very likely due to dilution, chemical precipitation, or changes in pH which result when the mine drainage reaches the main stream.

A water sample collected just below the confluence of Clear Creek and Quayle Creek (fig. 2) contained 2.0 μg of lead per liter, whereas samples taken from the mouth of Quayle Creek contained only 1.1 μg. Clear Creek just above Quayle Creek was not causing this higher figure, as waters collected here contained < 1.1 μg of lead per liter. Ground-water seepage may be be contributing lead to the stream in this area.

In using spectrochemical analysis as a technique in geochemical prospecting, one must expect to find waters where the concentrations of elements sought are sometimes higher or lower than would be expected. The overall increases, as well as individual variations, must be considered.

The data obtained in this study demonstrate that the combined chemical concentration-spectrochemical analysis method of analyzing stream waters for minor-element concentrations is so sensitive that mineralized areas many miles away can be detected by analysis of the main streams during geochemical prospecting.

REFERENCES

Lovering, T. S., and Goddard, E. N., 1950, Geology and ore deposits of the Front Range, Colorado: U.S. Geol. Survey Prof. Paper 223, 319 p.

Silvey, W. D., and Brennan, Robert, 1962, Concentration method for the spectrochemical determination of seventeen minor elements in natural water: Anal. Chem., v. 34, no. 7, p. 784–786.

USE OF THE DIFFRACTED-BEAM MONOCHROMATOR IN X-RAY DIFFRACTION OF CLAY MINERALS

By JOHN W. HOSTERMAN, Beltsville, Md.

Abstract.—The diffracted-beam crystal monochromator eliminates the unexplained fictitious peaks that may occur between 4° and 9° 2θ on X-ray diffraction traces of clay minerals that are exposed to high-intensity Cu radiation. The diffraction traces of clay minerals are also more easily duplicated regardless of how the sample is prepared. In addition, the monochromator completely eliminates Kβ radiation and secondary fluorescence, increases the peak-to-background ratio, and sharpens the resolution.

The large-target high-intensity X-ray tubes now available for diffraction work may cause false peaks on patterns of clay minerals. This and other undesirable features, such as Kβ peaks and secondary fluorescence, can be eliminated by using a diffraction-beam crystal monochromator.

The monochromator consists of a cylindrical doubly-bent lithium fluoride focusing crystal. The X-ray optical system is based on the Rowland focusing geometry in which the following equation must be fulfilled: $D=Rc \sin \theta$, where D is the receiving slit-to-crystal distance and the crystal-to-detector distance, Rc is the radius of the crystal, and θ is the Bragg angle (Koffman and Moll, 1964, p. 95). The crystal monochromator is designed so that the distance D is variable to allow it to be used for a variety of wavelengths. By adjusting the base plate which supports the crystal and detector, it is possible to select wavelengths from AgKα (0.56 angstrom) through CuKα (2.29 angstrom).

The 2θ angle between 4° and 12° is very important in identifying the 14A, 10A, and 7A clay minerals. Figure 1 shows the diffraction pattern of a powdered sample of flint clay from Clearfield County, Pa. This sample was prepared by sucking the water from a clay slurry through a porous ceramic tile. This leaves a

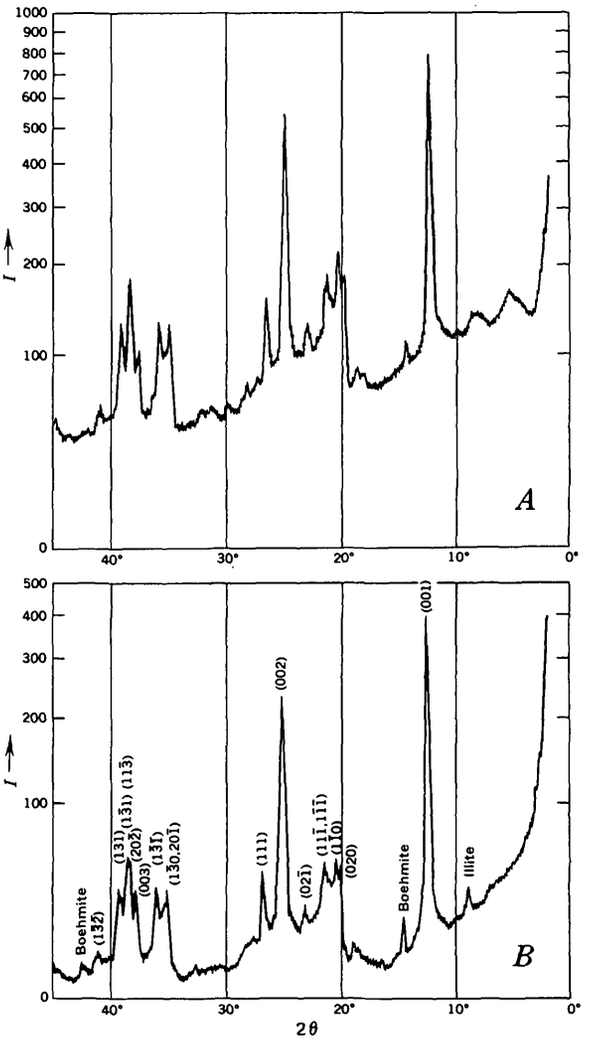

FIGURE 1.—Diffraction patterns of a powdered sample of flint clay (National Bureau of Standards No. 97) settled on a porous ceramic tile. *A*, traces made with a nickel filter; *B*, traces made with a diffracted-beam monochromator. (*I*=*intensity*.)

U.S. GEOL. SURVEY PROF. PAPER 600-B, PAGES B117-B118

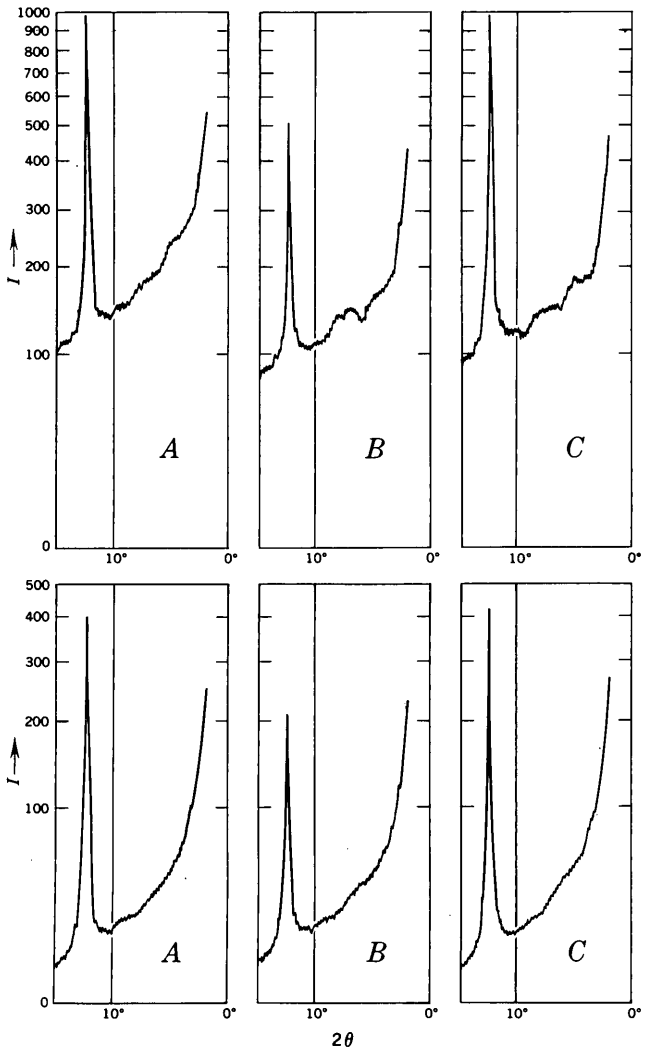

FIGURE 2.—Diffraction patterns of kaolinite (API H–1). *A*, sample pressed into a disk with methyl cellulose backing; *B*, sample packed into an aluminum holder; *C*, sample pressed into a disk without a backing. Top, traces made with a nickel filter; bottom, traces made with a diffracted-beam monochromator. (*I*=*intensity*.)

uniform layer of clay, slightly orientated, on the tile. Figure 1*A* illustrates two diffuse peaks, one at 4° and the other at 9° 2θ. These peaks could possibly be interpretated as mixed-layer clay and montmorillonite or chlorite. However, there is no shift in these peaks with heating or glycolation, and the existence of these peaks cannot be fully explained. Similar diffuse peaks occur on many diffraction traces of samples prepared on porous tile when irradiated with a high-intensity Cu-target tube. The diffuse peaks may represent white radiation caused by the tile and silicate minerals. Figure 1*B* shows that these diffuse peaks are not real when used with a diffracted-beam monochromator, and that the flint clay contains a minor amount of illite that was not discernible when the nickel filter was used.

Figure 2 shows three diffraction traces with more or less the same diffuse peaks between 4° and 9° 2θ that are shown on figure 1. The upper three traces are with a nickel filter, and the lower three are with a diffracted-beam monochromator. The three traces are of the same kaolinite sample (API H–1) prepared three different ways. For sample A, the kaolinite was pressed into a 1¼-inch disk about ¼ inch thick with methyl cellulose as a backing for strength; for sample B, the kaolinite was packed into an aluminum holder; and for sample C, the kaolinite was pressed into a disk without a backing. The diffraction-beam monochromator eliminates the false peaks between 4° and 9° 2θ. It also produces X-ray diffraction traces that can be be duplicated regardless of how the sample is mounted.

REFERENCE

Koffman, D. M., and Moll, S. H., 1964, A curved crystal monochromator for the X-ray diffractometer: Norelco Reporter, v. 11, no. 3, p. 95–98.

DETERMINATION OF MICRO AMOUNTS OF CESIUM IN GEOLOGIC MATERIALS

By WAYNE MOUNTJOY and JAMES S. WAHLBERG, Denver, Colo.

Abstract.—Cesium is concentrated from solutions of rock samples by ion-exchange onto ammonium molybdophosphate (AMP). Either X-ray fluorescence or atomic absorption spectrophotometry is used for the determination. Standard reference samples containing cesium in the range from about 1 to 10 ppm were analyzed and show good agreement with published results. The sensitivity for both methods is about 0.3 ppm on a 2-g sample.

Turekian and Wedepohl (1961) presented data to show that cesium in the major units of the earth's crust ranges in concentration from about 6 parts per million in clay and 5 ppm in shale to 0.X ppm in ultrabasic rocks. They also showed that in igneous rocks, cesium content ranges from 4 ppm in low-calcium granitic rocks to about 1 ppm in basalts. Goldschmidt (1954) estimated 3.2 ppm cesium in the upper lithosphere. The determination of cesium in rocks, therefore, requires either a very sensitive method or an efficient concentration procedure prior to the determination.

Cesium in shale was determined spectrographically by Canney (1952) using a 50-milligram sample and a short burning time to maintain a low background. Thus he achieved a detection limit of 1 ppm Cs. Annell (1964) attained about the same limit of detection, using a special focusing lens, a special filter, and potassium carbonate as a matrix. Concentration procedures followed by a flame-photometer determination using modified instruments enabled Horstman (1957), Collins (1963), and Feldman and Rains (1964) to determine cesium in rocks, waters, and brines. Smales and others (1964) determined cesium in meteorites by neutron activation and by mass spectrometry after concentrating the cesium by two different ion exchange methods.

The direct determination of cesium in rocks by either X-ray fluorescence or atomic absorption has not been reported in the literature. Furthermore, it has been confirmed in the laboratory that without preconcentration of the cesium no meaningful results can be obtained by either method on rocks containing only a few parts per million cesium.

The separation of the alkalis, using an ion exchange column of AMP (ammonium molybdophosphate), was investigated by Smit and others (1959). Feldman and Rains (1964) reported that cesium could be collected from a solution by a batch extraction with AMP. The separation is fast and efficient and provides a constant matrix for either the X-ray fluorescence or atomic absorption determination.

In the method presented here, cesium is collected on AMP followed by vacuum filtration onto a small filter disk which is pressed to prepare it for X-ray fluorescence analysis, or the AMP slurry is centrifuged and the AMP dissolved in dilute potassium hydroxide solution for determination of cesium by atomic absorption.

The combination of the optional Boling burner and the long-pass light filter, which is standard equipment on the newer models of the Perkin-Elmer model-303 atomic absorption spectrophotometer, gives a satisfactory signal-to-noise ratio so that 0.5 microgram of cesium in 5 milliliters of solution (0.1 ppm) may be detected with certainty.

APPARATUS AND REAGENTS

X-ray spectrometer: Norelco single-channel vacuum X-ray spectrometer equipped with a pulse height analyzer, a chromium target tube, a lithium fluoride analyzing crystal, and a gas-flow detector.

Hydraulic press: A press, with a 1⅛-inch diameter cylinder capable of exerting 40,000 pounds per square inch pressure for preparing the samples for X-ray.

Stirrer: Magnetic.

Filter: Millipore apparatus, 25-mm-diameter filter.

Shaking machine: Any type that will keep the AMP precipitate suspended.

U.S. GEOL. SURVEY PROF. PAPER 600-B, PAGES B119-B122

Centrifuge: Clinical type with trunions and cups for 50-ml and 15-ml centrifuge tubes.

Caplugs, No. EC–16: One-inch size available from Protective Closures Co., Buffalo, N. Y.

Mylar film: 0.25 mil thick.

Cover glasses: Microscope, 1-inch diameter.

Atomic absorption spectrophotometer: Perkin-Elmer model-303 equipped with the optional air-acetylene 3-slot Boling burner, a long-pass light filter which is standard on later models, and the accessory power source for the Osram lamps.

Centrifuge: International Equipment Co., size 2, equipped with cups, trunions, and head for 250-ml bottles.

Ammonium molybdophosphate (AMP): Free-flowing powder from Bio-rad Laboratories, Richmond, Calif. The powder was dried at 105°C and stored in a closed bottle.

Cesium standard solution, 1.00 ml=1.00 mg Cs: 1.468 g of $CsNO_3$ (dried 4 hrs at 110°C) dissolved in water and diluted to 1 liter. "Purified" $CsNO_3$ from Fisher Scientific Co. was found to be satisfactory.

PROCEDURE

Transfer 2.00 grams of sample to a 100-ml platinum dish. Add sufficient 20-percent v/v HCl to make a thin slurry. If there is much effervescence, heat to expel CO_2, add a few milliliters of additional 20-percent v/v HCl to make sure there is an excess of acid. Add about 15 ml of HF, cover, and set aside for several hours. Evaporate the solution to dryness on a hotplate. Add 5 ml more of HF and evaporate to dryness. Add 2 ml of concentrated $HClO_4$ and 1 ml of concentrated H_2SO_4, and fume to dryness. Add another 1 ml of $HClO_4$, 5 ml of water, and 3 ml of HCl. Heat the solution gently on a hotplate to fumes, and evaporate it to incipient dryness. Remove from heat and add 75 ml of 2-percent v/v HCl. Cover the dish and heat at near-boiling temperature until all the soluble material is dissolved. Transfer the supernatent solution to a 4-ounce polyethylene bottle. Unreacted material remaining may be tourmaline which accumulates cesium (Lyakhovich, 1963). Any unreacted residue must be fused with Na_2CO_3, the melt dissolved, and the solution neutralized with 20-percent v/v HCl and added to the primary solution. The volume of solution should be 75 to 100 ml.

Prepare a blank and 3 standards containing respectively 1, 5, and 25 micrograms of Cs in about 75 ml of 2-percent v/v HCl in 4-oz polyethylene bottles.

Add 50 mg of AMP to each solution. A convenient method of adding the AMP to a number of solutions is to prepare a mixture containing 0.5 g of AMP per 100 ml of 0.1-percent v/v HCl. Stir the mixture rapidly with a magnetic stirrer while pipetting a 10-ml aliquot of the slurry to each sample, standard solution, and blank.

Cap the bottles and shake them on a mechanical shaker for 30 minutes. Up to this point the procedure is the same for both X-ray fluorescence and atomic absorption.

X-ray fluorescence

Filter the sample through a 2.4-centimeter No. 540 Whatman filter paper or equivalent, with the aid of suction, using a 25-mm Millipore filter apparatus.

Wash the paper once with a small amount of 0.1-percent v/v HCl and twice with 50-percent v/v ethyl alcohol. Dry the paper and the precipitate for 15 minutes at 80°C.

Place the dry filter in the press cylinder, cover the AMP surface with a 1-inch microscope cover glass, and press at 40,000 psi for 30 seconds. The cover glass has been found necessary to give a smooth surface to the AMP and also to prevent contamination of the samples due to cesium sticking to the press cylinder. Remove the shattered glass from the AMP surface and place the filter paper on a Mylar film which has been stretched over a 1-inch Caplug. Stretch another Mylar film over the disk to hold it in place. The absorbance of a film of 0.25-mil thickness is negligible.

Place the sample in the X-ray fluorescence unit and take three 64-second counts using the following operating parameters: chromium target X-ray tube at 40 kilovolts and 30 milliamps; cesium Lα line diffracted with a lithium fluoride analyzing crystal at a 2θ angle of 91.92°; background corrections at a 2θ angle of 90.92° and 92.91°; flow proportional counter using P–10 gas. A pulse height analyzer was used. If it is found from the sample count and the background count that the sample contains less than 5μg of cesium, then two 64-second counts 1° on each side of the cesium L α peak should be made. The average of these counts is then used as the background correction for the peak count. It was found that the background of the various samples was constant enough so that little accuracy was gained by using an off-peak background correction for samples containing more than 5 μg of cesium.

The amount of cesium in the sample is read from a graph of count rate versus micrograms of cesium. A straight-line curve is obtained. Typical data are presented in table 1.

TABLE 1.—*X-ray counting rates for cesium on 50 mg of AMP*

Micrograms of cesium	*Counts per 64 seconds*
Blank	3,450
5	5,340
10	6,900
25	12,900

Atomic absorption

Centrifuge the samples in the plastic bottles in a large centrifuge equipped with 250-ml cups at 2,000

revolutions per minute for 5 minutes. Decant all but about 5 ml of supernatent into a beaker. Swirl the remaining liquid to suspend the AMP, and then transfer the slurry to a calibrated 15-ml centrifuge tube. Use some more of the supernatent solution to wash the last traces of the AMP to the centrifuge tube. Centrifuge in a clinical centrifuge for 2 minutes at high speed. Decant and reject the supernatent solution. Dissolve the residue in 1 ml of 15-percent KOH. Heat the tube with a small flame to aid solution if necessary. Dilute the solution to 5 ml with water and mix thoroughly. Determine the cesium by atomic absorption. The following conditions and settings have been found satisfactory:

Source: Osram arc-discharge lamp, operating at 350 milliamperes.
Wavelength: 852 millimicrons.
Sensitivity and meter response: As required for the instrument and concentration of cesium.
Silt: 5 (3 mm).
Filter: In.
Gas: Acetylene, pressure 8 psi flow rate, approximately 9½ arbitrary units.
Oxidant: Air, 30 psi gage pressure, flow rate approximately 9 arbitrary units.
Burner: Boling, 3-slot, premix.
Flame: Gas and air adjusted as described in the instructions for the Boling burner.

EXPERIMENTS

Several experiments using Cs^{134} were performed to check the efficiency of the AMP collection and to obtain optimum conditions. Two grams of each of six Pierre Shale samples were spiked by adding a solution of Cs^{134} to the dry powder before digestion. The samples were dissolved and the cesium collected. The radioactivity of the filtrate was used as a measure of the remaining cesium. Only 1.5 to 2.6 percent of the activity remained in solution after one extraction on 50 mg of AMP. Recovery of cesium from standard solutions averages 98 percent. The efficiency of the collection was not significantly different for acid concentrations ranging from 0.1 to 5 percent HCl and for volumes to 250 ml, the maximum tested.

An experiment to determine the smallest amount of AMP that is practical showed that 50 mg of AMP collected 98 percent of the Cs, 25 mg collected 96 percent, but 10 mg collected only 78 percent. The X-ray fluorescence response was twice as great for the same amount of Cs on 25 mg of AMP as for 50 mg. The reproducibility of the determination was not as good with the 25 mg, however.

In the X-ray fluorescence determination, if we consider the square root of the total counts to be the standard deviation and assume that a count that is three standard deviations above background is the practical limit of detection, then with the instrument used in this work, a lower limit of 0.3 μg of cesium can be detected by a 3-minute count. However owing to other experimental errors, 0.5 μg has been found to be a more practical limit. This is equivalent to less than 0.3 ppm in a 2-g sample. It should be noted that this limit could be reduced by longer counting times, by a constant potential unit, or by using less than 50 mg of AMP, possibly at the expense of precision and accuracy.

It is well known in atomic absorption work that an excess of one alkali enhances the absorption of another. This is due to the depression of the ionization of the alkali by an abundance of electrons supplied by the other alkali. Also, the ionization potential of the alkalis decreases with increasing atomic weight. Thus it was expected that potassium would enhance cesium more than either sodium or lithium. In order to verify and evaluate these effects, test solutions were prepared as shown in table 2, but some solutions contained the hydroxides of sodium and lithium instead of potassium as in the above procedure. The absorption of the solutions was read on the atomic absorption instrument using the three-slot burner and zeroing the instrument with the alkali being tested. No cesium impurity was detected in any of the alkalis tested. The results shown in table 2 verify that potassium has the greatest enhancing effect, and lithium the least. Another experiment showed that there was no difference in sensitivity whether the solution to be aspirated into the flame was basic or had been acidified with tartaric acid. The Boling burner, in preference to the 10-cm single-slot burner, is recommended because it gives greater sensitivity with less noise and permits the aspiration of more concentrated salt solutions.

TABLE 2.—*Enhancing effect of solvent alkalis on the atomic absorption determination of cesium*

Base	Composition of solutions		Absorption reading (× 5 scale)
	Cs (ppm)	AMP (mg/ml)	
None	0	None	0
	.1 1	None	2. 6
	1 4	None	15. 4
0.2*N* KOH	0	None	0
	1	None	22. 7
	4	None	74. 7
	0	10	0
	1	10	17. 5
	4	10	67.
0.2*N* NaOH	0	10	0
	1	10	8. 9
	4	10	38. 3
0.2*N* LiOH [2]	0	10	0
	1	10	6. 5
	4	10	22. 0
0.2*N* NH_4OH	0	10	0
	1	10	1. 0
	4	10	2. 8

[1] Cesium in distilled water.
[2] Lithium phosphate precipitated and was not dissolved.

DISCUSSION

Cesium values obtained by the X-ray fluorescence and atomic absorption methods and by other methods on reference samples are shown in table 3. The differences from the recommended values on samples G-1 and W-1 may be due at least in part to variations in sampling as shown by the two determinations of Butler and Thompson (*in* Fleischer, 1965), which were averages obtained on different bottles of G-1.

Cesium content of different splits of a series of five clay samples and of one synthetic sample as determined by the X-ray fluorescence method and by a spectrographic method is shown in table 4.

The acid digestion of National Bureau of Standards reference sample NBS-98 left an insoluble residue which was ignored in test 1, but in test 2 the residue was fused with sodium carbonate, dissolved, and added to the acid solution. This may account for the higher value on the second determination.

In summary, two methods have been developed for the determination of cesium in rocks. However, the methods are readily adaptable to almost any type of material. The combination of the single separation and the determination of either X-ray or atomic absorption is believed to be faster, more sensitive, and as accurate as any chemical methods that are available to most laboratories.

TABLE 3.—*Cesium content of rocks as determined by X-ray fluorescence, atomic absorption, and other techniques*

[Cesium in parts per million]

Sample No.	*Sample type*	*X-ray fluorescence*	*Atomic absorption*	*Other techniques*
National Bureau of Standards reference samples				
NBS-98	Plastic clay	11.2, 14.3		
NBS-91	Opal glass	8.2, 7.6		
NBS-99	Soda feldspar	.8, .9		
U.S. Geological Survey reference samples				
AGV-1	Andesite	1.7, 0.9	1.3, 1.6	
BCR-1	Basalt	1.1, 2.0	1.1, 1.4	
G-1	Granite	1.7, 1.8		[1] 1.5, [2] 1.6, [2] 2.35, [3] 4.7, [4] 2.1
G-2	do	1.7, .9	1.6, .9	
W-1	Diabase	1.1, 1.0	1.0,	[1] 1.1, [3] 2.3, [4] 0.8
GSP-1	Granodiorite	1.7, 1.7	1.1, 1.4	
PCC-1	Peridotite	<0.3, <0.3	<0.3	

[1] Recommended values (Fleischer, 1965).
[2] J. R. Butler and A. J. Thompson (in Fleischer, 1965), neutron activation.
[3] R. Brown and W. A. Wolstenholme (in Fleischer, 1965), mass spectrometer.
[4] S. R. Taylor (in Fleischer, 1965), mass spectrometer.

TABLE 4.—*Cesium content of rocks as determined by X-ray fluorescence and spectrographic techniques*

Description	*Sample No.*	*Cesium (ppm) in splits of sample*	
		X-ray fluorescence [1]	*Spectrographic* [2]
NBS–183 and perlite.	281085	12.1, 10.7	10.3, 11.2, 11.0, 10.6
Clay, Yavapai County, Ariz.	281080	12.2, 8.1	6.4, 7.2, 7.4, 6.8
	281069	10.3, 13.4	10.6, 9.9, 11.0, 11.8
	281081	8.9, 10.0	8.1, 8.7, 8.2, 8.6
	281067	4.3, 4.7	3.8, 4.2, 4.2, 5.4
	281083	1.0, 2.5	3.3, 2.9, 3.4, 3.6

[1] Determined by Wayne Mountjoy and J. S. Wahlberg, by X-ray fluorescence method described in this report.
[2] Determined by Charles Annell by a spectrographic method developed by him (Annell, 1964).

REFERENCES

Annell, Charles, 1964, A spectrographic method for the determination of cesium, rubidium, and lithium in tektites, *in* Geological Survey Research 1964: U.S. Geol. Survey Prof. Paper 501–B, p. B148–B151.

Canney, F. C., 1952, Some aspects of the geochemistry of potassium, rubidium, cesium, and thallium in sediments: Massachusetts Inst. Technology unpub. Ph.D. thesis, 256 p.

Collins, Gene, 1963, Flame spectrophotometric determination of cesium and rubidium in oil field waters: Anal. Chemistry, v. 35, p. 1258.

Feldman, Cyrus, and Rains, T. C., 1964, The collection and flame photometric determination of cesium: Anal. Chemistry, v. 36, p. 405–409.

Fleischer, Michael, 1965, Summary of new data on rock samples G–1 and W–1, 1962–1965: Geochim. et Cosmochim. Acta, v. 29, p. 1263–1283.

Goldschmidt, V. M., 1954, Geochemistry: London, Oxford Univ. Press, 730 p.

Horstman, E. L., 1957, The distribution of lithium, rubidium, and cesium in igneous and sedimentary rocks: Geochim. et Cosmochim. Acta, v. 12, nos. 1–2, p. 1–28.

Lyakhovich, V. V., 1963, Distribution of rare elements in a vertical section of a granitic massif: Akad. Nauk. SSSR Doklady, v. 153, p. 1424–1427.

Smales, A. A., Hughes, T. C., Mapper, D., McInnes, C. A. J., and Webster, R. K., 1964, The determination of rubidium and cesium in stony meteorites by neutron activation analysis and by mass spectrometry: Geochim. et Cosmochim. Acta, v. 28, p. 209–233.

Smit, J. van R., Robb, W., and Jacobs, J. J., 1959, Cation exchange on ammonium molybdophosphate I: Jour. Inorganic and Nuclear Chemistry, v. 12, p. 104–112.

Turekian, K. K., and Wedepohl, K. H., 1961, Distribution of the elements in some major units of the Earth's crust: Geol. Soc. America Bull., v. 72, no. 2, p. 175–192.

ATOMIC ABSORPTION DETERMINATION OF TELLURIUM

By H. M. NAKAGAWA and C. E. THOMPSON [1], Denver, Colo.

Abstract.—Tellurium in soils and rocks is solubilized by treatment of the sample with hydrobromic acid-bromine mixture, selectively extracted into methyl isobutyl ketone, and finally measured by atomic absorption spectrophotometry applied to the separated ketone. As little as 0.1 ppm of tellurium can be detected, and amounts of 0.2 ppm or more can be measured with an accuracy comparable to that for an existing catalytic procedure.

A simple and moderately accurate method for determining trace amounts of tellurium in soils and rocks was needed to meet the demands of an expanded program of the U.S. Geological Survey to develop new sources of heavy metals. Small amounts of tellurium occur in halos above deposits of less mobile elements such as gold, and its presence in abnormal amounts in soils or rocks may indicate targets of mineral potential such as were found in the Cripple Creek district of Colorado (Gott and others, 1967). Small amounts of tellurium also occur as a halo around the copper-rich core in the Ely district of Nevada (Gott and McCarthy, 1966). Thus as the need to exploit concealed ore deposits becomes more acute, the use of pathfinder elements such as tellurium increases, and its determination in soils and rocks becomes highly significant.

Several well-established and reliable colorimetric and catalytic procedures useful in geochemical exploration are being reexamined for possible modification to take advantage of the inherent simplicity and sensitivity of atomic absorption techniques. The procedure for determination of tellurium described in this paper is a modification of the catalytic procedure described by Lakin and Thompson (1963). The authors' original hopes to determine both tellurium and gold in the same sample solution had to be abandoned because the roasting of the soil or rock that is necessary to render gold soluble volatilized the tellurium.

[1] Present address: Skyline Labs, Inc., Wheatridge, Colo.; formerly of the U.S. Geological Survey.

Acknowledgments.—The authors are most grateful to R. L. Erickson, G. B. Gott, and J. H. McCarthy, Jr., of the U.S. Geological Survey, for collecting and supplying the samples used in this work.

PROCEDURE

Briefly, the procedure consists of sample dissolution in hydrobromic acid–bromine mixture, extraction of dissolved tellurium into methyl isobutyl ketone, and atomization of the organic extractant. The amount of absorption of the energy from the hollow cathode lamp is related to the concentration of the tellurium.

Reagents and apparatus

Standard tellurium solution (0.01 percent): Dissolve 0.0625 gram of TeO_2 in 500 milliliters of concentrated HBr.

Dilute tellurium solution (0.001 percent): Dilute 10 ml of 0.01-percent tellurium solution to 100 ml with concentrated HBr.

Bromine, reagent grade.

Hydrobromic acid, concentrated reagent grade.

Hydrobromic acid, 1*N*: Dilute 115 ml of concentrated HBr to 1 liter with water.

Hydrobromic acid, 3*N*: Dilute 345 ml of concentrated HBr to 1 liter with water.

Hydrobromic acid-bromine solution, 0.5 percent: Dissolve 5.0 ml of liquid bromine in 1 liter of concentrated HBr.

Methyl isobutyl ketone, reagent grade.

Hotplate, oscillating: A large electric hotplate that mounts on an oscillator base (which agitates the hot plate at a constant speed) and has temperature control from 200° to 700°F.

INSTRUMENTAL PARAMETERS

Set parameters of atomic absorption spectrophotometer as follows:

Wavelength, 2140 A.

Slit, 6.5 A.

Lamp current, 18 milliamperes.

Air pressure, 20 pounds per square inch; flow-meter setting of 5 on Perkin-Elmer model 303 spectrophotometer.

Fuel pressure, 8 psi; flow-meter setting of 4 or less.

U.S. GEOL. SURVEY PROF. PAPER 600-B, PAGES B123-B125

285-544 O—68——9

Solution of tellurium sample

Transfer a 5-g pulverized sample to a 50-ml beaker and add 20 ml of hydrobromic acid-bromine solution. Place the beaker on an oscillating hotplate and boil solution gently until the volume of the solution is reduced to approximately 10 ml. Remove the beaker from the hotplate and allow to cool.

Extraction of tellurium

Transfer the entire contents (sample and acid) of the beaker to a 25×200-millimeter test tube fitted with a screwcap. Rinse the beaker with three 5-ml portions of water and add each rinse portion to the tube. Add water to the 30-ml mark. Add 10 ml of methyl isobutyl ketone, screw on the cap and shake the tube vigorously for 1 minute. Let the contents of the tube settle, or centrifuge until the two layers separate. If the organic layer is colorless, proceed with estimation; however if the organic layer is colored, separate and transfer it to a clean screwcapped tube containing 25 ml of 1*N* HBr. Secure the cap and shake tube for 15 seconds. Allow phases to separate and proceed as below.

Estimation of tellurium

Atomize the organic extractant two times, average these readings and convert to parts per million, from a standard curve. Alternately, a digital concentration readout or a recorded readout may be used.

Preparation of standards

Transfer 0.25 ml, 2.5 ml, and 10.0 ml of 0.001-percent tellurium standard solution to three 100-ml volumetric flasks containing 50 ml of 3*N* HBr. Add 25 ml of methyl isobutyl ketone and shake the flasks for 1 minute. The ketone in each flask contains, respectively, 0.1, 1.0, and 4.0 ppm (micrograms per milliliter) of tellurium. Atomize the organic phase in each flask at least three times, average these readings and prepare a standard curve covering the range in tellurium concentration from 0.2 to 20 ppm in the original sample. Adjustments for other concentration ranges can be made as the analysts desire.

INTERFERENCE

Although interference from other elements is rare in atomic absorption spectrophotometry, several elements such as lead, zinc, calcium, and antimony whose resonance lines are near to that of tellurium were tested. None of these elements interfered in concentration ratios of element to tellurium up to 2,000. Large amounts of iron interfere, possibly by a process called "light scattering" as described by Billings (1965). Such amounts of iron, which color the organic layer during the initial extraction, are removed sufficiently to reduce the interference to less than 1 percent absorption by treatment of the separated ketone layer with 1*N* of HBr as directed in the extraction step of the procedure. Treatment with a less concentrated acid causes losses of tellurium and should be avoided.

PRECISION AND ACCURACY

The precision, or repeatability, of the atomic absorption method was established by making five replicate determinations on different kinds of geologic materials (table 1).

The accuracy of the proposed method was established by comparison of the tellurium content of several different samples as determined by the proposed method and by the established method (Lakin and Thompson, 1963) (table 2).

TABLE 1.—*Replicate atomic absorption determinations of tellurium*

[In parts per million]

Sample No.	*Description*	*Analyses of separate subsamples*				
		1	*2*	*3*	*4*	*5*
Samples from Cortez district, Nevada						
CS–760	Conglomerate, caliche-cemented	0.23	0.29	0.30	0.37	0.37
66–4237	Limestone, red-brown, leached	1.8	1.4	2.2	1.6	1.0
Samples from Cripple Creek district, Colorado						
CC–520B	Phonolite, iron-stained	5.0	4.4	4.5	4.4	5.4
516	Breccia, light-gray, manganese-stained	11.2	10.4	13.2	10.2	10.5
514B	Breccia, fractured	25.8	25.4	29.6	25.4	22.3

TABLE 2.—*Comparison of tellurium analyses by atomic absorption and catalytic procedures*

[In parts per million]

Sample No.	Description	Procedure	
		Atomic absorption	Catalytic
	Samples from Cortez district, Nevada		
66-4237	Limestone, red-brown, leached	2.2	2.0
4241	Limestone, red-brown; veined with white calcite and pyrite	1.0	.8
CS-600G	Limestone, dark-gray, vuggy	.28	.10
600I	Limestone breccia, brown, altered	.31	.20
66-4321	Limestone, light-gray, pyritic	2.1	1.5
4235	Limestone, red-brown, leached; contains white calcite	.60	1.0
4331	Chert, altered	1.4	1.2
	Samples from Cripple Creek district, Colorado		
CC-500	Phonolite, breccia	7.2	7.5
506A	Volcanic rock, fine-grained, with pyrite casts	11	13
512	Volcanic rock, fine-grained, with heavy iron stains	53	63

The results of the precision and accuracy tests show that the method is well suited for geochemical exploration and possibly for other applications. Better accuracy and precision will, undoubtedly, be achieved with improved instrumentation.

REFERENCES

Billings, G. K., 1965, Light scattering in trace element analysis by atomic absorption: Atomic Absorption Newsletter [Perkin-Elmer Corp.], v. 4, no. 10, p. 357–360.

Gott, G. B., and McCarthy, J. H., Jr., 1966, Distribution of gold, silver, tellurium, and mercury in the Ely mining district, White Pine County, Nevada: U.S. Geol. Survey Circ. 535, 5 p.

Gott, G. B., McCarthy, J. H., Jr., VanSickle, G. H., and McHugh, J. B., 1967, Distribution of gold, tellurium, silver, and mercury in part of the Cripple Creek district, Colorado: U.S. Geol. Survey Circ. 543, 9 p.

Lakin, H. W., and Thompson, C. E., 1963, Tellurium—A new sensitive test: Science, v. 141, no. 3575, p. 42–43.

AUTOMATIC SAMPLE CHANGER FOR ATOMIC ABSORPTION SPECTROPHOTOMETRY

By LEONARD SHAPIRO and C. J. MASSONI, Washington, D.C.

Abstract.—An automatic sample changer is described that sequentially carries 64 beakers to the intake aspirator tube of atomic absorption instruments. The aspirator tube is lowered into each beaker, in turn, and the measurement-printout circuitry is pulsed after a suitable pause. When are instruments having printout capability are used, the time for the entire cycle is 45 seconds per sample.

In the past several years, atomic absorption spectrophotometry has become a major method of analysis in the U.S. Geological Survey. The technique is based upon the measurement of the relative percentages of resonant light absorbed by atoms formed when solutions of samples and standards are aspirated into a flame. In most commercial instruments, solutions are manually placed into position for absorption. There are obvious advantages to performing this step automatically. For example, in conjunction with automatic measurement and read-out accessories commercially available, a major part of the analysis can be performed automatically without attention from the operator.

An automatic sample changer was designed and built for this purpose in the Geological Survey's laboratories during the past year (fig. 1). It is adopted from a changer previously designed for use in an X-ray quantometer (Shapiro and Massoni, 1965) but is much simpler to build as it is not required to operate under vacuum. This changer enables 64 solutions in 30-ml beakers to be run, unattended. Commercial automatic sample changers have been described in the literature (Gaumer and others, 1966; Slavin and Slavin, 1966), and some have become available recently (Beckman Instruments, Inc., 1967).

DESCRIPTION OF AUTOMATIC SAMPLE CHANGER

The automatic sample changer consists of three components: a sample carrier, a positioning drive mechanism, and a lifter arm to raise and lower the plastic aspirator tube. The whole unit is mounted on a small movable table so that it can be attached to the atomic absorption equipment or removed if desired. Tolerances of construction are nominal.

The sample carrier is made from a Lucite disk, 36 inches in diameter and ½ inch thick. Sixty-four depressions, each 1⅜ inches in diameter and ¼ inch deep, are uniformly spaced near the edge of the disk (fig. 2). A ¼-inch hole in the center of each depression provides drainage in case of spillage. A considerable amount of the Lucite is cut away to reduce weight, but six strong supporting spokes are left. A ½-inch-thick ring of Lucite, 2½ inches in internal diameter and 3½ inches in external diameter, is bolted to the bottom center of the Lucite sample carrier. Two holes are drilled and tapped into the outer edge of the ring from opposite sides; each hole has a steel ball, a spring, and a tension-adjusting screw. This ring is mounted around a 5-inch-diameter 64-tooth gear in such a way that spring tension presses the steel balls between the gear teeth and yet permits unimpeded rotation of the wheel by hand. The mechanism serves as a detent to allow reproducible positioning of the sample. The 64-tooth gear is fastened to a vertical shaft carrying a 100-tooth gear driven by a 25-tooth gear on the positioning drive mechanism.

Positioning drive mechanism

Automatic positioning of the beakers, sequentially and accurately, is controlled by an indexing wheel constructed after the Geneva drive design (fig. 3). This wheel is a round brass plate 6 inches in diameter with 16 semicircles and 16 radial slots that alternate around the periphery. The wheel is moved by a plate-mounted drive pin on a shaft rotated by a 1½-rpm motor which runs continuously. During the part of the rotation of the shaft when the pin is not in the radial slot of the index wheel, the wheel is locked in position by a semi-

U.S. GEOL. SURVEY PROF. PAPER 600-B, PAGES B126-B129

FIGURE 1.—Photograph of automatic sample changer in use.

circular lug of the Geneva drive design. A 45° miter gear on the upper part of the same shaft that carries the pin drive engages a mated gear on another shaft at right angles to the pin drive shaft. One cam on the driven shaft operates a leaf switch that activates the read-out of the atomic absorption equipment, and a second cam causes the lifter to rise and fall.

Lifter

The lifter is an aluminum arm about 11 inches long having its free end resting on a cam attached to the horizontal shaft that also carries the cam activating the read-out switch. The other end of the arm pivots on a fixed pin. This part of the assembly is shown in figure 2. The lifter must be raised about 1¾ inches if 30-ml beakers are used. Attached to the movable end of the lifter is a ⅛-inch aluminum rod about 15 inches long that extends slightly beyond the outer edge of the sample carrier. Two bends bring the end of the rod about 2 inches above the top surface of the sample carrier and about 1 inch back toward the center. A tightly fitting polyethylene sleeve slipped onto the last several inches of this rod is allowed to extend about 1 inch beyond the end of the rod. A hole large enough to accept insertion of the aspirator tube is drilled through the free part of the polyethylene sleeve.

Wiring

The 1½-rpm motor is controlled and powered by an on-off toggle switch and line cord. The atomic absorption equipment has a pushbutton switch used to control the read-out equipment when a printer is provided. This pushbutton, or read-out switch, is connected to the terminals of a normally open leaf switch.

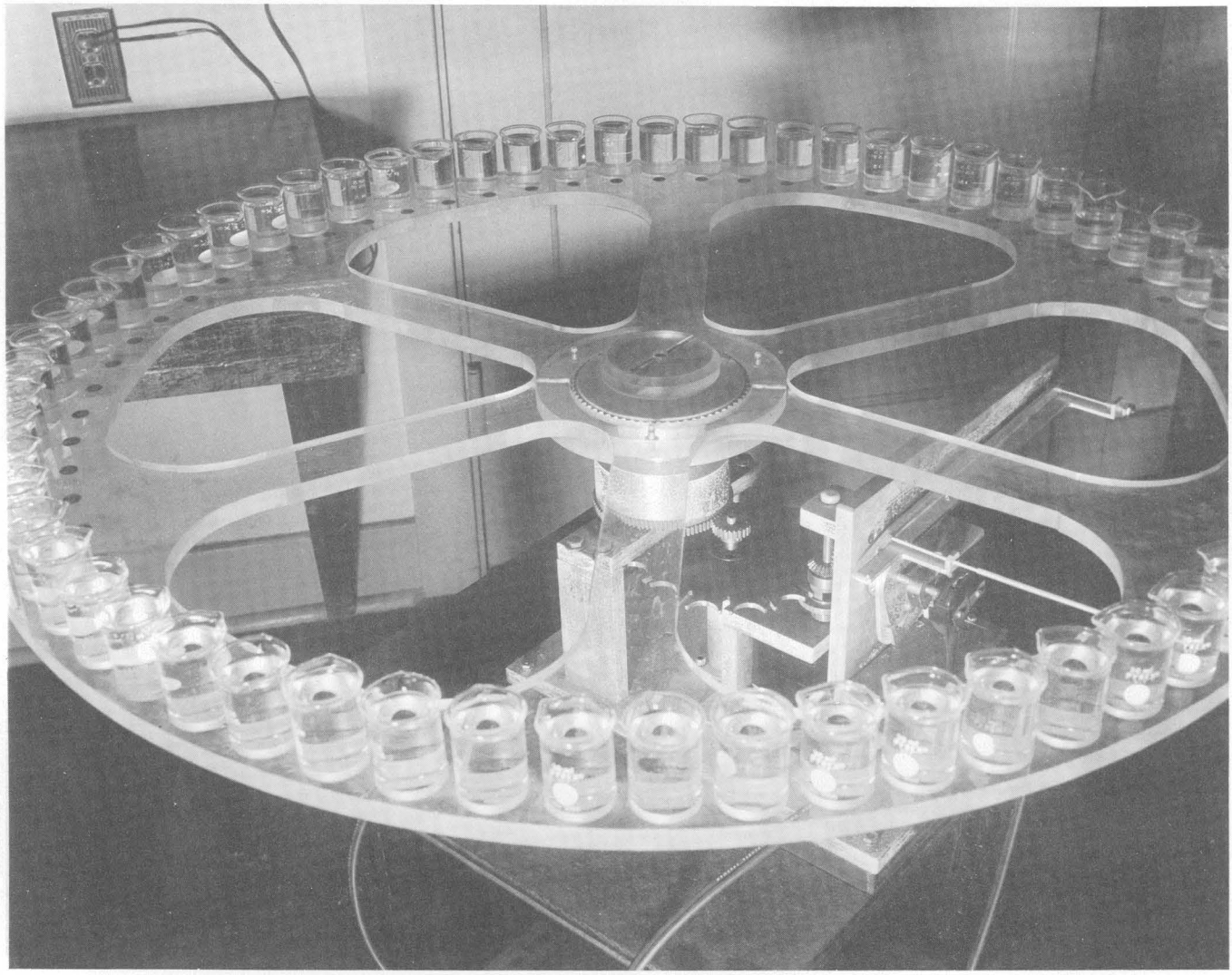

FIGURE 2.—Photograph showing general details of gear and cam mechanisms.

The leaf switch is positioned underneath the cam made for this purpose in such a way that as the cam rotates it closes the switch for 2–3 seconds. The exact position of the shaft at which this occurs need not be set until attachment is made to the aspirator tube.

ASSEMBLY AND OPERATION

The table is positioned so that the lifter arm is close to the aspirator tube. The aspirator tube is inserted through the drilled hole in the plastic sleeve. This is facilitated by passing a thin steel wire up through the drilled hole and into the aspirator tube for about 1 inch. The aspirator tube may then be brought through the hole without being crushed, after which the wire is removed. A beaker is placed in the sample-carrier depression just below the aspirator tube, and the motor switched on and allowed to run until the lifter arm is at its highest point. The aspirator tube is then positioned so that its tip is about $\frac{1}{8}$ inch above the top of the beaker.

The cam that activates the read-out switch is now loosened, the motor is turned on and allowed to run for 3 seconds after the time the lifter reaches its lowest point, and then the motor is turned off. The cam is retightened and is set to close the leaf switch. This procedure may have to be repeated a few times to set the exact position and degree of closing. The equipment is now ready for use and further adjustment should not be needed.

In our automatic operation, standards and samples are placed in a sequence of 6 standards followed by 15 samples. The flame position and electrical parameters are the same as in manual operation of the atomic absorption equipment when the blank and any one of

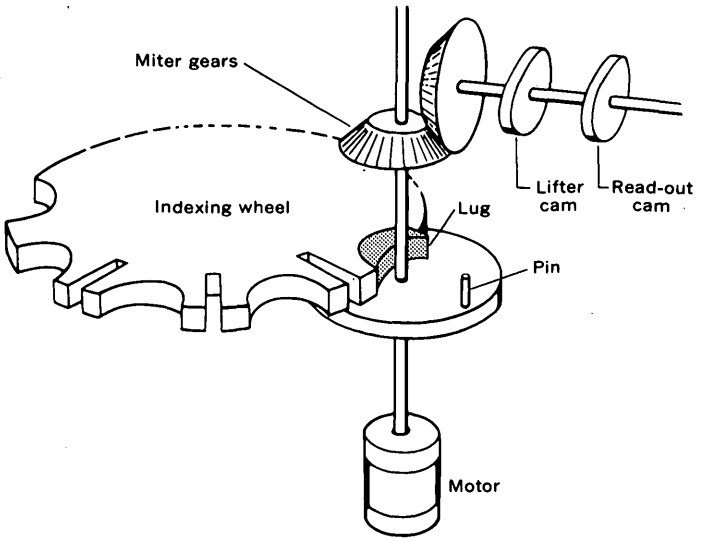

FIGURE 3.—Schematic diagram of pin drive of the Geneva mechanism and associated miter gears and cams.

the standards are used. When adjustments are correct, the sample carrier is positioned so that the aspirator tube is in the beaker preceding that of the blank, and the toggle is switched on. The rest of the operation is fully automatic.

The aspirator tube is lifted to its peak height, the table rotates to bring the first beaker into position, the aspirator tube is lowered into the beaker where it remains for 3 seconds, and then the read-out is activated. Our instrument makes four readings and displays the average in 12 seconds. The result is then printed out and the arm starts up again to repeat the cycle. We find that a slight amount of drift sometimes occurs in the readings of the standards before and after a batch of samples; therefore we always average the standard readings made before and after a given set of samples. The complete cycle of 64 solutions requires 48 minutes, or 45 seconds per sample.

REFERENCES

Beckman Instruments, Inc., 1967, Beckman automatic sample changer for Model 979 Atomic Absorption Spectrophotometer: Beckman Sci. Instrument Div., Bull. 7123, 2 p.

Gaumer, M. W., Sprague, Sabina, and Slavin, Walter, 1966, An automated procedure for the determination of trace metals by atomic absorption spectroscopy: Atomic Absorption Newsletter [Perkin-Elmer Corp.], v. 5, no. 3, p. 58–61.

Shapiro, Leonard, and Massoni, Camillo, 1965, Automatic sample changer and controller for an X-ray quantometer, *in* Geological Survey Research 1965: U.S. Geol. Survey Prof. Paper 525–D, p. D178–D183.

Slavin, Sabina, and Slavin, Walter, 1966, Fully automatic analysis of used aircraft lubricating oils: Atomic Absorption Newsletter [Perkin-Elmer Corp.], v. 5, no. 5, p. 106–112.

RAPID ANALYSIS FOR GOLD IN GEOLOGIC MATERIALS

By C. E. THOMPSON,[1] H. M. NAKAGAWA, and G. H. VanSICKLE,
Denver, Colo.

Abstract.—Trace amounts of gold in geologic materials are determined by atomic absorption spectrophotometry of an immiscible organic solvent containing the extracted gold. Samples are dissolved by either hot or cold hydrobromic acid-bromine mixtures. In the hot method the gold in the sample is dissolved by heating with hydrobromic acid and sodium bromate, and in cold method the sample is merely shaken with hydrobromic acid containing 0.5 percent bromine. In both methods, the gold is extracted from the acid solution with methyl isobutyl ketone which is atomized in an atomic absorption spectrophotometer for the estimation. The results compare favorably with those from assay methods. Up to 100 samples a day can be analyzed by the cold method and a sensitivity of 0.02 ppm is attained.

A relatively simple and precise method for determining trace amounts of gold in geologic materials was needed to meet the demand of an expanded program of the U.S. Geological Survey for the development of new sources of gold.

Metallic gold and most gold-bearing minerals are rapidly soluble in acid solutions of bromine even at room temperature. This provides a rapid and simple first step in the analysis of gold. Gold is easily extracted from hydrobromic acid by several organic solvents which provide a satisfactory medium for atomic absorption estimation. Tindall (1965) used methyl isobutyl ketone extraction prior to the determination of gold by atomic absorption spectrophotometry.

This report describes a method for the determination of gold after either hot or cold (room temperature) sample solution techniques, solvent extraction with methyl isobutyl ketone, and atomic absorption spectrophotometric estimation. Materials such as rocks, soils, stream sediments, and mineral concentrates can be analyzed for geochemical exploration purposes.

[1] Present address: Skyline Labs, Inc., Wheatridge, Colo.; formerly of the U.S. Geological Survey.

Of the two sample solution techniques, the hot digestion method was developed first and has been successfully used in Nevada and Colorado. The demands of an exploration program prompted an investigation to see if the hot method could be shortened, if a larger sample might be used without loss of speed, and if sensitivity or precision could be increased.

The cold method is our preference, because of its simplicity, and it is now exclusively used for the determination of gold in our exploration studies.

Both methods compare favorably with each other, and with the classical fire-assay method. These methods are not intended to replace the fire assay and should be used as supplemental methods or for exploration work where quick results are necessary.

LABORATORY REAGENTS AND APPARATUS

Reagents

Standard gold solution (0.1 percent): Dissolve exactly 1.000 gram of Au in hydrobromic acid-bromine solution and heat gently to expel excess bromine. Cool and dilute to 1,000 milliliters with concentrated HBr.

Dilute standard gold solution (0.01 percent): Dilute 10.0 ml of 0.1-percent Au solution to 100 ml with 1.5*N* HBr.

Dilute standard gold solution (0.001 percent): Dilute 1.0 ml of 0.1-percent Au solution to 100 ml with 1.5*N* HBr.

Hydrobromic acid, concentrated, reagent grade.

Hydrobromic acid, 0.1*N*: Dilute 23 ml of concentrated HBr to 2 liters with water.

Hydrobromic acid-bromine solution: Dissolve 10 ml of liquid bromine in 2 liters of concentrated HBr.

Methyl isobutyl ketone, reagent grade.

Sodium bromate, reagent grade.

Apparatus

Hotplate, oscillating: A large electric hotplate that mounts on an oscillator base (which agitates the hotplate at a constant speed) and has temperature control from 200° to 700°F.

U.S. GEOL. SURVEY PROF. PAPER 600-B, PAGES B130-B132

Shaking machine; Equipoise, heavy duty: Shaking-compartment space 5½ inches deep, 11½ inches wide, and 14¼ inches long; movable block adjusts length from 1/4 to 13 inches; 1/4 horsepower motor provides shaking speed of 265 cycles per minute and stroke amplitude of 2⅜ inches.
Atomic absorption spectrophotometer.

PROCEDURE

Solution of gold samples

1. Hot acid digestion: Ignite 2.0 g of rock or soil in a porcelain evaporating dish over a Meker burner until completely ashed. Stir the sample with a glass rod occasionally during the ashing. Transfer the ashed sample to a 50-ml beaker and add 0.5 g of $NaBrO_3$. Mix thoroughly and add 15 ml of concentrated HBr. Let stand overnight. Place the beaker on the oscillating hotplate and heat until the volume of acid is reduced to approximately 5 ml. Transfer the entire contents (unattacked sample and acid) of the beaker to a 25× 200-mm test tube fitted with a screwcap. Rinse the beaker with three 5-ml portions of water and add each rinse portion to the tube. Add 10 ml of methyl isobutyl ketone (MIBK) to the tube, shake the tube vigorously for 1 minute, and centrifuge or let solids settle. If the organic layer is colored, transfer the MIBK with an automatic pipet to a clean tube containing 25 ml of 0.1*N* HBr and shake for 15 seconds.
2. Cold acid treatment: Transfer 10 g of pulverized sample to a 25×200-mm screwcapped culture tube. If the sample contains much organic material or sulfides, it should first be ignited. Add 20 ml of hydrobromic acid-bromine solution to the sample. Cap the tube and place it in a shaking machine and shake the tube for 15 minutes. Add 20 to 30 ml of water and 10 ml of MIBK and again shake the tube for 2 minutes. Centrifuge the solution for 1 minute, transfer the MIBK with an automatic pipet to a similar tube containing 25 ml of 0.1*N* HBr, and shake for 15 seconds.

Estimation of gold

Atomize the ketone from either digestion (hot or cold) in an atomic absorption spectrophotometer. Compare with standard solutions atomized under the same conditions. Examples of atomic absorption spectrophotometer parameters are as follows:

Wavelength, 2,430 A
Spectral slit width, 20 A
Lamp current, 14 milliamperes
Air pressure, 20 pounds per square inch
Fuel pressure, 8 pounds per square inch

Preparation of standards

Pipet 0.06 and 0.6 ml of a 0.001 percent standard gold solution and 0.15, 0.6, and 1.5 ml of a 0.01 percent standard gold solution into five 100-ml volumetric flasks containing 30 ml of 1*N* HBr, and then add 30 ml of MIBK. Shake the flasks vigorously for 1 minute. Each milliliter of ketone of the five flasks contains, respectively, 0.02, 0.2, 0.5, 2.0, and 5.0 parts per million gold. Add water to bring the organic phase into the neck of the flask. Atomize the organic phase; use the reading obtained to prepare a standard curve or compare with the unknown directly.

DISCUSSION

Care must be taken when adding the hydrobromic acid-bromine reagent to a sample which contains much carbonate because all may effervesce from the tube or beaker. For rock samples or heavy-mineral concentrates that contain little organic materials or sulfides, it is not necessary to include the ignition step before the digesion.

Lakin and Nakagawa (1965) stated that any gold minerals completely enclosed in insoluble particles such as quartz would not be brought into solution and that the resulting values would be low. The sample must be ground to a powder to insure reasonable attack on the gold. However, if the sample is ground too fine, it is difficult to get a separation of the ketone layer. Fine grinding may also result in loss of gold by plating onto the grinding equipment. Thus a compromise must be reached. We have found, when a 10-g split of sample is used, that good reproducibility can be generally obtained if the sample is ground to pass a 100-mesh screen but is mostly held on a 150-mesh screen.

The only interference in the estimation was caused by the presence of an excessive amount of iron coextracted into the MIBK. The iron is presumed to interfere by causing light scattering. The iron is removed by washing the MIBK extract with the 0.1*N* HBr solution; the gold remains quantitatively in the ketone.

PRECISION

The repeatability of the cold method on placer-type samples is shown in table 1. Three samples of placer material were analyzed four times each by the 10-g-sample cold extraction method.

Table 2 presents a comparison of gold values obtained on several rock samples by hot and cold solution techniques with those obtained by fire assay.

Comparison of values obtained by the hot method with those by the cold method on rock samples is shown in table 3.

TABLE 1.—*Replicate gold analyses, in parts per million, obtained after cold digestion method was used on placer material from Routt County, Colo.*

Sample No.	Analyses of separate subsamples			
	1	2	3	4
AAE–146	0. 05	0. 03	0. 04	0. 04
649	1. 6	1. 9	1. 9	2. 1
654	. 20	. 22	. 20	. 24

TABLE 2.—*Comparison of gold analyses, in parts per million, obtained after hot digestion, cold digestion, and fire-assay methods were used on rocks from Cripple Creek, Teller County, Colo.*

Sample No.	Method		
	Fire assay [1]	Hot digestion	Cold digestion
CC–500	2. 0	2. 2	1. 9
503	. 7	. 1	. 2
506A	2. 5	3. 3	3. 5
508	14. 1	14. 6	15. 4
512	5. 4	6. 2	6. 5

[1] Assay by O. M. Parker, J. D. Mensik, and Claude Huffman, Jr., U.S. Geological Survey, Denver, Colo.

TABLE 3.—*Comparison of gold analyses, in parts per million, obtained after hot digestion and cold digestion methods were used on rocks from Cripple Creek, Teller County, Colo.*

Sample No.	Digestion method	
	Hot	Cold
66–7475–S	2. 2	1. 6
7476–S	1. 5	1. 2
7480–S	2. 0	2. 2
7481–S	. 8	. 7
7483–S	. 1	. 1
7493–S	3. 3	2. 6
7498–S	. 9	. 9
7478–S	. 6	. 4
7482–S	1. 1	1. 0
7491–S	. 1	. 2

The hot and cold methods of dissolution for a properly prepared sample combined with estimation of gold by atomic absorption spectrophotometry give adequately reproducible values for exploration purposes. The hot method was successfully used in analyzing the samples of anomalous gold areas located by Erickson (Erickson and others, 1966) and Gott (Gott and McCarthy, 1966; Gott and others, 1966). The cold method is now recommended because it is rapid, its larger samples are more representative, and it is more easily adaptable to field service.

REFERENCES

Erickson, R. L., VanSickle, G. H., Nakagawa, H. M., McCarthy, J. H., Jr., and Leong, K. W., 1966, Gold geochemical anomaly in the Cortez district, Nevada: U.S. Geol. Survey Circ. 534, 9 p.

Gott, G. B., and McCarthy, J. H., Jr., 1966, Distribution of gold, silver, tellurium, and mercury in the Ely mining district, White Pine County, Nevada: U.S. Geol. Survey Circ. 535, 5 p.

Gott, G. B., and McCarthy, J. H., Jr., VanSickle, G. H., and McHugh, J. B., 1966, Distribution of gold, tellurium, silver, and mercury in part of the Cripple Creek district, Colorado: U.S. Geol. Survey Circ. 543, 9 p.

Lakin, H. W., and Nakagawa, H. M., 1965, A spectrophotometric method for the determination of traces of gold in geologic materials, *in* Geological Survey Research 1965: U.S. Geol. Survey Prof. Paper 525–C, p. C168–C171.

Tindall, F. M., 1965, Silver and gold assay by atomic absorption spectrophotometry: Atomic Absorption Newsletter [Perkin-Elmer Corp.], v. 4, no. 9, p. 339–340.

SCHWAGERINA CRASSITECTORIA DUNBAR AND SKINNER, 1937, A FUSULINID FROM THE UPPER PART OF THE WICHITA GROUP, LOWER PERMIAN, COLEMAN COUNTY, TEXAS

By DONALD A. MYERS, Denver, Colo.

Abstract.—Specimens of *Schwagerina crassitectoria* Dunbar and Skinner, 1937, described in this report, were collected from the Talpa Limestone Member of the Clyde Formation (middle Permian) in north-central Texas. These forms are similar to the intergradational species of *S. crassitectoria* and *S. guembeli* from the Hess Formation, of early Leonard age, in the Glass Mountains, west Texas.

Fusulinid Foraminifera are little known from the upper part of the Wichita Group in central and north-central Texas. Thompson (1954) described specimens of fusulinids from the Coleman Junction Limestone Member at the top of the Putnam Formation of Wolfcamp age. Other than a note by Henbest (1958, p. 45), there have been no published reports of younger Wolfcamp or Leonard fusulinid faunas in this region. The purpose of this paper is to record the presence of *Schwagerina crassitectoria* Dunbar and Skinner, 1937 in the Talpa Limestone Member of the Clyde Formation, of early Leonard age, in Coleman County.

The stratigraphy of rocks of Permian age in the Colorado River valley is discussed by Moore (1949), and the following discussion is taken largely from his report. Rocks referred to the Permian System in Coleman County are assigned to the Wichita Group of Wolfcamp and early Leonard age, and to the Clear Fork Group of Leonard age. The Wichita Group was divided into seven formations, and each formation was subdivided into several members (Moore, 1949). The formations assigned to the Wichita Group are, in descending order:

Lueders Limestone
Clyde Formation
Belle Plains Formation
Admiral Formation
Putnam Formation
Moran Formation
Pueblo Formation

The boundary between the Leonard and Wolfcamp Series was placed by Moore at the top of the Admiral Formation.

The Clyde Formation, the base of which lies about 720 feet above the base of the Leonard Series, is about 500 feet thick. It consists of the Grape Creek Limestone Member below, and the Talpa Limestone Member. The Grape Creek, about 325 feet thick, is dominantly thin beds of blue-gray limestone (Moore, 1949). The Talpa, about 175 feet thick, is thin beds of blue-gray limestone and gray shale. Moore (1949) mapped three subdivisions of the Talpa: subdivision 1, a lower limestone and shale, about 75 feet thick; subdivision 2, a middle dominantly shale unit, about 25 feet thick; and subdivision 3, an upper limestone and shale, about 70 feet thick. Stafford (1960, p. 274, pl. 12) indicated a marked thinning of the Clyde Formation north and east of Coleman County to about 255 feet in west-central Throckmorton County.

Fusulinids were first reported from the Talpa Limestone Member by Henbest (1958, p. 45). He found

U.S. GEOL. SURVEY PROF. PAPER 600-B, PAGES B133-B139

"* * * a few immature specimens of a species of *Parafusulina* or *Schwagerina* suggesting *S. crassitectoria* Dunbar and Skinner, 1937, or *S. guembeli* Dunbar and Skinner, 1937 * * *" at the type locality of the Talpa. Two of Henbest's specimens are illustrated on figure 2, *k* and *l*. Henbest also reported rather rare *Boultonia* sp. Other than this citation, no fusulinids have been reported from outcropping rocks of Leonard age in central or north-central Texas.

In the spring of 1965, the writer was contacted by Mr. W. L. Gould, of Coleman, Tex., who had three specimens of fusulinids from a shale bed in the Talpa Limestone Member near the community of Novice in northwestern Coleman County. The locality was initially found by Mr. H. C. Fountain and Mr. Gould shortly before Fountain's death. The writer visited the Novice locality with Mr. Gould in the fall of 1965 and collected about 150 pounds of shale. Careful examination of the washed and sieved residue of all the shale yielded 17 specimens of fusulinids, all referable to *Schwagerina crassitectoria*.

The locality (fig. 1), U.S. Geological Survey locality f10119, is described as follows:

Texas, Coleman County, Talpa Limestone Member of the Clyde Formation, probably subdivision 2 of Moore (1949). Gray calcareous fossiliferous shale at a natural gas blowout in a field. The shale is found as pockets between and on erratic slabs of limestone around the perimeter of the crater. About 0.7 mile north of the community of Novice, on road at east end of town and between Farm Road 702 and U.S. Highway 84; F. M. Taylor Survey 80, Danoil Inc., Lou Gillespie Lease.

Shale beds in the Talpa that have similar lithology and probable stratigraphic equivalence to the shale bed of the Novice locality are exposed in roadcuts along U.S. Highway 84, about 2 miles north-northwest of Novice, east of the highway junction with Farm Road 702. A small sample of this shale was examined for fusulinids, with negative results.

The systematics and description of *Schwagerina crassitectoria*, from locality f10119 near Novice, Tex., are as follows:

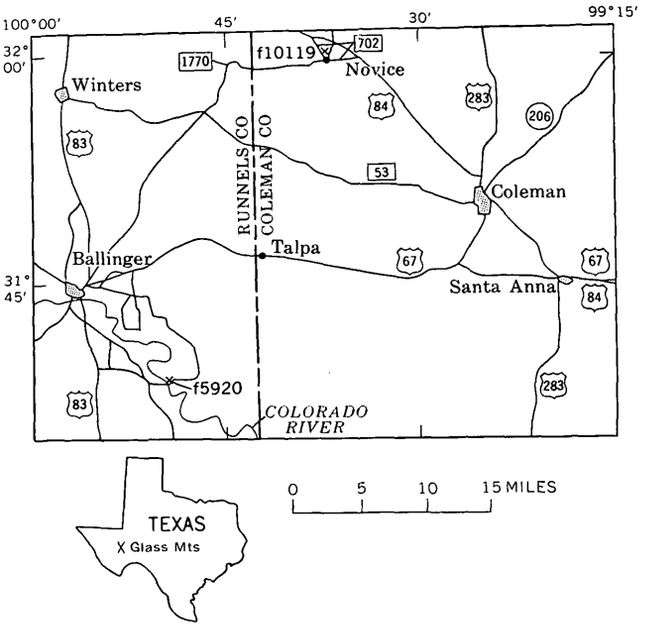

FIGURE 1.—Location of fusulinid collections from the Talpa Limestone Member of the Clyde Formation, Wichita Group, north-central Texas. Base from 1954 U.S. Geological Survey Brownwood 1:250,000, map.

Genus *Schwagerina* Möller, 1877, emend. Dunbar and Skinner, 1936

Schwagerina crassitectoria Dunbar and Skinner, 1937

Schwagerina crassitectoria Dunbar and Skinner, 1937, p. 641, pl. 65, figs. 1–15. Ross, 1960, p. 123, pl. 17, figs. 1–9; 1962, p. 9, pl. 1, figs. 15, 16; 1963, p. 118–120, pl. 9, figs. 10–15.

Description.—A fusiform species with convex lateral slopes and sharply rounded ends that is about 8 millimeters long and 3 mm wide in mature specimens. The form ratio of the exterior whorl is about 2.3.

Mature specimens have from 6 to 8 volutions. The height of the volution increases more or less uniformly from an average of 0.057 mm in the first volution to an average of 0.190 mm in the fifth. In the outer whorls, the height of the volution apparently decreases to about 0.185 mm; however, this decrease may be more

apparent than real. The form ratio averages 1.7 in the first volution; in succeeding volutions it is relatively constant, and averages between 2.0 and 2.2, with maximums and minimums of 2.3 and 1.6.

The proloculus has an average diameter of 0.205 mm, and ranges from 0.123 mm to 0.307 mm. The specimens with the smaller proloculi have a greater number of whorls and are larger than the specimens with the larger proloculi. The thickness of the proloculus wall ranges from 0.010 mm to 0.030 mm and averages 0.016 mm.

The average tunnel angle increases from 32° in the first volution to 37° in the third; it is about 36° in the fourth volution, 40° in the fifth, and 32° and 36° in the sixth (two specimens) and seventh (one specimen) volutions.

The septa are strongly fluted. Axial filling is present in varying amounts in all specimens examined, and it is restricted to the first 4 or rarely 5 volutions. The filling seems to be heavier in those specimens with the larger proloculi, and minimal in those specimens with the smaller proloculi. Septal pores were not noted. The number of septa in 2 specimens increases from 6 or 11 in the first volution to 18 or 24 in the fourth volution. Phrenothecae were noted in most of the specimens examined.

The spiral wall has an average thickness of 0.018 mm in the first volution. From the first volution, it increases more or less uniformly to an average thickness of 0.102 mm in the seventh volution. The wall thickness of a single specimen was 0.190 mm in the eighth volution. The wall consists of a tectum about 0.006 mm thick in the outer whorls, and a keriotheca in which 10 alveoli occupy 0.120 mm to 0.140 mm in the fifth volution, and 10 alveoli occupy 0.170 mm to 0.180 mm in the seventh and eighth volutions.

Discussion.—The described specimens are from the Talpa Limestone Member of the Clyde Formation, upper part of the Wichita Group, of early Leonard age. The material is from U.S. Geological Survey locality f10119. Henbest (1958, p. 45) reported fusulinids from the Talpa at U.S. Geological Survey locality f5920 in Runnels County (fig. 1) that are probably conspecific with the material from locality f10119 (fig. 2, *k* and *l*).

The referral of this species to *Schwagerina crassitectoria* rather than to *S. guembeli* is rather arbitrary, as the specimens described above are similar to both. Both species were originally described from the lower part of the Hess Formation in the Glass Mountains of west Texas. Ross (1960, p. 124) states that in the lower part of its range *S. crassitectoria* is very similar to *S. guembeli*, and that gradational forms between the two are common. In its type area, both species are apparently restricted to that part of the Hess Formation of early Leonard age (Ross, 1960, p. 123–125; 1962, p. 9–11; 1963, p. 118–120, 130–131).

The form from the Talpa Limestone Member differs from the one of the Glass Mountains in that the Talpa form has a slightly lower form ratio, slightly thicker wall, slightly greater tunnel angle in the early whorls and slightly less in the later whorls, and slightly lower radius vector in the fifth through seventh whorls. From *S. guembeli*, the Talpa form differs in having a larger tunnel angle in all but the last two whorls, and in having a slightly lower radius vector; the form ratio of the two is practically identical.

Measurements of *S. crassitectoria* from the Talpa Limestone Member have been plotted on figures 3 and 4. For comparative purposes, measurements given by Dunbar and Skinner (1937, p. 639–643) and Ross (1960, p. 123–125; 1962, p. 9–11; 1963, p. 118–120, 130–131) for the Hess Formation forms, *S. crassitectoria* and *S. guembeli*, have also been plotted on figures 3 and 4. The absence of plotted data for these two species indicates either that the necessary data were not given, or that the number of specimens measured was not sufficient to plot.

Parafusulina diabloensis Dunbar and Skinner, 1937, which resembles *S. crassitectoria*, possesses cunuculi, but is larger, has more septa and a smaller tunnel angle, has a higher form ratio in the outer whorls of mature specimens, has a greater radius vector, and has somewhat heavier axial fill than does *S. crassitectoria*.

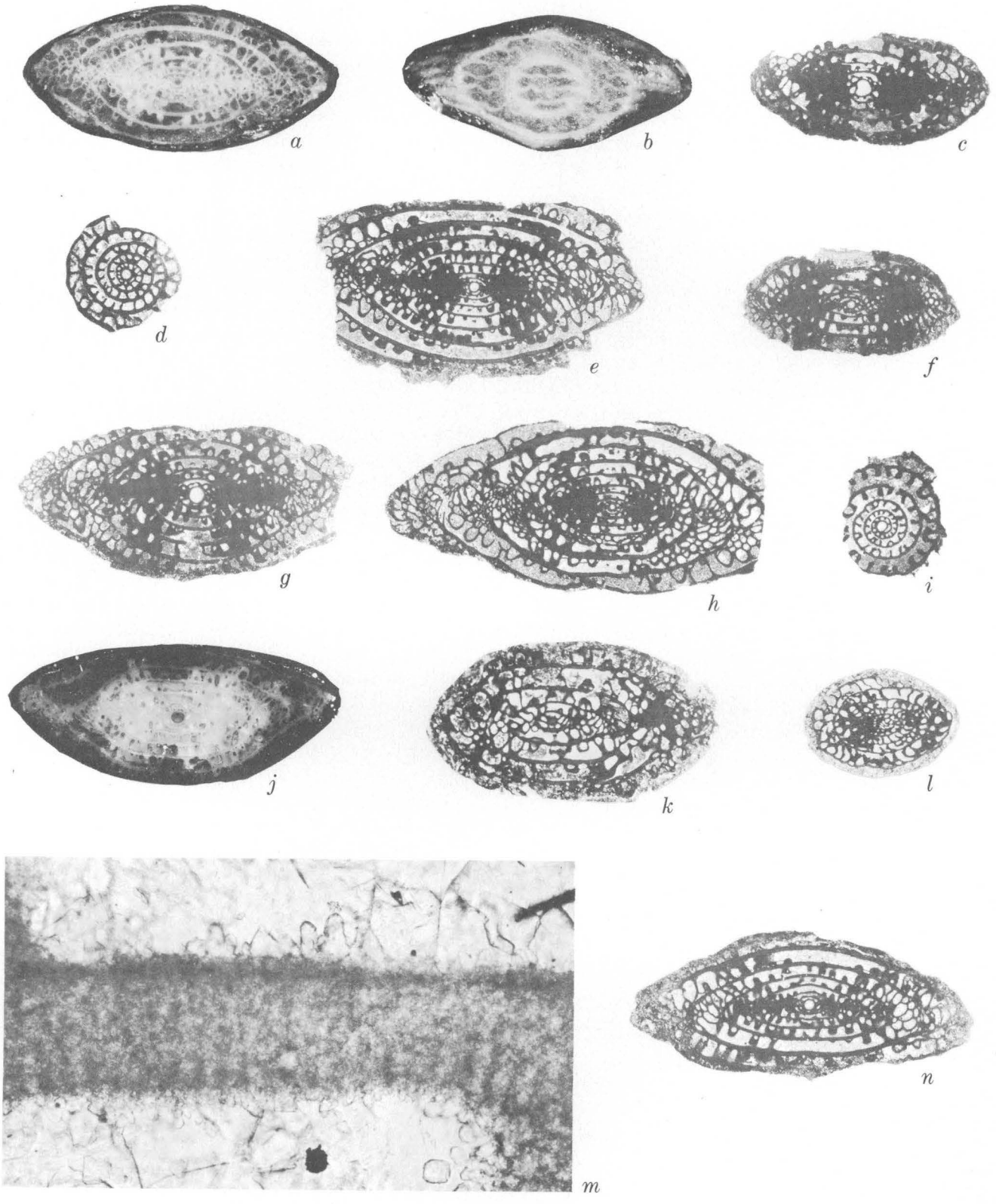

FIGURE 2.

FIGURE 2.—*Schwagerina crassitectoria* Dunbar and Skinner, 1937, from the Talpa Limestone Member of the Clyde Formation. All specimens from USGS loc. f10119, unless otherwise noted. Magnification, × 10, unless otherwise noted. All figured speciments deposited in the U.S. National Museum (USNM).
a, *b*. Polished sections of the same specimen. *a*. axial section; *b*, opposite side, tangential section. USNM 159054.
c, *c–g*. Axial sections of specimens that resemble *Schwagerina gucmbeli* Dunbar and Skinner, 1937. *c*. USNM 159055; *c*, USNM 159056; *f*, USNM 159057; *g*, USNM 159058.
d, *i*. Equatorial sections. *d*, USNM 159059; *i*, USNM 159060.
h. Axial section, USNM 159061.
j. Polished axial section of a specimen that resembles *S. gucmbeli* Dunbar and Skinner, 1937. USNM 159062.
k, *l*. Eccentric sections of specimens from USGS loc. f5920. *k*, USNM 159063; *l*, USNM 159064.
m. Photomicrograph (× 300) of a portion of the wall in the fifth whorl of specimen *n*. Shows the thin tectum and the keriotheca.
n. Axial section. USNM 159065.

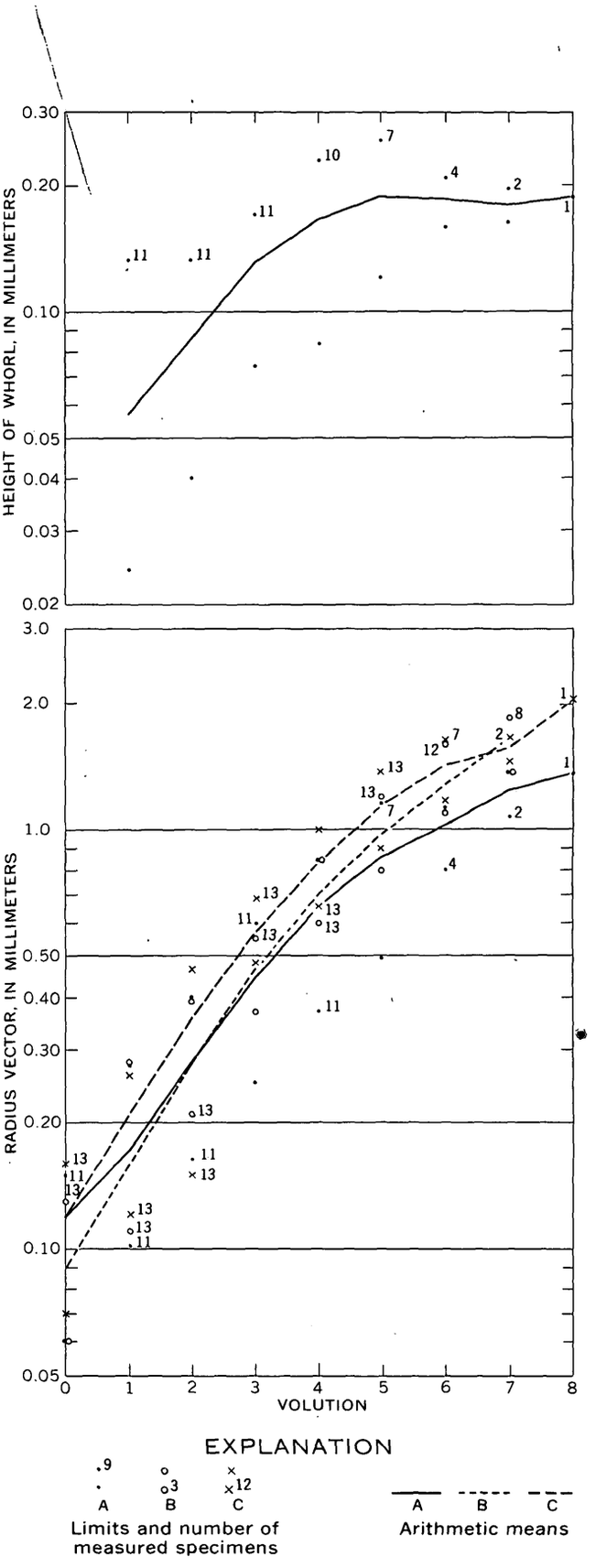

FIGURE 3.—Measurements of height of whorl and radius vector of *Schwagerina crassitectoria* Dunbar and Skinner, 1937, from the Talpa Limestone Member of the Clyde Formation (A) and from the Hess Formation (B), and *Schwagerina gucmbeli* Dunbar and Skinner, 1937, from the Hess Formation (C). Numbers adjacent to limit symbols indicate number of specimens. Data for specimens from Hess Formation from Dunbar and Skinner (1937) and Ross (1960, 1962, 1963).

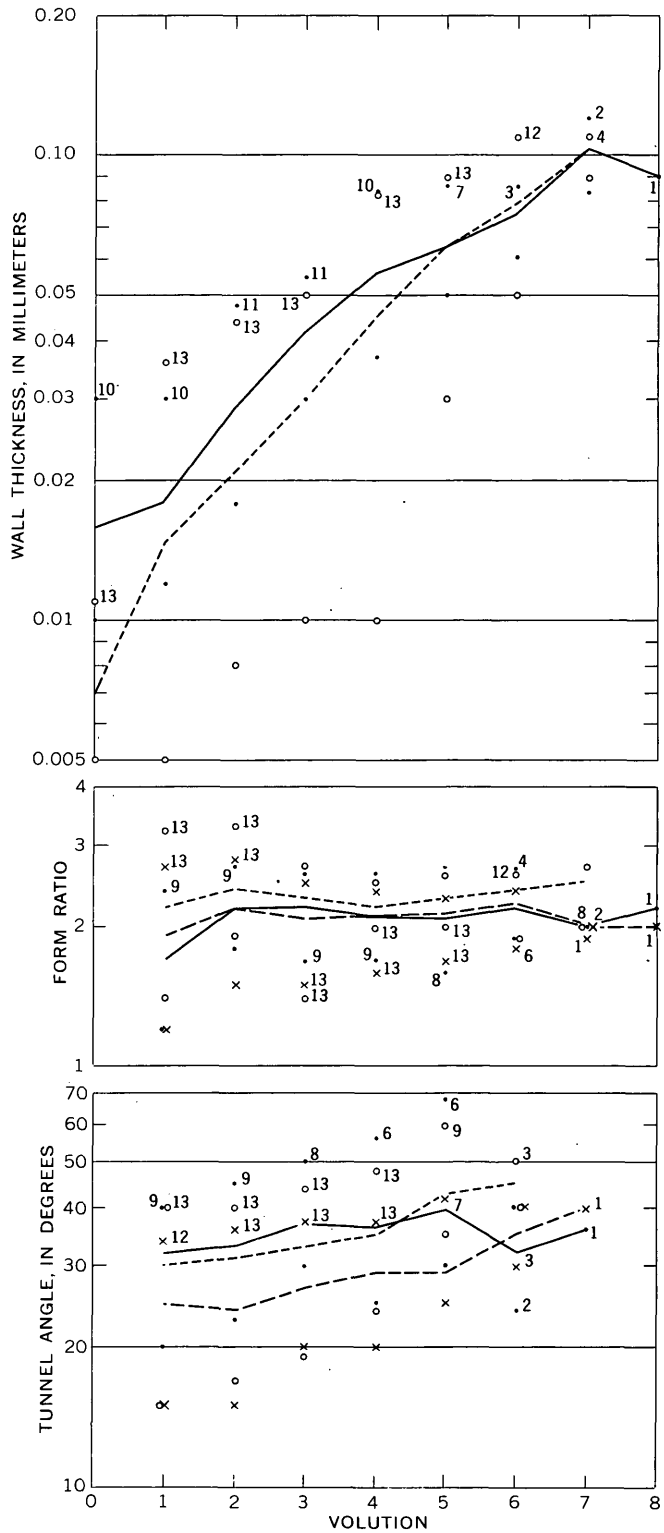

FIGURE 4.—Measurements of wall thickness, form ratio, and tunnel angle of *Schwagerina crassitectoria* Dunbar and Skinner, 1937, from the Talpa Limestone Member of the Clyde Formation (dot) and from the Hess Formation (open circle), and *Schwagerina guembeli* Dunbar and Skinner, 1937, from the Hess Formation (×). Numbers, symbols, and source of data explained in figure 3.

REFERENCES

Dunbar, C. O., and Skinner, J. W., 1936, *Schwagerina* versus *Pseudoschwagerina* and *Paraschwagerina:* Jour. Paleontology, v. 10, p. 83–91, pls. 10, 11.

——— 1937, The geology of Texas, v. 3, pt. 2, Permian Fusulinidae of Texas: Texas Univ. Bull. 3701, p. 517–825, pls. 42–81.

Henbest, L. G., 1958, Pennsylvanian-Permian boundary in north-central Texas, *in* The base of the Permian, a century of controversy: San Angelo Geol. Soc. Guidebook, field trip, April 17–19, 1958, p. 38–49.

Möller, Valerian von, 1877, Ueber Fusulinen und ähnliche Foraminiferenformen des russischen Kohlenkalkes: Neues Jahrb. Mineralogie, Geologie u. Paläontologie, v. 1877, p. 139–146.

Moore, R. C., 1949, Rocks of Permian(?) age in the Colorado River Valley, north-central Texas: U.S. Geol. Survey Oil and Gas Inv. Map 80.

Ross, C. A., 1960, Fusulinids from the Hess Member of the Leonard Formation, Leonard Series (Permian), Glass Mountains, Texas: Cushman Found. Foram. Research Contr., v. 11, p. 117–133, pls. 17–21.

——— 1962, Fusulinids from the Leonard Formation (Permian), western Glass Mountains, Texas: Cushman Found. Foram. Research Contr., v. 13, p. 1–21, pls. 1–6.

——— 1963, Standard Wolfcampian Series (Permian), Glass Mountains, Texas: Geol. Soc. America Mem. 88, 205 p., 29 pls.

Stafford, P. T., 1960, Stratigraphy of the Wichita group in part of the Brazos River Valley, north Texas: U.S. Geol. Survey Bull. 1081–G, p. 261–280, 2 pls., 1 fig.

Thompson, M. L., 1954, American Wolfcampian fusulinids: Kansas Univ. Paleon. Contr., Protozoa, Art. 5, 226 p., 52 pls., 14 figs.

285-544 O—68——10

RECENT FAULT SCARPS IN INDEPENDENCE VALLEY NEAR TUSCARORA, ELKO COUNTY, NEVADA

By R. R. COATS, Menlo Park, Calif.

Abstract.—In Independence Valley, near Tuscarora, Elko County, Nev., a system of northeast-trending faults cuts a late Quaternary gravel that veneers pediment surfaces cut on volcanic rocks of probable mid-Tertiary age. Some faults show erosionally degraded fault scarps up to 12 feet in height; the direction in which scarps face and the inferred direction of downthrow on the faults may be northwest or southeast, but most show the valleyward side downthrown. The faults are believed to be several hundred to several thousand years old. They have possible economic significance in prospecting for extensions of the gold-silver deposits of Tuscarora, or in the working of low-grade placers believed to exist in this district.

The purpose of this paper is to call attention to hitherto undescribed Recent fault scarps in a part of Nevada which displays little evidence of Recent faulting and to suggest the possible economic significance of the faulting, should mining be revived in this area.

Tuscarora is an old mining camp near the southwest corner of Independence Valley, an intermontane valley in western Elko County, Nev., (fig. 1) that is about 24 miles long and about 4 miles wide in the wider parts. The southern part of the valley trends northeast, and the northern part trends north. The slope of the eastern valley wall in the northern part is very steep and abrupt, and the outline is simple. The slope of the western side of the valley is much less abrupt, is more mature, and much of the west side of the valley is a broad pedimented fan. Tuscarora lies near the upper margin of the pediment surface.

CENOZOIC STRUCTURE

Little is known of the orientation of Cenozoic structures in the area. According to Nolan (1936, p. 22), most of the Tuscarora district is underlain by a bedded series of pyroclastic rocks intruded by irregular bodies of andesite. The bedded series dips generally southeast or east at angles of 15°–50°. It is cut by faults, some of which are mineralized. The mineralized faults commonly have a northerly strike and a steep westerly dip, but one productive vein described by Nolan (1936, p. 30) has a northeasterly strike and a northwest dip. The general strike of the mineralized belt is northeasterly.

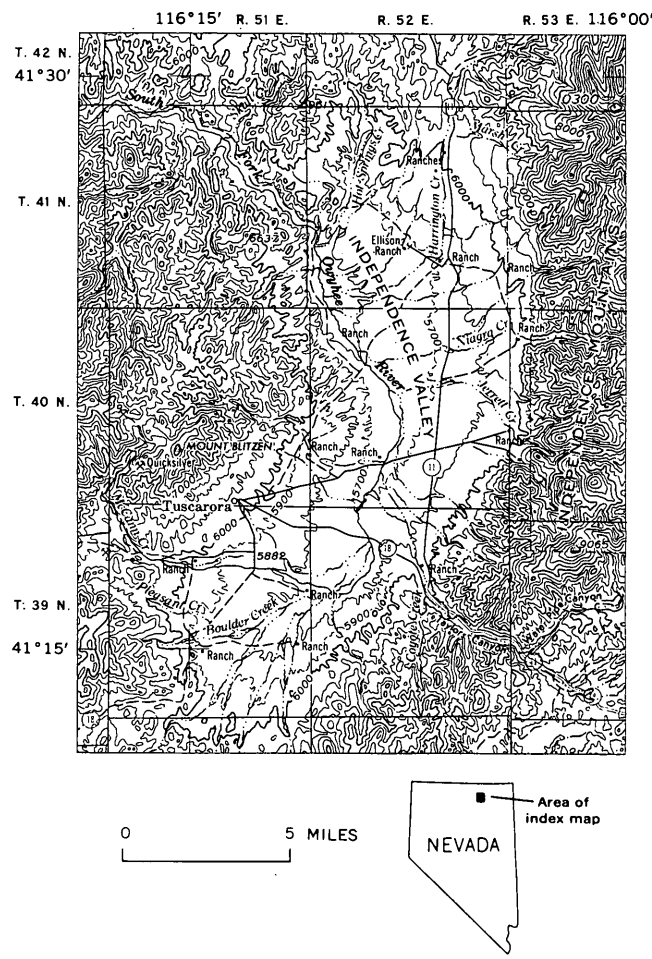

FIGURE 1.—Index map showing Tuscarora and Independence Valley, Nev.

U.S. GEOL. SURVEY PROF. PAPER 600-B, PAGES B140-B143

In the Independence Mountains, the geology has been recently mapped by Kerr (1962) for a distance of several miles north of Taylor Canyon. Kerr has mapped numerous high-angle faults with northeasterly and northwesterly trends that cut the Tertiary rocks. Either the northwest or the southeast side of the northeast-trending faults may be downthrown; the southwest sides of the mapped northwestward-trending faults are downthrown.

On both sides of Independence Valley, gently sloping pediment surfaces lie between the steeper mountain fronts and the flat-lying alluvium of the present flood plains of the South Fork of the Owyhee River and its larger tributaries.

The sloping pediment surface on the northwest side of the valley is underlain by the Tertiary volcanic rocks that form the wallrocks of the mines of the Tuscarora district; it is overlain by a thin sheet of gravel that feathers out in the vicinity of Tuscarora, at about the 6,080-foot contour, and increases in thickness southeastward, as the bedrock surface has a slightly steeper slope than the upper surface of the gravel. Sediment and gravel covering are dissected by shallow streamways, some occupied by perennial streams, others by intermittent streams. Some of these streamways rise on the pediment, others in the higher hills to the northwest.

The area that was placer mined in the period subsequent to the discovery of placer gold in 1867 is indicated on figure 2. Part of the worked ground was alluvium in the valleys of the shallow streamways mentioned above, but much of the area worked was eluvial material or disintegrated bedrock below the outcrops of the lodes. As indicated on the map (fig. 2), the width of alluvium worked was at many places so small that it can be shown only as a line on the scale used here.

RECENT FAULTS

Examination of aerial photographs (taken for the U.S. Soil Conservation Service in 1949) disclosed swarms of linear features here interpreted as fault traces, mostly of northeasterly trend, on both sides of Independence Valley, between 41°14′ N. and 41°20′ N., and between 106°06′ W. and 106°16′ W. As shown in figure 3, there is a small difference between the mean trend of the faults on the northwest side of the valley, which has a pronounced frequency maximum at about N. 30° E., and the mean trend on the southeast side of the valley, where the maximum is at about N. 35° E.

The faults, without exception, cut the dissected gravel surface that rests on the pediment and borders the flat Recent alluvial floor of Independence Valley. Some of the faults are marked on the ground by low inconspicuous scarps that may face either northwest or southeast; there seems to be a slight predominance of scarps facing toward the valley.

The fault scarps range in height from 12 feet downward to imperceptible. The slopes of the scarps have been degraded by erosion; the steepest slope measured has a gradient of about 1 foot in 10. All the faults, including those that do not have perceptible scarps, are marked by lines of darker and more vigorous vegetation, mostly sagebrush (*Artemisia tridentata* Nuttall). These vegetational differences are conspicuous in aerial photographs, but very difficult to make out on the ground. The differences in plant growth are probably due to the effect of the faults on ground-water flow. The scarps are interrupted where they intersect the shallow gullies that furrow the pediment; the gully floors, which have widths measured in tens to hundreds of feet, pass smoothly across the fault traces without perceptible dislocation or change of grade. A few faults may be traced across the gullies by the vegetational contrast. In one place, drainage was evidently diverted from a shallow gully to an adjacent deeper one when a fault, with upthrow on the downstream side, cut both of them. The beheaded remnant of the shallower gully is a few feet shallower than gullies that extend with unchanged gradient across faults. I infer that in this place erosion has lowered the grade of the gullies several feet since the faulting.

AGE OF FAULTING

The intersection of the slightly elevated and eroded pediment gravels by the faults suggests that the age of the faults does not extend back into the Tertiary. Roads that cut the faults are completely undisturbed. No written record of local earthquake activity has been found, and inquiry made locally disclosed no oral tradition of local earthquakes. The preservation in Tuscarora of mud-mortared rock walls dating from the early years of the camp suggests that no major seismic activity has occurred within the past hundred years. I would suggest that the age of faulting falls between the limits of several hundred and several thousand years.

POSSIBLE ECONOMIC SIGNIFICANCE

Nolan (1936, p. 22) pointed out that the well defined faults seen in the few accessible mine workings trend north to north-northeast and dip steeply west. The little information available about the veins suggests similar attitudes. The ages of these faults are not precisely determinable. Emmons (1910, p. 58) regarded the volcanic rocks that are cut by the veins as Miocene. The earliest faulting and the mineralization would then be

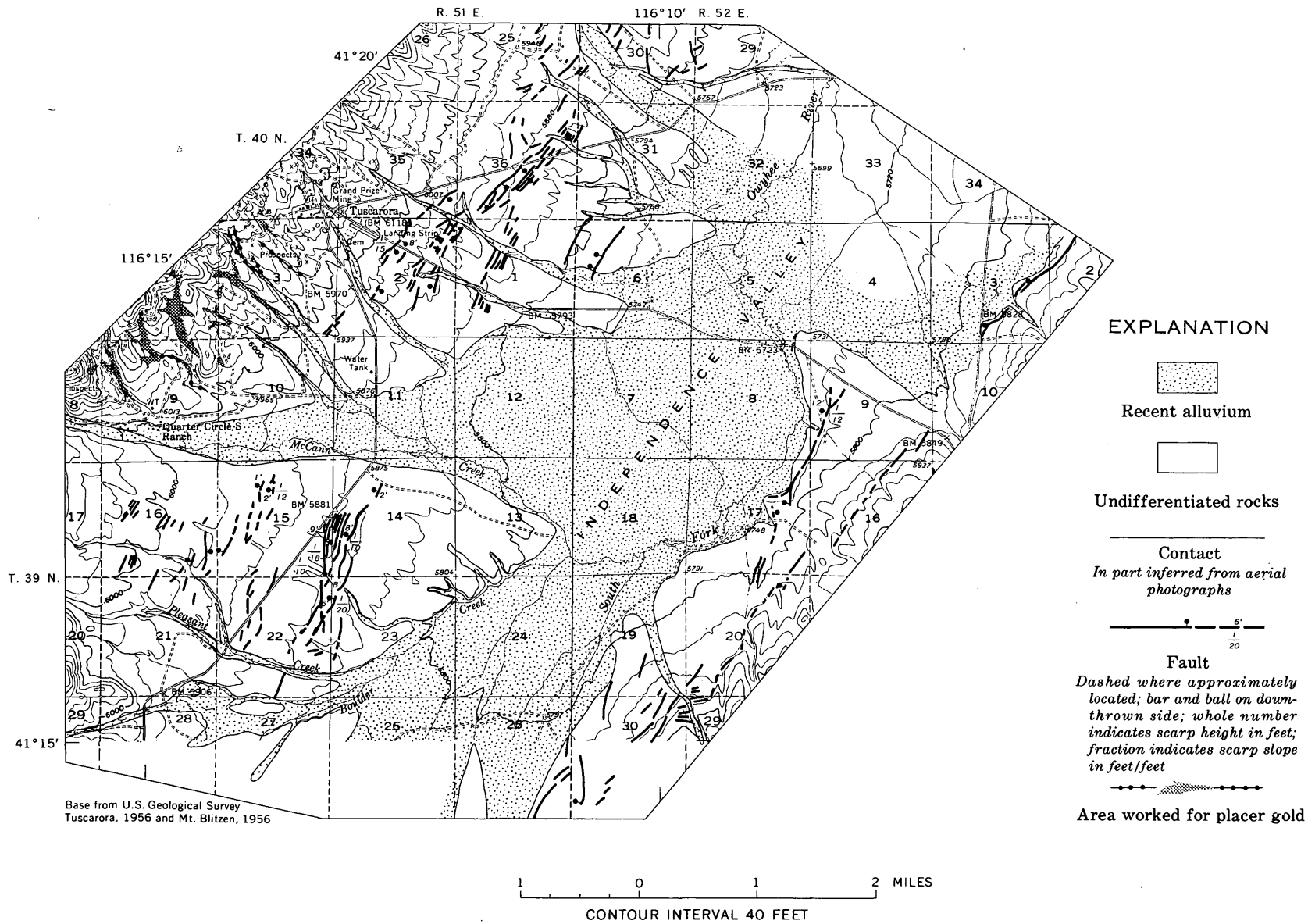

FIGURE 2.—Distribution of Recent faults near Tuscarora, Elko County, Nev., with respect to Recent alluvium and areas worked for placer gold.

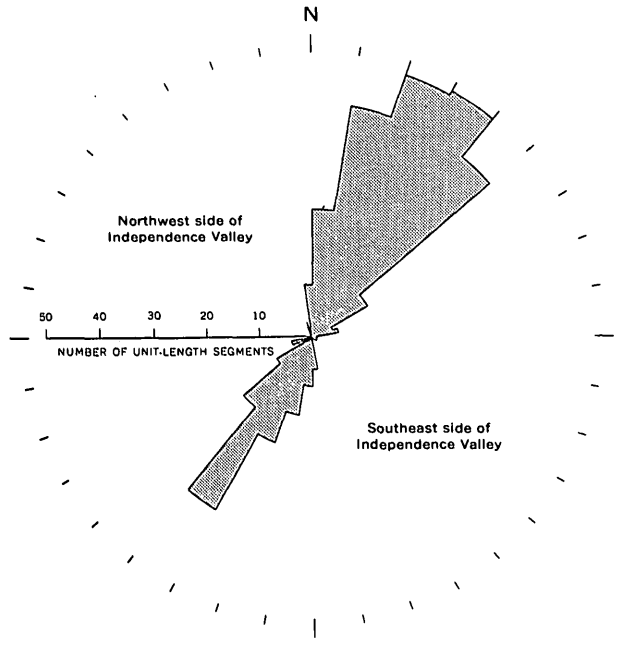

FIGURE 3.—Rose diagram showing distribution of orientations of Recent faults in the northwest (upper half of diagram) and southeast (lower half) sides of southern Independence Valley, Elko County, Nev. Measured in 400-foot segments; summed by 10° sectors.

post-Miocene and pre-Recent, probably pre-Quaternary. The area in which the Recent faults are traceable is southeast of the known mineralized area, but the correspondence in the trend of the earlier and Recent faults suggests that the strain field present in Recent time does not differ greatly from that present when the ore deposits were formed. The possible consequences of long-continued faulting on this pattern are numerous. They include shearing movements within the mineralized fissures and probable offset of ore shoots by gravity faults. Nolan (1936, p. 31) has indicated his reasons for believing that the bonanza silver ores of Tuscarora were the result of supergene enrichment. If faulting in the mineralized area has continued into the Recent, the relation of the enriched zone to the present ground-water table will have been affected by the faulting, and the zone of supergene enrichment will probably lie at deeper levels closer to Independence Valley.

Emmons (1910, p. 62) and Nolan (1936, p. 35) suggest that the lower portions of the stream courses that have furnished the placer-gold production might be economically workable by dredging. As this is the area in which the Recent faults have been active, it is probable that any placer paystreaks in this area would be affected by the normal faulting, which is predominantly southeast side down, on the northwest side of Independence Valley. It would be expected that the gold would be distributed through a greater thickness of gravel on the downthrown side of the fault, or that multiple paystreaks at different levels would be present. Increase of stream gradients over restricted reaches in the vicinity of faults with decrease farther downstream may result in the shortening and enriching of paystreaks. It is impossible to predict all the possible vagaries of distribution of placer gold that may be affected by the faulting, but it is evident that prospecting of this area should be conducted with these possibilities in mind.

REFERENCES

Emmons, W. H., 1910, A reconnaissance of some mining camps in Elko, Lander, and Eureka Counties, Nev.: U.S. Geol. Survey Bull. 408, 130 p.

Kerr, J. W., 1962, Paleozoic sequences and thrust slices of the Seetoya Mountains, Independence Range, Elko County, Nevada: Geol. Soc. America Bull., v. 73, no. 4, p. 430–460.

Nolan, T. B., 1936, The Tuscarora mining district, Elko County, Nev.: Nevada Univ. Bull., v. 30, no. 1, 38 p.

LATE TERTIARY SYNCLINE IN THE SOUTHERN ABSAROKA MOUNTAINS, WYOMING

By FREDERICK S. FISHER and KEITH B. KETNER, Denver, Colo.

Abstract.—A westward-trending syncline with at least 2,000 feet of structural relief occurs in Oligocene rocks of the southern Absaroka Mountains, Wyo. Alternate hypotheses of origin are: (1) the syncline was formerly a valley which was filled by sediments of the Oligocene Wiggins Formation; (2) the syncline is contemporaneous with the Wiggins Formation and is due to subsidence or collapse related to volcanism; or (3) the syncline was formed during regional deformation in late Tertiary time. Field relations, including the warping of a widespread erosion surface believed to have been cut prior to late Pliocene time, favor the third interpretation.

The Absaroka Mountains of northwestern Wyoming are composed largely of Tertiary volcanic sedimentary rocks, lava flows, and intrusives which have been uplifted and deeply dissected (Wilson, 1964; Parsons, 1958; Love, 1939; Rouse, 1935, 1937; Hague, 1899). Broad regional structural trends have not been described, although small- to medium-scale folds and faults in the southern Absarokas have been observed by Fisher (1967), Wilson (1964), Dunrud (1962), and Love (1939). Reconnaissance mapping in the Stratified Primitive Area (Ketner and others, 1966) revealed a regional northward dip of the base of the Wiggins Formation in the southern margin of the Absaroka Mountains. Subsequent comparison with data from other sources listed on figure 1 and table 1 indicated a large westward-trending syncline with at least 2,000 feet of structural relief (fig. 1).

The syncline was defined mainly by plotting elevations on the base of the early(?) Oligocene Wiggins Formation (Ketner and others, 1966; Wilson, 1963; Love, 1939) and equivalent rocks of the Late Basic Breccia of Hague (1899), although bedding attitudes are locally steep enough to be measured.

STRATIGRAPHIC AND STRUCTURAL RELATIONSHIPS

In the southern half of the map area (fig. 1) the Wiggins Formation lies on the middle and upper

TABLE 1.—*Source of data of control points shown on figure 1*

Map No.	*Source*	*Elevation (feet above sea level)*
Base of Wiggins Formation, top of Tepee Trail Formation		
1	Ketner and others (1966)	10, 000
2	----do----	9, 750
3	----do----	9, 950
4	----do----	9, 000
5	----do----	8, 550
6	----do----	8, 800
7	----do----	9, 150
8	----do----	9, 500
9	----do----	10, 200
10	----do----	10, 000
11	----do----	9, 400
12	----do----	8, 500
Base of Wiggins Formation, top of Pitchfork Formation		
13	W. H. Wilson (written commun., 1967); McGrew (1965).	8, 000
14	----do----	7, 300
15	----do----	8, 000
16	Ketner and others (1966)	8, 700
17	W. H. Wilson (written commun., 1967); McGrew (1965).	9, 000
Base of Wiggins Formation, top of Early Basalt flows		
18	Dunrud (1962)	10, 800
19	----do----	8, 825
20	----do----	8, 650
21	----do----	9, 000
22	----do----	9, 500
23	W. H. Wilson (written commun., 1967); McGrew (1965).	9, 440
24	----do----	9, 280
25	----do----	9, 760
26	----do----	9, 920
27	----do----	9, 760
28	----do----	10, 000
29	W. H. Wilson (written commun., 1967); McGrew (1965).	10, 000
30	Rouse (1935)	9, 300
31	----do----	9, 050
32	----do----	8, 700
33	Fisher (1967)	8, 200
34	----do----	7, 750
35	----do----	8, 100

U.S. GEOL. SURVEY PROF. PAPER 600-B, PAGES B144-B147

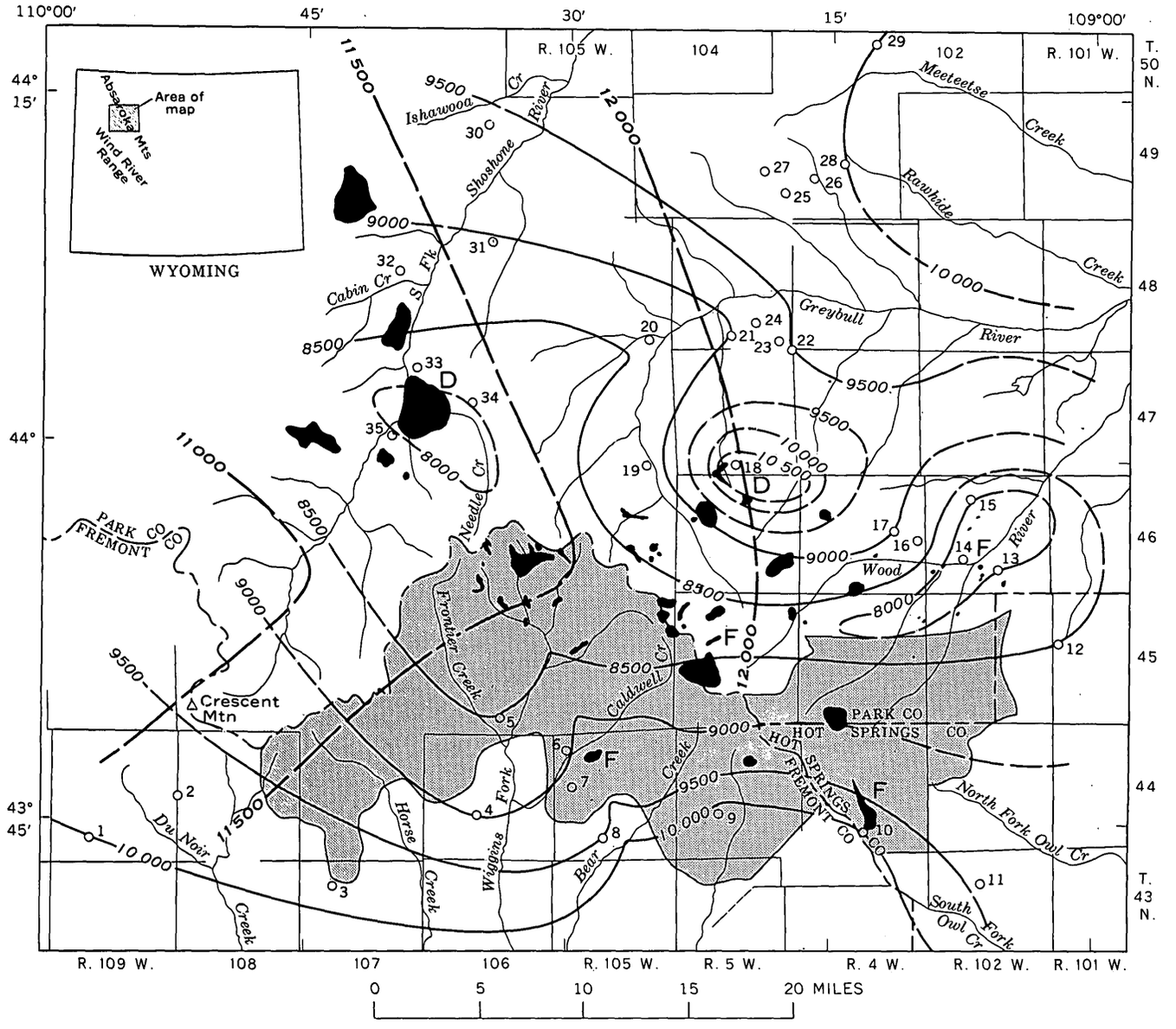

EXPLANATION

Intrusive body

Control point

Stratified Primitive Area

10 500 — Structure contour
Drawn on base of Wiggins Formation. Dashed where inferred. Interval 500 feet. Datum is mean sea level

12 000 — Structure contour
Drawn on old erosion surface. Interval 500 feet. Datum is mean sea level

D — Local doming and faulting

F — Local faulting

FIGURE 1.—Map showing structure contours on base of Wiggins Formation and on old erosion surface, southern Absaroka Mountains, Wyo. Map prepared from sources shown in table 1. Base from U.S. Geological Survey, 1:250,000-scale Thermopolis and Cody quadrangles.

Eocene Tepee Trail Formation and, in places, on Paleozoic rocks (Ketner and others, 1966). In the northwestern part of the area the Late Basic Breccia, which is stratigraphically equivalent to the Wiggins Formation in the southern Absaroka Mountains, lies on the Early Basalt flows (Wilson, 1963, 1964; Rouse, 1935; Hague, 1899). In the northeastern part of the area the Early Basalt flows are locally absent and the Wiggins Formation lies directly on the Pitchfork Formation (Wilson, 1963, 1964). For the purpose of this study we accept Wilson's assignment of the Blue Point Conglomerate Member as the basal unit of the Wiggins Formation.

ORIGIN OF THE SYNCLINE

To explain the origin of the synclinal structure three hypotheses are considered: (1) the syncline was formerly a structural or topographic sag in which the Wiggins Formation was deposited and the observed dips in the Wiggins represent initial bedding-plane attitudes; (2) the formation of the syncline was contemperaneous with the deposition of the Wiggins Formation, and was caused by subsidence or collapse into an underlying magma chamber as material was transferred to the surface during deposition of the Wiggins; (3) the syncline is of post-Wiggins age, and was formed by differential regional uplift or warping during late Tertiary deformation of the area.

Hypothesis 1 seems unlikely because several hundred to a few thousand feet of sedimentary and volcanic rocks, apparently centered around the belt of intrusives, accumulated in the area of the syncline prior to deposition of the Wiggins Formation. There appears to be no evidence that these rocks were subsequently folded or eroded to form a valley which was the size of the synclinal structure, and which could have been the site of Wiggins deposition. Hypothesis 2 may be partly supported by the distribution of intrusive bodies which locally coincide with the axis of the syncline. However, large intrusive bodies as a group are alined in a belt which trends northwest (Rouse, 1940, p. 1426, and fig. 1), whereas the synclinal structure has a more westerly trend. Some of the intrusions may represent plugs or vent fillings in volcanic conduits through which the material composing the rocks of the Wiggins Formation reached the surface (Fisher, 1967; Wilson, 1964). Hypothesis 3 appears to offer the best interpretation of the data now available. An erosion surface of relatively low relief was developed on the Wiggins Formation following its deposition (Ketner and others, 1966, p. E12; Wilson, 1964, p. 60; Love, 1939, p. 111–116). In the southwestern part of the map area (fig. 1) lava flows were deposited on the erosion surface, and in places partly filled some of the old valleys (Ketner and others, 1966, p. E12). Blackstone (1966) described an area of late Pliocene volcanism on Crescent Mountain (fig. 1), and stated (1966, p. 25) that pyroclastic material and basaltic lava flows from this vent area were deposited disconformably on the Wiggins Formation. Judged from the above evidence, the erosion surface cut on the Wiggins Formation must have been formed between early(?) Oligocene and late Pliocene time.

Uplifted remnants of the erosion surface are scattered throughout the southern Absarokas. The present configuration of the erosion surface is obtained by contouring plotted elevations (fig. 1). If the syncline is older than the erosion surface, rocks within the syncline would have been beveled when the surface was cut, and contours of equal elevation on the erosion surface should cross the syncline with relatively little or no change in trend. However, as seen in figure 1, the 11,000- and 11,500-foot contours show a distinct flexure and change in trend as they cross the syncline. This shift indicates that the synclinal warping took place after the old erosion surface was cut, between early Oligocene and late Pliocene times. If the old erosion surface in the Absaroka Mountains corresponds to Blackwelder's (1915, p. 198) middle(?) Pliocene summit peneplain in the Wind River Range, then the synclinal warping would be post-middle Pliocene in age. Regional deformation in the form of broad warping or differential uplift or a combination of both may have formed the syncline.

CONCLUSIONS

A broad, shallow, westward-trending syncline in the southern Absaroka Mountains may have been formed by post-middle Pliocene regional deformation. Both the proposed dating and mechanism of deformation, but not the existence of the syncline, depend on correct identification of remnants of the erosion surface as shown on old topographic maps of uncertain accuracy. As research continues in the area other hypotheses suggested above may gain favor. Previous workers in the Absaroka Mountains have experienced difficulty in correlating rock units throughout the range. Regardless of the origin of the syncline, knowledge of its existence should aid in interpreting the stratigraphic relationships and volcanic history in the region.

REFERENCES

Blackstone, D. L., Jr., 1966, Pliocene volcanism, southern Absaroka Mountains, Wyoming: Wyoming Univ. Contr. Geology, v. 5, no. 1, p. 21–30.

Blackwelder, Elliot, 1915, Post-Cretaceous history of the mountains of central western Wyoming: Jour. Geology, v. 23, p. 193–217.

Dunrud, C. R., 1962, Volcanic rocks of the Jack Creek area, southeastern Absaroka Range, Park County, Wyoming: Wyoming Univ. unpub. Master's thesis, 92 p.

Fisher, F. S., 1967, General geology and petrology of Tertiary intrusive rocks, pt. 1 *of* Geology of the Stinkingwater mining region, Park County, Wyoming: Wyoming Univ. Contr. Geology, v. 6, no. 1, p. 71–86.

Hague, Arnold, 1899, Description of Absaroka folio, Wyoming: U.S. Geol. Survey Geol. Atlas, Folio 52, 7 p.

Ketner, K. B., Keefer, W. R., Fisher, F. S., Smith, D. L., and Raabe, R. G., 1966, Mineral resources of the Stratified Primitive Area, Wyoming: U.S. Geol. Survey Bull. 1230–E, p. E1–E56.

Love, J. D., 1939, Geology along the southern margin of the Absaroka Range, Wyoming: Geol. Soc. America Spec. Paper 20, 134 p.

McGrew, A. R., 1965, Stratigraphy and mineralogy of the Blue Point Member of the Wiggins Formation, southeast Absaroka Range, Park County, Wyoming: Wyoming Univ. unpub. Master's thesis, 74 p.

Parsons, W. H., 1958, Origin, age, and tectonic relationships of the volcanic rocks in the Absaroka-Yellowstone-Beartooth region, Wyoming-Montana, *in* Billings Geol. Soc. Guidebook 9th Ann. Field Conf.: p. 36–43.

Rouse, J. T., 1935, The volcanic rocks of the Valley area, Park County, Wyoming: Am. Geophys. Union Trans., 16th Ann. Mtg., p. 272–284.

———1937, Genesis and structural relationships of the volcanic rocks, Wyoming: Geol. Soc. America Bull., v. 48, p. 1257–1296.

———1940, Structural and volcanic problems in the southern Absaroka Mountains, Wyoming: Geol. Soc. America Bull., v. 51, no. 9, p. 1413–1428.

Wilson, W. H., 1963, Correlation of volcanic rock units in the southern Absaroka Mountains, northwest Wyoming: Wyoming Univ. Contr. Geology, v. 2, p. 13–20.

———1964, The Wood-Greybull River area, pt. 1 *of* Geologic reconnaissance of the southern Absaroka Mountains, northwest Wyoming: Wyoming Univ. Contr. Geology, v. 3, no. 2, p. 60–77.

CYPRESS BAYOU, GRAND PRAIRIE REGION, ARKANSAS—AN EXAMPLE OF STREAM ALIENATION

By M. S. BEDINGER, Little Rock, Ark.

Abstract.—Stream drainage in the Grand Prairie region of Arkansas is predominantly toward the southeast, following the regional topographic slope. However, Cypress Bayou flows northward in the White River basin from a point near the Arkansas River, even though the valley of the bayou is open at its south end. The drainage divide between the Cypress Bayou basin and the Arkansas River basin is the summit of the natural levee of the Arkansas River. It is reasoned that the ancestral Cypress Bayou flowed southward into the Arkansas River, but that alluviation by the river blocked the mouth of the bayou, reversed the slope of the valley of the bayou, and forced the bayou to seek an outlet to the north over a low divide and into the White River basin. Thus, the mode of drainage-pattern change was the antithesis of stream piracy or capture and is herein referred to as "stream alienation."

The example of stream alienation cited here is found in the southern part of Arkansas County in the Grand Prairie region of Arkansas. The topography of the area is shown in the Gillett, Henrico, Red Fork, and Big Island quadrangles mapped by the U.S. Army Corps of Engineers. The Grand Prairie is an alluvial terrace extending northward from near a natural cutoff between the Arkansas and White Rivers to the vicinity of Lonoke, Ark., an airline distance of 65 miles. The flood plains of the Arkansas and White Rivers form the southern and eastern margins, respectively, of the Grand Prairie terrace. The regional topographic slope of the Grand Prairie is about 0.9 foot per mile to the southeast. With one notable exception, the streams that drain the Grand Prairie flow south or southeast, following the general topographic slope. The exception is Cypress Bayou (fig. 1), which flows northward from a point near the Arkansas River for a distance of 9 miles, thence northeastward for about 5 miles to its confluence with La Grue Bayou, a tributary of the White River. Although Cypress Bayou flows northward, its valley is open at the south end. The drainage divide between the bayou and the Arkansas River is the summit of the natural levee of the Arkansas River. It is assumed that the ancestral Cypress Bayou was a tributary of the Arkansas River and flowed southward, parallel to the trend of other streams and the slope of the Grand Prairie.

In its present north-trending segment, Cypress Bayou flows through Dismal Swamp, which occupies

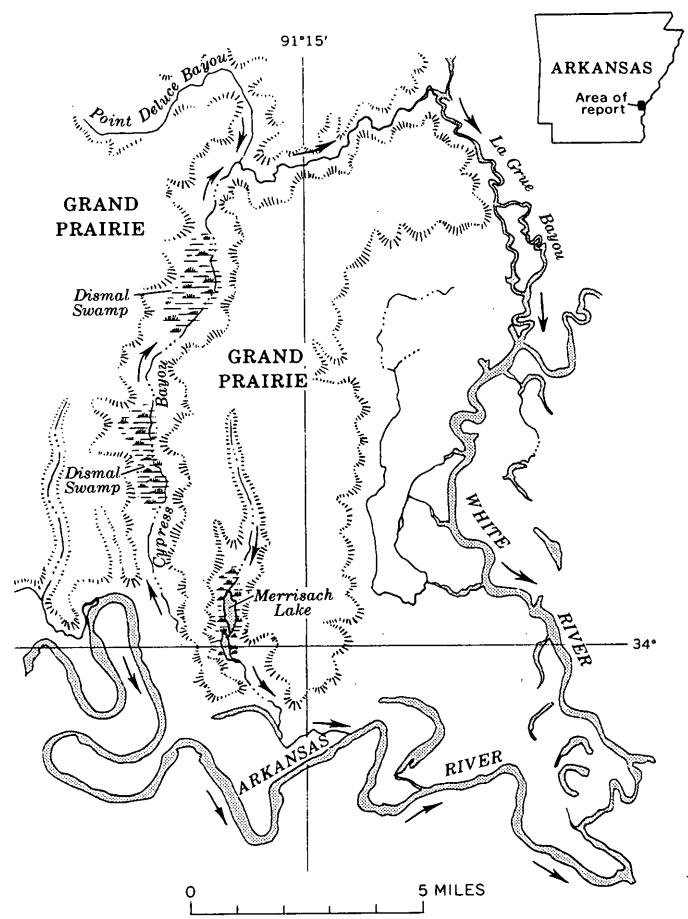

FIGURE 1.—Map of the southeastern Grand Prairie region, Arkansas County, Ark., showing present drainage pattern. Arrows indicate direction of flow.

U.S. GEOL. SURVEY PROF. PAPER 600-B, PAGES B148-B150

a broad, flat-bottomed valley. Except for its direction of slope, Cypress Bayou is similar to the stream which drains Merrisach Lake and to several other streams which drain from the Grand Prairie into the Arkansas River. Valleys of streams such as the one that drains Merrisach Lake have been termed marginal backswamps by Murray (1948, p. 11). The mouths of these valleys have been elevated by alluviation by the trunk stream, which in this case is the Arkansas River, during periods of overbank flow. The thickest overbank deposits are laid down at the mouth of the tributary valley and thus tend to dam the tributary.

Generally, the dam of overbank deposits is breached because there is no other outlet for the tributary stream, and a lake or swamp forms behind the alluvial dam because the drainage is poor, as demonstrated by the valley of Merrisach Lake. However, the valley of the ancestral Cypress Bayou was separated by only a low divide to the north from a tributary of La Grue Bayou in the White River basin. Thus, as alluviation of overbank deposits by the Arkansas River filled the lower part of the ancestral Cypress Bayou, the slope of the valley floor was reversed and the bayou was able to drain northward into the White River basin—the Arkansas River "alienated" Cypress Bayou.

Alienation of Cypress Bayou was dependent upon an outlet for drainage of lower elevation than the alluvial dam. An hypothesis of the sequence of events leading to alienation of Cypress Bayou by the Arkansas River is as follows:

1. At one time, the ancestral Cypress Bayou flowed southward and was a tributary of the Arkansas River. The drainage area of the ancestral Cypress Bayou most likely included that of Point Deluce Bayou, which is assumed primarily because a valley the size of the southern part of Cypress Bayou must have developed in response to a relatively large drainage area. A drainage divide, probably near point *X* (fig. 2*A*), separated the drainage basin of Cypress Bayou from that of La Grue Bayou.

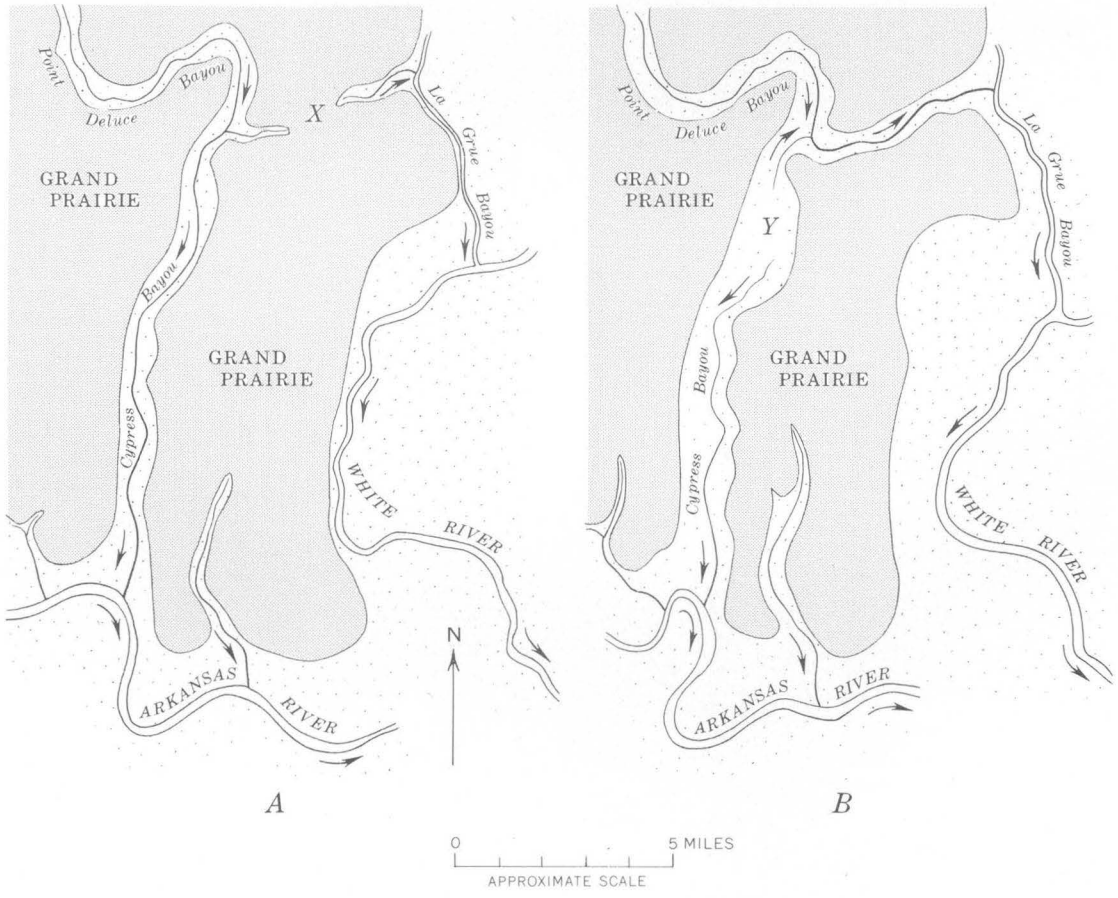

FIGURE 2.—Map showing stages in development of drainage pattern in the southeastern Grand Prairie region. Arrows indicate direction of flow. *A*, drainage pattern before capture of headwaters of Cypress Bayou. *B*, drainage pattern before alluviation of the Arkansas River natural levee alienated Cypress Bayou.

2. Headward erosion by the tributary of La Grue Bayou breached the divide at point *X* and captured the headwaters of the ancestral Cypress Bayou (now called Point Deluce Bayou). After the piracy, a very low divide near point *Y* (fig. 2*B*) separated Cypress Bayou, which flowed southward, from Point Deluce Bayou.

3. Alluviation by the Arkansas River tended to block the drainage of Cypress Bayou and the stream which now drains Merrisach Lake. Merrisach Lake and a lake in the valley of Cypress Bayou were thus formed by an alluvial dam at the mouth of their valleys.

4. Continued overbank deposition by the Arkansas River alluviated the valley of Cypress Bayou higher than the low divide at *Y* (fig. 2*B*). Cypress Bayou was thus "alienated" by the Arkansas River and forced to drain northward to La Grue Bayou (fig. 1).

REFERENCE

Murray, Grover E., 1948, Geology of DeSoto and Red River Parishes: Louisiana Dept. Conserv., Geol. Bull. 25, 312 p.

GEOLOGY AND RADIOCARBON AGES OF LATE PLEISTOCENE LACUSTRINE CLAY DEPOSITS, SOUTHERN PART OF SAN JOAQUIN VALLEY, CALIFORNIA

By M. G. CROFT, Sacramento, Calif.

Prepared in cooperation with the California Department of Water Resources

Abstract.—Five radiocarbon dates from the southern San Joaquin Valley, Calif., indicate that large lakes, which existed in the valley during late Pleistocene time, may be synchronous with similar lake deposits in the Great Basin physiographic province. Radiocarbon ages were determined from wood fragments obtained from test holes drilled during hydrologic investigations. A radiocarbon date of 26,780 ± 600 years B.P. (before present, 1950) was obtained from wood collected about 3 feet beneath a lacustrine clay deposit that underlies the dry bed of Tulare Lake. Wood obtained from sand overlying the lacustrine clay was determined to have a radiocarbon age of 13,350 ± 500 years and that obtained from sand beds that interfinger with a lacustrine clay deposit beneath the dry bed of Buena Vista and Kern Lakes an age of 9,040 ± 300 years.

During hydrologic investigations in the southern part of the San Joaquin Valley (fig. 1) by the California Department of Water Resources, the Buena Vista Water Storage District, and the U.S. Geological Survey, several hundred test holes were drilled to study water-bearing deposits. Wood fragments obtained from cores of several test holes drilled during the program were dated by radiocarbon methods by Meyer Rubin, of the U.S. Geological Survey. The areal geology, location of five wood samples from which significant radiocarbon dates were obtained, and selected well logs are shown in figures 1, 2, and 3. The well-numbering system used to identify test holes is described by Davis and others (1959, p. 12).

GEOMORPHOLOGY

The southern part of the San Joaquin Valley is a basin of interior drainage. The valley is bordered on the east by igneous and metamorphic rocks of the Sierra Nevada and on the west by deformed sedimentary and volcanic rocks of the Coast Ranges. The largest part of the valley floor consists of gently sloping alluvial plains and fans (fig. 1). Dissected uplands, which consist of eroded moderately tilted alluvial fans, flank the mountain areas. Overflow lands and lake bottoms form the central part of the valley trough. Davis and others (1959, p. 27) defined overflow land as "that land area in which the rivers splay out into numerous sloughs and which at times of highest flood under natural conditions has either been partly or wholly inundated."

The Kern, Kaweah, Kings, and Tule Rivers are major perennial streams that flow westward from the high Sierra Nevada to natural sumps on the valley floor. The Kings, Kaweah, and Tule Rivers discharge onto the north end of Tulare lakebed north of the area shown on figure 1. Kern River discharges into Buena Vista lakebed, but in the past it may have discharged through sloughs and distributaries onto Kern and Goose lakebeds or into Buena Vista Slough. Streams that flow eastward from the Coast Ranges are intermittent.

Davis and Green (1962, p. D89–D90) show that Tulare lakebed is the site of a structural downwarp where a lacustrine environment has long been maintained, and that active tectonic subsidence is the cause of the topographic depression. Buena Vista and Kern lakebeds also are sites of structural downwarp. Goose lakebed is a topographic low formed by structural downfolding of the area between two anticlinal ridges.

U.S. GEOL. SURVEY PROF. PAPER 600-B, PAGES B151-B156

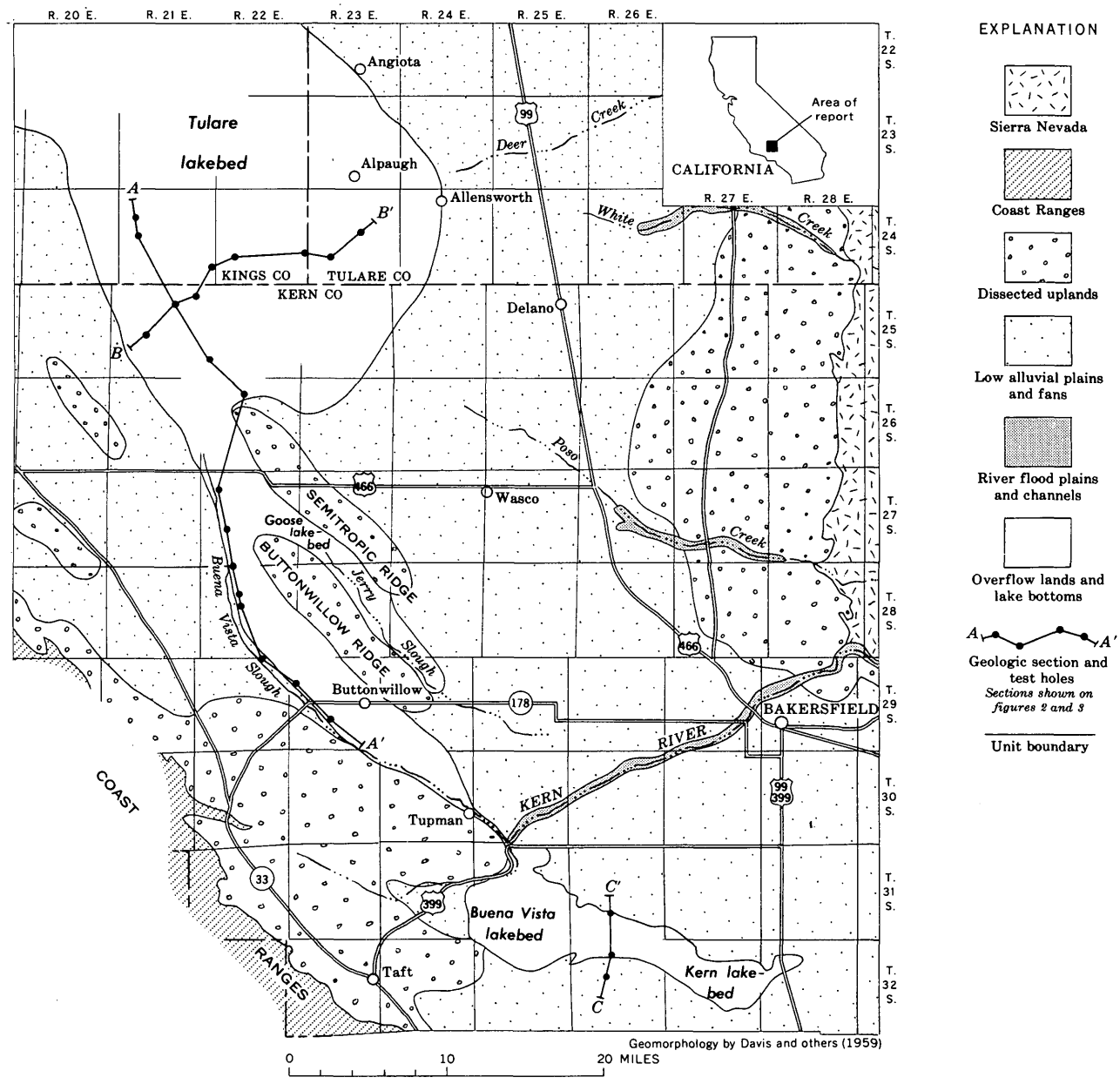

FIGURE 1.—Map of the geomorphic units in the southern part of the San Joaquin Valley, Calif.

Within historic times, Tulare, Buena Vista, Goose, and Kern lakebeds were sites for shallow lakes whose areal extent fluctuated widely with slight changes in water depth. The lakes occurred within the area shown as overflow lands and lake bottoms on figure 1. The lakes were connected by sloughs and surrounded by marshes. When Buena Vista Lake exceeded about 13 feet in depth, it overflowed into Tulare Lake by way of Buena Vista Slough. Tulare Lake overflowed to the north when the lake level reached a depth of about 30 feet, but overflow has not occurred since 1878 (Harding, 1949, p. 29–30). Presently, the lakes are dry owing to the diversion of water from tributary streams for irrigation.

GEOLOGY

The surficial deposits in the valley trough within the area of this investigation have been partially mapped by Hilton and others (1963), Wood and Dale (1964), and Wood and Davis (1959). They mapped the alluvial deposits of Quaternary age as younger alluvium, older alluvium, and as flood-basin deposits. The younger alluvium and older alluvium are undifferentiated in this report (figs. 2 and 3). They consist

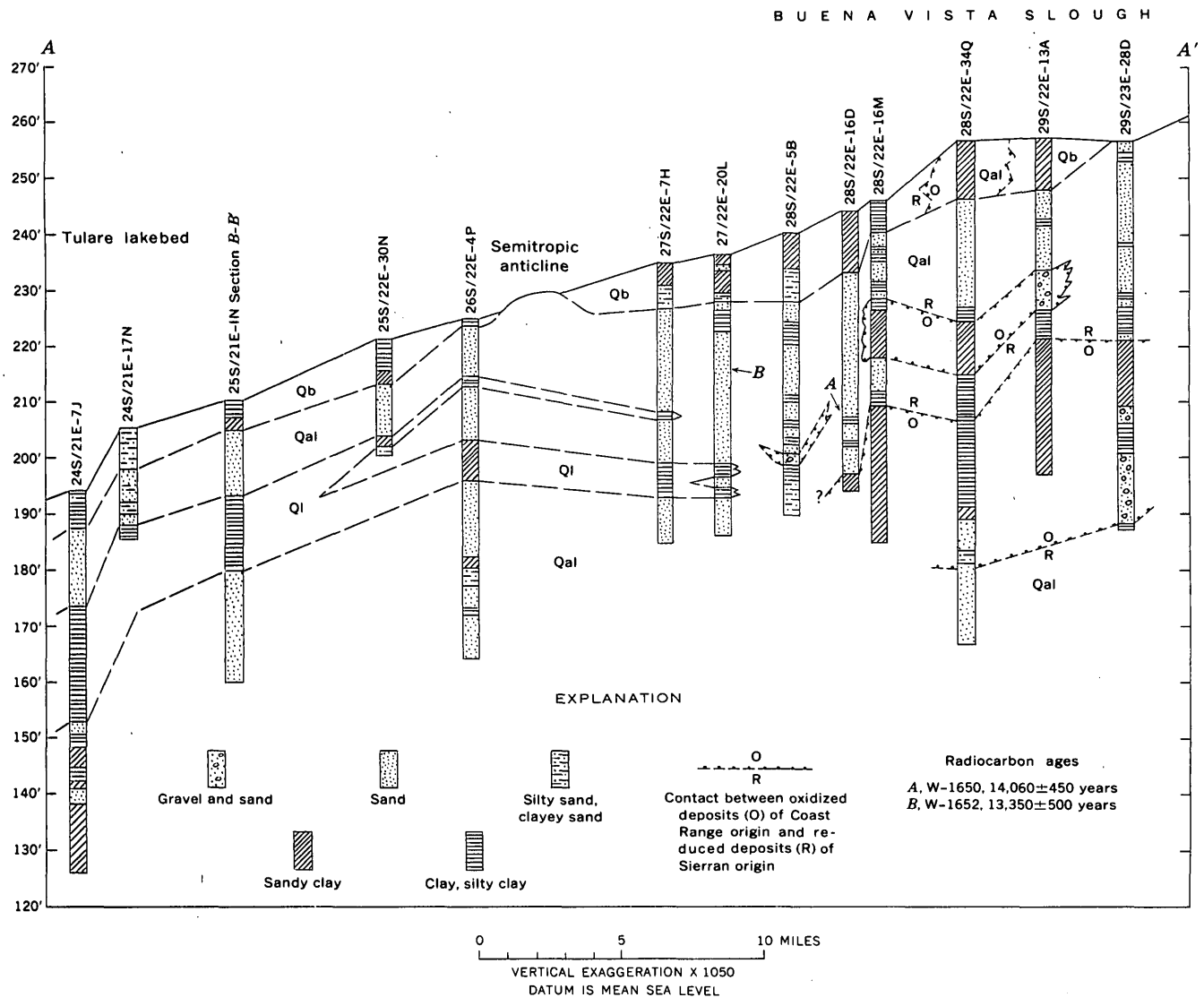

FIGURE 2.—Geologic section *A–A'*, southern part of the San Joaquin Valley, Calif. Qb, flood-basin deposits of Recent age; Qal, younger and older alluvium, undifferentiated, of Quaternary age; Ql, lacustrine clay deposits of Quaternary age. Location of section shown on figure 1.

of unconsolidated silt, clay, sand, and gravel derived from the Coast Ranges and from the Sierra Nevada. The alluvium interfingers with lacustrine clay deposits.

According to Davis and others (1959, p. 58), environment controls the degree of oxidation or reduction of the sediments and hence the color of the material in the San Joaquin Valley. Clastic material subjected to extensive weathering or oxidation on the surface of alluvial fans is red, yellow, or brown. Oxidized or reddish-brown beds in sections *A–A'* and *C–C'* (figs. 2 and 3), are subaerial alluvial deposits. They consist of gravel, sand, and clay derived mainly from sedimentary and volcanic rocks forming the Coast Ranges. The alluvium was deposited in Buena Vista Slough and in Buena Vista lakebed when the water level was low. Sediment deposited in lakes and marshes is reduced by chemical reactions that commonly produce black, gray, green, or blue colors. The chemically reduced deposits indicated in the three sections consist mainly of sand, silt, and clay derived from crystalline rocks of the Sierra Nevada. These beds contain fossils of fresh-water mollusks indicating they were deposited mainly in lakes or marshes.

Two lacustrine deposits, composed mainly of dark-greenish-gray silty clay, underlie much of Tulare lakebed and the northern part of Buena Vista Slough (figs. 2 and 3). They are shown as an upper lacustrine clay and as a lower lacustrine clay in the geologic sections. Data are insufficient to determine if the two lacustrine clays beneath Tulare lakebed are correlative

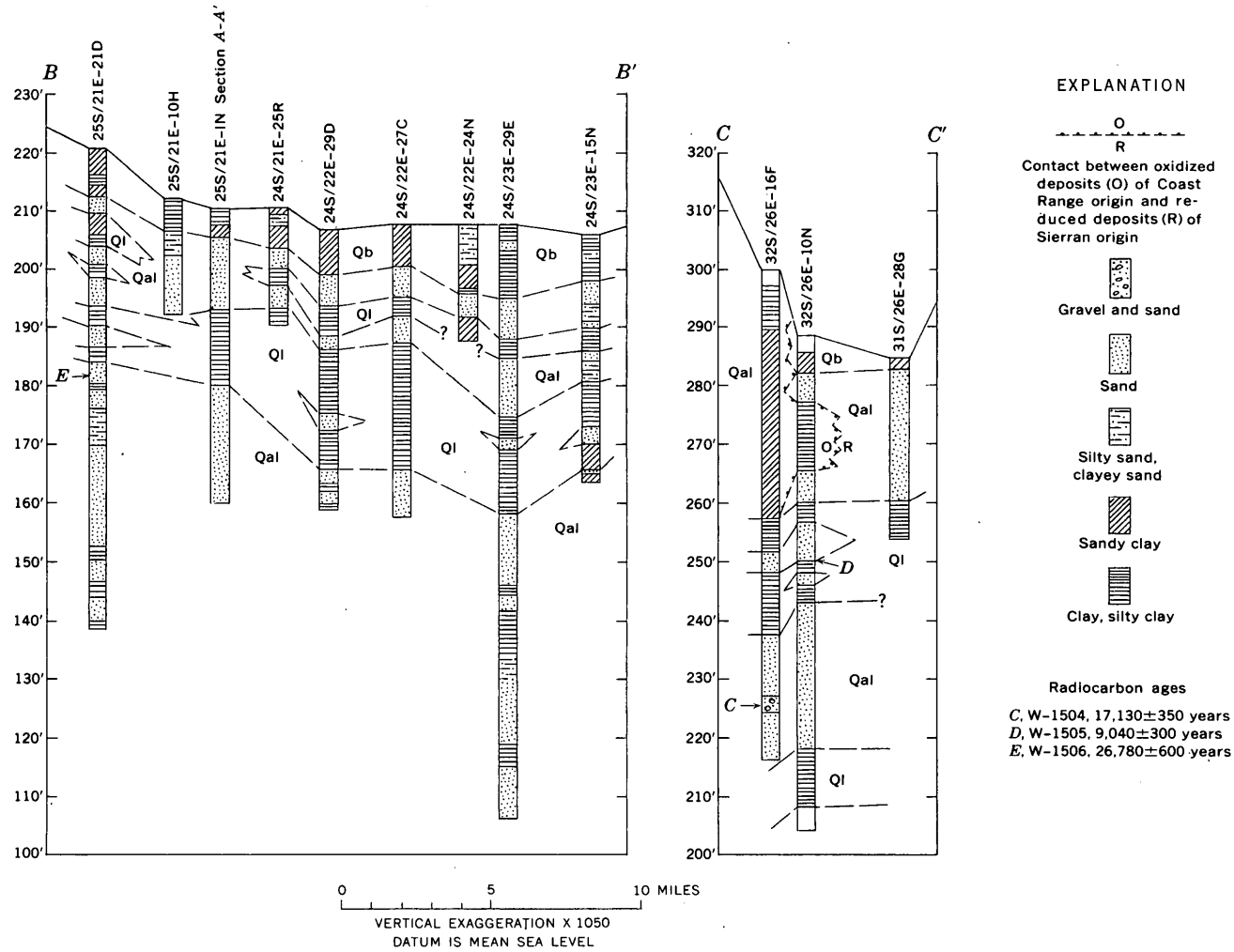

FIGURE 3.—Geologic sections *B–B′* and *C–C′*, southern part of the San Joaquin Valley, Calif. Qb, flood-basin deposits of Recent age; Qal, younger and older alluvium, undifferentiated, of Quaternary age; Ql, lucustrine clay deposits of Quaternary age. Location of sections shown on figure 1.

with those beneath Buena Vista lakebed. The lower lacustrine clay is widespread beneath Tulare lakebed, but its extent in the Buena Vista–Kern Lake area is unknown as it was penetrated by only a few test holes. The upper lacustrine clay was not found at the north end of Buena Vista Slough, adjacent to section *A–A′* (fig. 2), although it underlies most of Tulare lakebed. In addition, it underlies Buena Vista and Kern lakebeds where it interfingers with numerous beds of fine sand.

RADIOCARBON DATES

Pleistocene Lake Lahontan (Morrison, 1964) and Pleistocene Searles Lake (Flint and Gale, 1958) occurred in closed basins in the western part of the Great Basin physiographic province east of the Sierra Nevada. Deposits associated with these lakes indicate that the lake levels probably fluctuated widely with changes in precipitation and climate.

Five radiocarbon dates indicate that lacustrine clay deposits in the southern part of the San Joaquin Valley might be synchronous with similar lacustrine deposits in the Great Basin (fig. 4). This is logical since glaciers and storms over the high Sierra Nevada discharged both east and west simultaneously into lakes in the San Joaquin Valley and into the eastern part of the Great Basin. However, the similarity in age indicated by radiocarbon evidence could be fortuitous because of the limited data.

A radiocarbon date (W–1506) of 26,780 ± 600 years B.P. (before present, A.D. 1950) (*E*, table 1 and fig. 3), was obtained from wood found about 3 feet beneath the lower lacustrine clay deposit that underlies the southern part of Tulare lakebed. This date is in close agreement with the findings of several authors who believe that a pluvial period began in other basins about 24,000 years ago (fig. 4). Broecker and Kauf-

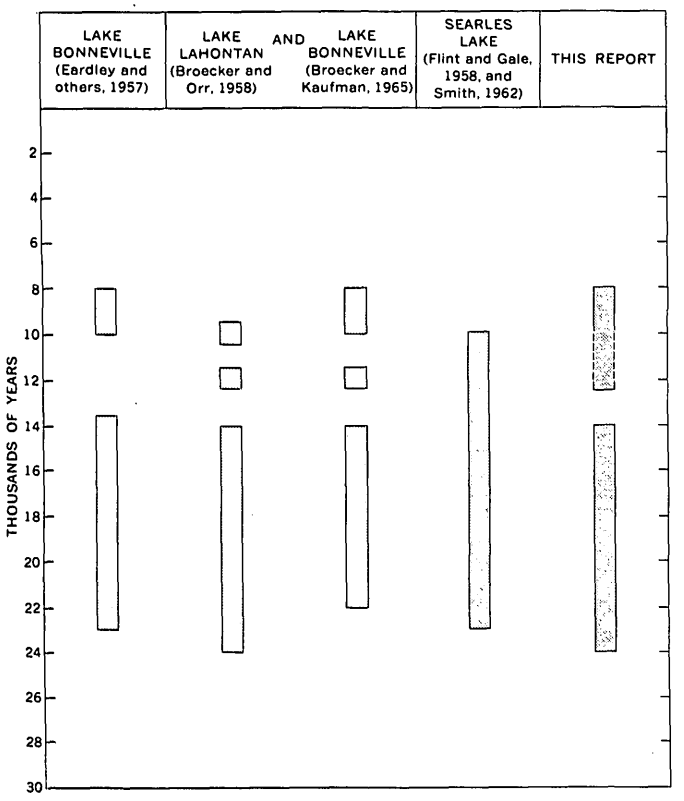

FIGURE 4.—Relative dates, in thousands of years before present (1950), of pluvial periods in the Western United States, based on radiocarbon data.

man (1965, p. 554), who use different values for the oxalic acid standard in their computations, believe that the pluvial period began about 22,000 years B.P. rather than 24,000 years B.P.

The pluvial period represented by the lower lacustrine clay beneath Tulare lakebed may have ended prior to 14,000 years ago (fig. 4). This is suggested by two radiocarbon ages that were obtained from samples of wood (*A* and *B*, table 1 and fig. 2) obtained from cores stratigraphically above the lower lacustrine clay.

TABLE 1.—*Radiocarbon data for samples of wood from test holes in lake deposits, southern San Joaquin Valley, Calif.*

[Radiocarbon determinations by Meyer Rubin, Radiocarbon Laboratory, U.S. Geological Survey]

Sample	Radiocarbon determination No.	Age (years)	Depth below land surface (feet)	Stratigraphic relation
A	(W-1650)	14,060±450	36	Above lower lacustrine clay, Buena Vista Slough; fig. 2, section *A-A'*.
B	(W-1652)	13,350±500	20	Above lower lacustrine clay, Buena Vista Slough; fig. 2, section *A-A'*.
C	(W-1504)	17,130±350	74	10 feet above lower lacustrine clay, Buena Vista lakebed; fig. 3, section *C-C'*.
D	(W-1505)	9,040±300	38	Middle of upper lacustrine clay, Buena Vista lakebed; fig. 3, section *C-C'*.
E	(W-1506)	26,780±600	39	3 feet beneath tongue of lower lacustrine clay, Tulare lakebed; fig. 3, section *B-B'*.

285-544 O—68——11

These radiocarbon dates provide an approximate time when oxidized alluvial deposits encroached into Buena Vista Slough. The alluvial beds in Buena Vista Slough could have been deposited during a period when the climate was arid or they could have been deposited when the Kern River bypassed Buena Vista Lake and Slough by discharging into Jerry Slough (fig. 1). The possibility of an arid climate beginning about 14,000 years ago in the San Joaquin Valley, agrees with concepts of Eardley and others (1957), Broecker and Orr (1958), and Broecker and Kaufman (1965).

A radiocarbon date of 17,130 ± 350 years B.P. (W-1504) was obtained from wood found in sand beds that occur stratigraphically between the upper and lower lacustrine clays that underlie Buena Vista and Kern lakebeds (*C*, fig. 3). If desiccation of the lower lacustrine clay was caused by an arid climate, the date, if accurate, indicates that desiccation began prior to 17,000 years ago rather than about 14,000 years ago. Also, desiccation could have been caused by the Kern River bypassing Buena Vista and Kern lakebeds by discharging its flow into lakes and sloughs to the north, or by an outlet draining the lake into Buena Vista Slough.

Broecker and Orr (1958), and Broecker and Kaufman (1965, p. 537), postulate that Lakes Lahontan and Bonneville were relatively high about 12,000 years ago and about 9,500 years ago (fig. 4). The radiocarbon date of 9,040 ± 300 years B.P. (*D*, table 1 and fig. 3), was obtained from wood found in sand beds that interfinger with the upper lacustrine clay that underlies Buena Vista and Kern lakebeds. Although the upper lacustrine clay beneath Buena Vista lakebed could possibly have formed during a period when the Kern River discharged most of its flow into Buena Vista or Kern Lakes, the age generally agrees with the concept of a pluvial period about 8,000 to 10,000 years ago (fig. 4).

REFERENCES

Broecker, W. S., and Kaufman, Aaron, 1965, Radiocarbon chronology of Lake Lahontan and Lake Bonneville II, Great Basin: Geol. Soc. America Bull., v. 76, no. 5, p. 537–566.

Broecker, W. S., and Orr, P. C., 1958, Radiocarbon chronology of Lake Lahontan and Lake Bonneville: Geol. Soc. America Bull., v. 69, p. 1009–1032.

Davis, G. H., Green, J. H., Olmsted, F. H., and Brown, D. W., 1959, Ground-water conditions and storage capacity in the San Joaquin Valley, California: U.S. Geol. Survey Water-Supply Paper 1469, 287 p., pls. 1–29.

Davis, G. H., and Green, J. H., 1962, Structural control of interior drainage, southern San Joaquin Valley, California: Art. 146 *in* U.S. Geol. Survey Prof. Paper 450–D, p. D89–D91.

Eardley, A. J., Gvosdetsky, Vasyl, and Marsel, R. E., 1957, Hydrology of Lake Bonneville and sediments and soils of its basin: Geol. Soc. America Bull., v. 68, no. 9, p. 1141–1202.

Flint, R. F., and Gale, W. A., 1958, Stratigraphy and radiocarbon dates at Searles Lake, California: Am. Jour. Sci., v. 256, p. 689–714.

Harding, S. T., 1949, Inflow to Tulare Lake from its tributary streams: Tulare Lake Basin Water Storage District open-file rept., 129 p.

Hilton, G. S., McClelland, E. J., Klausing, R. L., and Kunkel, Fred, 1963, Geology, hydrology, and quality of water in the Terra Bella–Lost Hills area, San Joaquin Valley, California: U.S. Geol. Survey open-file rept., 158 p.

Morrison, R. B., 1964, Lake Lahontan: Geology of southern Carson Desert, Nevada: U.S. Geol. Survey Prof. Paper 401, 156 p., 39 figs.

Smith, G. I., 1962, Subsurface stratigraphy of late Quaternary deposits, Searles Lake, California: Art. 82 *in* U.S. Geol. Survey Prof. Paper 450–C, p. C65–C69.

Wood, P. R., and Dale, R. H., 1964, Geology and ground-water features of the Edison-Maricopa area, Kern County, California: U.S. Geol. Survey Water-Supply Paper 1656, 108 p.

Wood, P. R., and Davis, G .H., 1959, Ground-water conditions in the Avenal-McKittrick area, Kings and Kern Counties, California: U.S. Geol. Survey Water-Supply Paper 1457, 141 p.

TREE-THROW ORIGIN OF PATTERNED GROUND ON BEACHES OF THE ANCIENT CHAMPLAIN SEA NEAR PLATTSBURGH, NEW YORK

By CHARLES S. DENNY and JOHN C. GOODLETT,[1] Beltsville, Md.

Abstract.—Patterns of stones and finer materials on beaches of the ancient Champlain Sea near the northeast end of the Adirondack Mountains, N.Y., look like sorted circles produced by repeated freeze and thaw and suggest that frost action was vigorous on the shores of the Champlain Sea about 11,000 years ago. These patterns, however, are only a few hundred years old. They are due to the formation and erosion of mounds and pits produced by the toppling of trees during the last few centuries. Whatever patterns may have been on the surface of these beaches during Champlain Sea time have been completely destroyed by the uprooting of trees since the beaches were first invaded by forest.

Fragments of rock arranged in patterns occur on beaches of the ancient Champlain Sea near Plattsburgh, N.Y., at the northeast end of the Adirondack Mountains. Angular slabs of thin-bedded arkose or arkosic sandstone, commonly 6 to 12 inches in diameter, form a pavement in which many fragments are upended. Pavements are interrupted by "islands" of finer material (silt, sand, and small fragments of rock), a few inches to several feet in diameter, that are covered by turf. Some pavements broken by many patches of fine material resemble the sorted circles described by Washburn (1956), a type of patterned ground commonly found in arctic or alpine regions and attributed to repeated cycles of freezing and thawing.

If the patterns on the beaches of the ancient Champlain Sea are the result of frost action, we must suppose that this process was active in the past, perhaps in late-glacial time, rather than at present. Present-day frost action in the forests of the Plattsburgh area is not forming ground patterns comparable to those on the ancient beaches. The assignment of these patterns to ancient frost action raises intriguing possibilities. Repeated freezing and thawing to depths much greater than at present may have been a widespread phenomenon in the area surrounding the Champlain Sea during a period that lasted from about 11,500 years Before Present to about 10,000 years B.P. (Gadd, 1964; Terasmae, 1965). At that time the edge of the waning ice sheet was at least as far away as Montreal, about 40 miles to the north. The climate would have been more rigorous than at present, and the land adjacent to the Champlain Sea was perhaps covered by some sort of tundra (Davis, 1965).

We are convinced, however, that the patterns are not the result of frost action, present or past. The surface of the beaches is a mosaic of mounds and pits, the result of tree throw in the presettlement forest within the last few hundred years. Small mounds and pits occur within the areas of pavement, whereas on adjacent parts of the beach ridges and swales, large mounds and pits are common. In the following pages we explain the sequence of events and the processes that have transformed the surface of rubbly beach ridges into patterned pavements of stones and fines. In this transformation, frost action plays only a minor role.

We wish to acknowledge the assistance of R. C. Zimmermann, Harvard University; and H. M. Raup and M. G. Wolman, the Johns Hopkins University, in the study of these patterns. Goodlett was supported by National Science Foundation grant GP–3963.

TREE-THROW MOUNDS AND PITS

Tree-throw mounds and pits are characteristic of areas in northeastern United States and adjacent Canada where the ground has never been plowed. When a tree falls the roots on one side of the trunk may form a hinge (Goodlett, 1954, pl. 5) and on the opposite side pull up a mass of earth and stones that stands as a vertical wall with the tree trunk on one side and a pit on the opposite side. As the binding roots decay, the

[1] Deceased; formerly of the Johns Hopkins University, Baltimore, Md.

mineral and organic materials fall down to form a mound that is generally on the same side of the pit as the fallen tree. The mound is gradually reduced in size by erosion, and the pit is filled. Leveling of the mound and pit is estimated to take place within 200 to 500 years. The more or less uniform orientation and age of mounds and pits in some areas indicate the toppling of many trees at one time, perhaps during a hurricane, whereas the random orientation in other areas suggests that the trees fell one by one.

Mounds and pits vary greatly in size. In northern Pennsylvania, mounds may be as much as 20 feet long and 15 feet wide. The adjacent pits are about the same size and may be as much as 2 feet deep. The relief from floor of pit to top of mound may be as much as 3½ feet. The large mounds in the plateaus of northern Pennsylvania are made of flaggy silt loam, whereas smaller mounds in southern New England are composed of pebbly sand.

The occurrence of mounds with a fallen tree trunk still preserved, the slightly curved form (in plan) of many mounds, and their internal structure distinguish tree-throw mounds from those that may result from the action of frost. (For maps and discussion of mound-and-pit microrelief, see Lutz, 1940; Goodlett, 1954; Stephens, 1956; Denny and Goodlett, 1956; and Lyford and MacLean, 1966.)

BEACHES OF THE CHAMPLAIN SEA

The patterned beaches are in a pasture about 1 mile north of Sciota and about 4 miles southeast of Mooers, in the Mooers 15-minute quadrangle (fig. 1). The site is north of the Mooers-Chazy town line and 0.6 mile east of State Route 22 (lat 44°54′44″ N., long 73°32′37″ W.).

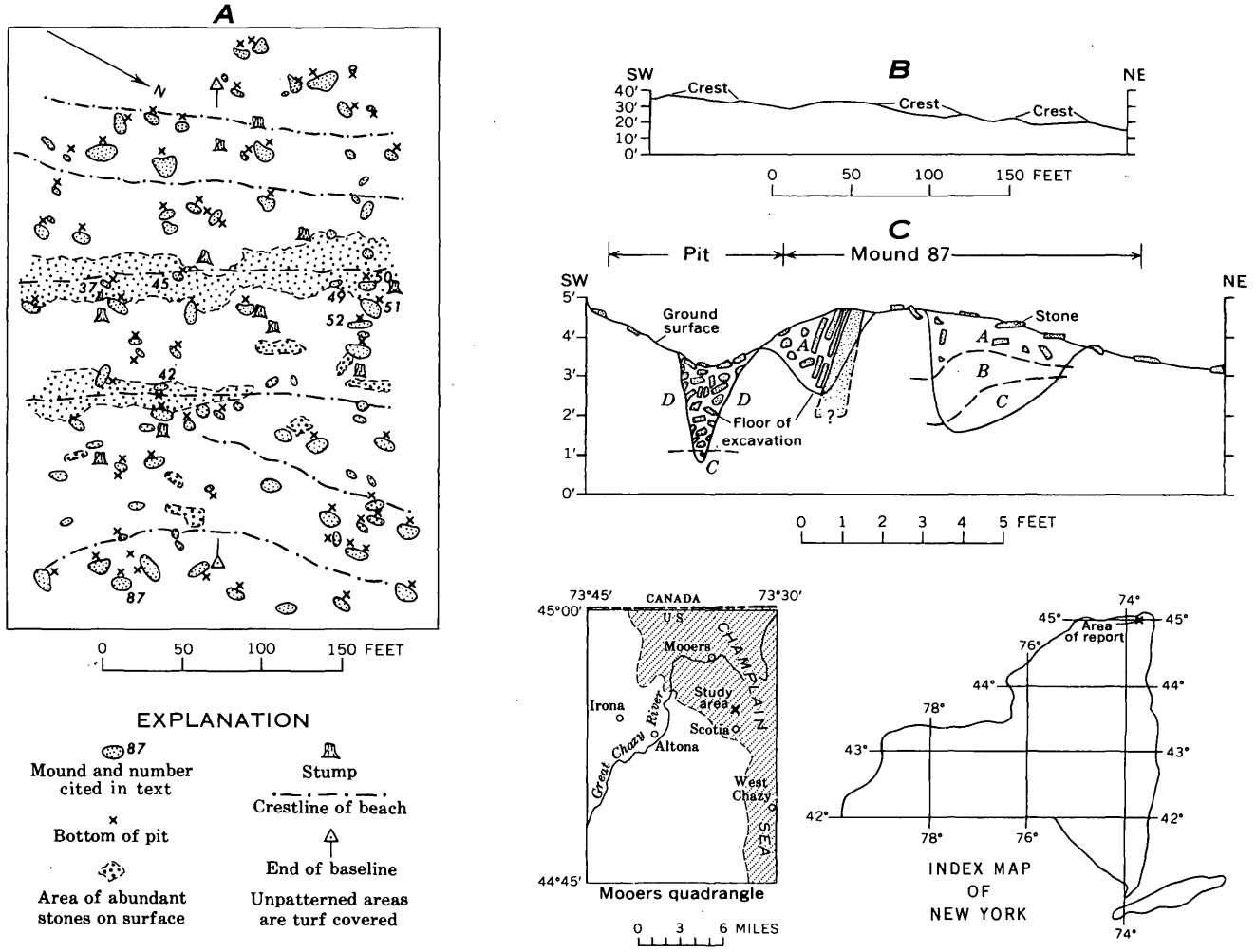

FIGURE 1.—Map and profile of some of the beaches of the ancient Champlain Sea, and cross section of a mound. *A*, map of mound-and-pit microrelief resulting from fallen trees. Locality is north of the Mooers-Chazy town line about 0.6 mile east of State Route 22, Mooers 15-minute quadrangle. *B*, profile of beach ridges along base line. *C*, partial cross section exposed in wall of excavation through mound 87 and adjacent pit; azimuth N. 65° E.; letter symbols identified in table 1.

Form

The beaches are low ridges 1 to 5 feet high that extend for about 1,000 feet (fig. 2). In the study area are six of these beaches (fig. 1*A*); the top of the westernmost beach is 17 feet above the one farthest east. Crests are broad, and side slopes range in grade from 5 to 20 percent. The ridges are 30 to 80 feet apart.

The beaches are covered with turf consisting mostly of wild fescue grass (*Festuca* sp.) interspersed with moss and lichen (figs. 2 and 3). Fragments of rock, hereafter called "stones," lie on the surface and in some places form a more or less continuous cover (fig. 1*A*).

Material

The beach ridges consist of loamy coarse sand containing abundant stones derived from sandy glacial drift. In a few places where bedrock is probably only 1 to 2 feet below the surface, the beach deposits consist of stones with only a little sandy matrix and abundant voids. Such rubbly beach deposits were probably derived from rubbly glacial drift by the action of waves and perhaps also that of sea ice.

The stones on the surface of beach ridges and in the beach deposits are fine- and very fine grained thin-bedded subarkose or arkose from the Potsdam Sandstone (Wiesnet, 1961; Wiesnet and Clark, 1966). The individual laminae range from 0.05 to 0.20 inch in thickness. On fresh surfaces the rocks are commonly either "pink" (grayish pink 5*R* 8/2 to pale red 5*R* 6/2) or "white" (pinkish gray 5*YR* 8/1 to yellowish gray 5*Y* 8/1). Color designations here and in following descriptions are based on the "Rock-color chart" of the National Research Council (Goddard and others, 1948).

The stones on the surface of the beach ridges are ½ to 40 inches in longest diameter; the mean of the longest diameter of 51 stones selected at random along a tape is about 4½ inches. The intermediate diameter ranges from ¼ to 20 inches; the mean of 51 stones is about 3 inches. The shortest diameter ranges from ¼ to 7 inches; the mean of 51 stones is about ¾ inch. The two largest fragments observed measure 40 by 15 by 7 inches and 36 by 20 by 6 inches. The stones are angular (fig. 3) as if they had been derived directly from the adjacent bedrock that is exposed in the county road just south of the pasture.

The stones on the beaches are fresh to slightly weathered. Weathering rinds are thin, and the fragments are firm. The most notable weathering change is color. The "pink" sandstones weather to pale red (10*R* 6/2) and grayish red (10*R* 4/2), and the "white" sandstones weather to a very light gray (*N*8) and yellowish gray (5*Y* 8/1). Most of the stones on the surface of the beach ridges are partly encrusted with lichen, commonly on the exposed side (fig. 3). Lichen on the underside of stones suggests recent overturning, probably since deforestation. Stones free of lichen (fig. 4) indicate recent uncovering or disturbance by present-day frost that breaks the turf and moves the individual stones (part of the process of mound erosion).

PATTERNED GROUND

On the beach ridges, the areas of abundant stones (fig. 1*A*) are not a continuous stone pavement. Patches

FIGURE 2.—View looking east across rubbly beach ridge, in middle distance. Ridge is near southeast edge of map area and passes just west of mounds 37, 45, 49, and 50 (fig. 1*A*). Scattered stones and turf in foreground. Tall grass is wild fescue (*Festuca* sp.). Dark area in foreground is moss and lichen. Tree at right is growing on stony beach.

FIGURE 3.—Oblique view of part of turf-covered circle with scale shown in figure 6*B*. Turf is largely moss and lichen. Prominent upended stones to left of 7-inch scale. View in taken from point directly above the lower right-hand corner of sketch (fig. 6*B*).

FIGURE 4.—View of part of a small circle of stones surrounded by turf. Some of the fragments in the circle are free of lichens (light colored). This is probably an area where stones and turf were disturbed by frost during the past frost season.

of stones and of turf form mosaics or patterns (fig. 5). Bands of stones surround centers of fines or of turf ½ to 6 feet in diameter. The centers are commonly a few inches higher than the surrounding stone-covered parts. Some stones are upended, their longer axes in a vertical plane. The patterns are illustrated in figure 6 by sketches made in the field. A few of the prominent stones were drawn in their true position, and the remainder of the sketch was filled in to show roughly the proportion of stones and fines or turf.

The patterns are similar to those defined by Washburn (1956) as sorted and nonsorted circles. Circles occur individually and in groups. A circle of fines may appear within an area of stones and resemble what Washburn calls a "debris island."

Circles of stones of varying size and shape are shown in figure 6*A*. Most of the long narrow fragments stand with their longer axes in a vertical plane. A low mound (37, fig. 1*A*) about 6 inches high forms the large oval-shaped area of fines in the upper right-hand part of the sketch. The lowest point on the stone rim is in the upper right-hand corner of the sketch. Near the lower right-hand end of the mound an irregular band of stones forms a small circle within the large oval. This large oval is the eroded remnant of a tree-throw mound. The mound-forming tree toppled

FIGURE 5.—Patterns of stones and turf on crest of beach ridge. View northward from point near mound 42 (fig. 1*A*). Twelve-inch planetable on beach in background, 7-inch white scale in foreground.

toward the lower left-hand corner of the area shown in the sketch, leaving a pit in the upper right-hand corner.

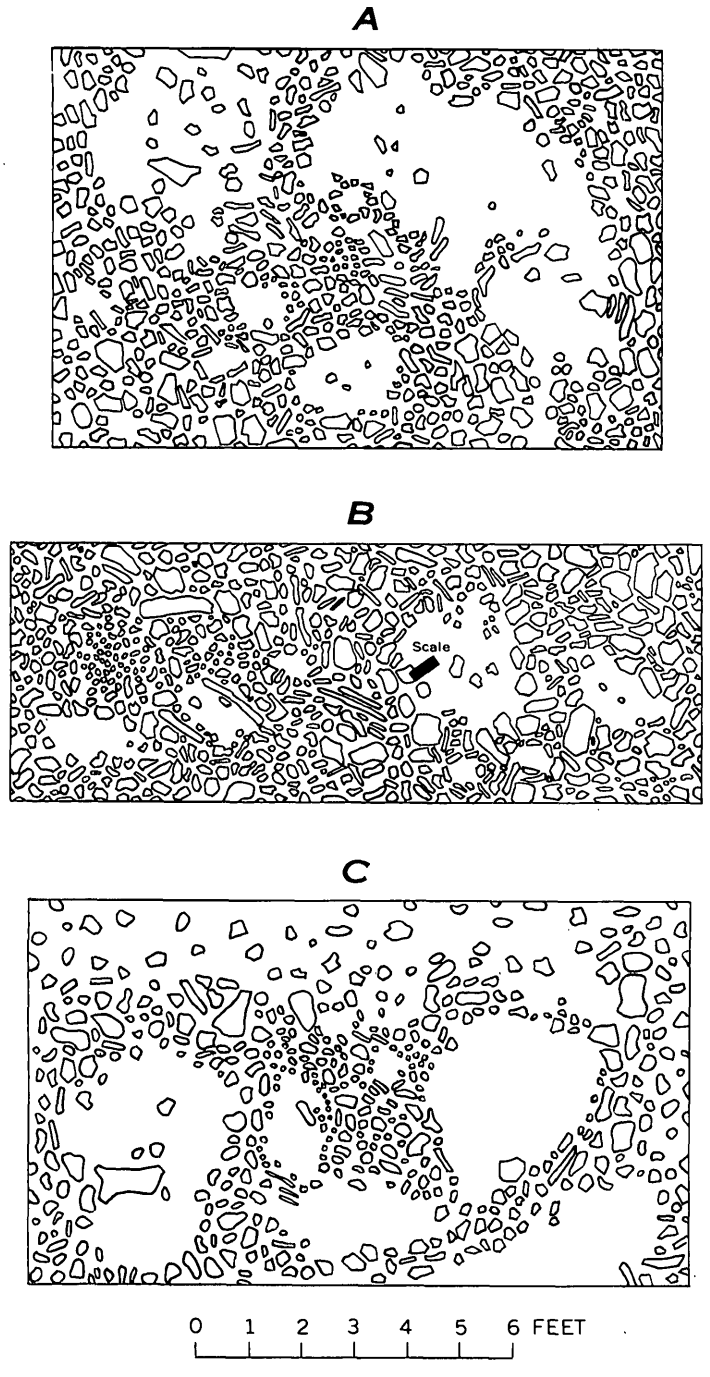

FIGURE 6.—Patterned ground on beach ridges. *A*, patterns of stones and fines. The large oval-shaped area of fines in upper right-hand part is mound 37. The adjacent pit in upper right-hand corner is floored with stones. *B*, sorted circles, with many upended fragments, especially to left of 7-inch scale. Area is about 12 feet south of mound 37. *C*, sorted circles near edge of area of abundant stones. Locality is 10 feet northwest of mound 42.

Figure 6*B* shows circles of fines ranging from less than 1 foot to several feet in diameter surrounded by stones that locally include many long upended stones. These patterns are about 12 feet south of mound 37 (fig. 1*A*). Figure 3 is an oblique view of a part of the circle shown in the sketch. The circle is largely turf covered. Prominent upended flagstones are to the left of the ruler. Most stones are lichen covered.

Circles of fines west of a beach crest near the edge of the area of abundant stones (fig. 6*C*) are ½ to 3 feet in diameter and stand 2 or 3 inches above the surrounding stony areas. Almost none of the stones are oriented with their long axes parallel to the rim of a circle.

MOUND-AND-PIT MICRORELIEF

Superimposed on the beach ridges is a microrelief of mounds and pits resembling that found in forested areas where the ground has never been plowed (fig. 7). The mounds are plentiful throughout the area mapped (fig. 1*A*), except in areas of abundant stones where mounds are few and small. Most mounds are associated with a well-defined pit.

The 95 mounds within the map area cover about 7 percent of the surface. They range in length from 3 to 20 feet, in width from 2 to 12 feet, and in height from about ¼ to 2 feet. The mean length is about 9½ feet, the mean width about 5½ feet, and the mean height about 0.25 foot. Seventy-five percent of the mounds are not more than 12 feet long, about 20 percent are 15 feet long, and 3 percent are 20 feet long. The largest mound is 20 by 12 by 2 feet. This mound is about the same size as the larger ones that we studied in Potter County, Pa., some years ago (Goodlett, 1954; Denny and Goodlett, 1956).

A trench (fig. 1*C* and table 1) was dug part way through mound 87 and the adjacent pit in further support of our interpretation of the microrelief as the result of tree throw. This mound is about 12 feet long, 10 feet wide, and 1 foot high. Excavations through tree mounds in other areas have shown that soil horizons are thickened and overturned and that fragments of woody material (roots, trunk, or bark) may be preserved in the mound when all trace of the fallen trunk has disappeared on the surface (Lutz and Griswold, 1939; Lutz, 1940; Goodlett, 1954; Denny and Goodlett, 1956).

The cross section (fig. 1*C*) shows that the existing pit is underlain by about 2 feet of rubble partly surrounded by an organic-rich silt (layer D). This material is interpreted as a partial filling of the pit that originally must have been almost 3 feet deep where crossed by the trench. Some of the larger stones in the

FIGURE 7.—Microrelief of mounds and pits on beaches of Champlain Sea. View looking northeast near north edge of map area (fig. 1*A*). Shovel rests on turf-covered mound 51. To right and behind is mound 52. Beach ridges cross in middle distance.

mound are upended; apparently they were turned up when the tree fell. On the northeast side of the mound the surface soil (layer A) is separated from the underlying beach gravel (layer C) by a brown organic-rich horizon (layer B) that contains amorphous organic matter and small fragments of bark. Layer B is interpreted as surface organic matter and remnants of the tree trunk buried by material carried up from lower horizons when the tree was uprooted and toppled over to the northeast.

TABLE 1.— *Material exposed in trench through tree mound*

[Mound 87 and adjacent pit, fig. 1*C*]

Layer A. Rubbly throughout.
Turf, 0–1 inch thick.
Sandy loam, 1–2 inches thick, dusky-brown (5*YR* 2/2).
Transition zone.
Loamy sand, light-brown (5*YR* 4/6).
Transition zone.
Loamy coarse sand, dark-yellowish-brown (10*YR* 4/2).

Layer B. Sandy loam, organic-rich, dusky-brown (5*YR* 2/2); contains amorphous organic matter, a few small fragments of bark <1 inch long.

Layer C. Rubbly loamy coarse sand, gray (10*YR* 5/4).

Layer D. Rubble, fragments 1–10 inches in diameter, little matrix of silty organic matter, black (5*YR* 2/1).

The mound-and-pit microrelief indicates that the map area was forested in presettlement times. The presettlement forest probably consisted mainly of sugar maple (*Acer saccharum* Marsh.), beech (*Fagus grandifolia* Ehrh.), paper and yellow birch (*Betula papyrifera* Marsh.; *B. lutea* Michx. f.), basswood (*Tilia americana* L.), shagbark hickory (*Carya ovata* (Mill.) K. Koch), black cherry (*Prunus serotina* Ehrh.), red oak (*Quercus rubra* L.), white ash (*Fraxinus americana* L.), red maple (*Acer rubrum* L.), and conifers such as northern white cedar (*Thuja occidentalis* L.), hemlock (*Tsuga canadensis* (L.) Carr.), white pine (*Pinus strobus* L.), pitch pine (*Pinus rigida* Mill.), and red spruce (*Picea rubens* Sarg.). The presence of trees is also shown by 12 tree stumps (fig. 1*A*) that stand more or less in growth position and postdate most, probably all, of the mounds.

The scarcity and small size of mounds within the areas of abundant stones at first suggest that these areas were not tree covered and therefore were never disturbed by tree roots. However, on beaches just outside the map area and elsewhere in the region, trees are now growing in areas of abundant stones. The small size of mounds made largely of stones compared with those that contain a high proportion of fines may be an

initial feature related to the cohesiveness of the mound-building material. Where the material is a flaggy silt loam, as in Potter County, Pa., tree mounds are much larger than where the mound-building material is commonly a gravelly sandy loam as in southern New England (Goodlett, 1954).

Large mounds (fig. 7) are easily recognized, but small ones merge into the low microrelief of the map area. There is no definite lower limit to the size of mounds. The mounds originated at different times and were initially of varying size. They are being reduced by erosion at different rates depending on many local factors such as slope, exposure, and nature of material.

We believe that the patterned ground on these beaches of the ancient Champlain Sea is due to the gradual erosion of tree mounds. The process may be somewhat as follows: Trees in the original forest are toppled. The trees may fall one by one, or they may fall in groups because of strong winds. Within the map area most of the mounds have pits on their western sides, suggesting that the trees were toppled by westerly winds (fig. 8). The mounds are then reduced by erosion and largely destroyed within a few hundred years (Goodlett, 1954; Denny and Goodlett, 1956).

Tree throw will also upend some of the stones, which may persist in this position and be exposed as the mound is lowered by erosion. In stony areas, with more fines at a depth of about 1 foot than at the surface, the roots of a tree that is toppled will bring up fines from below and produce a mound of fines and stones surrounded by stones. Or, conversely, in areas where the beach material has more fines at the surface than at a depth of a foot or so, the toppling of a tree will bring stones up from below into an area of fines. In this way, tree throw will produce mounds or islands of material of different texture from that which surrounds the mound. The forest floor is continually being disturbed both by the toppling of trees and by the erosion or reduction of the microrelief.

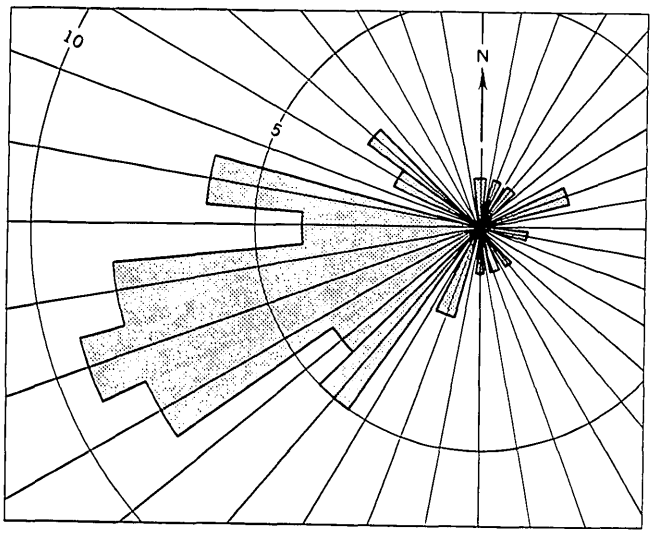

FIGURE 8.—Rose diagram of 59 measurements of mound-and-pit orientation indicating probable direction of winds that toppled the mound-forming trees.

Many of the mounds on the beaches are larger than those formed in recent years by trees in the adjacent woodlands; therefore, most of the mound-producing trees were in the presettlement forest. The spacing between mounds is variable. The mean distance from any mound to its closest neighbor is about 13½ feet. About 8 percent of the mounds are at least 30 feet from their nearest neighbor, and about 33 percent have a neighbor within 10 feet. Trees in the presettlement forest were probably spaced 20 to 30 feet apart (Goodlett, 1954). Some mounds are only a few feet apart, suggesting that they were not all formed at the same time but are probably the result of the toppling of trees over a period of many years.

CONCLUSIONS

Patterned ground on beaches of the ancient Champlain Sea results from the formation and reduction of tree-throw mounds and pits, not from ancient frost action on the shore of the Champlain Sea. The sorted circles on the beaches differ from those of undoubted frost origin. The patterns described here show a wide range in size within a small area, whereas those due to repeated freeze-thaw cycles are more uniform in size. The stones in circles on the shore of the Champlain Sea show little tendency to lie parallel to the border of a circle as do those in circles formed by frost action.

In favorable places within the map area frost action is eroding the mounds and filling the pits. Small stones free of lichens are found separated from their neighbors or adjacent turf probably by the wedging action of needle ice during the preceding year. Small circles of lichen-free stones surrounded by turf may have been exposed during the past frost season (fig. 4). On the east slope of the beaches in areas of abundant stones are places where small lichen-free stones form small tongues that appear to have moved a few inches downslope within the last year.

There may have been intense frost action on the shores of the Champlain Sea, and the surrounding slopes may have been treeless, but the existing patterns on these beaches are not evidence for such conditions in the past. The disturbance of the soil by tree roots has gone on at all times and in all places since the area was first invaded by forests.

REFERENCES

Davis, M. B., 1965, Phytogeography and palynology of northeastern United States, *in* Wright, H. E., Jr., and Frey, D. G., eds., The Quaternary of the United States: New Jersey, Princeton Univ. Press, p. 377–402.

Denny, C. S., and Goodlett, J. C., 1956, Microrelief resulting from fallen trees, *in* Denny, C. S., Surficial geology and geomorphology of Potter County, Pennsylvania: U.S. Geol. Survey Prof. Paper 288, p. 59–66.

Gadd, N. R., 1964, Moraines in the Appalachian region of Quebec: Geol. Soc. America Bull., v. 75, no. 12, p. 1249–1254.

Goddard, E. N., and others, 1948, Rock-color chart: Washington, D.C., Natl. Research Council, 6 p. [republished by Geol. Soc. America, 1951].

Goodlett, J. C., 1954, Vegetation adjacent to the border of the Wisconsin drift in Potter County, Pennsylvania: Harvard Forest Bull. 25, 93 p.

Lutz, H. J., 1940, Disturbance of forest soil resulting from the uprooting of trees: Yale Univ. School Forestry Bull. 45, 37 p.

Lutz, H. J., and Griswold, F. S., 1939, The influence of tree roots on soil morphology: Am. Jour. Sci., v. 237, no. 6, p. 389–400.

Lyford, W. H., and MacLean, D. W., 1966, Mound and pit microrelief in relation to soil disturbance and tree distribution in New Brunswick, Canada: Harvard Forest Paper 15, 18 p.

Stephens, E. P., 1956, The uprooting of trees, a forest process: Soil Sci. Soc. America Proc., v. 20, no. 1, p. 113–116.

Terasmae, Jaan, 1965, Surficial geology of the Cornwall and St. Lawrence Seaway project areas, Ontario: Canada Geol. Survey Bull. 121, 54 p.

Washburn, A. L., 1956, Classification of patterned ground and review of suggested origins: Geol. Soc. America Bull., v. 67, no. 7, p. 823–865.

Wiesnet, D. R., 1961, Composition, grain size, roundness, and sphericity of the Potsdam Sandstone (Cambrian) in northeastern New York: Jour. Sed. Petrology, v. 31, no. 1, p. 5–14.

Wiesnet, D. R., and Clark, T. H., 1966, The bedrock structure of Covey Hill and vicinity, northern New York and southern Quebec, *in* Geological Survey research 1966: U.S. Geol. Survey Prof. Paper 550–D, p. D35–D38.

QUALITY CONTROL OF ADJUSTMENT COEFFICIENTS USED IN SEDIMENT STUDIES

By HAROLD P. GUY, Fort Collins, Colo.

Abstract.—The means of a group or groups of sample data are often used to quantify a population. The algebraic method of evaluating a mean or the ratio of two means is rather cumbersome and therefore too infrequently used. This paper presents alinement charts and a simplified procedure for quality evaluation and control for such means and ratios. The evaluation of adjustment coefficients commonly used to adjust single-vertical measurements of suspended-sediment concentration by measurements of the cross-sectional concentration is illustrated.

Data from two sources are often used as a ratio to indicate a relationship between the two sources. This ratio can be considered as a coefficient useful for adjustment of data from one of the sources. When such data have a variation among observations caused by measurement error, or natural variation, it is essential that the user of the ratio, or coefficient, be aware of its quality or the relative error involved. For example, the average of several coefficients may indicate a mean adjustment of 1.07; but if most of these have a probable error of 9 or 10 percent, then the use of the average coefficient or adjustment ratio would be highly questionable.

The coefficient of adjustment, often used in sediment studies, is defined as the ratio between the mean concentration of sediment derived from a number of depth-integrated verticals representing the stream cross section and the concentration of a single depth-integrated vertical. Sediment measurement on most streams may require from 30 to 100 observations per month in a single vertical. Periodic measurements to represent a mean cross-sectional concentration of sediment may require as many as 20 vertical sampling locations for each sample or observation. The average of two or more sets of such cross-sectional measurements and the average of two or more single-vertical measurements taken at the same time as the cross-section measurement can thus be combined to form the ratio or coefficient useful to adjust the many values obtained at the single vertical. Adjustment to the single-vertical concentration is made only if the ratio is judged to be really different from 1.00 as determined by its probable error.

The purpose of this report is to provide statistical methods and tools to analyze ratios whose numerator and denominator are subject to possible errors in measurement resulting from natural fluctuations. The method is adapted from a discussion of the problem of evaluating groups and comparison of groups by Snedecor (1956). First, a procedure is presented that enables one to estimate the quality of the mean of a sample consisting of several members; second, a procedure is presented that enables one to estimate coefficient quality; and third, criteria are developed that enable one to determine the necessary number of observations required for the numerator and denominator of a desired ratio. In all instances, it will be assumed that the data or members of a sample have a normal distribution about the mean.

THE QUALTY OF THE MEAN OF A GROUP

The determination of the quality of the mean of a group of observations is an elementary statistical exercise that requires considerable time. The objective here is to simplify this exercise so it can be accomplished with simple tabulation and a nomograph. The standard error can be computed as

$$S_{\bar{x}} = \sqrt{\frac{s^2}{n}}$$

where s^2=variance=$\frac{\Sigma (x-\bar{x})^2}{n-1}$,

$(x-\bar{x})$=deviation of observation from the mean, and
n=number of observations in the group.

This forms the theoretical base for use of an alinement chart (fig. 1) and the tabulation of data (table 1) to determine the quality of a mean.

To illustrate, the 5 observations of table 1 range from 587 to 649 and have a mean of 618. The left line of the alinement chart (fig. 1) requires the sum of the squared deviations from the mean of the observations derived by reduction of the observations to a base of 100 for the mean; that is, divide each observation by the mean. The quality of the mean for the group of 5 observations is then determined by extension of a line from 82 on the left scale through 5 observations on the center scale to about 4.3 percent error on the right scale. In other words, if the data in table 1 represents a group of single-vertical sample concentrations, the true mean of the group has 9 chances out of 10 of being within 4.3 percent of 618.

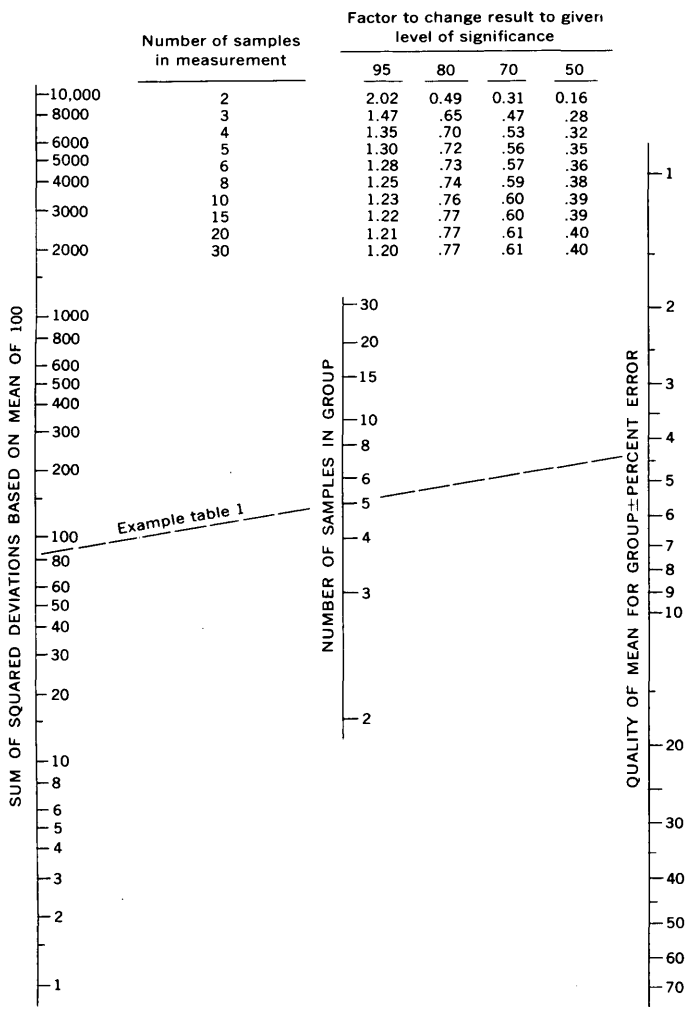

FIGURE 1.—Alinement chart to determine the quality of the mean for a group of samples given the sum of squared deviations at the 90-percent level of significance. The quality of the mean for other levels is obtained by use of the factors shown.

TABLE 1.—*Computations for quality of the mean of a group by alinement chart*

	Base of 100	
Measured observations	*Observations*	*Squared deviations*
643	104	16
618	100	0
593	96	16
649	105	25
587	95	25
Sum 3, 090		82
Mean 618		

Results obtained from the alinement chart are for the 90-percent level of significance or confidence interval. If a different level is required, the answer can be adjusted in accordance with the factor given on the chart for the specific number of samples in the group. Thus, for the 95-percent level, the quality of the mean in the above example would be 4.3 × 1.30, or 5.6-percent error.

THE QUALITY OF A COEFFICIENT

As previously mentioned, a coefficient is defined as the ratio of the means of two groups. In the evaluation of mean stream-sediment concentration, a common application would be the ratio of the mean of cross-sectional measurements to the mean of single-vertical measurements. A single-vertical measurement consists of a depth-integrated sample obtained at a specific vertical of the stream cross section. The sample usually is contained in a pint bottle having 250 to 400 milliliters of water-sediment mixture. Each cross-sectional measurement, on the other hand, may consist of several pint bottles, each representing only a portion of the stream cross section. The quality of a coefficient can be determined by expansion of the methods previously used to determine the quality of the mean of a single group.

Assume that a coefficient, obtained by the ratio of the mean concentration of two cross-sectional measurements (numerator) to the mean concentration of four single-vertical measurements, is to be evaluated. Such a coefficient, would be used for adjustment of the single-vertical samples. The coefficient for the data in table 2 would be $^{72}\%_{00}$, or 1.20. The pooled sum of the squared deviations, amounting to 44, is derived by changing the sample concentrations of the two groups to a base of 100. In figure 2, a line is extended from the left scale representing the pooled sum of the squared deviations at 44 through a point on the center scale representing the 2 and 4 samples in the numerator and denominator of the ratio and to the quality of the coefficient on the right scale, in this case ±6.0 percent. At the 90-percent

TABLE 2.—*Computations for the quality of a sediment-concentration coefficient by alinement chart*

Sample groups	Measured concentrations (mg/l)	Mean	Base of 100: Concentrations	Base of 100: Sum of squared deviations
Cross section	715	720	99	2
	725		101	
Single vertical	624	600	104	42
	606		101	
	600		100	
	570		95	
				44

level of significance, the lower and upper limits of the coefficient would then be approximately 1.20±0.06, or 1.14 to 1.26; or more precisely, 1.20±(0.06 × 1.20), or 1.13 to 1.27.

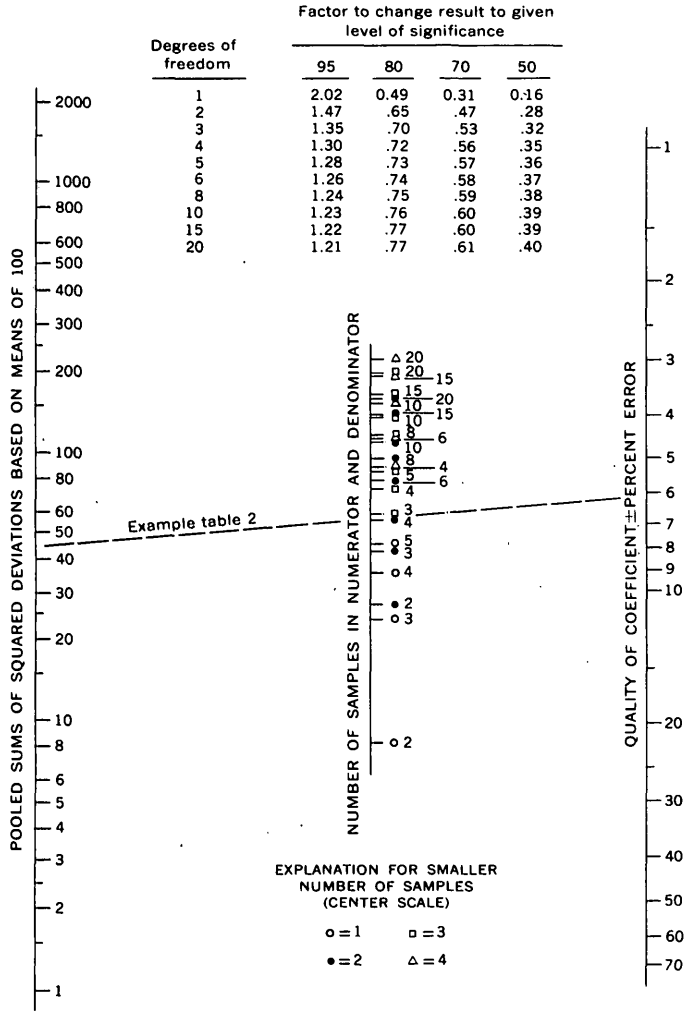

FIGURE 2.—Alinement chart to define the quality of a coefficient for a given sampling design and pooled sums of squared deviations at the 90-percent level of significance. The quality for other levels is obtained by the use of the factors shown. The legend used on the center scale indicates the smaller number of samples used for either the numerator or denominator.

Again note that the results can be changed to other levels of significance by use of the factors given on figure 2. Thus, if the 80-percent level is desired in this example, the quality of the coefficient having $n_1+n_2-2=4$ degrees of freedom would be 6.0×0.72, or 4.3 percent error.

In contrast to the use of the alinement graph, the above example may be solved with a commonly used algebraic procedure that does not reduce the concentrations to a base of 100. The computation is included here to illustrate the advantages of the alinement graphs. Symbols used are defined as follows:

$d.f.$ = degrees of freedom $= n_1+n_2-2$

n = number of samples in one group

$\bar{x}$ = difference in means of the two groups

Σd^2 = pooled sums of the squared deviations

s^2 = pooled variance $= \dfrac{\Sigma d^2}{d.f.}$

$s_{\bar{x}}$ = standard error $= \sqrt{\dfrac{s^2(n_1+n_2)}{n_1 n_2}}$ (for groups of unequal size)

t = test of significance $= \dfrac{\bar{x}}{s_{\bar{x}}}$

m = confidence limits $= \bar{x} \pm s_{\bar{x}} t$

The tabulations required for the algebraic procedure illustrating the example are included in table 3.

TABLE 3.—*Computations for the quality of a coefficient by the algebraic procedure*

Sample groups	Measured concentrations (mg/l)	Mean	Squared deviations from mean	Sum
Cross section	715	720	25	50
	725		25	
Single vertical	624	600	576	1,512
	606		36	
	600		0	
	570		900	
		$\bar{x}=120$		$\Sigma d^2=1,562$

Further, the pooled variance, $s^2 = \dfrac{1562}{1+3} = 390.5$, and the standard error, $s_{\bar{x}} = \sqrt{\dfrac{390.5\ (2+4)}{8}} = 17.1$. From a "$t$" table (Snedecor, 1956, p. 46), $t=2.13$ for 4 degrees of freedom and the 90-percent confidence level. Then the fiducial limits, $m=120\pm(17.1\times2.13)=120\pm36=84$ and 156.

Because $\bar{x}=120$ exceeds 42, the two groups of samples are adjudged from separate populations and that differences probably range from 84 to 156 mg/l. The coefficient $\dfrac{720}{600} = 1.20$ then has limits between $1.20\pm\dfrac{36}{720} = 1.20\pm0.05$, or 1.15 to 1.25, which agrees closely with the graphic method used above.

DETERMINING THE DESIRABLE NUMBER OF SAMPLES

The third item for consideration pertains to criteria for determining the number of samples necessary to define a coefficient within certain limits for a given set of data. Such a determination would only be applicable to sampling of the same population or stream from which the given set of data was obtained.

For example, it is desirable to define the daily concentration of stream sediment to the nearest 5 percent; therefore, coefficients, or the ratio of the cross-section concentration to the single-vertical concentration, for correcting the single vertical should be of similar quality, or ± 5 percent. For some streams, a probable definition within 10 percent may be adequate. It should also be stressed that the desirable number of samples determined by this method is based on the assumption that another set or group of samples will yield similar variation among the individual samples. Because the data at hand may not precisely represent the population, it is necessary to assign a level of significance or t value to the computation.

To determine the desired number of samples, remember that $t=\frac{\bar{x}}{s_{\bar{x}}}$, $s_{\bar{x}}=\sqrt{\frac{s^2(n_1+n_2)}{n_1 n_2}}$, and $s^2=\frac{\Sigma d^2}{d.f.}$. When $n=n_1=n_2$ (both groups the same size), then $s_{\bar{x}}=\sqrt{\frac{2s^2}{n}}$ and $n=\frac{2\times t^2\times \Sigma d^2}{\bar{x}^2\times d.f.}$.

The example of a set of data tabulated on table 4 for three samples of concentration in the cross section and three samples of concentration at the daily sampling vertical will be used to illustrate the computation. In order that the use of the above formula may be simplified, the concentrations of the samples are reduced to a base of 100, as in preceding examples using the alinement charts.

The computation table is completed by listing and totaling squared deviations from the means of the base of 100 ($\Sigma d_a^2=39$). Thus Σd_a^2 is the pooled sums of the squared deviations using the base of 100. To allow the maximum of 5 percent error for the coefficient, let $\bar{x}=5$ for the maximum difference in means of the two groups when the concentrations are reduced to a base of 100. With the $d.f.=4$, the formula then reduces to $n=\frac{2\times t^2\times \Sigma d_a^2}{5^2\times 4}=\frac{t^2\times \Sigma d_a^2}{50}$.

TABLE 4.—*Data to determine number of samples for defining a coefficient within certain limits*

Sample groups	Measured concentrations (mg/l)	Mean	Base of 100: Concentrations	Base of 100: Sum of squared deviations
Cross section	238	245	97	26
	242		99	
	255		104	
Single vertical	204	209	98	13
	215		103	
	208		100	
				$\Sigma d_a^2 = 39$

With $t=2.13$ for a 90-percent level of significance, this formula reduces to $n=0.091\Sigma d_a^2$. The required number of samples to define the coefficient within 5 percent should then be 0.091×39 or 4 samples each at the daily vertical and in the cross section unless a 1-in-10 chance has resulted in the available data being erratic.

The factors to be multiplied by Σd_a^2 to determine the necessary number of samples for desired coefficients within 5- and 10-percent accuracy at both the 80- and 90-percent level of significance and for a given number of samples of the available data are tabulated in table 5.

TABLE 5.—*Factors for use with computed* Σd_a^2 *to determine n*

Available samples in each group	Desired coefficient within 5 percent: 90-percent level	Desired coefficient within 5 percent: 80-percent level	Desired coefficient within 10 percent: 90-percent level	Desired coefficient within 10 percent: 80-percent level
2	0.34	0.14	0.085	0.035
3	.091	.047	.023	.012
4	.050	.028	.012	.0069
5	.035	.020	.0086	.0049

REFERENCE

Snedecor, G. W., 1956, Statistical methods, fifth edition; Iowa State College Press, 534 p.

ORIGIN OF ORDOVICIAN QUARTZITE IN THE CORDILLERAN MIOGEOSYNCLINE

By KEITH B. KETNER, Denver, Colo.

Abstract.—Ordovician quartzite deposits in the Cordilleran miogeosyncline extend from the Peace River, British Columbia, to Owens River, southern California. The hypothesis is offered that almost all the sand composing these deposits was eroded from Cambrian sandstone formerly covering the Peace River–Athabaska arch in northern Alberta. This sand probably entered the geosyncline at about lat 56°N. and was swept southward at least as far as southern California. The evidence is as follows: (a) the presence of an adequate source of sand in northern Alberta and the apparent absence of adequate sources elsewhere, (b) the progressively decreasing age of basal quartzite beds from north to south, (c) the southerly decreasing thickness and increasing width of the deposits, (d) the southerly decreasing grain size, and (e) a southerly trend toward improved sorting.

Quartzite is a well-known component of the Ordovician System in the Cordilleran miogeosyncline, where it composes large parts of the following formations: Eureka Quartzite (Hague, 1883; Kirk, 1933; Webb, 1958; Nolan and others, 1956), Swan Peak Quartzite (Richardson, 1913; R. J. Ross, Jr., 1951), Kinnikinic Quartzite (C. P. Ross, 1934, 1937), Toquima Formation (Ferguson, 1924), Convict Lake Formation (Rinehart and Ross, 1964), Johnson Spring Formation (D. C. Ross, 1966), Wonah Quartzite (Walcott, 1924), and Mt. Wilson Quartzite (Norford, 1966). It composes minor parts of the Pogonip Group (Nolan and others, 1956), the Copenhagen Formation (Merriam, 1963a), and the Palmetto Formation (Ferguson and Muller, 1949; Albers and Stewart, 1965).

The purpose of this paper is to develop the hypothesis that Ordovician quartzite beds throughout the miogeosyncline were derived mainly from a common provenance in northern Canada and were deposited in a single marine trough.

In the following discussion, to avoid repetition, the unqualified word "quartzite" means Ordovician quartzite of the miogeosyncline and of the transition zone between miogeosyncline and eugeosyncline. Eugeosynclinal quartzite is considered a separate problem (Ketner, 1966) and is not discussed here. No claim is made that quartzite units are exactly correlative; in fact, it is certain that the onset of quartz sand deposition varied considerably from place to place. Nor is any claim made that quartzite is, or ever was, present in a continuous sheet; depositional and erosional gaps are normal. Although formations such as the Eureka and Swan Peak Quartzites include carbonate and shale beds in addition to quartzite, these nonquartzite beds are not discussed in the present paper, which is concerned solely with the properties and origin of quartzite, not with entire stratigraphic units of which quartzite is a part.

Unusual features of the quartzite, such as its great extent, uniformity, and purity, have stimulated speculation on its provenance and environment of deposition. Among those who have published hypotheses of origin are Kirk (1933), Webb (1958), Kay (1960), Merriam (1963a), and R. J. Ross, Jr. (1964a). The paleontologic evidence pointing to southward and westward migration of sand in Utah and Nevada presented by R. J. Ross Jr. (1964a) and research on the northern part of the geosyncline by B. S. Norford (1964, 1966), of the Geological Survey of Canada, have been especially useful in developing the present hypothesis. Special thanks are due to Norford for the loan of representative suites of quartzite from Canada.

EXTENT, THICKNESS, AND VOLUME OF QUARTZITE

Quartzite is coextensive with the southern part of the Cordilleran miogeosyncline south of the Peace River, British Columbia (figs. 1, 2) but, significantly, it is absent in the northern part, north of the Peace River (Norford, 1964, 1966). It tends to be relatively narrow and thick in Canada, thinning rapidly eastward toward the craton and westward toward the eugeosyncline (North and Henderson, 1954, p. 67; Norford, 1966, p. 45). In contrast, it is relatively wide and thin in Nevada and Utah and thins gradually to the east

U.S. GEOL. SURVEY PROF. PAPER 600-B, PAGES B169-B177

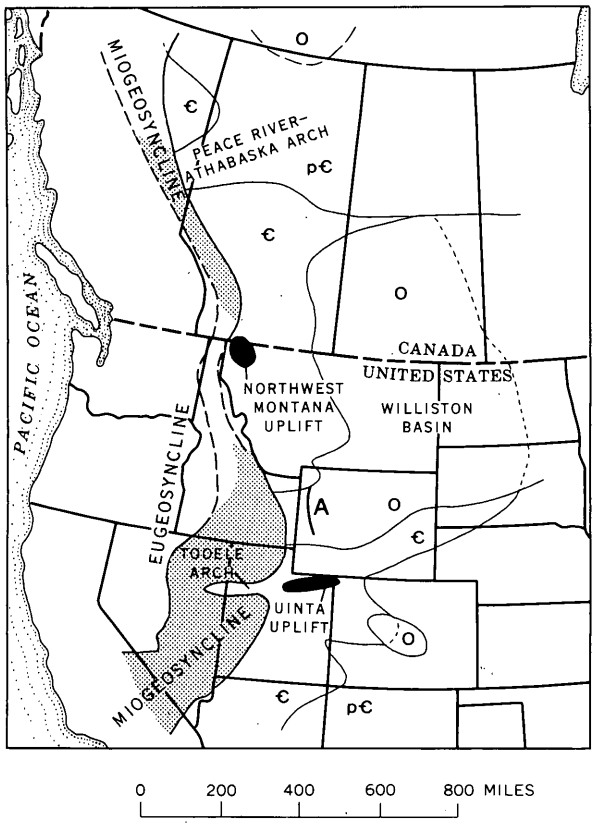

FIGURE 1.—Western North America, showing extent of Ordovician quartzite (stippled) in the miogeosyncline; and Precambrian (Pc), Cambrian (c), and Ordovician (O) terranes east of the geosyncline. *A*, Western limit of Ordovician quartz sand in the Williston basin.

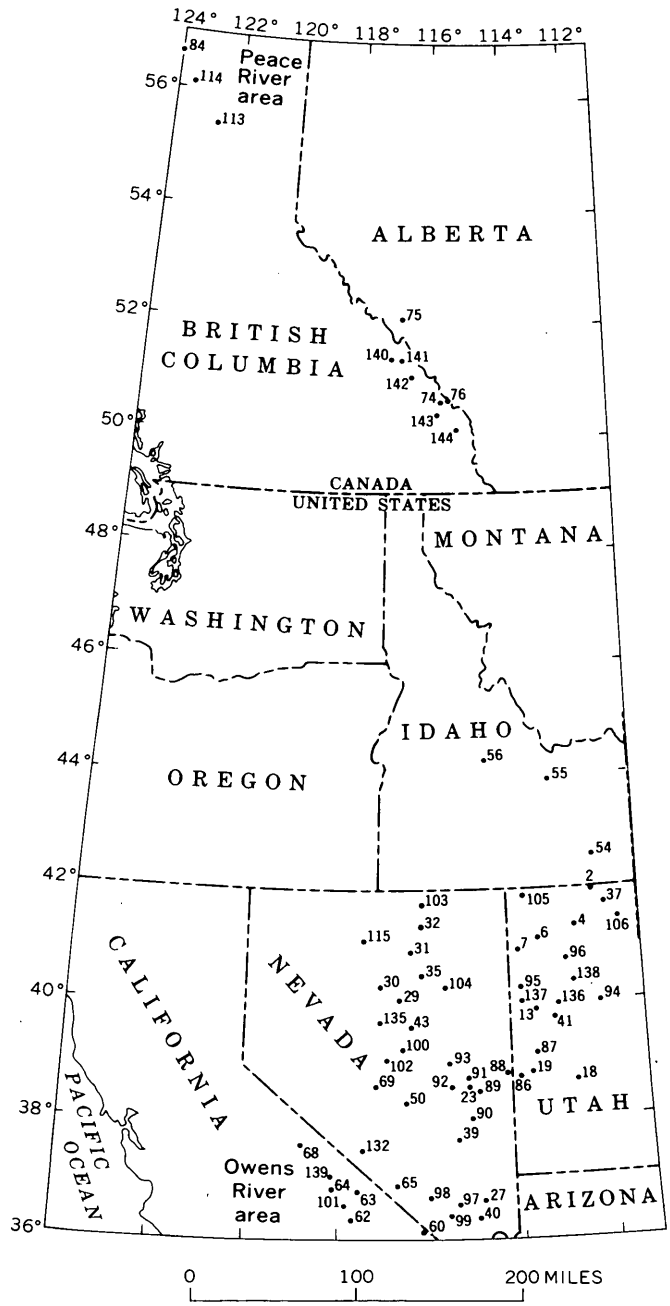

FIGURE 2.—Index map showing sites to which references are made.

and west (fig. 3, table 1). It terminates abruptly at its widest part in southern California, possibly owing to Paleozoic erosion. Thickness trends in Idaho indicate that quartzite may have extended some distance northward, possibly as far as Canada, before it was obliterated by intrusion of the Idaho batholith.

In Canada, quartzite originally covered 15,000 square miles, a figure based on the assumption that quartzite having an average width of 50 miles (Norford, 1966, figs. 4–9) extended continuously (before Cenozoic erosion) from the Peace River to southeastern British Columbia. In Idaho, Utah, Nevada, and California, quartzite covered (before Cenozoic erosion) 110,000 square miles. If quartzite is assumed to have occupied the area between central Idaho and southeastern British Columbia and the area between Owens River, Calif., and the Pacific Ocean, then 15,000 and 35,000 square miles must be added, respectively. The total is 175,000 square miles, of which about 50,000 is debatable.

If the average thickness of quartzite in Canada is estimated (conservatively) at 400 feet, the volume of quartzite would be 2,000 cubic miles. South of central Idaho, thickness data are abundant (fig. 3) and the volume of quartzite can therefore be determined accurately at 7,000 cubic miles. The uncertain areas in Idaho and California might add 3,000 cubic miles. The total volume would then be 12,000 cubic miles, of which 3,000 are in doubt. Although the areal extent of quartzite is relatively small, its volume in the miogeosyncline is about double that of correlative sandstones on the craton (Dapples, 1955).

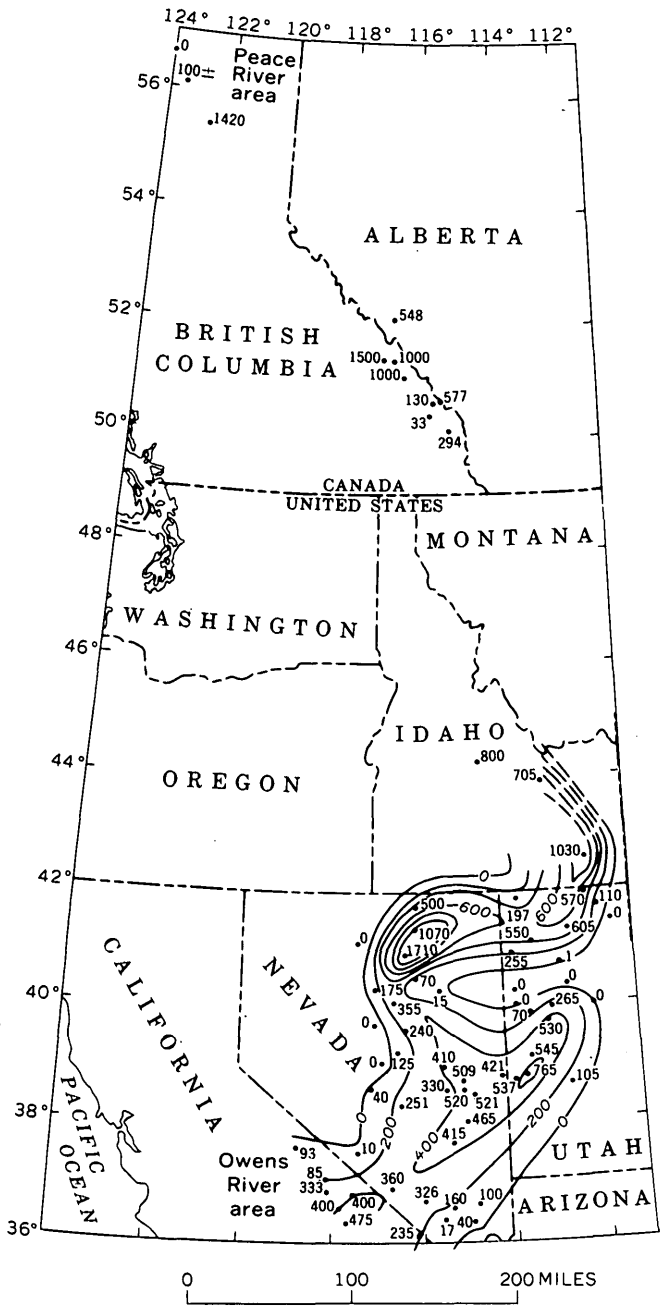

FIGURE 3.—Thickness, in feet, of Ordovician quartzite in the miogeosyncline. Contour interval 200 feet, dashed where approximately located.

STRATIGRAPHY AND REGIONAL VARIATIONS IN AGE

In the miogeosyncline, Ordovician quartzite is sandwiched between Lower Ordovician shaly limestone (Pogonip Group, Garden City Limestone, Mons-Sarbach unit) and Upper Ordovician dolomite (Ely Springs Dolomite, Hanson Creek Formation, Fish Haven Dolomite, Beaverfoot-Brisco Formation). In

TABLE 1.—*Thickness of Ordovician quartzite, Cordilleran miogeosyncline*

Site (fig. 2)	Thickness [1] (feet)	Source of data
2	570	R. J. Ross., Jr. (1953, p. 24).
4	605	Present report.
6	550	Do.
7	255	Do.
13	70	Do.
18	105	Do.
19	765	Do.
23	520	Do.
27	100	Do.
29	355	Do.
30	175	Gilluly and Gates (1965, p. 15).
31	1, 710	Present report.
32	1, 070	Do.
35	70	Do.
37	110	Do.
39	415	Do.
40	40	Do.
41	530	Do.
43	240	Do.
50	251	R. J., Ross, Jr. (1964b, p. C66).
54	1, 030	Present report.
55	705	Do.
56	[2] 800	W. S. Hobbs (oral commun., 1965).
60	235	Present report.
62	475	Do.
63	400	R. J. Ross, Jr (1964b, p. C32).
64	333	D. C. Ross (1966, p. 47).
65	360	Cornwall and Kleinhampl (1961).
68	93	Present report.
69	40	Do.
74	130	B. S. Norford (written commun., 1965).
75	545	Do.
76	577	Norford (1966, p. 47).
84	0	Irish (1963).
86	537	G. W. Webb (1956, p. 39).
87	545	(1956, p. 41).
88	421	(1956, p. 45).
89	521	(1956, p. 47).
90	465	(1956, p. 50).
91	509	(1956, p. 53).
92	330	(1956, p. 56).
93	410	(1956, p. 58).
94	0	Morris and Lovering (1961, p. 57).
95	0	Nolan (1935, p. 16).
96	1	Young (1955).
97	160	R. J. Ross, Jr. (1964b, p. C14).
98	326	(1964b, p. C48).
99	17	(1964b, p. C60).
100	125	Merriam (1963a, p. 28).
101	400	(1963b, p. 8).
102	0	Kay and Crawford (1964, p. 450).
103	500	Decker (1962, map).
104	15	Ronald Willden (oral commun., 1965).
105	197	Felix (1956, p. 83).
106	0	R. J. Ross, Jr. (1949, p. 489).
113	1, 420	Norford (1966, p. 47).
115	0	Hotz and Willden (1964, p. 20).
132	10	Present report.
135	0	Stewart (1967).
136	265	Staatz and Carr (1964, p. 37).
137	0	Nolan (1935, map).
138	0	Rigby (1958, map).
139	85	D. C. Ross, (1966, p. 53).
140	1, 500	North and Henderson (1954, p. 67).
141	1, 000	Do.
142	1, 000	Do.
143	33	Norford (1966, p. 47).
144	294	(1966, p. 45).

[1] Interbeds of other lithologies are excluded.
[2] Estimated thickness.

a few places (sites 55, 56, 29, 31, fig. 2) Lower Ordovician limestone is missing and quartzite lies directly on Cambrian or older rocks. In the transition zone between the miogeosyncline and eugeosyncline (sites 68, 132, 69, fig. 2) quartzite beds lithically similar to those of the miogeosyncline commonly overlie limestone of miogeosynclinal aspect, but are overlain by black bedded chert and siltstone of eugeosynclinal aspect.

The quartzite-bearing interval commonly consists of two quartzite units: a lower lenticular bed and an upper persistent bed composed, in turn, of three indistinct quartzite strata (fig. 4). In some places carbonate units commonly present within the quartzite sequence are thick enough to have been given separate names such as Crystal Peak Dolomite (Webb, 1958), Copenhagen Formation (Merriam, 1963a), and Skoki Formation (Norford, 1966). The comparative petrographic data of this report were derived from the upper persistent unit of quartzite.

Although precise correlation among the many named and unnamed stratigraphic units is beyond the scope of this report, the relative age from place to place of basal quartzite beds is discussed because of its bearing on the location of the source areas. Because lower beds of quartzite alternate with fossiliferous carbonate and shale, their ages commonly can be determined with reasonably good precision. Upper beds of quartzite cannot be closely dated.

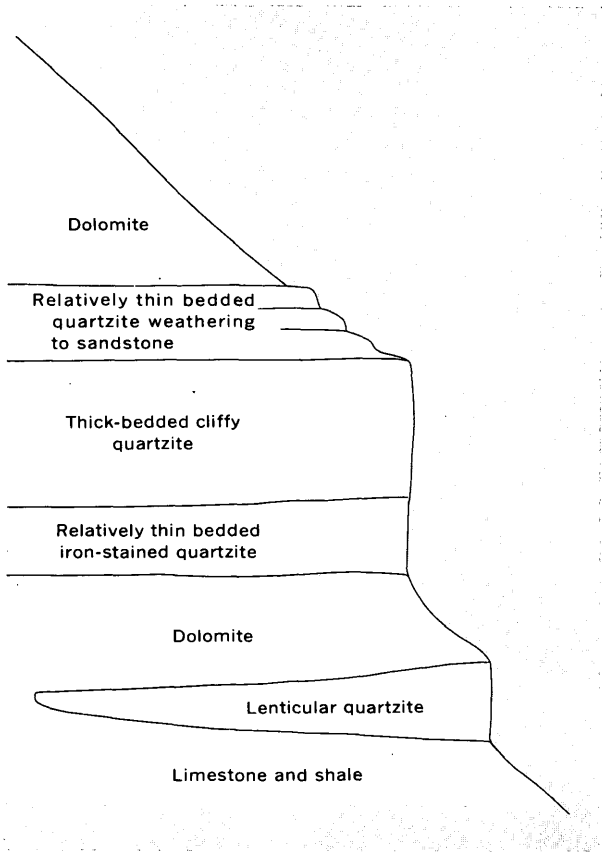

FIGURE 4.—Typical profile of Ordovician quartzite in the miogeosyncline.

Two trends in the age of basal quartzite beds are evident: a dominant trend parallel to the axis of the geosyncline and a subordinate transverse trend (fig. 5). Among well-dated quartzite beds, the oldest are in the north at Mount Hunter (site 113) and Tipperary Lake, British Columbia (site 76), where they have been dated as late Early to early Middle Ordovician by Norford (1966, p. 46; written commun. 1965). R. J. Ross, Jr., (1964a, p. 1547) has demonstrated a southerly decrease in age from Whiterock age in northern Utah to Porterfield age in southern Nevada.

Ross (1964b, p. C86) also presents evidence for a transverse trend in the southern part of the geosyncline: well-dated quartzite beds at the Nevada Test Site (site 98), Meiklejohn Peak (site 65), and the Inyo Range of California (site 64)) indicate a probable westward decrease in age. This trend is strengthened by data from Convict Lake, Calif. (site 68; Rinehart and Ross, 1964, p. 21) where miogeosynclinal quartzite overlies a unit containing graptolites of probable Wilderness age (zone 10 of Elles and Wood, 1914).

REGIONAL VARIATIONS IN GRAIN SIZE AND SORTING

The diameters of 200 randomly chosen grain sections were measured in randomly chosen thin sections from the upper quartzite bed at each of 19 representative sites. These data were combined and plotted as five cumulative curves, each representing a segment of the miogeosyncline (fig. 6). Cumulative curves show relative grain size by their lateral position on the diagram—the farther to the right, the finer the grain. Sorting is shown by the slope of the straight parts of the curves—the steeper the slope, the better the sorting.

Grain size as shown by these size frequency curves tends to decrease progressively southward between western Canada and the Tooele arch (fig. 6*A*), south of which there is a slight increase in average size mainly due to a decreased proportion of fine grains (fig. 6*B*).

The diameters of the largest quartz grains at each site[1] show no systematic variation between central Idaho and southern California (Ketner, 1966, fig. 2). A few quartz grains observed in 270 thin sections from this area were as much as 1 millimeter in diameter. However, a similar study of 18 thin sections from Mount Wilson, Alberta (site 75), showed many grains with diameters greater than 1 mm, which tends to con-

[1] Determined by scanning thousands of grains in thin sections rather than by measuring diameters in a small random sample as was done in deriving the curves of figure 6.

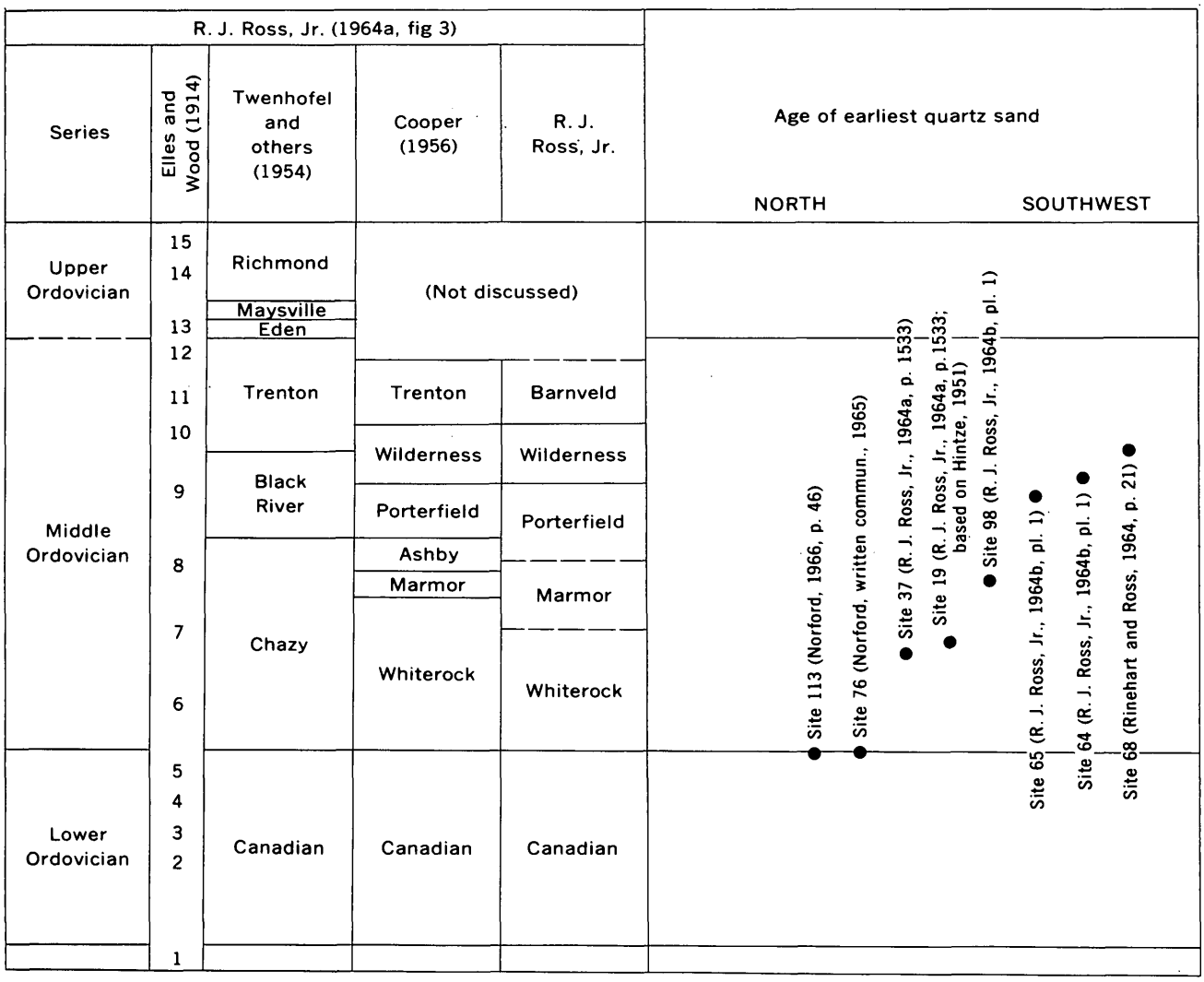

FIGURE 5.—Age of earliest quartz sand deposition, showing progressive shift to younger deposits from north to southwest.

firm the southerly trend toward finer size shown by cumulative curves (fig. 6).

Sorting of grains tends to improve southward and northward from Idaho (table 2), but the southerly trend is stronger.

ENVIRONMENT OF DEPOSITION

Abundant definite evidence of an aqueous and, specifically, a marine environment of deposition is opposed by local ambiguous evidence of subaerial conditions.

TABLE 2.—*Coefficients of sorting*[1] *derived from composite size frequency curves (fig. 6)*

Southern British Columbia and Alberta	1.34
Idaho	1.41
Northern Nevada and Utah	1.31
Central Nevada and Utah	1.26
Southern Nevada and California	1.22

[1] Perfect sorting is indicated by a coefficient of 1.00.

A marine environment of deposition is indicated by the common occurrence of limestone and dolomite lenses containing marine fossils within the quartzite sequence (Gilluly and Masursky, 1965, p. 18; Webb, 1958, p. 2339; Mansfield, 1927, p. 57; D. C. Ross, 1966, p. 19; R. J. Ross, Jr., 1964a, p. 1539); overlying and underlying formations are unquestionably marine, and the contact between underlying units and the quartzite is commonly gradational. Worm borings in all areas (Ketner, 1966, p. C55) and organic collophane along the eastern margin of the geosyncline (Mansfield, 1927, p. 57; R. J. Ross, Jr., 1964a, p. 1551) indicate an aqueous environment.

Opposed to a marine environment are uncommon examples of large-scale crossbeds possibly of subaerial origin (Gilluly and Masursky, 1965, p. 17) and frosted surfaces of quartz grains (Ketner, 1966, p. C59) which

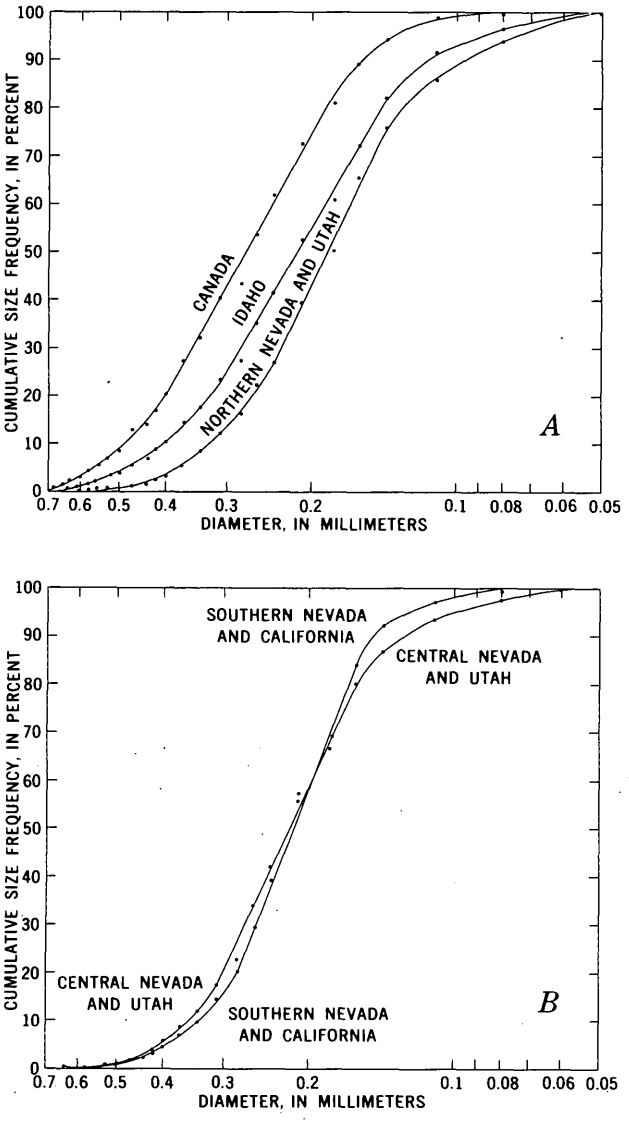

FIGURE 6.—Curves showing the cumulative size frequency distribution of diameters of quartz grain sections, Ordovician quartzite. *A*, each curve based on at least 600 measurements; *B*, each curve based on 1,000 measurements.

have been interpreted as being due to subaerial abrasion (Pettijohn, 1949, p. 58).

The quartzite is a shallow-water deposit. It cannot be a deep-water turbidite because it has none of the characteristic features of turbidites (Dzulynski and Walton, 1965). Crossbeds indicate strong currents which are likely to have been near-shore phenomena.

PROVENANCE AREAS

An adequate provenance of Ordovician quartzite must be a widespread, exposed quartz-bearing terrane, preferably of sandstone, having a viable connection with the miogeosyncline and a logical geographic position with respect to regional variations in the deposit. Features of six possible provenance areas are discussed here, but only the Peace River–Athabaska arch in northern Alberta adequately fulfills the requirements.

Cambrian rocks border the Cordilleran geosyncline on the east from central Alberta to Mexico (fig. 1). Generally the sequence includes basal sandstone, as much as 500 feet thick, and overlying shales and carbonate rocks. In most of the region—including southern Alberta, nearly all of Montana, eastern Utah, western Colorado, and much of Arizona—Cambrian carbonate rocks had not been breached in Ordovician time, and these areas therefore could not have supplied sand to the geosyncline. Moreover, large areas of this region were the sites of deposition in Middle Ordovician time and therefore were unlikely to be major source areas of Middle Ordovician sediments. These areas include (1) the Williston basin and connecting passages to the miogeosyncline through Wyoming where the Lander Sandstone Member of the Bighorn Dolomite was being deposited, (2) central Colorado where the Harding Sandstone was deposited, and (3) the cratonic basin whose western edge extended from Lake Superior to northwestern Mexico and where the St. Peter Sandstone, Simpson Group, and Cable Canyon Sandstone Member of the Montoya Dolomite were being deposited.

Cambrian rocks were uplifted and eroded away some time before Late Devonian time in (1) the Peace River–Athabaska arch of northern Alberta, (2) northwestern Montana and southwestern British Columbia, and (3) the Uinta uplift of northern Utah. The capacity of each these uplifts to supply quartz sand to the geosyncline is estimated, in the following discussion, on the assumption that it achieved its maximum uplift and erosion in Middle Ordovician time.

The Peace River–Athabaska arch of northern Alberta (deMille, 1958, p. 61) is a large positive area extending from the Canadian Shield to the Cordilleran geosyncline. The exact age of uplift is uncertain, but the area was high enough in Middle Cambrian time to slightly affect sedimentation patterns (Hees, 1959, p. 81 and figs. 2 and 5) and had become subdued by Middle Devonian time (deMille, 1958, fig. 5). Except for scattered residual Cambrian sand deposits, the Cambrian, Ordovician, and Silurian Systems are absent from the arch (Webb, 1954, figs. 3 and 4).

On the Peace River–Athabaska arch, about 150,000 square miles of Cambrian rocks was exposed to erosion. After removal of Cambrian shale and carbonate rocks, basal sandy rocks averaging 500 feet in thickness (Hees, 1966, p. 22) were eroded. On the assumption that quartz sand made up about three-fourths of the content of these sandy beds, the volume of sand removed was at least 10,000 cubic miles.

Sporadic remnants of Cambrian sands still preserved beneath Devonian strata suggest that erosion failed to penetrate Precambrian rocks to great depths. This is confirmed by the absence, in Ordovician rocks, of metamorphic minerals and compound grains. Loosely consolidated Cambrian sands may have been stripped off the metamorphic Precambrian basement by near-surface turbulence and sea currents with little or no exposure to subaerial erosion.

In northwest Montana and southeast British Columbia an area of about 10,000 square miles was elevated in Late Cambrian to Late Devonian time, and Cambrian rocks were eroded away. Because the basal Cambrian Flathead Sandstone thins rapidly toward the uplifted area (Theodosis, 1955, p. 66; Hees, 1959, p. 74), it is unlikely that the thickness of sandstone which overlay the uplift exceeded 50 feet. Thus the maximum possible volume of sand available from Cambrian rocks was about 100 cubic miles. Underlying Precambrian rocks of the Belt Series contain a negligible amount of sand in the uplifted area (Ross and Rezak, 1959, p. 436), and therefore could not have added a significant amount of sand to the total.

In the Uinta uplift of northern Utah, Mississippian rocks lie unconformably on Cambrian and Precambrian sandstones, sandy shale, and quartzite. On the assumptions that all of the pre-Mississippian erosion took place in Middle Ordovician time and that the present mountainous area roughly coincides with pre-Mississippian uplift, the maximum possible volume of quartz sand contributed to the Cordilleran geosyncline in Middle Ordovician time can be estimated. The maximum area of pre-Mississippian erosion of the Cambrian Tintic and Lodore Formations is about 2,000 square miles (Stokes and Madsen, 1961). If 330 feet is taken as the original average thickness (Lochman-Balk, 1955, p. 30), and if it is assumed that about half of this thickness was quartz sand (Kinney, 1955, p. 22), the volume of eroded Cambrian sand is about 60 cubic miles.

In the 2,000-square-mile area of the Uinta uplift that was stripped of Cambrian rocks before Mississippian time, Precambrian shales and quartzites were eroded to various depths. Before Mississippian time, the Red Pine Shale of Williams (1953), the topmost formation of the Precambrian, was not significantly eroded in the west half of the area, but Precambrian quartzite was eroded to depths ranging from 0 to 5,000 feet in the east half of the area (Hansen, 1965, p. 148). If the average depth of erosion in the east half of the area is 2,500 feet, then about 500 cubic miles of Precambrian rocks was removed, or 400 cubic miles of sand, assuming that one-fifth of the rocks was shale. The maximum volume of sand eroded from the Uinta uplift before Mississippian time, from the combined Cambrian and Precambrian sources, is thus about 460 cubic miles.

Northern Idaho has been suggested as a possible source of Ordovician quartizite. It seems unlikely that this area could have been a major provenance for the following reasons: (1) Central Idaho was the site of deposition of a full thickness of Ordovician quartzite including basal dolomitic beds (sites 55 and 56), and the lithology of this quartzite gives no hint of proximity to a source area; impure, coarse-grained quartzite exposed near site 56 is of pre-Ordovician age according to recent work by S. W. Hobbs and W. H. Hays of the U.S. Geological Survey (oral commun., 1967). (2) The Ledbetter Slate (Park and Cannon, 1943) of northern Washington and the Phi Kappa Formation of central Idaho (Umpleby and others, 1930) show little evidence, in the form of immature deposits, of proximity to an uplifted area. (3) Ordovician sediments are absent from western Montana immediately east of the postulated provenance area. (4) Belt Series rocks which must underlie the postulated provenance area are composed predominantly of silt- and clay-sized material, not sand-sized quartz.

The area near Hudson Bay, Canada, may have contributed sand to the Cordilleran geosyncline by way of the Williston basin. However, this area seems unlikely to have been an important provenance of Cordilleran quartzite because the eastern edge of the geosyncline tended to remain high relative to the Williston basin (fig. 1) and probably restricted the westward flow of sand. Ordovician rocks deposited in a marine passageway between the Williston basin and the geosyncline in western Wyoming and adjacent parts of Idaho are quartz-free carbonate (W. R. Keefer, oral commun., 1967; Staatz and Albee, 1966).

Although eugeosynclinal quartzite may have been derived from west of the geosyncline (Ketner, 1966), it is unlikely that a westerly source has provided sand to both the eugeosyncline and the miogeosyncline because of the following factors: (1) Eugeosynclinal quartzite does not merge into sand of the miogeosyncline. Rather, from a point of maximum thickness near the type locality of the Valmy Formation (Roberts, 1964, p. 18) it pinches out in the more easterly Vinini and Phi Kappa Formations short of the miogeosyncline. (2) Miogeosynclinal quartzite wedges out westward short of the eugeosyncline (fig. 3). (3) The eugeosyncline probably lay at a lower level than the miogeosyncline, which prevented sediments from being carried eastward. Briefly, the evidence for this last factor is in the nature of eugeosynclinal sediments which are carbo-

naceous and finely laminated and which lack carbonates and bottom-dwelling organisms. Stagnant conditions over an area of thousands of square miles implied by these characteristic features can be accounted for most easily by postulating a cover of very deep water.

CONCLUSION

Almost all the sand composing Ordovician quartzite of the Cordilleran miogeosyncline was derived from Cambrian sandstone eroded from the Peace River–Athabaska arch. The evidence for this, as is summarized from the foregoing discussions, is (1) the presence of an adequate source of quartz in northern Alberta and the apparent absence elsewhere of adequate sources, (2) the progressively decreasing age of basal quartzite beds from north to south, (3) the southerly decreasing thickness and increasing width of the deposit, (4) the southerly decreasing grain size, and (5) the southerly trend toward improved sorting.

REFERENCES

Albers, J. P., and Stewart, J. H., 1965, Preliminary geologic map of Esmeralda County, Nevada: U.S. Geol. Survey Mineral Inv. Field Studies Map MF-298.

Cooper, G. A., 1956, Chazyan and related brachiopods [U.S.-Canada]: Smithsonian Misc. Colln., v. 127, pt. 1, p. 1–1024; pt. 2, plates, p. 1025–1245.

Cornwall, H. R., and Kleinhampl, F. J., 1961, Geology of the Bare Mountain quadrangle, Nevada: U.S. Geol. Survey Geol. Quad. Map GQ–157.

Dapples, E. C., 1955, General lithofacies relationship of St. Peter sandstone and Simpson group: Am. Assoc. Petroleum Geologists Bull., v. 39, no. 4, p. 444–467.

Decker, R. W., 1962, Geology of the Bull Run quadrangle, Elko County, Nevada: Nevada Bur. Mines Bull. 60, 65 p.

deMille, George, 1958, Pre-Mississippian history of the Peace River Arch, *in* Scott, J. C., ed., Symposium on the Peace River Arch: Alberta Soc. Petroleum Geologists Jour., v. 6, no. 3, p. 61–68.

Dzulynski, Stanislaw, and Walton, E. K., 1965, Sedimentary features of flysch and greywackes: New York, American Elsevier Publishing Co., 274 p.

Elles, G. L., and Wood, E. M. R., 1914, A monograph of British graptolites, pt. 10: Paleont. Soc. Pub., v. 67, p. 487–526, pls. 50–52.

Felix, C. E., 1956, Geology of the eastern part of the Raft River Range, Box Elder County, Utah, *in* Utah Geol. Soc. Guidebook to the geology of Utah: no. 11, p. 76–97.

Ferguson, H. G., 1924, Geology and ore deposits of the Manhattan district, Nevada: U.S. Geol. Survey Bull. 723, 163 p.

Ferguson, H. G., and Muller, S. W., 1949, Structural geology of the Hawthorne and Tonopah quadrangles, Nevada: U.S. Geol. Survey Prof. Paper 216, 55 p.

Gilluly, James, and Gates, Olcott, 1965, Tectonic and igneous geology of the northern Shoshone Range, Nevada, *with sections on* Gravity in Crescent Valley, by Donald Plouff, *and* Economic geology, by K. B. Ketner: U.S. Geol. Survey Prof. Paper 465, 153 p.

Gilluly, James, and Masursky, Harold, 1965, Geology of the Cortez quadrangle, Nevada, *with a section on* Gravity and aeromagnetic surveys,, by D. R. Mabey: U.S. Geol. Survey Bull. 1175, 117 p.

Hague, Arnold, 1883, Geology of the Eureka district, Nevada: U.S. Geol. Survey 3d Ann. Rept., p. 237–290.

Hansen, W. R., 1965, Geology of the Flaming Gorge area, Utah-Colorado-Wyoming: U.S. Geol. Survey Prof. Paper 490, 196 p.

Hees, Hendrik van, 1959, Middle Cambrian of the southern Alberta Plains, *in* Alberta Soc. Petroleum Geologists 9th Ann. Field Conf., Sept. 1959: p. 73–85.

———1966, Cambrian of the plains, *in* Geological history of western Canada: Alberta Soc. Petroleum Geologists, Canadian Sed. Basins Symposium, chap. 3, pt. 1, p. 20–28.

Hintze, L. F., 1951, Lower Ordovician detailed stratigraphic sections for western Utah: Utah Geol. and Mineralog. Survey Bull. 39, 100 p.

Hotz, P. E., and Willden, Ronald, 1964, Geology and mineral deposits of the Osgood Mountains quadrangle, Humboldt County, Nevada: U.S. Geol. Survey Prof. Paper 431, 128 p.

Irish, E. J. W., 1963, Halfway River, British Columbia: Canada Geol. Survey Map 22–1963.

Kay, Marshall, 1960, Paleozoic continental margin in central Nevada, western United States: Internat. Geol. Cong., 21st, Copenhagen, 1960, Rept., pt. 12, p. 94–103.

Kay, Marshall, and Crawford, J. P., 1964, Paleozoic facies from the miogeosynclinal to the eugeosynclinal belt in thrust slices, central Nevada: Geol. Soc. America Bull., v. 75, no. 5, p. 425–454.

Ketner, K. B., 1966, Comparison of Ordovician eugeosynclinal and miogeosynclinal quartzites of the Cordilleran geosyncline, *in* Geological Survey Research 1966: U.S. Geol. Survey Prof. Paper 550–C, p. C54–C60.

Kinney, D. M., 1955, Geology of the Uinta River–Brush Creek area, Duchesne and Uinta Counties, Utah: U.S. Geol. Survey Bull. 1007, 185 p.

Kirk, Edwin, 1933, The Eureka quartzite of the Great Basin region: Am. Jour. Sci., 5th ser., v. 26, no. 151, p. 27–44.

Lochman-Balk, Christina, 1955, Cambrian stratigraphy of the south and west margins of Green River Basin [Utah-Wyo.], *in* Wyoming Geol. Assoc. Guidebook 10th Ann. Field Conf., 1955: p. 29–37.

Mansfield, G. R., 1927, Geography, geology, and mineral resources of part of southeastern Idaho: U.S. Geol. Survey Prof. Paper 152, 453 p.

Merriam, C. W., 1963a, Paleozoic rocks of Antelope Valley, Eureka and Nye Counties, Nevada: U.S. Geol. Survey Prof. Paper 423, 67 p.

———1963b, Geology of the Cerro Gordo mining district, Inyo County, California: U.S. Geol. Survey Prof. Paper 408, 83 p. [1964].

Morris, H. T., and Lovering, T. S., 1961, Stratigraphy of the East Tintic Mountains, Utah: U.S. Geol. Survey Prof. Paper 361, 145 p.

Nolan, T. B., 1935, The Gold Hill mining district, Utah: U.S. Geol. Survey Prof. Paper 177, 172 p.

Nolan, T. B., Merriam, C. W., and Williams, J. S., 1956, The stratigraphic section in the vicinity of Eureka, Nevada: U.S. Geol. Survey Prof. Paper 276, 77 p.

Norford, B. S., 1964, Reconnaissance of the Ordovician and Silurian rocks of northern Yukon Territory: Canada Geol. Survey Paper 63–69, 139 p.

Norford, B. S., 1966, Ordovician-Silurian of the Cordillera, *in* Geological history of western Canada: Alberta Soc. Petroleum Geologists, Canadian Sed. Basins Symposium, chap. 4, pt. 2, p. 42–48.

North, F. K., and Henderson, G. G. L., 1954, Summary of the geology of the southern Rocky Mountains of Canada, *in* Alberta Soc. Petroleum Geologists Guidebook 4th Ann. Field Conf.: p. 15–81.

Park, C. F., Jr., and Cannon, R. S., Jr., 1943, Geology and ore deposits of the Metaline quadrangle, Washington: U.S. Geol. Survey Prof. Paper 202, 81 p.

Pettijohn, F. J., 1949, Sedimentary rocks: New York, Harper & Bros., 526 p.

Richardson, G. B., 1913, The Paleozoic section in northern Utah: Am. Jour. Sci., 4th ser., v. 36, p. 406–416.

Rigby, J. K., 1958, Geology of the Stansbury Mountains, eastern Tooele County, Utah, *in* Utah Geol. Soc. Guidebook to the geology of Utah: no. 13, p. 1–134.

Rinehart, C. D., and Ross, D. C., 1964, Geology and mineral deposits of the Mount Morrison quadrangle, Sierra Nevada, California, *with a section on* A gravity study of Long Valley, by L. C. Pakiser: U.S. Geol. Survey Prof. Paper 385, 106 p.

Roberts, R. J., 1964, Stratigraphy and structure of the Antler Peak quadrangle, Humboldt and Lander Counties, Nevada: U.S. Geol. Survey Prof. Paper 459–A, 93 p. [1965].

Ross, C. P., 1934, Correlation and interpretation of Paleozoic stratigraphy in south-central Idaho: Geol. Soc. America Bull., v. 45, no. 5, p. 937–1000.

———1937, Geology and ore deposits of the Bayhorse region, Custer County, Idaho: U.S. Geol. Survey Bull. 877, 161 p. [1938].

Ross, C. P., and Rezak, Richard, 1959, The rocks and fossils of Glacier National Park [Mont.]—the story of their origin and history: U.S. Geol. Survey Prof. Paper 294–K, p. 401–439.

Ross, D. C., 1966, Stratigraphy of some Paleozoic formations in the Independence quadrangle, Inyo County, California: U.S. Geol. Survey Prof. Paper 396, 64 p.

Ross, R. J., Jr., 1949, Stratigraphy and trilobite faunal zones of the Garden City formation, northeastern Utah: Am. Jour. Sci., v. 247, no. 7, p. 472–491.

———1951, Stratigraphy of the Garden City formation in northeastern Utah, and its trilobite faunas: Yale Univ., Peabody Mus. Nat. History Bull. 6, 161 p.

———1953, The Ordovician system in northeastern Utah and southeastern Idaho, *in* Intermountain Assoc. Petroleum Geologists Guidebook 4th Ann. Field Conf., 1953: p. 22–26.

Ross, R. J., Jr., 1964a, Relations of Middle Ordovician time and rock units in Basin Ranges, Western United States: Am. Assoc. Petroleum Geologists Bull., v. 48, no. 9, p. 1526–1554.

———1964b, Middle and Lower Ordovician formations in southernmost Nevada and adjacent California: U.S. Geol. Survey Bull. 1180–C, p. C1–C101.

Staatz, M. H., and Albee, H. F., 1966, Geology of the Garns Mountain quadrangle, Bonneville, Madison, and Teton Counties, Idaho: U.S. Geol. Survey Bull. 1205, 122 p.

Staatz, M. H., and Carr, W. J., 1964, Geology and mineral deposits of the Thomas and Dugway Ranges, Juab and Tooele Counties, Utah: U.S. Geol. Survey Prof. Paper 415, 188 p.

Stewart, J. H., 1967, Newly discovered window in the Roberts thrust, Toiyabe Range, central Nevada—the Callaghan Window [abs.]: Geol. Soc. America 63d Ann. Mtg., Program, p. 63.

Stokes, W. L., and Madsen, J. H., Jr., compilers, 1961, Geologic map of Utah, northeast quarter: Utah Geol. and Mineralog. Survey.

Theodosis, S. D., 1955, Cambrian system in northwestern Montana, *in* Billings Geol. Soc. Guidebook 6th Ann. Field Conf., Sept. 1955: p. 64–69.

Twenhofel, W. H., chm., and others, 1954, Correlation of the Ordovician formations of North America: Geol. Soc. America Bull., v. 65, no. 3, p. 247–298.

Umpleby, J. B., Westgate, L. G., and Ross, C. P., 1930, Geology and ore deposits of the Wood River region, Idaho: U.S. Geol. Survey Bull. 814, 250 p.

Walcott, C. D., 1924, Cambrian geology and paleontology, V; No. 1, Geological formations of Beaverfoot-Brisco-Stanford Range, British Columbia, Canada: Smithsonian Misc. Colln., v. 75, no. 1, p. 1–51.

Webb, G. W., 1956, Middle Ordovician detailed stratigraphic sections for western Utah and eastern Nevada: Utah Geol. and Mineralog. Survey Bull. 57, 77 p.

———1958, Middle Ordovician stratigraphy in eastern Nevada and western Utah: Am. Assoc. Petroleum Geologists Bull., v. 42, no. 10, p. 2335–2377.

Webb, J. B., 1954, Geological history of plains of western Canada, *in* Clark, L. M., ed., Western Canada sedimentary basin—a symposium: Am. Assoc. Petroleum Geologists. Ralph Leslie Rutherford Memorial Volume: p. 3–28.

Williams, N. C., 1953, Late pre-Cambrian and early Paleozoic geology of western Uinta Mountains, Utah: Am. Assoc. Petroleum Geologists Bull., v. 37, no. 12, p. 2734–2742.

Young, J. C., 1955, Geology of the southern Lakeside Mountains, Utah: Utah Geol. and Mineralog. Survey Bull. 56, 116 p.

DARK-MINERAL ACCUMULATIONS IN BEACH AND DUNE SANDS OF CAPE COD AND VICINITY [1]

By JAMES V. A. TRUMBULL and JOHN C. HATHAWAY,
Woods Hole, Mass.

Abstract.—Accumulations of dark minerals were observed along 23 percent of the shoreline of Cape Cod and vicinity on January 23–24, 1967. The largest single accumulation observed was only 15 cm thick and 6 by 20 m in area. Streams are not effective concentrating agents in the area studied. Wind is an effective agent, but the largest accumulations of dark minerals are wave caused and occur where the largest amounts of sand are in transport along the beach. More dark-mineral accumulations originate from outwash than from till. Material from coastal-plain sediments may form a significant part of the glacial deposits in areas of abundant accumulations.

Dark-mineral accumulations on a portion of the Massachusetts coast were observed January 23–24, 1967, and their location, extent, and relative concentration were mapped (fig. 1). The area examined includes the shorelines of Cape Cod, Monomoy Island, the Elizabeth Islands except Penikese, and the mainland north of Cape Cod as far as Scituate. The entire shoreline shown by the solid line on figure 1 was flown by helicopter at heights usually less than 30 meters and at a usual speed of 100 kilometers per hour. Landings were made at 25 places, and 10 additional sites were later visited on the ground.

Observations of beaches from a helicopter allowed us to detect even very slight dark-mineral concentrations in the surface layer; we estimate that a concentration of 5 percent or more dark minerals was detectable. We had no difficulty distinguishing darkening associated with greater than usual grain size (and the accompanying increase in dark rock fragments) or darkening caused by organic layers, films, or encrustations. Many places, however, that seemed to show very light dustings of dark minerals below the berm were actually areas of greater than usual moisture content.

By this method 255 km (160 miles) of shoreline was covered in 6 hours of flying each day. This included time for an average of 12 landings a day to examine the beach, for departures from the coast for refueling, and for transit to and from an inland airport.

A similar study of the distribution of coastal dark-mineral accumulations in North Carolina, South Caroline, and Georgia had been made earlier by McKelvey and Balsley (1948), using a fixed-wing aircraft. They concluded that the distribution of accumulations in those areas was related to the configuration of the shoreline.

The present report concerns field observations only. Mineralogical information on the samples will be reported separately if it proves to be of sufficient interest.

We thank Robert G. Weeks, pilot, Woods Hole Oceanographic Institution, for technical advice and logistic support, and John Connelly, helicopter pilot, for skillful piloting and enthusiastic assistance.

NATURE OF DARK-MINERAL ACCUMULATIONS

In the present study, accumulations of dark minerals were observed along about 23 percent, or 120 km (74 statute miles) of the total of 515 km (320 statute miles), of shoreline shown on the map. Relative con-

[1] Contribution No. 1944 of the Woods Hole Oceanographic Institution.

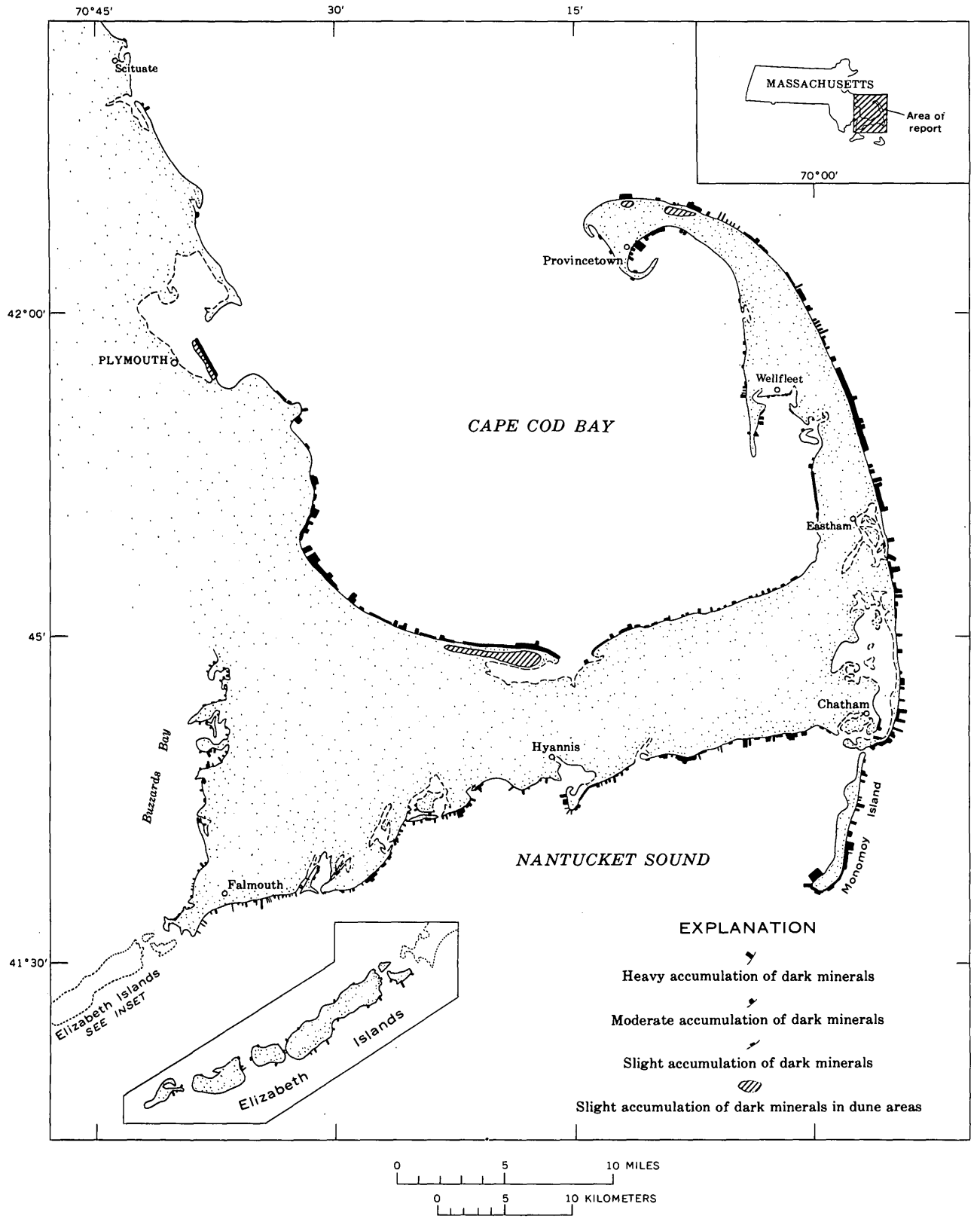

FIGURE 1.—Map of the beaches of Cape Cod and vicinity, showing distribution of observed dark-mineral accumulations as of January 23 and 24, 1967. That part of the shoreline shown by dashed line was not surveyed.

centrations of the dark-mineral accumulations along the total length of coastline are shown below:

Estimated concentration of dark minerals in surface layer of accumulations	*Distance*		*Percentage of total shoreline*
	Km	*Miles*	
Heavy (50 percent)	20	12	3.9
Moderate (10 to 50 percent)	47	29	9.1
Slight (10 percent)	53	33	10.3
None present	395	246	76.7
Total	515	320	100.0

Moderate and heavy accumulations were widely distributed. The accumulations of greatest linear extent were about 8 km (5 miles) long. Width of accumulations in the direction normal to the shoreline rarely exceeded 10 m and was commonly much less, except where wind-caused accumulations were thinly spread over dunes or sand flats behind the beach proper.

Roughly half the accumulations were caused by wave action and half by wind action. Wave-caused accumulations had thicker individual dark-mineral strata and more such strata in the top 25 centimeters of section than wind-caused accumulations. Characteristic wave-caused accumulations had dark strata 3 to 10 millimeters thick, several such strata being in the upper 10 to 20 cm of section, as in figure 2. The maximum observed thickness of a single stratum of dark minerals was 15 cm, at Coast Guard Beach, Eastham; it covered an area 6 by 20 m. Few moderate and heavy accumulations exceeded 100 m in length, though some, especially on the east-facing beach of the outer Cape, were considerably longer.

Wave-caused accumulations were found mostly near the storm high-water mark; figure 3 shows a typical occurrence. Some accumulations were on the foreshore. Few accumulations were on the berm crest itself, and none that we detected was seaward of the plunge line at the time of observation. The few wave-caused accumulations revisited after 6 days were being dissipated by wave action.

Wind-caused dark strata rarely exceeded a few millimeters in thickness (see figs. 4 and 5), and tended to be separated by 25 cm or more of barren sand. The most common type of wind-caused accumulation was a long, narrow (3 m or less) strip of slight to moderate concentration at the extreme upper beach, just at the base of the dune, cliff, or wall that limits the beach. Except for the outer beaches of Cape Cod, the coast in the areas studied has many groins, roughly 100 m apart and 50 to 80 m long. We observed many accumulations in the triangular accretion areas at the groins;

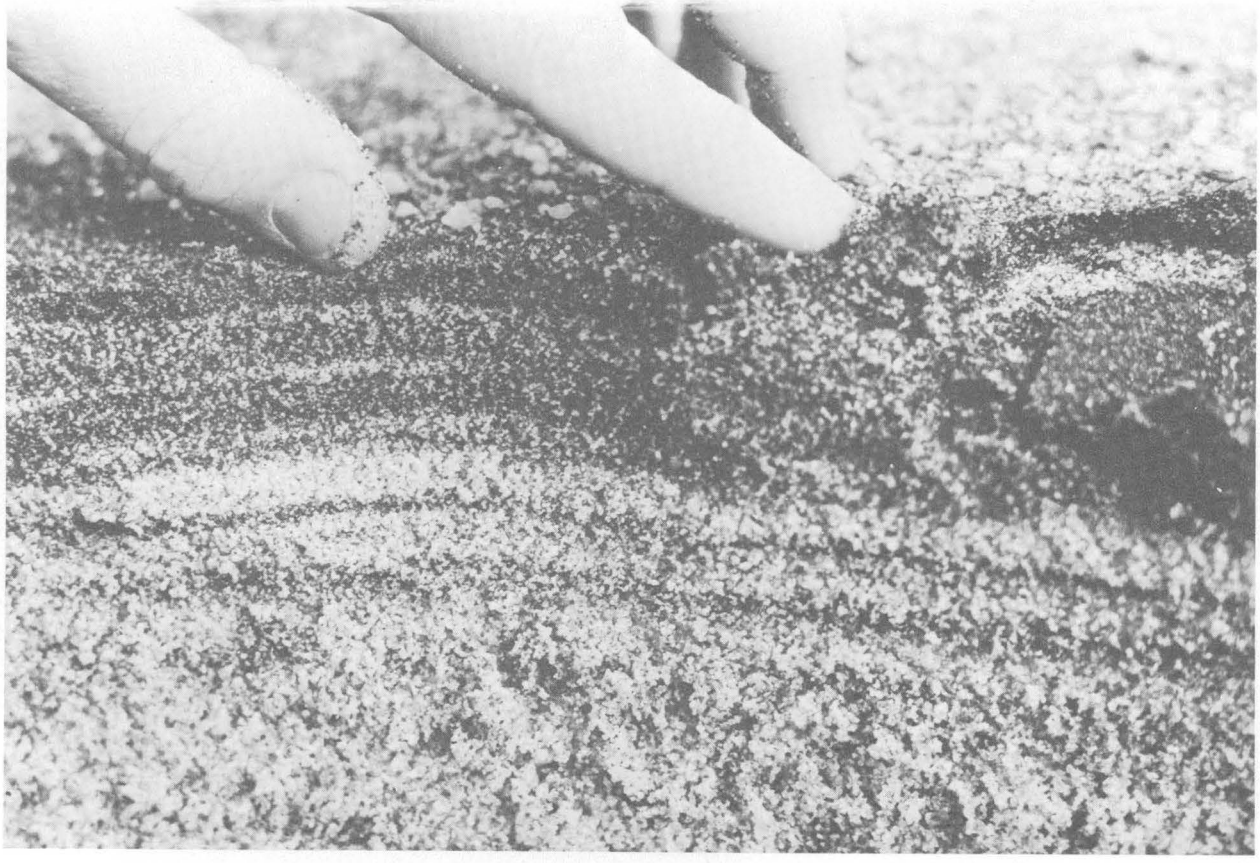

FIGURE 2.—Closeup view of typical wave-caused dark-mineral accumulation. Nauset Beach near Chatham.

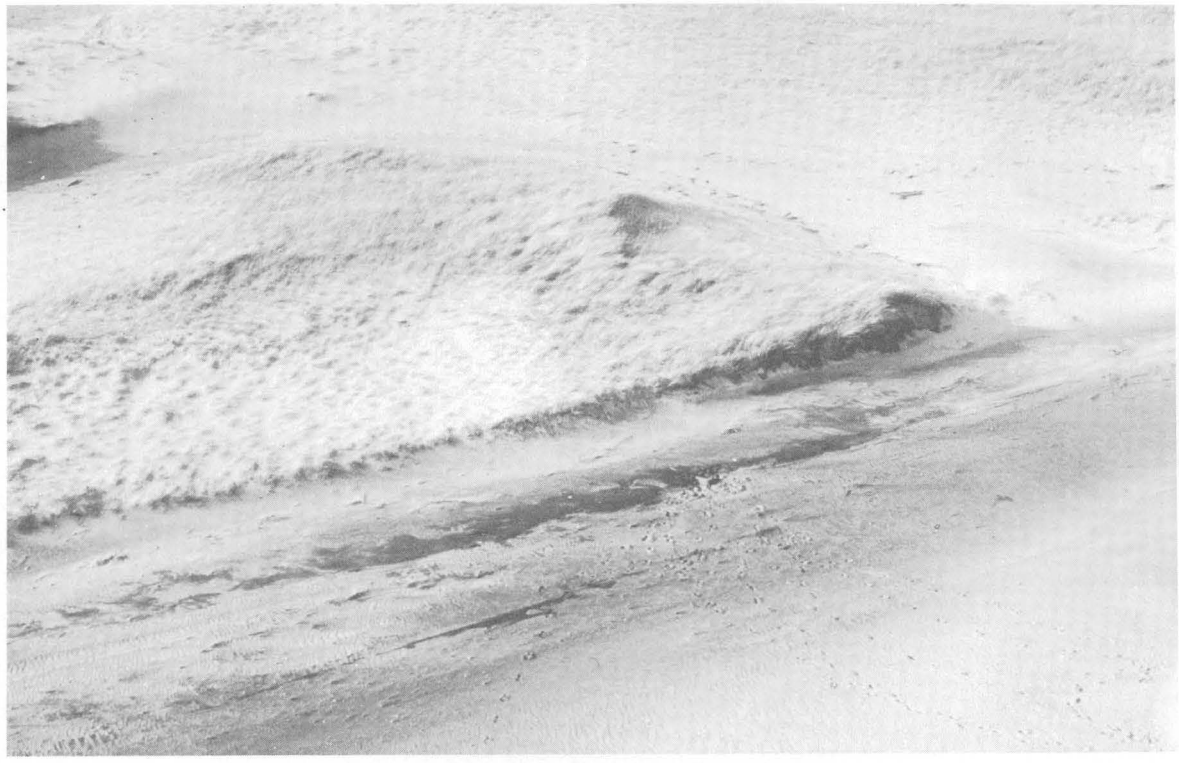

FIGURE 3.—General view of typical occurrence of wave-caused dark-mineral accumulation. East side of Monomoy Island; sea is toward lower right. Human footprints give scale.

most of these accumulations seemed to be caused by wind.

Some dunes, notably the large active ones near Provincetown, had outcrops of dark strata on their tops and sides. Both dune fields and flat sand areas behind the beach commonly had a light dusting of dark grains.

Some storm scarps at the upper edges of beaches contained several dark-mineral strata. These strata were usually thin and seemed to be caused by wind.

Nearly all accumulations examined on the ground had one or more dark strata beneath the one on the surface. This suggests that dark minerals tend to accumulate repeatedly in the same place, at least during a rather short period of time.

The factors controlling the specific location of dark-mineral concentrations within a local area were commonly not apparent to us.

The color of the accumulations shows some relation to general area. Many of the accumulations on the southeastern corner of Cape Cod and on Monomoy Island are a garnetlike purplish red, as are several accumulations on the outer arm of the Cape. Accumulations on the mainland beaches north of Cape Cod and on the western part of the Cape are generally blacker than elsewhere. The color characteristics suggest differences in parent material, or perhaps mineralogical differentiation during concentration.

No information is yet available on possible seasonal differences in occurrence of dark-mineral accumulations. The information in this report is based on the synoptic situation on the dates of the field observations.

RELATIONS BETWEEN ACCUMULATIONS AND PARENT MATERIAL

No clear-cut principles governing the location of dark-mineral accumulations are evident, nor does any strong relationship between accumulations and parent material emerge, but a few generalizations can be made.

The 18 km (11 statute miles) of coast at the northwest end of the survey area is formed on both crystalline bedrock and glacial till. The beach sediments of this area are predominantly cobbles; the few sand beaches are nearly lacking in dark-mineral accumulations. Long sand beaches from that area south to Plymouth are probably derived from the same material and are also notably poor in dark-mineral accumulations. It is not clear why dark-mineral accumulations are so sparse north of Plymouth. It may be significant, however, that the only two areas of Cape Cod whose beaches are derived directly from glacial till are also

FIGURE 4.—Typical wind-caused dark-mineral accumulation in dunes developed on barrier beach. Plymouth Beach; sea is toward lower left, Plymouth Harbor is in background. Automobile tracks give scale.

deficient in dark-mineral accumulations. These areas are the western or Buzzards Bay shore of Cape Cod and the shores of the Elizabeth Islands.

The beaches and dunes of the remainder of Cape Cod and of Monomoy Island are formed largely from glacial outwash material, though till contributes material in some places, and interglacial deposits are present in the eroding cliffs of the outer (east-facing) Cape. The greatest concentrations of dark minerals are in the outer Cape beaches and their continuation on Monomoy Island, and in some parts of the beaches adjoining Nantucket Sound. Beaches derived primarily from outwash thus seem to have more accumulations of dark minerals than those derived primarily from till.

All beaches in the area are derived primarily from the erosion of glacial deposits. These deposits in turn were derived from the terrain over which the glaciers passed. For some parts of the Cape this terrain may have included Tertiary coastal-plain sediments, inasmuch as Eocene material has been reported from the northern part of outer Cape Cod (Zeigler and others, 1960) and from Third Cliff at Scituate on the coast north of Cape Cod (Chute, 1965). If the coastal-plain sediments already contained accumulations of dark minerals, then glacial materials incorporating large amounts of such sediments would provide a ready source for further concentration. The scarcity of accumulations north of Plymouth suggests that the older crystalline bedrock terrain provided a poor source of dark minerals. In turn, the predominance of dark-mineral accumulations in the outer Cape area may be the result of large amounts of coastal-plain sediments in the glacial drift. Although coastal-plain Cretaceous clay occurs on Nonamessett Island of the Elizabeth Island chain (Woodworth and Wigglesworth, 1934), the proximity of these islands to the older crystalline rocks across Buzzards Bay probably results in a dominance of debris from these crystalline rocks rather than from coastal-plain sediments in the Elizabeth Islands area. This, together with the lack of glacial outwash, could account for the scarcity of dark-mineral concentrations on the Elizabeth Islands and the Buzzards Bay shore of Cape Cod.

FIGURE 5.—Closeup view of typical moderate wind-caused dark-mineral accumulation in dunes. Plymouth Beach.

RELATIONS BETWEEN ACCUMULATIONS AND GEOLOGIC PROCESSES

The outer Cape and Monomoy Island beaches are in general the areas where the greatest volumes of sand are being transported. The beaches of Cape Cod facing Cape Cod Bay do not have such large volumes of sand in transport and do not have such heavy accumulations of dark minerals. Volume of sand being transported may thus be another factor related to accumulation of dark minerals. South of Plymouth the areas of largest and most closely spaced accumulations tend to be on shores that are normal to the northeast quadrant, the direction of approach of the largest waves (Giese, 1964). The northwest-facing beaches of Cape Cod Bay tend to be protected by extensive offshore shoals. Concentration of dark minerals cannot be related entirely to intensity of wave action, because some moderate to heavy dark-mineral accumulations occur on relatively protected shores such as Provincetown Harbor, Chatham Harbor, Wellfleet Harbor, and parts of the Buzzards Bay shore.

Correlation is poor between dark-mineral accumulations and the type of beach, whether long low barrier beach or beaches at the foot of eroding cliffs.

Streams are not important sources of coastal sediments in this area, and aerial observations revealed no dark-mineral concentrations in the lower courses of streams.

Because no part of Cape Cod lies more than about 9 km from open salt water, and the Cape is underlain primarily by highly permeable unconsolidated sandy deposits, streams are poorly developed. Longer streams discharge to the ocean along the mapped mainland coast, but, as with the smaller streams of the Cape, their lower reaches are tidal estuaries. They seem to deliver only particles of silt and clay size to the ocean, and particles of these sizes do not in general occur on the relatively high-energy beaches of the area. We feel that the streams of the area are too small, flow is at too low a gradient, and most of the streams have courses too stabilized by vegetation to have formed concentrations of dark minerals.

SUMMARY

The two-day investigation resulted in a synoptic view under winter conditions of the distribution and relative concentration of dark-mineral accumulations visible at the surface.

Dark-mineral accumulations were observed along about 23 percent of the shoreline. Roughly half the accumulations were wave caused and half were wind caused, but the wave-caused ones had more and thicker dark-mineral strata. Individual dark-mineral strata were commonly 3 to 10 mm thick; the thickest seen was 15 cm. Accumulations were usually not greater than 10 by 100 m in area, except for widespread but light accumulations in dune and sand-flat areas. No accumulations were seen on flats or bars seaward of the plunge line.

Where one dark-mineral stratum occurred, more were usually present, suggesting that certain sites favor accumulation as time passes. Orientation of a beach relative to the direction of approach of the largest waves seems to be a factor in some, but not in all, areas. Correlation between amount of dark-mineral accumulations and beach type is poor. Subtle details of topography seem to control the location of accumulations within a local area.

No controls of localization or relations to parent material are obvious, but we suggest three general principles: (1) Beaches formed directly from glacial till seem to have fewer and smaller dark-mineral accumulations than beaches formed from predominantly outwash material. (2) The glacial deposits in areas of abundant dark-mineral accumulations may incorporate more coastal-plain material than those in areas with fewer accumulations. (3) Beaches on which a large volume of sand is being transported seem to have more dark-mineral accumulations than beaches on which less sand is being transported.

REFERENCES

Chute, N. E., 1965, Geologic map of the Scituate quadrangle, Plymouth County, Massachusetts: U.S. Geol. Survey Geol. Quad. Map GQ 497, scale 1:24,000.

Giese, G. S., 1964, Coastal orientations of Cape Cod Bay: Univ. Rhode Island, Master's thesis, 70 p.

McKelvey, V. E., and Balsley, J. R., Jr., 1948, Distribution of coastal black-sands in North Carolina, South Carolina, and Georgia, as mapped from an airplane: Econ. Geology, v. 43, no. 6, p. 518–524.

Woodworth, J. B., and Wigglesworth, Edward, 1934, Geography and geology of the region including Cape Cod, the Elizabeth Islands, Nantucket, Martha's Vineyard, No Mans Land, and Block Island: Harvard Univ. Mus. Comp. Zoology Mem. 52, 332 p.

Zeigler, J. M., Hoffmeister, W. S., Giese, G. S., and Tasha, Herman, 1960, Discovery of Eocene sediments in subsurface of Cape Cod: Science, v. 132, no. 3437, p. 1397–1398.

SKETCH MAP SERIES FOR ANTARCTICA

By WILLIAM R. MacDONALD, Washington, D.C.

Abstract.—Shaded-relief sketch maps of areas in Antarctica at 1:500,000 scale, compiled from tricamera photographs, are furnishing valuable basic source data needed for long-range scientific programing, logistic coordination, geodetic control, and other U.S. Antarctic Research Program activities. Maps of this new series are prepared to provide data until 1:250,000-scale reconnaissance maps of the same areas can be published. The conventional procedures were simplified to produce relatively inexpensive but comprehensive maps.

The U.S. Geological Survey has the primary responsibility for producing maps needed to support scientific investigations of the U.S. Antarctic Research Program (USARP). Activities are funded by the National Science Foundation, which determines the priorities and level of Antarctic mapping operations. The current mapping is aimed at producing 1:250,000-scale reconnaissance topographic maps for the mountainous areas of Antarctica between long 15° E. westward to long 158° E., excluding the Antarctic Peninsula north of lat 68° S. Two hundred sixty three maps at the 1:250,000 scale may be required during the next decade to meet the National Science Foundation's long-range mapping needs for scientific exploration of Antarctica, and to furnish source material for updating air navigation charts required by U.S. Navy air support personnel. Of these 263 maps, 34 are published and 36 are programed for publication by 1970.

SKETCH MAP TO PROVIDE INTERIM DATA

The most recent answer to the increasing demand for maps of Antarctica is a series of shaded-relief sketch maps at 1:500,000 scale. This series is intended to provide map data during the period between the time that aerial photography of an area is obtained and the time (about 4 to 5 years later) when the 1:250,000-scale maps of the same area are published. This delay is due to a combination of the following factors: (1) lack of complete field control at the time photography is acquired, (2) the need for flying photographic fill lines for 1:250,000-scale compilation, (3) the normal process of map compilation and reproduction, (4) delays in getting international agreement on Antarctic place names, (5) lack of logistic support for immediate field control operations, and (6) the amount of available funds for mapping.

The time lag in obtaining map data has existed for several years in Antarctica. However, after the ski-equipped C–130 Hercules airplane and the UH–1B helicopters were introduced into Antarctic operations, demands for mapping increased and the lag became serious. The scientific exploration program was accelerated as parties were airlifted by the C–130's to base camps in remote areas years ahead of previous plans. The versatility of the UH–1B's eliminated most of the transportation problem associated with field operations and allowed the scientific field parties to accomplish in a single season what previously would have taken years. Thus it became obvious that map requirements for field parties could no longer be satisfied by furnishing copies of planimetric manuscript bases at 1:50,000 scale, a normal byproduct of the 1:250,000-scale map compilation process.

To solve the pressing map-data problem, the Geological Survey compiled a 1:500,000-scale experimental sketch map of the northern coast of Victoria Land. The results were promising, and the area was enlarged to include all of Victoria Land north of lat 73° S.—approximately 50,000 square miles. Because of the additional time and money that would have been required to show contours, they were omitted. Inasmuch as many USARP scientists and pilots were unable to read the planimetric symbolization (fig. 1) without considerable study, shaded-relief was added to facilitate map use (fig. 2).

U.S. GEOL. SURVEY PROF. PAPER 600-B, PAGES B185-B189

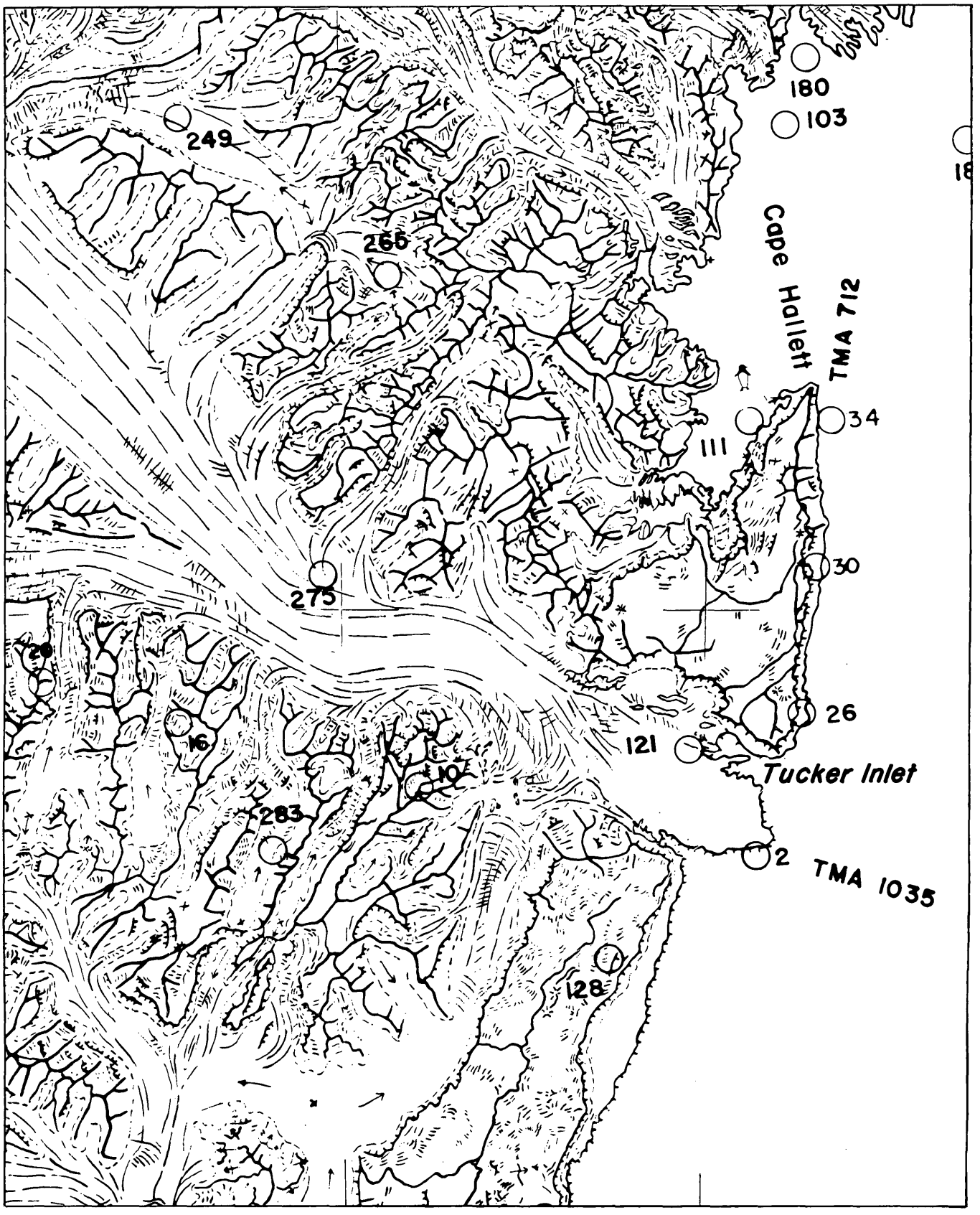

FIGURE 1.—Planimetric sketch map of an area in Antarctica. Scale 1 : 500,000.

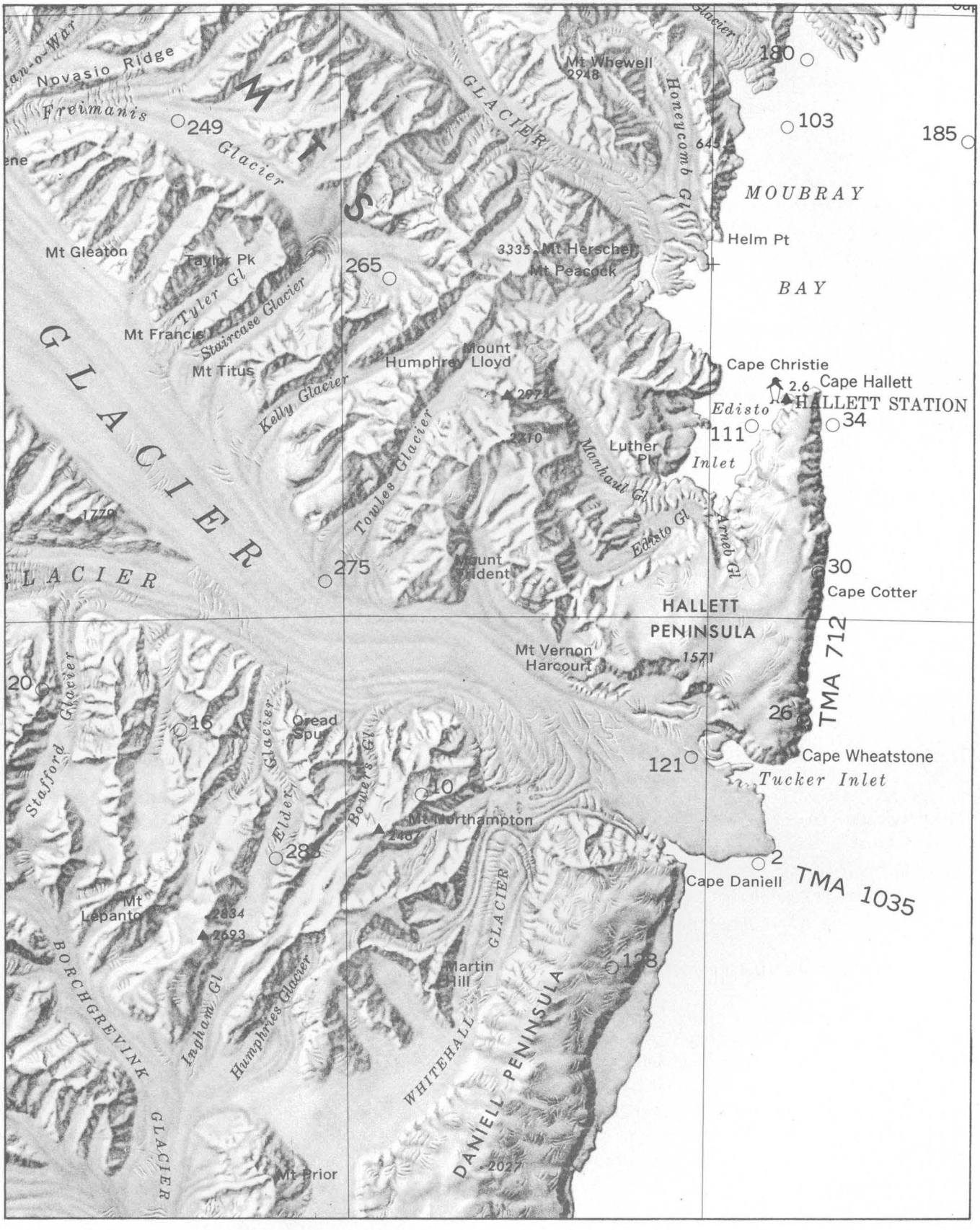

FIGURE 2.—Shaded-relief sketch map of the area of Antarctica shown in figure 1.

285-544 O—68——13

The first shaded relief sketch map received immediate and sustained support from the National Science Foundation, USARP scientists, aircraft commanders, and government mapping agencies using Geological Survey compilations to revise their maps and charts of Antarctica. With National Science Foundation support, maps of other unmapped areas of Antarctica have been compiled in advance of field operations, and the USARP is now dependent on the availability of sketch maps to coordinate and plan scientific and logistic operations for the complex multidisciplinary helicopter-supported projects in remote areas of Antarctica.

TRIMETROGON SYSTEM

Although the sketch-map series is compiled by using the basic trimetrogon system, there are significant cost-reducing and time-saving modifications that are in keeping with the purpose of the new series.

The new 1:500,000-scale sketch maps are compiled from selected tricamera photographs taken by the U.S. Navy for the Geological Survey at a width-height ratio of about 5.0, appropriate for 1:250,000-scale mapping. The tricamera system used in Antarctica has three planigon cameras rigidly mounted in a photographic aircraft so that one camera is in a vertical position and the other two are pointed to the right, and to the left, respectively, depressed 30° from the horizon so that coverage is complete from horizon to horizon. The cameras take simultaneous exposures at an interval that will give 60-percent forward overlap on the vertical photographs. The flight height of the photographic aircraft is usually between 20,000 and 25,000 feet above sea level. The trimetrogon system of photogrammetric compilation, developed by the Geological Survey during World War II for reconnaissance mapping, is considered to be the best available system for the Antarctic mapping.

COMPILATION PROCEDURES

For sketch mapping at 1:500,000 scale, the major modification to normal trimetrogon procedures is compilation at publication scale, about one-tenth the scale of the vertical photographs. (Standard 1:250,000-scale production compilation is done on 1:50,000-scale manuscripts.) The only photogrammetric instruments used are the Lewis Rectoblique Plotter, the photoangulator, and a stereoscope.

Because only every third or fourth flight is used, all primary photogrammetric control (tie points) must be selected beyond the x axes of the oblique photographs. Also, a greater number of image points are required to control the hand sketching.

The oblique photographs are rectified with the rectoblique plotter. A constant depression angle of 30° is assumed when making templets on the plotter. Paper templets are reduced to approximately a 9- × 18-inch format and contain radials to all primary control. The paper templets are assembled directly on top of the manuscript. The flight having the best distribution of ground control is selected as the base flight. All nadir points and photogrammetric control are then pricked through the templets and marked on the manuscript. Additional sets of templets are assembled, constrained by the ground control, and adjusted to the previously established photogrammetric points. Individual pullups are made of each combined flight strip so that all flights can be worked concurrently during the angulating and sketching phases. Secondary photogrammetric control (image-point positions) required for the sketching operations is established by photoangulation. Detail is then hand sketched on the individual pullup strips, transferred to the manuscript, and refined to make all detail join between flight strips. When the pencil manuscript has been completed, a clean ink copy is prepared on Cronaflex 0.007-inch thick.

CARTOGRAPHIC PROCEDURES

Cartographic procedures are simplified because the maps are printed only in black. The procedures for the shaded-relief techniques are standard, but the artist must use indicated ridge and foot-of-slope lines for vertical reference, because no contours are available. Symbolization, projection, and the 1:500,000 map scale conform to recommendations of the Scientific Committee on Antarctic Research, composed of representatives of the 12 nations which are active in Antarctic scientific exploration. Only names approved by the U.S. Board on Geographic Names are used.

CONCLUSIONS

The new 1:500,000-scale sketch maps are furnishing valuable basic source data needed for long-range scientific programing, logistic coordination, geodetic control, and other USARP field activities in the international cooperative effort to probe the Antarctic. Although preparation of the maps is relatively inexpensive—about one-tenth as costly as 1:250,000-scale top-

ographic mapping—the sketch maps are a product of comprehensive photointerpretation by selected, skillful photointerpreters and cartographers.

As of July 1967, about 115,750 square miles of sketch mapping have been completed, and 201,500 square miles are in compilation. It is anticipated that the program will grow and will cover all the areas programed for aerial photography. Most of these areas will also eventually be mapped as part of the 1:250,000-scale topographic series. Some areas, however, will not be included because they lack features of significant interest to USARP scientists. In the meantime, the sketch maps provide the only reliable coverage of these areas.

284-544 O—68——14

RELATION BETWEEN LAND USE AND CHEMICAL CHARACTERISTICS OF LAKES IN SOUTHWESTERN ORANGE COUNTY, FLORIDA

By F. L. PFISCHNER, JR., Ocala, Fla.

Work done in cooperation with the Orange County Board of County Commissioners

Abstract.—A fairly representative, random sampling of lakes in southwestern Orange County was conducted during May to November, 1966. An analysis of selected physical and chemical parameters of these lakes reveals a fair correlation between quality of lake water and land-use practices in the lake basin. Physical features of lake basins, such as size of lake and drainage basin and the presence of inlets or outlets, appear to have no determinable effect on the quality of lake water. The specific conductance values of the lake-water samples have a log-normal distribution with a range from 40 to 550 micromhos.

The area studied includes about 250 square miles in southwestern Orange County, west of Orlando and south of Lake Apopka (fig. 1). The more than 300 lakes and ponds in this area range in surface area from less than an acre to about 2,500 acres. Most of the land is planted in citrus. The remaining land contains several small towns, housing developments, swamp, pasture, and native scrub. There is very little manufacturing in the area.

The purpose of this study was to obtain data on the physical and chemical characteristics of lakes, to find if a correlation exists between certain physical and chemical parameters, and to determine if this information can be used to define the hydrologic relation between lakes and ground water in Orange County.

The physical characteristics determined for 71 lakes—69 in southwestern Orange County and 2 in Lake County—include lake and drainage basin areas, location and capacity of surface inlets and outlets, and land use within each lake basin. Chemical characteristics determined include the sulfate content and the specific conductance of lake water. Several complete chemical analyses were made to determine the more common dissolved constituents in selected lakes.

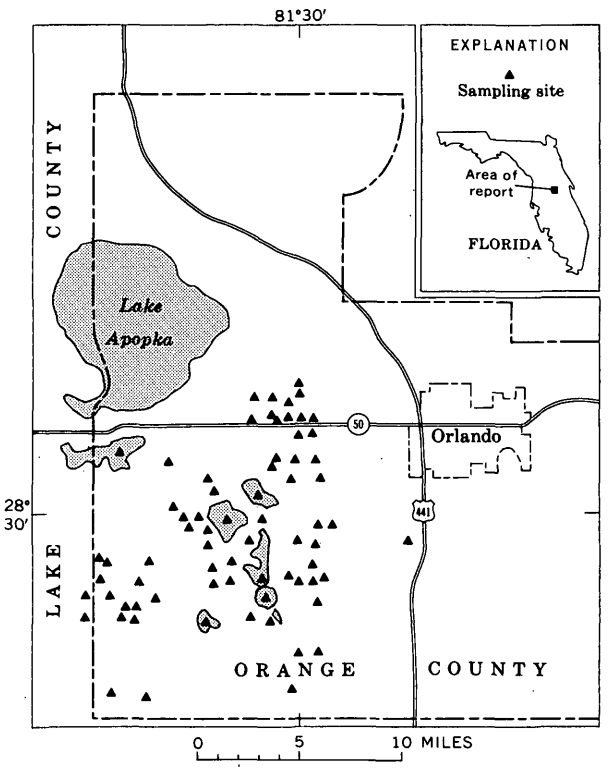

FIGURE 1.—Location of lake sampling sites in southwestern Orange County, Fla. Two sites are in Lake County and are adjacent to the Orange County line.

This investigation is a part of an intensive study of lakes in Orange County currently being conducted by the U.S. Geological Survey in cooperation with the Orange County Board of Commissioners and the Florida Geological Survey.

METHODS OF INVESTIGATION

The fieldwork was conducted during May to November 1966. Initially, five lakes were surveyed with a portable temperature and specific conductance probe, and a fathometer. Lakes Florence, Herrick, Johio, Little Sand, and Marsha were sampled to determine if differences in water quality existed due to incomplete mixing of the lake water. No appreciable areal differences in specific conductance were found in open water. One factor that appears to affect conductance is aquatic vegetation along the shallow edges of the lakes which traps surface runoff and rainfall and prevents thorough mixing with the main body of water. Life processes of vegetation and associated biota along the shoreline also may account for differences in conductance. It was determined that a representative conductivity sample could be collected at the lake edge if there was no aquatic vegetation present or if the sample was collected beyond the ring of vegetation; about 90 percent of the samples were collected in this manner. Several conductance observations were made in November at sites which had been sampled in May. These observations indicated that no significant change in conductivity had taken place in the interim, even though at one lake the level had risen more than 5 feet due to heavy rainfall during the spring and summer. Locations of sample sites are shown on figure 1.

Specific electrical conductance was used to define the quality of water because it is proportional to the mineral content of the water and it can be measured easily with field equipment. Conductance values used in this analysis are averages where more than one reading was obtained at a given site. The accuracy of the field conductivity measurements is limited by the accuracy of the meter, and is estimated at ±10 micromhos.

Standard complete chemical analyses of water from 13 representative sites were made by the U.S. Geological Survey Laboratory in Ocala, Florida. The laboratory also ran analyses for sulfates and conductivity on four additional samples.

The latest topographic maps were used to determine lake surface drainage areas, elevations, and the location of inlets and outlets. Land-use information was obtained from a map "General Land Use 1963" that was published by the East Central Florida Regional Planning Council and was based on 1963 aerial photographs. Additional information was obtained by field reconnaissance and from 1963 aerial photographs.

SUMMARY OF PHYSICAL CHARACTERISTICS OF LAKES INVESTIGATED

Most of Orange County's lakes occupy closed depressions with no natural surface inlets or outlets. In this report, lakes are classified as confined, or not confined, at most stages. Those lakes that are classified as being confined have no surface inflow and no surface outflow, except at high or extremely high stages. Those classified as being not confined at most stages have surface inlets or outlets, or both, that flow at most lake stages.

Of the lakes sampled, 37.1 percent have a surface area of less than 25 acres; 12.9 percent have a surface area between 25 and 50 acres; and the remainder have a surface area of more than 50 acres. Most of the lakes have drainage areas which are more than 6 times as large as the lake areas, and the range in drainage areas is from 2.5 to 17,000 acres.

Land in the area can be classified as: (a) relatively undeveloped swamp, pasture, and scrub, (b) citrus grove, and (c) urban and suburban housing.

SUMMARY OF SPECIFIC CONDUCTANCE VALUES OF LAKES INVESTIGATED

The specific conductance values range from 40 to 550 micromhos at 25° C, with an average of 136 micromhos, a standard deviation of 100 micromhos, and a coefficient of variation of 0.77.

Because of the large variation in conductance values from lake to lake, the normalcy of statistical distribution was tested. Figure 2 is a percentage-frequency distribution of conductance values based on a class interval of 50 micromhos for the 71 lakes. A semilog

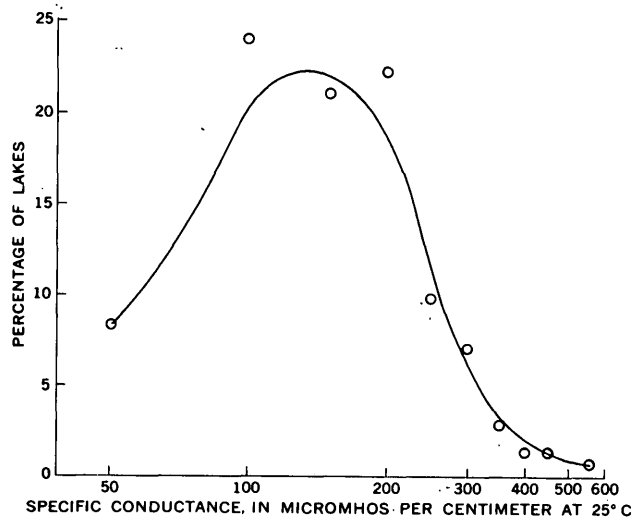

FIGURE 2.—Percentage-frequency distribution of conductance values for 50-micromho intervals for 71 lakes sampled.

plot of these data exhibits a statistically "normal" curve and is termed a log-normal distribution. These same data lie on a nearly straight line on a log-probability plot (fig. 3). A perfect log-normal distribution would be a straight line on a log-probability plot.

RELATION OF CHEMICAL CHARACTERISTICS TO LAND USE

A perusal of the chemical data showed several interesting relations, but some seemingly lacked correlation with the physical setting.

A plot of conductance versus sulfate and versus dissolved solids showed straight-line relations. Sulfate is the major mineral constituent in most of the samples. In waters of low sulfate content (and low conductivity), the chlorides predominate.

As the specific conductance data proved to have a near log-normal distribution, it was statistically compared with various land-use classifications.

Figure 4 shows a frequency distribution of conductance related to the major land use within the basin of each lake. This figure shows the wide variation of conductance values for lakes in basins that are primarily in groveland. Many of the low-conductance lakes are in virtually their native state. The few lakes whose basins are used primarily for housing have water with about average or slightly above average conductance.

Percentage-frequency distributions showing the effect of citrus areas on lake-water quality are shown in figure 5. The percentage of grove coverage is the acres in groves divided by the total acres in each basin.

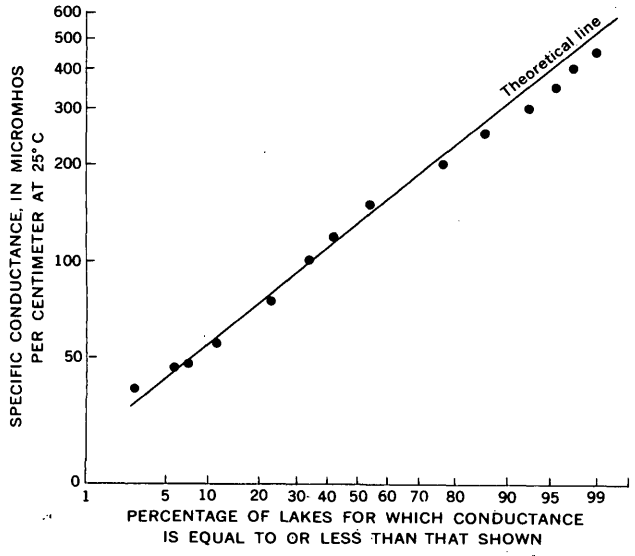

FIGURE 3.—Cumulative frequency curve of specific conductance for 71 lakes sampled.

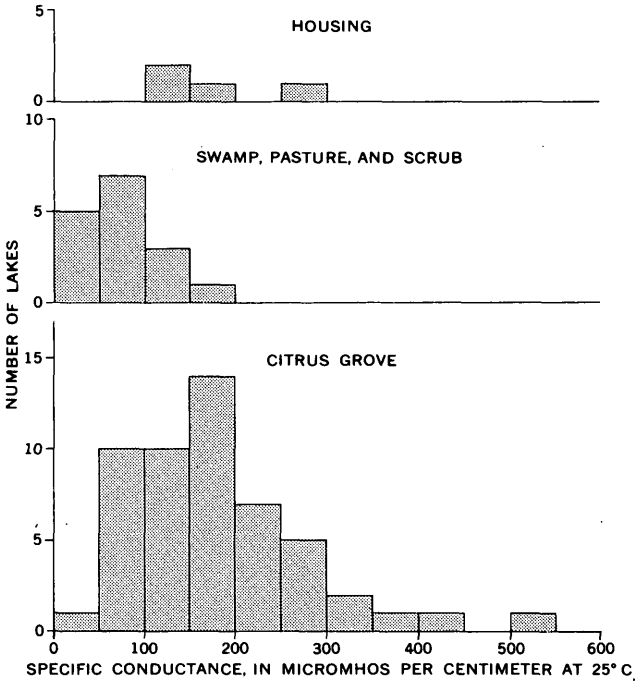

FIGURE 4.—Frequency distribution of specific conductance for lakes in basins having different major land uses.

The three classes of grove coverage were chosen so that the data split into three groups of similar size.

The frequency distribution of specific conductance for lakes in basins having 0- to 30-percent grove coverage is markedly skewed and indicates generally lower conductivity values for the 23 lakes in this category. The frequency distribution of specific conductance for lakes in basins having 31- to 60-percent grove coverage is a more normal distribution with generally higher conductivity values for the 27 lakes in this category. The frequency distribution of specific conductance for lakes in basins having 61- to 100-percent grove coverage for 21 lakes, is slightly skewed with even higher conductivity values, including the two highest values observed. A statistical comparison of the 3 curves shows that they are significantly different at a level of significance of 5 percent (5 chances out of 100 that any 1 curve occurred by chance alone). This figure indicates that the amount of grove coverage in the lake basin has some effect on surface-water quality. The lakes with the higher percentage of their basin area in groves tend to be more highly mineralized. It was concluded that the higher conductivity values were caused by higher sulfates which are probably due largely to the frequent application of wettable sulfur on surrounding citrus groves to control spider mites and rust. The sulfur may reach the lake directly as windblown spray, or indirectly through surface- and ground-water drainage.

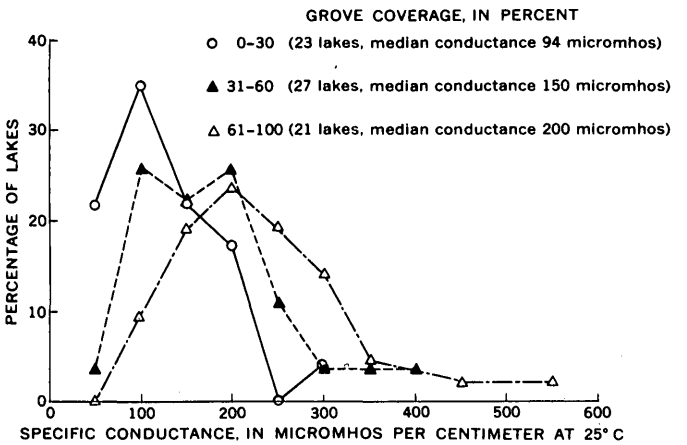

FIGURE 5.—Percentage-frequency distribution of specific conductance for lakes in basins having different percentages of the land in citrus groves.

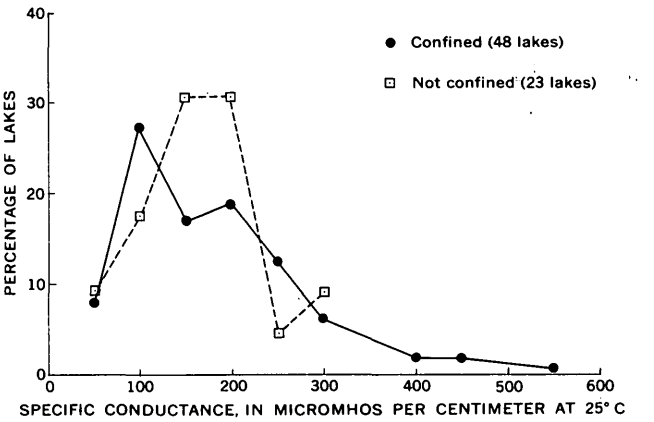

FIGURE 6.—Percentage-frequency distribution of specific conductance for lakes which are either confined or not confined at most stages.

The effect of the age of citrus groves on the quality of water in nearby lakes is a factor that needs to be examined in more detail. Preliminary information for a few groves indicates that the more highly mineralized lakes are surrounded by the older groves. This factor may account for the variation of quality of water for lakes in basins with similar percentages of grove coverage.

RELATION OF CHEMICAL CHARACTERISTICS TO OTHER FACTORS

Although a comparison of conductance values of waters from lakes not confined at most stages with values from lakes confined at most stages appeared to show no trend, a percentage-frequency distribution plot on figure 6 reveals certain distinctive differences between the two groups of conductance values.

The plot for the 48 confined lakes was a skewed distribution with a large degree of dispersion. This class includes most of the lakes with low-conductance waters and all of the lakes with the extreme high-conductance waters.

The plot for the 23 unconfined lakes was a normal distribution with little dispersion. The distribution is influenced by the inclusion of the Butler chain of lakes, which had conductivity values between 108 and 200 micromhos, for 8 lakes sampled. These lakes are all connected but there was little, if any, flow between them during the period that the samples were taken. The conductivity values for the chain of lakes decreased toward the chain's outlet.

The fact that a lake is confined or not confined at most stages does not appear to have a great affect on the quality of lake water. The difference in size of the two samples and the inclusion of the Butler chain of lakes precludes any meaningful statistical comparison for the two groups of data.

Davis (1966) has shown that the frequency distribution of dissolved-solids content of ground water in geologically and climatologically homogeneous terrane units approximates a log-normal distribution. It is interesting and possibly significant that the conductance data for the lakes sampled in Orange County follow a log-normal distribution.

The shallow aquifer in southwestern Orange County is composed primarily of fairly homogeneous unconsolidated marine sediments.

The high degree of variation in the conductance data for the lakes sampled may be due partially to differences in the aquifer materials adjacent to a particular lake, however, it appears that most of the variation is related to local land-use practices.

CONCLUSIONS

The conductance values obtained from water samples from 71 lakes exhibit a log-normal distribution with an average value of 136 micromhos, a range from 40 to 550 micromhos, and a standard deviation of 100 micromhos.

All the lakes sampled are in a similar geologic and climatologic setting. The size of a lake in relation to the size of its drainage area, and the presence of inlets or outlets were not found to appreciably affect the quality of water in a lake. The variation in quality of water among the lakes is due primarily to land-use practices in the lake basin. The higher conductivity of some lake waters is probably due to the presence of sulfates which results from the application of wettable sulfur to the citrus groves in the vicinity of the lake.

In a nonleaky closed lake, concentrations of dissolved minerals increase with time until the water is saline.

The presence of water having conductance values of no more than 550 micromhos indicates that the "closed" lakes in this area constantly drain to a ground-water body. The closed lakes, largely in grove environments, that contain the lowest conductance water may leak or otherwise exchange water at a faster rate than those that contain the highest conductance water, although the age of the groves is probably a more significant variable.

REFERENCE

Davis, G. H., 1966, Frequency distribution of dissolved solids in ground water: Ground Water, v. 4, no. 4, p. 5–12.

RESERVOIR EFFECT ON DOWNSTREAM WATER TEMPERATURES IN THE UPPER DELAWARE RIVER BASIN

By OWEN O. WILLIAMS, Trenton, N.J.

Work done in cooperation with the Delaware River Basin Commission

Abstract.—Seasonal water-temperature data are being obtained at five sites in the upper reaches of the Delaware River. A graphical analysis of these data illustrates the effect that significant reservoir releases can have on downstream water temperature. Releases from New York City's Cannonsville Reservoir have caused a drop in water temperature of 26°F, 8.1 miles downstream, and of 8°F, 44.3 miles downstream. Releases from New York City's Pepacton Reservoir have caused a drop of 20°F, 31 miles downstream, and of 5°F, 59.4 miles downstream.

An investigation of stream temperature in the upper reaches of the Delaware River (fig. 1) has been conducted since the spring of 1964. The objectives of this temperature study are (1) to determine the effect of reservoir releases on downstream water temperatures, (2) to define the variations in water temperature during the summer months, (3) to design a mathematical model to predict the effect of future releases from existing and proposed reservoirs on downstream water temperature, and (4) to determine the thermal suitability of water in the study area for the spawning of anadromous fish.

This paper presents a graphical analysis of the effect of significant releases from New York City's Pepacton and Cannonsville Reservoirs on downstream water temperature. It is based on records collected during May through September 1966. An analysis of the records of this period clarifies the downstream effect of reservoir releases more readily than those collected during 1964 or 1965. The choice of 1966 is due to the pattern of reservoir releases. One reservoir releasing for a period of time while the other is not, allows the downstream effect from each reservoir to be analyzed separately.

The reach under study (fig. 1) extends 17.5 miles from the Cannonsville Reservoir on the West Branch Delaware River to its confluence with the East Branch; from the Pepacton Reservoir on the East Branch, 32.6 miles to the West Branch confluence; and 54.5 miles along the mainstem Delaware River from the confluence of the East and West Branches to Barryville, N.Y. The drainage areas controlled by the Cannonsville and Pepacton Reservoirs are 454 square miles and 371 sq mi, respectively. The drainage area of the Delaware River at Barryville, N.Y. is approximately 2,610 sq mi. Pertinent information on mileages and drainage areas in the study area are presented in table 1.

During the study, the Cannonsville Reservoir was under construction. However, limited detention and storage were maintained, some of which was diverted out of the basin for municipal supply and some released downstream for streamflow augmentation. The Pepacton Reservoir, which was constructed by 1954, also diverts for municipal supply and provides flow augmentation. Both reservoirs have low level outlets.

It is noted that during the three years of study, drought conditions existed in the study area.

PROCEDURE

To determine the effect of the reservoirs on downstream water temperature, five waterproof thermographs were installed at selected locations (fig. 1) in the upper Delaware River basin. The locations selected were at Hancock on the East Branch, and at Lordville, Callicoon, Narrowsburg, and Barryville on the mainstem. Each temperature recorder was chained to two 100-pound concrete blocks and placed on the

U.S. GEOL. SURVEY PROF. PAPER 600-B, PAGES B195-B199

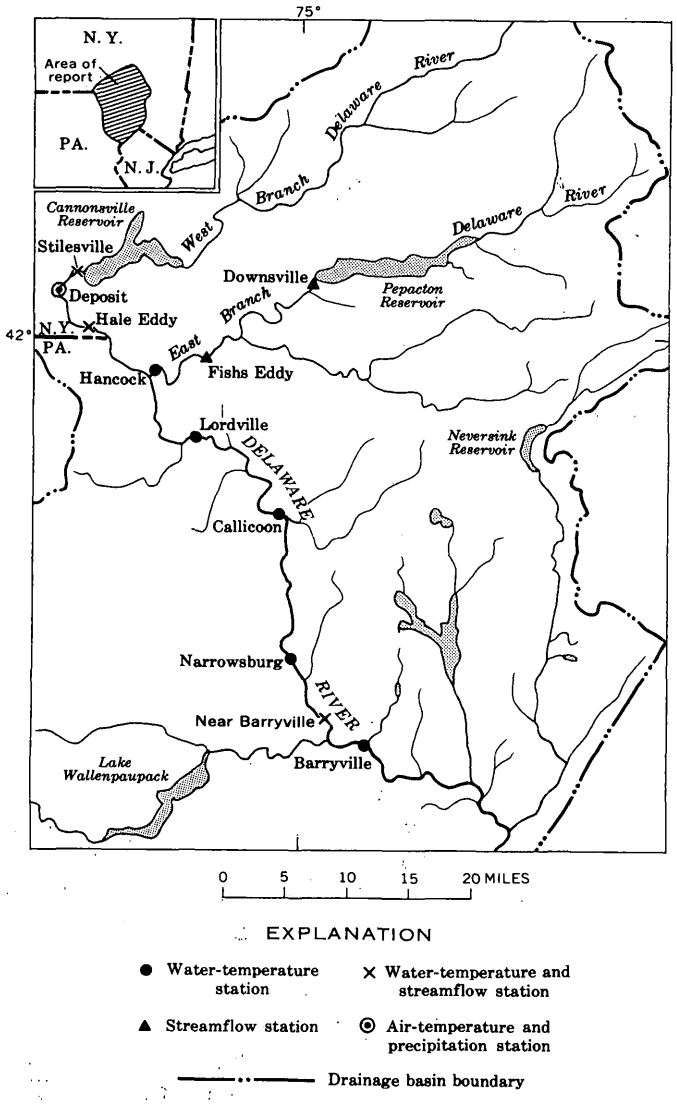

FIGURE 1.—Temperature-monitoring sites and streamflow-gaging stations in the upper Delaware River basin.

streambed in flowing water from 3 to 6 feet deep. They were in operation for approximately six months, May through October, of each year from 1964 to 1966. They were serviced once every 20 to 25 days. Data obtained are within an accuracy of 2°F. Additional water-temperature data, collected at Stilesville and Hale Eddy on the West Branch and near Barryville on the mainstem by the U.S. Geological Survey in its continuing cooperative program with the City of New York, were used to augment and supplement the records collected as part of this investigation.

Maximum and minimum air-temperature and precipitation records were obtained from the Weather Bureau station at Deposit (fig. 1). Streamflow records were obtained from continuous-recording gaging stations at Stilesville and Hale Eddy on the West Branch,

TABLE 1.—*Distances from New York City Reservoir sites and drainage areas at water-temperature sampling sites*

Drainage-area features	Distance (in miles) From Cannonsville Reservoir	Distance (in miles) From Pepacton Reservoir	Drainage area (sq mi)
Pepacton Reservoir	----	----	371
Cannonsville Reservoir	----	----	454
Stilesville	1.5	----	456
Hale Eddy	8.1	----	593
Downsville	----	0.5	371
Fishs Eddy	----	21.6	780
Hancock	----	31.0	[1] 840
Confluence, East and West Branches Delaware River	17.5	32.6	[1] 1,500
Lordville	26.6	41.7	[1] 1,570
Callicoon	44.3	59.4	[1] 1,700
Narrowsburg	55.9	71.0	[1] 1,860
Near Barryville	66.5	81.6	2,023
At Barryville	72.0	87.1	[1] 2,610

[1] Estimated.

at Downsville and Fishes Eddy on the East Branch, and on the Delaware River near Barryville.

The data were graphically analyzed by plotting and comparing both daily and hourly hydrographs, and by plotting double-mass curves. The procedures of double-mass-curve analyses are described by Searcy and Hardison (1960). An average of the maximum and minimum daily water temperature was used to represent the mean for the day. Future analyses of the data will include the computation of multiple-regression correlations and frequency analyses using automatic data-processing techniques.

RESULTS

A graphic illustration of the effect that colder water released from Pepacton and Cannonsville Reservoirs exerted on seasonal downstream temperatures during 1966 is shown in figure 2. Water temperatures of the West Branch Delaware River at Hale Eddy, of the East Branch at Hancock, and of the mainstem of Callicoon are shown for May through September. Air temperature at Deposit also is plotted to represent regional air temperature. Streamflows at Stilesville and Downsville representing the release from Cannonsville and Pepacton Reservoirs, respectively, are plotted on the upper section of the figure.

The upper section of the figure shows that reservoir releases were insignificant until the latter part of June. On June 23, significant releases began from Cannonsville Reservoir into the West Branch Delaware River. Although air temperatures at Deposit rose 7°F, the water temperature at Hale Eddy, 8.1 miles downstream of the damsite, dropped 13°F. When releases were cut back on June 25, the water temperature at Hale Eddy rose 22°F during the next few days while the air temperature dropped about 4°F.

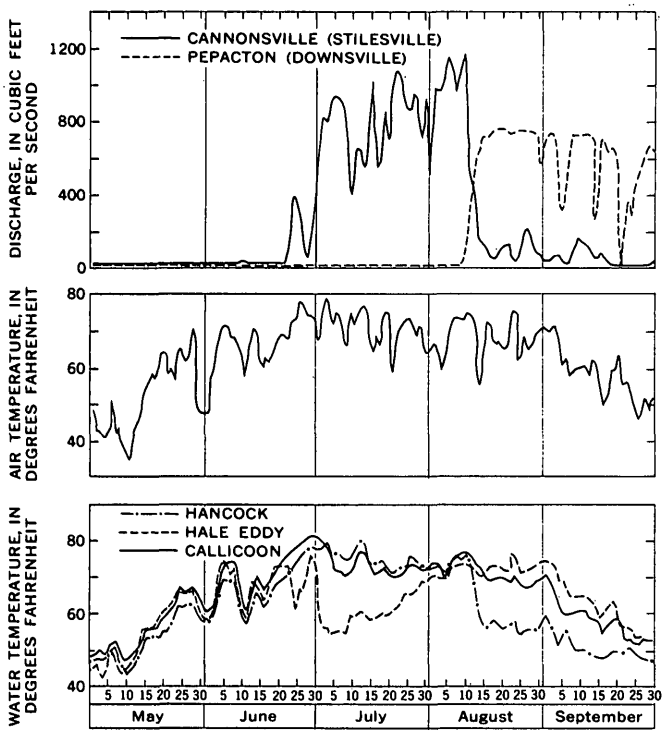

FIGURE 2.—Water temperature and discharge in the upper Delaware River basin and regional air temperature for May through September 1966.

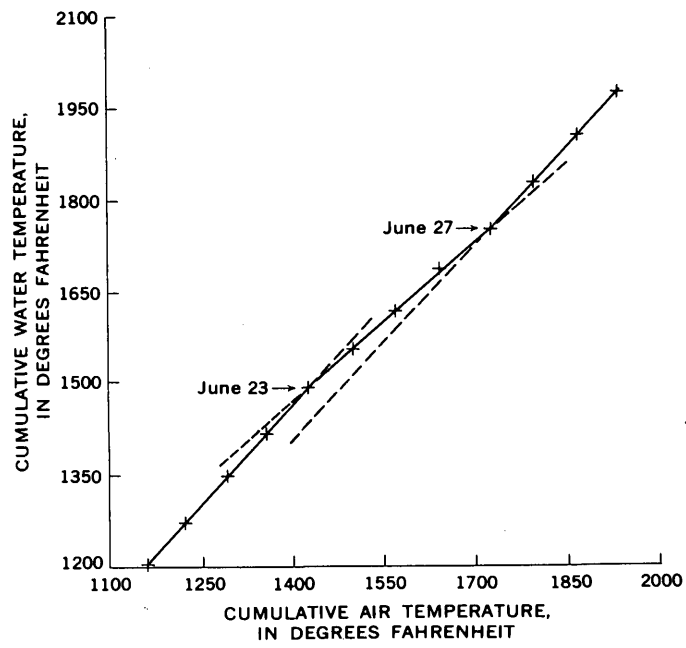

FIGURE 3.—Double-mass curve–cumulative air temperature at Deposit, N.Y., versus cumulative water temperature at Hale Eddy, N.Y., June 19–30, 1966.

In order to confirm that a change in the proportionality between climatologic conditions and that of water temperature had occurred at the time reservoir releases began, a double-mass curve was plotted. This consisted of plotting cumulative air-temperature values at Deposit against cumulative water-temperature values at Hale Eddy (fig. 3) for the period of June 19–30, 1966. The change in slope noted on June 23 indicates a change in proportionality between the climatologic conditions and the water temperature, and suggests that the rate of increase of water temperature decreased in relation to the rate of increase of air temperature. As releases from the reservoir were reduced (June 27), the slope approximated that defined prior to releases. Dashed lines, representing extensions of defined linear relations, have been added to this and a later illustration (fig. 5) to facilitate their interpretation.

To further illustrate the effect that reservoir releases have on downstream water temperature, hourly plots were prepared of the water temperatures at Hale Eddy, Hancock, and Callicoon, and the plots were compared with those of air temperature. The combined plot of water and air temperature during the period June 20–26, 1966 is shown in figure 4. Temperatures plot as sinusoidal curves with the curve for temperature at Hale Eddy having the largest amplitude of the three water-temperature curves. Releases from Cannonsville Reservoir began at 3 p.m. on June 23. The lowering of the axis of the sine curve by about 3 a.m. on June 24 suggests a traveltime of about 12 hours from Cannonsville Reservoir.

These releases began to effect the Callicoon temperatures on the morning of June 25. This is suggested by noting that water temperatures at Callicoon were usually 3° to 5°F above those at Hancock until the morning of June 25. Then, the water temperature at Callicoon began to level off, while the water temperature at Hancock, not affected by releases from Cannonsville, continued to rise with the air temperature to within 2°F of the temperature at Callicoon late in the evening.

Referring again to figure 2, it appears that there was no effect on water temperature at Callicoon during June 20–26. However, a comparison of temperatures at Hancock with those at Callicoon, on figure 4, shows that some effect was present. Although there was no drop in water temperature at Callicoon, there was a change in its rate of rise, thus indicating that the effect of the release from Cannonsville was shadowed by climatological conditions.

At the end of June and beginning of July, significant releases again were made from Cannonsville Reservoir and the water temperature dropped 26°F at Hale Eddy (fig. 2). Such releases from Cannonsville produce this effect at Hale Eddy because the water released through

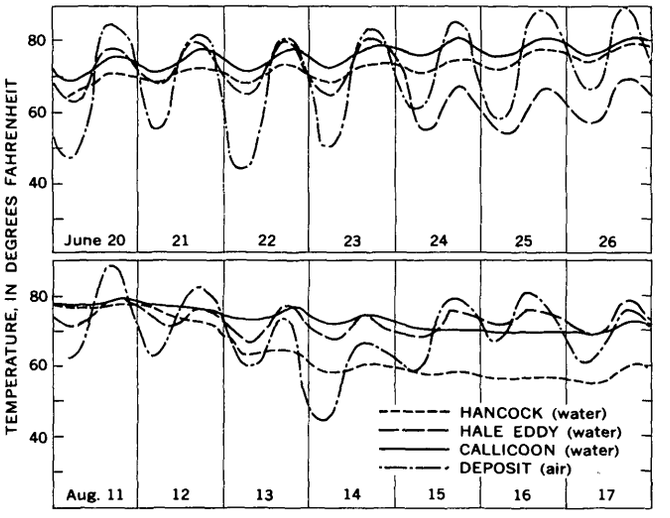

FIGURE 4.—Hourly air and water temperatures in the upper Delaware River basin, June 20–26, and August 11–17, 1966.

the low level outlet is from the hypolimnion—the lower strata of the reservoir—which is colder than is normal for the area streams during summer months.

Throughout July and into the middle of August, significant releases from Cannonsville were continued (fig. 2). Water temperatures at Hale Eddy increased through the month of July until they approximated those on the East Branch Delaware River at Hancock. The temperatures of the East Branch were not affected by upstream reservoir releases. This could indicate that colder water from the hypolimnion had been completely released from Cannonsville and that warmer upper strata water was then being released. It should be noted that at no time prior to or during these observations was Cannonsville filled to more than half capacity.

When releases from both reservoirs were insignificant, as in May and June (fig. 2), water temperatures at both Hale Eddy and Hancock were within a few degrees of each other. When one reservoir was releasing, and the other was not, the effect of this release and that of climatologic conditions can be estimated by comparing the respective downstream variations in water temperature with those of local air temperature. For example, on July 20, the water temperature at Hale Eddy was 61°F while that at Hancock was 72°F. If releases from Cannonsville had been insignificant, the water temperature at Hale Eddy could be assumed to be similar to that at Hancock, or approximately 72°F. Thus, the effect of Cannonsville's release on Hale Eddy on that day is estimated to be the difference between 72°F and 61°F, or approximately 11°F. Mean air temperature on July 20 was 70°F, a decrease of 5°F from the previous day. Water temperature at Hancock had dropped 3°F from the previous day, but at Hale Eddy it had risen 2°F. This 2°F rise at Hale Eddy, while the temperature dropped 3°F at Hancock, suggests that the effect of the climatological conditions on water temperature at Hale Eddy is overshadowed by the effect of the reservoir release at Cannonsville.

Water temperature records collected at Stilesville, indicative of the water temperature of the Cannonsville Reservoir release, verify that the rise in water temperature at Hale Eddy is the result of warmer water being released from the reservoir. Mean water temperature at Stilesville was 48°F on July 1, 10°F lower than that at Hale Eddy. The water temperature continued to rise at Stilesville through July. On August 2, the water temperatures at both stations were within 1°F of each other; 69°F at Stilesville and 70°F at Hale Eddy. Throughout the rest of August and September, the water temperatures at both stations continued to approximate each other.

Water temperatures at Callicoon, 26.8 miles below the confluence of the East and West Branches, usually were 1° to 4°F higher than those at Hancock (fig. 2) until early July, after which they were 1° to 4°F lower than those at Hancock. This change suggests that releases from Cannonsville had produced a drop in water temperature of as much as 8°F at Callicoon, 44.3 miles below the damsite.

Releases began from Pepacton Reservoir at noon on August 10 (fig. 2). During the short period after the releases, water temperature at Hancock dropped 20°F, and at Callicoon 9°F. Air temperature during this period dropped 25°F but recovered 23°F within a few days. At the same time, water temperatures at Hancock and Callicoon continued to drop. Water temperatures at Hale Eddy, which are not affected by releases from Pepacton, fell and rose with air temperatures.

A double-mass curve (fig. 5) was plotted with cumulative air-temperature values at Deposit against cumulative water-temperature values at Hancock. The change in slope noted on August 14 indicated a change in proportionality between the air and water temperatures. Had the change in proportionality been due only to the reservoir release, a traveltime of one to two days would have been expected. In short, a change in slope would have been noted on August 11 or 12 on the double-mass curve. However, a change in climatologic conditions occurred at the same time, and its effect must also be taken into account. This change is described in the next paragraphs.

The lower section of figure 4 is an hourly plot of water temperature for the period August 11–17 at Hancock, Hale Eddy, and Callicoon, and of air temperature at Deposit. At Hale Eddy, the water temperature, which is not affected by releases from Pepacton, rises and falls diurnally with air temperature. At

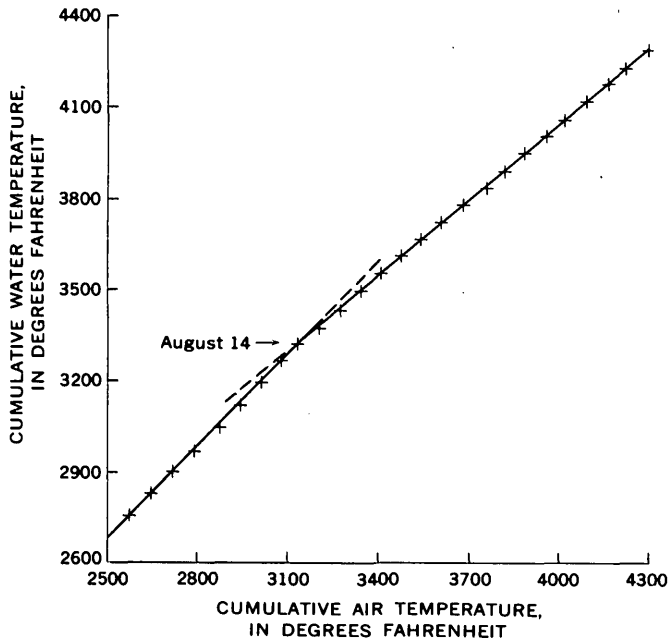

FIGURE 5.—Double-mass curve–cumulative air temperature at Deposit, N.Y., versus cumulative water temperature at Hancock, N.Y., August 5–31, 1966.

Hancock they decline from August 11 through August 16. On August 11, the water temperature at Hancock approximates that at Hale Eddy. The indication is that the release initiated on August 10 began to affect the water temperature at Hancock late August 11 or early August 12.

A change in slope of the double-mass curve (fig. 5) was not noted until August 14–15 because the short term change in climatological conditions was concurrent with the change in water temperature.

The effect of reservoir releases has been observed as far downstream as Narrowsburg, which is 71.0 miles below the Pepacton Reservoir and 55.9 miles below the Cannonsville Reservoir. By the same method used to determine reservoir effect at Callicoon, a 3°F drop from the Cannonsville releases and a 5°F drop from the Pepacton releases were observed. However, little, if any, effect could be detected at Barryville, 87.1 miles below Pepacton Reservoir and 72.0 miles below Cannonsville Reservoir.

Similar studies of the effect of reservoir releases during 1964 and 1965 suggest that water temperature at Hancock drops as much as 20°F after releases from the Pepacton Reservoir and that water temperature at Narrowsburg drops as much as 3° to 5°F. The effect of reservoir releases from Cannonsville during 1964 and 1965 was not observed at Narrowsburg. This can be explained with the knowledge that large water storage in Cannonsville Reservoir, which was under construction, was not attempted prior to the fall of 1965. Therefore, the volume of water in the hypolimnion most likely was not as large as, or the water as cold as, that found in 1966 when the effect on temperatures of the releases was observed at Narrowsburg.

SUMMARY

A primary purpose for studying the effect of reservoir releases is to be able to predict downstream water temperature with some degree of accuracy. The results of a multiple-regression correlation, which is being prepared at present, will be applied to this end. However, hydrographs, temperature records, and double-mass curves can be used to determine and substantiate both climatologic and release effects on downstream water temperatures. Comparison of water-temperature records not affected by the reservoir releases with those collected on a stream which is affected, combined with a knowledge of local climatologic conditions, can be used to estimate the effect of these releases on stream temperatures.

Through these methods significant reservoir releases from Pepacton have been observed to lower water temperature as much as 20°F, 31.0 miles downstream, and 5°F, 71.0 miles downstream. Significant releases from the Cannonsville Reservoir were more effective in lowering water temperature in 1966 than in 1964 or 1965 because of increasing storage. Thus, significant releases from this reservoir during 1966 were observed to drop the water temperature as much as 26°F, 8.1 miles downstream, and 3°F, 55.9 miles downstream.

An approximate traveltime of one-half day for the reservoir releases from Cannonsville to affect the downstream water temperature at Hale Eddy was estimated from hourly plots. Similarly, the traveltime from the Pepacton Reservoir to Hancock was estimated to be approximately one and a half days.

REFERENCE

Searcy, J. K., and Hardison, C. H., 1960, Double-Mass Curves, *with a section on* Fitting curves to cyclic data, by W. B. Langbein: U.S. Geol. Survey Water-Supply Paper 1541–B, p. 31–66.

PRELIMINARY ASSESSMENT OF GROUND WATER IN THE GREEN RIVER FORMATION, UINTA BASIN, UTAH

By R. D. FELTIS, Billings, Mont.

Work done in cooperation with, and publication authorized by, the Utah Oil and Gas Conservation Commission

Abstract.—The Green River Formation of Eocene age contains not only large reserves of hydrocarbons in the form of bituminous sand and oil shale but also aquifers that yield small to large quantities of water to wells and springs. Thus, sufficient water for processing the hydrocarbons may be locally available from subsurface sources. The ground water ranges from fresh to briny. Detailed hydrologic studies are needed to determine the quantity and quality of water in the formation.

The Green River Formation in the Uinta Basin in northeastern Utah contains large reserves of hydrocarbons in the form of oil shale and bituminous sand. Whether these reserves can be developed economically depends in large measure on the available quantities of process water of suitable chemical quality. This article summarizes the available information on the yields of wells and springs that are known to derive water from the Green River Formation and on the chemical character of that water.

Most of the available data are from wells drilled for oil and gas exploration. As yet little effort has been made to determine the number of aquifers in the Green River Formation, their extent and hydrologic characteristics, and the variations in the quality of water contained in them.

The Uinta Basin is an asymmetric syncline; its axis is concave southward and generally parallel to the eastward-trending Uinta Mountains (fig. 1). Beds that form the north flank of the basin dip steeply southward away from the Uinta Mountains. Although the beds that form the south flank dip as much as 5° northward toward the axis of the syncline, they are nearly horizontal in the southernmost part of the basin.

The Green River Formation, which crops out extensively on the south flank of the basin and forms the south-facing Roan Cliffs, consists wholly, or almost wholly, of evenly stratified lakebeds. From a 4-mile width near the west end of the basin the outcrop widens southeastward to about 50 miles where the basin is broadest; thence it narrows northeastward to about 10 miles where it crosses to the north side of the synclinal axis. The outcrop on the north flank is much less extensive than on the south flank and is limited to the easternmost part of the basin. In the central part of the basin the Green River Formation is overlain by younger sediments that are 3,000 feet or more thick.

The average amount of annual precipitation in the basin is closely related to the altitude of the land surface. Altitudes in the basin range from about 4,650 feet above sea level near Ouray on the Green River to 10,000 feet along the Roan Cliffs. Less than 12 inches of precipitation falls annually on most of the basin, but 20 to 30 inches falls on the high areas along the Roan Cliffs and on the west end of the basin.

YIELD OF WATER FROM GREEN RIVER FORMATION

The yield of water from the Green River Formation, as indicated by tests at 17 oil and gas wells, ranges from 17 to 7,200 barrels per day, or 0.5 to 220 gallons per minute. Two gas wells, one in sec. 35, T. 10 S., R. 20 E. (about 12 miles south of Ouray), and the other in sec. 17, T. 10 S., R. 22 E. (about 15 miles southeast of Ouray) (fig. 1), were converted to water wells; and in 1964 they flowed at rates of 2,700 bpd (80 gpm) and 340 bpd (10 gpm) (table 1). The larg-

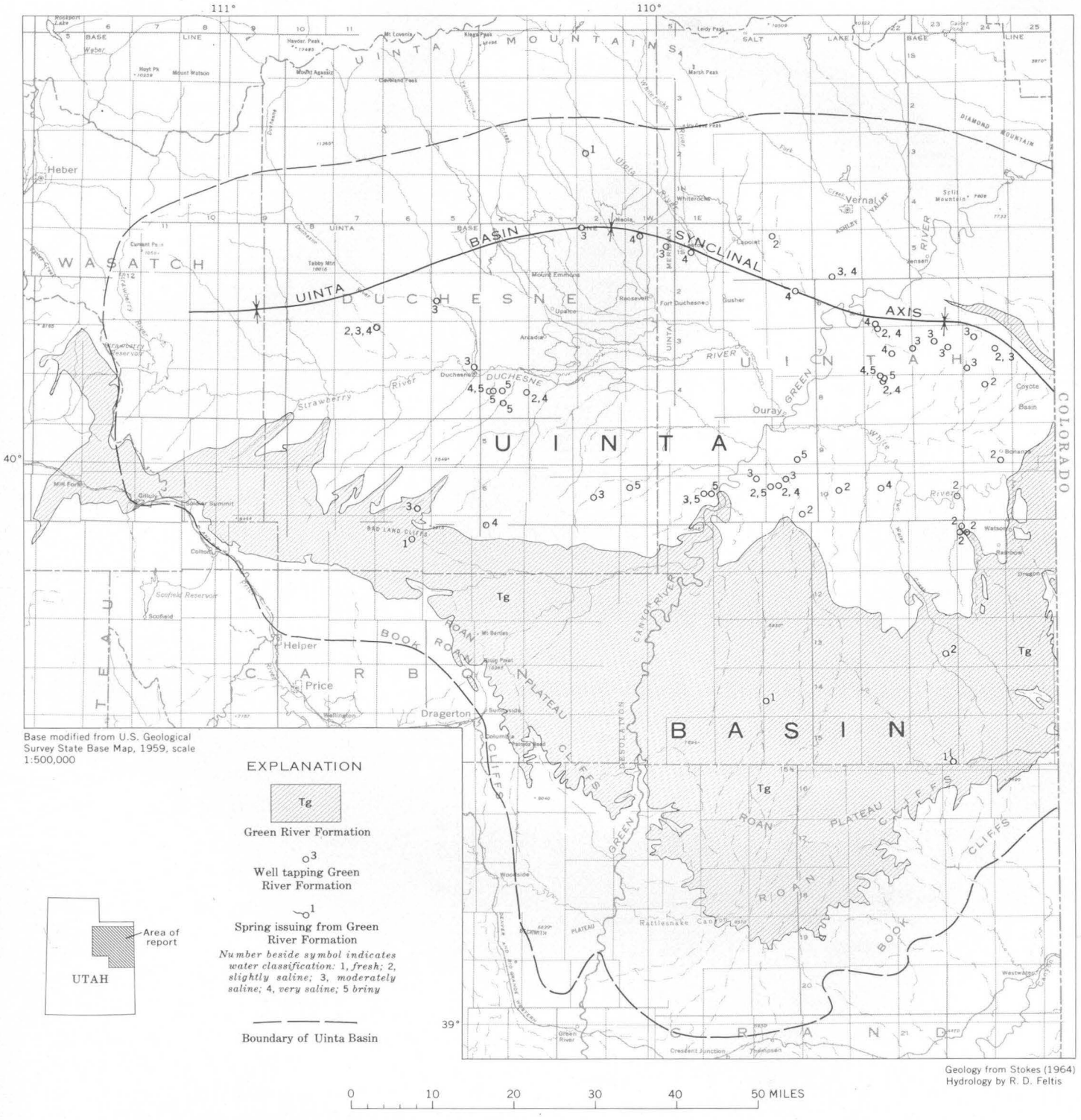

FIGURE 1.—Map showing locations of wells and a spring in the Green River Formation in the Uinta Basin.

TABLE 1.—*Selected chemical analyses of water from wells and*

Source: O, oil or gas well;
Operator or owner: Name of operator or owner at
Yield (at time water sample was collected for chemical analysis): bpd, barrels per day; gpm, gallons per minute; E, estimated;
34 bpd and 1 bpd
Analysis by: CGL, Chemical and Geological Laboratories, Casper, Wyo.;

Location			Source	Operator or owner	Depth to top of formation (ft)	Interval sampled (ft)	Yield	Date of collection	Chemical constituents (ppm)		
T.	R.	Section							Silica (SiO_2)	Iron (Fe)	Calcium (Ca)
Uinta meridian and base line											
2 N.	2 W.	C NW¼NW¼	20	O	Standard Oil Co. of California	4,030	4,115–4,143	----------	8-31-56	----	----	63
3 S.	7 W.	SW¼NW¼SW¼	1	O	California Oil Co.	2,490	4,075–4,089	----------	2-? -62	----	----	4
4 S.	4 W.	C SE¼SE¼	13	O	Carter Oil Co----	3,075	3,281–3,569	----------	2-23-52	----	----	------
							5,871–5,936	----------	4-11-52	----	----	16
Salt Lake meridian and base line											
5 S.	20 E.	C NE¼SW¼	5	O	Carter Oil Co----	4,480	6,475–6,495	----------	3- 8-51	----	----	21
							6,894–6,915	----------	3-19-51	----	----	------
7 S.	22 E.	C NE¼NE¼	5	O	Pan American Petroleum Corp.	3,212	5,332–5,337	----------	6-11-63	----	0.0	42
							6,116–6,126	----------	6-11-63	----	.0	112
7 S.	24 E.	C SW¼SW¼	14	O	Sunray-Mid-Continent Oil.	2,587	4,991–5,121	----------	4- 9-61	3.8	----	9.2
							5,155–5,216	----------	4-11-61	.5	----	18
8 S.	22 E.	SE¼SW¼SE¼	4	O	Belco Petroleum Corp.	2,480	4,469–4,482	----------	4-16-65	----	----	58
8 S.	24 E.	C NE¼NE¼	9	O	Standard Oil Co. of California	1,748	1,818–1,836	----------	5-? -56	----	----	35
9 S.	24 E.	C NW¼SE¼	27	O	Pacific Natural Gas Exploration Co.	1,240	At 1,932	7,200 bpd (R) or 220 gpm	2-? -63	----	----	------
10 S.	20 E.	NW¼SE¼SW¼	7	O	Mountain Fuel Supply Co.	1,335	2,070–2,096	----------	10-16-60	----	----	11
							3,102–3,142	----------	10-21-60	----	----	11
10 S.	20 E.	C NE¼SW¼	8	O	----do----------	1,235	3,310–3,337	----------	7-10-62	----	----	6
							3,488–3,514	----------	7-12-64	----	----	272
10 S.	20 E.	SW¼NW¼NW¼	35	W	U.S. Bur. of Land Management	750	(4)	4,800 bpd (E) or 140 gpm	7-24-64	15	----	.0
10 S.	21 E.	SE¼SE¼NE¼	16	O	DeKalb Agr. Association, Inc.	1,250	1,900–3,520	(5)	4- 2-64	13	----	.0
10 S.	23 E.	NE¼NW¼NW¼	24	O	Shell Oil Co-----	375	3,066	----------	10-15-61	----	----	2
11 S.	12 E.	NE¼NE¼NW¼	14	O	King Oil Co-----	0	635–650	17 bpd or 0.5 gpm (E)	7-22-65	9.8	----	6.4
11 S.	24 E.	SW¼NW¼SE¼	6	O	Shamrock Oil and Gas Corp.	-----	223–2,207	----------	8-26-65	12	----	3.2
11 S.	24 E.	SW¼NE¼SW¼	7	O	----do----------	-----	216–2,396	(7)	8-26-65	12	----	3.2
11 S.	24 E.	NE¼NE¼SW¼	8	O	----do----------	0	At 1,275	----------	9- 6-61	13	.36	3.6
13 S.	23 E.	SE¼SW¼NE¼	26	O	Skyline Oil Co---	0	At 2,000	----------	6-? -60	40.8	----	10.4
14 S.	20 E.	C NE¼NW¼	30	O	Phillips Petroleum Co.	0	1,883–1,910	360 bpd (R) or 11 gpm	7-22-63	----	----	10
15 S.	23 E.	SE¼SE¼	36	S	----------	0	--------	34 bpd or 1 gpm (M)	9-17-64	17	----	65

[1] Trace. [2] Analysis supplied by Carter Oil Co. [3] Calculated from specific conductance.
[4] Water from annulus behind 5½-inch casing from 168 to approximately 4,000 feet. Water sample collected before final conversion of abandoned gas well to water well. Water encountered while drilling from about 2,000 to 4,000 feet at rate of 200 to 250 barrels per hour (140 to 170 gpm). Completed water well production, 80 gpm (2,700 bpd).

a spring in the Green River Formation, Uinta Basin, Utah

S, spring; W, water well.
time water sample was collected for chemical analysis.
M, measured; R, reported. The E, M, or R is beside the given quantity. The other quantity is calculated as 1 gpm equals equals 0.03 gpm.
GS, U.S. Geological Survey; ShO, Shell Oil Co.; UC, Utah State Chemist.

Chemical constituents (ppm)—Continued															
Magnesium (Mg)	Na + K: Sodium (Na)	Na + K: Potassium (K)	Bicarbonate (HCO_3)	Carbonate (CO_3)	Sulfate (SO_4)	Chloride (Cl)	Nitrate (NO_3)	Dissolved solids (sum)	Hardness as $CaCO_3$	Noncarbonate hardness as $CaCO_3$	Percent sodium	Sodium-adsorption ratio (SAR)	Specific conductance (micromhos/cm at 25°C)	Resistivity (ohms at 68°F)	pH	Analysis by
Uinta meridian and base line—Continued																
26	14		132	-----	180	(1)	----	348	----	----	----	----	-----	19.	8. 2	CGL
1	886		1, 110	552	(1)	80	----	2, 070	----	----	----	----	-----	3. 70	9. 0	CGL
-----	1, 117		1, 550	271	164	380	----	2, 695	----	----	----	----	-----	2. 70	9. 0	(2)
7	4, 287		1, 730	251	79	5, 300	----	10, 792	----	----	----	----	-----	. 70	8. 5	(2)
Salt Lake meridian and base line—Continued																
(1)	975		1, 450	180	21	470	----	2, 381	----	----	----	----	-----	2. 90	8. 9	(2)
-----	697		1, 075	141	140	180	----	1, 687	----	----	----	----	-----	4. 20	8. 9	CGL
(1)	1, 015	90	85	96	290	1, 350	----	2, 926	----	----	----	----	-----	2. 25	10	CGL
43	9, 550	54	476	60	1, 450	13, 700	----	25, 207	----	----	----	----	-----	. 30	8. 3	CGL
16	949		2, 340	0	120	78	1. 3	2, 330	90	0	96	43	3, 190	----	8. 0	GS
12	1, 520		4, 000	0	52	51	3. 2	3, 630	95	0	97	68	5, 230	----	8. 1	GS
13	997	11	1, 610	-----	215	604	-----	2, 693	----	----	----	-----	-----	2. 65	8. 1	CGL
9	894		630	84	205	850	----	2, 387	----	----	----	-----	-----	2. 85	8. 3	CGL
-----	----------		-----	-----	-------	126	----	[3] 1, 360	----	----	----	-----	2, 090	----	----	GS
8	39, 367		9, 150	8, 520	525	45, 000	----	97, 937	----	----	----	-----	-----	. 10	9. 7	CGL
1	812		1, 379	216	107	140	----	1, 966	----	----	----	-----	-----	3. 55	8. 7	CGL
-----	928		1, 440	228	54	296	----	2, 221	----	----	----	-----	-----	3. 30	8. 8	CGL
92	10, 506		1, 720	-----	3, 870	13, 100	----	28, 489	----	----	----	-----	-----	. 27	8. 0	CGL
7. 3	859		1, 420	189	9. 1	290	. 3	2, 070	30	0	98	68	3, 340	----	9. 0	GS
2. 4	785		1, 480	128	14	195	. 7	1, 870	10	0	99	108	3, 080	----	8. 8	GS
1	572		1, 078	48	145	99	----	1, 941	8	----	----	-----	-----	[6] 4. 2	8. 9	ShO
4. 4	221		392	0	179	5. 1	. 1	619	34	0	93	16	942	----	7. 8	GS
. 5	438		644	0	334	60	1. 6	1, 170	10	0	99	60	1, 800	----	8. 2	GS
. 5	418		691	0	310	21	1. 4	1, 110	10	0	99	58	1, 720	----	8. 2	GS
1. 5	437	1. 6	606	12	422	4. 0	. 6	1, 200	15	0	98	49	1, 820	----	8. 5	GS
7. 1	261		-----	-----	423	17	----	1, 086	----	----	----	-----	-----	----	7. 6	UC
7	274	13	366	12	290	32	----	818	----	----	----	-----	-----	9. 35	8. 7	CGL
36	17		302	0	94	2. 8	. 5	381	312	64	11	. 4	606	----	7. 7	GS

[5] Reported flow on 9-29-59 was 125 gpm (4,300 bpd).
[6] Resistivity at 73°F.
[7] Reported yield of 250 barrels of water per hour (175 gpm) while drilling at 1,159 feet.

est reported yield of water from the Green River Formation is from an oil well in sec. 27, T. 9 S., R. 24 E. (about 27 miles southeast of Ouray), which produced 7,200 bpd (220 gpm) from a depth of 1,932 feet.

QUALITY OF WATER IN GREEN RIVER FORMATION

The chemical quality of the water in the Green River Formation ranges from fresh to briny. The classification of the water is based on the concentration of dissolved solids as follows:

Class	*Dissolved solids (ppm)*
Fresh	0–1, 000
Slightly saline	1, 000–3, 000
Moderately saline	3, 000–10, 000
Very saline	10, 000–35, 000
Briny	>35, 000

Analyses of 73 water samples collected from 51 wells and 1 spring indicate that 4 samples were fresh, 18 were slightly saline, and the remaining 51 were moderately saline to briny (fig. 1). The 22 chemical analyses of fresh and slightly saline water and 5 analyses of moderately saline to briny water are listed in table 1; the remainder have been published in a report by Feltis (1966). The 5 samples of moderately saline to briny water were from 5 wells that also yielded slightly saline water from a higher or lower zone. They are included to illustrate the wide range in concentration of dissolved solids in water from different depths at the same location.

Samples of fresh water were obtained from a gas well in T. 11 S., R. 12 E., an oil well in T. 14 S., R. 20 E., and a spring in T. 15 S., R. 23 E.—all on the south flank of the Uinta Basin. These samples contained 619, 818, and 381 parts per million of dissolved solids, respectively. The fourth sample of fresh water was obtained from the oil well in T. 2 N., R. 2 W. (Uinta meridian), near the north edge of the basin and contained only 348 ppm of dissolved solids. Of the 18 samples of slightly saline water, 16 came from wells on the south flank of the basin and the remaining 2 came from different zones in the same well on the north flank.

QUALITY OF WATER IN RELATION TO TOPOGRAPHIC POSITION AND GEOLOGY

Despite the widely scattered grouping of the data, it is apparent from examination of the water-quality classifications in figure 1 that fresh and slightly saline water is found in and near the exposed area of the Green River Formation near the middle of the basin.

The occurrence of fresh and slightly saline water along the south flank of the basin indicates that the aquifers are recharged where they crop out in the area of high precipitation north of the Roan Cliffs. Fresh or slightly saline water is known to occur in at least some places on the north flank also; recharge in that part of the basin probably is by interformational leakage along the base of the Uinta Mountains. The more saline ground water in the middle of the basin is probably connate water or water that has picked up salts during percolation through the formation.

CONCLUSIONS

Relatively fresh ground water occurs in moderately large quantities in at least parts of the area where the Green River Formation is exposed in the Uinta Basin. Because development of the large hydrocarbon reserves can be economically more feasible if moderate to large sources of relatively fresh water are available, it is important to complete a comprehensive appraisal of the occurrence, distribution, quantity, and quality of the ground-water resources of the Green River Formation.

REFERENCES

Feltis, R. D., 1966, Water from bedrock in the Colorado Plateau of Utah: Utah State Engineer Tech. Pub. 15, 82 p.

Stokes, W. L., 1964, Geologic map of Utah: Utah Univ., scale 1:250,000, 4 sheets.

DOUBLE-MASS-CURVE ANALYSIS OF THE EFFECTS OF SEWERING ON GROUND-WATER LEVELS ON LONG ISLAND, NEW YORK

By O. L. FRANKE, Mineola, N.Y.

Work done in cooperation with the Nassau County Department of Public Works; New York State Department of Conservation, Division of Water Resources; Suffolk County Board of Supervisors; and Suffolk County Water Authority

Abstract.—Double-mass-curve analysis of ground-water levels in Nassau County, Long Island, shows that ground-water levels in a 50-square-mile area sewered in the early 1950's have declined an average of about 10 feet relative to the unsewered area farther east. An analysis of the various factors causing this relative decline indicates that about 7 feet of the decline was caused by the sewering. The decline in ground-water levels has been accompanied by a pronounced reduction in streamflow within the sewered area.

Change in the methods of disposing of waste water is one of the many factors associated with the rapid urban development in western Long Island, N.Y. The change, locally, from disposal of waste water through individual cesspools and septic tanks to disposal through extensive communal sewers has resulted in a significant decrease in recharge to the shallow ground water and has been suspected of causing a lowering of the water table. Extensive data on ground-water levels have been collected during the last 30 years in a continuing program of water-resources studies on Long Island by the U.S. Geological Survey in cooperation with agencies of New York State and Nassau and Suffolk Counties. However, even with these data, the quantitative effects of sewering have been difficult to assess because water-level changes related to that cause must be separated from water-level changes resulting from other causes such as pumping, variations in precipitation, and creation of impervious areas by paving and building. In the present study, certain of those water-level data have been analyzed by a graphical-statistical procedure to determine the effects of the installation and operation of an extensive sewer system in part of Nassau County on ground-water levels and streamflow in that part of Long Island.

Nassau County, one of the four counties comprising Long Island, N.Y., is bordered by Queens County on the west and Suffolk County on the east (fig. 1). In contrast to the water supply for the New York City part of Long Island (Kings and Queens Counties), which is obtained mostly from upstate surface-water sources, virtually the entire public and industrial water supply for Nassau County (population about 1.6 million) is derived from the local ground-water reservoir. For the past several decades, most of the public-supply water in Nassau County has been pumped from deep confined aquifers, and only small quantities have been derived from a shallow unconfined aquifer. Until the early 1950's, a large percentage of the water from the deep aquifers was returned to the shallow aquifer through cesspools and septic tanks throughout the county. As a result, the amounts of dissolved solids and of synthetic detergents in the water from the shallow aquifer have increased sharply, particularly in the densely populated southern and western parts of the county.

To minimize further contamination and to provide efficient waste-water disposal in areas of shallow ground water near the south shore where cesspools and septic tanks are virtually inoperative, Sewer District 2, comprising about 70 square miles in the western and southwestern part of the county (fig. 1), was established in the early 1950's. The Bay Park sewage-treatment plant, which began operations in 1953, was

U.S. GEOL. SURVEY PROF. PAPER 600-B, PAGES B205-B209

285-544 O—68——15

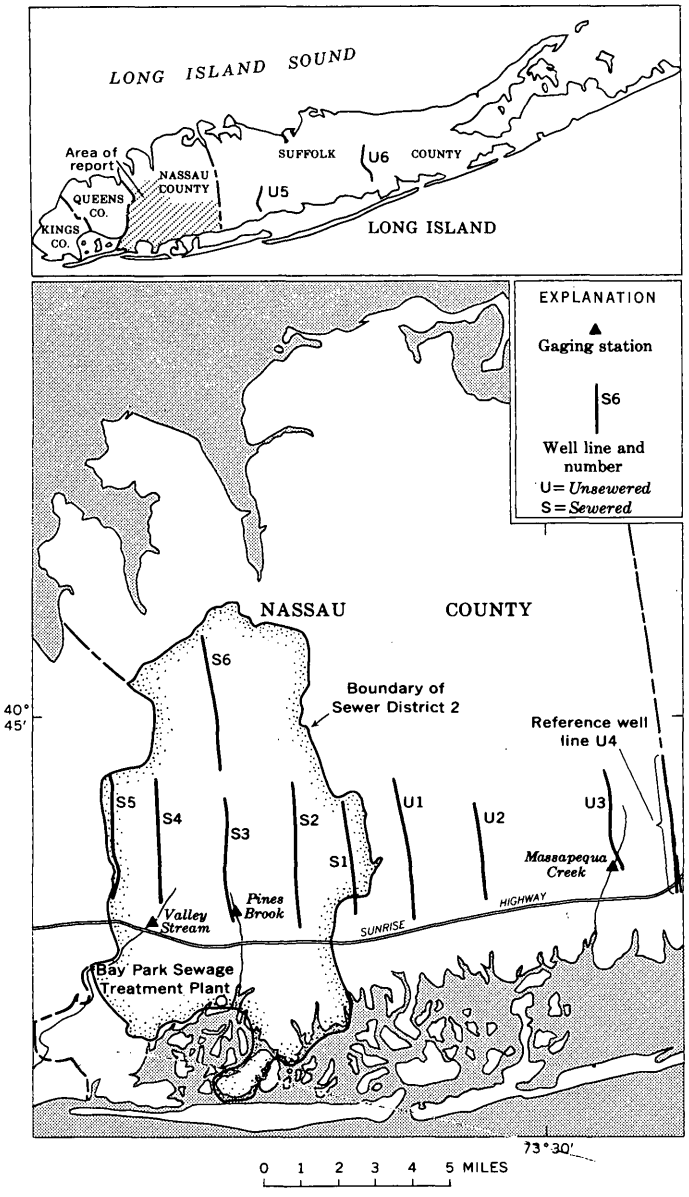

FIGURE 1.—Location of Nassau County, Sewer District 2, and well lines and streams selected for study in this investigation.

constructed near the south shore to handle the sewage from this district. Construction and hookup of the sewers in the district were virtually completed in 1964.

After the sewer system began operating fully, most of the waste water that had previously recharged the ground-water reservoir in that area by way of cesspools and septic tanks was discharged to the sea after being treated in the plant. The amount of treated waste water that was discharged from the plant to the sea since 1953 averaged about 31 million gallons per day and was about 50 mgd in 1966. The effect that this abrupt and marked decrease in recharge to the shallow aquifer has had on ground-water levels in the sewered area is the main information sought in the present analysis.

METHODS OF ANALYSIS

The first step in the analysis was to determine if shallow ground-water levels in the present sewered area were proportional to those in the present unsewered area before sewering, and whether such proportionality changed with time. The second step was to determine the extent to which the changes in proportionality were caused by sewering.

Proportionality between ground-water levels in the present sewered and unsewered areas was tested by means of double-mass curves. A double-mass curve is a graph of cumulative values of one variable plotted against the cumulative values of another variable for the same period (Linsley and others, 1958; and Searcy and Hardison, 1960). The data are proportional if the plotted points lie on a straight line, and the constant of proportionality between the quantities is represented by the slope of the line. A break in the slope of the double-mass curve indicates that a change has occurred in the relation between the two variables. Moreover, if the break in slope is not a result of a change in the method of collecting the data, the departure from linearity (direction and curvature) of the double-mass curve can be used to identify and quantitatively assess the nature of the change.

The effects of sewering on ground-water levels in the study area had to be differentiated from the effects of ground-water withdrawals, urbanization, and, especially, the pronounced drought of the past five years (1961–66) which caused a marked decline in ground-water levels throughout Long Island. One of the major inducements to use of the double-mass-curve technique was that the effects of the drought were cancelled in the analysis because the drought had roughly the same effect on water-levels in wells inside and wells outside the sewered area.

The variables that were studied by means of double-mass curves were average ground-water levels in comparable groups of wells. Water levels along 12 lines of wells were analyzed (fig. 1); 6 well lines are inside and 6 are outside the sewered area. Each well line includes either 4 or 5 wells, depending on the availability of wells and of comparable data for them. All the well lines except S4, S5, and S6 (fig. 1) are approximately parallel to the general direction of ground-water movement. Where possible, the lines of wells were chosen so that the water level in the southernmost well in each line has an average altitude between 10 and 20 feet; the water level in the next well northward has an average altitude between 20 and 30 feet; and so on. In general, the lines of wells are 3 to 4 miles long.

The effects of sewering on ground-water levels were studied mainly in the 50-square-mile area of Sewer District 2, north of Sunrise Highway (fig. 1). Ground-water levels in the shallow aquifer south of Sunrise Highway are less sensitive to changes in the hydrologic regimen, inasmuch as this area is closer to a positive hydraulic boundary—the bays connected to the Atlantic Ocean. An east-west line of wells (not shown on figure 1, nor tabulated in table 1) was used to study water-level changes in the area south of Sunrise Highway and is discussed in a later part of the paper.

The annual-average water level was calculated for each well for the period of investigation (1938–66), and the average levels for the individual wells in a particular well line were, in turn, averaged to determine a composite annual-average value for each line. The composite annual-average water levels for each well line were cumulated (added algebraically), and double-mass curves were constructed by plotting the cumulative annual-average water levels for one well line as the ordinate (y-axis) and the cumulative annual-average water level for another well line as the abscissa (x-axis). If the initial part of the curve of best fit was a straight line and the latter part deviated from an extension of that straight line, the departure in the y direction (vertical) was calculated by multiplying the observed x values by the slope of the straight line, and subtracting this calculated value from the corresponding observed y value (table 1).

The double-mass curves were evaluated to select a reference well line—that is, a line of wells in an area where ground-water levels were unaffected by sewering but where virtually all other pertinent conditions were closely comparable to those in the sewered area. The well-line U4 (U for unsewered), which is farther from the sewered area than any of the other suitable lines of wells in Nassau County, was chosen as the reference well line for this study.

Double-mass curves relating annual-average water levels for reference well-line U4 and for each of the other U well lines except well-line U6 are virtually straight. However, double-mass curves relating annual-average water levels for reference well-line U4 and for each of the S well lines (S for sewered) in the sewered area have initial straight segments which are followed by a distinct break in slope. Figure 2 shows a typical curve relating the reference well-line U4 and one of the S well lines.

RESULTS OF ANALYSIS

The calculated vertical (y-direction) departures from a straight line for the double-mass curves relat-

TABLE 1.—*Calculated departures, in feet, of the average ground-water levels of selected well lines from the average water level of the reference well-line U4*

[Italicized figures are for the first calculated departures exceeding 1 foot that are consistently followed by departures exceeding 1 foot]

	Lines of wells										
Year	U1	U2	U3	U5	U6	S1	S2	S3	S4	S5	S6
1938	−2.4	−0.3	−0.1	+0.5	------	+1.4	+0.4	+1.0	+0.4	------	−0.6
1939	+1.3	+.7	+.7	+1.2	------	+0.4	+.3	−0.4	+2.0	------	+2.9
1940	−.4	−.6	−.2	+.1	------	−.5	−1.3	−.9	−1.0	−0.3	−.5
1941	+.6	.0	+.8	+.2	------	+1.0	+.1	+.2	−.1	+.5	+.7
1942	+1.4	+.9	+1.7	+1.1	------	+1.9	+.8	+.3	+.1	+.7	+1.2
1943	−.4	+.5	+.4	−.1	------	+1.1	+.2	−.1	−.2	+.6	−.6
1944	−.2	.0	−.5	−1.1	------	+.4	−.7	−.9	−.9	−.5	−2.5
1945	.0	.0	−.9	−.4	−0.3	+.5	−.3	−.2	.0	+.9	+.2
1946	.0	.0	.0	−.5	+.2	+.5	−.1	−.4	+.2	+.5	+.8
1947	+.4	+.2	+.5	−.2	+.8	+.6	.0	+.2	+.2	+.7	+1.5
1948	−.5	+.2	−.9	−1.0	−1.4	+.5	−.8	−.9	−1.4	−1.1	−3.1
1949	+.2	−.1	+.2	−.2	+1.6	+.7	+.1	−.1	+.1	+.5	+.8
1950	+.7	+.3	+.7	+.2	+1.5	+1.4	−.3	+.1	+.1	−.1	+2.0
1951	+.4	+.5	.0	−.4	+.1	+.5	−.4	.0	−.9	−.8	−.7
1952	−.3	.0	−.1	−.4	−.3	+3.1	−.5	−.7	−.5	−.8	*−1.4*
1953	−.5	−.1	−.4	.0	+.8	+1.2	*−1.5*	*−1.2*	*−3.0*	−.8	−1.1
1954	−.2	−.9	−.2	+.7	*+1.5*	−.5	−1.4	−1.0	−2.3	*−1.5*	−1.0
1955	−.6	−.9	−.4	+.3	+2.0	−.8	−1.5	−1.3	−2.4	−2.1	−1.7
1956	−.2	−1.3	−.3	+.7	+2.3	*−1.0*	−1.7	−2.0	−2.4	−2.1	−2.9
1957	−1.1	−1.2	.0	−.1	+1.6	−1.3	−1.2	−1.8	−3.9	−2.8	−2.3
1958	−1.1	−1.5	−.8	.0	+2.4	−1.0	−2.0	−2.2	−4.6	−3.9	−5.0
1959	−.9	−1.7	−.1	+.1	+2.9	−1.5	−2.3	−3.0	−5.6	−5.2	−4.4
1960	−.9	−1.3	−.3	.0	+1.4	−2.2	−2.5	−3.6	−7.1	−6.2	−6.1
1961	−1.2	−1.3	−.7	+.3	+1.6	−2.3	−2.4	−3.4	−7.3	−6.0	−5.7
1962	−1.2	−1.3	−.8	−.4	+1.9	−2.9	−3.3	−4.3	−8.8	−4.9	−7.1
1963	−.9	−.9	−.2	−.4	+2.0	−3.1	−3.4	−4.2	−10.3	−7.1	−7.6
1964	−.9	−.8	−.1	−.6	+1.5	−2.9	−3.9	−5.4	−12.1	−10.4	−10.1
1965	−.6	−.6	+.1	−.6	+1.9	−2.8	−4.0	−6.3	−13.2	−12.2	−11.3
1966	.0	−.1	+.6	−.4	+1.4	−2.9	−4.5	−7.2	−14.4	−13.1	−13.5

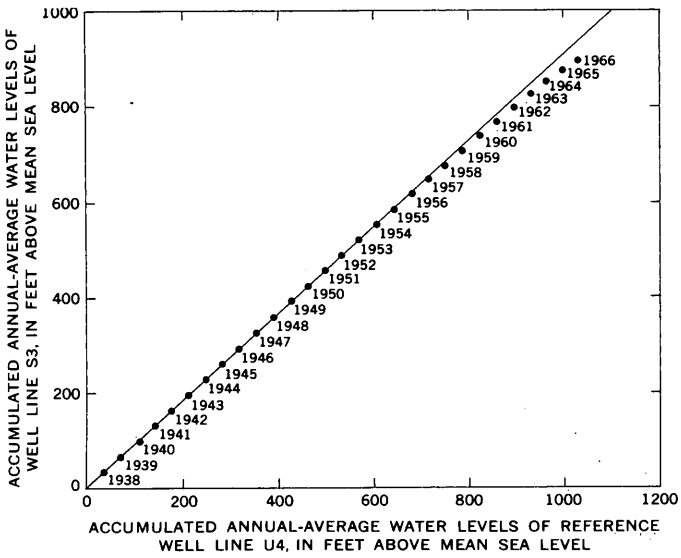

FIGURE 2.—Double-mass plot of composite annual-average ground-water levels along the reference well-line U4 and along well-line S3, in the sewered area.

ing the reference well-line U4 (plotted on x-axis) to the other lines of wells studied are listed in table 1. Except for the calculated departures for well-line U6, which are discussed subsequently, the departures for the U well lines are small, and probably largely reflect numerous minor local factors, such as nearby pumping and slight differences in recharge from place to place. The small calculated departures for the U well-lines data, which generally are less than one foot, are an indication of the "noise" in the data. With only minor discrepancies, the calculated departures for data of the S well lines increase steadily from the early 1950's through 1966. These calculated departures are consistently negative, which shows that average ground-water levels in the S well lines have declined relative to water levels in the reference well line. The largest departures are for the well lines in the northern and western parts of the sewered area (fig. 1). The first calculated departure for each well line that exceeded 1 foot and that was consistently followed by departures exceeding 1 foot is italicized in table 1. For three of the S well lines (S2, S3, and S4), the year in which this occurred was 1953—the year that the Bay Park sewage-treatment plant first began limited operations. For one S well line (S6), the year was 1952. These data suggest that the calculated departures of the S well lines in table 1 are not entirely the result of sewering, but are at least partly related to other factors which are discussed subsequently.

The magnitude of the decline in ground-water levels in the sewered area relative to water levels in the area of the reference well-line U4 was evaluated from the data in table 1, by weighting the departures for each line of wells in the sewered area according to the relative size of the area for which each was believed to be representative. By this means, the average cumulative water-level decline in the 50 square-mile sewered area north of Sunrise Highway, relative to the reference well-line U4, was calculated to be about 10 feet by 1966.

For the previously described east-west well line of 5 wells in the sewered area south of Sunrise Highway, the annual-average water levels also showed a departure from a straight-line relationship when plotted against the corresponding water levels of the reference well-line U4. However, the calculated departure—about 1.5 feet by 1966—was considerably smaller than those for the lines of wells in the area north of Sunrise Highway.

Because streams on Long Island function as ground-water drains, a significant decline of ground-water levels within the sewered area should have been reflected by a corresponding decrease in streamflow. To test this hypothesis, double-mass curves were plotted relating the annual-average discharge of Massapequa Creek (the nearest gaged stream to the reference well-line U4) in the unsewered area and the discharges of Pines Brook and Valley Stream in the sewered area. The resulting curves also were characterized by marked negative departures from initial best-fit straight-line segments. The calculated departures of annual-average streamflow for Pines Brook and Valley Stream are given in table 2.

The double-mass-curve analyses indicate that a marked decline in ground-water levels has occurred in the sewered area relative to the unsewered area in Nassau County. However, in addition to sewering, other factors have contributed to the decline. The major factors are (a) the effects of ground-water pumping and (b) changes in direct runoff and ground-water recharge owing to urban development.

Pumping from two sources probably affected ground-water levels in the sewered area, namely (1) the New York City system, which is located in southern Nassau County south of Sunrise Highway, and (2) public-supply wells in neighboring Queens County, to the west. Although more than 25 mgd was pumped from the New York City system for short periods, the pumping averaged less than 5 mgd from the entire system between 1951 and 1966, and was divided about equally between the sewered and unsewered areas. Therefore, relative water-level declines related to this pumping were negligible and can be disregarded as a significant factor in this analysis.

Intensive pumping in neighboring Queens County and the resulting cone of depression have affected

TABLE 2.—*Calculated departures, in cubic feet per second, of annual-average discharge of Pines Brook and Valley Stream from the annual-average discharge of Massapequa Creek*

Year	Calculated departures	
	Pines Brook	Valley Stream
1940	−0.4	−0.1
1941	+.3	.0
1942	+1.1	+.5
1943	+.4	+.6
1944	−.7	−.5
1945	+.9	−.3
1946	−.6	−.1
1947	+.1	−.3
1948	−.8	−.3
1949	−.4	−.2
1950	−.2	+.1
1951	+.5	−.1
1952	−1.3	−.5
1953	−2.7	−1.5
1954	−1.7	.0
1955	−2.2	+1.7
1956	−2.5	+.9
1957	−.4	+1.3
1958	−1.3	−.2
1959	−2.4	−1.8
1960	−2.4	−1.4
1961	−5.0	−4.5
1962	−3.6	−3.5
1963	−3.3	−3.4
1964	−3.1	−3.3
1965	−2.6	−2.8
1966	−1.2	−1.2

ground-water levels in the sewered area. The center of the cone of depression, about 5½ miles west of the Nassau County border, has been at or somewhat below sea level since the early 1930's. A detailed evaluation of the effects of this feature is beyond the scope of this report; however, the average water-level decline in the sewered area of Nassau County resulting from pumping in Queens County is estimated to be about 3 feet or less. This estimate is based on consideration of several factors including (1) the distance of the center of this pumping from the sewered area, (2) the magnitude of the pumping relative to the discharge at Bay Park, and (3) the location of a recharge boundary (the ocean), which is closer to the pumping in Queens County than to the sewered area in Nassau County.

Decreased ground-water recharge resulting from the construction of impervious surfaces and consequent increased direct runoff to the streams in the urbanized areas under study also has affected ground-water levels in the sewered and unsewered areas. To investigate the magnitude of this effect, water-level data for the reference well-line U4 were plotted against data for well-line U6—a line of wells located in an area in eastern Suffolk County that is virtually free of urban development. The calculated departures from the initial straight portion of the double-mass curve relating the two well lines are listed in table 1 (well-line U6). Since 1954, the water levels in wells of line U6 have averaged about 2 feet higher than those of the reference well-line U4. In other words, water levels in the wells of reference line U4 have declined relative to water levels in the wells of the U6 line by about 2 feet. All the lines except U6 are in areas where a significant percentage of the water from precipitation falls upon impervious surfaces resulting from urban development, and leaves the areas as direct runoff to streams. The effects of this factor, therefore, probably are about the same at the present time in both the sewered area and the parts of the unsewered area that were studied. However, during the period of rapid development in southern Nassau County, starting in the early 1950's, one of the two areas may have been affected by this factor more than the other area for a short period of years. Such unequal variation in the effects of urban development may partly explain the calculated departures of more than 1 foot for some of the S well lines beginning in and prior to 1953 (table 1).

CONCLUSIONS

The results of the double-mass-curve analyses indicate that an average water-level decline of 10 feet for the 50-square-mile area under investigation is the maximum that could be attributed to the sewering if no other factors were involved. If it is assumed that 3 feet of the decline resulted from pumping in Queens County, the estimated water-level decline resulting from sewering in the area averaged about 7 feet. However, the water-level decline at specific locations within the study area that is attributable to sewering ranged from about 1 to 15 feet.

If the specific yield of the shallow aquifer is assumed to be 20 percent, the estimated average loss of ground water from storage in the sewered area as a result of sewering is on the order of 3 mgd since 1953.

The losses of flow in the two gaged streams within the sewered area (Pines Brook and Valley Stream), in relation to streamflow in the unsewered area, correspond to an average of about 5.7 cubic feet per second since 1958 and about 3.3 cfs (2 mgd) for the period since 1953. As with the associated declines of ground-water levels, most of that decrease in streamflow is attributed to the sewering.

REFERENCES

Linsley, R. K., Kohler, M. A., and Paulhus, J. L., 1958, Hydrology for engineers: New York, McGraw-Hill Book Company, 340 p.

Searcy, J. K., and Hardison, C. H,. 1960, Double-mass curves; *with a section on* Fitting curves to cyclic data: U.S. Geol. Survey Water-Supply Paper 1541–B, p. 31–66.

TEMPERATURE PROFILES IN WATER WELLS AS INDICATORS OF BEDROCK FRACTURES

By FRANK W. TRAINER, Washington, D.C.

Work done in cooperation with the New York Water Resources Commission

Abstract.—Wells in the gently dipping Lockport Dolomite in Niagara County, western New York, are characterized by downward flow of water from fractures in the upper part of the rock to deeper fracture zones. Temperature profiles for these wells can be used to determine the vertical distribution of water-bearing fractures because the profiles show inflections which mark the levels of the fracture zones receiving the water. The areal distribution of the fractures can be studied by correlation of these fracture zones from one well to another.

Temperature profiles in wells characterized by internal flow of water have been used to study the distribution of fractures in the Lockport Dolomite in western New York. In a typical well, ground water from fractures in the upper part of the rock flows down the well bore and out into deeper fracture zones. This downward movement leads to much more effective transfer of heat than can occur where the rock is not penetrated by wells. Discontinuities in a temperature profile for the well mark the levels of the fracture zones that receive most of the flow. This interpretation was presented briefly in an earlier report (Trainer and Eddy, 1964) which described a periscope for use in wells. Subsequent study has shown a considerable variety in the character of the measured profiles. This report describes representative temperature profiles and illustrates their use in interpretation of the distribution of fractures in the Lockport Dolomite.

The Lockport Dolomite, of Silurian age, crops out in a belt a few miles wide that extends across western New York and into Ontario. Near Sanborn, N.Y. (fig. 1), in Niagara County about 10 miles east of the city of Niagara Falls, the dolomite is about 120 feet thick and dips very gently to the south. Two types of fractures—bedding joints and vertical joints—are well developed in the rock. The bedding joints are present in most surface exposures and have been observed with a periscope in numerous wells. Vertical joints are most abundant near the bedrock surface; they commonly extend to depths of less than 10 to 15 feet. A few vertical and steeply dipping joints have also been observed in wells. Johnston (1964) examined the entire thickness of the Lockport Dolomite where it was exposed in deep construction excavations near Niagara Falls. He (1964, p. 23–29) found that below the level of the near-surface vertical fractures the dolomite is cut by at least seven distinct zones of bedding joints. Each zone consists of a single open joint or of a group of several joints. These zones commonly occur in thin-bedded rock or at distinct lithologic breaks in the dolomite. The zones are separated from one another by thick or massive beds that are relatively impermeable, and each zone is a separate and distinct artesian aquifer. Observations in the excavations showed that some of these zones of bedding joints extend laterally for distances of several miles.

Johnston (1964, p. 50–55) concluded that recharge of the zones of bedding joints is almost entirely from precipitation, and that the water, after moving through the thin cover of glacial drift, enters the bedding joints where they intersect the buried bedrock surface or where they are intersected by vertical fractures near that surface. In most wells the piezometric level for each zone of bedding joints is lower than that for the water-bearing zone next above it, and in wells which penetrate two or more zones water moves

U.S. GEOL. SURVEY PROF. PAPER 600-B, PAGES B210-B214

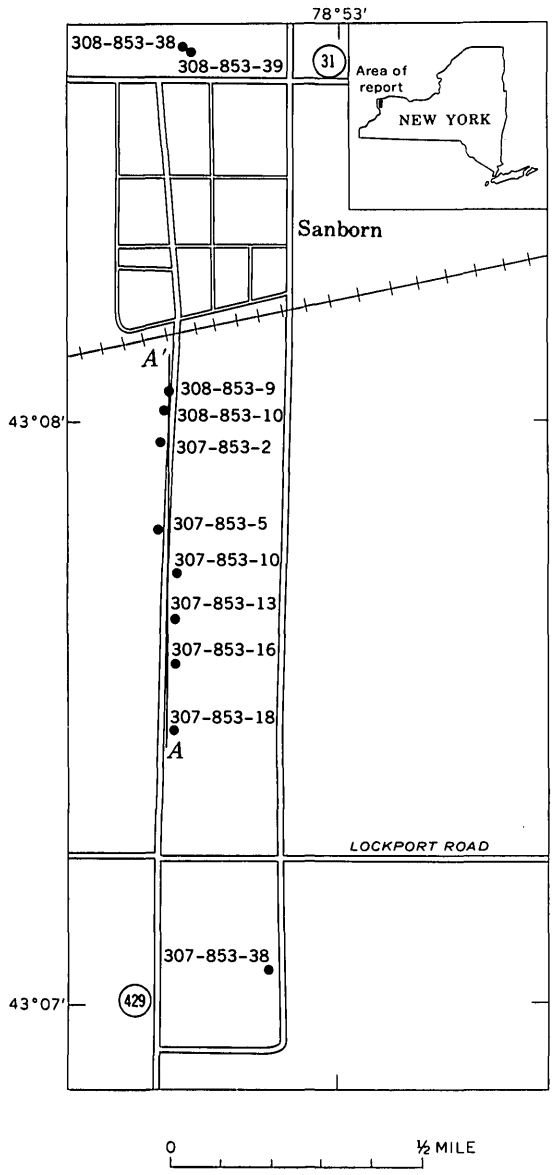

FIGURE 1.—Index map showing area in vicinity of Sanborn, N.Y. Solid circles are wells for which temperature data are presented in this report. Number beside well symbol is well number referred to in text. *A-A'*, line of section shown in figure 3.

into and down the wells from the upper zone(s) of higher head (Johnston, 1964, p. 29). In the Sanborn area, in April and May 1967, the velocity of downward flow in the several wells tested was found to be less than the lower limit of measurement with the current meter (about 2 feet per minute). In one well in which a flow guide could be used to channel all the flow through the meter, a maximum velocity down the well bore of about 2.3 feet per minute (about 3.3 gallons per minute) was measured.

TEMPERATURE PROFILES AS INDICATORS OF THE VERTICAL DISTRIBUTION OF FRACTURES

An earlier study at Sanborn (Trainer and Eddy, 1964, p. D205) showed that the form of measured temperature profiles departs markedly from that of ideal profiles computed on the assumption that heat flow is entirely by conduction through the dolomite. The measured profiles, rather than being smooth curves as are the ideal profiles, are marked by conspicuous breaks in slope, or inflections. Fractures or groups of fractures were found at or near the positions of the inflections, and the inflections are taken to indicate the principal levels at which water moving down the well bore flows out into the rock. Thus, during winter and early spring, when the near-surface ground water is relatively cold, the rock wall of the well loses heat to the downward-moving water. The flow of water and the loss of heat become progressively less below the level of each fracture or group of fractures which receives water, and these largely stepwise changes are expressed as inflections in the temperature profile. A similar but temperature-reversed process occurs later in the season when the downward-moving water is warmer than the rock penetrated by the well.

The data presented in 1964 were from well 307–853–10. Figure 2 shows five temperature profiles for this well. Fractures or groups of fractures were observed with a periscope at the following depths (in feet below the land surface): 8, 12, 13, 18, 19, 22–24, 29–30, 32, 38, and 40. The principal inflections in the temperature profiles (see fig. 2) are at about 12, 16–19, 21–24, 29–30, 32–34, and 39 feet. Because the temperature profiles were constructed from temperature measurements made at intervals (commonly 1 or 2 feet) down the well, some inflections cannot be located precisely; those which represent zones of fractures rather than single fractures may be complex changes of slope over several feet of profile.

More than a hundred temperature profiles have been measured in about 60 bedrock wells in the Sanborn area. Most of these profiles are characterized by inflections similar to those in the profiles for well 307–853–10, and in most wells the positions of fractures or fracture zones can be determined from the profiles. Thus, in this area of strong seasonal differences in surface temperature and of horizontally stratified rocks with layered permeability, temperature profiles in wells serve to identify water-bearing zones in the rock.

SEASONAL CHANGES IN TEMPERATURE PROFILES

Passage of the seasons brings changes in the quantity and temperature of the shallow ground water

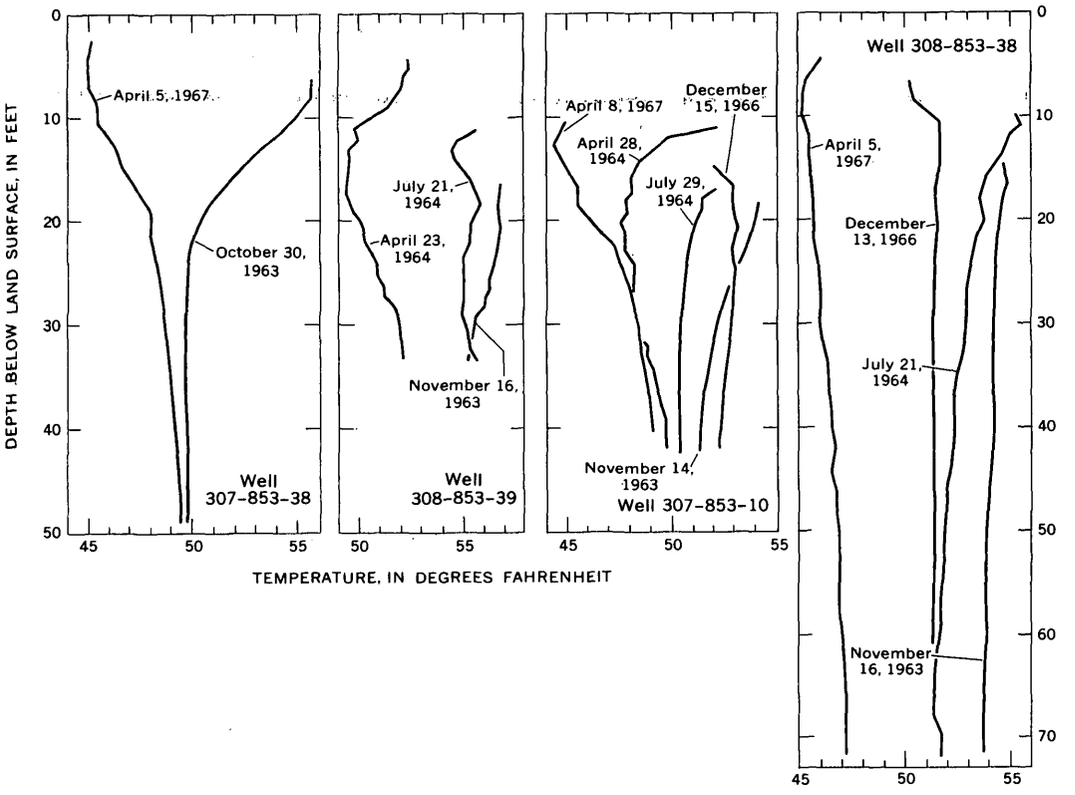

FIGURE 2.—Temperature profiles for four wells in and near Sanborn, N.Y. See figure 1 for locations of wells. Well 307–853–10: profile for April 28, 1964, at 29–31 feet, approximately duplicates profile for April 8, 1967.

which recharges the deeper fracture zones by flow down wells. Temperature profiles made in 1963–64 in well 308–853–39 (fig. 2), together with other data from this well, provide a key to the interpretation of these seasonal changes. The effects of these changes can be seen in the profiles for well 307–853–10, already discussed, and in many of the other profiles made in the Sanborn area.

A periscope survey of well 308–853–39 showed the presence of 25 fractures which are rather regularly distributed between the bottom of the casing, 8 feet below the land surface, and the bottom of the well at 34 feet. No fractures were seen in the intervals from 8.8 to 11.3 feet and from 28.4 to 31.4 feet. These data do not reveal zonation of the fractures. However, inflections in temperature profiles for well 308–853–39 (fig. 2) suggest zones of hydraulically significant fractures at about 11–17 feet, at about 20–22 feet, and at several places between 23 and 29 feet. Because the profiles are based on measurements made 1 foot apart, down the well bore, inflections cannot be located with precision greater than about 1 foot.

Current-meter measurements made at 1-foot intervals of depth in well 308–853–39 on May 23, 1967 showed a downward flow of about 2.3 feet per minute (about 3.3 gallons per minute) between 11 and 16 feet inclusive. No flow was detected by measurements above 11 feet and below 16 feet. (The lower limit of sensitivity of the meter, used with a flow guide which channels all the flow through the meter, is about 1 foot per minute.) The position of greatest flow thus nearly coincides with the fracture zone at about 11–17 feet which, according to the interpretation of the temperature data given above, is a water-bearing zone. The form of the profile for April 1964, between 11 and 17 feet, suggests that the fracture zone consists of two parts: a thin member at about 11 feet; and a thick member, between 13 and 17 feet, which because of the near-vertical slope of the temperature profile is believed to have been receiving water through several fractures distributed over its entire thickness. Shallower fractures in which the water is under higher head are the source of the water which moves down the well. Two fractures were seen at 8.6 and 8.8 feet. The current-meter data show that they did not provide all the downward-moving water. Part of it may have come from a fracture seen at 11.3 feet, in the "thin member" noted above, or from unrecognized fractures between 8.8 and 11.3 feet.

By July 1964 the fractures in the uppermost part of the rock had been drained, the prominent bulge in the April temperature profile had largely decayed, and the column of water and walls of the well had been warmed through several degrees. The temperature change at the bottom of the well over this 3-month period was about 3½°F. Before the uppermost part of the rock was dewatered, heat required for these changes must have been provided by the unconfined ground water, which in this area is warmed markedly in late spring and early summer. Probably the downward flow from the unconfined aquifer exceeded the transmissive capacity of the fracture zone at 11–17 feet, and a small part of the water bypassed that zone. After complete drainage of the unconfined aquifer, heat was carried down the well by water from the zone at 11–17 feet, which now had the highest hydraulic head among water-bearing fractures tapped by the well. Thus this zone now lost water rather than gaining it, and also began to lose its conspicuous expression in the temperature profile. The strongly convex form of the bulge in the July profile, with a residual cool "peak" at about 13 feet, is interpreted as follows: the downward-moving water was by now derived from the rock just below the 13-foot level, and it was warming the rock adjacent to the deeper part of the well; the water standing in the well above 13 feet also was gaining some heat from the air in the uncapped casing.

No further observations were made in 1964, but study of a temperature profile for well 308–853–39 made in November 1963 (fig. 2) suggests that continuation of the processes postulated in the preceding paragraph leads to extensive dewatering of the fracture zone at 11–17 feet, and to further warming of the column of water and of the rock adjacent to the well.

Temperature profiles measured during the spring differ considerably in wells 308–853–39 and 308–853–38, which are about 50 feet apart. The downward-moving water seems to be carried more rapidly to greater depths in well 308–853–38, so that temperature is more nearly uniform down the well bore (the profile is more nearly vertical) during the early part of the year when the downward flow of water is at its maximum. (Later in the year, profiles in the two wells are more similar.) Well 308–853–38, being nearly 40 feet deeper than well 308–853–39, penetrates a greater total number of fractures to a greater depth. This facilitates the more rapid movement of water down well 308–853–38 which is implied by the near-vertical form of the profiles, and is thought the likely explanation of the differences in spring profiles for these wells.

The wide annual range in temperature at the bottoms of most wells at Sanborn is the most striking seasonal effect of the flow of water down these wells. Comparison of profiles for well 307–853–38 (fig. 2) with the profiles already discussed illustrates the magnitude of this effect. Well 307–853–38 penetrates 40 feet of unconsolidated sediment, and is cased to the top of the bedrock. It is common practice of drillers in this area to drive well casing into the dolomite to prevent leakage of water around the end of the casing and into the well. The nature of the unconsolidated material penetrated by the well, and the significance of inflections in the upper parts of temperature profiles for the well, are not known. However, the lower parts of the profiles for well 307–853–38 indicate that the annual range in temperature at depth, in a well not characterized by internal flow of water, is much smaller than in wells where flow occurs. Thus, in well 307–853–38 the range at 30 feet, between the dates of the profiles, is about 1°F. In contrast, at 30 feet in well 308–853–38 and for approximately the same dates, the range is about 8°F.

This relatively large annual temperature fluctuation at depth, caused by the movement of water down wells, provides a means of estimating how widespread such flow is in the Sanborn area. For the purpose of this estimate a temperature of 50°F at a depth of 30 feet (see well 307–853–38, fig. 2) is arbitrarily taken as a maximum value for the autumn temperature in a well where internal movement of water is insignificant. In October and November, 1963, temperature measurements were made at the bottoms of 69 wells which are more than 30 feet deep. Of these 69 wells, 7 percent had bottom temperatures lower than 50.0° and 93 percent had bottom temperatures of 50.0° or higher. These data strongly suggest that downward flow of water occurs in most bedrock wells deeper than 30 feet in the Sanborn area. By extension they imply the widespread occurrence of zones of bedding fractures such as Johnston (1964) found near Niagara Falls.

LATERAL DISTRIBUTION OF FRACTURE ZONES

If zones of bedding fractures are as widely developed near Sanborn as is suggested above, it should be practicable to correlate these zones through the use of temperature data, much as lithologic, water-quality, or other parameters inferred from electric logs are correlated. Figure 3 illustrates such a correlation along a cross section extending south from Sanborn. Using the interpretation of temperature data from well 308–853–39, already described, inflections were marked on the temperature profiles. The positions of these inflections were translated laterally to the vertical lines which represent the wells. The dashed lines and pattern in figure 3 show the correlation of fracture zones inferred.

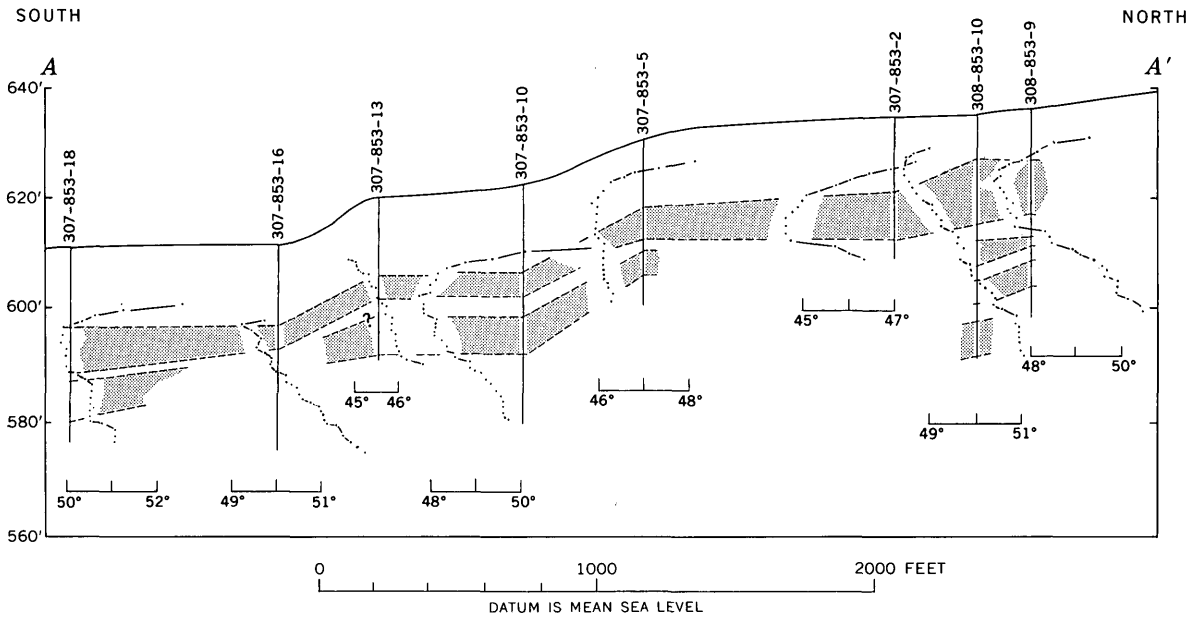

FIGURE 3.—Cross section extending south from Sanborn, N.Y., showing wells (vertical lines) and temperature profiles (curved lines) measured in them during April 1964. (See figure 1 for locations of wells and section.) Temperature scale (in degrees Fahrenheit) is shown beneath each profile. Dashed lines and pattern show inferred correlation of fracture zones.

The uppermost zone is expressed by a variety of forms among the profiles, but most of them are consistent with the two-member form of the zone at 11–17 feet in well 308–853–39. The zone at 11–17 feet in well 308–853–39 is believed to be the same as the uppermost zone shown in figure 3. This correlation implies that the top of the zone of bedding fractures declines 33 feet over the distance from well 308–853–39 to well 307–853–18 (about 1.3 miles), and thus that the dip of the strata averages about 25 feet per mile. Johnston (1964, p. 14) states that the strata near Niagara Falls dip southward about 30 feet per mile. The correlation in figure 3 also implies local changes of dip of a few feet per mile. These changes are credible; dips of several degrees, with appreciable changes over short distances laterally, can be seen in outcrops of the dolomite.

At least one deeper fracture zone can be inferred with confidence from the data shown in figure 3; it rather closely parallels the overlying fracture zone. Deeper zones are also suggested at the north end of the section, where well 308–853–10 penetrates the Lockport Dolomite to the lowest stratigraphic level shown in this section.

ACKNOWLEDGMENTS

The cooperation of property owners in the Sanborn area, who permitted study of their wells, and the assistance of R. V. Allen, O. K. Wirkki, and J. A. Ziarno in the collection of well records, are gratefully acknowledged.

REFERENCES

Johnston, R. H., 1964, Ground water in the Niagara Falls area, New York, with emphasis on the water-bearing characteristics of the bedrock: New York Water Resources Comm. Bull. GW–53, 93 p.

Trainer, F. W., and Eddy, J. E., 1964, A periscope for the study of borehole walls, and its use in ground-water studies in Niagara County, New York, *in* Geological Survey Research 1964: U.S. Geol. Survey Prof. Paper 501–D, p. D203–D206.

RELATION OF CHANNEL WIDTH TO VERTICAL PERMEABILITY OF STREAMBED, BIG SANDY CREEK, COLORADO

By DONALD L. COFFIN, Helena, Mont.

Abstract.—The upper 38 miles of Big Sandy Creek is mostly perennial, and the lower 140 miles mostly ephemeral. The channel widens downstream through the upper reach and narrows downstream through the lower. As the decrease in channel width in the lower reach is the result of adjustment to long-term downstream decrease in flood discharge, the rate of decrease in channel width between any two points along the channel affords a basis for estimation of the average vertical permeability of the streambed between those two points. The estimated values of vertical permeability may be used for computation of water losses from the stream to the valley-fill alluvium.

Big Sandy Creek, a tributary of the Arkansas River, is about 178 miles long and drains an area of about 3,600 square miles in east-central Colorado (fig. 1). An interesting feature of this stream is that its channel is widest in the vicinity of River Bend, about 140 miles upstream from its mouth. As measurements of flow indicate that the stream begins to lose water at about River Bend, the downstream decrease in channel width obviously is an adjustment to downstream decrease of flood discharge. Therefore, in any section of the

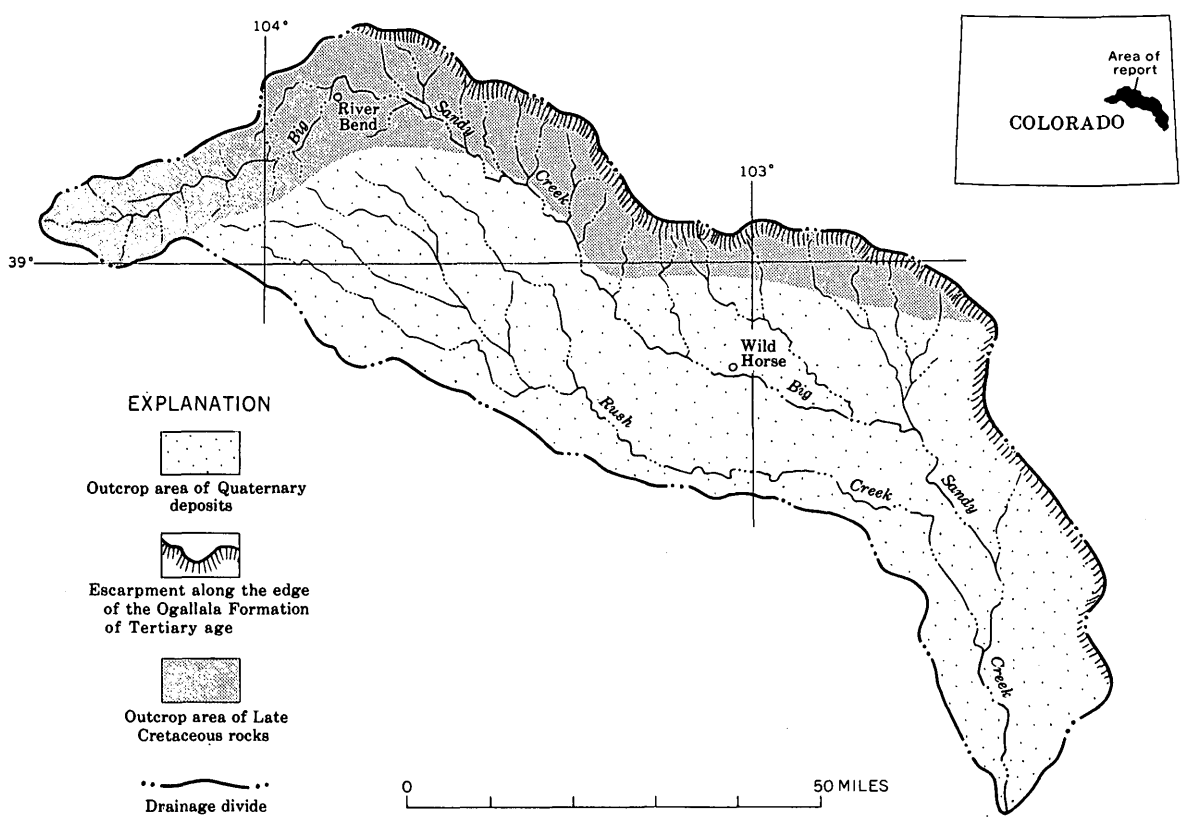

FIGURE 1.—Map showing Big Sandy Creek drainage basin, eastern Colorado, and the type of rocks exposed in the basin.

U.S. GEOL. SURVEY PROF. PAPER 600-B, PAGES B215-B218

channel below River Bend, the rate of decrease in channel width is related to the long-term average water loss, which in turn is related to the average vertical permeability of the streambed. As will be shown later, these relationships afford a method of evaluating the average vertical permeability of the streambed in any given section of the stream below River Bend.

GEOLOGY OF THE DRAINAGE BASIN

Rocks of Late Cretaceous age underlie the entire drainage basin of Big Sandy Creek and are the oldest rocks that crop out (fig. 1). West and southwest of River Bend the uppermost Cretaceous rocks are mostly fine-grained sandstone, sandy shale, and shale, but throughout the remainder of the basin they are mostly black shale, chalky shale, marl, and limestone. The sandstone is slightly permeable, whereas the shale, marl, and limestone are nearly impermeable.

Unconsolidated to consolidated rocks of Tertiary age crop out in the south- and southwest-facing escarpment that forms the basin margin north and east from River Bend. They overlie the Cretaceous rocks and comprise a complex of gravel, sand, silt, and clay lenses, the coarser grained of which are moderately permeable. Many of the smaller tributaries to the middle and lower reaches of Big Sandy Creek head in the escarpment.

Unconsolidated deposits of Quaternary age consist of sheetlike colluvium, eolian sand, and valley-fill alluvium. Except for the eolian sand, a small part of which was derived from outside the basin, the Quaternary deposits were derived wholly from Cretaceous and Tertiary rocks within the basin boundaries.

Colluvium overlies the Cretaceous rocks in a small upland area drained by the streams tributary to Rush Creek and in a small area northeast of Wild Horse. In the Rush Creek drainage area the colluvium is interbedded conglomeratic sandstone, clay, and silt. Northeast of Wild Horse the colluvium includes some gravel near its base, but the remainder is mostly silt and sand. A cover of eolian sand mantles the colluvium in most places.

Eolian sand is the most widespread of the Quaternary deposits. Except for the valley-fill alluvium and outcrop area of the Cretaceous rocks, it covers the entire drainage basin of Big Sandy Creek. In most places the sand forms dunes and is as much as 70 feet thick.

The valley-fill alluvium occupies channels that have been cut into the Cretaceous rocks. Along Big Sandy Creek these deposits generally are 30–40 feet thick and grade from coarse grained at their base to fine grained in their upper part. The basal valley fill in the upper reach consists primarily of gravel containing some cobbles (McLaughlin, 1946, p. 94) but grades downstream to medium and fine gravel. The basal gravel is overlain by coarse to medium sand that is gravelly in part, and the coarse to medium sand is overlain by sandy silt, silt, and clay. The topmost fine-grained deposits are of similar particle size the full length of the flood plain but differ in thickness. In the middle reach, where flood flows are almost completely absorbed by the valley-fill alluvium, the average thickness of the topmost fine-grained deposits increases downstream from 2 to 5 feet, but no further increase is detectable below the middle reach. The increase in thickness probably is related to the downstream decrease in the discharge of flood flows as they traverse the middle reach; the decreasing discharge causes deposition of part of the suspended load. The flood plain is about a mile wide in the middle reach and decreases to about half a mile in the lower reach.

Particle-size analyses indicate that coarse to very coarse sand constitutes 70–80 percent of the channel-floor sediment in the upper reach and 45–50 percent in the lower reach. Fine sand to clay increases from 1–2 percent in the upper reaches to 5–10 percent in the lower reaches. The banks of the channel consist of very fine to coarse sand intermixed with silt and clay. Visual inspection of the banks revealed no significant downstream decrease in grain size.

HYDROLOGY OF THE DRAINAGE BASIN

The average annual precipitation ranges from about 16 inches in the uppermost part of the basin to about 12 inches in the middle and lower parts. Generally, about 70 percent of the annual precipitation occurs during late spring and summer thunderstorms. Nearly all the storms are of small areal extent, and most produce runoff only from exposures of the Cretaceous rocks (fig. 1). Where Quaternary rocks are at the surface, all the precipitation not promptly evaporated generally is completely absorbed. Ordinarily most, if not all, of the absorbed precipitation is returned to the atmosphere through evaporation and vegetal transpiration. However, in places where the Quaternary rocks are thick enough for some of the absorbed precipitation to infiltrate to depths below the reach of plant roots, the infiltrating water eventually is added to the zone of saturation.

The 38-mile reach of Big Sandy Creek above River Bend is about 70 percent perennial, whereas the 140-mile reach below River Bend is ephemeral except in short sections below the mouths of tributaries, which contribute enough underflow to raise the water table. In the 38-mile reach the valley-fill alluvium generally

is saturated to capacity, and seepage from the zone of saturation into the stream channel occurs whenever the surface of the stream is below the adjacent water table. In the 140-mile reach, the water table in the valley-fill alluvium generally is below the floor of the stream channel and seepage from the zone of saturation into the stream channel occurs only after very large quantities of water infiltrate the alluvium and temporarily raise the water table above the stream-channel floor.

When precitipation on the area drained by the 38-mile reach is heavy enough to produce direct overland runoff to Big Sandy Creek and its tributaries, the Big Sandy generally floods because the valley-fill alluvium in that reach has little capacity to store additional water. The flood volume increases downstream commensurate with the increase in runoff-contributing area, but as soon as the floodwater passes River Bend it begins to sink into the valley-fill alluvium. Seldom is the volume of floodwater great enough for a residual flow to reach the mouth of the creek. Local heavy rains in the middle and lower parts of the drainage basin are unlikely to result in flooding because the permeable Quaternary deposits afford temporary storage space for large volumes of water.

VEGETATION OF THE DRAINAGE BASIN

Vegetation in the Big Sandy Creek basin is typical of a semiarid climate. Perennial grasses grow along the banks of the channel throughout most of the valley and tend to stabilize the banks. Scattered cottonwood trees grow along the banks and flood plain of the Big Sandy. Their distribution is not uniform along the valley, for they usually grow in irregularly shaped areas 1 or 2 miles long and several miles apart. The cottonwoods have little influence on channel width except in a few places where the density is much greater than average. In these places, the channel narrows, and the depth is slightly greater than average.

DOWNSTREAM CHANGE IN CHANNEL WIDTH

Channel width was measured at 19 places; figure 2 shows the relation of the widths plotted against their respective distances from the head of Big Sandy Creek. Channel width is defined as width near bankfull stage. Bankfull stage was estimated in the field, and the width measured with a steel tape.

In places the bankfull stage, and hence true channel width, was difficult to estimate exactly, which probably explains much of the scatter of points in figure 2. Throughout the course of the stream, channel width increases sharply below the mouths of the larger tributaries, and the corresponding points lie above the trend shown on figure 2. Several points lying below the line

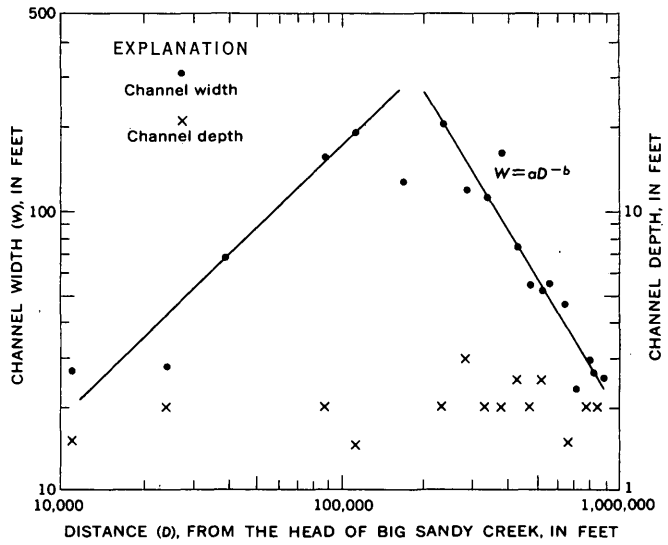

FIGURE 2.—Relation of channel width and channel depth to distance from the head of Big Sandy Creek.

represent measurements of width near short perennial reaches, where the width is restricted by abundant vegetation. Except for possible variations of gradient in these short reaches, the rate of change of channel slope does not change significantly between perennial and ephemeral reaches.

Channel width begins to decrease in about the same place that the stream becomes ephemeral for 140 miles. In this reach the water table generally is from 2 to 5 feet below the channel bed. Therefore, the valley-fill alluvium can absorb and transmit the entire flow of the usual short-duration floods.

Channel depth changes little throughout the length of the creek. Measurements of depth are plotted on figure 2. A "best-fit" line to these data would be almost horizontal, indicating that there is little if any trend to downstream changes in channel depth. Over long periods of time, the channel of Big Sandy Creek apparently adjusts to changes in discharge by changing width rather than by changing depth.

The downstream decrease in discharge is illustrated by rough data collected during the summer of 1960. On July 6, about 3 inches of rain fell on the upper reaches of the Big Sandy basin. Although the resulting flood produced a flow of about 300 acre-feet at Wild Horse in the middle reach, where there had been no rain, within one day the flow was almost completely absorbed within 22 miles of stream channel downstream from Wild Horse. The area of wetted material was about 110 acres. Therefore, absorption was about 14 acre-feet per mile of stream channel and about 3 acre-feet per acre wetted. Water levels in observation wells about 80 feet from the channel rose during the

flow. Rises ranging from 0.09 to 0.25 foot were measured, but as the water-level fluctuation was not recorded continuously, it is not known whether the maximum rise was measured.

As the rate of decrease in discharge between any two points in the ephemeral reach is governed by the vertical permeability of the streambed between the two points, the average vertical permeability of those sediments can be expressed in terms of the changes in channel width, depth, slope, and channel roughness within that reach and distance of the reach from the head of the stream.

If saturated seepage is assumed and horizontal seepage into the banks is ignored, the seepage rate, Q, into the streambed may be expressed as

$$Q=P_v IA, \tag{1}$$

where P_v is the coefficient of vertical permeability, I is the gradient (change in depth of flow), and A is the area through which seepage occurs.

The area (A) through which vertical seepage occurs may be found by integrating the curve on figure 2 between any two points e and f in the ephemeral reach or

$$\begin{aligned} A&=\int_e^f W\delta D \\ &=\int_e^f aD^{-b}\delta D \\ &=\frac{a}{1-b}(f-e)^{1-b} \end{aligned} \tag{2}$$

where a is a numerical coefficient, W is channel width, D is the distance from the head of the stream, and $-b$ is the slope of the right side of the curve in figure 2. If there are no surface-water additions or withdrawals within the reach, seepage into the streambed is equal to the decrease of discharge between two cross sections on the stream channel, e and f. The decrease in discharge, ΔQ, which is the rate of seepage into the streambed between e and f, may be expressed as the difference between approximations of Mannings equation at the cross sections, or

$$\Delta Q=\left[\frac{1.5}{n}d^{5/3}S^{1/2}W\right]_f-\left[\frac{1.5}{n}d^{5/3}S^{1/2}W\right]_e \tag{3}$$

where d is mean depth, W is width, S is slope of the stream bed, and n is a roughness factor, assumed to be the same at both e and f. Setting equation 1 equal to equation 3 and substituting equation 2

$$\begin{aligned} P_v I\left[\frac{a}{1-b}(f-e)^{1-b}\right]&=\frac{1.5}{n}[(d^{5/3}S^{1/2}W)_f-(d^{5/3}S^{1/2}W)_e] \\ P_v&=\left[\frac{1.5}{nIa}(1-b)(f-e)^{b-1}\right][(d^{5/3}S^{1/2}W)_f-(d^{5/3}S^{1/2}W)_e] \end{aligned} \tag{4}$$

Equation 4 relates some of the hydraulic variables of the stream to the hydraulic coefficients of the underlying deposits and permits estimation of P_v. Even though the equation represents only one of several approaches that can be made with these or similar data, it does point out one of the cause-and-effect relations and the complexity of the relation between the stream and its alluvial deposits.

Many ephemeral streams, which flow over permeable deposits, exhibit a downstream decrease in channel width. If careful study shows the cause to be a downstream decrease in discharge due to infiltration, then the rate of decrease of channel width may be used to estimate recharge to the underlying aquifers. Direct measurements of recharge from ephemeral streams commonly involve measurements of flood flow, and these measurements may be difficult and expensive. Measurement and analysis of channel-width data may result in a relatively inexpensive tool to estimate recharge, or at least to compare rates of recharge by ephemeral streams in similar geologic settings.

REFERENCE

McLaughlin, T. G., 1946, Geology and ground-water resources of parts of Lincoln, Elbert, and El Paso Counties, Colorado: Colorado Water Conserv. Board Bull. 1, 193 p., 6 pls., 15 figs.

ANALYSIS OF STRESSES CAUSING LAND SUBSIDENCE

By BEN E. LOFGREN, Sacramento, Calif.

Abstract.—Land subsidence in areas of intensive groundwater withdrawal is attributed to the compaction of deposits caused by increased effective loading stresses. As demonstrated at the Pixley recorder site, subsidence is related directly to effective-stress changes computed from water-level data. Effective-stress changes are sometimes difficult to calculate in a complex of aquifer systems, even with ample water-level data. Effective stresses are changed in two principal ways: (1) Water-table fluctuations change the buoyant support of grains in the zone of the change, and (2) a change of the water table or of the piezometric head, or both, may induce hydraulic gradients and seepage stresses in the deposits. These stress changes are additive in their effect, and together cause compaction.

Nowhere have the activities of man produced more extensive land subsidence than in the San Joaquin Valley of central California (fig. 1). Here, the accelerated pumping of ground water for irrigation, especially since 1940, has caused more than 3,000 square miles of land to subside. In the area of maximum subsidence 10 miles southwest of Mendota, a water-level decline of 300 feet has resulted in 26 feet (1966) of settlement since 1930. Wherever studied in the San Joaquin Valley, a correlation exists between subsidence and water-level decline. The magnitude of the subsidence is dependent on the effective-stress increase, the compressibility of the deposits, the thickness of the compressible beds, the time the increased stress has been applied, and possibly the rate and type of stress applied. It is also dependent on the past stress history —whether the increased stress is being applied for the first time or has been attained or exceeded previously.

Depending on the nature of the deposits, compaction may be (1) largely elastic, in which case stress and strain are proportional, independent of time, and reversible, or (2) principally nonelastic, resulting from a rearrangement of the granular structure in such a way that the volume of the deposits is permanently decreased. In general, if the deposits are coarse sand and gravel, the compaction will be small and chiefly

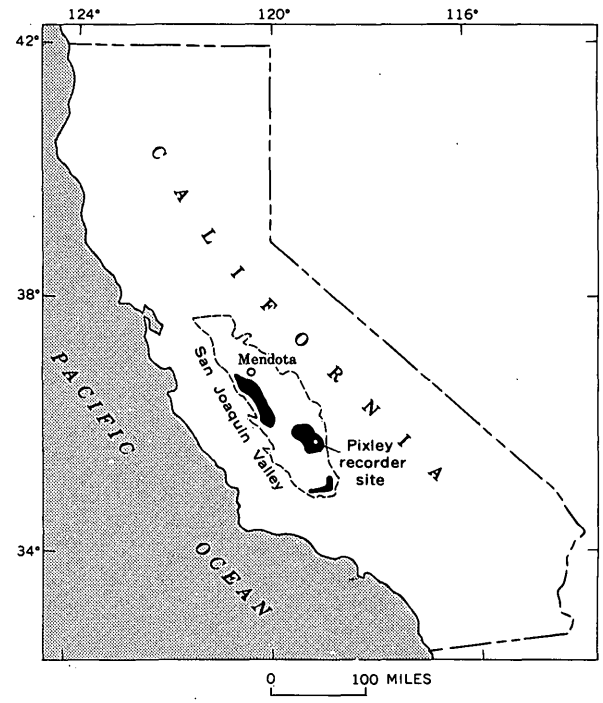

FIGURE 1.—Principal subsidence areas (shaded) in the San Joaquin Valley, and location of the Pixley recorder site.

elastic and reversible, whereas if they contain fine-grained clayey beds, the compaction will be much greater and chiefly inelastic and permanent. In either case, a one-directional compression of the deposits occurs which results in a subsidence of the land surface.

Figure 2 shows the correlation that exists in the confined aquifer system near Pixley (fig. 1) between water-level change and compaction of the unconsolidated deposits. At this location, both the confined water level in well 23/25–16N3 and the recorded compaction in well 23/25–16N1 show an immediate response to pumping effects of nearby irrigation wells. The compaction recorder (for description, see Lofgren, 1961) is anchored at a depth of 760 feet and measures the

U.S. GEOL. SURVEY PROF. PAPER 600-B, PAGES B219-B225

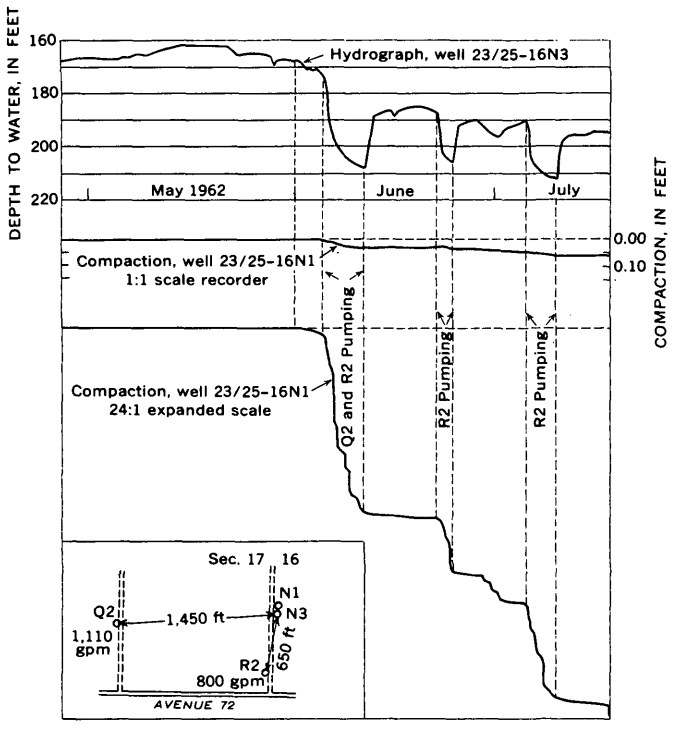

FIGURE 2.—Water-level change and compaction near Pixley.

vertical shortening that occurs in the formation, principally in the depth interval from 355 to 760 feet. As shown in the lower graph (24:1 expanded scale), compaction of the aquifer system begins immediately after the water level in nearby observation well 23/25–16N3 begins to fall, and compaction virtually stops soon after the water level in the observation well starts to recover.

Figure 3 shows the interrelationship between compaction, land subsidence, water-level fluctuations in the semiconfined (hydrograph, 23/25–16N4) and confined (hydrograph, 23/25–16N3) aquifer systems, and change in effective stress at this same recorder site near Pixley for 6 years of record. Subsidence of bench mark Q945 is determined by U.S. Coast and Geodetic Survey levelings from distant and stable bench marks. During this period measured compaction to a depth of 760 feet was 75 percent of the total subsidence. Thus, 25 percent of the vertical shortening was due to compaction below 760 feet.

Comparison of the compaction rate with fluctuations in water level in the semiconfined and confined aquifer systems indicates that compaction began each year during the period of rapid head decline in the aquifer system, continued through the pumping season, and ceased during the early stages of head recovery. Although the correlation between compaction and artesian-head change in the confined aquifer system is good, the correlation with changes in effective stress in the confined aquifer system (center graph, fig. 3) is closer. Of special interest in relating compaction to changes in effective stress is the position of straight line X–X'. Most of the compaction occurred when the effective-stress curve was below line X–X' (that is, when the stress was higher), whereas little or no compaction occurred when the effective stress was above line X–X'. Compaction continued for several weeks each year after the date of maximum effective stress and, in all instances, terminated before line X–X' was reached during recovery. In general, the amount of compaction in any year is related to the area below line X–X' bounded by the effective-stress curve.

TYPES OF STRESSES

Three different types of stresses are involved in the compaction of an aquifer system. These are closely interrelated, yet of such different nature that a clear distinction is of utmost importance. The first of these is a gravitational stress, caused by the effective weight of overlying deposits, which is transmitted downward through the grain-to-grain contacts in the deposits. The second, a hydrostatic stress due to the weight of the interstitial water, is transmitted downward through the water. The third is a dynamic seepage stress exerted on the grains by the viscous drag of vertically moving interstitial water. The first and third are additive in their effect and together comprise the grain-to-grain stress which effectively changes the void ratio and mechanical properties of the deposit; it is commonly known as the "effective stress." The second type of stress, although it tends to compress each individual grain, has virtually no tendency to change the void ratio of the deposit and is referred to as a "neutral stress."

Of the various methods used in analyzing the effect of these stresses in a compacting aquifer system (Taylor, 1948, p. 203), only two are considered here. Although they vary in their conceptual approach, these methods give the same mathematical results and can be used to check one another. The classical method, the approach most often used in practical soil-mechanics problems, considers the geostatic load, or combined total weight of grains and water in the system, and the neutral, or hydrostatic, stress. The second method considers the static gravitational stress of the grains, which comprises their true weight above the water table and submerged (buoyed) weight below the water table, and the vertical seepage stresses that may exist in the system. Inasmuch as changes in the effective grain-to-grain stress (both gravitational and stress due to seepage) are directly responsible for the com-

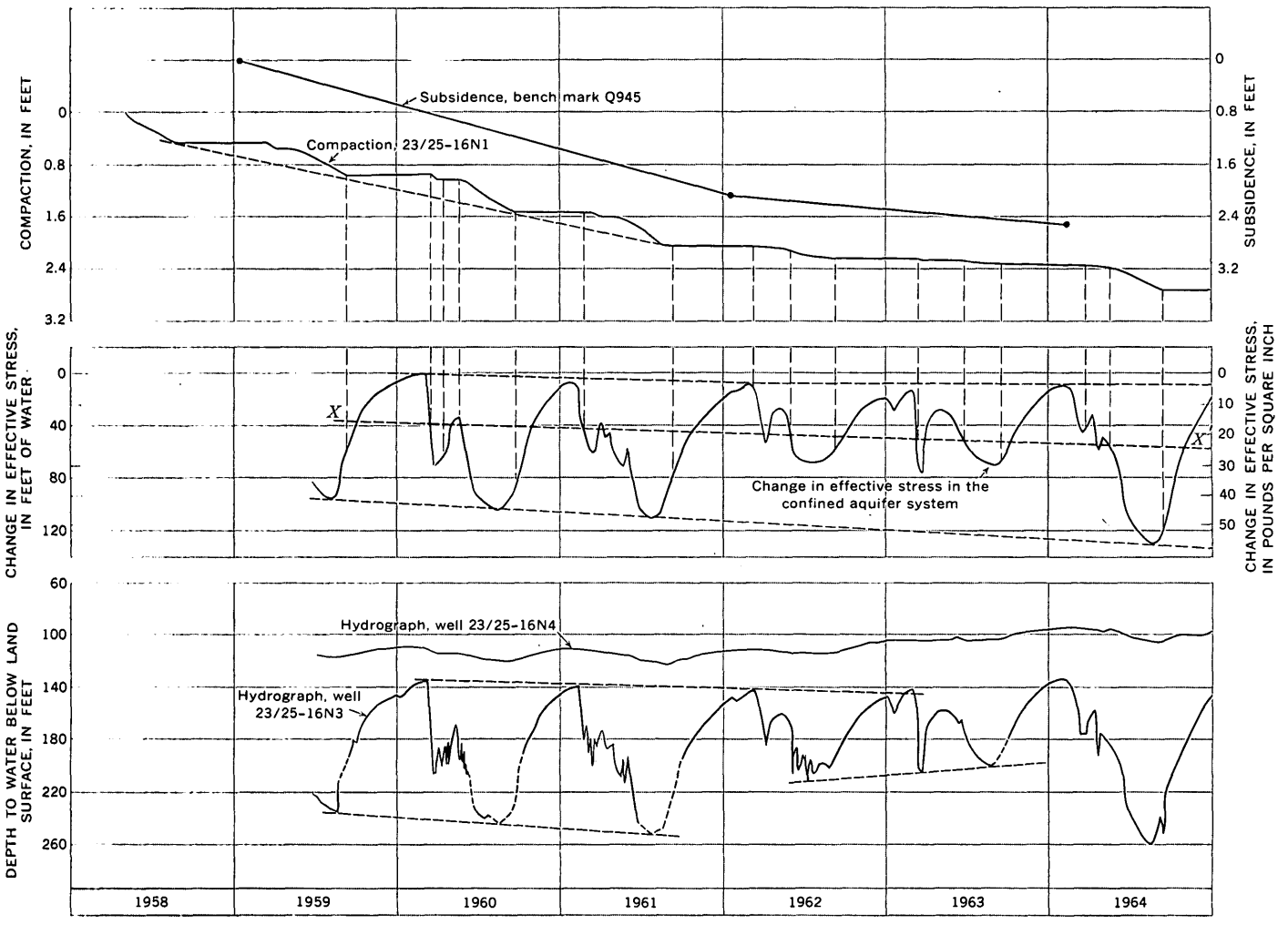

FIGURE 3.—Land subsidence, compaction, water-level fluctuations, and change in effective stress, 3 miles south of Pixley.

paction of the deposits and are directly related to changes in head in an aquifer system, this second approach has proved the simplest and clearest in our subsidence investigation.

The Terzaghi theory of consolidation (Terzaghi and Peck, 1948, p. 233) commonly is used to estimate the magnitude and rate of compaction that will occur in fine-grained clayey deposits under a given change in stress. According to the theory, compaction results from the slow escape of pore water from the stressed deposits, accompanied by a gradual transfer of stress from the pore water to the granular structure of the deposits. When an increment of loading stress is applied to an aquitard (fine-grained interbed), the entire stress increase first is borne by the interstitial water because no increase in grain-to-grain stress can occur until drainage from the aquitard begins. A high hydraulic gradient at the surface of the aquitard causes rapid drainage from the pores near that surface. Then, as the excess pressure gradually decreases, the intergranular stress increases and the void ratios decrease; this slow process always is in a more advanced state near the surfaces of the aquitard and at a less advanced state near its middle.

Effective stress increases and compaction occurs in a water-bearing bed only as rapidly as water can move out. A slowly draining aquitard may take weeks or years to adjust to an applied stress increase, whereas a coarse-grained aquifer will adjust quickly. In either case, one-dimensional consolidation results, which is directly related to the change in effective grain-to-grain stress.

RELATION OF CHANGE IN EFFECTIVE STRESS TO WATER-LEVEL FLUCTUATIONS

Water-level fluctuations in subsidence areas change effective stresses in the following two ways:

1. A rise of the water table increases the buoyant support of grains in the zone of the change, and a decline decreases the buoyant support; these changes in gravitational stress are transmitted downward to all underlying deposits.

2. A change in position of the water table or the piezometric surface (artesian head), or both, may induce vertical hydraulic gradients across confining or semiconfining beds and thereby produce a seepage stress; this stress is algebraically additive to the gravitational stress that is transmitted downward to all underlying deposits. A change in effective stress also results if preexisting seepage stresses are altered in direction or magnitude by a change in head.

In the following analysis of stresses, consideration will be given to compaction under two different hydraulic regimes, namely (1) water-table (unconfined) conditions in which no vertical hydraulic gradients exist, and (2) artesian (confined) conditions, in which vertical gradients exist and result in seepage stresses that usually represent the major part of the change in effective stress. Generally, changes in effective stress involve changes in both buoyant support and in seepage forces, with both time and depth.

Figure 4 shows the components of effective stress at three depths in an assumed hydrologic system that consists of a confined aquifer system having an interbedded aquitard and an overlying unconfined aquifer.

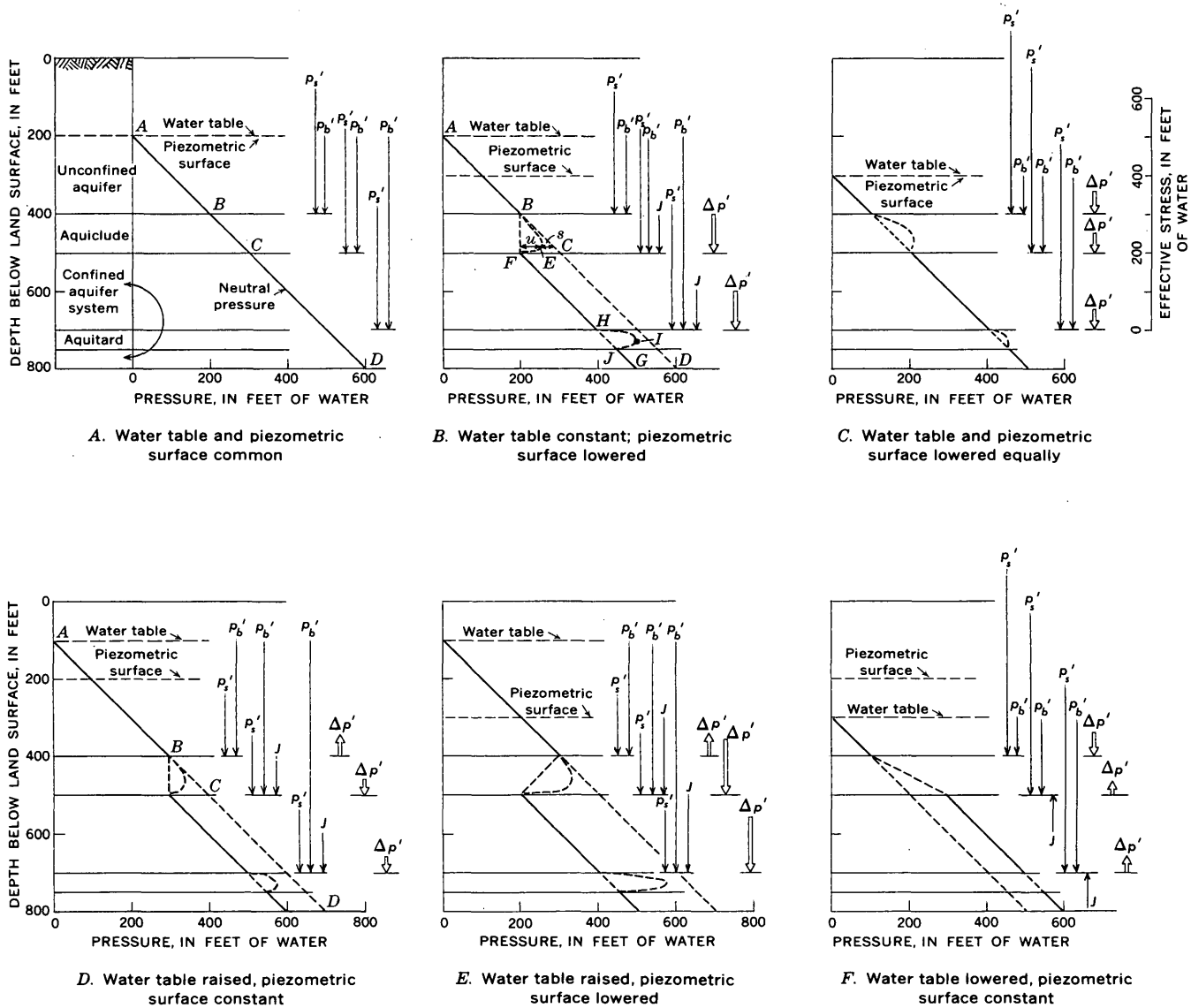

All stresses in feet of water; based on assumed porosity=0.40 and specific gravity=2.70

p_s' =effective stress due to weight of unsaturated deposits

p_b' =effective stress due to buoyant weight of submerged deposits

J =seepage stress

$\Delta p'$=change in total effective stress from condition A

FIGURE 4.—Effective-stress diagrams for a confined aquifer system overlain by an unconfined aquifer.

For purposes of demonstration, a porosity, n, of 40 percent and an average specific gravity, G, of 2.7 for the individual mineral grains are assumed. All stresses in the system are expressed in units of feet of water (1 foot of water equals 0.43 pounds per square inch) so that they are directly additive and are relatable to changes in hydraulic head. Thus, the unit weight of deposits above the water table (ignoring the contained moisture), γ_d, may be expressed as

$$\gamma_d=(1-n)\cdot G\cdot\gamma_w,$$

in which γ_w is the unit weight of water.

Correspondingly, the buoyant (submerged) unit weight, γ', of the deposits below the water table equals

$$\gamma'=(1-n)(G-1)\gamma_w$$

Using the above assumed numerical values for n and G and expressing γ_w as 1 foot of water, the effective stress due to the weight of deposits above the water table equals about 1.6 feet of water per foot of thickness, and the effective stress due to the weight of deposits below the water table equals approximately 1.0 foot of water per foot of thickness.

UNCONFINED (WATER-TABLE) CONDITIONS

Before pumping lowers the water table in an unconfined aquifer, the deposits are generally in equilibrium with the natural effective stresses. For any element of the deposit, these effective stresses equal the true weight (per unit area) of the unsaturated deposits and the buoyant weight (per unit area) of the saturated deposits that overlie the element. As the water table is lowered, the effective unit weight of the deposits in the dewatered zone increases from the submerged unit weight, γ', (weight of solids minus the weight of the displaced water) to the unit weight, γ_d, of the solids. Thus, the effective grain-to-grain stress in the aquifer below the dewatered zone is increased by the loss of buoyant support in the dewatered zone and the increase in effective stress at any depth below the lowered water table is equal to the increase in unit weight of the dewatered deposits multiplied by the dewatered thickness. Use of the assumed unit weights indicates that the effective stress below the lowered water table is increased 0.6 foot for each foot of water-table lowering.

CONFINED (ARTESIAN) CONDITIONS

Under simple hydrostatic conditions in a confined aquifer system (fig. 4*A*), the hydraulic heads above and below the confining layer stand at the same altitude. Therefore no hydraulic gradient exists across the confining layer and, consequently, no seepage occurs through the confining layer. The effective stresses under these hydrostatic conditions are the same as in the unconfined case, that is, equal to the gravitational stress of the overlying deposits.

If both the water table and the piezometric head in the confined aquifer are 200 feet below land surface (fig. 4*A*), the two components of effective stress exerted downward on the grains, due to the weight of deposits above the water table (vector p_s') and due to the buoyant weight of deposits below the water table (vector p_b') are 320 feet and 200 feet, respectively, on the top of the confining layer; 320 feet and 300 feet on the top of the confined aquifer system, and 320 feet and 500 feet on the top of the aquitard at a depth of 700 feet.

If the artesian pressure in a confined aquifer system, under the hydrostatic condition of figure 4*A*, is drawn down below an unchanging water table by pumping (fig. 4*B*), gravitational stresses remain the same; however, the downward hydraulic gradient developed across the confining layer (aquiclude) induces downward seepage. The loss of hydraulic head through the aquiclude represents the energy expended in moving the water through the pore passages. As head is dissipated by viscous flow through the confining layer, the energy in the moving water is transferred by viscous drag to the granular skeleton of the deposit. The force corresponding to this energy transfer is exerted in the direction of flow and is algebraicly additive with the gravitational stresses that tend to compact the deposits.

As commonly used, the term "seepage force" refers to the energy transfer that occurs within the body through which the seepage takes place. As defined by Scott (1963, p. 96, equation 4–20), the seepage force, f, exerted on the grains can be represented by the expression

$$f=h\cdot\gamma_w\cdot A,$$

in which h is equal to the head loss across an incremental thickness, and A is equal to the cross sectional area.

Within an aquiclude that is compacting under the stress of downward seepage (fig. 4*B*), the hydraulic gradient, and therefore the seepage force per unit thickness, varies from a minimum at the upper surface to a maximum at the lower surface until steady-state conditions are reached. The loading effect of the incremental seepage force developed through each unit volume vertically through the aquiclude is additive downward. Thus, the net effect of these incremental units of seepage force at any point in the structure of the aquiclude is equal to the summation of the incremental forces above that point. Although the distribution of these forces within the aquiclude may be indeterminate, the total seepage force accumulated through the aquiclude is equal to the total head dif-

285-544 O - 68 - 16

ferential across it. Thus, at the base of the aquiclude, the total seepage force, F, may be expressed as

$$F=H\cdot\gamma_w\cdot A,$$

and the seepage force per unit area, J, hereafter referred to as the seepage stress, is

$$J=\frac{F}{A}=H\cdot\gamma_w.$$

This seepage stress is transmitted downward through the intergranular structure of the aquifer system below the aquiclude. If stress or pressure is expressed as equivalent head of water instead of force per unit area, the specific weight of water, γ_w, which serves to convert head into pressure units, is not required, and the expression is simply $J=H$.

In the assumed ground-water systems of figure 4*B*, straight line *A–B–C–D* represents the hydrostatic pressure (neutral pressure) gradient that existed before pumping began. The deposits are adjusted to the overburden load which equals the actual weight of the deposits above the water table plus the buoyant weight of the submerged deposits. After pumping has lowered the head in the permeable members of the confined aquifer system to 300 feet, the effective stresses shown by vectors in figure 4*B* would prevail at the depths represented by the arrow points. The length *C–F* represents the 100 feet of head decline, and *F–G* represents the reduced fluid pressure in the confined aquifer system. With a 100-foot head loss through the confining layer, a 100-foot seepage stress is immediately developed across the confining layer and transmitted through grain-to-grain contacts to the underlying aquifer system. Even though normal hydrostatic pressure gradients exist in both the unconfined (line *A–B*) and the confined (line *F–G*) aquifers, hydraulic gradients and transient flow conditions within the confining aquiclude gradually change until a steady hydrodynamic gradient (line *B–F*) is established between the heads at the upper and lower surfaces of the aquiclude. The initial head distribution through the confining aquiclude is approximated by lines *B–C* and *C–F*, and the transient distribution of head in the confining layer at some intermediate time before steady flow is established is approximated by the curved line *B–E–F*.

As shown in figure 4*B*, the length, s, indicates the magnitude of the seepage stress at a particular depth in the aquiclude, and the length, u, indicates the excess over steady-state head (Taylor, 1948, p. 221, 236) that remains in the interstitial voids at that depth. Also, the area *BCFEB* is proportional to the part of the ultimate compaction that has occurred and area *BEFB* to the part of the ultimate compaction that has not taken place. Domenico and Mifflin (1965, p. 571) referred to the combined area *BCFB* as the "effective-pressure area". As adjustment continues, excess pore pressures are reduced and compaction occurs within the aquiclude. After equilibrium conditions have been established, head distribution through the aquiclude follows straight line *B–F* (assuming uniform permeability), and uniform flow conditions and a constant seepage gradient prevail through the aquiclude. Under these conditions, 1 foot of head is lost (transferred to the grains) through each foot of thickness of the aquiclude. The accumulated downward seepage thrust exerted on the grains by the moving water thus varies linearly from 0 at the upper surface of the aquiclude to 100 feet at its lower surface. The total seepage stress, equal to the head differential across the aquiclude, is exerted on the granular structure of all underlying beds in the aquifer system. The time involved in reaching complete adjustment is dependent chiefly on the thickness, compressibility, and permeability of the confining layer.

At all times after the head in the confined aquifer system is lowered to 300 feet, the magnitude of the seepage stress (increased effective stress) exerted downward on all beds within the confined system (below the aquiclude) is 100 feet (distance *C–F*, fig. 4*B*). In the more permeable, less compactible aquifers of the confined systems, the increase in effective stress occurs rapidly. Within the aquitards, however, no change in effective stress can occur until water escapes from these slow-draining, compacting beds. The reduction in head in the permeable aquifers creates a two-directional hydraulic gradient outward from the center of the aquitard and thereby induces drainage from and compaction of the aquitard. The drainage is two-directional and excess pore pressures are transient (curved line *H–I–J*, fig. 4*B*) until equilibrium conditions (straight line *H–J*) are established. Although upward and downward seepage stresses occur within the aquitard during this adjustment, they have no net external effect on the rest of the aquifer system.

The open arrows ($\Delta p'$) at two depths in the hydrologic section of figure 4*B* are vectors indicating the change in effective stress from the hydrostatic conditions of figure 4*A*. Thus, the net effect of lowering the piezometric head in the confined aquifer system 100 feet below the water table is to create a seepage stress through the confining layer and, ultimately, to increase the effective stress in all beds in the confined aquifer system by 100 feet. No change in effective stress occurs in the unconfined aquifer overlying the confining layer. Although a small part of the resulting deformation of the confined aquifer system is elastic

and reversible, a large part represents an irreversible rearrangement of fine particles in the clayey sediments to a more dense state.

Figure 4*C* represents a dual water-level lowering, with both the water table and piezometric surface lowered 100 feet below the level in figure 4*A*. A normal hydrostatic gradient of pressure with depth exists in the aquifers and is ultimately achieved in both the aquiclude and the aquitard. However, effective stresses throughout the section are considerably different from the conditions of either figure 4*A* or figure 4*B*. Loss of buoyant support in the dewatered zone causes the effective stress changes shown in figure 4*C*. The net change in stress from conditions of figure 4*A* is shown at three depths by the open arrow vectors. Although the effective stress throughout the section is increased from conditions of figure 4*A* by the loss of buoyant support, the stresses in the confined aquifer system are less than those of figure 4*B* because there is no seepage stress component. It is apparent that if the head in the confined aquifer system had been drawn down to the condition of figure 4*B* before the hydrostatic conditions of figure 4*C* were established, rebound would tend to occur throughout the confined aquifer system as the water table was drawn down.

If the piezometric surface remains constant and the water table is raised 100 feet above the conditions of figure 4*A*, the effective stresses shown by vectors in figure 4*D* are produced. The raised water table reduces the gravitational stress below the raised level by providing buoyant support of the grains in the zone of water-table rise; it also creates a downward seepage stress across the confining layer. The net change from the conditions in figure 4*A* is to increase effective stress throughout the confined aquifer system. It is noteworthy that rebound would tend to occur in the unconfined aquifier when the conditions of figure 4*A* are changed to the conditions of figure 4*D*, whereas a 40-foot increase in stress would occur in the underlying confined system.

If the water table is raised 100 feet above the hydrostatic conditions of figure 4*A*, and the piezometric surface is lowered 100 feet, the effective stresses shown in figure 4*E* will prevail. Increase in buoyant support causes reduced gravitational stress in the unconfined aquifer, as it did under the conditions of figure 4*D*. The 200 feet of head differential across the confining layer represents a seepage stress of 200 feet exerted downward on the deposits in the confined aquifer system. Under these conditions, the change in effective stress in the confined aquifer system, due to the combined changes in gravitational and seepage stress from the hydrostatic condition of figure 4*A*, is 140 feet, which is considerably greater than for conditions illustrated in figures 4*B*, *C*, and *D*.

Figure 4*F* shows the effective stresses under the sixth general condition where the water table is lowered 100 feet below the piezometric surface of figure 4*A*. Here the effective stress in the unconfined aquifer is increased 60 feet due to the loss of buoyant support in the zone of lowered water table. Because of upward seepage stresses that are developed through the aquiclude, however, the effective stress throughout the confined aquifer system is reduced by 40 feet from the hydrostatic condition of figure 4*A*.

SUMMARY

The following generalizations are made with respect to analysis of effective stress:

1. A ground-water reservoir may act as an unconfined aquifer system if no significant vertical head differentials (seepage stresses) occur within it under ordinary pumping stress. It includes one or more confined (artesian) systems if vertical head differentials within the reservoir are significant.
2. If the porosity of an unconfined aquifer is 40 percent, the effective stress in the aquifer would increase 0.6 foot for each foot of water-table decline and would decrease 0.6 foot for each foot of water-table rise. For larger or smaller values of porosity the values of effective-stress change would be somewhat different. The change in effective stress equals the change in buoyant support of the deposits in the interval of water-table change and is independent of the specific gravity of the grains.
3. If a confined aquifer is overlain by an unconfined aquifer, the effective stress is affected by changes in both the water table and the piezometric surface. If the porosity is 40 percent, a water-table rise of 1 foot would cause a 0.4-foot increase in effective stress whereas a decline of 1 foot in the piezometric surface would cause a 1-foot increase in effective stress.

REFERENCES

Domenico, P. A., and Mifflin, M. D., 1965, Water from low-permeability sediments and land subsidence: Am. Geophys. Union, Water Resources Research, v. 1, no. 4, p. 563–576.

Lofgren, Ben E., 1961, Measurement of compaction of aquifer systems in areas of land subsidence: Art. 24 *in* U.S. Geol. Survey Prof. Paper 424–B, p. B49–B52.

Scott, R. F., 1963, Principles of soil mechanics: Palo Alto, Calif., Addison-Wesley Pub. Co., Inc., 550 p.

Taylor, D. W., 1948, Fundamentals of soil mechanics: New York, John Wiley and Sons, 700 p.

Terzaghi, Karl, and Peck, R. B., 1948, Soil mechanics in engineering practice: New York, John Wiley and Sons, 566 p.

NEUTRON MOISTURE MEASUREMENTS BY CONTINUOUS- AND POINT-LOGGING PROCEDURES

By ROBERT C. PRILL and WALTER R. MEYER, Garden City, Kans.

Work done in cooperation with the State Geological Survey of Kansas, the Environmental Health Services of the Kansas State Department of Health, and the Kansas State Board of Agriculture

Abstract.—A recently developed neutron meter records moisture measurements by continuous and point-logging procedures. Field calibration of the meter shows a linear relationship between the instrument reading and the moisture content over a range of 5 to 40 percent moisture by volume. Comparison of neutron moisture logs obtained by different logging procedures illustrates that a compromise must be made between logging time, bed definition, and curve reproducibility. Tests indicate that the point-logging procedure, using close logging intervals, provides the more accurate logs. However, the continuous-logging procedure, which requires much less time and manual operation, can provide acceptable logs for many moisture studies.

Measurement of moisture content in earth materials by nuclear methods has become commonplace in the last decade. One important application is the measurement, in drill holes, of moisture changes with time in the unsaturated zone. In the point-logging procedure, generally used for these measurements, the probe is stationed at specified depths and the neutron count is recorded for a selected time period at each depth. A recently developed neutron moisture meter reduces the time required for logging by continuously recording the measurements. This paper compares data obtained by the continuous-logging and point-logging procedures in drill holes cased with aluminum tubing and discusses the problem of logging time versus accuracy for continuous logging. The aluminum tubing, which has a 2-inch outside diameter and a 1/16-inch wall thickness, was driven and cleaned from the inside as the hole was drilled. The tests were performed in Finney County, Kans. in 1966.

NEUTRON MOISTURE PROBE AND METER

The neutron moisture probe used for this study is designed to be adaptable to a logger generally used with electric and gamma-ray logging probes. The neutron probe contains a 100-millicurie americium-beryllium source for emission of high-energy neutrons and a lithium iodide crystal coupled to a photomultiplier tube for detection of slow neutrons. Alpha particles emitted from the americium strike the beryllium nuclei and release fast neutrons from the probe. The emitted neutrons are slowed down by collision with the low-atomic-weight nuclei. Because the hydrogen nuclei in water are the predominant low-atomic-weight nuclei present, the number of slow neutrons that strike the lithium iodide crystal reflects the amount of moisture in the soil. The light signal that is emitted when the slow neutrons strike the lithium iodide crystal is amplified by the photomultiplier tube. The amplified signal is transmitted to a rate meter and recorded on pressure-sensitive paper.

A selection of 5 time constants (2, 7, 15, 20, and 30) is available on the rate meter. These constants represent the time period required for the original charge on the condenser to be reduced 37 percent (Pirson, 1963). Because the values of the constants are approximate, each rate meter should be individually evaluated for best results. The signal recorded for each constant represents an average current for a series of discrete bursts charged by a capacitor and discharged through a resistor. Thus, the inherent averaging process smooths out variations due to statistical fluctuation. The logger has been adapted so that the speed at which

the probe is moved can be varied from less than 1 foot to 60 feet per minute.

CALIBRATION OF PROBE

The relation of the amplitude of the neutron signal or readings in instrument units to volumetric moisture content was determined by field calibration. Strata of uniform lithology were selected where the readings were constant for a vertical distance of at least half a foot. Samples were collected from these strata, and their volumetric moisture content was determined gravimetrically. The readings in instrument units and gravimetric moisture values for these strata were used in the preparation of the calibration curve shown in figure 1. The relationship between instrument units and volumetric moisture content is linear from 5 to 40 percent. Below 5 percent the slope of the curve decreases with decreasing instrument units.

The equation for the linear portion of the curve is

$$Y = 1.3X - 8.1,$$

in which Y is the volumetric moisture content; 1.3, the slope of the line; X, the instrument reading; and —8.1, the Y intercept.

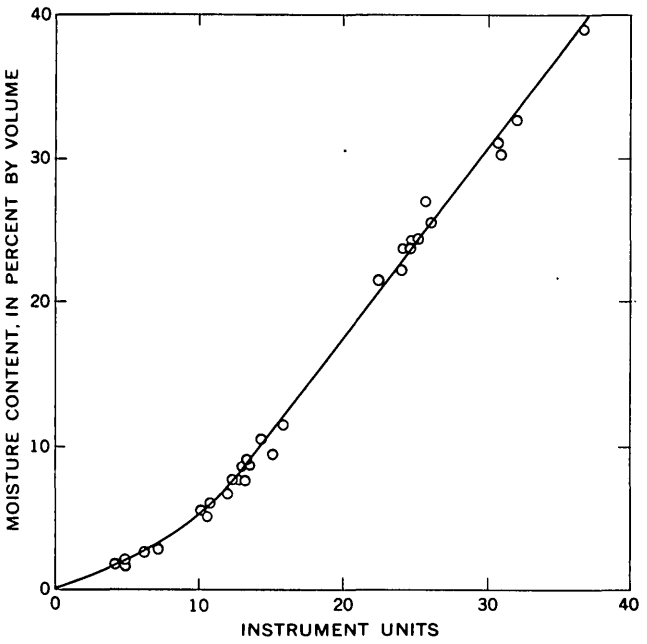

FIGURE 1.—Instrument calibration curve.

LOGGING PROCEDURES

The random decay process inherent in radioactive measurements causes statistical values to fluctuate from a mean value (Pirson, 1963; Tittman, 1956). Thus, the received neutron count must be averaged for a period of time to obtain an accurate reading. When the probe is moved, the averaging process tends to smooth out variations with depth, and details of the moisture-depth profile are obscured. The loss of detail is increased when long time constants or fast logging speeds are used. When the time constant is short, the readings are more erratic and duplicated with less accuracy than readings for a longer time constant. Reducing the logging speed to obtain accuracy, however, increases the time necessary to make a log. Consequently, it is not possible to obtain both speed and accuracy when operating the neutron logger. In the selection of the most desirable logging procedure, a compromise is required between good bed definition, curve reproducibility, and logging time.

Data presented in figures 2 and 3 illustrate some of the considerations in the selection of a logging procedure. These data show the definition of a 0.25-foot-thick bed of sandy clay obtained by different logging procedures. At this site, several feet of sand and gravel occurs both above and below the sandy clay bed, and the lithologic contacts are sharp. Samples for gravimetric moisture determinations were obtained as the tubing was installed. The sand and gravel contained 4.5 and 7 percent moisture by volume.

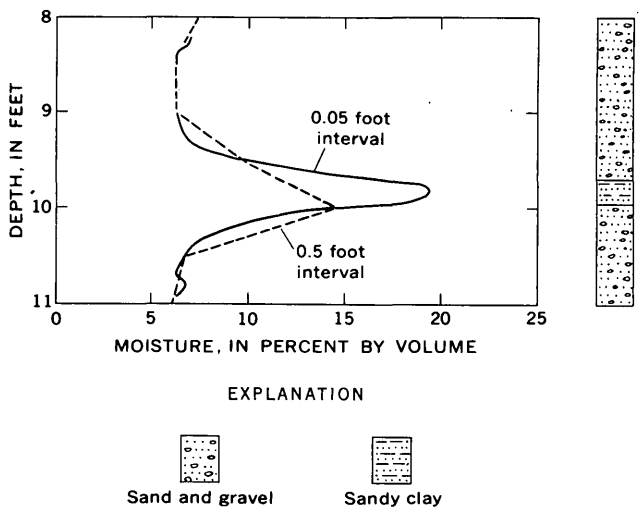

FIGURE 2.—Point log showing effect of depth interval on neutron moisture curve.

Continuously recorded neutron logs were run from the bottom of the hole to the top. Continuous moisture logs were made by plotting moisture values (converted from instrument units by using the calibration curve) at 0.125-foot intervals. Point moisture logs were made by plotting the moisture values based on the average instrument reading at the indicated depth intervals.

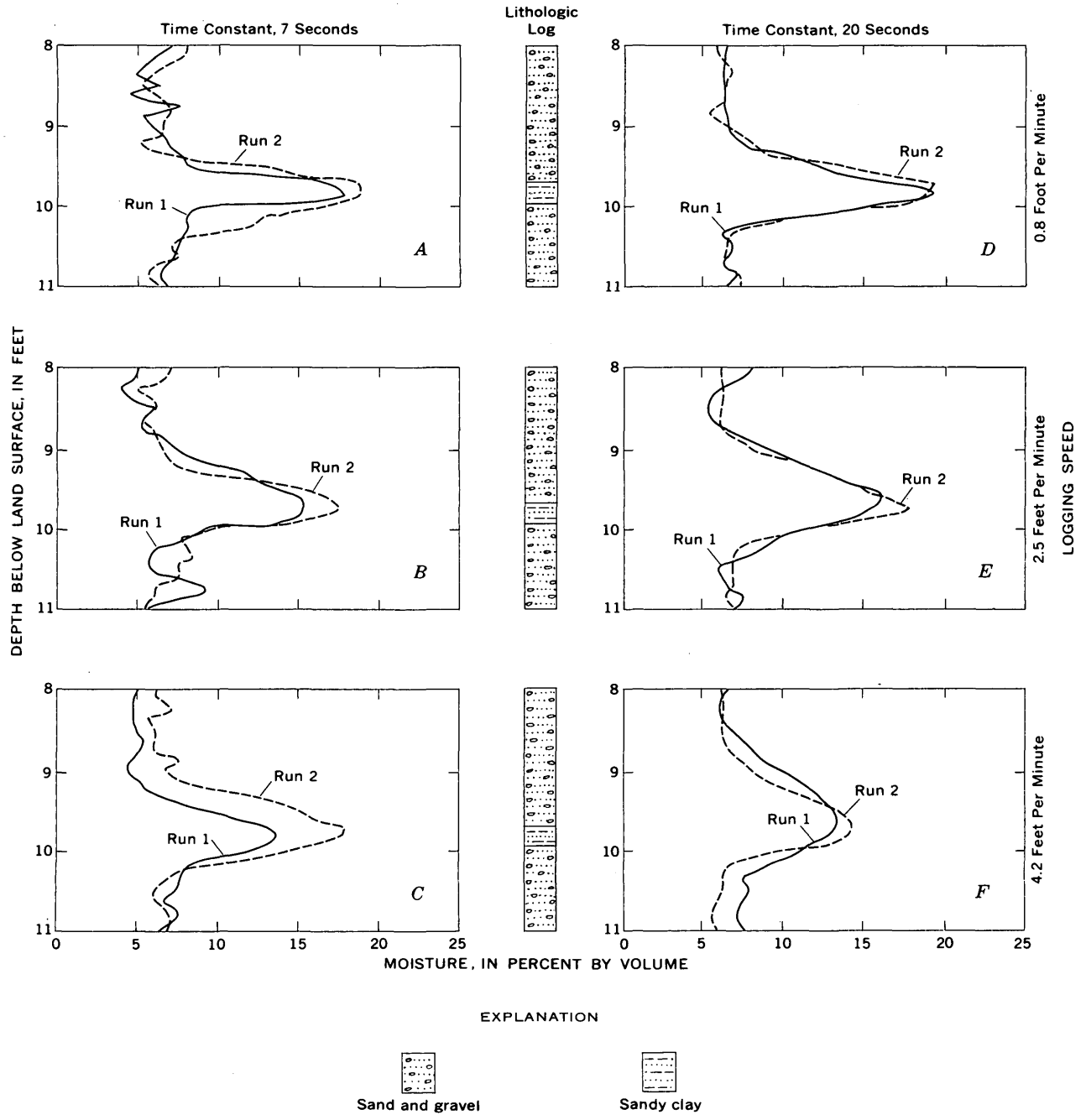

FIGURE 3.—Continuous logs showing effects of logging speed and time constant on reproducibility of neutron moisture curve.

Point logging

The logs shown in figure 2 were obtained by point logging. The neutron log shown by the solid line is from data at 0.05-foot depth intervals obtained by recording for 3-minute periods with the time constant set at 20 seconds. The time required to run this log was 4 hours. The dashed line represents a plot of data from the same neutron log using only the moisture values for 0.5-foot intervals. By comparison, the time required to run this log would have been about 25 minutes.

The neutron log for 0.05-foot intervals approximates the maximum definition of the moisture-depth profile obtainable with the neutron moisture-meter. With the probe positioned at the center of the sandy clay strata, the moisture reading was 19 percent compared to a gravimetric measurement for this zone of 35 percent.

The neutron signal was evidently affected by the lower moisture values in the adjacent sand and gravel.

Data obtained at other neutron-logging sites during this study suggest that a minimum of 1 foot of sandy clay would be required to obtain a maximum moisture reading. This is comparable to the minimum thickness reported for other types of neutron probes (McHenry, 1963).

Although the neutron point log at 0.05-foot intervals gives a maximum zone definition, the time required to obtain these data would be prohibitive in most soil-moisture studies. Thus, in a practical application, a depth interval of much more than 0.05 foot would be required. As illustrated in figure 2, measurements at the 0.5-foot intervals showed a deflection on the log, caused by the sandy clay bed that poorly defined the moisture profile. The positioning of the probe can be critical when the point-logging technique is used. For example, a 0.1-foot depth error at the 10-foot depth interval in the example shown in figure 2 would result in an error of moisture measurement of about 4 percent.

Continuous logging

The effect of the time constant and speed on the continuous neutron moisture log is illustrated in figure 3. Duplicate neutron moisture logs were run at time constants of 7 and 20 seconds, and at speeds of 0.8, 2.5, and 4.2 feet per minute. The logs run with the time constant at 20 seconds show much better reproducibility and are less erratic than those run with the time constant at 7 seconds. The logs run at a speed of 0.8 foot per minute have moisture-depth curves similar to the log obtained by point logging at 0.05-foot interval. The duplicate logs obtained with the time constant at 20 seconds and a logging speed of 0.8 foot per minute show the best reproducibility.

When the logging speed is increased, the amplitude of the deflection caused by the sandy clay bed is reduced and the deflection is spread over a larger depth interval. These effects are more pronounced for the logs obtained with the time constant at 20 seconds than for logs obtained with a time constant of 7 seconds as the longer averaging process had a tendency to smooth out the moisture variations and obscure details of the moisture-depth profile.

The reproducibility of the continuous neutron moisture log is further illustrated in figure 4. Logs run in the morning (a.m.) and the afternoon (p.m.) of the same day are shown for a 16-foot section. The logs were run at a time constant of 20 seconds and a logging speed of 0.8 foot per minute. A comparison of moisture values at the same depth interval for the two logs shows that the moisture values are generally within 1 percent. The peak moisture value at 15.2 feet is the same for both logs, at 24.5 to 25 feet is slightly higher on the afternoon log, and at 26.5 feet is slightly higher on the morning log. The moisture values in the sand between 16.5 and 22.5 feet have a maximum difference of slightly more than 1 percent; neither log shows a tendency for higher or lower values in this 6-foot interval. The random occurrence in moisture-value differences indicates that the principal cause for these variations is statistical fluctuation.

SELECTION OF LOGGING PROCEDURES

Selection of the best logging procedure depends upon the purpose for which the neutron moisture log is intended. The point-logging procedure using close inter-

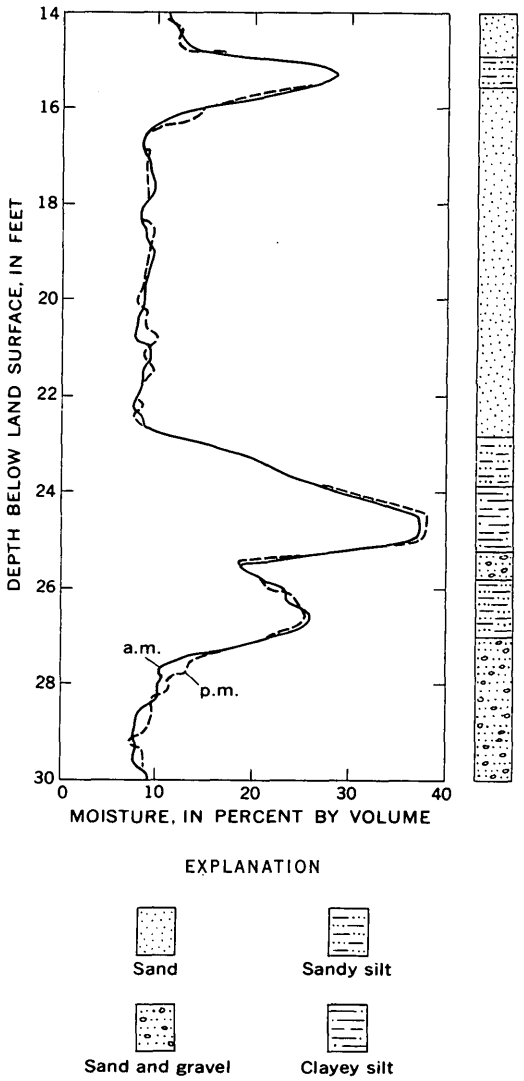

FIGURE 4.—Reproducibility of continuous neutron moisture logs. Time constant is 20 seconds and logging speed is 0.8 foot per minute.

vals provides the most accurate moisture measurements but requires much more time and manual operation than continuous logging. The use of a long time constant in both procedures appears desirable for the quantitative measurements of moisture changes because the effects of statistical fluctuations are minimized. Good zone definition and moisture-change accuracy are obtainable in continuous logging at a speed of 0.8 foot per minute and a time constant of 20 seconds. Faster logging speeds may be advantageous in some studies, although the zone definition will be reduced and moisture measurements will be less accurate. For example, increased logging speeds may be needed to reflect rapid moisture changes due to drainage during a pumping test or due to the advancement of a wetting front during an infiltration experiment. At these times, a short time constant may be desirable where zone definition is a principal concern. The selection of the most appropriate logging speed and time constant should be based on the required accuracy and zone definition and the time required to obtain the moisture log.

REFERENCES

McHenry, R. J., 1963, Theory and application of neutron scattering in the measurement of soil moisture: Soil Sci., v. 95, p. 294–307.

Pirson, S. J., 1963, Handbook of well log analysis: Prentice-Hall, Inc., Englewood Cliffs, N. J., 326 p.

Tittman, Jay, 1956, Radiation logging, fundamentals of logging: Petroleum Eng. Conf., Univ. Kansas, April 2, 3, 1956, p. 115–154.

SUBJECT INDEX

[For major headings such as "Economic geology," "Geophysics," "Paleontology," see under State names or refer to table of contents]

AUTHOR INDEX

U. S. GOVERNMENT PRINTING OFFICE : 1968 O - 285-544